



**UNIwersYTET  
MIKOŁAJA KOPERNIKA  
W TORUNIU**  
Wydział Chemii

Uniwersytet Mikołaja Kopernika w Toruniu

Wydział Chemii

Katedra Chemii Fizycznej i Fizykochemii Polimerów

**Mgr Guoqiang Li**

**Rozprawa doktorska**

**Polymeric membranes and mixed matrix membranes (MMMs) for carbon dioxide separation**

**Promotor**

**Prof. dr hab. Wojciech Kujawski**

**Promotor pomocniczy**

**Dr hab. Joanna Kujawa, prof. UMK**

Toruń 2024

## Acknowledgements

Firstly, I would like to express my sincere gratitude to my supervisor Prof. Wojciech Kujawski for providing me the opportunity to make my PhD in his group – Membranes and Membrane Techniques Research Group. I would like to thank him for his selfless help, inspirational guidance, fruitful discussions, valuable suggestions and tremendous effort for reviewing and correcting the manuscripts of my PhD thesis and scientific publications. During my whole PhD study life, Prof. Wojciech Kujawski encourages and supports me to take advantage of every opportunity such as internships, competitions, grants, and conferences, which enriches my research life and achievements. He sets a good example to show me how to be a good researcher, how to work as a team member in the research group, how to prepare the manuscript for articles, and how to exhibit research results in conferences. Moreover, he provides me the financial support by letting me work in his research projects since he knows I am a self-funded student. I am truly grateful to Prof. Wojciech Kujawski for all the opportunities and strong support in my research and daily life.

I would like to specially thank dr hab. Joanna Kujawa for her help in characterizations of my samples, and the preparation of applications for grants and competition, and suggestions in the experimental data analysis, manuscript preparation, and the preparation of presentations and posters for conferences.

I would like to express my sincere gratitude to dr Katarzyna Knozowska for her help in the synthesis of MOFs, preparation of membranes, demonstration of pervaporation experiment, and problem-solving in the daily laboratory life.

I would like to particularly thank dr Edyta Rynkowska for her help and suggestions in the preparation and publication of my first scientific article.

I would like to express my deep gratitude to dr Anna Kujawska for her help in my first year of PhD study and her kind “push” in my Polish language.

I would like to specially thank my colleagues Waldemar Jankowski, Mohammad Ebrahimi, and dr Mariusz Banach for their help in the laboratory and exams, for the fruitful discussions about research and life, conferences we attended together, and for the support in my PhD study life.



I would like to express my sincere gratitude to the members of Department of Physical Chemistry and Physiochemistry of Polymers at the NCU in Toruń: dr Piotr Adamczak, dr Magdalena Gierszewska, prof. Stanisław Koter, dr Izabela Koter, dr hab. Jacek Nowaczyk, dr hab. Ewa Olewnik-Kruszkowska, dr hab. Piotr Szczepański for all the help, and suggestions.

I would like to particularly thank dr Robert Válek from MemBrain for his help and demonstration for the fabrication of hollow fibers, dr Andrius Tonkonogovas from Lithuanian Energy Institute and prof. Pavel Izák and dr Petr Stanovský from Institute of Chemical Process Fundamentals of the CAS for their help in the gas permeance measurements.

I would like to express my deep gratitude to all my friends Yi Zhou, Yi Zhang, Haitian, Chengcheng, Lianjie, Xiaomei, Yuan, Wen, Xiao, Yangyu, Haopeng, Ziyun, Xiaochen, Xiaorong, Guodong, and Leilei for their help, accompany, friendship and support during my study in Poland.

Last but not least, I would like to thank my family, especially my parents and my wife, for their unconditional support and love. 家人的爱，理解，和默默的支持是我前进路上源源不绝的动力。是你们成就了今天的我，我会永远的爱你们，为我们的家庭贡献出自己的力量。

## Table of contents

Acknowledgements.....	2
Abbreviations and nomenclature .....	6
1. Introduction.....	8
1.1 The background review of the work.....	8
1.2 Motivation and objectives of the work.....	19
2. Research conducted in this thesis .....	21
2.1 Fabrication and characterization of hollow fiber membranes (HFMs) .....	23
2.1.1 A review of the development of hollow fiber membranes for gas separation processes (Publication I).....	23
2.1.2 The effects of PEI hollow fiber substrate characteristics on PDMS/PEI hollow fiber membranes for CO <sub>2</sub> /N <sub>2</sub> separation (Publication II). .....	24
2.1.3 Fabrication of polydimethylsiloxane (PDMS) dense layer on polyetherimide (PEI) hollow fiber support for the efficient CO <sub>2</sub> /N <sub>2</sub> separation membranes (Publication III). .....	27
2.1.4 Thin film mixed matrix hollow fiber membrane fabricated by incorporation of amine functionalized metal-organic framework for CO <sub>2</sub> /N <sub>2</sub> separation (Publication IV).....	30
2.2 Fabrication and characterization of flat sheet mixed matrix membranes (FS-MMMs) .....	34
2.2.1 Evaluation of CO <sub>2</sub> separation performance with enhanced features of materials - Pebax <sup>®</sup> 2533 mixed matrix membranes containing ZIF-8-PEI@[P(3)HIm][Tf <sub>2</sub> N] (Publication V).....	34
2.2.2 Pebax <sup>®</sup> 2533/PVDF thin film mixed matrix membranes containing MIL-101 (Fe)/GO composite for CO <sub>2</sub> capture (Publication VI).....	38
3. Conclusions.....	42
4. Future work and research directions .....	44
5. References.....	45
6. Abstract.....	52

7. Streszczenie: .....	53
8. List of publications included in this dissertation .....	55
9. Academic achievements.....	56
10. Statements of co-authors.....	63
11. Copies of publications included in the thesis.....	78

## Abbreviations and nomenclature

[Bmim][Tf <sub>2</sub> N]	1-butyl-3-methylimidazolium bis(trifluoromethanesulfonyl)imide
[P(3)HIm][Tf <sub>2</sub> N]	1-allyl-3H-imidazolium bis(trifluoromethanesulfonyl)imide
BET	Brunauer-Emmett-Teller
bPEI	Branched polyethyleneimine
CA	Cellulose acetate
DLS	Dynamic light scattering
EDX	Energy-dispersive X-ray spectroscopy
FSM	Flat sheet membrane
FS-MMM	Flat sheet mixed matrix membrane
FTIR-ATR	Fourier Transform Infrared Spectroscopy with Attenuated Total Reflectance
GO	Graphene oxide
HFM	Hollow fiber membrane
HF-MMM	Hollow fiber mixed matrix membrane
HKUST	Hong Kong University of Science and Technology
MIL	Materials of Institut Lavoisier
MMM	Mixed matrix membrane
MOF	Metal organic framework
MUF	Massey University Framework
MWCNT	Multi-wall carbon nanotubes
PA	Polyamide
PDMS	Poly(dimethylsiloxane)
Pebax	Poly(ether block amide)
PEGDE	Poly(ethylene glycol) diglycidyl ether
PEI	Polyetherimide
PES	polyethersulfone
PI	Polyimide
PIM	Polymers of intrinsic microporosity
PP	Polypropylene
PPO	Poly(p-phenylene oxide)
PSF	Polysulfone
PVA	Poly (vinyl alcohol)
PVAc	Polyvinlyl acetate
PVAm	Polyvinylamine
RTIL	Room temperature ionic liquids
SEM	Scanning electron microscope
STEM	Scanning transmission electron microscopy
TFC-HFM	Thin film composite hollow fiber membrane

TFN	Thin film nanocomposite
TGA	Thermogravimetric analysis
UiO	University of Oslo
XRD	X-ray diffraction
ZIF	Zeolitic imidazolate framework

# 1. Introduction

## 1.1 The background review of the work

Gas separation plays an important role in various industrial processes, *e.g.*, oxygen enrichment, helium separation, hydrocarbons recovery, inert gas separation, air dehumidification, flue gas treatment, biogas upgrading, hydrogen purification, and natural gas sweetening [1-4]. Natural gas mainly contains methane and some gas impurities (*e.g.*, CO<sub>2</sub>, and H<sub>2</sub>S). The presence of gas impurities undermines the energy quality of natural gas and creates pipeline corrosion in the transporting process, which is problematic for its practical applications. Therefore, the gas impurities must be removed to purify the natural gas [5, 6]. Biogas containing 60-70 vol% CH<sub>4</sub> and 30–40 vol% CO<sub>2</sub> is an important renewable energy resource since the limited fossil fuels are under depletion. However, in order to improve the energy quality and prevent the corrosion of the transporting pipelines, CO<sub>2</sub> must be removed to purify biogas [7]. Hydrogen is a sustainable and environmental friendly energy source. However, raw hydrogen generated from thermochemical process or dark fermentation process is not able to meet the purity requirements in many cases. Therefore, it is essential to purify hydrogen to meet the purity requirements of various potential applications [1, 8].

Chemical absorption [9], adsorption [10], and cryogenic separation [11] are widely used for gas separation. Chemical absorption is a mature technology which can provide better purification performance in the CO<sub>2</sub> separation process [12]. However, the heat energy used for the regeneration of chemical solvents such as amine solvents is substantial, which makes chemical absorption an energy intensive process. Additionally, chemical absorption requires a large area to install the necessary equipment such as absorber, solvent pumps, strippers, heat exchanger and so on [12]. Cryogenic separation can also provide a good CO<sub>2</sub> capture performance. Comparing with the chemical absorption, cryogenic separation is a simpler process which is more environmentally friendly since no chemical reaction is involved [12]. However, it requires the refrigeration equipment and consumes a lot of energy. Therefore, in order to achieve the goal of carbon neutrality, more efficient CO<sub>2</sub> separation technology is highly needed.

Membrane separation technology was developed for gas separation processes, such as CO<sub>2</sub> separation process. Membrane-based technologies for gas separation have shown many advantages, such as lower capital and processing cost, high compactness and light weight, easy upscaling, low labour intensity, low maintenance, lower energy consumption, and environmental

friendliness, in comparison to the traditional gas separation technologies, *e.g.*, chemical absorption and cryogenic process [1, 13]. Polymeric membranes can be assembled into membrane modules such as spiral wound module and hollow fiber module, which significantly increased their compactness and separation efficiency in the separation processes [14]. Comparing with chemical absorption process, there is no chemicals nor high amount of energy involved in the membrane separation process. Moreover, the membrane separation is much simpler than chemical absorption process. Comparing with the cryogenic separation process, the membrane separation process is operated in mild temperature conditions instead of extremely low temperature conditions. As a result, much less energy is needed to maintain the operation conditions [12-14]. Therefore, membrane technology shows great potential and practical value in the industrial gas separation processes. However, the research on the development of membrane technology, such as the research on the membrane material, the membrane fabrication techniques, the optimization of the membrane gas separation processes, is still highly demanded.

The proper selection of polymer materials is important to obtain membranes with high gas separation performance. Commercial polymers such as polysulfone (PSF), polyvinylamine (PVAm), polyvinyl alcohol (PVA), polycarbonates, poly(phenylene oxides) (PPO), cellulose acetate (CA), polyether block amide (Pebax), polydimethylsiloxane (PDMS), polyetherimide (PEI) and polyimides (PI), are used for the fabrication of gas separation membranes [15, 16]. In addition to the commercial polymers, some emerging polymer materials such as the thermally rearranged polymers [17], perfluoropolymers [18], polymers of intrinsic microporosity (PIMs) [19], and polymerized room temperature ionic liquids (poly(RTIL)s) [20], have been used to fabricate membranes and subsequently investigated in gas separation processes [15]. The gas permeability and selectivity of polymeric membranes are mainly dependent on the intrinsic properties of polymer materials. The selection of polymers and the optimization of the fabrication conditions are crucial to obtain membranes possessing high gas separation performance.

Both flat sheet membranes (FSMs) and hollow fiber membranes (HFMs) are used in gas separation processes. Comparing with FSMs, HFMs possess several advantages. HFMs possess a self-supporting structure and high packing density [21, 22], which makes them highly efficient for large scale gas separation processing. The asymmetric HFMs are generally fabricated by using dry-jet wet spinning technique [23]. However, in comparison to the fabrication of flat sheet membranes, the fabrication of HFMs is much more complex, this is because a lot of parameters

should be controlled in the HFMs fabrication processes. For instance, the morphology and structure of HFMs are influenced by the following parameters: the composition of the dope and bore fluid, the composition and temperature of the external coagulant, the temperatures of dope and bore fluid, the structure and dimension of the spinneret, the flow rate of the bore fluid, the dope extrusion rate, the length of air gap, and the take-up speed [24, 25]. To obtain desirable HFMs, each parameter should be controlled as it can influence the resulting performance of hollow fibers [26-29].

In addition to the asymmetric HFMs, the thin film composite hollow fiber membranes (TFC-HFMs) [30, 31] possess a porous support and a dense selective layer which are prepared from different materials. In general, the porous support is fabricated by using a phase inversion method, and the dense selective layer is fabricated by using dip-coating [32], plasma polymerization [31], interfacial polymerization [33, 34], and dual-layer spinning [33]. The totally integral asymmetric HFMs are usually fabricated by the non-solvent induced phase inversion techniques [35]. Additionally, dual-layer asymmetric hollow fiber membranes can be fabricated if a triple orifice spinneret is applied [36]. The preparation of hollow fiber mixed matrix membranes (HF-MMMs) can further enhance the gas separation performance of HFMs. UiO-66-NH<sub>2</sub> particles, an amine functionalized metal organic frameworks (MOFs), were incorporated into the Pebax<sup>®</sup> 2533 coating solution. Subsequently, the Pebax<sup>®</sup> 2533 selective layer containing UiO-66-NH<sub>2</sub> was formed on the outer surface of polypropylene (PP) hollow fibers. The prepared HF-MMMs demonstrated increased gas permeance and selectivity owing to the porous structure and the amine functional group of UiO-66-NH<sub>2</sub> [37]. More detailed review and discussion related to the development and fabrication of asymmetric HFMs, TFC-HFMs, and HF-MMMs can be found in publications I [16], II [38], III [39], and IV [37] from this thesis.

The trade-off relationship exists for polymeric membranes, that is, the selectivity decreases when the permeability of more permeable gas increases. As it is shown in Figure 1, the upper bound sets a limit for obtaining polymeric membranes with high gas permeability along with high selectivity, owing to the trade-off relationship [40]. Therefore, the preparation of heterogenous membranes can be a good solution to exceeding the upper bound. Surface modification [41] and the preparation of MMMs [42] are effective ways to exceeding the upper bound limit. Additionally, carbon molecular sieving membranes prepared by the carbonization of aromatic polymeric membranes is another approach to break the upper bound limitation [43].



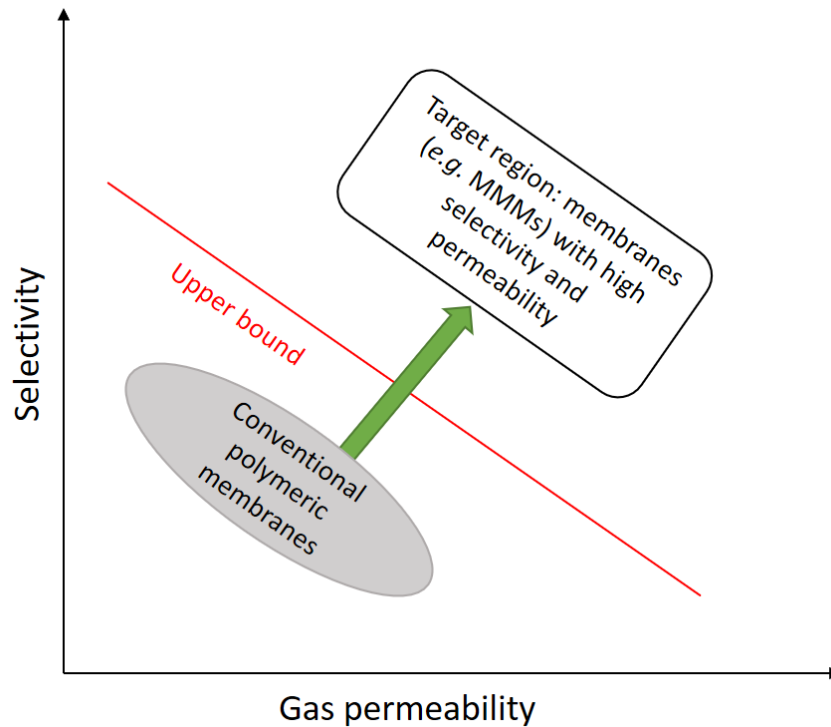


Figure 1. Illustration of the trade-off relationship for polymeric membranes in gas separation.

MMMs are organic-inorganic heterogenous membranes, which can be obtained by incorporating inorganic fillers into a polymeric matrix. MMMs combine the advantages of the desirable processability of polymers with the high gas separation performance of inorganic fillers, resulting in the enhanced gas permeability and selectivity [44]. The presence of inorganic fillers can increase the gas permeability of MMMs since the porous structure of inorganic fillers increases the free volume of membranes and provides additional pathways for gas molecules, resulting in the increased diffusivity coefficient [42]. In some cases, the inorganic fillers show higher affinity to the more permeable gas molecules, resulting in the increased solubility coefficient [45]. The high gas selectivity of MMMs results from the size sieving effect derived from the specific pore sized of inorganic fillers, the increased solubility coefficient, and the facilitated transport mechanism for the more permeable gas molecules [45, 46].

Although MMMs have shown enhanced gas separation performance in comparison to the pristine polymeric membranes, there are still challenges and problems existing for the preparation of defect-free MMMs. The main problem is the poor compatibility between inorganic fillers and polymer matrix, which creates nonideal interfacial morphology in MMMs such as the nonselective interface voids, the aggregation of fillers, the polymer rigidification around the fillers, and the pore

blockage of fillers [44, 47]. The filler aggregation can generate nonselective defects in membranes and the interfacial voids can form bypass for gas molecules, resulting in the decrease in the separation efficiency. The polymer rigidification restricts the mobility of polymer chains, resulting in the increased resistance for gas transport and the decreased gas permeability. Similarly, the blockage of filler pores can change the porous structure of fillers into impermeable particles, which results in the higher tortuosity for gas molecules transport and the decreased permeability [48].

In order to fabricate the defect-free MMMs, the above mentioned challenges and problems must be mitigated. Several approaches have been applied to improve the interfacial morphology and compatibility, such as an addition of plasticizer, blending of polymer additives, the utilization of copolymers, and the surface modification of inorganic fillers [42]. The surface modification of inorganic fillers can effectively adjust the interfacial morphology since the modified fillers show high compatibility with polymer matrix by forming hydrogen bonds, electrostatic interaction, and coordination bonds.

The proper selection of inorganic fillers is also important to obtain the defect-free MMMs. Among various types of inorganic fillers, MOFs are desirable fillers for the preparation of MMMs. MOFs are porous crystals consisting of metal nodes and organic ligands. MOFs possess uniform pore sizes, various topologies, high surface areas, connected channels for molecules transport and tailored functionalities, which makes MOFs suitable for various separation processes, especially the gas separation process by using membranes [49]. Wang et al. [50] synthesized ZIF-301 and incorporated into 6FDA-DAM polyimide matrix to fabricate ZIF-301/6FDA-DAM MMMs for CO<sub>2</sub>/CH<sub>4</sub> separation. It was found that the synthesized ZIF-301 possessed the Langmuir BET surface equal to 623.5 m<sup>2</sup>/g and higher adsorption capacity for CO<sub>2</sub> (25.31 cm<sup>3</sup>/g) over CH<sub>4</sub> (9.30 cm<sup>3</sup>/g). The ZIF-301 crystals were homogeneously dispersed in polyimide matrix without agglomeration when the filler loading was up to 20 wt%. The MMMs containing 20 wt% of ZIF-301 showed the highest CO<sub>2</sub> permeability equal to 891 Barrer and CO<sub>2</sub>/CH<sub>4</sub> selectivity equal to 29.3, which is attributed to the high CO<sub>2</sub> affinity and the aperture molecular sieving effect of ZIF-301. The CO<sub>2</sub>/CH<sub>4</sub> separation performance surpassed the 2008 Robeson upper-bound. Chen et al. [51] synthesized MOF-801 and prepared MMMs by incorporating MOF-801 into PIM-1 polymer matrix. The prepared MMMs were used for CO<sub>2</sub> separation. The prepared MOF-801/PIM-1 MMMs showed high CO<sub>2</sub> permeability equal to 9686 Barrer along with a CO<sub>2</sub>/N<sub>2</sub> ideal selectivity equal to 27, which is owing to the uniform dispersion of the CO<sub>2</sub>-philic MOF-801 providing

channels for the rapid and selective transport of CO<sub>2</sub> molecules. In comparison to the pristine membranes, the prepared MMMs enhanced their resistance to aging since the gas permeability remained over 70% after 90 days aging test, which is attributed to the enhanced binding force between fillers and PIM-1 polymer chains, and the increased rigidity, resulting from the good compatibility of MOF-801 with PIM-1.

In the preparation of MMMs for gas separation, the pore size and surface functionality of MOFs can be controlled *via* physical and chemical modification, endowing MOFs with precise molecular size sieving effect and high adsorption affinity for the target gas molecules. Wang et al. [52] synthesized nanoporous NH<sub>2</sub>-ZIF-7 by partially replacing benzimidazole with 2-aminobenzimidazole in ZIF-7. The synthesized NH<sub>2</sub>-ZIF-7 nanoparticles were incorporated into polymers of intrinsic microporosity (PIM-1) to prepared MMMs for biogas upgrading. It was found that NH<sub>2</sub>-ZIF-7 nanoparticles possess bigger window size than ZIF-7, which is beneficial for the CO<sub>2</sub> transport. In addition, NH<sub>2</sub>-ZIF-7 showed high specific surface area and the ability of forming hydrogen bond with polymer chains, which is helpful to avoid the formation of non-selective voids in MMMs. As a result, the mechanical properties and the aging resistance of MMMs were improved. In comparison to the pristine PIM membranes, the prepared MMMs containing 20 wt% NH<sub>2</sub>-ZIF-7 demonstrated CO<sub>2</sub> permeability of 2953 Barrer and 65% higher CO<sub>2</sub>/CH<sub>4</sub> selectivity of 21. The improvement of gas separation performance can be attributed to the interfacial rigidification of polymer chains and the intrinsic properties of NH<sub>2</sub>-ZIF-7, resulting in the increased diffusion selectivity of MMMs.

In addition to the *in-situ* modification of MOFs by using mixing linkers, Chuah et al. [53] modified HKUST-1 by using the post-synthetic method. The synthesized HKUST-1 was modified with 3-picolyamine. Subsequently, the MMMs were prepared by incorporating the amine modified HKUST-1 into the Matrimid matrix in order to improve the CO<sub>2</sub>/N<sub>2</sub> selectivity. It was found that the crystal structure of HKUST-1 was preserved after amine modification. While the BET surface area and the total micropore volume decreased after amine modification. The gas permeation results demonstrated that the incorporation of unmodified HKUST-1 significantly increased the CO<sub>2</sub> permeability without changing the CO<sub>2</sub>/N<sub>2</sub> selectivity. However, the prepared MMMs containing 20 wt% amine modified HKUST-1 showed 25% higher CO<sub>2</sub> permeability of 13 Barrer and 38% higher CO<sub>2</sub>/N<sub>2</sub> selectivity of 43, comparing with the pristine Matrimid membranes. The amine modified HKUST-1 could suppress the diffusivity and solubility of N<sub>2</sub> but

increase the diffusivity of CO<sub>2</sub> significantly. Chen et al. [54] modified MOF-801 with [bmim][Tf<sub>2</sub>N] *via* wet impregnation since [bmim][Tf<sub>2</sub>N] possesses high CO<sub>2</sub> affinity owing to the interaction between the quadrupole moment of CO<sub>2</sub> and the electrical charge of [bmim][Tf<sub>2</sub>N]. Subsequently, the [bmim][Tf<sub>2</sub>N]@MOF-801 nanocomposite was incorporated into PIM matrix to prepare MMMs with enhanced gas separation performance. It was found that MMMs containing 5 wt% of [bmim][Tf<sub>2</sub>N]@MOF-801 exhibited 129% higher CO<sub>2</sub> permeability of 9420 Barrer and 45% higher CO<sub>2</sub>/N<sub>2</sub> selectivity of 29, comparing with pristine PIM-1 membranes. More active sites in [bmim][Tf<sub>2</sub>N]@MOF-801 were exposed, resulting in the improvement of CO<sub>2</sub> adsorption since MOF-801 could well dispersed [bmim][Tf<sub>2</sub>N] in the polymer matrix. The porous structure of MOF could also enhance the gas adsorption and diffusion. MMMs showed desirable anti-plasticization and anti-aging features owing to the good chemical stability of [bmim][Tf<sub>2</sub>N]@MOF-801.

Table 1 summarized the gas separation performance of FS-MMMs containing MOFs. Various types of MOFs were synthesized and used as fillers in MMMs for CO<sub>2</sub> separation, such as UiO [55-59], ZIF [50, 52, 60-62], HKUST [53, 63], and MIL [64-66]. These MOFs used for CO<sub>2</sub> separation usually possess relatively high BET surface area, high CO<sub>2</sub> adsorption capacity, ease of functionalization, and size sieving effects. According to the aforementioned discussion and Table 1, MOFs could be directly incorporated into polymer matrix for the fabrication of MMMs for gas separation. MOFs could increase the gas permeability without decreasing the gas selectivity, owing to its porous structure and high affinity to CO<sub>2</sub> molecules. Moreover, the material properties of MMMs were also enhanced. For example, the MMMs usually possess high mechanical and thermal stability, and good anti-aging and anti-plasticization properties. In order to further enhance the compatibility between MOFs and polymer chains and obtain more homogeneous distribution of MOFs in polymer matrix, MOFs could be modified by using the *in-situ* modification method [52, 56] and the post-synthetic modification method [53, 57]. The surface modification also tune the pore size, surface area, and the CO<sub>2</sub> affinity of MOFs. As a result, the fabricated MMMs possess uniform distribution of MOFs and enhanced CO<sub>2</sub> separation performance.

Table 1. Comparison of gas separation performance of FS-MMMs containing MOFs (SG - single gas, MG - mixed gas).

Polymers	MOFs	MOF content [wt%]	Gas pairs	$P_{CO_2}$ [Barrer]	Selectivity	Testing conditions	Ref.
Matrimid <sup>®</sup>	UiO-66-NH <sub>2</sub> @ICA	10	CO <sub>2</sub> /CH <sub>4</sub>	40.1	65	25 °C, 3 bar, MG	[55]
Matrimid <sup>®</sup>	UiO-67-33	10	CO <sub>2</sub> /CH <sub>4</sub>	26	75	30 °C, 5 bar, MG	[56]
Matrimid <sup>®</sup>	HKUST-1-25NH <sub>2</sub>	20	CO <sub>2</sub> /N <sub>2</sub>	13	43	35 °C, 1 bar, MG	[53]
Matrimid <sup>®</sup>	ZIF-68	20	CO <sub>2</sub> /N <sub>2</sub>	27	30	35 °C, 10 bar, MG	[60]
		20	CO <sub>2</sub> /CH <sub>4</sub>	25	35		
6FDA-durene	NH <sub>2</sub> -MIL-125 (Ti)	7	CO <sub>2</sub> /CH <sub>4</sub>	1116	37	25 °C, 3.5 bar, SG	[64]
6FDA-DAM	ZIF-301	20	CO <sub>2</sub> /CH <sub>4</sub>	891	29	25 °C, 4 bar, SG	[50]
6FDA-ODA	UiO-66-PEI@[bmim][Tf <sub>2</sub> N]	15	CO <sub>2</sub> /CH <sub>4</sub>	26	60	35 °C, 1 bar, MG	[57]
ODPA-TMPDA	UiO-66	20	CO <sub>2</sub> /N <sub>2</sub>	169	32	35 °C, 1 bar, MG	[58]
	UiO-66-NH <sub>2</sub>			142	37		
	UiO-66-Br			200	35		
	UiO-66-(OH) <sub>2</sub>			125	39		
6FDA-DAM	UiO-66	14	CO <sub>2</sub> /CH <sub>4</sub>	1912	31	35 °C, 2 bar, MG	[59]
	UiO-66-NH <sub>2</sub>	16	CO <sub>2</sub> /CH <sub>4</sub>	1223	30		
	UiO-66-NH-COCH <sub>3</sub>	16	CO <sub>2</sub> /CH <sub>4</sub>	1263	33		
P84	ZIF-8	27	CO <sub>2</sub> /CH <sub>4</sub>	11	93	25 °C, 3 bar, MG	[61]
6FDA-durene	HKUST-Emim[Tf <sub>2</sub> N]	10	CO <sub>2</sub> /N <sub>2</sub>	1102	27	25 °C, 2 bar, SG	[63]
		10	CO <sub>2</sub> /CH <sub>4</sub>	1102	29		
PES	Etched ZIF-8	10	CO <sub>2</sub> /N <sub>2</sub>	15.7	7	25 °C, 1 bar, SG	[67]
PIM-1	Mg-MOF-74	8	CO <sub>2</sub> /CH <sub>4</sub>	1935	12	30 °C, 0.5 bar, SG	[65]
	Mg-MOF-74	8	CO <sub>2</sub> /N <sub>2</sub>	1935	17		
	MIL-53	4	CO <sub>2</sub> /CH <sub>4</sub>	953	13		
	MIL-53	4	CO <sub>2</sub> /N <sub>2</sub>	953	17		
	TIFSIX-3	4	CO <sub>2</sub> /CH <sub>4</sub>	1000	14		
	TIFSIX-3	4	CO <sub>2</sub> /N <sub>2</sub>	1000	19		
PIM-1	NH <sub>2</sub> -ZIF-7	20	CO <sub>2</sub> /CH <sub>4</sub>	2953	21	30 °C, 2 bar, SG	[52]

PIM-1	ZIF-67	15	CO <sub>2</sub> /CH <sub>4</sub>	2800	21	30 °C, 2 bar, SG	[62]
PIM-1	MUF-15	15	CO <sub>2</sub> /N <sub>2</sub>	23000	15	20 °C, 1 bar, SG	[68]
PIM-1	MOF-801	5	CO <sub>2</sub> /N <sub>2</sub>	9686	27	35 °C, 4 bar, SG	[51]
PIM-1	[Bmim][NTf <sub>2</sub> ] @MOF- 801	5	CO <sub>2</sub> /N <sub>2</sub>	9420	29	35 °C, 4 bar, SG	[54]
PIM-1	[bmim][Tf <sub>2</sub> N ] @UiO-66- NH <sub>2</sub>	10	CO <sub>2</sub> /N <sub>2</sub>	8283	23	20 °C, 1 bar, SG	[69]
PIM-1	TSILs@ZIF- 67	10	CO <sub>2</sub> /CH <sub>4</sub>	12848	11	23 °C, 1 bar, SG	[70]
PVA+PVA m/PS	PEGDE- UiO-66-NH <sub>2</sub>	28.5	CO <sub>2</sub> /N <sub>2</sub>	1295 GPU	91	25 °C, 3 bar, MG	[71]
PSF	Bio-MOF-1	30	CO <sub>2</sub> /CH <sub>4</sub>	17	43	25 °C, 10 bar, SG	[72]
PSF	ZIF-11	24	CO <sub>2</sub> /CH <sub>4</sub>	23	43	25 °C, 3 bar, MG	[73]
PVAc	Mg-MOF-74	20	CO <sub>2</sub> /CH <sub>4</sub>	5	25	25 °C, 6 bar, MG	[74]
Pebax	[bmim][Tf <sub>2</sub> N ] @ZIF-8	15	CO <sub>2</sub> /N <sub>2</sub>	105	84	25 °C, 1 bar, SG	[75]
Pebax-1657	MIL-101	15	CO <sub>2</sub> /N <sub>2</sub>	28	89	-20 °C, 3.5 bar, SG	[66]
Pebax-1657	NH <sub>2</sub> -MIL- 101	5	CO <sub>2</sub> /N <sub>2</sub>	30	96	-20 °C, 2 bar, SG	[66]

PIM – Polymers of intrinsic microporosity, PES – Polyethersulfone, PEGDE – Poly(ethylene glycol) diglycidyl ether, PVA – polyvinyl alcohol, PSF – Polysulfone, PEI – branched polyethyleneimine, PVAc – Polyvinyl acetate, Pebax – Poly (ether block amide), UiO – University of Oslo, ZIF – Zeolitic imidazolate framework, MIL – Materials of Institut Lavoisier, MUF – Massey University Framework.

The decoration of porous MOFs on GO nanosheets is an effective way to improve the gas separation performance of MMMs. The MOF@GO composite fillers showed higher compatibility with polymer matrix and can be homogeneously dispersed in polymer matrix owing to the strong steric effect of GO. MOFs possess high porosity, surface area, high affinity to CO<sub>2</sub> molecules, and good thermal stability [76]. Therefore, the combination of MOFs and GO could significantly improve the gas separation performance of MMMs.

Yang et al. [77] synthesized ZIF-8@GO composite fillers by forming a ZIF-8 layer on the GO surface to overcome the stacking and folding issues of GO in MMMs. The prepared ZIF-8@GO composite fillers were incorporated into Pebax matrix to prepare MMMs. The prepared MMMs containing 20 wt% of ZIF-8@GO showed the highest CO<sub>2</sub> permeability of 136 Barrer and CO<sub>2</sub>/N<sub>2</sub> ideal selectivity of 78. Comparing with the pristine membranes, the CO<sub>2</sub> permeability increased by 66% and the CO<sub>2</sub>/N<sub>2</sub> ideal selectivity increased by 60%. It was found that the high porosity of ZIF-8 provided the transporting pathways around GO nanosheets for gas molecules to reduce the mass transfer resistance of GO. As a result, the CO<sub>2</sub> permeability increased. The CO<sub>2</sub>/N<sub>2</sub> selectivity was enhanced by abundant oxy-groups on GO surface. Dong et al. [78] synthesized ZIF-8@GO composite filler and prepared ZIF-8@GO/Pebax MMMs for gas separation. It was found that MMMs containing 6 wt% of ZIF-8@GO showed the CO<sub>2</sub> permeability of 249 Barrer and CO<sub>2</sub>/N<sub>2</sub> ideal selectivity of 47.6 which are 191% and 174% higher than those of pristine Pebax membranes, respectively. The synergistic effects of ZIF-8 and GO resulted in the enhancement of gas separation of MMMs. The high porosity of ZIF-8 could increase the solubility selectivity, while the tortuous diffusion pathways created by GO nanosheets could increase the diffusivity selectivity.

Jia et al. [79] synthesized UiO-66-NH<sub>2</sub>@GO composite by growing UiO-66-NH<sub>2</sub> crystals on GO nanosheets. The synthesized UiO-66-NH<sub>2</sub>@GO composite was incorporated into polyimide to prepare MMMs for CO<sub>2</sub>/N<sub>2</sub> separation. It was found that the composite filler was homogeneously dispersed in polyimide matrix owing to the high-aspect GO nanosheets. The gas separation performance of MMMs was significantly improved owing to the high porosity and the high CO<sub>2</sub> adsorption capacity of UiO-66-NH<sub>2</sub>@GO composite filler. The fabricated MMMs containing 5 wt% of UiO-66-NH<sub>2</sub>@GO exhibited the highest CO<sub>2</sub>/N<sub>2</sub> selectivity of 52, along with the CO<sub>2</sub> permeability of 7 Barrer. Comparing with the pristine polyimide membranes, the CO<sub>2</sub>/N<sub>2</sub> selectivity increased by 80% and the CO<sub>2</sub> permeability increased by 220%. Castarlenas et al. [80]

synthesized UiO-66-GO composite by growing UiO-66 on GO nanosheets *via* the hydrothermal synthesis. Subsequently, the synthesized UiO-66-GO composite was incorporated into polyimide matrix to fabricate MMMs for gas separation. It was found that the UiO-66-GO composite showed good compatibility with polymer chains. The gas separation performance of MMMs was enhanced owing to the barrier effect of GO and the porosity of UiO-66. When 24 wt% UiO-66-GO composite was incorporated into polyimide membranes, the prepared MMMs showed the highest CO<sub>2</sub>/CH<sub>4</sub> selectivity of 51, along with the CO<sub>2</sub> permeability of 21 Barrer.

According to the aforementioned discussion, the incorporation of MOF based composite materials could enhance the gas separation performance of MMMs owing to the synergistic effects of MOFs and carbon nanomaterials *e.g.* GO. Table 2 summarized the gas separation performance of FS-MMMs containing MOF based composite nanomaterials. For the synthesis of MOF composite nanomaterials, ZIF-8 [77, 81-83], UiO-66 [79, 80], and MIL-101[84] are the commonly used MOFs and GO [77, 79, 80, 83] and CNT [82, 84] are the commonly used carbon nanomaterials.

Table 2. Comparison of gas separation performance of FS-MMMs containing MOF based composite nanomaterials (SG - single gas, MG - mixed gas).

Polymers	MOF composites	Filler content [wt%]	Gas pairs	P <sub>CO2</sub> [Barrer]	Selectivity	Testing conditions	Ref.
Matrimid®	UiO-66-NH <sub>2</sub> @GO	5	CO <sub>2</sub> /N <sub>2</sub>	7	52	25 °C, 3 bar, SG	[79]
PEDM	ZIF-8@GO	6	CO <sub>2</sub> /N <sub>2</sub>	475	58	25 °C, 1 bar, SG	[81]
Matrimid®	NiDOBDC/GO	20	CO <sub>2</sub> /CH <sub>4</sub>	10	58	25 °C, 1 bar, MG	[85]
Pebax	MWCNTs@ZIF-8	8	CO <sub>2</sub> /N <sub>2</sub>	186	61	35 °C, 5 bar, SG	[82]
Matrimid®	UiO-66-GO	24	CO <sub>2</sub> /CH <sub>4</sub>	21	51	35 °C, -, MG	[80]
6FDA-durene	NH <sub>2</sub> -MIL-101@CNT	10	CO <sub>2</sub> /CH <sub>4</sub>	1037	25	25 °C, 2 bar, SG	[84]
PES	rGO-ZIF-8	2	CO <sub>2</sub> /CH <sub>4</sub>	8955 GPU	14	25 °C, 4 bar, SG	[83]
Pebax	ZIF-8@GO	20	CO <sub>2</sub> /N <sub>2</sub>	136	78	25 °C, 3 bar, SG	[77]

PEDM – P(PEGMA-co-DEAEMA-co-MMA) copolymer, Pebax – Poly (ether block amide),

PES – Polyethersulfone, UiO – University of Oslo, ZIF – Zeolitic imidazolate framework, MIL – Materials of Institut Lavoisier, GO – Graphene oxide, MWCNTs – Multi-wall carbon nanotubes.



## 1.2 Motivation and objectives of the work

The excess CO<sub>2</sub> emission into the atmosphere results in the serious environmental problems such as global warming and climate change. The control of the CO<sub>2</sub> emission has drawn the global concern. Therefore, it is important to develop environmentally friendly technologies to capture CO<sub>2</sub> and reduce the emission of CO<sub>2</sub> into atmosphere. Separation of CO<sub>2</sub> from natural gas and synthesis gas is necessary to improve the energy quality and to meet the requirements for practical utilization. Comparing with other technologies such as cryogenic distillation, adsorption, and absorption, membrane technology is a promising solution for CO<sub>2</sub> separation, owing to its environmental friendliness, high compactness, lower energy consumption, small footprint, simplicity in operation, and lower capital cost [86]. Therefore, the study of membrane fabrication, membrane characterization, and gas transport properties of membrane is crucial for the development of membrane technology for CO<sub>2</sub> separation.

Both flat sheet membranes and hollow fiber membranes can be used in gas separation processes. Comparing with flat sheet membranes, hollow fiber membranes have high packing density and self-supporting structure. Hollow fiber membranes are highly productive for large scale gas separation processes. Therefore, the study of fabrication of hollow fiber membranes and the effect of spinning parameters on the morphology, pore structure and gas transport properties of hollow fiber membranes is highly needed.

Polymeric membranes show the trade-off relationship between gas permeability and selectivity, limiting their application in gas separation processes [40, 87]. In order to break the trade-off relationship, the incorporation of inorganic fillers into polymer matrix to prepare MMMs is a promising alternative to enhance the permeability and selectivity simultaneously. The preparation of MMMs by the incorporation of inorganic fillers into polymer matrix can overcome the disadvantages of individual polymer and inorganic membranes, but take advantage of the merits of both components. Therefore, it is crucial to select the inorganic fillers and polymer matrix to obtain MMMs with high gas separation performance. Metal organic frameworks (MOFs) have drawn great attention in the preparation of MMMs for gas separation, owing to their various topologies suitable for various separation processes, uniform pore size to achieve precise molecular size sieving effects, high surface area and feasible surface modification to show high affinity to the target gas molecules, and the permanent connected channels to promote the gas permeation [49]. In the past 10 years, more than 20 000 structures of MOFs have been reported

and investigated. However, only a small fraction of MOFs were utilized for the preparation of MOF-based MMMs owing to the requirements of pore size, stability, gas selectivity, solubility and diffusivity for membrane applications [88].

Even though the incorporation of MOFs into polymeric membranes can enhance their thermal stability, mechanical strength, and gas separation performance. The challenges in the preparation of MMMs, such as the selection of proper MOFs and polymers, the stability and dispersion of fillers in polymer matrix, and the interfacial defects, should be considered and tackled [88]. Therefore, the surface modification for MOFs is required to obtain defect-free MMMs. The surface modification for MOFs can be achieved by using the post-synthetic modification methods such as component replacement, chemical function decoration, defect sealing with flexible coatings, and *in-situ* modification methods such as *in-situ* hybridization, and encapsulation in the cages [49].

According to the aforementioned discussion, the following objectives were formulated:

- i. to fabricate polyetherimide (PEI) HFMs by using the dry-jet-wet spinning technique and to investigate the effects of spinning parameters on the morphology, pore structure, and gas permeance of HFMs;
- ii. to fabricate PDMS/PEI TFC-HFMs by using dip-coating method and to investigate the effects of coating conditions on the morphology and thickness of PDMS layer and the gas permeance of TFC-HFMs;
- iii. to synthesize and characterize ZIFs (pristine and modified ZIF-8), MOFs (UiO-66-HN<sub>2</sub>, MIL-101 (Fe)), and MOF@GO composite (MIL-GO composite);
- iv. to fabricate and characterize Pebax<sup>®</sup> 2533 based HF-MMMs and FS-MMMs containing pristine and modified ZIFs, MOFs or MOF@GO composite;
- v. to investigate the effects of pristine and modified ZIFs, MOFs or MOF@GO composite on the morphology, structure, thermal stability, mechanical strength, and gas transport properties of MMMs.

## 2. Research conducted in this thesis

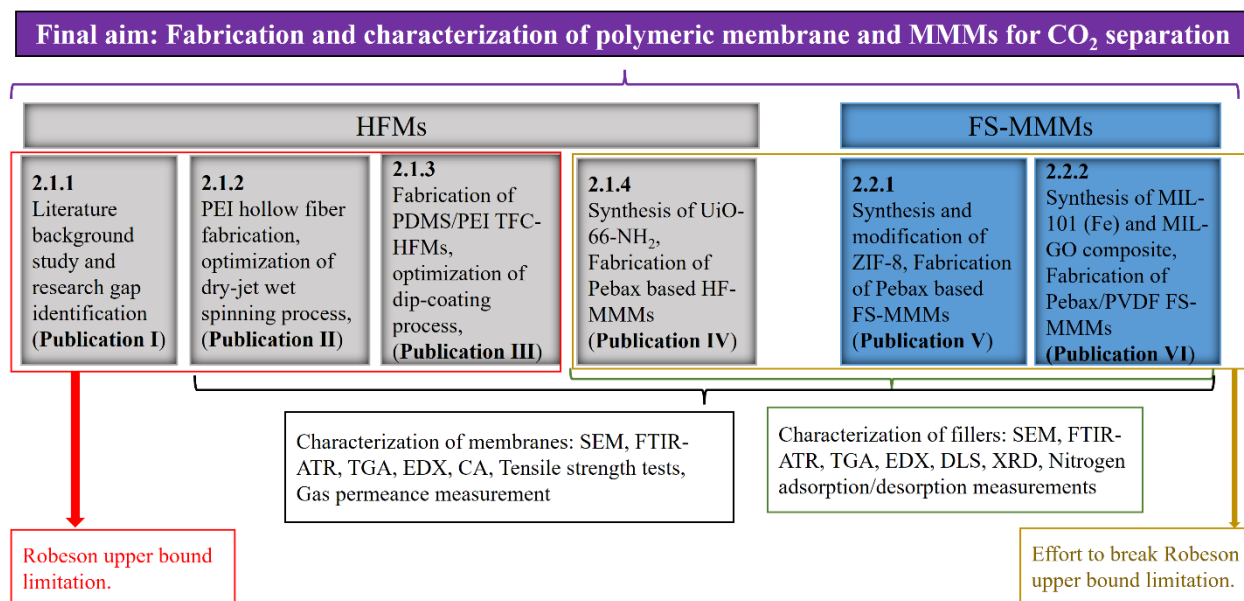


Figure 2. Scheme of research tasks completed in this PhD thesis.

Figure 2 illustrates the logic behind the design of this PhD thesis and the completed research tasks. As it is shown in Figure 2, the PhD thesis consists of two major topics which are the fabrication and characterization of hollow fiber membranes (HFMs) and the fabrication and characterization of flat sheet mixed matrix membranes (FS-MMMs). One review article (Publication I) and three research articles (Publication II, III, and IV) are included in this thesis for the study of HFMs for gas separation. Firstly, the review article was prepared to understand the recent development of HFMs in gas separation and to indicate the research gaps. Subsequently, three research articles were prepared for the study of the fabrication of hollow fibers by using dry-jet-wet spinning technique, preparation of thin film composite hollow fiber membranes (TFC-HFMs) consisting of PDMS dense layer on hollow fiber support by using dip-coating method, and the preparation of hollow fiber mixed matrix membranes (HF-MMMs) by the incorporation of amine functionalized metal organic framework (MOF). As a result, the membrane properties and gas permeance of HFMs, TFC-HFMs, and HF-MMMs were comprehensively studied and compared. In order to make a comparative study on the membrane properties and gas permeance of hollow fiber MMMs and flat sheet MMMs, two research articles (Publication V, and VI) related to the preparation and characterization of the free-standing and PVDF supported FS-MMMs for

gas separation were also included in this thesis. The preparation of MMMs aimed to overcome the Robeson upper bound [40] existing in polymeric membranes.

The details of experimental part related to the preparation of HFMs and MMMs, the synthesis and modification of fillers, the material characterizations and the gas permeance measurements were presented in the publications (II-VI). The synthesized fillers and the prepared membranes were fully characterized to obtain the complementary results for a detailed and comprehensive discussion. The fabricated HFMs and FS-MMMs were characterized by scanning electron microscope (SEM), Fourier transform infrared spectroscopy with attenuated total reflectance (FTIR-ATR), thermogravimetric analysis (TGA), energy dispersive X-ray (EDX), tensile strength tests, contact angle (CA) measurements, and gas permeance measurements. The synthesized fillers were characterized by SEM, FTIR-ATR, TGA, EDX, dynamic light scattering (DLS), X-ray diffraction (XRD), the nitrogen adsorption/desorption measurements, and scanning transmission electron microscopy (STEM).

## **2.1 Fabrication and characterization of hollow fiber membranes (HFMs)**

### **2.1.1 A review of the development of hollow fiber membranes for gas separation processes (Publication I).**

The main aim of the review article (Publication I) was to fully understand the recent development of HFMs for gas separation, such as the fabrication methods for various types of HFMs, the effects of polymer materials and fabrication conditions on the membrane properties and gas separation performance of membranes, and the application of HFMs in various gas separation processes. Additionally, the research gaps and the future directions of HFMs in gas separation were identified, which paved the way for designing the experiments for my PhD research work.

In this literature review, the recent advancement of HFMs, TFC-HFMs and HF-MMMs for gas separation processes was comprehensively reviewed and discussed from the viewpoint of polymer materials, membrane fabrication methods, and the gas separation performance. For the asymmetric HFMs, the effects of spinning parameters such as dope concentration, bore fluid composition, air gap, and the flow rates of dope and bore fluid, on the morphology, structure, selective layer thickness and gas permeance and selectivity of asymmetric HFMs were discussed. For the TFC-HFMs, dip-coating and interfacial polymerization are the two main methods used for the formation of thin selective layer on the porous supports. The effects of dip-coating conditions, such as the coating solution composition and concentration, the coating time, and the coating temperature, and the interfacial polymerization conditions, such as the monomer used in aqueous phase and organic phase, on the morphology, structure, thickness, and gas permeance properties of the thin selective layer were discussed. Additionally, the co-extrusion method, a one-step method to fabricate dual-layer HFMs, was presented. The effects of polymer material selection and the spinning parameters on the interfacial morphology and gas separation performance of dual-layer HFMs were discussed. For the HF-MMMs, the effects of the inorganic filler types, the filler content, and the surface modification of inorganic fillers on the material properties and gas separation performance of MMMs were thoroughly discussed.

This review work served as a very important starting point for my PhD thesis since it provided a comprehensive vision on the development of hollow fiber membranes in gas separation processes. The fabrication methods and the most important factors which affect the membrane structure, and the gas separation performance were summarized.

### 2.1.2 The effects of PEI hollow fiber substrate characteristics on PDMS/PEI hollow fiber membranes for CO<sub>2</sub>/N<sub>2</sub> separation (Publication II).

#### *Overview*

Publication II described the fabrication of PEI hollow fibers by using the dry-jet wet spinning technique. The effects of spinning parameters such as the polymer solution concentration, the bore fluid composition, and the flow rate of bore fluid on the morphology of the cross-section and the inner and outer surfaces, the pore structure, the outer and inner diameters, the wall thickness, and the gas permeance of hollow fibers were studied and discussed. The hollow fibers prepared under various conditions are gathered in Table 3. The PDMS thin selective layer was subsequently formed on the outer surface of hollow fibers prepared using different spinning conditions to study the effect of characteristics of hollow fiber support on the gas permeation properties of PDMS/PEI TFC-HFMs. The prepared hollow fibers and TFC-HFMs were assembled into the hollow fiber module for gas permeance measurements. The CO<sub>2</sub> and N<sub>2</sub> permeances of the fabricated hollow fibers and TFC-HFMs were measured. The ideal selectivity was calculated by using the ratio of CO<sub>2</sub> permeance over N<sub>2</sub> permeance.

Table 3. The name codes and the spinning conditions of the fabricated hollow fibers.

<b>Hollow Fibers</b>	<b>PEI (wt%)</b>	<b>Bore Fluid</b>	<b>Flow Rate of Bore Fluid (cm<sup>3</sup>/min)</b>
HF1	16	H <sub>2</sub> O	6
HF2	18	H <sub>2</sub> O	6
HF3-1	20	H <sub>2</sub> O	3
HF3-2	20	H <sub>2</sub> O	6
HF3-3	20	H <sub>2</sub> O	9
HF3-4	20	H <sub>2</sub> O	12
HF3-5	20	H <sub>2</sub> O/NMP 50/50 (wt%)	9
HF3-6	20	H <sub>2</sub> O/NMP 30/70 (wt%)	9
HF4	22	H <sub>2</sub> O	6
HF5	24	H <sub>2</sub> O	6

#### *The selected results*

As it is shown in Figure 3, all the fabricated hollow fibers showed high gas permeance but low selectivity for CO<sub>2</sub>/N<sub>2</sub> separation. The gas permeance decreased dramatically with the increase of PEI concentration (Figure 3a), which resulted from the increase of skin layer thickness and the

change of pore structure from finger-like to sponge-like. Among the prepared hollow fibers, hollow fibers prepared from 20 wt% of PEI solution showed the desirable pore structure and high gas permeance around 6000 GPU. Therefore, 20 wt% of PEI solution was selected as the optimal dope for hollow fiber preparation. Hollow fibers were spun from 20 wt% of PEI solution at various bore fluid flow rate to study the effect of bore fluid flow rate on their structure and gas permeance. It was found that the increase of bore fluid flow rate resulted in a slight decrease of gas permeance from 7000 GPU to 4500 GPU (Figure 3b). The CO<sub>2</sub> and N<sub>2</sub> permeance increased when NMP was added to the bore fluid, rising from 6500 GPU and 6000 GPU to 9000 GPU and 8000 GPU, respectively (Figure 3c). The increased porosity on the inner surface of hollow fibers and the modest reduction in the skin layer on the inner and outer surfaces of hollow fibers could be the reasons for the increase in gas permeances.

To study the effect of hollow fiber substrate characteristics on the gas permeance of PDMS/PEI composite hollow fiber membranes, a PDMS layer was formed on the outer surface of hollow fibers fabricated from 20 wt% of PEI solution at different spinning conditions. In comparison to the hollow fiber substrates, PDMS/PEI composite membranes showed decreased CO<sub>2</sub> permeance and increased CO<sub>2</sub>/N<sub>2</sub> ideal selectivity (Figure 4). This is because the PDMS selective layer was successfully formed on the outer surface of hollow fiber substrates and the defects on the outer surface was covered by PDMS layer. As is shown in Figure 4, the CO<sub>2</sub> permeance and increased CO<sub>2</sub>/N<sub>2</sub> ideal selectivity of PDMS/PEI composite membranes M3-2, M3-3, and M3-4 increased when the bore fluid flow rate increased. In comparison of the CO<sub>2</sub> permeance and increased CO<sub>2</sub>/N<sub>2</sub> ideal selectivity of PDMS/PEI composite membranes M3-3, M3-5, and M3-6, it was found that the addition of NMP in bore fluid dramatically increased the CO<sub>2</sub> permeance but decreased the CO<sub>2</sub>/N<sub>2</sub> ideal selectivity.

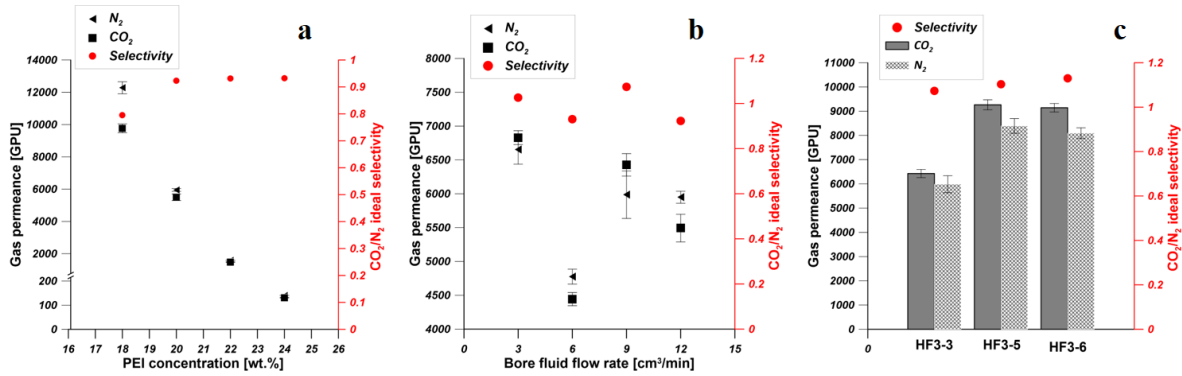


Figure 3. The effect of PEI concentration (a), bore fluid flow rate (b), and bore fluid composition (c) on the gas permeance and ideal selectivity of the fabricated hollow fibers.

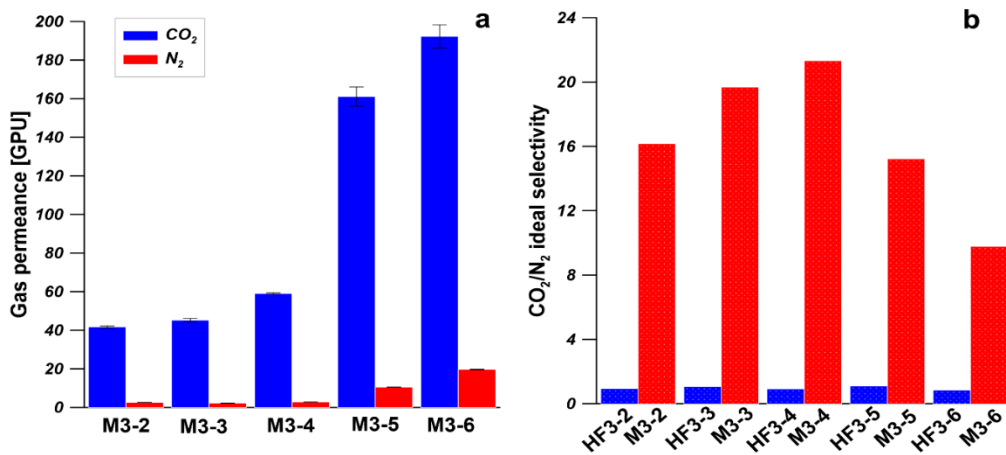


Figure 4. (a) The gas permeance of PDMS/PEI TFC-HFMs. (b) The ideal selectivity of PEI hollow fibers and PDMS/PEI TFC-HFMs (PDMS solution concentration—15 wt% and coating time—10 min).

### Key findings

The characteristics of structure and morphology of hollow fibers were affected by spinning conditions. PEI concentration showed significant effect on the pore structure, skin layer thickness, outer diameter of hollow fibers, and gas permeance. The bore fluid flow rate imparted predominant effects on the wall thickness and inner skin layer thickness rather than the outer diameter, gas permeance, and the structure of hollow fibers. The addition of NMP into the bore fluid resulted in the decrease in the length of finger-like macrovoids near the lumen side and the increase of gas permeance owing to the formation of more porous inner surface and the decrease of skin layer thickness. As the support, the gas permeance and CO<sub>2</sub>/N<sub>2</sub> ideal selectivity of PDMS/PEI TFC-HFMs were affected by the hollow fibers spun under different spinning conditions.



### **2.1.3 Fabrication of polydimethylsiloxane (PDMS) dense layer on polyetherimide (PEI) hollow fiber support for the efficient CO<sub>2</sub>/N<sub>2</sub> separation membranes (Publication III).**

#### ***Overview***

Publication III described the fabrication of PDMS/PEI TFC-HFMs by using dip-coating technique. The hollow fiber substrates were fabricated by using the dry-jet-wet spinning technique under the optimized spinning conditions found in Publication II. The effects of coating conditions such as the coating solution concentration, coating time, curing temperature, and the number of coating layer on the thickness of PDMS selective layer and the gas permeation properties of PDMS/PEI TFC-HFMs were studied.

#### ***The selected results***

PDMS/PEI TFC-HFMs were prepared by submerging PEI supports in 15 wt% of PDMS solution for different time intervals between 0.5 and 15 minutes and cured at 25 °C to study the effect of coating time on the gas permeance. Figure 5a depicts the trends of CO<sub>2</sub> and N<sub>2</sub> permeances, and the ideal selectivity of PDMS/PEI TFC-HFMs fabricated at different coating time. When the coating time increased from 0.5 min to 5 min, it was evident that the CO<sub>2</sub> and N<sub>2</sub> permeances dramatically decreased. The CO<sub>2</sub> permeance continued to decrease while the N<sub>2</sub> permeance remained constant over the coating time from 5 to 15 minutes. This is because the kinetic diameter of N<sub>2</sub> molecule (0.36 nm) is larger than that of CO<sub>2</sub> molecule (0.33 nm). Furthermore, CO<sub>2</sub> molecules have a greater affinity to PDMS [89]. Therefore, CO<sub>2</sub> molecules are transported considerably faster than N<sub>2</sub> molecules, and they are more susceptible to differences in PDMS layer thickness (Figure 5a). The CO<sub>2</sub>/N<sub>2</sub> ideal selectivity reached its maximum of 21 as the coating time approached 10 minutes. Afterwards, the CO<sub>2</sub>/N<sub>2</sub> ideal selectivity decreased slightly. This is owing to the fact that as the coating time rose, a layer of defect-free PDMS was generated, resulting in a rise in the ideal selectivity value. However, if the coating time is extended, the PDMS could be re-dissolved in the solvent. Consequently, defects could have arisen and the selectivity was slightly decreased. The ideal coating time for preparing PDMS/PEI TFC-HFMs with a high gas separation performance was equal to 10 minutes. Figure 5b depicts the effect of PDMS layer thickness on CO<sub>2</sub> permeance. It can be seen that CO<sub>2</sub> permeance decreases as PDMS layer thickness increases owing to higher mass transfer resistance [90, 91]. According to the solution-diffusion model, the gas permeance is inversely proportional to the thickness of selective layer

[92]. Figure 5b reveals that the CO<sub>2</sub> permeance is directly proportional to the reciprocal of the PDMS layer thickness, confirming the solution-diffusion mechanism hypothesis for gas transport through the PDMS layer.

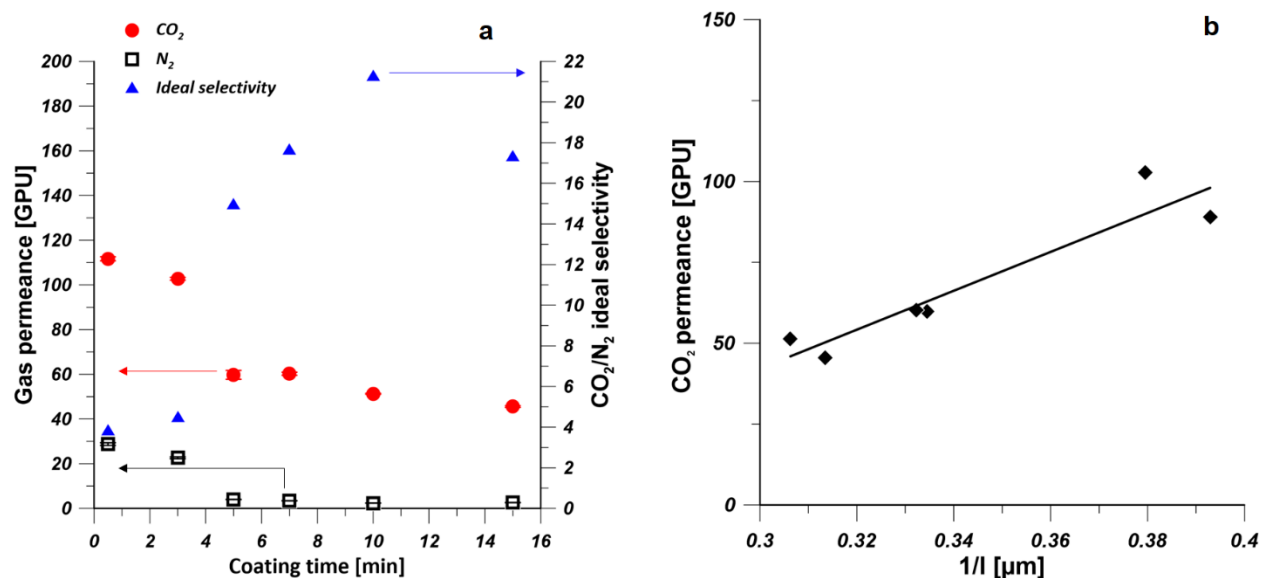


Figure 5. (a) The influence of coating time on gas permeance and ideal selectivity of PDMS/PEI TFC-HFMs. (b) The influence of PDMS layer thickness ( $l$ ) on CO<sub>2</sub> permeance of PDMS/PEI TFC-HFMs prepared at various coating time.

As seen in Figure 6a, when the PDMS concentration was raised from 1.5 wt% to 20 wt%, the CO<sub>2</sub> permeance and N<sub>2</sub> permeance reduced substantially from 1360 GPU to 40 GPU and 2.4 GPU, respectively. Gas permeance decreased, owing to the rise in PDMS layer thickness. The CO<sub>2</sub>/N<sub>2</sub> ideal selectivity reached its maximum value of 21 when the concentration of PDMS was raised to 15 wt%. When 20 wt % PDMS solution was utilized as the coating solution, the resulting TFC-HFMs had the lowest CO<sub>2</sub> permeance, owing to the formation of a thicker PDMS selective layer. The decrease in CO<sub>2</sub>/N<sub>2</sub> ideal selectivity might be explained by the substantially higher drop in CO<sub>2</sub> permeance compared to the N<sub>2</sub> permeance, owing to the sensitivity of CO<sub>2</sub> to the change in PDMS layer thickness. As it is shown in Figure 6b, CO<sub>2</sub> permeance is linearly proportional to the reciprocal of PDMS layer thickness which is in good agreement with solution-diffusion model [92].

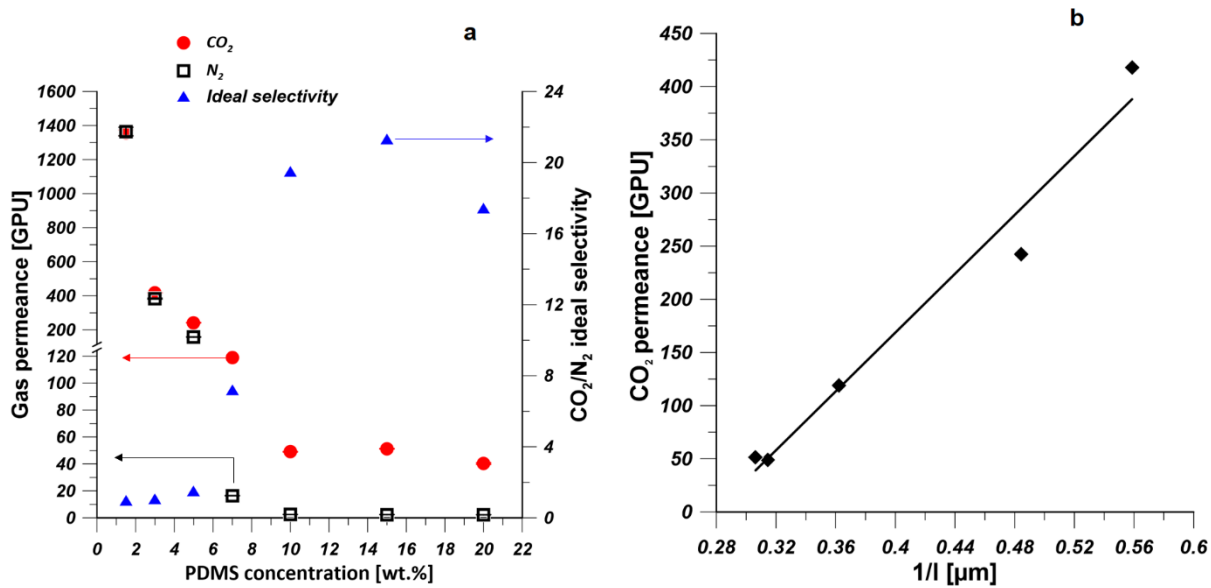


Figure 6. (a) The influence of PDMS concentration on gas permeance and ideal selectivity of PDMS/PEI TFC-HFMs. (b) The influence of PDMS layer thickness on CO<sub>2</sub> permeance of PDMS/PEI TFC-HFMs prepared from various PDMS concentration.

### Key findings

The thickness of the PDMS layer was affected by the coating solution concentration and the coating time. The increase in coating time and PDMS solution concentration resulted in the increase in its thickness. The TFC-HFMs fabricated from a 15 wt % PDMS solution coated for 10 minutes exhibited the highest gas separation performance with a CO<sub>2</sub> permeance of 51 GPU and a CO<sub>2</sub>/N<sub>2</sub> selectivity of 21. The relationship between gas permeance and PDMS layer thickness followed the solution-diffusion model. The gas separation performance was adversely affected by the increase in curing temperature and the number of coating layers.

#### **2.1.4 Thin film mixed matrix hollow fiber membrane fabricated by incorporation of amine functionalized metal-organic framework for CO<sub>2</sub>/N<sub>2</sub> separation (Publication IV).**

##### ***Overview***

The upper bound relationship sets a limit for the preparation of polymeric membranes with high gas permeability and selectivity in the same time [40]. Therefore, the fabrication of Pebax-UiO-66-NH<sub>2</sub>/PP HF-MMMs for gas separation was presented in Publication IV. Polyether block amide (Pebax<sup>®</sup>) materials are used for MMMs fabrication because of their advantages, *e.g.*, desirable separation performance and high processability [93]. They are good candidates for polymeric membrane matrix for CO<sub>2</sub>/N<sub>2</sub> separation owing to their desirable CO<sub>2</sub> permeance, high ideal selectivity, and tunability of gas separation properties *via* the incorporation of nanofillers [94]. Amine-functionalization is an effective strategy for enhancing the CO<sub>2</sub> affinity of MOFs crystals [58]. UiO-66-NH<sub>2</sub> shows high CO<sub>2</sub> adsorption capacity, which offers great potential for the fabrication of MMMs for CO<sub>2</sub> separation [94]. Therefore, Pebax<sup>®</sup> 2533 and UiO-66-NH<sub>2</sub> were chosen as the polymer matrix and filler for the preparation of HF-MMMs.

Publication IV described the synthesis of UiO-66-NH<sub>2</sub> by using solvothermal method. Subsequently, the synthesized UiO-66-NH<sub>2</sub> particles were incorporated into the Pebax<sup>®</sup> 2533 coating solution for the preparation of Pebax-UiO-66-NH<sub>2</sub>/PP HF-MMMs. In the dip-coating process, the polypropylene (PP) hollow fiber support was firstly dipped into the 3 wt% Pebax<sup>®</sup> 2533 coating solution to fabricate a gutter layer on the outer surface of PP hollow fibers. Subsequently, the obtained PP hollow fiber support with a gutter layer was dipped into the 6 wt% Pebax<sup>®</sup> 2533 coating solution containing UiO-66-NH<sub>2</sub> particles to prepare the defect-free Pebax-UiO-66-NH<sub>2</sub>/PP HF-MMMs. Finally, the effects of the filler content on the morphology, surface chemistry and gas permeation properties of HF-MMMs were investigated.

##### ***The selected results***

Figure 7 displays surface and cross-section SEM images of the HF-MMMs, pristine Pebax<sup>®</sup> 2533 membrane, and polypropylene (PP) hollow fiber support. Figure 7A demonstrates the porous structure (A1 and A2) and porous outer surface of the PP hollow fiber supports (A3 and A4). The average pore size of PP hollow fiber is 0.3 μm, and porosity ranges from 50% to 60%. On the shell side of PP hollow fiber support, a defect-free Pebax<sup>®</sup> 2533 selective layer was formed by dip-coating with 3 and 6 wt% Pebax<sup>®</sup> 2533 solutions (Figure 7B). The HF-MMM was properly

developed on the outside of PP hollow fiber support after the addition of UiO-66-NH<sub>2</sub> to the Pebax<sup>®</sup> 2533 matrix (Figure 7C–G). The thickness of the Pebax<sup>®</sup> 2533-UiO-66-NH<sub>2</sub> hybrid selective layer was in the range of 5.40–6.97 μm. The roughness of the shell side of the fabricated HF-MMMs increased when the amount of UiO-66-NH<sub>2</sub> rose from 0 to 50 wt% (Figure 7B4–G4). When the amount of UiO-66-NH<sub>2</sub> was low (5 and 10 wt %), a homogenous dispersion of UiO-66-NH<sub>2</sub> particles was observed in the Pebax<sup>®</sup> 2533 matrix (Figure 7B,C). At the high amounts of MOF particles (15, 20, and 50 wt %), UiO-66-NH<sub>2</sub> aggregated in the polymeric matrix (Figure 7E–G). It is reported that the MOF aggregation in polymeric matrix could lead to the formation of non-selective defects during the fabrication process [95].

The CO<sub>2</sub> and N<sub>2</sub> permeance of the fabricated membranes were tested at 2 bar and 25 °C. Figure 8 demonstrates that the UiO-66-NH<sub>2</sub> content in the Pebax<sup>®</sup> 2533 matrix affected the gas permeance and ideal selectivity of Pebax<sup>®</sup> 2533-UiO-66-NH<sub>2</sub>/PP HF-MMMs. As shown in Figure 8a, the CO<sub>2</sub> permeance considerably rose from 19 to 30 GPU as the UiO-66-NH<sub>2</sub> content increased from 0 to 50 wt%. N<sub>2</sub> permeance hardly increased when the UiO-66-NH<sub>2</sub> content rose from 0 to 10 wt%. N<sub>2</sub> permeance, however, rose to 0.91, 1.14, and 1.42 GPU when the UiO-66-NH<sub>2</sub> content increased to 15, 20, and 50 wt%, respectively. As seen in Figure 8b, the CO<sub>2</sub>/N<sub>2</sub> ideal selectivity rose from 30 to 37 as the UiO-66-NH<sub>2</sub> content increased from 0 to 10 wt %. The CO<sub>2</sub>/N<sub>2</sub> ideal selectivity then reduced to 21 as the UiO-66-NH<sub>2</sub> content increased to 50 wt%. Both the CO<sub>2</sub> permeance and CO<sub>2</sub>/N<sub>2</sub> ideal selectivity increased when the UiO-66-NH<sub>2</sub> content increased to 10 wt%, indicating the presence of defect-free thin mixed matrix membrane on the PP hollow fiber support. The increased CO<sub>2</sub> permeance and CO<sub>2</sub>/N<sub>2</sub> ideal selectivity were attributed to the interrupted chain packing in the polymer matrix and the CO<sub>2</sub>-philic nature of UiO-66-NH<sub>2</sub>.

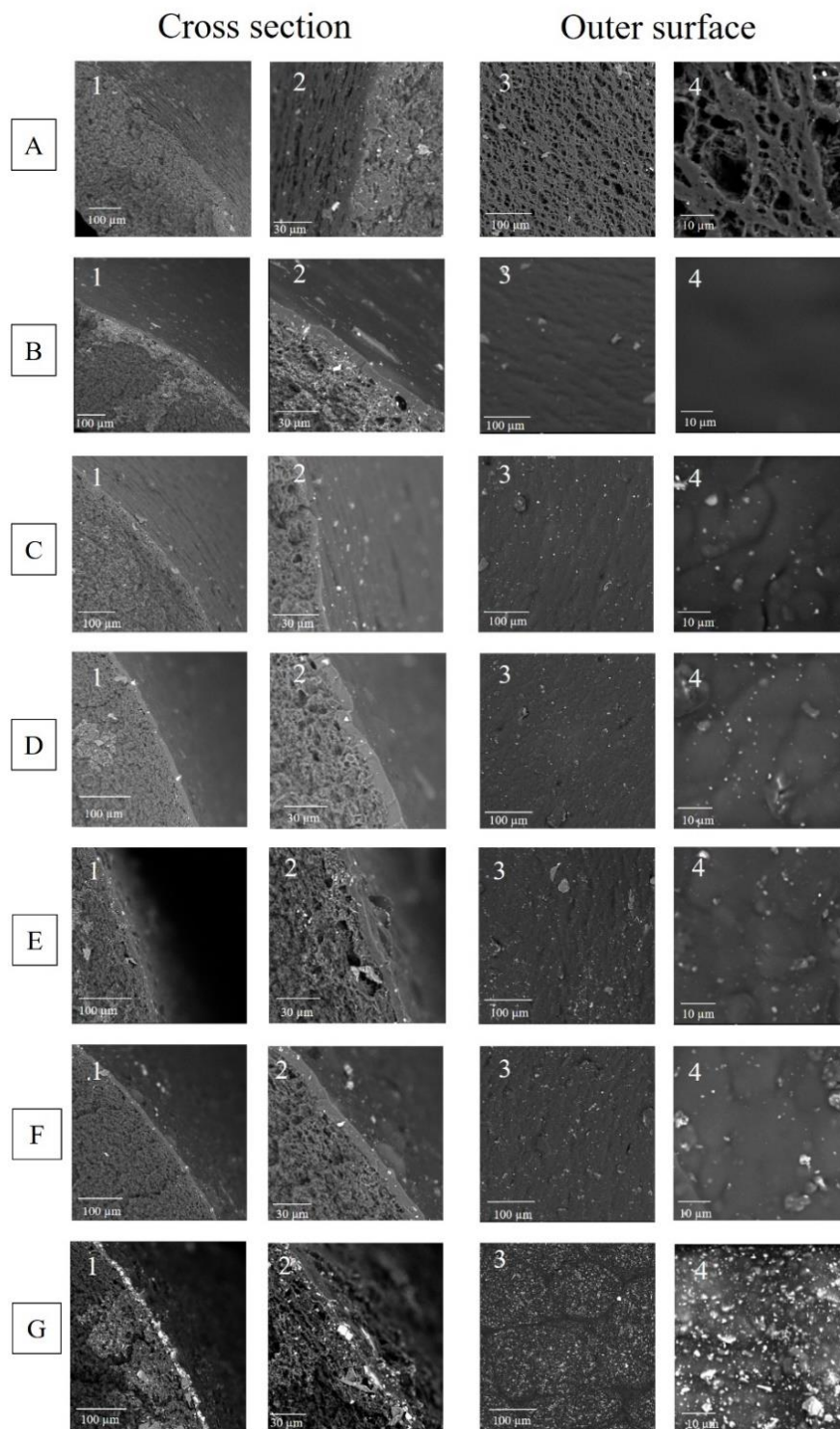


Figure 7. SEM pictures of cross-section (1 and 2) and outer surface (3 and 4) of Pebax<sup>®</sup> 2533-UiO-66-NH<sub>2</sub>/PP HF-MMMs —(A) PP hollow fiber support, (B) 0 wt% UiO-66-NH<sub>2</sub>, (C) 5 wt% UiO-66-NH<sub>2</sub>, (D) 10 wt% UiO-66-NH<sub>2</sub>, (E) 15 wt% UiO-66-NH<sub>2</sub>, (F) 20 wt% UiO-66-NH<sub>2</sub>, and (G) 50 wt% UiO-66-NH<sub>2</sub>.

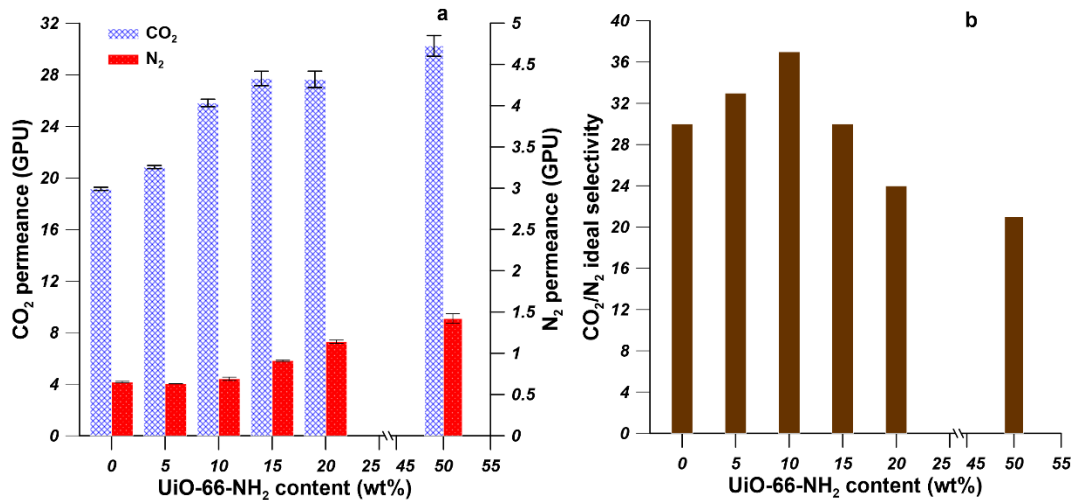


Figure 8. The effect of UiO-66-NH<sub>2</sub> content on the CO<sub>2</sub> and N<sub>2</sub> permeances (a) and CO<sub>2</sub>/N<sub>2</sub> ideal selectivity (b) of Pebax<sup>®</sup> 2533-UiO-66-NH<sub>2</sub>/PP HF-MMMs.

### ***Key findings***

By dip-coating PP hollow fibers with 3 wt % Pebax<sup>®</sup> 2533 solution, the outer surface of hollow fiber supports could be smoothed, therefore facilitating the fabrication of a defect-free selective layer. The addition of UiO-66-NH<sub>2</sub> nanoparticles to the Pebax<sup>®</sup> 2533 coating solution altered the morphology, surface chemistry, and gas separation performance of Pebax<sup>®</sup> 2533-UiO-66-NH<sub>2</sub>/PP HF-MMMs. The aggregation of UiO-66-NH<sub>2</sub> nanoparticles was observed at higher amounts of UiO-66-NH<sub>2</sub> nanoparticles in the Pebax<sup>®</sup> 2533 matrix.

## **2.2 Fabrication and characterization of flat sheet mixed matrix membranes (FS-MMMs)**

### **2.2.1 Evaluation of CO<sub>2</sub> separation performance with enhanced features of materials - Pebax<sup>®</sup> 2533 mixed matrix membranes containing ZIF-8-PEI@[P(3)HIm][Tf<sub>2</sub>N] (Publication V).**

#### *Overview*

ZIF-8 consisting of zinc ion centers coordinated with 2-methyl imidazolate is used as fillers for the fabrication of MMMs for CO<sub>2</sub> separation owing to its intrinsic properties and the small aperture equal to 3.4 Å which is bigger than the kinetic diameter of CO<sub>2</sub> (3.3 Å) but smaller than the kinetic diameter of N<sub>2</sub> (3.6 Å) and CH<sub>4</sub> (3.8 Å) [96, 97]. Both polyethyleneimine (PEI) and ionic liquids possess high affinity to CO<sub>2</sub> molecules and the ability to enhance the compatibility between ZIF-8 and polymer matrix. In addition, they can act as CO<sub>2</sub> carriers to facilitate the transport of CO<sub>2</sub> molecules through membranes. Therefore, they were selected as the ZIF-8 modifiers.

Publication V discussed the synthesis of ZIF-8 by using solvothermal method and the modification with PEI and ionic liquids [P(3)HIm][Tf<sub>2</sub>N] by using the post-synthetic modification strategy. The pristine and modified ZIF-8 were characterized by using various techniques. The effects of surface modification on the morphology, BET surface area, pore size, total pore volume, thermal stability, crystal structure and surface chemistry were investigated. The pristine and modified ZIF-8 were incorporated into Pebax matrix to fabricate the free-standing dense FS-MMMs. The free-standing dense FS-MMMs were fabricated by using the solution casting along with the solvent evaporation method. The effects of filler types (pristine and modified ZIF-8) and the content of modified ZIF-8 on the morphology, mechanical strength, thermal stability and gas permeation properties of FS-MMMs were investigated. Additionally, the effect of temperature on the gas permeation properties of FS-MMMs was studied.

#### *The selected results*

The characteristic XRD peaks of ZIF-8 were also found in the modified ZIF-8 (Figure 9a), which indicates that the crystal structure of ZIF-8 was well preserved after PEI modification and IL decoration. However, the intensity of these peaks gradually decreased after PEI modification and IL decoration, owing to the decrease of electron density resulting from the presence of PEI



polymer chains and IL in the cage and on the surface of ZIF-8 [57]. As is shown in Figure 9b, type-I adsorption behavior was observed for both unmodified and modified ZIF-8, suggesting the microporous nature of the synthesized fillers [98, 99]. After PEI surface modification and ILs decoration, the microporous structure of ZIF-8 was maintained. For ZIF-8-PEI and ZIF-8-PEI@IL, the BET surface area, total pore volume and average pore size reduced owing to the presence of PEI and ionic liquid in ZIF-8. FTIR spectra were conducted to analyze the chemical structure of ZIF-8, ZIF-8-PEI, and ZIF-8-PEI@IL (Figure 9c). It was found that ZIF-8-PEI@IL contains not only the characteristic peaks for ZIF-8, but also the characteristic peaks from PEI, *e.g.* peaks at  $1458\text{ cm}^{-1}$  and  $1585\text{ cm}^{-1}$  correspond to the N-H vibrations of main and secondary amino groups, and [P(3)HIm][Tf<sub>2</sub>N], *e.g.* peaks at  $1186\text{ cm}^{-1}$ ,  $1134\text{ cm}^{-1}$ , and  $1055\text{ cm}^{-1}$  correspond to the [Tf<sub>2</sub>N] anion's C-F stretching, S=O stretching, and S-N-S stretching, respectively [100]. As illustrated in Figure 9d, there was a small mass loss between 100 and 200 °C, indicating the elimination of H<sub>2</sub>O, DMF, ethanol, and methanol molecules. Owing to the thermal decomposition of ZIF-8, the greatest mass loss occurred between 550 and 900 °C, confirming the high thermal stability of synthesized ZIF-8 [101]. For ZIF-8-PEI and ZIF-8-PEI@IL, there was an additional mass loss between 200 °C and 500 °C, which was related to the decomposition of PEI polymer chains and ILs.

The gas permeability and selectivity of prepared MMMs were compared with the Robeson's upper bound (Figure 10) [40]. ZIF-8-PEI@IL/Pebax<sup>®</sup> 2533 MMMs showed better permselectivity than pristine Pebax<sup>®</sup> 2533 membranes for CO<sub>2</sub>/N<sub>2</sub> and CO<sub>2</sub>/CH<sub>4</sub> separations. The CO<sub>2</sub>/N<sub>2</sub> separation performance of ZIF-8-PEI@IL/Pebax<sup>®</sup> 2533 MMMs exceeded the Robeson's upper bound (2008). While the CO<sub>2</sub>/CH<sub>4</sub> separation performance of ZIF-8-PEI@IL/Pebax<sup>®</sup> 2533 MMMs is reaching the Robeson's upper bound (2008). MMMs containing 15 wt% ZIF-8-PEI@IL showed the best performance in CO<sub>2</sub>/N<sub>2</sub> and CO<sub>2</sub>/CH<sub>4</sub> separations. The performance of MMMs containing ZIF-8-PEI@IL is analogous to reported performances of Pebax based MMMs, as shown in Figure 10. Owing to the additional gas molecule transport pathways, improved filler affinity to CO<sub>2</sub>, and improved compatibility between filler and polymer matrix, the modification of ZIF-8 with PEI along with the decoration of ILs is an encouraging way to improve the gas separation performance of MMMs.

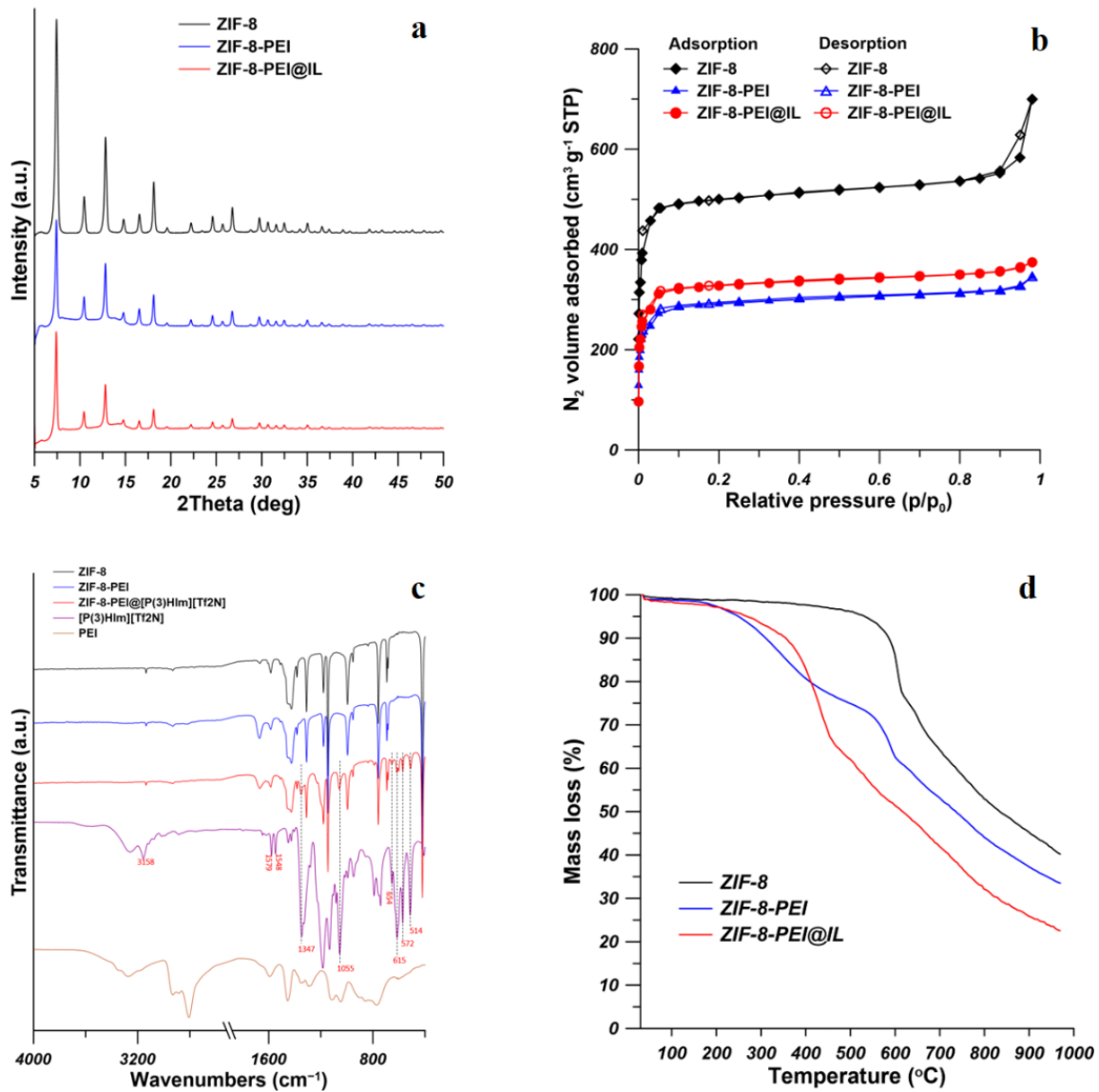


Figure 9. (a) XRD patterns, (b) N<sub>2</sub> adsorption-desorption isotherms, (c) FTIR spectra, and (d) TGA curves of ZIF-8, ZIF-8-PEI, and ZIF-8-PEI@IL.

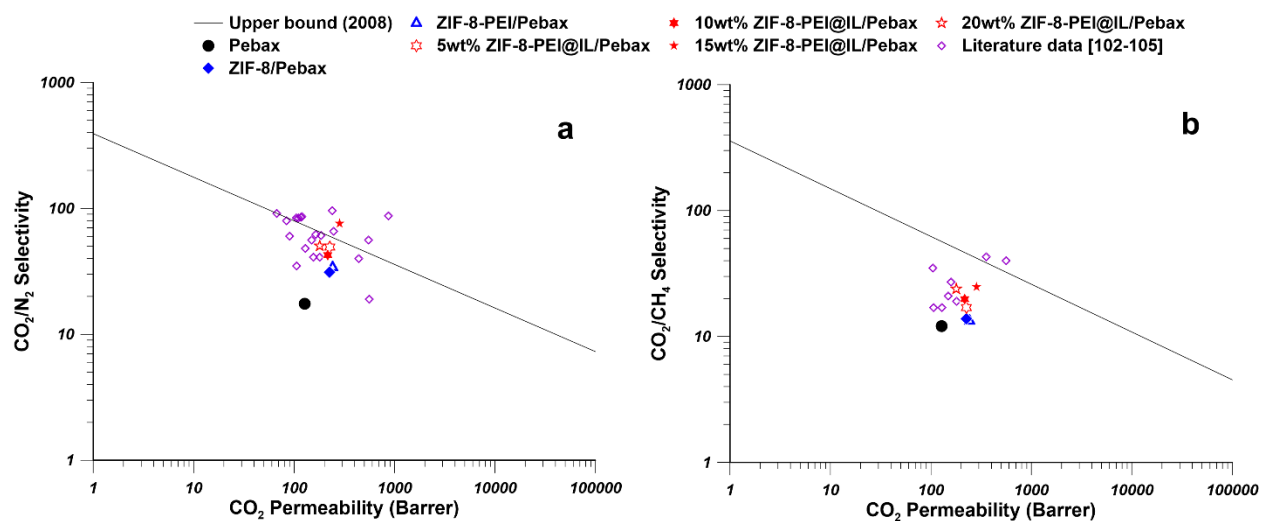


Figure 10. The comparison of the performance of MMMs with Robeson upper bound (2008) for (a)  $\text{CO}_2/\text{N}_2$  and (b)  $\text{CO}_2/\text{CH}_4$ .

### ***Key findings***

Owing to the presence of PEI and ILs in ZIF-8, the BET surface area, total pore volume, and average pore diameter reduced after modification while the crystal structure of ZIF-8 was well preserved. It was discovered that the improved molecular interactions between the amino groups in the PEI and Pebax polymer chains considerably improved the compatibility between the filler and polymer matrix. The amine and ionic liquid modification on ZIF-8 significantly increased the  $\text{CO}_2$  permeability, and  $\text{CO}_2/\text{N}_2$  ideal selectivity of the prepared MMMs, owing to the size sieving effect of ZIF-8-PEI@IL, the additional facilitated  $\text{CO}_2$  molecules transport pathways from amino groups on PEI, and the enhanced  $\text{CO}_2$  affinity to fillers by ILs.

## 2.2.2 Pebax<sup>®</sup> 2533/PVDF thin film mixed matrix membranes containing MIL-101 (Fe)/GO composite for CO<sub>2</sub> capture (Publication VI).

### *Overview*

MIL-101 (Fe) consists of the high-valence metal sites (Fe<sup>3+</sup>) and the strongly polarizing terephthalic acid, which can enhance the molecular interaction with CO<sub>2</sub> molecules owing to the electrical difference. The nontoxic MIL-101 (Fe) showed higher adsorption capacity for CO<sub>2</sub> than N<sub>2</sub> [106]. In MMMs, GO nanosheets improve the gas diffusivity selectivity owing to the formation of tortuous pathways, allowing small gas molecules to transport through membranes more easily than big gas molecules [78]. Therefore, MIL-101 (Fe) and MIL-GO composite were used as fillers to enhance the gas separation performance of FS-MMMs resulted from the synergistic effects of MOF and GO.

Publication VI described the synthesis of MIL-101 (Fe) and MIL-GO composite fillers by using as solvothermal method. MIL-101 (Fe) and MIL-GO composite fillers were characterized by using various techniques to study the effects of GO on the morphology, BET surface area, pore size, total pore volume, thermal stability, crystal structure and surface chemistry of MIL-101 (Fe). Subsequently, Pebax-MIL-GO/PVDF FS-MMMs were fabricated by casting the Pebax solution containing MIL-101 (Fe) or MIL-GO composite fillers onto the surface of PVDF support. The freshly cast membranes were dried at 25 °C for 24 h then dried in an oven at 60 °C for 8 h to completely evaporate solvent. The composition of the selective layer, and the names of the fabricated membranes are presented in Table 4. In the nomenclature of the fabricated membranes, P represented Pebax<sup>®</sup> 2533, M represented MIL-101 (Fe), G represented GO. The effects of filler types and the content of MIL-GO-2 on the morphology, thermal stability, and gas permeation properties of FS-MMMs were investigated.

Table 4 Compositions and fabrication conditions of the prepared Pebax-based MMMs.

Membrane	Composition of selective layer (wt%)		
	Pebax <sup>®</sup> 2533	Filler type	Filler content
Pebax <sup>®</sup> 2533/PVDF	100	-	0
9-PM/PVDF	90.9	MIL-101 (Fe)	9.1
9-PMG2/PVDF	90.9	MIL-GO-2	9.1
9-PMG5/PVDF	90.9	MIL-GO-5	9.1
9-PMG10/PVDF	90.9	MIL-GO-10	9.1
5-PMG2/PVDF	95.2	MIL-GO-2	4.8
13-PMG2/PVDF	87.0	MIL-GO-2	13.0

### *The selected results*

Figure 11 shows the morphology of the cross-section and top surface of pure Pebax<sup>®</sup> 2533 membrane and MMMs containing various amounts of MIL-GO-2 composite filler. With the increasing amounts of MIL-GO-2 composite filler, the surfaces of MMMs became rougher. As evidenced by the cross-section of the prepared MMMs, the MIL-GO-2 composite fillers were uniformly distributed in the polymer matrix at a low filler percentage, suggesting that the interfacial cavities or apparent agglomerates were not detected. However, when the filler content reached 13 wt%, agglomeration was detected. No interfacial gaps were identified in the MMMs.

To evaluate the gas permeation performance of the prepared MMMs, the single gas permeation measurements were performed. In this study, permeability of pure gas (CO<sub>2</sub> and N<sub>2</sub>) were determined at 2 bar and 20 °C. The influence of filler types, *e.g.* MIL-101 (Fe), MIL-GO-2, MIL-GO-5, and MIL-GO-10 on the gas permeability, and the ideal selectivity of MMMs was presented in Figure 12a. The addition of fillers into Pebax<sup>®</sup> 2533 had a substantial effect on the gas transport properties of the fabricated membranes. The CO<sub>2</sub> permeability of 9.1 wt% MIL-101 (Fe)/Pebax<sup>®</sup> 253 MMMs increased by 59% to 323 Barrer compared to the pristine Pebax<sup>®</sup> 2533 membranes, while the ideal selectivity of 17 was barely altered. The addition of MIL-GO-2 and MIL-GO-5 in MMMs enhanced CO<sub>2</sub> permeability and CO<sub>2</sub>/N<sub>2</sub> ideal selectivity. In contrast, the addition of MIL-GO-10 had detrimental impacts on the gas separation capabilities of MMMs. MMMs containing 9.1 wt% MIL-GO-2 showed CO<sub>2</sub> permeability (equal to 303 Barrer) and CO<sub>2</sub>/N<sub>2</sub> ideal selectivity (equal to 24), which were 50% and 41% higher than the pristine

membranes, respectively. This is because the porous structure of MIL-GO-2, the additional free volume in MMMs and the higher affinity to CO<sub>2</sub> of MIL-GO-2 strongly enhanced the CO<sub>2</sub> permeability rather than N<sub>2</sub> permeability. The highly tortuous diffusion paths and the inter-distance between GO nanosheets inhibited the N<sub>2</sub> transport through MMMs. However, the MMMs containing 9.1 wt% MIL-GO-10 showed worse gas separation performance than that of pristine Pebax<sup>®</sup> 2533 membranes, which could be related to the decreased porosity and GO behavior of MIL-GO-10 composite filler.

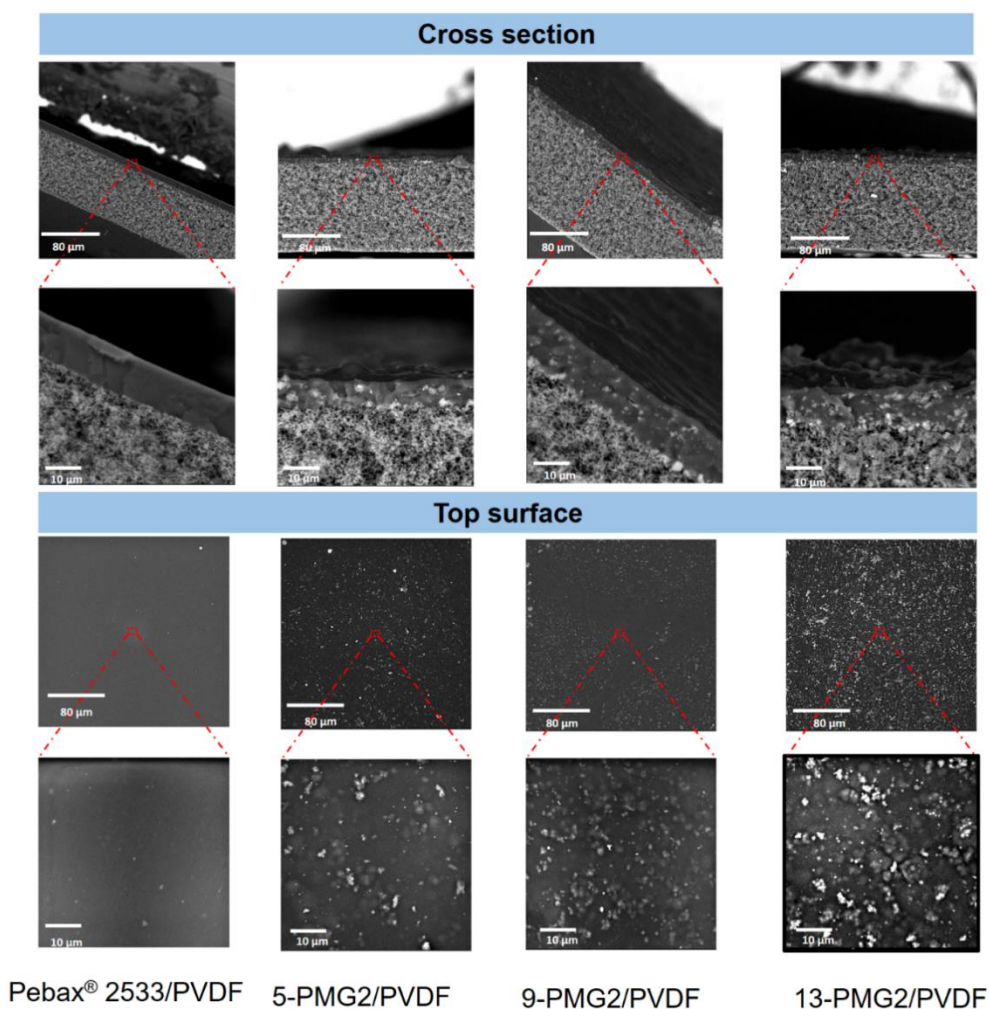


Figure 11. SEM images of cross-section and surface of the pristine Pebax<sup>®</sup> 2533 membrane; MMMs with 4.8 wt%, 9.1 wt%, and 13.0 wt% of MIL-GO-2 composite filler.

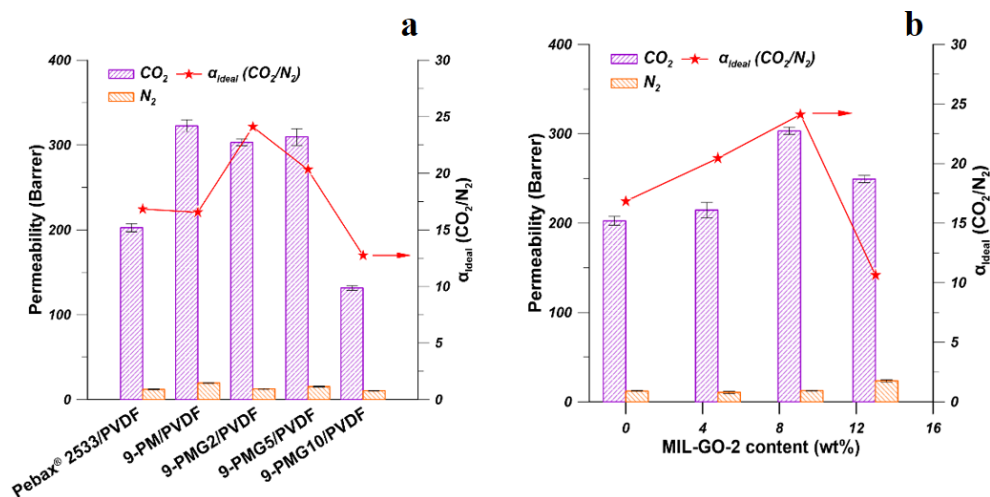


Figure 12. Gas permeability and ideal selectivity of MMMs containing (a) 9.1 wt% of various types of fillers, and (b) various amount of MIL-GO-2 (Experimental condition: 20 °C and 2 bar).

The influence of MIL-GO-2 amount in MMMs on the gas permeability and ideal selectivity was presented in Figure 12b. When the MIL-GO-2 content increased to 9.1 wt%, the  $CO_2$  permeability and  $CO_2/N_2$  ideal selectivity were improved dramatically, while the  $N_2$  permeability was unaffected. MMMs having 9.1% MIL-GO-2 composite filler displayed the maximum  $CO_2$  permeability equal to 303 Barrer and  $CO_2/N_2$  ideal selectivity equal to 24. The further increase of MIL-GO-2 content in MMMs to 13.0 wt% resulted in the decrease of  $CO_2$  permeability and  $CO_2/N_2$  ideal selectivity. This could be related to the over-loading of MIL-GO-2, resulting in filler agglomeration and rigidified interface between filler and polymer chains [107].

### Key findings

Comparing with MIL-101 (Fe), the BET surface area and total pore volume of MIL-GO composite decreased owing to the coverage of nonporous GO nanosheets on MIL-101 (Fe). The high amount of GO in the MIL-101 (Fe) synthesis process could inhibit the growth of MIL-101 (Fe) crystals. The utilization of MOF-GO composite filler in MMMs is a promising way to enhance the gas separation performance of membranes since the gas permeability and selectivity increased significantly simultaneously owing to the synergistic effects of the additional gas molecules pathways provided by MOFs and the tortuous diffusion pathways created by GO.

### 3. Conclusions

PEI (polyetherimide) hollow fibers, PDMS/PEI TFC-HFMs, Pebax<sup>®</sup> 2533-based HF-MMMs and flat sheet MMMs were fabricated and characterized in the gas separation process. UiO-66-NH<sub>2</sub>, ZIF-8, ZIF-8-PEI (polyethyleneimine), ZIF-8-PEI@IL, MIL-101 (Fe), and MIL-GO composites were synthesized by using solvothermal method and used as fillers for the fabrication of MMMs.

For the fabrication of PEI hollow fibers by using a dry-jet-wet spinning technique and PDMS/PEI TFC-HFMs by using the dip-coating method, the most important conclusions are following:

- The polymer concentration, the bore fluid flow rate, and the composition of bore fluid showed significant influence on the pore structure, skin layer thickness, the wall thickness, outer diameter, and gas permeance of PEI hollow fibers.
- The spinning conditions showed significant influence on the gas permeance and CO<sub>2</sub>/N<sub>2</sub> ideal selectivity of PDMS/PEI TFC-HFMs.
- PDMS/PEI TFC-HFMs were fabricated by using the dip-coating method. The thickness of PDMS layer, the gas permeability, and CO<sub>2</sub>/N<sub>2</sub> ideal selectivity were predominantly influenced by the concentration and composition of coating solution and the coating time.

For the fabrication of Pebax<sup>®</sup> 2533-based HF-MMMs and flat sheet MMMs, the most important conclusions are following:

- The incorporation of proper amount of fillers, such as 10 wt% of UiO-66-NH<sub>2</sub>, and 15 wt% ZIF-8-PEI@IL, into the Pebax<sup>®</sup> 2533 matrix significantly increased the CO<sub>2</sub> permeability and the ideal selectivity of the prepared MMMs.
- The aggregation of fillers occurred when too high amount of fillers was incorporated into Pebax<sup>®</sup> 2533 matrix, resulting in the adverse effects on the gas separation performance of MMMs.
- ZIF-8-PEI@IL showed enhanced compatibility with polymer matrix and enhanced gas separation performance owing to its size sieving effect, the additional facilitated CO<sub>2</sub> molecules transport path from amino groups on PEI, and the enhanced CO<sub>2</sub> affinity to fillers by ILs.



- MIL-GO-2-Pebax<sup>®</sup> 2533/PVDF MMMs showed increased CO<sub>2</sub> permeability and the CO<sub>2</sub>/N<sub>2</sub> ideal selectivity, owing to the additional gas molecules pathway, the high affinity of MIL-GO-2 to CO<sub>2</sub>, and the tortuous diffusion pathways created by GO nanosheets.

#### **4. Future work and research directions**

In this thesis, the gas transport properties of the prepared membranes were studied by using pure gas in the gas permeance measurements. In the future works, the gas mixture should be used to measure the gas separation performance of membranes. The presence of another gas in the gas mixture affects the gas permeability of the target gas and the gas selectivity owing to the competitive effects and the interaction between gas molecules and polymer materials. Moreover, the presence of water vapors in the gas mixture can also affect the gas separation performance of membranes. The water molecules can increase the permeability of CO<sub>2</sub> molecules owing to the facilitated transport mechanism for CO<sub>2</sub> molecules, which enhances the CO<sub>2</sub> separation performance [108]. Therefore, the use of gas mixture along with the saturated steams as feed for gas permeability testing can provide a more comprehensive picture on the gas transport behavior in membranes. The influence of the type of gas mixture and the presence of water molecules on the diffusion coefficient, solubility coefficient, and the structure change of membranes should be investigated.

The further utilization of MOFs in the MMMs preparation is highly needed. The synthesis of various types of MOFs including 2D MOFs and the subsequent modification should be conducted. The effects of synthesis conditions and the modifiers on the crystal structure, BET surface area, pore size, and total pore volume of MOFs should be investigated. The effects of modified MOFs on the structure, morphology, mechanical strength, and thermal stability of MMMs should be studied. Finally, the gas transport properties of MMMs should be systematically investigated to understand the influence of MOF fillers in MMMs.

## 5. References

- [1] P. Li, Z. Wang, Z. Qiao, Y. Liu, X. Cao, W. Li, J. Wang, S. Wang, Recent developments in membranes for efficient hydrogen purification, *Journal of membrane science*, 495 (2015) 130-168.
- [2] M.S. Seong, C.I. Kong, B.R. Park, Y. Lee, B.K. Na, J.H. Kim, Optimization of pilot-scale 3-stage membrane process using asymmetric polysulfone hollow fiber membranes for production of high-purity CH<sub>4</sub> and CO<sub>2</sub> from crude biogas, *Chemical Engineering Journal*, 384 (2020) 123342.
- [3] J. Adewole, A. Ahmad, S. Ismail, C. Leo, Current challenges in membrane separation of CO<sub>2</sub> from natural gas: A review, *International Journal of Greenhouse Gas Control*, 17 (2013) 46-65.
- [4] S.E. Kentish, C.A. Scholes, G.W. Stevens, Carbon dioxide separation through polymeric membrane systems for flue gas applications, *Recent Patents on Chemical Engineering*, 1 (2008) 52-66.
- [5] L.D. Biondo, J. Duarte, M. Zeni, M. Godinho, A Dual-mode model interpretation of CO<sub>2</sub>/CH<sub>4</sub> permeability in polysulfone membranes at low pressures, *Anais da Academia Brasileira de Ciências*, 90 (2018) 1855-1864.
- [6] G. George, N. Bhoria, S. AlHallaq, A. Abdala, V. Mittal, Polymer membranes for acid gas removal from natural gas, *Separation and Purification technology*, 158 (2016) 333-356.
- [7] X.-Y. Gong, Z.-H. Huang, H. Zhang, W.-L. Liu, X.-H. Ma, Z.-L. Xu, C.Y. Tang, Novel high-flux positively charged composite membrane incorporating titanium-based MOFs for heavy metal removal, *Chemical Engineering Journal*, 398 (2020) 125706.
- [8] P. Bakonyi, G. Kumar, K. Bélafi-Bakó, S.-H. Kim, S. Koter, W. Kujawski, N. Nemestóthy, J. Peter, Z. Pientka, A review of the innovative gas separation membrane bioreactor with mechanisms for integrated production and purification of biohydrogen, *Bioresource Technology*, 270 (2018) 643-655.
- [9] L. Ji, L. Zhang, X. Zheng, L. Feng, Q. He, Y. Wei, S. Yan, Simultaneous CO<sub>2</sub> absorption, mineralisation and carbonate crystallisation promoted by amines in a single process, *Journal of CO<sub>2</sub> Utilization*, 51 (2021) 101653.
- [10] A.A. Abd, M.R. Othman, S.Z. Naji, A.S. Hashim, Methane enrichment in biogas mixture using pressure swing adsorption: process fundamental and design parameters, *Materials Today Sustainability*, 11-12 (2021) 100063.
- [11] A.M. Yousef, W.M. El-Maghlany, Y.A. Eldrainy, A. Attia, New approach for biogas purification using cryogenic separation and distillation process for CO<sub>2</sub> capture, *Energy*, 156 (2018) 328-351.
- [12] T. He, Z. Liu, H. Son, T. Gundersen, W. Lin, Comparative analysis of cryogenic distillation and chemical absorption for carbon capture in integrated natural gas liquefaction processes, *Journal of Cleaner Production*, 383 (2023) 135264.
- [13] J. Xu, H. Wu, Z. Wang, Z. Qiao, S. Zhao, J. Wang, Recent advances on the membrane processes for CO<sub>2</sub> separation, *Chinese Journal of Chemical Engineering*, 26 (2018) 2280-2291.
- [14] A. Basu, J. Akhtar, M. Rahman, M. Islam, A review of separation of gases using membrane systems, *Petroleum science and technology*, 22 (2004) 1343-1368.
- [15] D.F. Sanders, Z.P. Smith, R. Guo, L.M. Robeson, J.E. McGrath, D.R. Paul, B.D. Freeman, Energy-efficient polymeric gas separation membranes for a sustainable future: A review, *Polymer*, 54 (2013) 4729-4761.
- [16] G. Li, W. Kujawski, R. Válek, S. Koter, A review - The development of hollow fibre membranes for gas separation processes, *International Journal of Greenhouse Gas Control*, 104 (2021) 103195.

- [17] K.A. Stevens, Z.P. Smith, K.L. Gleason, M. Galizia, D.R. Paul, B.D. Freeman, Influence of temperature on gas solubility in thermally rearranged (TR) polymers, *Journal of Membrane Science*, 533 (2017) 75-83.
- [18] C.A. Scholes, Blended perfluoropolymer membranes for carbon dioxide separation by miscible and immiscible morphologies, *Journal of Membrane Science*, 618 (2021) 118675.
- [19] Y. Wang, X. Ma, B.S. Ghanem, F. Alghunaimi, I. Pinnau, Y. Han, Polymers of intrinsic microporosity for energy-intensive membrane-based gas separations, *Materials Today Nano*, 3 (2018) 69-95.
- [20] S.N.A. Shafie, N.A.H. Md Nordin, S.M. Racha, M.R. Bilad, M.H.D. Othman, N. Misdan, J. Jaafar, Z.A. Putra, M.D.H. Wirzal, Emerging ionic liquid engineered polymeric membrane for carbon dioxide removal: A review, *Journal of Molecular Liquids*, 358 (2022) 119192.
- [21] H.M. Tham, K.Y. Wang, D. Hua, S. Japip, T.-S. Chung, From ultrafiltration to nanofiltration: Hydrazine cross-linked polyacrylonitrile hollow fiber membranes for organic solvent nanofiltration, *Journal of membrane science*, 542 (2017) 289-299.
- [22] J. Gao, Z. Thong, K.Y. Wang, T.-S. Chung, Fabrication of loose inner-selective polyethersulfone (PES) hollow fibers by one-step spinning process for nanofiltration (NF) of textile dyes, *Journal of Membrane Science*, 541 (2017) 413-424.
- [23] E.W. Tow, D.M. Warsinger, A.M. Trueworthy, J. Swaminathan, G.P. Thiel, S.M. Zubair, A.S. Myerson, Comparison of fouling propensity between reverse osmosis, forward osmosis, and membrane distillation, *Journal of membrane science*, 556 (2018) 352-364.
- [24] N. Peng, N. Widjojo, P. Sukitpaneenit, M.M. Teoh, G.G. Lipscomb, T.-S. Chung, J.-Y. Lai, Evolution of polymeric hollow fibers as sustainable technologies: Past, present, and future, *Progress in Polymer Science*, 37 (2012) 1401-1424.
- [25] C. Feng, K. Khulbe, T. Matsuura, A. Ismail, Recent progresses in polymeric hollow fiber membrane preparation, characterization and applications, *Separation and Purification Technology*, 111 (2013) 43-71.
- [26] I. Ullah Khan, M.H.D. Othman, A.F. Ismail, T. Matsuura, H. Hashim, N.A.H.M. Nordin, M.A. Rahman, J. Jaafar, A. Jilani, Status and improvement of dual-layer hollow fiber membranes via co-extrusion process for gas separation: A review, *Journal of Natural Gas Science and Engineering*, 52 (2018) 215-234.
- [27] M.L. Jue, V. Breedveld, R.P. Lively, Defect-free PIM-1 hollow fiber membranes, *Journal of Membrane Science*, 530 (2017) 33-41.
- [28] J.-J. Qin, J. Gu, T.-S. Chung, Effect of wet and dry-jet wet spinning on the shear-induced orientation during the formation of ultrafiltration hollow fiber membranes, *Journal of Membrane Science*, 182 (2001) 57-75.
- [29] X. Ding, Y. Cao, H. Zhao, L. Wang, Interfacial morphology between the two layers of the dual-layer asymmetric hollow fiber membranes fabricated by co-extrusion and dry-jet wet-spinning phase-inversion techniques, *Journal of Membrane Science*, 444 (2013) 482-492.
- [30] P. Sukitpaneenit, T.-S. Chung, Fabrication and use of hollow fiber thin film composite membranes for ethanol dehydration, *Journal of membrane science*, 450 (2014) 124-137.
- [31] H. Zhou, Y. Su, X. Chen, J. Luo, S. Tan, Y. Wan, Plasma modification of substrate with poly (methylhydrosiloxane) for enhancing the interfacial stability of PDMS/PAN composite membrane, *Journal of Membrane Science*, 520 (2016) 779-789.
- [32] I. Jesswein, T. Hirth, T. Schiestel, Continuous dip coating of PVDF hollow fiber membranes with PVA for humidification, *Journal of Membrane Science*, 541 (2017) 281-290.

- [33] H.-A. Tsai, Y.-L. Chen, S.-H. Huang, C.-C. Hu, W.-S. Hung, K.-R. Lee, J.-Y. Lai, Preparation of polyamide/polyacrylonitrile composite hollow fiber membrane by synchronous procedure of spinning and interfacial polymerization, *Journal of Membrane Science*, 551 (2018) 261-272.
- [34] E.-S. Jo, X. An, P.G. Ingole, W.-K. Choi, Y.-S. Park, H.-K. Lee, CO<sub>2</sub>/CH<sub>4</sub> separation using inside coated thin film composite hollow fiber membranes prepared by interfacial polymerization, *Chinese Journal of Chemical Engineering*, 25 (2017) 278-287.
- [35] A.K. Hołda, I.F. Vankelecom, Understanding and guiding the phase inversion process for synthesis of solvent resistant nanofiltration membranes, *Journal of Applied Polymer Science*, 132 (2015) 42130.
- [36] D.F. Li, T.-S. Chung, R. Wang, Y. Liu, Fabrication of fluoropolyimide/polyethersulfone (PES) dual-layer asymmetric hollow fiber membranes for gas separation, *Journal of Membrane Science*, 198 (2002) 211-223.
- [37] G. Li, W. Kujawski, K. Knozowska, J. Kujawa, Thin film mixed matrix hollow fiber membrane fabricated by incorporation of amine functionalized metal-organic framework for CO<sub>2</sub>/N<sub>2</sub> separation, *Materials*, 14 (2021) 3366.
- [38] G. Li, W. Kujawski, K. Knozowska, J. Kujawa, The Effects of PEI Hollow Fiber Substrate Characteristics on PDMS/PEI Hollow Fiber Membranes for CO<sub>2</sub>/N<sub>2</sub> Separation, *Membranes*, 11 (2021) 56.
- [39] G. Li, K. Knozowska, J. Kujawa, A. Tonkonogovas, A. Stankevičius, W. Kujawski, Fabrication of Polydimethylsiloxane (PDMS) Dense Layer on Polyetherimide (PEI) Hollow Fiber Support for the Efficient CO<sub>2</sub>/N<sub>2</sub> Separation Membranes, *Polymers*, 13 (2021) 756.
- [40] L.M. Robeson, The upper bound revisited, *Journal of Membrane Science*, 320 (2008) 390-400.
- [41] J.-T. Chen, Y.-J. Fu, K.-L. Tung, S.-H. Huang, W.-S. Hung, S. Jessie Lue, C.-C. Hu, K.-R. Lee, J.-Y. Lai, Surface modification of poly(dimethylsiloxane) by atmospheric pressure high temperature plasma torch to prepare high-performance gas separation membranes, *Journal of Membrane Science*, 440 (2013) 1-8.
- [42] A.R. Kamble, C.M. Patel, Z.V.P. Murthy, A review on the recent advances in mixed matrix membranes for gas separation processes, *Renewable and Sustainable Energy Reviews*, 145 (2021) 111062.
- [43] H.-j. Li, Y.-d. Liu, A review of polymer-derived carbon molecular sieve membranes for gas separation, *New Carbon Materials*, 37 (2022) 484-507.
- [44] Y. Cheng, Y. Ying, S. Japip, S.D. Jiang, T.S. Chung, S. Zhang, D. Zhao, Advanced porous materials in mixed matrix membranes, *Advanced Materials*, 30 (2018) 1802401.
- [45] H. Daglar, S. Keskin, Recent advances, opportunities, and challenges in high-throughput computational screening of MOFs for gas separations, *Coordination Chemistry Reviews*, 422 (2020) 213470.
- [46] G. Li, W. Kujawski, A. Tonkonogovas, K. Knozowska, J. Kujawa, E. Olewnik-Kruszkowska, N. Pedišius, A. Stankevičius, Evaluation of CO<sub>2</sub> separation performance with enhanced features of materials – Pebax® 2533 mixed matrix membranes containing ZIF-8-PEI@[P(3)HIm][Tf2N], *Chemical Engineering Research and Design*, 181 (2022) 195-208.
- [47] Z. Wang, D. Wang, S. Zhang, L. Hu, J. Jin, Interfacial design of mixed matrix membranes for improved gas separation performance, *Advanced Materials*, 28 (2016) 3399-3405.
- [48] Y. Cheng, Z. Wang, D. Zhao, Mixed matrix membranes for natural gas upgrading: Current status and opportunities, *Industrial & Engineering Chemistry Research*, 57 (2018) 4139-4169.

- [49] C. Zhu, Y. Peng, W. Yang, Modification strategies for metal-organic frameworks targeting at membrane-based gas separations, *Green Chemical Engineering*, 2 (2021) 17-26.
- [50] Z. Wang, J. Yuan, R. Li, H. Zhu, J. Duan, Y. Guo, G. Liu, W. Jin, ZIF-301 MOF/6FDA-DAM polyimide mixed-matrix membranes for CO<sub>2</sub>/CH<sub>4</sub> separation, *Separation and Purification Technology*, 264 (2021) 118431.
- [51] W. Chen, Z. Zhang, L. Hou, C. Yang, H. Shen, K. Yang, Z. Wang, Metal-organic framework MOF-801/PIM-1 mixed-matrix membranes for enhanced CO<sub>2</sub>/N<sub>2</sub> separation performance, *Separation and Purification Technology*, 250 (2020) 117198.
- [52] Y. Wang, Y. Ren, H. Wu, X. Wu, H. Yang, L. Yang, X. Wang, Y. Wu, Y. Liu, Z. Jiang, Amino-functionalized ZIF-7 embedded polymers of intrinsic microporosity membrane with enhanced selectivity for biogas upgrading, *Journal of Membrane Science*, 602 (2020) 117970.
- [53] C.Y. Chuah, W. Li, S.A.S.C. Samarasinghe, G.S.M.D.P. Sethunga, T.-H. Bae, Enhancing the CO<sub>2</sub> separation performance of polymer membranes via the incorporation of amine-functionalized HKUST-1 nanocrystals, *Microporous and Mesoporous Materials*, 290 (2019) 109680.
- [54] W. Chen, Z. Zhang, C. Yang, J. Liu, H. Shen, K. Yang, Z. Wang, PIM-based mixed-matrix membranes containing MOF-801/ionic liquid nanocomposites for enhanced CO<sub>2</sub> separation performance, *Journal of Membrane Science*, 636 (2021) 119581.
- [55] Y. Jiang, C. Liu, J. Caro, A. Huang, A new UiO-66-NH<sub>2</sub> based mixed-matrix membranes with high CO<sub>2</sub>/CH<sub>4</sub> separation performance, *Microporous and Mesoporous Materials*, 274 (2019) 203-211.
- [56] R. Thür, N. Van Velthoven, S. Sloopmaekers, J. Didden, R. Verbeke, S. Smolders, M. Dickmann, W. Egger, D. De Vos, I.F.J. Vankelecom, Bipyridine-based UiO-67 as novel filler in mixed-matrix membranes for CO<sub>2</sub>-selective gas separation, *Journal of Membrane Science*, 576 (2019) 78-87.
- [57] B. Liu, D. Li, J. Yao, H. Sun, Improved CO<sub>2</sub> separation performance and interfacial affinity of mixed matrix membrane by incorporating UiO-66-PEI@[bmim][Tf2N] particles, *Separation and Purification Technology*, 239 (2020) 116519.
- [58] C.Y. Chuah, J. Lee, J. Song, T.-H. Bae, CO<sub>2</sub>/N<sub>2</sub> Separation Properties of Polyimide-Based Mixed-Matrix Membranes Comprising UiO-66 with Various Functionalities, *Membranes*, 10 (2020) 154.
- [59] M.Z. Ahmad, M. Navarro, M. Lhotka, B. Zornoza, C. Téllez, W.M. de Vos, N.E. Benes, N.M. Konnertz, T. Visser, R. Semino, G. Maurin, V. Fila, J. Coronas, Enhanced gas separation performance of 6FDA-DAM based mixed matrix membranes by incorporating MOF UiO-66 and its derivatives, *Journal of Membrane Science*, 558 (2018) 64-77.
- [60] M. van Essen, L. van den Akker, R. Thür, M. Houben, I.F.J. Vankelecom, Z. Borneman, K. Nijmeijer, The influence of pore aperture, volume and functionality of isorecticular gmelinite zeolitic imidazolate frameworks on the mixed gas CO<sub>2</sub>/N<sub>2</sub> and CO<sub>2</sub>/CH<sub>4</sub> separation performance in mixed matrix membranes, *Separation and Purification Technology*, 260 (2021) 118103.
- [61] A. Guo, Y. Ban, K. Yang, W. Yang, Metal-organic framework-based mixed matrix membranes: Synergetic effect of adsorption and diffusion for CO<sub>2</sub>/CH<sub>4</sub> separation, *Journal of Membrane Science*, 562 (2018) 76-84.
- [62] C. Ye, X. Wu, H. Wu, L. Yang, Y. Ren, Y. Wu, Y. Liu, Z. Guo, R. Zhao, Z. Jiang, Incorporating nano-sized ZIF-67 to enhance selectivity of polymers of intrinsic microporosity membranes for biogas upgrading, *Chemical Engineering Science*, 216 (2020) 115497.

- [63] R. Lin, L. Ge, H. Diao, V. Rudolph, Z. Zhu, Ionic Liquids as the MOFs/Polymer Interfacial Binder for Efficient Membrane Separation, *ACS Applied Materials & Interfaces*, 8 (2016) 32041-32049.
- [64] N.H. Suhaimi, Y.F. Yeong, N. Jusoh, T.L. Chew, M.A. Bustam, S. Suleman, Separation of CO<sub>2</sub> from CH<sub>4</sub> using mixed matrix membranes incorporated with amine functionalized MIL-125 (Ti) nanofiller, *Chemical Engineering Research and Design*, 159 (2020) 236-247.
- [65] E. Aliyev, J. Warfsmann, B. Tokay, S. Shishatskiy, Y.-J. Lee, J. Lillepaerg, N.R. Champness, V. Filiz, Gas Transport Properties of the Metal–Organic Framework (MOF)-Assisted Polymer of Intrinsic Microporosity (PIM-1) Thin-Film Composite Membranes, *ACS Sustainable Chemistry & Engineering*, 9 (2021) 684-694.
- [66] C. Song, R. Li, Z. Fan, Q. Liu, B. Zhang, Y. Kitamura, CO<sub>2</sub>/N<sub>2</sub> separation performance of Pebax/MIL-101 and Pebax /NH<sub>2</sub>-MIL-101 mixed matrix membranes and intensification via sub-ambient operation, *Separation and Purification Technology*, 238 (2020) 116500.
- [67] Y. Zhou, M. Jia, X. Zhang, J. Yao, Etched ZIF-8 as a Filler in Mixed-Matrix Membranes for Enhanced CO<sub>2</sub>/N<sub>2</sub> Separation, *Chemistry – A European Journal*, 26 (2020) 7918-7922.
- [68] H. Yin, A. Alkaş, Y. Zhang, Y. Zhang, S.G. Telfer, Mixed matrix membranes (MMMs) using an emerging metal-organic framework (MUF-15) for CO<sub>2</sub> separation, *Journal of Membrane Science*, 609 (2020) 118245.
- [69] J. Lu, X. Zhang, L. Xu, G. Zhang, J. Zheng, Z. Tong, C. Shen, Q. Meng, Preparation of Amino-Functional UiO-66/PIMs Mixed Matrix Membranes with [bmim][Tf<sub>2</sub>N] as Regulator for Enhanced Gas Separation, *Membranes*, 11 (2021) 35.
- [70] J. Han, L. Bai, H. Jiang, S. Zeng, B. Yang, Y. Bai, X. Zhang, Task-Specific Ionic Liquids Tuning ZIF-67/PIM-1 Mixed Matrix Membranes for Efficient CO<sub>2</sub> Separation, *Industrial & Engineering Chemistry Research*, 60 (2021) 593-603.
- [71] R. Xu, Z. Wang, M. Wang, Z. Qiao, J. Wang, High nanoparticles loadings mixed matrix membranes via chemical bridging-crosslinking for CO<sub>2</sub> separation, *Journal of Membrane Science*, 573 (2019) 455-464.
- [72] S. Ishaq, R. Tamime, M.R. Bilad, A.L. Khan, Mixed matrix membranes comprising of polysulfone and microporous Bio-MOF-1: Preparation and gas separation properties, *Separation and Purification Technology*, 210 (2019) 442-451.
- [73] A. Guo, Y. Ban, K. Yang, Y. Zhou, N. Cao, M. Zhao, W. Yang, Molecular sieving mixed matrix membranes embodying nano-fillers with extremely narrow pore-openings, *Journal of Membrane Science*, 601 (2020) 117880.
- [74] S. Majumdar, B. Tokay, V. Martin-Gil, J. Campbell, R. Castro-Muñoz, M.Z. Ahmad, V. Fila, Mg-MOF-74/Polyvinyl acetate (PVAc) mixed matrix membranes for CO<sub>2</sub> separation, *Separation and Purification Technology*, 238 (2020) 116411.
- [75] H. Li, L. Tuo, K. Yang, H.-K. Jeong, Y. Dai, G. He, W. Zhao, Simultaneous enhancement of mechanical properties and CO<sub>2</sub> selectivity of ZIF-8 mixed matrix membranes: Interfacial toughening effect of ionic liquid, *Journal of Membrane Science*, 511 (2016) 130-142.
- [76] J. Kujawa, S. Al-Gharabli, T.M. Muzioł, K. Knozowska, G. Li, L.F. Dumée, W. Kujawski, Crystalline porous frameworks as nano-enhancers for membrane liquid separation – Recent developments, *Coordination Chemistry Reviews*, 440 (2021) 213969.
- [77] K. Yang, Y. Dai, X. Ruan, W. Zheng, X. Yang, R. Ding, G. He, Stretched ZIF-8@GO flake-like fillers via pre-Zn(II)-doping strategy to enhance CO<sub>2</sub> permeation in mixed matrix membranes, *Journal of Membrane Science*, 601 (2020) 117934.

- [78] L. Dong, M. Chen, J. Li, D. Shi, W. Dong, X. Li, Y. Bai, Metal-organic framework-graphene oxide composites: A facile method to highly improve the CO<sub>2</sub> separation performance of mixed matrix membranes, *Journal of Membrane Science*, 520 (2016) 801-811.
- [79] M. Jia, Y. Feng, J. Qiu, X.-F. Zhang, J. Yao, Amine-functionalized MOFs@GO as filler in mixed matrix membrane for selective CO<sub>2</sub> separation, *Separation and Purification Technology*, 213 (2019) 63-69.
- [80] S. Castarlenas, C. Téllez, J. Coronas, Gas separation with mixed matrix membranes obtained from MOF UiO-66-graphite oxide hybrids, *Journal of Membrane Science*, 526 (2017) 205-211.
- [81] B. Chen, C. Wan, X. Kang, M. Chen, C. Zhang, Y. Bai, L. Dong, Enhanced CO<sub>2</sub> separation of mixed matrix membranes with ZIF-8@GO composites as fillers: Effect of reaction time of ZIF-8@GO, *Separation and Purification Technology*, 223 (2019) 113-122.
- [82] X. Li, S. Yu, K. Li, C. Ma, J. Zhang, H. Li, X. Chang, L. Zhu, Q. Xue, Enhanced gas separation performance of Pebax mixed matrix membranes by incorporating ZIF-8 in situ inserted by multiwalled carbon nanotubes, *Separation and Purification Technology*, 248 (2020) 117080.
- [83] N. Jamil, N.H. Othman, N.H. Alias, M.Z. Shahrudin, R.A. Roslan, W.J. Lau, A.F. Ismail, Mixed matrix membranes incorporated with reduced graphene oxide (rGO) and zeolitic imidazole framework-8 (ZIF-8) nanofillers for gas separation, *Journal of Solid State Chemistry*, 270 (2019) 419-427.
- [84] R. Lin, L. Ge, S. Liu, V. Rudolph, Z. Zhu, Mixed-Matrix Membranes with Metal–Organic Framework-Decorated CNT Fillers for Efficient CO<sub>2</sub> Separation, *ACS Applied Materials & Interfaces*, 7 (2015) 14750-14757.
- [85] W. Li, C.Y. Chuah, L. Nie, T.-H. Bae, Enhanced CO<sub>2</sub>/CH<sub>4</sub> selectivity and mechanical strength of mixed-matrix membrane incorporated with NiDOBDC/GO composite, *Journal of Industrial and Engineering Chemistry*, 74 (2019) 118-125.
- [86] Y. Han, W.S.W. Ho, Polymeric membranes for CO<sub>2</sub> separation and capture, *Journal of Membrane Science*, 628 (2021) 119244.
- [87] M. Wang, Z. Wang, S. Zhao, J. Wang, S. Wang, Recent advances on mixed matrix membranes for CO<sub>2</sub> separation, *Chinese Journal of Chemical Engineering*, 25 (2017) 1581-1597.
- [88] R. Lin, B. Villacorta Hernandez, L. Ge, Z. Zhu, Metal organic framework based mixed matrix membranes: an overview on filler/polymer interfaces, *Journal of Materials Chemistry A*, 6 (2018) 293-312.
- [89] G. Aguilar-Armenta, M.E. Patiño-Iglesias, R. Leyva-Ramos, Adsorption kinetic behaviour of pure CO<sub>2</sub>, N<sub>2</sub> and CH<sub>4</sub> in natural clinoptilolite at different temperatures, *Adsorption Science & Technology*, 21 (2003) 81-91.
- [90] G. Firpo, E. Angeli, L. Repetto, U. Valbusa, Permeability thickness dependence of polydimethylsiloxane (PDMS) membranes, *Journal of Membrane Science*, 481 (2015) 1-8.
- [91] R. Selyanchyn, M. Ariyoshi, S. Fujikawa, Thickness Effect on CO<sub>2</sub>/N<sub>2</sub> Separation in Double Layer Pebax-1657®/PDMS Membranes, *Membranes*, 8 (2018) 121.
- [92] J.G. Wijmans, R.W. Baker, The solution-diffusion model: a review, *Journal of membrane science*, 107 (1995) 1-21.
- [93] L. Liu, A. Chakma, X. Feng, CO<sub>2</sub>/N<sub>2</sub> separation by poly (ether block amide) thin film hollow fiber composite membranes, *Industrial & engineering chemistry research*, 44 (2005) 6874-6882.
- [94] J. Shen, G. Liu, K. Huang, Q. Li, K. Guan, Y. Li, W. Jin, UiO-66-polyether block amide mixed matrix membranes for CO<sub>2</sub> separation, *Journal of Membrane Science*, 513 (2016) 155-165.



- [95] X. Bi, Y.a. Zhang, F. Zhang, S. Zhang, Z. Wang, J. Jin, MOF Nanosheet-Based Mixed Matrix Membranes with Metal–Organic Coordination Interfacial Interaction for Gas Separation, *ACS Applied Materials & Interfaces*, 12 (2020) 49101-49110.
- [96] W.S. Chi, S. Hwang, S.-J. Lee, S. Park, Y.-S. Bae, D.Y. Ryu, J.H. Kim, J. Kim, Mixed matrix membranes consisting of SEBS block copolymers and size-controlled ZIF-8 nanoparticles for CO<sub>2</sub> capture, *Journal of Membrane Science*, 495 (2015) 479-488.
- [97] V. Nafisi, M.-B. Hägg, Gas separation properties of ZIF-8/6FDA-durene diamine mixed matrix membrane, *Separation and Purification Technology*, 128 (2014) 31-38.
- [98] Z.A. AlOthman, A Review: Fundamental Aspects of Silicate Mesoporous Materials, *Materials*, 5 (2012) 2874-2902.
- [99] G. Leofanti, M. Padovan, G. Tozzola, B. Venturelli, Surface area and pore texture of catalysts, *Catalysis today*, 41 (1998) 207-219.
- [100] S. Abdollahi, H.R. Mortaheb, A. Ghadimi, M. Esmaili, Improvement in separation performance of Matrimid<sup>®</sup>5218 with encapsulated [Emim][Tf<sub>2</sub>N] in a heterogeneous structure: CO<sub>2</sub>/CH<sub>4</sub> separation, *Journal of Membrane Science*, 557 (2018) 38-48.
- [101] W. Zheng, R. Ding, K. Yang, Y. Dai, X. Yan, G. He, ZIF-8 nanoparticles with tunable size for enhanced CO<sub>2</sub> capture of Pebax based MMMs, *Separation and Purification Technology*, 214 (2019) 111-119.
- [102] S. Meshkat, S. Kaliaguine, D. Rodrigue, Mixed matrix membranes based on amine and non-amine MIL-53(Al) in Pebax<sup>®</sup> MH-1657 for CO<sub>2</sub> separation, *Separation and Purification Technology*, 200 (2018) 177-190.
- [103] J. Shen, G. Liu, K. Huang, Q. Li, K. Guan, Y. Li, W. Jin, UiO-66-polyether block amide mixed matrix membranes for CO<sub>2</sub> separation, *Journal of Membrane Science*, 513 (2016) 155-165.
- [104] W. Zheng, R. Ding, K. Yang, Y. Dai, X. Yan, G. He, ZIF-8 nanoparticles with tunable size for enhanced CO<sub>2</sub> capture of Pebax based MMMs, *Separation and Purification Technology*, 214 (2019) 111-119.
- [105] M. Li, X. Zhang, S. Zeng, L. bai, H. Gao, J. Deng, Q. Yang, S. Zhang, Pebax-based composite membranes with high gas transport properties enhanced by ionic liquids for CO<sub>2</sub> separation, *RSC Advances*, 7 (2017) 6422-6431.
- [106] H.R. Mahdipoor, R. Halladj, E. Ganji Babakhani, S. Amjad-Iranagh, J. Sadeghzadeh Ahari, Adsorption of CO<sub>2</sub>, N<sub>2</sub> and CH<sub>4</sub> on a Fe-based metal organic framework, MIL-101(Fe)-NH<sub>2</sub>, *Colloids and Surfaces A: Physicochemical and Engineering Aspects*, 619 (2021) 126554.
- [107] G. Li, W. Kujawski, K. Knozowska, J. Kujawa, Pebax<sup>®</sup> 2533/PVDF thin film mixed matrix membranes containing MIL-101 (Fe)/GO composite for CO<sub>2</sub> capture, *RSC Advances*, 12 (2022) 29124-29136.
- [108] Z. Dai, J. Deng, H. Aboukeila, J. Yan, L. Ansaloni, K.P. Mineart, M. Giacinti Baschetti, R.J. Spontak, L. Deng, Highly CO<sub>2</sub>-permeable membranes derived from a midblock-sulfonated multiblock polymer after submersion in water, *NPG Asia Materials*, 11 (2019) 53.

## 6. Abstract

Gas separation is very important to many industrial processes, such as flue gas treatment, the upgrading of biogas and natural gas, and hydrogen purification. Comparing with other technologies such as cryogenic distillation, membrane technology is a promising solution for CO<sub>2</sub> separation, owing to its environmental friendliness, high compactness, low energy consumption, simplicity in operation, and low capital cost. Polymeric membranes possess the trade-off relationship between gas permeability and selectivity, limiting their application in gas separation processes. In order to break the trade-off relationship, the incorporation of inorganic fillers into polymer matrix to prepare MMMs is a promising alternative to enhance the gas separation performance. MOFs have drawn great attention in the preparation of MMMs for gas separation.

This doctoral thesis aims to fabricate polymeric membranes and MMMs for gas separation. PEI hollow fibers, PDMS/PEI TFC-HFMs, Pebax<sup>®</sup> 2533-based HF-MMMs and flat sheet MMMs were fabricated and characterized by various characterization methods, such as SEM, FTIR-ATR, TGA, EDX, Tensile strength tests, and gas permeance measurement. UiO-66-NH<sub>2</sub>, pristine and modified ZIF-8, MIL-101 (Fe), and MIL-GO composites were synthesized by using solvothermal method and used as fillers for the fabrication of MMMs. The synthesized fillers were characterized by SEM, FTIR-ATR, TGA, EDX, DLS, XRD, and nitrogen adsorption/desorption measurements.

For the fabrication of PEI hollow fibers and PDMS/PEI TFC-HFMs, the parameters of dry-jet wet spinning process and dip-coating process were optimized. The polymer concentration, and the composition and flow rate of bore fluid affected the morphology, pore structure, and the gas permeance of PEI hollow fibers. The thickness of PDMS layer, the gas permeability, and CO<sub>2</sub>/N<sub>2</sub> ideal selectivity were predominantly influenced by the concentration of coating solution and the coating time.

For the fabrication of Pebax<sup>®</sup> 2533-based MMMs, the incorporation of a proper amount of fillers into polymer matrix could simultaneously increase the gas permeability and ideal selectivity. However, the filler agglomeration occurred when high amount of fillers were incorporated, resulting in the adverse effect on gas separation performance. ZIF-8 was synthesized and modified with branched polyethyleneimine (PEI) with subsequent IL ([P(3)HIm][Tf<sub>2</sub>N]) decoration. The crystal structure of ZIF-8 was preserved, while the BET surface area, total pore volume, and average pore diameter decreased after modification. The ZIF-8-PEI@IL/Pebax<sup>®</sup> 2533 MMMs showed enhanced compatibility between filler and polymer matrix and significant improvement of gas separation performance. The BET surface area and total pore volume of MIL-GO composite were lower than MIL-101 (Fe), owing to the coverage of nonporous GO nanosheets on MIL-101 (Fe). The incorporation of MIL-GO-2 into Pebax matrix simultaneously increased the CO<sub>2</sub> permeability and the CO<sub>2</sub>/N<sub>2</sub> ideal selectivity of the fabricated MIL-GO-2-Pebax<sup>®</sup> 2533/PVDF MMMs.

## 7. Streszczenie:

Separacja gazów jest bardzo ważna w wielu procesach, takich jak oczyszczanie gazów spalinowych, uszlachetnianie biogazu i gazu ziemnego oraz oczyszczanie wodoru. W porównaniu z innymi technikami, takimi jak destylacja kriogeniczna lub sorpcje, separacja z wykorzystaniem membran jest obiecującym rozwiązaniem do separacji CO<sub>2</sub> ze względu na przyjazność dla środowiska, dużą kompaktowość, niskie zużycie energii i niskie koszty inwestycyjne. W przypadku membran polimerowych, kompromis pomiędzy właściwościami materiału, tj. albo dobrą przepuszczalnością gazu albo odpowiednią selektywnością organiczną ich szersze zastosowanie w procesach separacji gazów. Aby móc polepszyć jednocześnie przepuszczalność jak i selektywność, należy membrany odpowiednio zmodyfikować. Jednym z efektywnych rozwiązań, które skupiły uwagę naukowców, jest wprowadzenie do matrycy polimerowej nieorganicznych nanonapełniaczy, w szczególności sieci metalo organicznych (MOF, ang. *metal organic framework*). Tak przygotowane materiały separacyjne określane są jako membrany heterogeniczne (MMM, ang. *mixed matrix membranes*).

Celem nadrzędnym pracy doktorskiej było wytworzenie membran polimerowych lub membrany o matrycy mieszanej do separacji gazów. Przygotowano membrany o strukturze włókien kanalikowych (ang. *hollow fibre*) na bazie następujących polimerów PEI, PDMS/PEI TFC-HFM, HF-MMM oraz Pebax<sup>®</sup> 2533. Ponadto przygotowane zostały płaskie membrany heterogeniczne (MMM). Wszystkie przygotowane materiały zostały szczegółowo scharakteryzowane z wykorzystaniem technik analitycznych i instrumentalnych, m.in., SEM, FTIR-ATR, TGA, EDX. Ponadto zbadano właściwości mechaniczne membran (m.in. odporność na zerwanie) i określono przepuszczalność membran w kontakcie z wybranymi gazami. Nanonapełniacze, UiO-66-NH<sub>2</sub>, natywny i zmodyfikowany ZIF-8, MIL-101 (Fe) oraz kompozytowy MIL-GO zsyntetyzowano metodą solwotermiczną. Nieorganiczne dodatki zostały również szczegółowo scharakteryzowane, w tym wykonano pomiary niskotemperaturowej adsorpcji/desorpcji azotu.

Podczas wytwarzania membran o strukturze włókien kanalikowych na bazie polimeru PEI oraz PDMS/PEI TFC-HFMs, zoptymalizowano parametry procesu przędzenia włókien i procesu powlekania przez zanurzenie. Stwierdzono, że stężenie polimeru oraz skład i prędkość przepływu roztworu polimerowego wpływa na morfologię, strukturę porów i przepuszczalność membran na bazie PEI. Jednak, na właściwości transportowe i selektywne (przepuszczalność gazu, idealną selektywność CO<sub>2</sub>/N<sub>2</sub>) oraz strukturę membran (grubość warstwy PDMS), w największym stopniu wpływały stężenie roztworu powlekającego i czas powlekania.

W przypadku wytwarzania MMM na bazie Pebax<sup>®</sup> 2533, wprowadzenie odpowiedniej ilości napełniaczy do matrycy polimerowej umożliwiło jednoczesne polepszenie przepuszczalności gazu i wzrost selektywności idealnej. Jednakże, w przypadku wysokich stężeń, zaobserwowano aglomerację napełniacza w matrycy, co w negatywny sposób wpływało na wydajność separacji gazów. ZIF-8 zsyntetyzowano i zmodyfikowano polietylenoiminą o rozgałęzionej strukturze, a następnie funkcjonalizowano cieczą jonową ([P(3)HIm][Tf<sub>2</sub>N]). Istotnym efektem było zachowanie struktury krystalicznej ZIF-8 po procesie funkcjonalizacji, jednakże zaobserwowano, że powierzchnia właściwa, całkowita objętość porów i średnia

średnica porów uległy zmniejszeniu. MMM ZIF-8-PEI@IL/Pebax<sup>®</sup> 2533 wykazały lepszą kompatybilność pomiędzy napelniaczem a matrycą polimerową oraz znaczną poprawę wydajności separacji gazów. Powierzchnia właściwa i całkowita objętość porów kompozytu MIL-GO były mniejsze niż MIL-101 (Fe), ze względu na pokrycie nieporowatymi nanoarkuszami GO struktury MIL-101 (Fe). Włączenie MIL-GO-2 do matrycy Pebax jednocześnie zwiększyło przepuszczalność CO<sub>2</sub> i idealną selektywność CO<sub>2</sub>/N<sub>2</sub> wytworzonych MMM MIL-GO-2-Pebax<sup>®</sup> 2533/PVDF.

## 8. List of publications included in this dissertation

The list includes 6 publications in the Journal Citation Reports database (JCR) (IF<sub>total</sub>=24.3; MNiSW<sub>total</sub>= 720).

- I. **G. Li**, W. Kujawski\*, R. Válek, S. Koter, A review of the development of hollow fiber membranes for gas separation processes, *International Journal of Greenhouse Gas Control*, 104 (2021) 103195. (IF=3.9, Q1, MNiSW =140)  
Contribution of the first author: 60 %
- II. **G. Li**, W. Kujawski\*, K. Knozowska, J. Kujawa, The effects of PEI hollow fiber substrate characteristics on PDMS/PEI hollow fiber membranes for CO<sub>2</sub> /N<sub>2</sub> separation, *Membranes*, 11 (2021) 56. (IF=4.2, Q2, MNiSW =100)  
Contribution of the first author: 65 %
- III. **G. Li**, K. Knozowska, J. Kujawa, A. Tonkonogovas, A. Stankevičius, W. Kujawski\*, Fabrication of polydimethylsiloxane (PDMS) dense layer on polyetherimide (PEI) hollow fiber support for the efficient CO<sub>2</sub>/N<sub>2</sub> separation membranes, *Polymers* 13 (2021) 756. (IF=5.0, Q1, MNiSW =100)  
Contribution of the first author: 55 %
- IV. **G. Li**, W. Kujawski\*, K. Knozowska, J. Kujawa, Thin film mixed matrix hollow fiber membrane fabricated by incorporation of amine functionalized metal-organic framework for CO<sub>2</sub>/N<sub>2</sub> separation, *Materials*, 14 (2021) 3366. (IF=3.4, Q2, MNiSW =140)  
Contribution of the first author: 65 %
- V. **G. Li**, W. Kujawski\*, A. Tonkonogovas, K. Knozowska, J. Kujawa, E. Olewnik-Kruszkowska, N. Pedišius, A. Stankevičius, Evaluation of CO<sub>2</sub> separation performance with enhanced features of materials - Pebax<sup>®</sup> 2533 mixed matrix membranes containing ZIF-8-PEI@[P(3)HIm][Tf<sub>2</sub>N], *Chemical Engineering Research and Design*, 181 (2022) 195-208. (IF=3.9, Q1, MNiSW =140)  
Contribution of the first author: 45 %
- VI. **G. Li**, W. Kujawski\*, K. Knozowska, J. Kujawa, Pebax<sup>®</sup> 2533/PVDF thin film mixed matrix membranes containing MIL-101 (Fe)/GO composite for CO<sub>2</sub> capture, *RSC Advances*, 12 (2022) 29124-29136 (IF=3.9, Q1, MNiSW =100)  
Contribution of the first author: 65 %

\* Corresponding author.

## 9. Academic achievements

**Publications (IF<sub>total</sub>=152.9; MNiSW<sub>total</sub>=2950; H-index=13, Citation Index=364)**

### a) Publications from the dissertation

- I. **G. Li**, W. Kujawski\*, R. Válek, S. Koter, A review of the development of hollow fiber membranes for gas separation processes, *International Journal of Greenhouse Gas Control*, 104 (2021) 103195. (IF=3.9, Q1, MNiSW =140)
- II. **G. Li**, W. Kujawski\*, K. Knozowska, J. Kujawa, The effects of PEI hollow fiber substrate characteristics on PDMS/PEI hollow fiber membranes for CO<sub>2</sub>/N<sub>2</sub> separation, *Membranes*, 11 (2021) 56. (IF=4.2, Q2, MNiSW =100)
- III. **G. Li**, K. Knozowska, J. Kujawa, A. Tonkonogovas, A. Stankevičius, W. Kujawski\*, Fabrication of polydimethylsiloxane (PDMS) dense layer on polyetherimide (PEI) hollow fiber support for the efficient CO<sub>2</sub>/N<sub>2</sub> separation membranes, *Polymers* 13 (2021) 756. (IF=5.0, Q1, MNiSW =100)
- IV. **G. Li**, W. Kujawski\*, K. Knozowska, J. Kujawa, Thin film mixed matrix hollow fiber membrane fabricated by incorporation of amine functionalized metal-organic framework for CO<sub>2</sub>/N<sub>2</sub> separation, *Materials*, 14 (2021) 3366. (IF=3.4, Q2, MNiSW =140)
- V. **G. Li**, W. Kujawski\*, A. Tonkonogovas, K. Knozowska, J. Kujawa, E. Olewnik-Kruszkowska, N. Pedišius, A. Stankevičius, Evaluation of CO<sub>2</sub> separation performance with enhanced features of materials - Pebax<sup>®</sup> 2533 mixed matrix membranes containing ZIF-8-PEI@[P(3)HIm][Tf<sub>2</sub>N], *Chemical Engineering Research and Design*, 181 (2022) 195-208. (IF=3.9, Q1, MNiSW =140)
- VI. **G. Li**, W. Kujawski\*, K. Knozowska, J. Kujawa, Pebax<sup>®</sup> 2533/PVDF thin film mixed matrix membranes containing MIL-101 (Fe)/GO composite for CO<sub>2</sub> capture, *RSC Advances*, 12 (2022) 29124-29136 (IF=3.9, Q1, MNiSW =100)

### b) Other publications

1. X. Chen, **G. Li**, M. Głodek, K. Knozowska, J. Kujawa, P. Zhang, W. Kujawski, Efficient surface engineering of aluminum foil by using piranha solution strategy, *Surfaces and Interfaces*, 43 (2023) 103566. (IF=6.2, Q1, MNiSW=70)
2. J. Kujawa, S. Al-Gharabli, A. Szymczyk, A. P. Terzyk, S. Boncel, K. Knozowska, **G. Li**, W. Kujawski, On membrane-based approaches for rare earths separation and extraction – Recent

- developments, *Coordination Chemistry Reviews*, 493 (2023) 215340. (IF=20.6, Q1, MNiSW=200)
3. W. Jankowski, **G. Li**, W. Kujawski, J. Kujawa, Recent development of membranes modified with natural compounds: Preparation methods and applications in water treatment, *Separation and Purification Technology*, 302 (2022) 122101. (IF=8.6, Q1, MNiSW=140)
  4. **G. Li**, W. Kujawski, E. Rynkowska, Advancements in proton exchange membranes for high-performance high-temperature proton exchange membrane fuel cells (HT-PEMFC), *Reviews in Chemical Engineering*, 38 (2022) 327-346. (IF=4.7, Q1, MNiSW=140)
  5. K.S.Burts, T.V.Plisko, A.V.Bildyukevich, **G. Li**, J.Kujawa, W.Kujawski, Development of dynamic PVA/PAN membranes for pervaporation: Correlation between kinetics of gel layer formation, preparation conditions, and separation performance, *Chemical Engineering Research and Design*, 182 (2022) 544-557. (IF=3.9, Q1, MNiSW=140)
  6. J. Kujawa, M. Głodek, I. Koter, **G. Li**, K. Knozowska, W. Kujawski, Bioconjugation Strategy for Ceramic Membranes Decorated with *Candida Antarctica* Lipase B—Impact of Immobilization Process on Material Features, *Materials* 15 (2022) 671. (IF=3.4, Q2, MNiSW=140)
  7. K. Knozowska, A. Kujawska, **G. Li**, J. Kujawa, M. Bryjak, W. Kujawski, F. Lipnizki, L. Ahrné, J. Kujawski, Membrane assisted processing of acetone, butanol, and ethanol (ABE) aqueous streams, *Chemical Engineering and Processing*, 166 (2021) 108462. (IF=4.3, Q1, MNiSW=140)
  8. J. Kujawa, M. Głodek, **G. Li**, S. Al-Gharabli, K. Knozowska, W. Kujawski, Highly effective enzymes immobilization on ceramics: Requirements for supports and enzymes, *Science of The Total Environment*, 801 (2021) 149647. (IF=9.8, Q1, MNiSW=200)
  9. J. Kujawa, S. Al-Gharabli, T. M.Muzioł, K. Knozowska, **G. Li**, L. F.Dumée, W. Kujawski, Crystalline porous frameworks as nano-enhancers for membrane liquid separation – Recent developments, *Coordination Chemistry Reviews*, 440, (2021) 213969. (IF=20.6, Q1, MNiSW=200)
  10. **G. Li**, E. Rynkowska, K. Fatyeyeva, J. Kujawa, K. Dzieszowski, A.Wolan, S. Marais, C. Chappey, Z. Rafinski, W. Kujawski, The Impact of Reactive Ionic Liquids Addition on the Physicochemical and Sorption Properties of Poly(Vinyl Alcohol)-Based Films, *Polymers*, 12 (2020) 1958. (IF=5.0, Q1, MNiSW=100)

11. D. S. Lakshmi, S. Sankaranarayanan, T. K Gajaria, **G. Li**, W. Kujawski, J. Kujawa, R. Navia, A Short Review on the Valorization of Green Seaweeds and Ulvan: FEEDSTOCK for Chemicals and Biomaterials, *Biomolecules*, 10 (2020) 991. (IF=5.5, Q2, MNiSW=100)
12. W. Kujawski, **G. Li**, B. V. Bruggen, N. Pedišius, J. Tonkonogij, A. Tonkonogovas, A. Stankevicius, J. Šreika, N. Jullok, J. Kujawa, Preparation and Characterization of Polyphenylsulfone (PPSU) Membranes for Biogas Upgrading, *Materials*, 13 (2020) 2847. (IF=3.4, Q2, MNiSW=140)
13. K. Knozowska, **G. Li**, W. Kujawski, J. Kujawa, Novel heterogeneous membranes for enhanced separation in organic-organic pervaporation, *Journal of Membrane Science*, 599 (2020) 117814. (IF=9.5, Q1, MNiSW=140)
14. A. Kujawska, K. Knozowska, J. Kujawa, **G. Li**, W. Kujawski, Fabrication of PDMS based membranes with improved separation efficiency in hydrophobic pervaporation, *Separation and Purification Technology*, 234 (2020) 116092. (IF=8.6, Q1, MNiSW=140)
15. J. Kujawa, W. Kujawski, S. Cerneaux, **G. Li**, S. Al-Gharabli, Zirconium dioxide membranes decorated by silanes based-modifiers for membrane distillation – Material chemistry approach, *Journal of Membrane Science*, 596 (2020) 117597. (IF=9.5, Q1, MNiSW=140)
16. J. Kujawa, E. Rynkowska, K. Fatyeyeva, K. Knozowska, A. Wolan, K. Dzieszowski, **G. Li**, W. Kujawski, Preparation and characterization of cellulose acetate propionate films functionalized with reactive ionic liquids, *Polymers*, 11 (2019) 1217. (IF=5.0, Q1, MNiSW=100)

## Participation in conferences

### a) Oral communications

1. **G. Li**, K. Knozowska, J. Kujawa, W. Kujawski, Pebax<sup>®</sup> 2533 Mixed Matrix Membranes Containing Modified ZIF-8 for the Separation of Carbon Dioxide, 2nd Conference "Membrane Materials - Modification and Separation" (M3-S), 26-28.9.2023, Toruń, Poland.
2. **G. Li**, W. Kujawski, M. Kapkowski, K. Knozowska, Efficiency of Dense PVA Based Membranes in Pervaporative Dehydration of Postreaction Mixtures, 2nd Conference "Membrane Materials - Modification and Separation" (M3-S), 26-28.9.2023, Toruń, Poland.
3. **G. Li**, K. Knozowska, J. Kujawa, W. Kujawski, Pebax<sup>®</sup> 2533-zeolitic imidazolate framework mixed matrix membrane for the separation of carbon dioxide, MEMPEP 2023, 21–24.6.2023, Zakopane/Kościelisko, Poland. (1<sup>st</sup> prize awarded)



4. W. Kujawski, M. Kapkowski, **G. Li**, K. Knozowska, Application of pervaporation for removal of water from the postreaction mixture, EuroMembrane 2022, 20–24.11.2022, Sorrento, Italy.
5. **G. Li**, W. Kujawski, Fabrication of thin film composite hollow fiber membranes for CO<sub>2</sub>/N<sub>2</sub> separation, Workshop of Students' Presentations 2022, 20.10.2022, Membrane Innovation Centre, Straz pod Ralskem, Czech Republic.
6. **G. Li**, W. Kujawski, K. Knozowska, J. Kujawa, Pebax/PVDF thin film mixed matrix membranes containing HKUST-1@GO composite for CO<sub>2</sub> capture, MELPRO 2022, 18–21.09.2022, Prague, Czech Republic. (**1<sup>st</sup> prize awarded**)
7. **G. Li**, W. Kujawski, A. Tonkonogovas, K. Knozowska, J. Kujawa, N. Pedišius, A. Stankevičius, Pebax<sup>®</sup> 2533 mixed matrix membranes containing ionic liquid decorated zeolitic imidazolate framework (ZIF-8@IL) for CO<sub>2</sub> separation, Online Workshop of Students' Presentations 2021, 24.11.2021, Membrane Innovation Centre, Straz pod Ralskem, Czech Republic.
8. **G. Li**, W. Kujawski, A. Tonkonogovas, K. Knozowska, J. Kujawa, N. Pedišius, A. Stankevičius, Preparation and characterization of Pebax<sup>®</sup> 2533 based mixed matrix membranes for CO<sub>2</sub> capture, Membrane Materials - Modification and Separation (M3-S) Conference, 6–8.9.2021, Torun, Poland.
9. **G. Li**, W. Kujawski, K. Knozowska, J. Kujawa, Fabrication of thin film PDMS/PEI and PEBAX/PEI composite hollow fiber membranes for CO<sub>2</sub>/N<sub>2</sub> separation, XIII Scientific Conference “Membranes and Membrane Processes in Environmental Protection” MEMPEP 2021 (online), 10–11.6.2021, Zakopane, Poland. (**2<sup>nd</sup> prize awarded**)
10. T. Plisko, A. Bilyukevich, K. Burts, J. Kujawa, **G. Li**, W. Kujawski, Development of Thin film composite PVA/PAN membranes for pervaporation *via* controlled fouling technique, 6th International Scientific Conference on Pervaporation, Vapor Permeation, Gas Separation, and Membrane Distillation, 14–17.5.2019, Torun, Poland

#### **b) Posters**

1. **G. Li**, W. Kujawski, K. Knozowska, J. Kujawa, Pebax/PVDF thin film mixed matrix membranes containing MIL-101 (Fe)@GO composite for CO<sub>2</sub> capture, XVI Polish Membrane Society Summer School, 20–22.7.2022, Szczecin, Poland.
2. **G. Li**, W. Kujawski, K. Knozowska, J. Kujawa, Thin Film Mixed Matrix Hollow Fiber Membrane Fabricated by Incorporation of Amine Functionalized Metal-Organic Framework

for CO<sub>2</sub>/N<sub>2</sub> separation, IV Ogólnopolskie Forum Chemii Nieorganicznej, 7–9.9.2021, Torun, Poland.

3. **G. Li**, W. Kujawski, B. V. Bruggen, N. Pedišius, J. Tonkonogij, A. Tonkonogovas, A. Stankevičius, J. Šreika, J. Kujawa, Investigation on gas separation properties of polyphenylsulfone (PPSU) membranes for biogas upgrading, MELPRO 2020 conference (online), 8 – 11.11.2020, Prague, Czech Republic.
4. **G. Li**, R. Válek, J. Peter, W. Kujawski, Hollow fibre membranes for gas separation: preparation and characterization, XV Polish Membrane Society Summer School, 21–22.9.2019, Wrocław, Poland.
5. **G. Li**, W. Kujawski, J. Kujawa, S. Koter, Fabrication of polysulfone hollow fibers as the support of nanocomposite capillary membranes for gas separation, 6th International Scientific Conference on Pervaporation, Vapor Permeation, Gas Separation, and Membrane Distillation, 14–17.5.2019, Torun, Poland.

## Grants

1. Grants4NCUStudents II edycja 2021, Nicolaus Copernicus University in Torun, File number: 90-SIDUB.6102.74.2021.G4NCUS1 – individual project: The fabrication of amine-functionalized GO@HKUST-1/Pebax/PVDF thin film mixed matrix membranes for CO<sub>2</sub> capture.
2. Granty Młodych Naukowców 2022, Faculty of Chemistry, Nicolaus Copernicus University in Torun, for the implementation of the project: Conference MELPRO 2022 – The fabrication of GO@HKUST-1/Pebax/PVDF thin film mixed matrix membranes for CO<sub>2</sub>/N<sub>2</sub> separation.
3. Granty Młodych Naukowców 2021 (Grant number: PDB/granty wydziałowe), Faculty of Chemistry, Nicolaus Copernicus University in Torun, for the implementation of the project: Mixed matrix thin film composite hollow fiber membranes for CO<sub>2</sub> and N<sub>2</sub> separation.
4. Granty Młodych Naukowców 2020 (Grant number: 492/2020), Faculty of Chemistry, Nicolaus Copernicus University in Torun, for the implementation of the project: Novel nanocomposite capillary membranes for gas separation and pervaporation – preparation, characterization, and transport-separation properties.
5. Granty Młodych Naukowców 2019 (Grant number: 2092/2019), Faculty of Chemistry, Nicolaus Copernicus University in Torun, for the implementation of the project: Novel

nanocomposite capillary membranes for gas separation and pervaporation – preparation, characterization, and transport-separation properties.

### **Travel awards**

1. Mobility for doctoral students edition II 2022, Nicolaus Copernicus University in Torun, File number: 90-SIDUB.6102.3.2022.MD2 – travel award for research stay.
2. Mobility for doctoral students edition I 2020, Nicolaus Copernicus University in Torun, – travel award for international conference.
3. Grants4NCUStudents IV edycja 2022, Nicolaus Copernicus University in Torun, File number: 90-SIDUB.6102.7.2022.G4NCUS4 – travel award for international conference.
4. Project PROM 2020 – travel award for research stay.
5. Project PROM 2019 – travel award for research stay.

### **Participation in research projects**

1. V4-Korea Joint Research Program + National Centre for Research and Development in Poland – “Towards the sustainable production of valuable chemicals from microalgae based on the sequestration of refused-CO<sub>2</sub> in a novel, circular-loop gas separation membrane bioreactor system”, 10.2017 – 09.2020.
2. Emerging Field 2020-2022 – Polymer Sciences and Multifunctional Nanomaterials, 01.2020 – 12.2022.
3. Emerging Field 2023-2025 – Applied polymers, nanomaterials, membranes, and composites, 01.2023 – 12.2025.
4. Canaletto NAWA (PPN/BIT/2021/1/00088 ) – joint project with Institute on Membrane Technology, Rende, Italy "Formation, characterization and properties of separation innovative bio-membranes for pervaporation and thermopervaporation" I.2021 – XII.2023.
5. Polish-Chinese cooperation – Ministry of Science and Higher Education (37-4), “Novel mixed matrix membranes (MMMs) for separation of liquid and gas mixtures”, 2018 – 2019.

### **Research stays**

1. Institute on Membrane Technology (ITM), Rende, Italy, 23<sup>rd</sup> July – 1<sup>st</sup> August 2023. The preparation of biopolymeric membranes for pervaporation. This internship was funded by Canaletto project (NAWA) 2021.
2. Institute of Chemical Process Fundamentals, Prague, Czech Republic, 3<sup>rd</sup> – 30<sup>th</sup> October 2022. Gas permeation measurements and MOF gas sorption measurements. This internship

was funded by Mobility for doctoral students edition II 2022.

3. Lithuanian Energy Institute, Kaunas, Lithuania, 1<sup>st</sup> – 21<sup>st</sup> August 2021. Gas permeation measurements. This internship was funded by Project PROM (NAWA) 2020.
4. Membrain Innovation Centre, Czech Republic, 1<sup>st</sup> - 28<sup>th</sup> July 2019. Hollow fiber membranes for gas separation: preparation and characterization. This internship was funded by Project PROM (NAWA) 2019.
5. State Key Laboratory of Material-Oriented Chemical Engineering, College of Chemical Engineering, Nanjing Tech University, Nanjing, China, 12<sup>th</sup> – 27<sup>th</sup> October 2019. This internship was funded by project Polish-Chinese cooperation – Ministry of Science and Higher Education (37-4).

### **Prizes/Awards**

1. 1<sup>st</sup> prize for the best oral presentation in MEMPEP 2023 XIV scientific conference
2. 1<sup>st</sup> prize for the best oral presentation in MELPRO 2022 international conference
3. 2<sup>nd</sup> prize for the best oral presentation in MEMPEP 2021 XIII scientific conference.
4. Zespołowa Nagroda Rektora Uniwersytet Mikołaja Kopernika w Toruniu I stopnia, za osiągnięcia uzyskane w dziedzinie naukowej w 2022 roku.
5. Zespołowa Nagroda Rektora Uniwersytet Mikołaja Kopernika w Toruniu II stopnia, za osiągnięcia w dziedzinie naukowej w 2021 roku.
6. Zespołowa Nagroda Rektora Uniwersytet Mikołaja Kopernika w Toruniu III stopnia, za osiągnięcia w dziedzinie naukowo-badawczej w 2020 roku.

## **10. Statements of co-authors**

Toruń, 16.12.2023

mgr Guoqiang Li  
Wydział chemii, Uniwersytetu Mikołaja Kopernika w Toruniu

**Rada Dyscypliny Nauki Chemiczne  
Uniwersytetu Mikołaja Kopernika w Toruniu**

## **Oświadczenie o współautorstwie**

Niniejszym oświadczam, że w pracy [G. Li, W. Kujawski\*, R. Válek, S. Koter, 2021, A review of the development of hollow fiber membranes for gas separation processes, International Journal of Greenhouse Gas Control, 104, 103195] mój udział polegał na [Opracowanie koncepcji i metodologii, przygotowanie pierwszej wersji tekstu, recenzja i redakcja tekstu]. Mój udział w powstaniu pracy wynosi [60]%.

Niniejszym oświadczam, że w pracy [G. Li, W. Kujawski\*, K. Knozowska, J. Kujawa, 2021, The effects of PEI hollow fiber substrate characteristics on PDMS/PEI hollow fiber membranes for CO<sub>2</sub>/N<sub>2</sub> separation, Membranes, 11, 56] mój udział polegał na [Opracowanie koncepcji i metodologii, analiza formalna, opracowanie wizualizacji, przygotowanie pierwszej wersji tekstu, recenzja i redakcja tekstu]. Mój udział w powstaniu pracy wynosi [65]%.

Niniejszym oświadczam, że w pracy [G. Li, K. Knozowska, J. Kujawa, A. Tonkonogovas, A. Stankevičius, W. Kujawski\*, 2021, Fabrication of polydimethylsiloxane (PDMS) dense layer on polyetherimide (PEI) hollow fiber support for the efficient CO<sub>2</sub>/N<sub>2</sub> separation membranes, Polymers, 13, 756] mój udział polegał na [Opracowanie koncepcji i metodologii, analiza formalna, weryfikacja danych, przeprowadzanie badań, opracowanie wizualizacji, przygotowanie pierwszej wersji tekstu, recenzja i redakcja tekstu]. Mój udział w powstaniu pracy wynosi [55]%.

Niniejszym oświadczam, że w pracy [G. Li, W. Kujawski\*, K. Knozowska, J. Kujawa, 2021, Thin film mixed matrix hollow fiber membrane fabricated by incorporation of amine functionalized metal-organic framework for CO<sub>2</sub>/N<sub>2</sub> separation, Materials, 14, 3366] mój udział polegał na [Opracowanie koncepcji i metodologii, analiza formalna, weryfikacja danych, przeprowadzanie badań, opracowanie wizualizacji, pozyskanie finansowania i zasobów, przygotowanie pierwszej wersji tekstu, recenzja i redakcja tekstu]. Mój udział w powstaniu pracy



Załącznik nr 5 do uchwały Nr 38 Senatu UMK z dnia 26 września 2023 r.  
w sprawie postępowania o nadanie stopnia doktora  
na Uniwersytecie Mikołaja Kopernika w Toruniu

wynosi [65]%

Niniejszym oświadczam, że w pracy [G. Li, W. Kujawski\*, A. Tonkonogovas, K. Knozowska, J. Kujawa, E. Olewnik-Kruszkowska, N. Pedišius, A. Stankevičius, 2022, Evaluation of CO<sub>2</sub> separation performance with enhanced features of materials - Pebax<sup>®</sup> 2533 mixed matrix membranes containing ZIF-8-PEI@[P(3)HIm][Tf<sub>2</sub>N], Chemical Engineering Research and Design, 181, 195-208] mój udział polegał na [Opracowanie koncepcji i metodologii, analiza formalna, weryfikacja danych, przeprowadzanie badań, opracowanie wizualizacji, przygotowanie pierwszej wersji tekstu, recenzja i redakcja tekstu]. Mój udział w powstaniu pracy wynosi [45]%

Niniejszym oświadczam, że w pracy [G. Li, W. Kujawski\*, K. Knozowska, J. Kujawa, 2022, Pebax<sup>®</sup> 2533/PVDF thin film mixed matrix membranes containing MIL-101 (Fe)/GO composite for CO<sub>2</sub> capture, RSC Advances, 12, 29124-29136] mój udział polegał na [Opracowanie koncepcji i metodologii, analiza formalna, weryfikacja danych, przeprowadzanie badań, opracowanie wizualizacji, pozyskanie finansowania i zasobów, przygotowanie pierwszej wersji tekstu, recenzja i redakcja tekstu]. Mój udział w powstaniu pracy wynosi [65]%

Guoqiang Li  
(podpis)



Toruń, 16.11.2023

Prof. dr hab. Wojciech Kujawski  
Wydział chemii, Uniwersytetu Mikołaja Kopernika w Toruniu

**Rada Dyscypliny Nauki Chemiczne  
Uniwersytetu Mikołaja Kopernika w Toruniu**

**Oświadczenie o współautorstwie**

Niniejszym oświadczam, że w pracy [G. Li, W. Kujawski\*, R. Válek, S. Koter, 2021, A review of the development of hollow fiber membranes for gas separation processes, International Journal of Greenhouse Gas Control, 104, 103195] mój udział polegał na: pomoc przy opracowaniu koncepcji i metodologii, pozyskanie finansowania, nadzór, redakcja tekstu. Mój udział w powstaniu pracy wynosi [20]%.

Niniejszym oświadczam, że w pracy [G. Li, W. Kujawski\*, K. Knozowska, J. Kujawa, 2021, The effects of PEI hollow fiber substrate characteristics on PDMS/PEI hollow fiber membranes for CO<sub>2</sub>/N<sub>2</sub> separation, Membranes, 11, 56] mój udział polegał na pomoc przy opracowaniu koncepcji i metodologii, pozyskanie finansowania, nadzór, redakcja tekstu. Mój udział w powstaniu pracy wynosi [20]%.

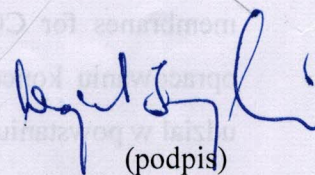
Niniejszym oświadczam, że w pracy [G. Li, K. Knozowska, J. Kujawa, A. Tonkonogovas, A. Stankevičius, W. Kujawski\*, 2021, Fabrication of polydimethylsiloxane (PDMS) dense layer on polyetherimide (PEI) hollow fiber support for the efficient CO<sub>2</sub>/N<sub>2</sub> separation membranes, Polymers, 13, 756] mój udział polegał na: pomoc przy opracowaniu koncepcji i metodologii, pozyskanie finansowania, nadzór, redakcja tekstu, weryfikacja danych, analiza formalna. Mój udział w powstaniu pracy wynosi [15]%.

Niniejszym oświadczam, że w pracy [G. Li, W. Kujawski\*, K. Knozowska, J. Kujawa, 2021, Thin film mixed matrix hollow fiber membrane fabricated by incorporation of amine functionalized metal-organic framework for CO<sub>2</sub>/N<sub>2</sub> separation, Materials, 14, 3366] mój udział polegał na: pomoc przy opracowaniu koncepcji i metodologii, pozyskanie finansowania, weryfikacja danych, analiza formalna, nadzór, redakcja tekstu. Mój udział w powstaniu pracy wynosi [20]%.



Niniejszym oświadczam, że w pracy [G. Li, W. Kujawski\*, A. Tonkonogovas, K. Knozowska, J. Kujawa, E. Olewnik-Kruszkowska, N. Pedišius, A. Stankevičius, 2022, Evaluation of CO<sub>2</sub> separation performance with enhanced features of materials - Pebax<sup>®</sup> 2533 mixed matrix membranes containing ZIF-8-PEI@[P(3)HIm][Tf<sub>2</sub>N], Chemical Engineering Research and Design, 181, 195-208] mój udział polegał na: pomoc przy opracowaniu koncepcji i metodologii, pozyskanie finansowania, weryfikacja danych, analiza formalna, nadzór, redakcja tekstu. Mój udział w powstaniu pracy wynosi [15]%

Niniejszym oświadczam, że w pracy [G. Li, W. Kujawski\*, K. Knozowska, J. Kujawa, 2022, Pebax<sup>®</sup> 2533/PVDF thin film mixed matrix membranes containing MIL-101 (Fe)/GO composite for CO<sub>2</sub> capture, RSC Advances, 12, 29124-29136] mój udział polegał na pomoc przy opracowaniu koncepcji i metodologii, pozyskanie finansowania, weryfikacja danych, analiza formalna, nadzór, redakcja tekstu. Mój udział w powstaniu pracy wynosi [20]%



(podpis)



Toruń, 27.11.2023

Dr hab. Joanna Kujawa, prof. UMK  
Wydział chemii, Uniwersytetu Mikołaja Kopernika w Toruniu

**Rada Dyscypliny Nauki Chemiczne**  
**Uniwersytetu Mikołaja Kopernika w Toruniu**

## **Oświadczenie o współautorstwie**

Niniejszym oświadczam, że w pracy [G. Li, W. Kujawski\*, K. Knozowska, J. Kujawa, 2021, The effects of PEI hollow fiber substrate characteristics on PDMS/PEI hollow fiber membranes for CO<sub>2</sub>/N<sub>2</sub> separation, Membranes, 11, 56] mój udział polegał na [weryfikacja danych, pomoc w wyborze metodologii, praca z oprogramowaniem, nadzór, redakcja tekstu]. Mój udział w powstaniu pracy wynosi [5]%.

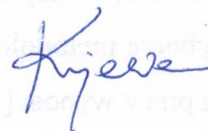
Niniejszym oświadczam, że w pracy [G. Li, K. Knozowska, J. Kujawa, A. Tonkonogovas, A. Stankevičius, W. Kujawski\*, 2021, Fabrication of polydimethylsiloxane (PDMS) dense layer on polyetherimide (PEI) hollow fiber support for the efficient CO<sub>2</sub>/N<sub>2</sub> separation membranes, Polymers, 13, 756] mój udział polegał na [analiza formalna, nadzór, redakcja tekstu]. Mój udział w powstaniu pracy wynosi [5]%.

Niniejszym oświadczam, że w pracy [G. Li, W. Kujawski\*, K. Knozowska, J. Kujawa, 2021, Thin film mixed matrix hollow fiber membrane fabricated by incorporation of amine functionalized metal-organic framework for CO<sub>2</sub>/N<sub>2</sub> separation, Materials, 14, 3366] mój udział polegał na [analiza formalna, pomoc w wyborze metodologii, praca z oprogramowaniem, nadzór, redakcja tekstu]. Mój udział w powstaniu pracy wynosi [5]%.

Niniejszym oświadczam, że w pracy [G. Li, W. Kujawski\*, A. Tonkonogovas, K. Knozowska, J. Kujawa, E. Olewnik-Kruszkowska, N. Pedišius, A. Stankevičius, 2022, Evaluation of CO<sub>2</sub> separation performance with enhanced features of materials - Pebax<sup>®</sup> 2533 mixed matrix membranes containing ZIF-8-PEI@[P(3)HIm][Tf<sub>2</sub>N], Chemical Engineering Research and Design, 181, 195-208] mój udział polegał na [analiza formalna, pomoc w wyborze metodologii, praca z oprogramowaniem, nadzór, redakcja tekstu]. Mój udział w powstaniu pracy wynosi [5]%.

Załącznik nr 5 do uchwały Nr 38 Senatu UMK z dnia 26 września 2023 r.  
w sprawie postępowania o nadanie stopnia doktora  
na Uniwersytecie Mikołaja Kopernika w Toruniu

Niniejszym oświadczam, że w pracy [G. Li, W. Kujawski\*, K. Knozowska, J. Kujawa, 2022, Pebax® 2533/PVDF thin film mixed matrix membranes containing MIL-101 (Fe)/GO composite for CO<sub>2</sub> capture, RSC Advances, 12, 29124-29136] mój udział polegał na [pomoc w wyborze metodologii, analiza formalna, praca z oprogramowaniem, nadzór, redakcja tekstu]. Mój udział w powstaniu pracy wynosi [5]%



(podpis)



Toruń, 20.11.2023

Dr Katarzyna Knozowska  
Wydział chemii, Uniwersytetu Mikołaja Kopernika w Toruniu

**Rada Dyscypliny Nauki Chemiczne  
Uniwersytetu Mikołaja Kopernika w Toruniu**

## **Oświadczenie o współautorstwie**

Niniejszym oświadczam, że w pracy [G. Li, W. Kujawski\*, K. Knozowska, J. Kujawa, 2021, The effects of PEI hollow fiber substrate characteristics on PDMS/PEI hollow fiber membranes for CO<sub>2</sub>/N<sub>2</sub> separation, Membranes, 11, 56] mój udział polegał na [weryfikacja danych, analiza formalna, praca na oprogramowaniu, opracowanie wizualizacji, opracowanie części tekstu]. Mój udział w powstaniu pracy wynosi [10]%.

Niniejszym oświadczam, że w pracy [G. Li, K. Knozowska, J. Kujawa, A. Tonkonogovas, A. Stankevičius, W. Kujawski\*, 2021, Fabrication of polydimethylsiloxane (PDMS) dense layer on polyetherimide (PEI) hollow fiber support for the efficient CO<sub>2</sub>/N<sub>2</sub> separation membranes, Polymers, 13, 756] mój udział polegał na [analiza formalna, przeprowadzanie badań, pomoc w wyborze metodologii, opracowanie wizualizacji]. Mój udział w powstaniu pracy wynosi [10]%.

Niniejszym oświadczam, że w pracy [G. Li, W. Kujawski\*, K. Knozowska, J. Kujawa, 2021, Thin film mixed matrix hollow fiber membrane fabricated by incorporation of amine functionalized metal-organic framework for CO<sub>2</sub>/N<sub>2</sub> separation, Materials, 14, 3366] mój udział polegał na [weryfikacja danych, analiza formalna, praca na oprogramowaniu, opracowanie wizualizacji, redakcja tekstu]. Mój udział w powstaniu pracy wynosi [10]%.

Niniejszym oświadczam, że w pracy [G. Li, W. Kujawski\*, A. Tonkonogovas, K. Knozowska, J. Kujawa, E. Olewnik-Kruszkowska, N. Pedišius, A. Stankevičius, 2022, Evaluation of CO<sub>2</sub> separation performance with enhanced features of materials - Pebax<sup>®</sup> 2533 mixed matrix membranes containing ZIF-8-PEI@[P(3)HIm][Tf<sub>2</sub>N], Chemical Engineering Research and Design, 181, 195-208] mój udział polegał na [pomoc w wyborze metodologii, analiza formalna, praca na oprogramowaniu, opracowanie wizualizacji, redakcja tekstu]. Mój udział w powstaniu pracy wynosi [10]%.

Załącznik nr 5 do uchwały Nr 38 Senatu UMK z dnia 26 września 2023 r.  
w sprawie postępowania o nadanie stopnia doktora  
na Uniwersytecie Mikołaja Kopernika w Toruniu

Niniejszym oświadczam, że w pracy [G. Li, W. Kujawski\*, K. Knozowska, J. Kujawa, 2022, Pebax<sup>®</sup> 2533/PVDF thin film mixed matrix membranes containing MIL-101 (Fe)/GO composite for CO<sub>2</sub> capture, RSC Advances, 12, 29124-29136] mój udział polegał na [weryfikacja danych, analiza formalna, praca na oprogramowaniu, opracowanie wizualizacji]. Mój udział w powstaniu pracy wynosi [10]%.

*Katarzyna Knozowska*

(podpis)



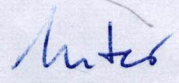
Toruń, 17.11.2023

Prof. dr hab. Stanisław Koter  
Wydział chemii, Uniwersytetu Mikołaja Kopernika w Toruniu

**Rada Dyscypliny Nauki Chemiczne  
Uniwersytetu Mikołaja Kopernika w Toruniu**

## **Oświadczenie o współautorstwie**

Niniejszym oświadczam, że w pracy [G. Li, W. Kujawski\*, R. Válek, S. Koter, 2021, A review of the development of hollow fiber membranes for gas separation processes, International Journal of Greenhouse Gas Control, 104, 103195] mój udział polegał na [redakcja tekstu]. Mój udział w powstaniu pracy wynosi [10]%.

  
(podpis)



Toruń, 16.11.2023

Dr hab. Ewa Olewnik-Kruszkowska, prof. UMK  
Wydział chemii, Uniwersytetu Mikołaja Kopernika w Toruniu

**Rada Dyscypliny Nauki Chemiczne  
Uniwersytetu Mikołaja Kopernika w Toruniu**

### **Oświadczenie o współautorstwie**

Niniejszym oświadczam, że w pracy [G. Li, W. Kujawski\*, A. Tonkonogovas, K. Knozowska, J. Kujawa, E. Olewnik-Kruszkowska, N. Pedišius, A. Stankevičius, 2022, Evaluation of CO<sub>2</sub> separation performance with enhanced features of materials - Pebax<sup>®</sup> 2533 mixed matrix membranes containing ZIF-8-PEI@[P(3)HIm][Tf<sub>2</sub>N], Chemical Engineering Research and Design, 181, 195-208] mój udział polegał na [pomoc w próbach rozciągania do charakterystyki właściwości mechanicznych próbek membran i konsultacja analizy uzyskanych wyników]. Mój udział w powstaniu pracy wynosi [5] %.

(podpis)

*Ewa Olewnik-Kruszkowska*

Załącznik nr 5 do uchwały Nr 38 Senatu UMK z dnia 26 września 2023 r.  
w sprawie postępowania o nadanie stopnia doktora  
na Uniwersytecie Mikołaja Kopernika w Toruniu

Stráž pod Ralskem, 18.12.2023

Dr Robert Válek  
MemBrain

**Rada Dyscypliny Nauki Chemiczne  
Uniwersytetu Mikołaja Kopernika w Toruniu**

### **Declaration of co-authorship**

I hereby declare that in the work [G. Li, W. Kujawski\*, R. Válek, S. Koter, 2021, A review of the development of hollow fiber membranes for gas separation processes, International Journal of Greenhouse Gas Control, 104, 103195] my participation consisted of [writing – reviewing and editing]. My share in the creation of the work is [10]%.



Signature



Załącznik nr 5 do uchwały Nr 38 Senatu UMK z dnia 26 września 2023 r.  
w sprawie postępowania o nadanie stopnia doktora  
na Uniwersytecie Mikołaja Kopernika w Toruniu

Kaunas, 17.11.2023

Dr Nerijus Pedišius  
Lithuanian Energy Institute  
Breslaujos st. 3, Kaunas, Lithuania

**Rada Dyscypliny Nauki Chemiczne  
Uniwersytetu Mikołaja Kopernika w Toruniu**

### **Declaration of co-authorship**

I hereby declare that in the work [G. Li, W. Kujawski\*, A. Tonkonogovas, K. Knozowska, J. Kujawa, E. Olewnik-Kruszkowska, N. Pedišius, A. Stankevičius, 2022, Evaluation of CO<sub>2</sub> separation performance with enhanced features of materials - Pebax<sup>®</sup> 2533 mixed matrix membranes containing ZIF-8-PEI@[P(3)HIm][Tf<sub>2</sub>N], Chemical Engineering Research and Design, 181, 195-208] my participation consisted of [writing—reviewing and editing]. My share in the creation of the work is [5]%



Signature

Kaunas, 17.11.2023

Dr Arūnas Stankevičius  
Lithuanian Energy Institute  
Breslaujos st. 3, Kaunas, Lithuania

**Rada Dyscypliny Nauki Chemiczne  
Uniwersytetu Mikołaja Kopernika w Toruniu**

### **Declaration of co-authorship**

I hereby declare that in the work [G. Li, K. Knozowska, J. Kujawa, A. Tonkonogovas, A. Stankevičius, W. Kujawski\*, 2021, Fabrication of polydimethylsiloxane (PDMS) dense layer on polyetherimide (PEI) hollow fiber support for the efficient CO<sub>2</sub>/N<sub>2</sub> separation membranes, *Polymers*, 13, 756] my participation consisted of [methodology, validation, writing—reviewing and editing]. My share in the creation of the work is [5]%.

I hereby declare that in the work [G. Li, W. Kujawski\*, A. Tonkonogovas, K. Knozowska, J. Kujawa, E. Olewnik-Kruszkowska, N. Pedišius, A. Stankevičius, 2022, Evaluation of CO<sub>2</sub> separation performance with enhanced features of materials - Pebax<sup>®</sup> 2533 mixed matrix membranes containing ZIF-8-PEI@[P(3)HIm][Tf<sub>2</sub>N], *Chemical Engineering Research and Design*, 181, 195-208] my participation consisted of [writing—reviewing and editing]. My share in the creation of the work is [5]%.

  
Signature

Kaunas, 17.11.2023

Dr Andrius Tonkonogovas  
Lithuanian Energy Institute  
Breslaujos st. 3, Kaunas, Lithuania

**Rada Dyscypliny Nauki Chemiczne  
Uniwersytetu Mikołaja Kopernika w Toruniu**

### **Declaration of co-authorship**

I hereby declare that in the work [G. Li, K. Knozowska, J. Kujawa, A. Tonkonogovas, A. Stankevičius, W. Kujawski\*, 2021, Fabrication of polydimethylsiloxane (PDMS) dense layer on polyetherimide (PEI) hollow fiber support for the efficient CO<sub>2</sub>/N<sub>2</sub> separation membranes, *Polymers*, 13, 756] my participation consisted of [formal analysis, methodology, validation, writing—reviewing and editing]. My share in the creation of the work is [10]%.

I hereby declare that in the work [G. Li, W. Kujawski\*, A. Tonkonogovas, K. Knozowska, J. Kujawa, E. Olewnik-Kruszkowska, N. Pedišius, A. Stankevičius, 2022, Evaluation of CO<sub>2</sub> separation performance with enhanced features of materials - Pebax<sup>®</sup> 2533 mixed matrix membranes containing ZIF-8-PEI@[P(3)HIm][Tf<sub>2</sub>N], *Chemical Engineering Research and Design*, 181, 195-208] my participation consisted of [the help of the measurements of gas permeance for Pebax<sup>®</sup> 2533 mixed matrix membranes, the consultation of the obtained results of gas permeance measurements, writing—reviewing and editing]. My share in the creation of the work is [10]%.



Signature

## **Publication I**

**G. Li**, W. Kujawski, R. Válek, S. Koter, A review of the development of hollow fiber membranes for gas separation processes, *International Journal of Greenhouse Gas Control*, 104 (2021) 103195.





Contents lists available at ScienceDirect

## International Journal of Greenhouse Gas Control

journal homepage: [www.elsevier.com/locate/ijggc](http://www.elsevier.com/locate/ijggc)

## A review - The development of hollow fibre membranes for gas separation processes

Guoqiang Li<sup>a</sup>, Wojciech Kujawski<sup>a,b,\*</sup>, Robert Válek<sup>c</sup>, Stanisław Koter<sup>a</sup><sup>a</sup> Nicolaus Copernicus University in Toruń, Faculty of Chemistry, 7, Gagarina Street, 87-100, Toruń, Poland<sup>b</sup> National Research Nuclear University MEPhI, 31, Kashira Hwy, Moscow, 115409, Russia<sup>c</sup> MemBrain, 87, Pod Vinicí, 471 27, Stráž pod Ralskem, Czech Republic

## ARTICLE INFO

## Keywords:

Gas separation  
Hollow fibre membranes  
Thin film composite membranes  
Mixed matrix membranes  
Dry-jet wet spinning parameters

## ABSTRACT

Gas separation is an important separation process to many industries, and membrane separation using hollow fibre membranes (HFMs) has become one of the emerging technologies. In this article, the gas separation concepts, gas transport mechanism, and the fabrication and gas separation performance of HFMs including asymmetric HFMs, thin film composite hollow fibre membranes (TFC-HFMs), and mixed matrix hollow fibre membranes (MM-HFMs), are reviewed and discussed. Dope composition and spinning parameters directly influence the structure of HFMs and subsequently the gas separation performance of HFMs. The gas separation performance of TFC-HFMs can be improved by the design of the coating solution, surface modification, and the addition of both a gutter layer and a protective layer. Mixed matrix membranes (MMMs) have been intensively investigated in flat sheet membranes and the inspiring gas separation results have been obtained. Therefore, the incorporation of nanoparticles into hollow fibre membranes is a desirable solution to increase the gas permeability and selectivity simultaneously. The functionalization of nanoparticles and fabrication methods of MM-HFMs are also presented.

## 1. Introduction

Gas separation is indispensable in many industrial processes, including biogas upgrading, natural gas sweetening, flue gas treatment, hydrogen purification, and nitrogen production (Adewole et al., 2013; Kentish et al., 2008; Li et al., 2015a; Seong et al., 2020). Natural gas which contains mainly methane is the cleanest, safest, and most efficient energy source. To meet the quality standards for its practical applications, raw natural gas needs further purification. For example, CO<sub>2</sub> as an acid gas must be removed to enhance energy content and to reduce pipeline corrosion (Adewole et al., 2013; Biondo et al., 2018; George et al., 2016). Because of the depletion of fossil fuels, biogas consisting of 60–70 vol% CH<sub>4</sub> and 30–40 vol% CO<sub>2</sub>, becomes an important renewable energy resource. However, CO<sub>2</sub>, as one of the unavoidable impurities of biogas, should be removed to increase the energy grade, prevent pipeline corrosion, and mitigate climate change (Gong et al., 2020). Hydrogen is an environmental friendly and sustainable energy carrier and storage medium. However, raw hydrogen produced from thermochemical process or dark fermentation process cannot meet the purity demands in many cases. For example, high purity hydrogen (> 99.99 vol

%) is needed for its application in fuel cells. Therefore, it is essential to perform hydrogen purification to meet the purity requirements of various potential applications (Li et al., 2015a).

In 1980, Monsanto became the first company to establish a commercial application of gas separation by launching the Prism membrane for hydrogen separation. By the mid-1980s, Cynara, Separex, and Grace Membrane Systems had established membrane plants to remove carbon dioxide from methane in natural gas. At about the same time, the first commercial membrane system was launched by Dow to separate nitrogen from air (Baker, 2012; Kentish et al., 2008). Membranes for natural gas processing were first commercialized in the 1980s for CO<sub>2</sub> removal (Scholes et al., 2012). Nowadays, membrane technology has found its application in many gas separation processes, including the removal of carbon dioxide from methane, hydrogen, and nitrogen. Compared with conventional technologies such as pressure swing adsorption, chemical absorption, and cryogenic process, membrane separation processes show many advantages, including lower energy consumption, lower capital and processing costs, smaller unit size, easy upscaling, and lower environmental impact (Dai et al., 2016c; Li et al., 2015a; Xu et al., 2018).

The membrane plays a crucial role in the membrane separation

\* Corresponding author at: Nicolaus Copernicus University in Toruń, Faculty of Chemistry, 7, Gagarina Street, 87-100, Toruń, Poland.

E-mail address: [kujawski@chem.umk.pl](mailto:kujawski@chem.umk.pl) (W. Kujawski).

<https://doi.org/10.1016/j.ijggc.2020.103195>

Received 29 June 2020; Received in revised form 24 September 2020; Accepted 21 October 2020

Available online 6 December 2020

1750-5836/© 2020 Elsevier Ltd. All rights reserved.

Abbreviations	
APTES	3-aminopropyltriethoxysilane
CHMA	1,3-cyclohexanebis-methylamine
CoTPP	cobalt tetraphenylporphyrin
CTA	cellulose triacetate
CuZnIF	copper zinc bimetallic imidazolate framework
DA	dopamine
DBX	$\alpha,\alpha'$ -dibromo-p-xylene
DMAc	N,N-dimethylacetamide
DMF	dimethylformamide
EDA	ethanediamine
EG	ethylene glycol
GO	graphene oxide
GPU	gas permeation unit
HFM	hollow fibre membrane
HPAAc	poly(amid acid)
ICA	imidazole-2-carbaldehyde
IL	ionic liquid
ImGO	imidazole functionalized graphene oxide
MC	methylcarbamate
MEA	monoethanolamine
MG	mixed gas
MM-HFM	mixed matrix hollow fibre membrane
MM-HFMs	mixed matrix hollow fibre membranes
MMM	mixed matrix membrane
MMMs	mixed matrix membranes
MMT	montmorillonite
MOF	metal-organic framework
NMP	N-methyl-2-pyrrolidone
OPM	oxygen permeation membranes
PAN	polyacrylonitrile
PANi	polyaniline
PBI	polybenzimidazole
PDMS	polydimethylsiloxane
PEBA/PEBAX	poly(ether block amide)
PEG	polyethylene glycol
PEI	polyetherimide
PEO	polyethylene oxide
PESU/PES	polyethersulfone
PFI	post-(membrane)-fabrication infiltration
PG	piperazine glycinate
PIMs	polymers of intrinsic microporosity
PIP	piperazine
PPO	poly(p-phenylene oxide)
ProK	potassium proline
PS/PSf	polysulfone
PTFPMS	poly(fluoropropylmethylsiloxane)
PTMSP	poly[1-(trimethylsilyl)-1-propyne]
PTPESU	poly trimethyl phenylene ethersulfone
PVA	poly (vinyl alcohol)
PVAm	polyvinylamine
PVDF	polyvinylidene fluoride
PVP	polyvinyl pyrrolidone
SG	single gas
sPPSU	sulfonated polyphenylsulfone
SR	silicon rubber
STP	standard temperature and pressure
TEGMC	triethylene glycol monoesterified crosslinkable
TFC	thin film composite
TFC-HFM	thin film composite hollow fibre membrane
THF	tetrahydrofuran
TMC	trimesoyl chloride
TNT	titania nanotube
TPESU	trimethyl phenylene ethersulfone
TR-PBO	thermally rearranged polybenzoxazole
YSZ	yttrium-stabilized zirconia
ZIF	zeolitic imidazolate framework
<b>Symbols</b>	
D	diffusion coefficient [ $\text{cm}^2 \text{s}^{-1}$ ]
J	gas flux [ $\text{cm}^3 \text{ (STP) cm}^{-2} \text{ s}^{-1}$ ]
l	membrane thickness [cm]
P	permeability [Barrer]
p	pressure [ $\text{cmHg}^{-1}$ ]
S	solubility coefficient [ $\text{cm}^3 \text{ (STP) cmHg}^{-1}$ ]
V	permeate volume [ $\text{cm}^3$ ]
$\alpha$	ideal selectivity [-]

process. The separation efficiency depends on the membrane performance. A number of polymers were applied to develop different types of membranes including asymmetric hollow fibre membranes, thin film composite flat sheet and hollow fibre membranes, (HFMs), and mixed matrix membranes (MMMs) for gas separation. A summary of materials used in the fabrication of membranes for gas separation is collected in Table 1.

Compared to flat sheet membranes, HFMs have a promising future in various separation processes, providing a number of advantages. HFMs possess a self-supporting structure and high packing density (Gao et al., 2017; Tham et al., 2017). For instance, a spiral-wound module 20 cm in diameter and 1 m long would contain about 20-40  $\text{m}^2$  of membrane area, while the equivalent hollow fibre module, filled with fibres with a diameter of 100  $\mu\text{m}$ , will contain approximately 300  $\text{m}^2$  of membrane area (Baker, 2012). Therefore, HFMs are highly productive for large scale gas separation processing. Thin film composite hollow fibre membranes (TFC-HFMs) (Sukitpameenit and Chung, 2014; Zhou et al., 2016) consist of a very thin dense selective layer and a porous sublayer which are made from different materials. Generally, the porous substrate is prepared by a phase inversion method, and the top dense selective layer is prepared using plasma polymerization (Zhou et al., 2016), dip-coating (Jesswein et al., 2017), dual-layer spinning (Tsai et al., 2018), and interfacial polymerization (Jo et al., 2017; Tsai et al.,

2018). The wholly integral asymmetric membranes including flat membranes and HFMs are usually fabricated by the non-solvent induced phase inversion techniques (Hoida and Vankelecom, 2015) and the dense selective layer is formed by controlling the phase inversion conditions. In the case of asymmetric membranes, the porous support layer is made from the same material as the dense selective layer which is the main difference from thin film composite membranes. Additionally, dual-layer asymmetric hollow fibre membranes can be fabricated if a triple orifice spinneret is applied (Li et al., 2002).

Dry-jet wet spinning (Tow et al., 2018) is the most commonly used technique to fabricate HFMs. However, the fabrication of HFMs is much more complex than the preparation of flat membranes, because many more parameters must be controlled in the former process, i.e., the structure and dimension of the spinneret, the composition of the dope and bore fluid, the temperatures of dope and bore fluid, the dope extrusion rate, the flow rate of the bore fluid, the composition and temperature of the external coagulant, the length of air gap, and the take-up speed (Feng et al., 2013; Peng et al., 2012). To get a desirable membrane, each parameter should be controlled as it can influence the structure and morphology of the prepared membranes, and consequently the performance of hollow fibres (Ding et al., 2013; Jue et al., 2017; Qin et al., 2001; Ullah Khan et al., 2018).

Xu et al. (Xu et al., 2018) and Siagian et al. (Siagian et al., 2019)

**Table 1**  
Polymers used in the fabrication of different types of membranes for gas separation.

Polymers	Filler/additives	Membrane type	Gas separation	Ref.
Polyvinylamine (PVAm)	Ethanediamine (EDA) Piperazine (PIP) Monoethanolamine (MEA) Methylcarbamate (MC)	Flat sheet membrane	CO <sub>2</sub> /CH <sub>4</sub> CO <sub>2</sub> /N <sub>2</sub> CO <sub>2</sub> /H <sub>2</sub>	(Qiao et al., 2013)
Polysulfone (PS)	Polyethylene glycol (PEG)	Flat sheet membrane	CO <sub>2</sub> /N <sub>2</sub> CO <sub>2</sub> /CH <sub>4</sub>	(Karimi et al., 2019)
Polyamide/PDMS/PS	–	Flat sheet thin film composite membrane	CO <sub>2</sub> /N <sub>2</sub>	(Wang et al., 2013)
PDMS/polyetherimide (PEI)	–	Flat sheet thin film composite membrane	H <sub>2</sub> /CH <sub>4</sub>	(Shamsabadi et al., 2014)
Poly(ether block amide) (PEBA)/ polysulfone (PS)	–	Hollow fibre thin film composite membrane	CO <sub>2</sub> /N <sub>2</sub>	(Liu et al., 2004a)
PEBA/polysulfone (PS)	–	Hollow fibre thin film composite membrane	O <sub>2</sub> /N <sub>2</sub>	(Chong et al., 2018)
PDMS/polysulfone (PS)	–	Hollow fibre thin film composite membrane	CO <sub>2</sub> /N <sub>2</sub>	(Liang et al., 2017)
PDMS/polyacrylonitrile (PAN)	–	Hollow fibre thin film composite membrane	CO <sub>2</sub> /N <sub>2</sub> O <sub>2</sub> /N <sub>2</sub>	(Liang et al., 2017)
Pebax®1657/polyvinylidene fluoride (PVDF)	Ionic liquid	Hollow fibre thin film composite membrane	CO <sub>2</sub> /N <sub>2</sub> CO <sub>2</sub> /CH <sub>4</sub>	(Fam et al., 2017b)
Pebax 1657	Modified two-dimensional (2D) imidazole framework (hZIF-L)	Mixed matrix membrane	CO <sub>2</sub> /CH <sub>4</sub>	(Zhu et al., 2019b)
Pebax 1657	MOF-801 nanoparticles	Mixed matrix membrane	CO <sub>2</sub> /N <sub>2</sub>	(Sun et al., 2019)
Poly (vinyl alcohol) (PVA)	ZIF-8	Mixed matrix membrane	CO <sub>2</sub> /N <sub>2</sub>	(Barooah and Mandal, 2019)
Poly (dimethyl siloxane) (PDMS)	Piperazine glycinate (PG) Graphene oxide	Mixed matrix membrane	CO <sub>2</sub> /H <sub>2</sub>	(Nigiz and Hilmioğlu, 2020)

described and discussed the membranes separation processes for carbon dioxide separation in their review works. Wang et al. (Wang et al., 2017) and Xie et al. (Xie et al., 2019) reviewed the development of MMMs and polymeric thin film membranes for gas separation, respectively. Ullah Khan et al. (Ullah Khan et al., 2018) discussed the improvements of dual-layer HFMs via co-extrusion process for gas separation. Liang et al. (Liang et al., 2019) reviewed the fabrication of TFC-HFMs and gas transport through composite membranes. The objective of this review is focused on the development of various types of HFMs for the gas separation process from the point of view of materials, methods of fabrication and the performance of gas separation process. It provides a direction to design innovative HFMs for the applications in gas separation.

## 2. Gas separation concepts and gas transport mechanisms

The gas separation process is a pressure driven process, in which the flux ( $J$ ) of a specific gas through the membrane is proportional to the pressure difference between the feed side ( $p_1$ ) and permeate side ( $p_2$ ), but inversely proportional to the membrane thickness ( $l$ ) (Wijmans and Baker, 1995; Xie et al., 2019):

$$J = P \frac{p_1 - p_2}{l} \quad (1)$$

$P$  is the permeability expressed in Barrers

$$P \text{ (1 Barrer)} = 10^{-10} \frac{V \text{ [cm}^3 \text{ STP]} \times l \text{ [cm]}}{A \text{ [cm}^2 \text{]} \times t \text{ [s]} \times (p_1 - p_2) \text{ [cmHg]}} \quad (2)$$

In Eq. (2),  $V$  is the permeate volume of a specific gas,  $l$  is the membrane thickness,  $A$  is the membrane area,  $t$  represents the time, and ( $p_1 - p_2$ ) is the pressure difference between the feed and permeate side.

The ratios of the permeability of pure gas  $i$  and pure gas  $j$  is defined as an ideal selectivity  $\alpha_{i/j}$  (Xie et al., 2019)

$$\alpha_{i/j} = \frac{P_i}{P_j} \quad (3)$$

The permeability depends merely on the intrinsic properties of membrane material. However, the experimental parameters such as temperature, pressure, and interactions between gas molecules and

polymer can influence the properties of membrane material, resulting in the variations of permeability (Xie et al., 2019).

Permeance is usually used to assess the gas permeation rate through membranes. It is expressed in Gas Permeation Unit (GPU), where  $1 \text{ GPU} = 10^{-6} \text{ cm}^3 \text{ (STP) cm}^{-2} \text{ s}^{-1} \text{ cmHg}^{-1}$ .

The main transport mechanisms for gas separation are Knudsen diffusion, molecular sieving, surface diffusion, capillary condensation, solution-diffusion, and facilitated transport (Kentish et al., 2008). In this review, molecular sieving, solution-diffusion, and facilitated transport are introduced more in detail since these three mechanisms are commonly applied for the polymeric membranes and mixed matrix membranes (MMM).

The pore size of membrane and the molecular size play critical roles in the molecular sieving mechanism. The gas molecules with smaller kinetic diameter than the pore diameter diffuse faster than the gas molecules with bigger kinetic diameter than the pore diameter. Microporous metal-organic frame works (MOFs) are a growing class of molecular sieves and are incorporated into the polymer matrix to form MMMs for gas separation. To achieve the precise molecular sieving, the effective cage size of ZIF-8 was tuned to be between CO<sub>2</sub> and N<sub>2</sub> by confining an imidazolium based ionic liquid [bmim][Tf<sub>2</sub>N] into ZIF-8's sodalite cages by in-situ ionothermal synthesis. The MMMs containing ionic liquid modified ZIF-8 showed remarkable gas separation performance which transcended the upper bound of polymer membranes for CO<sub>2</sub>/N<sub>2</sub> and CO<sub>2</sub>/CH<sub>4</sub> separation (Ban et al., 2015). ZIF-11 particles with extremely narrow pore-openings (~3.0 Å of aperture windows) were dispersed into the polysulfone matrix to form MMMs for CO<sub>2</sub>/CH<sub>4</sub> separation. It was found that the diffusion coefficient of CO<sub>2</sub> of MMMs with 24 wt.% of ZIF-11 nanoparticles increased by 48.8 % compared with that of the pure polymer membrane, but the diffusion coefficient of CH<sub>4</sub> decreased by 42.7 %. Accordingly, the CO<sub>2</sub>/CH<sub>4</sub> diffusion selectivity increased by 160 %, indicating that the restricted aperture windows of ZIF-11 permit CO<sub>2</sub> to pass through but impede CH<sub>4</sub>. A clear molecular sieving process was realized in MMMs with ZIF-11 fillers (Guo et al., 2020).

In addition to the inorganic fillers, organic macrocyclic molecules e.g. 4-sulfocalix[4]arene (SCA4) with size-sieving open cavities were incorporated into polymer membranes to endow polymer membrane strong molecular sieving capability for gas separation (Wu et al., 2020).

SCA4 molecules possess an intrinsic 3-dimensional bowl-shape cavity with a small range of bottom opening sizes around the mean value of 0.3 nm. Therefore, they can act as size-sieving molecular gatekeepers in membranes, which allows gases with a size smaller than or similar to 0.3 nm, e.g. H<sub>2</sub> (0.29 nm) to pass easily, while impedes the transport of larger gases, e.g. N<sub>2</sub> (0.36 nm) and CH<sub>4</sub> (0.38 nm). Wu et al. (Wu et al., 2020) incorporated SCA4 molecules into amidoxime-functionalized PIM1 (AOPIM1) membranes by using an unconventional post-(membrane)-fabrication infiltration (PFI) method. Comparing with the conventional method of MMMs preparation, PFI method guarantees the homogeneity of composite membrane and avoids the issue of interfacial nanodefects and pore blockage in composite membrane due to the hydrogen and ionic bonding between SCA4 molecules and AOPIM1 chains. Consequently, the prepared AOPIM1-SCA4 membranes exhibited high gas separation performance which is attributed to their molecule sieving ability endowed by SCA4 molecules (Wu et al., 2020).

2D membranes including graphene based membranes, metal-organic framework membranes, layered double hydroxides membranes, and MXene membranes are promising materials for efficient separation of gas pairs, such as H<sub>2</sub>/CO<sub>2</sub>, CO<sub>2</sub>/N<sub>2</sub>, and CO<sub>2</sub>/CH<sub>4</sub>, due to their exciting molecular sieving properties (Cheng et al., 2019). Wang et al. (Wang et al., 2016b) manipulated the interlayer nanochannel size of ultrathin (< 10 nm) graphene oxide (GO) membranes by borate-crosslinking. The interlayer spacing between two-dimensional GO nanosheets could be accurately tailored by covalently bonded borate groups and associated water of hydration. The prepared membranes showed high CO<sub>2</sub> permeance up to 650 GPU and CO<sub>2</sub>/CH<sub>4</sub> selectivity of 75 due to the excellent molecular sieving effect. Ding et al. (Ding et al., 2018) reported lamellar stacked MXene membranes with aligned and regular subnanometer channels, which exhibited excellent gas separation performance with H<sub>2</sub> permeability >2200 Barrer and H<sub>2</sub>/CO<sub>2</sub> selectivity >160. It was found that the subnanometer interlayer spacing between the neighbour MXene nanosheets was acting as molecular sieving channels for gas separation.

The solution-diffusion mechanism (Favvas et al., 2017) is based on the solubility of specific gases and their diffusion in the membrane matrix. In this mechanism, each of the gases is absorbed and dissolved on the upstream surface of the membrane and moves across the membrane by diffusion. The diffusion flux of each gas is proportional to the difference of chemical potential between both sides of the selective layer. Moreover, the solubility and diffusion coefficient of gases, the characteristics of the polymer, and the physical-chemical interaction between gas species and polymers have a critical influence on the gas separation performance (Kentish et al., 2008). The relationship between permeability, diffusivity and solubility can be described by (Favvas et al., 2017; Wijmans and Baker, 1995):

$$P = D \times S \quad (4)$$

where P is the permeability coefficient (Barrer), D - the diffusivity coefficient (cm<sup>2</sup> s<sup>-1</sup>), and S - the solubility coefficient (cm<sup>3</sup> (STP) cmHg<sup>-1</sup>).

$$\alpha_{i/j} = \frac{P_i}{P_j} = \frac{D_i}{D_j} \times \frac{S_i}{S_j} \quad (5)$$

where P<sub>i</sub> and P<sub>j</sub> represent the single gas permeability, D<sub>i</sub> and D<sub>j</sub> represent the diffusivity coefficient, and S<sub>i</sub> and S<sub>j</sub> represent the solubility coefficient of gas species i and j, respectively. Eq. (5) is obtained by combining Eq.s (3) and (4).

The diffusivity is significantly influenced by the free volume between the polymer chains and the gas molecular size, while the solubility is mainly dependent on the interaction between the gas molecules and polymers. For instance, the solubility is the predominant factor to affect the selectivity for CO<sub>2</sub>/N<sub>2</sub> separation owing to the high condensability of CO<sub>2</sub> and the high interaction with polymer chains (Xie et al., 2019; Favvas et al., 2017). The ideal selectivity is dependent on the differences of diffusivity and solubility of gas species.

The facilitated transport mechanism is based on the reversible chemical reaction between the gas molecules and the carrier loaded onto the membrane. Four types of reversible reaction including proton transfer reaction, nucleophilic addition reaction, π-complexation reaction, and electro-chemical reaction are used to explain the facilitated transport mechanism (Li et al., 2015b). Proton transfer reaction is one type of acid-base reaction, which can facilitate the transport of proton itself, as well as the transport of small molecules with Brønsted acidity or basicity, e.g. H<sub>2</sub>S, and NH<sub>3</sub>. The reactive carries in this mechanism are Brønsted base-acid pairs, e.g. H<sub>2</sub>O/H<sub>3</sub>O<sup>+</sup>, NH<sub>3</sub>/NH<sub>4</sub><sup>+</sup>. Nucleophilic addition reaction allows the facilitated transport of small molecules, e.g. CO<sub>2</sub> and SO<sub>2</sub>. In the case of facilitated CO<sub>2</sub> transport, OH<sup>-</sup>, CO<sub>3</sub><sup>2-</sup>, PO<sub>4</sub><sup>3-</sup>, -COO<sup>-</sup>, amino groups, and water can be used as CO<sub>2</sub> carriers. The π-complexation reaction allows the facilitated transport of unsaturated small molecules, e.g. olefins, aromatic compounds, O<sub>2</sub> and CO<sub>2</sub>. Transition metal ions are generally used as carriers in this reaction. For instance, Co<sup>2+</sup>, Fe<sup>2+</sup> and Mn<sup>2+</sup> are used as carriers for the transport of O<sub>2</sub>. The electro-chemical reaction is used for the facilitated transport of oxygen. Electrons and O<sup>2-</sup> generally act as reactive carriers for O<sub>2</sub> transport (Li et al., 2015b). The reactive gas species are carried across the membrane easily, whereas the transport of non-reactive gases is inhibited. Different reactive carriers can be used to increase the permeability and selectivity of the reactive gas species (Li et al., 2015b; Xie et al., 2019).

### 3. Development of HFMs

#### 3.1. Asymmetric HFMs

Asymmetric HFMs are generally prepared by the dry-jet wet spinning process. It is well-known that polymer is a crucial factor in obtaining membranes with high performance. What is more, the membrane fabrication parameters play important roles in the dry-jet wet spinning process. The preparation of asymmetric HFMs is more complex since more fabrication parameters should be controlled than with the fabrication of flat sheet membranes. Therefore, many researchers have focused on the optimization of fabrication parameters to prepare asymmetric HFMs with high performance.

Hasbullah et al. (Hasbullah et al., 2011) developed the asymmetric HFMs from polyaniline (PAni) and investigated the effects of air gap on the morphology, gas permeation, and the mechanical properties of HFMs. It was found that with the increase of air gap length, the gas permeance decreased while the selectivity increased; the wall thickness of hollow fibre decreased while the skin layer thickness increased; and the tensile strength, stress at break, and Young's modulus increased. All these findings were attributed to the elongation stress which results in increased molecular orientation and more packed structure during the dry phase separation in air gap and to the increase of the skin layer thickness owing to the longer evaporation time (Hasbullah et al., 2011).

Sharpe et al. (Sharpe et al., 1999) investigated the effect of extrusion shear and forced convection residence time on polysulfone HFMs for gas separation. Their results showed that the phase inversion dynamics and the alignment of polymer chains in the active layer were influenced by extrusion shear. Selectivity can be enhanced by increasing extrusion shear. An optimized residence time is helpful to form a thinner and more highly oriented defect-free active layer (Sharpe et al., 1999). Similar results were obtained by Ismail et al. (Ismail et al., 1999). In their study, they prepared highly selective polysulfone HFMs by the dry-jet wet spinning process and investigated the effect of extrusion rate and bore fluid composition on the gas separation performance. It was found that reducing the water activity in bore and the increase in extrusion rate play important roles in the preparation of highly selective polysulfone HFMs. It is because the oriented and highly ordered membrane active layer provides higher selectivity than the intrinsic value for the isotropic polymer. Zuhairun et al. (Zuhairun et al., 2015) prepared asymmetric polysulfone HFMs by dry-jet wet spinning process and a PDMS



protective layer was coated on the outer surface of hollow fibres to seal the defects on HFMs. It is interesting that  $\text{Cu}_3(\text{BTC})_2$  metal organic framework (MOF) particles were incorporated into the protective layer. It was found that the  $\text{CO}_2$  permeance increased from 69.7 GPU to 109.2 GPU after 5 consecutive coatings. This is because the unsaturated copper sites in MOF particles provided high adsorptive capability for polar molecules. In addition, the  $\text{CO}_2/\text{CH}_4$  and  $\text{CO}_2/\text{N}_2$  selectivities increased as well.

Xu et al. (Xu et al., 2014) prepared defect-free 6FDA-DAM polyimide asymmetric HFMs for gas separation by the dry-jet wet spinning process. It is challenging for fibre spinning of 6FDA based materials owing to their relatively low phase separation rate in a water bath. Thus, the optimization of the dope composition is crucially important to overcome such a challenge. In their study, when the influence of non-solvent dope additives was investigated by ternary phase diagram, it was found that water is less advantageous as a non-solvent dope additive compared with ethanol and the addition of lithium nitrate is beneficial for the asymmetric hollow fibre formation. The  $\text{O}_2/\text{N}_2$  selectivities of spun hollow fibres with and without lithium nitrate are 3.9 and 3.5, respectively. These results are in agreement with the intrinsic  $\text{O}_2/\text{N}_2$  selectivity of such polymers. Defect-free fibres with smaller skin thickness and

smaller fibre size were formed when lithium nitrate was added (Xu et al., 2014). Their results provide a good guideline for the design of dope solution.

Wang et al. (Wang et al., 2002) prepared asymmetric PEI HFMs with high gas selectivity by introducing volatile organic compounds as additives into the dope solutions. It was found that methanol, acetone and a mixture of methanol/acetone are good additives for the preparation of highly selective membranes owing to their good coagulant miscibility and high volatility. The hollow fibres prepared from the higher polymer concentration exhibited higher selectivity and lower permeability. The increase in air gap results in an increase in the thickness of the skin layer. The PEI hollow fibres prepared from 30 wt.% polymer solution, 30 cm air gap, and a 50 % acetone/methanol mixture as additive possess the best gas separation performance with 11.9 GPU He permeance and 95  $\text{He}/\text{N}_2$  selectivity (Wang et al., 2002).

Woo et al. (Woo et al., 2015) fabricated thermally rearranged poly-benzoxazole (TR-PBO) HFMs from a poly(amid acid) (HPAAC) precursor through the dry-jet wet spinning process. The dope composition and spinning conditions were optimized and their effects on the structure and performance of HFMs were investigated. It was found that the addition of THF is beneficial in order to suppress the finger-like

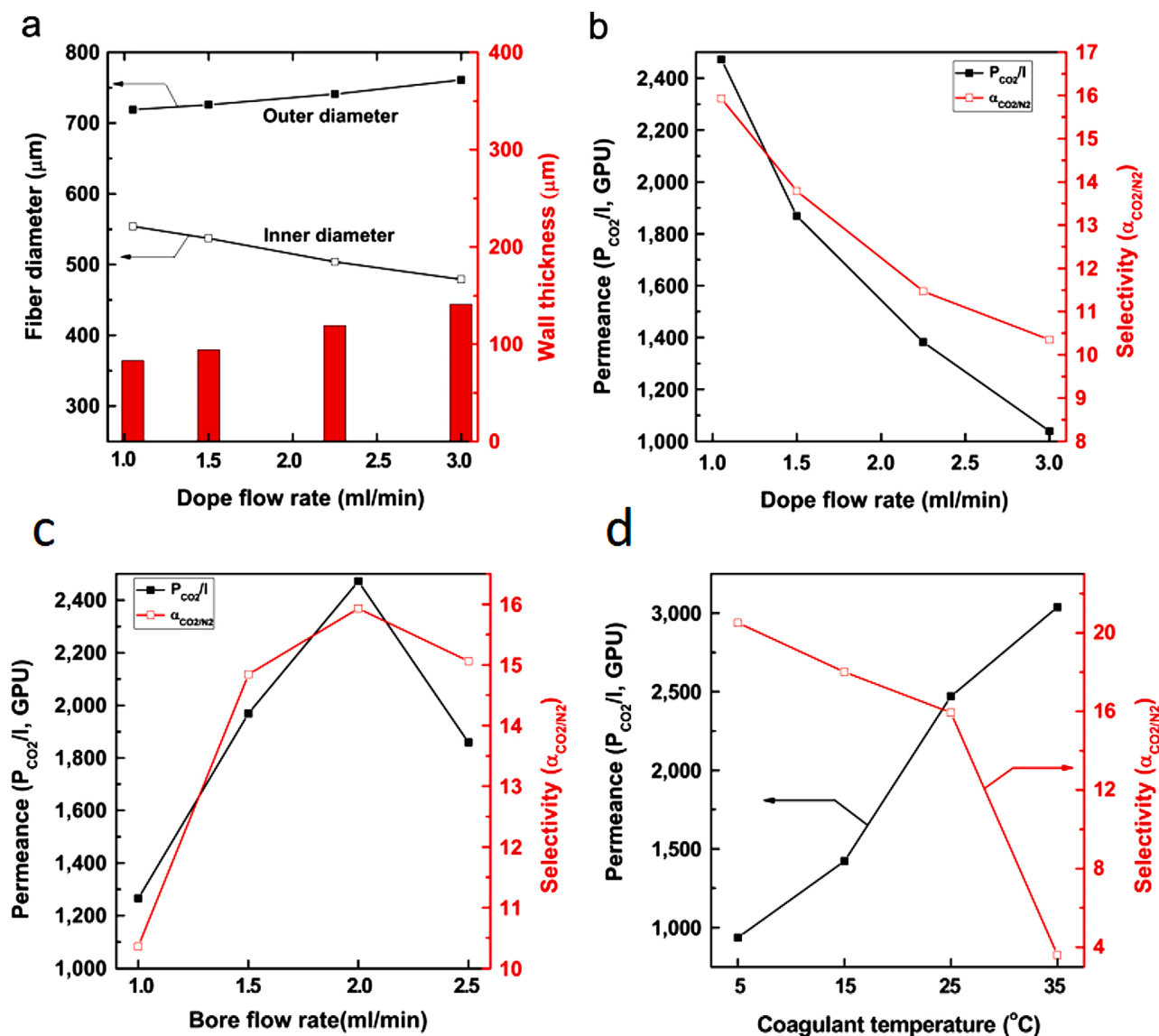


Fig. 1. The profiles of (a) fiber diameter and wall thickness, and (b) gas permeation properties as a function of the dope flow rates, gas permeation properties as a functional of the bore flow rate (c) and coagulant temperature (d) (Woo et al., 2015). Reproduced with the permission from ELSEVIER.

macro-voids and to form a dense selective layer. The addition of LiCl salt is good for the suppression of finger-like macro-voids. In terms of the optimization of spinning conditions, the increase in bore flow rate results in an increase in the outer and inner diameter and a decrease in the wall thickness and dense layer thickness of a hollow fibre. Consequently the gas permeance increased with the increase in bore flow rate up to 2 ml/min (Fig. 1). The increasing dope flow rate led to larger outer and inner diameters and thicker fibre wall, which was reflected by the decrease of gas permeance (Fig. 1). The prepared HFMs showed superior performance with CO<sub>2</sub> permeance of 2500 GPU and CO<sub>2</sub>/N<sub>2</sub> selectivity of 16 (Woo et al., 2015).

Kumbharkar et al. (Kumbharkar et al., 2011) prepared polybenzimidazole (PBI) based asymmetric HFMs by the dry-jet wet spinning process for H<sub>2</sub>/CO<sub>2</sub> separation at high temperatures. It was found that increasing the solvent concentration in bore fluid is helpful to the formation of loose skin on the inner surface and the suppression of finger-like macro-voids in the substructure of hollow fibres. Consequently, the gas separation performance and mechanical properties were enhanced. When the temperature increased from 100 °C to 400 °C, the H<sub>2</sub> permeance and CO<sub>2</sub> permeance increased by 8 times and 2 times, respectively. As a result, the H<sub>2</sub>/CO<sub>2</sub> selectivity increased 3.5 times up to 27.3 (Kumbharkar et al., 2011).

The polymeric membranes suffer from plasticization and physical aging problems in the real mixed gas separation process. David et al. (David et al., 2012) investigated the gas permeation behaviour through Matrimid asymmetric HFMs by testing four types of pure gas and gas mixtures containing H<sub>2</sub> (H<sub>2</sub>/N<sub>2</sub>, H<sub>2</sub>/CO, H<sub>2</sub>/CO<sub>2</sub>). It was found that the permeance of H<sub>2</sub>, CO, and N<sub>2</sub> remained almost constant when the pressure increased from 2 bar to 10 bar in the pure gas permeation measurements. However, the permeance of CO<sub>2</sub> increased by 42 %. This tendency in the permeation of condensable gas such as CO<sub>2</sub> was explained by the plasticization phenomenon (Simons et al., 2010). The gas permeation behaviour of a gas mixture is different from that of pure gas through asymmetric HFMs owing to the CO<sub>2</sub> induced plasticization and competitive sorption effects between gas components (David et al., 2012). Cao et al. (Cao et al., 2002) fabricated 6FDA-2,6-DAT polyimide asymmetric HFMs for CO<sub>2</sub>/CH<sub>4</sub> separation. It was found that plasticization and physical aging occurred in the prepared membranes reflected by the decrease in CO<sub>2</sub> permeance from 300 GPU at the initial state to 76 GPU at a steady state. However, the membranes still showed a good performance with CO<sub>2</sub>/CH<sub>4</sub> selectivity of 40 and CO<sub>2</sub> permeance of 59 GPU in mixed gas tests (Cao et al., 2002).

The plasticization phenomenon and physical aging problem should be mitigated by some physical and chemical treatment on polymer membranes. Heat treatment is an effective method to suppress CO<sub>2</sub> plasticization and achieve better membrane performance. Ismail et al. (Ismail and Lorna, 2003) investigated the permeation behaviour of CO<sub>2</sub> and CH<sub>4</sub> in heat treated and untreated asymmetric polysulfone membranes. It was found that CH<sub>4</sub> permeance was almost constant, while CO<sub>2</sub> permeance increased with the increasing feed pressure indicating the CO<sub>2</sub> induced plasticization. However, the CO<sub>2</sub> induced plasticization was inhibited after treatment at 140 °C (Ismail and Lorna, 2003). To improve the performance of polyimide asymmetric HFMs, Babu et al. (Babu et al., 2018) fabricated TEGMC (TriEthylene Glycol Mono-esterified Crosslinkable) polyimide asymmetric HFMs to study their stability and permselectivity under sour gas feed conditions. Moreover, a PDMS layer was coated on the skin to seal the morphological defects so as to further improve the performance. It was found that crosslinked HFMs showed higher H<sub>2</sub>S/CH<sub>4</sub> and CO<sub>2</sub>/CH<sub>4</sub> permselectivity than that of a dense film membrane, which is because of the polymer chain alignment induced during the spinning process. The CO<sub>2</sub>/CH<sub>4</sub> and H<sub>2</sub>S/CH<sub>4</sub> selectivities of prepared HFMs are 55 and 29, respectively at 35 °C. PDMS coated crosslinked hollow fibre membranes were able to resist H<sub>2</sub>S and CO<sub>2</sub> induced plasticization under the sour gas feed condition (Babu et al., 2018).

Physical aging is a common characteristic of glassy polymer

membranes with unrelaxed free volume and is due to rapid quenching from the rubbery state or casting from solutions. Ma et al. (Ma and Koros, 2018) investigated the physical aging of propane-diol mono-esterified cross-linkable polyimide HFMs. It was found that physical aging caused a loss of CO<sub>2</sub> permeance with a small degree of CO<sub>2</sub>/CH<sub>4</sub> selectivity increase for cross-linked HFMs (Ma and Koros, 2018). To overcome the rapid physical aging problem of polyethersulfone (PESU) asymmetric HFMs, Yong et al. (Yong et al., 2018) synthesized poly trimethyl phenylene ethersulfone (TPESU) and fabricated HFMs based on this material. The TPESU HFMs showed good gas separation performance, but significantly less aging phenomena. The permeances of O<sub>2</sub> and CO<sub>2</sub> are 16 GPU and 85.1 GPU, respectively and the O<sub>2</sub>/N<sub>2</sub> and CO<sub>2</sub>/N<sub>2</sub> selectivities are 6.5 and 34.0, respectively (Yong et al., 2018).

The gas separation performance (permeance and selectivity) of asymmetric HFMs is dependent on the membrane material and structure properties. Table 2 summarizes the effects of spinning parameters on the structure, morphology, diameter, selective layer thickness and gas separation performance of hollow fibres. And Table 3 presents the fabrication conditions, e.g. dope composition, bore fluid composition, and temperature of hollow fibres discussed in 3.1. As is shown in Table 2 and Table 3, dope composition plays an important role in the phase inversion process which has an influence on the structure and morphology of hollow fibres. Increasing the solvent concentration in bore fluid results in the formation of loose skin on the inner surface and the suppression of finger-like macro-voids. As well as the dope and bore fluid composition, spinning parameters also have a significant influence on the structure of

**Table 2**  
The effects of spinning parameters on hollow fibre membranes.

Parameters	Effects on hollow fibre membranes	Ref.
	The addition of lithium nitrate in dope resulted in the increased dope viscosity, increased fibre spinning efficiency, smaller selective layer thickness, and reduced fibre size.	(Xu et al., 2014)
Dope composition	Higher polymer concentration resulted in higher selectivity and lower permeability. The addition of volatile organic compounds such as methanol/acetone mixture can minimize the finger-like macrovoids and increase the selectivity. The addition of THF and LiCl salt is favourable to suppress the finger-like macrovoids and form a dense selective layer.	(Wang et al., 2002) (Woo et al., 2015)
Bore fluid composition	The increase in solvent concentration in bore fluid is helpful to the formation of loose skin on the inner surface and the suppression of finger-like macro-voids in the substructure of hollow fibres.	(Kumbharkar et al., 2011)
Dope flow rate	The increasing dope flow rate led to larger outer and inner diameters and a thicker fibre wall.	(Woo et al., 2015)
Bore flow rate	The increase in bore flow rate resulted in an increase in outer and inner diameter and a decrease in wall thickness and dense layer thickness of hollow fibre.	(Woo et al., 2015)
Extrusion shear	The increase in extrusion shear resulted in the decreased active layer thickness, increased gas permeance and higher selectivity than the intrinsic value of amorphous membrane polymer.	(Sharpe et al., 1999)
Extrusion shear	The increased shear resulted in an oriented and highly ordered membrane active layer and a significant increase in selectivity.	(Ismail et al., 1999)
Air gap	The increase in air gap resulted in decreased gas permeance, increased selectivity, decreased hollow fibre wall thickness, increased skin layer thickness, and the enhanced mechanical properties.	(Hasbullah et al., 2011) (Wang et al., 2002)
Residence time	Excessive residence time induced harmful non-solvent intrusion from the lumen.	(Sharpe et al., 1999)

**Table 3**  
Summary of the important fabrication parameters of HFMs from Section 3.1.

Dope [wt.%]	Bore fluid [wt.%]	Bore fluid T [°C]	Coagulation bath [wt.%]	Coagulation bath T [°C]	Skin layer location	Ref.
PAni/NMP/THF 17.5/41.25/41.25	H <sub>2</sub> O/NMP 80/20	–	H <sub>2</sub> O	25	Outer surface	(Hasbullah et al., 2011)
PSf/DMAc/THF/EtOH 22/31.8/31.8/14.4	H <sub>2</sub> O/CH <sub>3</sub> CO <sub>2</sub> K 80/20	20	H <sub>2</sub> O	14	Outer surface	(Sharpe et al., 1999)
PSf/DMAc/THF/EtOH 30/35/30/5	H <sub>2</sub> O/CH <sub>3</sub> CO <sub>2</sub> K 80/20	25	H <sub>2</sub> O	25	Outer surface	(Zulhairun et al., 2015)
6FDA-DAM /NMP/THF/EtOH 22/43/10/25	H <sub>2</sub> O/NMP 80/20	70	H <sub>2</sub> O	20, 50	Outer surface	(Xu et al., 2014)
PEI/NMP/MeOH 30/59.3/10.7	H <sub>2</sub> O/EtOH 50/50	25	H <sub>2</sub> O	25	Outer surface	(Wang et al., 2002)
PEI/NMP/THF 30/60/10	H <sub>2</sub> O/EtOH 50/50	25	H <sub>2</sub> O	25	Outer surface	(Wang et al., 2002)
PEI/NMP/Acetone 25/53.94/21.06	H <sub>2</sub> O/EtOH 50/50	25	H <sub>2</sub> O	25	Outer surface	(Wang et al., 2002)
HPAAc/NMP/THF/EG/LiCl 27/54/7.6/ 11.4/3	H <sub>2</sub> O/NMP 80/20	25	H <sub>2</sub> O	25	Outer surface	(Woo et al., 2015)
PBI/DMAc/LiCl 13/85.8/1.2	H <sub>2</sub> O/DMAc 20/80 50/50	–	H <sub>2</sub> O	25	Outer surface	(Kumbharkar et al., 2011)
Matrimid/NMP/EtOH 26.2/58.9/14.9	H <sub>2</sub> O/NMP 4/96	22	H <sub>2</sub> O	20	Outer surface	(David et al., 2012)
6FDA-2,6-DAT/NMP 28/72	H <sub>2</sub> O/NMP 5/95	40	H <sub>2</sub> O	25	Outer surface	(Cao et al., 2002)
TEGMC/NMP/THF/EtOH/LiNO <sub>3</sub> 25/ 23.5/10/35/6.5	H <sub>2</sub> O/NMP 20/80	70	H <sub>2</sub> O	40	Outer surface	(Babu et al., 2018)

hollow fibres. Air gap and extrusion rate influence the orientation of polymer molecules in selective layer and thickness of skin layer. The flow rates of dope solution and bore fluid influence the outer and inner diameters of hollow fibres and the thickness of the hollow fibres wall and skin layer. Therefore, the design of dope and bore fluid composition and the optimization of spinning parameters are critical in the fabrication of asymmetric HFMs with high gas separation performance. During the gas separation process, plasticization and physical aging have adverse effects on gas permeance and selectivity. To mitigate plasticization and physical aging, heat treatment, crosslinking, and the modification on the polymer chain have been applied.

### 3.2. Thin film composite hollow fibre membranes (TFC-HFMs)

#### 3.2.1. TFC-HFMs prepared by multi-step method

Generally, thin film composite membranes contain a selective layer deposited on a support hollow fibre. Compared with the preparation of asymmetric HFMs, the preparation of thin film composite membranes shows several advantages, such as the reduction of cost when expensive materials were used, the possibility of using highly selective, but brittle polymers when it is difficult to use them for asymmetric hollow fibre fabrication, and the ease of obtaining defect free membranes in a composite form (Chung et al., 1999).

Dip-coating is a commonly used method to prepare thin film composite hollow fibre membranes. Liu et al. (Liu et al., 2004b) prepared PEBA/PSf TFC-HFMs for CO<sub>2</sub>/N<sub>2</sub> separation. The hollow fibre substrate was fabricated by the dry-jet wet spinning/phase inversion process. The PEBA thin film was coated on the substrate by dip-coating method. It was found that the defect-free PEBA layer cannot be formed when the concentration of coating solution is low (0.5 wt.%). The support hollow fibres with larger pores on the surface are not favourable for the PEBA/PSf composite HFMs. The defect free PEBA/PSf composite HFMs with a CO<sub>2</sub> permeance equal to 61 GPU and a CO<sub>2</sub>/N<sub>2</sub> selectivity equal to 30 were obtained by using 3 wt.% coating solution and 23 wt.% polysulfone solution. The CO<sub>2</sub> permeance increased with an increase in feed pressure owing to the CO<sub>2</sub> induced membrane plasticization (Liu et al., 2004b).

Chong et al. (Chong et al., 2018) fabricated TFC-HFMs by dip-coating

a PDMS layer or PEBAX layer on the outer surface of PSf hollow fibres for the oxygen enhancement process. The effect of the concentration of coating solution on the gas separation performance was investigated. It was found that PDMS/PSf composite membranes showed higher gas permeance and selectivity compared with PEBAX/PSf composite membranes. The PSf hollow fibre coated five times with 3 wt.% PDMS possessed O<sub>2</sub> permeance equal to 18.31 GPU and O<sub>2</sub>/N<sub>2</sub> selectivity equal to 4.56. The PSf hollow fibre coated five times with 1 wt.% PEBAX possessed O<sub>2</sub> permeance equal to 12.23 GPU and O<sub>2</sub>/N<sub>2</sub> selectivity equal to 3.94 (Chong et al., 2018).

Dai et al. (Dai et al., 2016a) prepared defect free poly(fluropropylmethylsiloxane) (PTFPMS)/polyetherimide (PEI) hollow fibre composite membrane by the dip-coating method. It was found that the gas permeance decreased in the following order: CO<sub>2</sub> > C<sub>3</sub>H<sub>6</sub> > H<sub>2</sub> > O<sub>2</sub> > CH<sub>4</sub> > N<sub>2</sub>. The selectivity for C<sub>3</sub>H<sub>6</sub>/N<sub>2</sub>, O<sub>2</sub>/N<sub>2</sub> and CH<sub>4</sub>/N<sub>2</sub> were independent with the PTFPMS concentration, whereas CO<sub>2</sub>/N<sub>2</sub> selectivity increased and H<sub>2</sub>/N<sub>2</sub> selectivity decreased when the PTFPMS concentration increased (Dai et al., 2016a).

Surface modification on the coated thin film selective layer is used to further improve the gas separation efficiency. Hu et al. (Hu et al., 2017) modified the PDMS membrane supported on PAN hollow fibres with 3-aminopropyltriethoxysilane (APTES) by using the crosslinking method. It was found that the polarity of membranes increased and the water contact angle decreased from 114° to 87.5° with the increase in APTES content. The CO<sub>2</sub> permeability increased, but the CO<sub>2</sub>/H<sub>2</sub>, CO<sub>2</sub>/CH<sub>4</sub> and CO<sub>2</sub>/N<sub>2</sub> selectivities decreased (Hu et al., 2017). To further improve the surface polarity, Hu et al. (Hu et al., 2018) modified the amino functionalized PDMS membranes supported on PAN hollow fibres by using the surface grafting method. The PDMS/PAN composite membranes were immersed in polyvinyl pyrrolidone (PVP) solution and PVP was connected to the membrane surface by reacting with amine groups. It was found that the water contact angle of PDMS membranes decreased from 98° to 28° and the surface roughness increased after surface grafting modification. The CO<sub>2</sub>/H<sub>2</sub>, CO<sub>2</sub>/CH<sub>4</sub>, and CO<sub>2</sub>/N<sub>2</sub> selectivities were improved as a result of 10 s surface modification, with the simultaneous CO<sub>2</sub> permeance decrease from 2500 GPU to 2440 GPU (Hu et al., 2018).

Different additives are mixed into the coating solution to form a

hybrid thin film selective layer with enhanced gas separation performance. Li et al. (Li et al., 2016) synthesized cobalt tetraphenylporphyrin (CoTPP), and a prepared PDMS coating solution containing CoTPP. The coating solution was coated on polyethersulfone (PES) hollow fibres to form TFC-HFMs. It was found that the prepared membranes showed  $O_2/N_2$  selectivity of 2.8 and  $O_2/CO_2$  selectivity of 1.5, and oxygen permeance of 53 GPU at 0.05 bar. The incorporation of CoTPP is helpful to facilitate the oxygen transport through membranes resulting in higher  $O_2/N_2$  and  $O_2/CO_2$  selectivity compared with pristine membranes (Li et al., 2016). Park et al. (Park et al., 2019) incorporated the Nafion/ $TiO_2$  (Nf/ $TiO_2$ ) nanoparticles into PEBA solution and coated on the inner side of polyethersulfone support hollow fibre to form TFC-HFMs for the removal of  $SO_2$  gas. It was found that the addition of Nf/ $TiO_2$  nanoparticles improved the membrane performance by introducing sulfonate and hydroxyl functional groups to the membrane, and thus increased  $SO_2$  permeance and selectivity. The ideal selectivities achieved for  $SO_2/N_2$  and  $SO_2/CO_2$  were 2928 and 72, respectively. The water contact angle decreased with the increase in the content of Nf/ $TiO_2$  nanoparticles (Park et al., 2019). Dai et al. (Dai et al., 2019) fabricated defect free TFC-HFMs by dip-coating poly(p-phenylene oxide) (PPO) hollow fibres into 0.5 wt.% PVA solution containing amino acid salts. It was found that the incorporation of amino acid salts into PVA membranes significantly increased the  $CO_2$  permeance without changing the  $CO_2/N_2$  selectivity. The addition of 40 % potassium proline (ProK) into the PVA matrix increased the  $CO_2$  permeance from 399 to 791 GPU (Dai et al., 2019).

A polyamide selective layer is generally formed on the inner or outer surface of the hollow fibres by using the interfacial polymerization method. Jo et al. (Jo et al., 2017) prepared inside coated TFC-HFMs by interfacial polymerization of 1,3-cyclohexanebis-methylamine (CHMA) and trimesoyl chloride (TMC) on the inner surface of PSf hollow fibres. It was found that the CHMA concentration governs the crosslinking extent of skin layer, whereas TMC concentration determines the skin layer thickness. The CHMA-TMC/PSf composite membrane showed a  $CO_2$  permeance of 25 GPU and  $CO_2/CH_4$  selectivity of 28 in the  $CO_2/CH_4$  (30/70 vol%) mixed gas permeation test (Jo et al., 2017). Baig et al. (Baig et al., 2016) fabricated TFC-HFMs by incorporating modified  $TiO_2$  nanoparticles in the polyamide selective layer for water vapour removal from flue gas. It was found that the addition of modified nanoparticles increased the hydrophilicity of the prepared membrane and provided the water vapour permeation path. Consequently, the water vapour permeance and selectivity were improved and a maximum water vapour permeance of 1340 GPU and selectivity of 486 were obtained (Baig et al., 2016).

Multilayer thin film composite membranes are prepared for use to improve the gas separation efficiency of thin film composite membranes. Generally, the protective layer is coated on the surface of the selective layer to seal the existing defects and to protect the selective layer from abrasion or detrimental chemical attacks (Liang et al., 2018; Ye et al., 2005). The gutter layer is coated on the surface of substrate to improve the adhesion between substrate and selective layer. Moreover, the gutter layer can minimize the mass transport resistance since it is usually made from highly permeable materials (Liang et al., 2018; Ye et al., 2005).

Chung et al. (Chung et al., 1999) fabricated multilayer composite HFMs consisting of a silicon rubber protective layer, a poly (4-vinylpyridine) selective layer, and a polysulfone support substrate for gas separation. It was found that the substrates with a smooth surface can reduce defects in the selective layer whereas substrates with a high surface porosity can enhance the permeance of composite membranes. The concentration of material for the selective layer plays a crucial role to form the composite membranes with high gas separation performance. Pre-wetting does not show significant improvement of the membrane performance when a highly permeable substrate is used. The prepared membranes exhibited high gas separation performance. The permeances of  $H_2$ ,  $CO_2$  and  $O_2$  were 100 GPU, 40 GPU, and 8 GPU, respectively. The selectivities of  $H_2/N_2$ ,  $CO_2/CH_4$ , and  $O_2/N_2$  were 100,

50, and 7, respectively (Chung et al., 1999).

Ye et al. (Ye et al., 2005) prepared polysulfone/polyethylene oxide/silicone rubber (PSf/PEO/SR) multilayer composite membrane by using the dip-coating method. The PEO layer was selective and the SR layer was used as a protective layer. It was found that the prepared composite membranes showed high gas separation performance for hydrogen recovery. The  $H_2$  permeance,  $N_2$  permeance and  $H_2/N_2$  selectivity are 49.51 GPU, 0.601 GPU, and 82.3, respectively (Ye et al., 2005).

Choi et al. (Choi et al., 2019) prepared multilayer TFC-HFMs for helium extraction. The polyamide selective layer was formed on the PAN hollow fibres by the interfacial polymerization method from 1,3,5-benzenetricarbonyl trichloride and m-phenylenediamine. Finally the prepared composite membranes were dipped into poly [1-(trimethylsilyl)-1-propyne] (PTMSP) solution to seal the defects in the polyamide layer. It was found that the prepared membranes showed a high ideal  $He/CO_2$  selectivity in the range of 30–38. The separation factor varied from 2.3 to 11.9, while the helium permeance varied from 3.4 to 46.2 GPU depending on operating parameters in a mixed gas system (Choi et al., 2019).

Chen et al. (Chen et al., 2014) prepared PEBA/PDMS/PAN multilayer composite HFMs by the dip-coating method for flue gas treatment and hydrogen purification. The coating conditions such as polymer concentration and coating time were investigated and optimized. It was found that the composite membranes prepared under optimal conditions displayed a  $CO_2$  permeance of 481.5 GPU,  $CO_2/H_2$  selectivity of 8.1, and  $CO_2/N_2$  selectivity of 42.0. The  $CO_2$  permeance decreased with the increase in polymer concentration. However, it decreased initially and subsequently increased with the increase of coating time. The PDMS gutter layer mitigated the intrusion of coating solution into the porous support (Chen et al., 2014).

Liang et al. (Liang et al., 2018) prepared defect-free PIM-CD/PDM-S/PAN three-layer TFC-HFMs by a dip-coating process (Fig. 2). It was found that the  $O_2$  and  $CO_2$  permeances were 69 and 483 GPU, respectively, whereas the  $O_2/N_2$  and  $CO_2/N_2$  selectivities were equal to 3.2 and 22.5, respectively. Moreover, the  $O_2/N_2$  and  $CO_2/N_2$  selectivities are further increased to 4.2 and 29.5, respectively in air separation and flue gas tests. The PDMS gutter layer is crucial for the preparation of composite membranes owing to the mitigation of the detrimental solvent effect, the enhancement of PIM adhesion on support layer, and the redistribution of gas transport through membranes (Liang et al., 2018).

Ionic liquids exhibited the potential for  $CO_2$  separation owing to their affinity to  $CO_2$ . Fam et al. (Fam et al., 2017a) blended  $CO_2$  selective ionic liquid (IL) with Pebax 1657 polymer to fabricate Pebax 1657/[emim][BF<sub>4</sub>] TFC-HFMs to improve the  $CO_2$  separation efficiency. PTMSP was coated on the surfaces of PVDF substrate as a gutter layer and coated on the surface of the selective layer as a sealing layer. It was found that the TFC-HFMs with 80 wt.% IL loading showed a  $CO_2$  permeance of 300 GPU and  $CO_2/N_2$  and  $CO_2/CH_4$  selectivities of 36 and 15, respectively. The prepared membranes showed high mechanical and chemical stabilities and high  $CO_2$  separation efficiency under harsh conditions (Fam et al., 2017a).

Dip-coating is a flexible and frequently-used method to form a thin selective layer on the outer surface of hollow fibres (Table 4). PEBA and PDMS are used as coating material, and the concentration of coating solution plays a critical role in the preparation of TFC-HFMs with desirable separation performance. Interfacial polymerization is commonly used to fabricate the polyamide selective layer (Table 4). The membrane separation performance can be controlled by the design of the aqueous phase and organic phase. It can be seen from Table 4, that the gas permeance and selectivity are usually measured at mild conditions, such as room temperature and low pressure. Multilayer TFC-HFMs were designed and prepared by dip-coating method or interfacial polymerization method or the combination of both methods to further enhance the gas separation performance of TFC-HFMs.

Surface modification was conducted by a crosslinking and grafting to



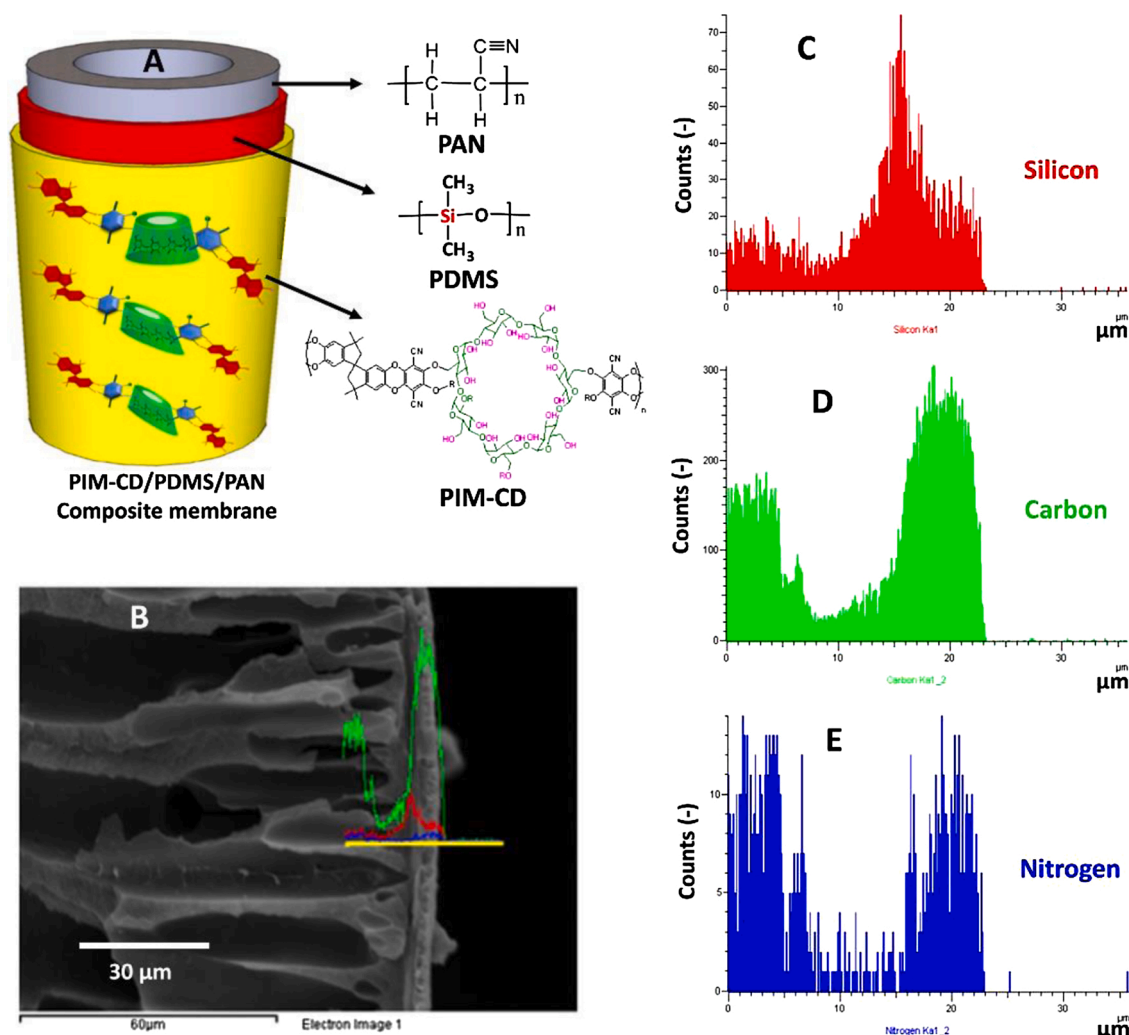


**Fig. 2.** The architecture and element analyses of the optimal PIM-CD/PDMS/PAN membrane. (A) The chemical composition in each layer, (B) The cross-section image, and (C, D, E) the SEM-EDX element spectra of silicon (Si), carbon (C), nitrogen (N), respectively (Liang et al., 2018). Reproduced with the permission from ELSEVIER.

**Table 4**

Comparison of gas separation performance of TFC-HFMs prepared by multi-step method (SG - single gas, MG - mixed gas).

Membrane materials	Fabrication method	Fast gas/slow gas	Permeance of faster gas [GPU]	Selectivity	Testing conditions	Ref.
PEBA/PSf	Dip-coating	CO <sub>2</sub> /N <sub>2</sub>	61	30.0	25 °C, 7.9 bar, SG	(Liu et al., 2004b)
PEBA/PSf	Dip-coating	O <sub>2</sub> /N <sub>2</sub>	12.23	3.1	28 °C, 5 bar, SG	(Chong et al., 2018)
PDMS/PSf	Dip-coating	O <sub>2</sub> /N <sub>2</sub>	18.31	4.6	28 °C, 5 bar, SG	(Chong et al., 2018)
PTFPMS/PEI	Dip-coating	CO <sub>2</sub> /N <sub>2</sub>	61.63	17.2	25 °C, 3 bar, SG	(Dai et al., 2016a)
PDMS/PAN	Dip-coating	CO <sub>2</sub> /N <sub>2</sub>	2440	8.3	30 °C, 3 bar, SG	(Hu et al., 2018)
		CO <sub>2</sub> /CH <sub>4</sub>		3.6		
		CO <sub>2</sub> /H <sub>2</sub>		2.5		
PDMS-CoTPP/PES	Dip-coating	O <sub>2</sub> /N <sub>2</sub>	53	2.8	30 °C, 0.05 bar, SG	(Li et al., 2016)
		O <sub>2</sub> /CO <sub>2</sub>		1.5		
PEBA-(Nafion/TiO <sub>2</sub> )/PES	Dip-coating	SO <sub>2</sub> /N <sub>2</sub>	1671	2928.0	25 °C, 2.5 bar, SG	(Park et al., 2019)
		SO <sub>2</sub> /CO <sub>2</sub>		72.0		
PVA-amino acid salt/PPO	Dip-coating	CO <sub>2</sub> /N <sub>2</sub> (10/90 vol%)	791	40.0	25 °C, 2 bar, MG	(Dai et al., 2019)
PDMS-Cu <sub>3</sub> (BTC) <sub>2</sub> /PSf	Dip-coating	CO <sub>2</sub> /N <sub>2</sub>	109.2	31.0	25 °C, 5 bar, SG	(Zulhairun et al., 2015)
		CO <sub>2</sub> /CH <sub>4</sub>		28.0		
PSf/PEO/SR	Dip-coating	H <sub>2</sub> /N <sub>2</sub>	49.5	82.3	30 °C, 5.1 bar, SG	(Ye et al., 2005)
PEBA/PDMS/PAN	Dip-coating	CO <sub>2</sub> /H <sub>2</sub>	481.5	8.1	25 °C, 2 bar, SG	(Chen et al., 2014)
		CO <sub>2</sub> /N <sub>2</sub>		42.0		
PIM/PDMS/PAN	Dip-coating	O <sub>2</sub> /N <sub>2</sub>	69	3.2	25 °C, 2 bar, SG	(Liang et al., 2018)
		CO <sub>2</sub> /N <sub>2</sub>	483	22.5		
PTMSP/Polyamide/PAN	Interfacial polymerization	He/ CO <sub>2</sub>	7.79	28.3	25 °C, 21.7 bar, SG	(Choi et al., 2019)
	Interfacial polymerization	He/ CH <sub>4</sub>		40.1		
Polyamide/PSf	Interfacial polymerization	CO <sub>2</sub> /CH <sub>4</sub> (30/70 vol %)	25	28.0	30 °C, 1–5 bar MG	(Jo et al., 2017)

tune the surface properties. The membrane performance was influenced by the change of surface properties. Therefore, surface modification is a facile solution to improve membrane performance. The addition of additives into coating solution further improves the gas separation performance by the specific interaction between additives and gas species and endows the dip-coating method with more versatility by designing the coating solution. Moreover, the surface properties of the selective layer changed owing to the presence of additives. For instance, the addition of MOF particles into PDMS coating solution improves the CO<sub>2</sub> permeance and CO<sub>2</sub>/CH<sub>4</sub> and CO<sub>2</sub>/N<sub>2</sub> selectivities owing to the high affinity between MOF particles and CO<sub>2</sub>.

As was stated before, the formation and surface modification of thin selective layer are crucial to obtain TFC-HFMs possessing superior gas separation performance. On the other hand, the selection of materials for the fabrication of hollow fibre substrate is important to the mechanical stability and the long term stability of gas separation performance since the hollow fibre substrate provides the mechanical support for TFC-HFMs. The most commonly used polymer materials for the fabrication of hollow fibre substrate in TFC-HFMs are PSf, PES, PAN, PPO and PEI (Table 4). Those polymers are glassy polymers possessing good mechanical properties, high thermal stability, and chemical resistance (Chen et al., 2014, 2011; Dai et al., 2019; Hu et al., 2018; Li et al., 2004; Liang et al., 2017; Park et al., 2019). The hollow fibre substrate with surface porosity is generally fabricated by using dry-jet wet spinning and nonsolvent induced phase inversion method. Therefore, the polymer materials should possess processability into hollow fibres (Esposito et al., 2015). What is more, hollow fibre supports possessing a uniform pore size and a narrow pore size distribution are favorable for the formation of a uniform coating layer. The chemical compatibility between the support material and the solvent used for dissolving the coating material is also very important to the fabrication of TFC-HFMs when selecting the support material (Choi et al., 2019). Last but not least, the support materials should be easily available with low price (Jo et al., 2017).

### 3.2.2. Dual-layer HFMs prepared by co-extrusion method

Compared with the dip-coating and the interfacial polymerization methods, the co-extrusion is a one-step method to prepare dual-layer HFMs. Dual-layer HFMs prepared by using co-extrusion method possess the following advantages: reduced material cost, less time consumption, and fewer defects induced in membrane owing to the one-step process. What is more, some potential materials with high separation efficiency are not advisable for the fabrication of asymmetric hollow fibres, whereas they can be used to form the outer layer of dual-layer hollow fibres by applying co-extrusion method (Ding et al., 2008).

It is crucial to investigate and optimize the fabrication conditions, such as polymers for outer and inner layers, solvents used for dope solution, and spinning parameters of co-extrusion process to prepare dual-layer HFMs with high gas separation performance. A desirable dual-layer HFM should be delamination free and possess a defect-free selective layer on the outer surface of hollow fibres. The morphology of the outer surface of the inner layer and the interface between two layers should be controlled to reduce the mass transfer resistance. Ding et al. (Ding et al., 2008) fabricated matrimid/PSf dual-layer HFMs by using the co-extrusion technique and investigated the effects of the spinning dope composition, spinneret temperature, and air gap length on the gas separation performance. In their study, a mixture of NMP/H<sub>2</sub>O (95/5 wt.%) was used as bore fluid and tap water was used as coagulant. It was found that the delamination-free dual layer HFMs showed a high O<sub>2</sub> permeance equal to 9.36 GPU and a high selectivity of O<sub>2</sub>/N<sub>2</sub> equal to 7.5. The morphology between two layers was influenced by thermodynamic and kinetic property of spinning dopes.

Ding et al. (Ding et al., 2013) fabricated dual layer HFMs with Matrimids 5218 by using the co-extrusion method (Fig. 3). PSf, PES and PEI were dissolved in different solvents such as N-methyl-2-pyrrolidone (NMP), N,N-dimethylacetamide (DMAc), and dimethylformamide (DMF) to prepare the dope solution for the inner layer. NMP/H<sub>2</sub>O (95/5 wt.%) and tap water were used as bore fluid and external coagulant, respectively. The effects of polymers and solvents for inner dope

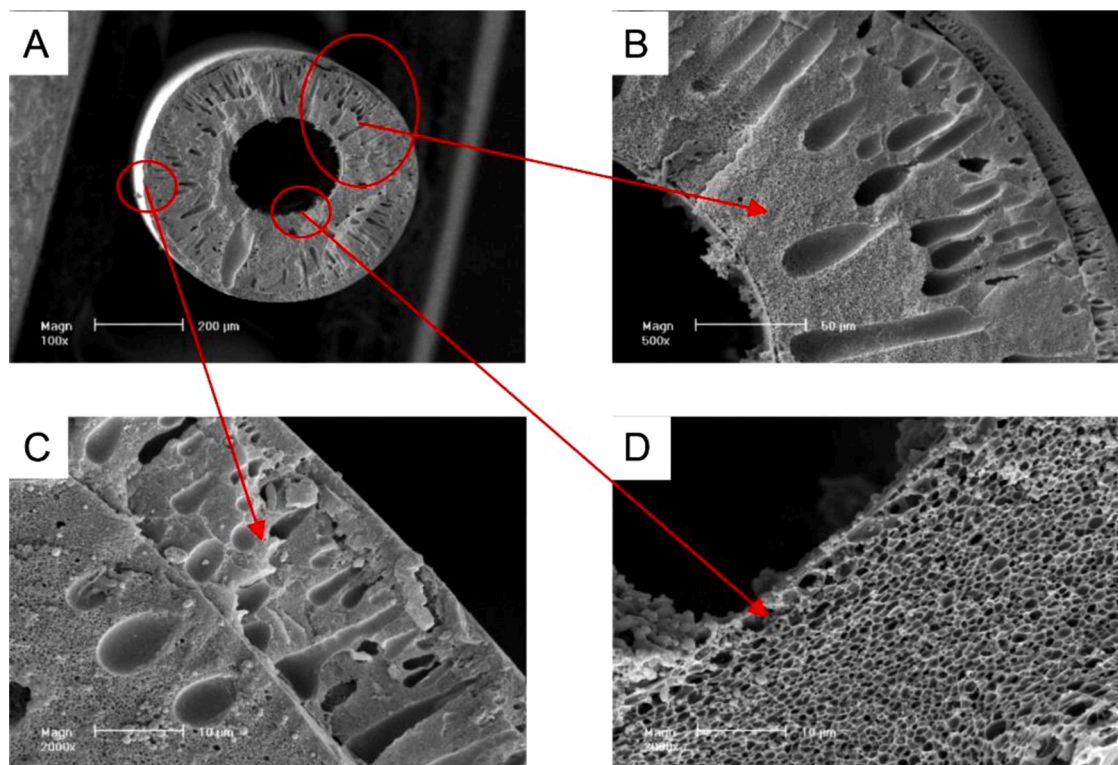


**Fig. 3.** Cross-section images of the dual-layer asymmetric hollow fiber membrane: (A) overall profile:  $\times 100$ ; (B) part of cross-section:  $\times 500$ ; (C) outer edge of outer layer:  $\times 2000$ ; and (D) inner edge of inner layer:  $\times 2000$  (Ding et al., 2013). Reproduced with the permission from ELSEVIER.

solution on the interfacial morphology between two layers were investigated to optimize the fabrication parameters of the co-extrusion process. It was found that the morphologies of the outer surfaces of inner and outer layers were strongly affected by the demixing rates of inner dope and outer dope. If the outer dope demixes first, the dense skin forms only on the outer surface of outer layer. On the contrary, the dense skin would also be formed on the outer surface of the inner layer, which would increase the mass transfer resistance and decreased the gas permeance (Ding et al., 2013).

Jiang et al. (Jiang et al., 2004) investigated the effects of spinning parameters on the structural properties and gas performance of Matrimid/PES dual-layer HFMs prepared by using the co-extrusion method. NMP/H<sub>2</sub>O (80/20 wt.%) and water were used as bore fluid and external coagulant, respectively. It was found that the coagulant temperature influences the thickness and interfacial structure of dual-layer HFMs. The outer dope flow rate has an important effect on the gas separation performance. The dual-layer HFMs prepared at 25 °C for both spinneret and coagulant showed an O<sub>2</sub>/N<sub>2</sub> selectivity equal to 6.26 in pure gas tests and CO<sub>2</sub>/CH<sub>4</sub> selectivity equal to 40 in mixed gas tests (Jiang et al., 2004).

Li et al. (Li et al., 2002) fabricated delamination-free fluoropolyimide/PES dual layer HFMs for gas separation by using the co-extrusion method. It was revealed that the inner layer dope concentration, bore fluid composition (H<sub>2</sub>O, NMP/H<sub>2</sub>O (95/5 wt.%), and the sequent solvent exchange play important roles in the preparation of delamination-free dual-layer HFMs. Tap water was used as external coagulant. The prepared membranes showed an O<sub>2</sub>/N<sub>2</sub> ideal selectivity equal to 4.7 and O<sub>2</sub> permeance equal to 28 GPU (Li et al., 2002).

Naderi et al. (Naderi et al., 2019) prepared dual layer HFMs consisting of an outer-selective layer made from PBI and sulfonated polyphenylsulfone (sPPSU) blends, and an inner-support layer made of PSf by using co-extrusion method for H<sub>2</sub>/CO<sub>2</sub> separation at elevated temperatures. NMP/H<sub>2</sub>O (95/5 wt.%) and tap water were used as bore fluid and external coagulant, respectively. The prepared dual-layer HFMs are delamination-free and have a defect-free microstructure. It was found that the dual-layer HFMs crosslinked by 3 %  $\alpha,\alpha'$ -dibromo-p-xylene (DBX) and annealed at 120 °C showed a H<sub>2</sub> permeance equal to 16.7 GPU and H<sub>2</sub>/CO<sub>2</sub> ideal selectivity equal to 9.7 at 90 °C and 14 atm. The interaction between sPPSU and PBI increased the interchain space in PBI resulting in the increase in H<sub>2</sub> permeance. The H<sub>2</sub>/CO<sub>2</sub> ideal selectivity was improved because DBX covalently crosslinked PBI resulting in the outer-selective layer with a smaller free volume (Naderi et al., 2019).

The post-treatment on dual-layer HFMs is as important as the fabrication conditions of the dry-jet wet spinning process to the formation of high performance membranes. Li et al. (Li et al., 2004) prepared dual-layer PES HFMs with an ultrathin dense selective layer of 40.7 nm by using the co-extrusion method and heat treatment. NMP/H<sub>2</sub>O (95/5 wt.%) and tap water were used as bore fluid and external coagulant, respectively. It was found that the O<sub>2</sub>/N<sub>2</sub> ideal selectivity increased from 5.26 to 6.00 when the membranes were heat-treated at 75 °C for 3 h. However, the gas selectivity and permeance decreased when the membranes were heat-treated at 150 °C for 1 h (Li et al., 2004). Peng et al. (Peng et al., 2010) applied a new amorphous thermoplastic PEI (Extem®) to fabricate Extem® asymmetric HFMs by using the dry-jet wet spinning method and dual-layer HFMs with an ultrathin dense selective layer by using the co-extrusion method for gas separation. NMP/H<sub>2</sub>O (95/5 wt.%) and water were used as bore fluid and external coagulant, respectively. They compared the gas separation performance of single-layer and dual-layer HFMs. It was found that the defects in asymmetric HFMs could not be sealed by coating with PDMS, while the heat treatment could inhibit the formation of defects. However, the gas permeance decreased owing to the heat treatment. Compared with the asymmetric HFMs, the prepared dual-layer Extem® HFMs showed better O<sub>2</sub>/N<sub>2</sub> selectivity equal to 6.15. It is concluded that this material is not suitable for the asymmetric HFMs fabrication, however, it can be used in the dual-layer HFMs fabrication by using the

co-extrusion method (Peng et al., 2010).

Askari et al. (Askari et al., 2012) fabricated cross-linkable dual layer HFMs consisting of an outer-selective layer made from 6FDA-Durene/-DABA (9/1) grafted with  $\beta$ -Cyclodextrin (PI-g- $\beta$ CD) and an inner layer made from 6FDA-Durene for natural gas purification and olefin/paraffin separation. NMP/H<sub>2</sub>O (95/5 wt.%) and tap water were used as bore fluid and external coagulant, respectively. The effects of take-up velocities, outer layer dope flow rates, heat treatment and silicon rubber coating on the gas separation performance and hollow fibre morphology were investigated. It was found that when the take-up velocity increased, permeances of all gases decreased while the selectivity firstly increased then decreased, which can be attributed to the influence of elongational draw ratio and change in surface porosity of membranes. The permeances increased with a decrease in outer layer dope flow rate due to the thinner skin layer. However, selectivity decreased with a decrease in outer layer dope flow rate due to the defect formation. Membranes heat treated at 400 °C showed higher selectivity but lower permeance due to the skin densification and a higher degree of cross-linking. Moreover, the heat treatment enhanced the anti-plasticization properties of membranes.

As is shown in Table 5, polyimide-based materials are frequently used to form the selective layer of dual-layer HFMs prepared by using the co-extrusion method. Such prepared membranes with a polyimide selective layer are generally used for O<sub>2</sub>/N<sub>2</sub> separation. The interfacial morphology between the inner layer and outer layer influences significantly the gas permeance. The mass transfer resistance increases when the inner layer possesses a skin layer which results from the difference of the phase inversion processes of two layers. Therefore, the composition of outer dope and inner dope must be strictly designed to control the phase inversion process. The spinning parameters such as the flow rates

**Table 5**

Comparison of gas separation performance of dual-layer HFMs prepared by co-extrusion method (SG - single gas, MG - mixed gas).

Membrane materials	Fast gas/slow gas	Permeance of faster gas [GPU]	Selectivity	Testing conditions	Ref.
Matrimid/PSf	O <sub>2</sub> /N <sub>2</sub>	9.36	7.55	25 °C, 5.07 bar, SG	(Ding et al., 2008)
Matrimid/PES	O <sub>2</sub> /N <sub>2</sub>	4.57	6.26	25 °C, 13.8 bar, SG	(Jiang et al., 2004)
Matrimid/PES	CO <sub>2</sub> /CH <sub>4</sub> (40/60 mol %)	11	40	22 °C, 17.2 bar, MG	(Jiang et al., 2004)
Fluoropolyimide/PES	O <sub>2</sub> /N <sub>2</sub>	4.7	28	25 °C, 13.8 bar, SG	(Li et al., 2002)
PBI-sPPSU/PSf	H <sub>2</sub> /CO <sub>2</sub>	16.7	9.7	90 °C, 14.2 bar, SG	(Naderi et al., 2019)
PEI/PEI	O <sub>2</sub> /N <sub>2</sub>	12.02	6.15	25 °C, 13.8 bar, SG	(Peng et al., 2010)
PI-g- $\beta$ CD/6FDA-Durene	CO <sub>2</sub> /CH <sub>4</sub>	130	15.5	25 °C, 13.8 bar, SG	(Askari et al., 2012)
	C <sub>3</sub> H <sub>6</sub> /C <sub>3</sub> H <sub>8</sub>	73	10.5	25 °C, 3.5 bar, SG	
PI-g- $\beta$ CD/6FDA-Durene with silicon coating	CO <sub>2</sub> /CH <sub>4</sub>	82	20.0	25 °C, 13.8 bar, SG	(Askari et al., 2012)
	C <sub>3</sub> H <sub>6</sub> /C <sub>3</sub> H <sub>8</sub>	29	15.3	25 °C, 3.5 bar, SG	



of outer and inner dope solution, air gap, the spinneret design, and coagulant temperature must be optimized to fabricate delamination-free dual-layer HFMs with high gas separation performance (Ding et al., 2013, 2008; Jiang et al., 2004; Li et al., 2004; Naderi et al., 2019).

### 3.3. Mixed matrix hollow fibre membranes (MM-HFMs)

It is well known that polymeric membranes possess the tradeoff relation between gas permeability and selectivity, which limits the application of polymeric membranes in gas separation processes to some extent (Robeson, 2008; Wang et al., 2017). Incorporating inorganic fillers into polymer matrix to prepare MMMs is a promising alternative to enhance the permeability and selectivity for breaking the tradeoff relation in gas separation processes. Nanomaterials such as carbon fillers (Xin et al., 2019; Zhao et al., 2018), zeolite and related fillers (Chen et al., 2015; Hu et al., 2020), metal oxide nanoparticles (Dilshad et al., 2019; Shamsabadi et al., 2017), and metal organic frameworks (MOFs) (Ding et al., 2020; Jiang et al., 2019; Meshkat et al., 2020; Ozen and Ozturk, 2019) are widely applied to prepare MMMs. However, due to the undesirable compatibility between inorganic particles and polymers, the imperfect particle dispersion e.g. particle agglomeration in the polymer matrix and the non-ideal interfacial morphology between fillers and polymer matrix e.g. non-selective voids restrict the gas separation performance and mechanical strength of MMMs (Zhang et al., 2019). It is important to tackle these issues during the fabrication of high-performance MMMs. Therefore, this section will summarize and discuss the strategies of inorganic filler modification to improve the interfacial compatibility and the affinity to target gas species.

#### 3.3.1. The fillers and their modification strategies

Graphene oxide (GO) has attracted considerable research interest because the strong interaction between polymer chains and graphene oxide may favourably mediate polymer chain packing and significantly enhance gas diffusion behaviour. Moreover, the surface can be easily functionalized to improve the physicochemical properties and the compatibility with the polymer matrix (Wang et al., 2019). It is possible to control the molecular sieving separation property, the interlayer space channels diameter, and the diversity of functional groups. What is more, the high surface ratio and high mechanical and thermal properties have helped GO and its derivatives to become the best nanofiller

candidates for carbon dioxide separation (Mohammed et al., 2019). Zhang et al. (Zhang et al., 2019) prepared the MMMs comprising aminosilane-functionalized GO for CO<sub>2</sub> separation (Fig. 4). The organosilanes modification on filler improved the interfacial compatibility and resulted in a more uniform distribution of these nanoparticles. Moreover, the amino groups on the grafted GO surface act as CO<sub>2</sub> carriers, which provide facilitated transport pathway along the polymer-filler interface. As a result, the CO<sub>2</sub> separation performances surpass Robeson's upper bounds (Robeson, 2008). Comparing with the pristine membrane, the Young's modulus to 2.7 times higher, and the break strength increased to 2.1 times higher. This might be attributed to the superior mechanical strength of modified GO, the good interfacial adhesion between the modified GO and the polymer.

Dong et al. (Dong et al., 2016) prepared MMMs by incorporating porous reduced GO into Pebax to improve CO<sub>2</sub> permeability and CO<sub>2</sub>/N<sub>2</sub> selectivity. Huang et al. (Huang et al., 2018) prepared facilitated transport MMMs by incorporating ionic liquid functionalized GO (GO-IL) into Pebax 1657. It was found that the CO<sub>2</sub> separation was improved owing to the higher affinity between CO<sub>2</sub> molecules and GO-IL. A homogeneous dispersion of GO-IL was obtained owing to the improved compatibility between Pebax and fillers. The presence of GO and GO-IL fillers dose not significantly influence the thermal properties of MMMs. The MMM comprising GO-IL sheets showed less change in mechanical properties compared with GO based MMMs that could be due to the higher miscibility and stronger interaction between GO-IL fillers and Pebax matrix.

Dai et al. (Dai et al., 2016b) prepared MMMs composed of imidazole functionalized GO (ImGO) and PEBA for CO<sub>2</sub> capture. The ionic liquid modification improve the interfacial compatibility and the ImGO nanosheets are distributed in the polymer matrix uniformly. The T<sub>g</sub> of ImGO/PEBAX MMMs is higher than that of pristine PEBAX membrane, which is attributed to the restricted mobility of polymer chain by the fillers. The tensile strength of the MMMs is significantly increased compared to that of pristine PEBAX membrane because of the strong interfacial adhesion, which is caused by the H-bonding interactions formed between graphene and the polymer matrix. The addition of ImGO as a CO<sub>2</sub>-philic filler enhanced the CO<sub>2</sub> separation.

Metal oxide nanoparticles have been widely used as fillers in polymeric membranes to form MMMs. The modification of inorganic fillers is a desirable way to tune the filler properties. TiO<sub>2</sub> nanoparticles and

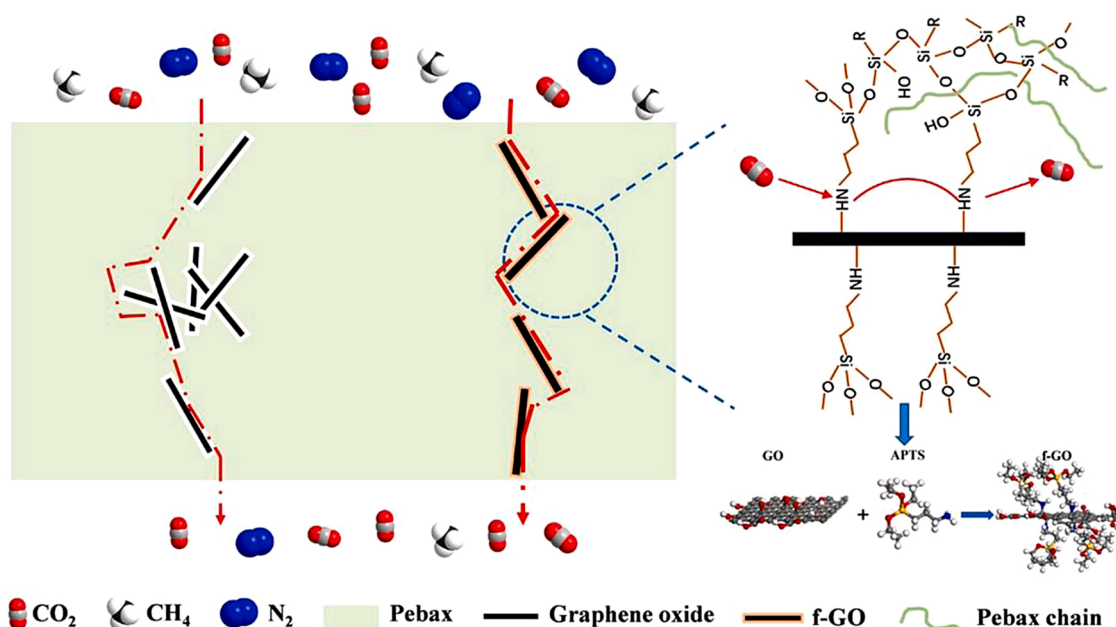


Fig. 4. Illustration of surface modification of GO and gas separation through MMMs (Zhang et al., 2019). Reproduced with the permission from ELSEVIER.



surface modified TiO<sub>2</sub> nanoparticles were used as the filler in the PEBA matrix to improve the CO<sub>2</sub> removal efficiency. In the modification process, the TiO<sub>2</sub> nanoparticles were grafted with 3-aminopropyl-diethoxymethylsilane and modified with carboxymethyl chitosan (Shamsabadi et al., 2017). The MMMs with modified TiO<sub>2</sub> nanoparticles showed higher compatibility between filler and polymer, better thermal stability, and satisfactory dispersion of fillers into polymer matrix. The MMMs containing silane modified fillers showed significant higher apparent elastic moduli due to the strong interfacial interactions between modified fillers and polymer matrix (Shamsabadi et al., 2017).

Another approach to modify the TiO<sub>2</sub> nanoparticles was proposed by Zhu et al. (Zhu et al., 2019a). In their research, TiO<sub>2</sub> nanoparticles were synthesized and the amine groups were grafted onto the fillers (Fig. 5). Homogeneous dispersion was obtained in all the modified TiO<sub>2</sub>/PEBA MMMs due to the improved compatibility between the inorganic and organic phase, which is resulted from the interactions between amine groups on the PEI and PEBA chains. It was found that the modified TiO<sub>2</sub>/PEBA MMMs showed improve CO<sub>2</sub>/N<sub>2</sub> separation performance because the amine groups are conducive to transfer CO<sub>2</sub> (Zhu et al., 2019a).

MOFs are porous crystalline solids composed of metal ions centre and organic ligands. The structure of MOFs is defined by nodes of metal ions or clusters of metal ions held in the lattice by organic linkers (He et al., 2020). MOFs possess plenty of advantages such as high surface area, tailoring pore size, high adsorption capacity, and greater chemical and thermal properties. Moreover, the organic moiety of MOFs enhances the compatibility between the polymer matrix and fillers (Vinoba et al., 2017). Therefore, MMMs incorporated with MOFs showed remarkable gas separation properties.

Jiang et al. (Jiang et al., 2019) synthesized UiO-66-NH<sub>2</sub> and grafted imidazole-2-carbaldehyde (ICA) onto UiO-66-NH<sub>2</sub> (Fig. 6). It was found that the grafted ICA reduced the pore volume of UiO-66-NH<sub>2</sub> but increased the number of nitrogen atoms as the binding site of CO<sub>2</sub>. The modified UiO-66-NH<sub>2</sub> showed a higher CO<sub>2</sub>/CH<sub>4</sub> adsorption selectivity. The CO<sub>2</sub>/CH<sub>4</sub> selectivity increased by 40 % when the modified UiO-66-NH<sub>2</sub> was incorporated. The modified UiO-66-NH<sub>2</sub> particles were well dispersed in the polymeric phase due to the good compatibility and adhesion between modified particles and polymers, resulting in MMMs without visible defects, agglomerate and phase separation at particle

loading of under 20 % (Jiang et al., 2019).

Shen et al. (Shen et al., 2016) synthesized CO<sub>2</sub>-philic UiO-66-NH<sub>2</sub> nanoparticles and incorporated them into PEBA membranes for CO<sub>2</sub> separation. The poor dispersion of UiO-66 nanoparticles was observed, which is attributed to the weak interaction between pristine particles and polymer chains. The amine modification improved the particle dispersion in the polymer matrix owing to the enhanced hydrogen bonding frameworks between UiO-66-NH<sub>2</sub> and PEBA. It was found that amine functionalized UiO-66-NH<sub>2</sub> particles showed stronger CO<sub>2</sub> affinity compared with UiO-66. The UiO-66-NH<sub>2</sub>-PEBA MMMs showed higher CO<sub>2</sub>/N<sub>2</sub> selectivity and slightly decreased CO<sub>2</sub> permeance compared with UiO-66-PEBA membranes. Comparing with pristine PEBA membrane, the mechanical properties of UiO-66-NH<sub>2</sub>-PEBA MMMs was significantly improved. UiO-66-NH<sub>2</sub>-PEBA (20) membrane showed 52 % and 29.4 % enhancement in hardness and elastic modulus, respectively (Shen et al., 2016).

Ding et al. (Ding et al., 2020) proposed a microemulsion based mixed linkers strategy to introduce amino groups into ZIF-8. According to their method, the mixed ligands (2-aminobenzimidazole and 2-methylimidazole) instead of 2-methylimidazole were used to synthesize NH<sub>2</sub>-ZIF-8. Compared with post-synthetic modification, this method presents less reduction in S<sub>BET</sub> of ZIF-8, which is beneficial for CO<sub>2</sub> adsorption. The prepared MMMs with incorporated NH<sub>2</sub>-ZIF-8 showed a desirable dispersion of fillers in polymer matrix owing to interaction between the amino groups in ZIF-8 and the amide in the Pebax chain. It was observed that the NH<sub>2</sub>-ZIF-8/Pebax MMMs possess a uniform structure and without any obvious interfacial voids on the surface and cross-section, indicating the outstanding compatibility between NH<sub>2</sub>-ZIF-8(15) and Pebax. NH<sub>2</sub>-ZIF-8 showed higher affinity with CO<sub>2</sub> than that of pristine ZIF-8, which results in an enhancement in the CO<sub>2</sub>/N<sub>2</sub> separation performance (Ding et al., 2020). Gao et al. (Gao et al., 2020) synthesized three partially NH<sub>2</sub>-, OH- and CH<sub>3</sub>OH- functionalized ZIF-7 by applying mixed linkers strategy and incorporated the functionalized ZIF-7 into the Pebax polymer to form MMMs. It was found that the introduction of functional groups in the ZIF-7 framework was beneficial for CO<sub>2</sub> adsorption and all MMMs composed of ZIF-7-NH<sub>2</sub>, ZIF-7-OH and ZIF-7-CH<sub>3</sub>OH offered better CO<sub>2</sub>/N<sub>2</sub> separation performance than the MMMs composed of ZIF-7.

Since the incorporation of another metal can enhance the optical,

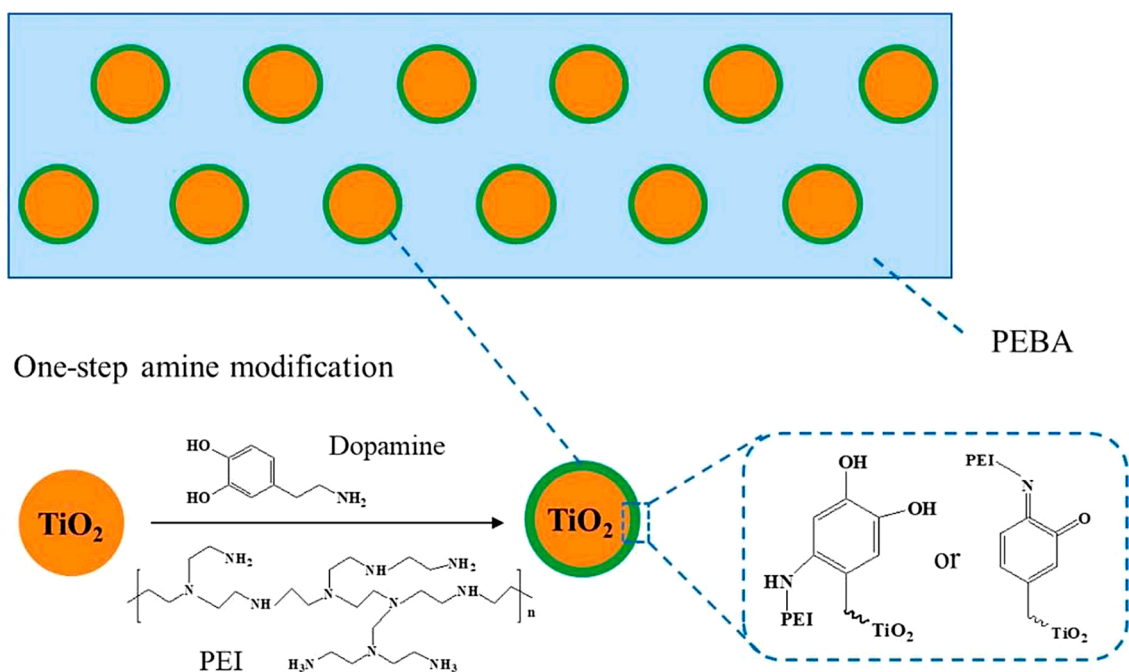


Fig. 5. Schematic structure of the DP/PEI grafted TiO<sub>2</sub>/PEBA MMM (Zhu et al., 2019a). Reproduced with the permission from ELSEVIER.

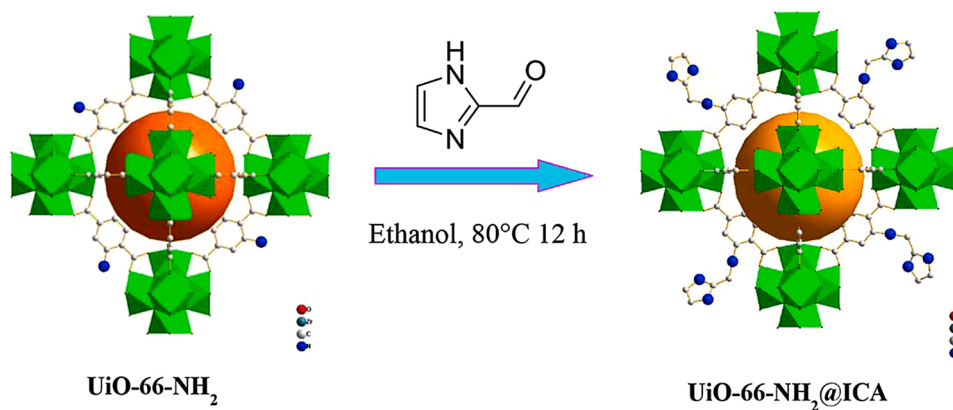


Fig. 6. Scheme of synthesis of UiO-66-NH<sub>2</sub>@ICA by post-synthetic modification method (PSM) through amine condensation reaction (Jiang et al., 2019). Reproduced with the permission from ELSEVIER.

electronic, magnetic, and adsorption properties of MOFs and the bimetallic MOFs usually provide higher surface area, porosity, and adsorption properties, Kardani et al. (Kardani et al., 2020) synthesized a copper, zinc, bimetallic, imidazolite, framework (CuZnIF) particles and introduced them into a PEBA matrix to form MMMs. It was found that CO<sub>2</sub> permeability significantly increased owing to the enhanced free volume content induced by the intrinsic cavities of CuZnIF nanoparticles as well as the disruption of polymer chain packing and the strong affinity between CO<sub>2</sub> molecules and CuZnIF domains (Kardani et al., 2020). Zhang et al. (Zhang et al., 2018) synthesized nickel zinc bimetallic imidazolite framework (Zn/Ni-ZIF-8) particles by solvothermal method and incorporated them into a PEBA matrix to form MMMs. It was found that the synthesized Zn/Ni-ZIF-8 particles exhibited higher CO<sub>2</sub> adsorption capacities than ZIF-8 owing to the dual metal sites. The CO<sub>2</sub>/N<sub>2</sub> separation performance was significantly improved and surpasses the 2008 Robeson's upper bound (Robeson, 2008). The prepared MMMs showed excellent mechanical properties as a result of good compatibility between the polymer and Zn/Ni-ZIF-8 particles, which is a result of the electron-rich properties of the Zn/Ni-ZIF-8 framework that facilitates strong electrostatic interactions between Zn/Ni-ZIF-8 and the PEBA-polymer chains. The tensile strength and elongation at break of the Zn/Ni-ZIF-8-PEBA MMMs increased slightly as the filler loading was increased to 10 %, due to the homogeneous distribution of Zn/Ni-ZIF-8 and its good adhesion to PEBA. However, the tensile strength and elongation at break of the ZIF-8-PEBA MMMs decreased steadily with increasing ZIF-8 loading.

As was stated before, the surface modification of inorganic fillers is an effective way to improve the compatibility between inorganic nanoparticles and polymer matrix and to tune the interfacial morphology between inorganic and organic phase in MMMs, consequently, the gas separation performance of MMMs. Moreover, the physicochemical properties of inorganic fillers such as the size of nanoparticles, pore size of porous fillers, roughness, surface chemistry, and affinity to gas species are changed after surface modification. Post-synthetic modification e.g. covalently grafting silane coupling agents or ionic liquid onto the surface of fillers and in-situ modification e.g. microemulsion based mixed linkers strategy to introduce amino groups into MOF nanoparticles can be used to realize the surface modification with desirable functional groups. For instance, amine groups are grafted on the surface of GO (Zhang et al., 2019), TiO<sub>2</sub> nanoparticles (Zhu et al., 2019a), ZIF-8 (Ding et al., 2020), and UiO-66-NH<sub>2</sub> (Shen et al., 2016) to improve their compatibility with polymer matrix and affinity to CO<sub>2</sub>. The incorporation of surface modified fillers into polymer matrix not only improves the gas separation performance of MMMs, but also maintains or enhances the mechanical properties of MMMs arising from the high compatibility, desirable interfacial morphology, and interactions between functional groups in fillers and polymer chains.

### 3.3.2. Examples of MM-HFMs

Although plenty of research was focused on the preparation and characterization of flat sheet MMMs for gas separation processes, the strategy of synthesis and modification of inorganic fillers could be also used to fabricate MM-HFMs. Some research works presented inspiring results of MM-HFMs for the gas separation process (Etxeberria-Benavides et al., 2020b; Magueijo et al., 2013b; Zhu et al., 2018).

Zulhairun et al. (Zulhairun et al., 2017) prepared polysulfone (PSf) MM-HFMs incorporated with titania nanotubes (TNTs) for gas separation. It was found that the incorporation of 0.4 wt.% TNTs into the PSf matrix increased the gas permeance by 1.5 times. The gas permeances of H<sub>2</sub>, CO<sub>2</sub>, O<sub>2</sub> are 269 GPU, 120 GPU, and 26 GPU, respectively. Moreover, the O<sub>2</sub>/N<sub>2</sub>, H<sub>2</sub>/CH<sub>4</sub>, CO<sub>2</sub>/CH<sub>4</sub>, and CO<sub>2</sub>/N<sub>2</sub> selectivities were enhanced compared with pristine membranes.

Jamil et al. (Jamil et al., 2018) prepared polyetherimide-montmorillonite MM-HFMs for CO<sub>2</sub>/CH<sub>4</sub> separation. I-MMT and O-MMT were incorporated into the polyetherimide matrix and their effects on gas separation were investigated. The MM-HFMs were prepared by the phase inversion method and coated with a PDMS layer. It was found that the developed MM-HFMs with I-MMT showed a decrease in CO<sub>2</sub>/CH<sub>4</sub> separation performance compared to the PEI membrane. In contrast, the MM-HFMs with O-MMT showed enhanced CO<sub>2</sub>/CH<sub>4</sub> separation performance. The maximum ideal selectivity achieved was 18.35 with a 2 wt.% loading of O-MMT at 4 bar. To improve the filler dispersion in polymer matrix, Jamil et al. (Jamil et al., 2017) modified montmorillonite by replacing the inorganic cations with organic cation of aminolauric acid to impart organophilicity to enhance compatibility with organic polymer matrix. The prepared MM-HFMs with 2 wt.% modified montmorillonite showed a 39 % increment in ideal selectivity for CO<sub>2</sub>/CH<sub>4</sub> separation compared to pristine PEI hollow fibre membranes. The uniform dispersion of modified filler enhanced the thermal properties of MM-HFMs.

Wahab et al. (Wahab et al., 2012) prepared asymmetric MM-HFMs by incorporating nanosized fume silica into a polysulfone matrix for gas separation. It was found that the gas separation performance was improved when 0.1 wt.% of particles was incorporated. The permeances of CO<sub>2</sub> and CH<sub>4</sub> were 90.04 and 2.75 GPU, respectively. Moreover, the CO<sub>2</sub>/CH<sub>4</sub> ideal selectivity was 32.74 which was higher than that for pristine PSf membranes. However, when the filler content increased to 10 wt.%, the permeance of CH<sub>4</sub> was increased owing to the severe agglomeration of fillers, resulting in the lower selectivity of 7.43. The MM-HFMs showed improved thermal stability and an increase in glass transition temperature.

Magueijo et al. (Magueijo et al., 2013a) prepared MM-HFMs by incorporating carbon xerogel into polysulfone matrix. When 5 wt.% of xerogel was added, the prepared membranes showed higher mechanical strength than the pristine membranes. Most importantly, the prepared

membranes gave a higher CO<sub>2</sub> permeance without sacrificing the CO<sub>2</sub>/CH<sub>4</sub> selectivity compared to the pristine membranes.

Khan et al. (Khan et al., 2020) incorporated ZIF-8 nanoparticles into a polysulfone matrix to form asymmetric MM-HFMs for natural gas purification. It was found that the prepared membranes with 0.5 wt.% ZIF-8 showed significant improvement in CO<sub>2</sub> permeance (36 %), and CO<sub>2</sub>/CH<sub>4</sub> selectivity (28 %), at 6 bar feed pressure, owing to the uniform dispersion of ZIF-8 particles across the membrane surface which hindered CH<sub>4</sub> permeation with enhanced CO<sub>2</sub>/CH<sub>4</sub> selectivity. However, the higher ZIF-8 loading reduced the separation performance. The glass transition temperature was increased owing to the excellent interaction between filler and polymer matrix.

Ettxeberria-Benavides et al. (Ettxeberria-Benavides et al., 2020a) incorporated ZIF-8 particles into a PBI matrix to prepare MM-HFMs for H<sub>2</sub>/CO<sub>2</sub> separation. It was found that the incorporation of ZIF-8 into the PBI matrix resulted in a strong increase in hydrogen permeance from 65 GPU to 107 GPU at 150 °C and 7 bar, while the ideal H<sub>2</sub>/CO<sub>2</sub> selectivity remained constant at  $\alpha = 18$ . The prepared membranes were able to be applied for the treatment of gas streams in pre-combustion and syngas processes.

Zhu et al. (Zhu et al., 2017a) functionalized MIL-53 particles by aminosilane grafting and incorporated them into a polyetherimide matrix to fabricate MM-HFMs for gas separation. It was found that the filler particles were uniformly dispersed in the polymer matrix and the thermal stability of the membrane was improved. The prepared MM-HFMs achieved excellent gas permeance and CO<sub>2</sub>/N<sub>2</sub> selectivity. The CO<sub>2</sub> permeance increased from 12.2 GPU to 30.9 GPU and the ideal CO<sub>2</sub>/N<sub>2</sub> selectivity was simultaneously enhanced from 25.4 to 34.7.

The dual-layer MM-HFMs for gas separation have been prepared and investigated by several researchers. Widjojo et al. (Widjojo et al., 2008) fabricated polyethersulfone (PES)-beta zeolite/PES-Al<sub>2</sub>O<sub>3</sub> dual-layer MM-HFMs for gas separation. It was found that the prepared dual-layer MM-HFMs containing 20 wt.% beta zeolite in the outer selective layer and 60 wt.% Al<sub>2</sub>O<sub>3</sub> in the inner layer showed an increased O<sub>2</sub>/N<sub>2</sub> selectivity equal to 6.89. The high draw ratios caused the uniform distribution of Al<sub>2</sub>O<sub>3</sub> particles towards both edges of the inner layer resulting in the increased mechanical stability.

Dai et al. (Dai et al., 2012) prepared dual-layer MM-HFMs via co-extrusion of the inner and outer dopes with a bore fluid solution through a composite spinneret. PEI was used to prepare inner and outer dopes while 13 wt.% of ZIF-8 particles were dispersed into the outer dope to form MM-HFMs. It was found that the MM-HFMs showed increased permeance and 20 % selectivity enhancements compared with pristine membranes. Furthermore, the separation factor is as high as 32 in the mixed gas separation test.

Li et al. (Li et al., 2006) prepared dual-layer PES-zeolite beta/P84

MM-HFMs by using the co-extrusion method. The outer selective layer was controlled as thin as 0.55  $\mu\text{m}$  by adjusting the ratio of outer layer flow rate to inner layer flow rate. It was found that the prepared membranes showed enhanced O<sub>2</sub>/N<sub>2</sub> and CO<sub>2</sub>/CH<sub>4</sub> selectivity compared with the pristine PES dense films. Increasing the air gap length can mitigate the formation of defects in membranes. Heat treatment at 235 °C and silica rubber coating further improved the gas separation performance by reducing the voids formation and sealing the defects, respectively.

As Table 6 and the aforementioned examples show, different fillers can be incorporated into a polymer matrix to prepare MM-HFMs. The incorporation of inorganic fillers improves the gas separation performance, by either increasing the gas permeability without sacrificing the gas selectivity or by increasing the gas permeability and selectivity simultaneously. What is also important is that the incorporation of inorganic particles influences the physico-chemical properties, such as mechanical properties and thermal stability, of hollow fibres. However, it is crucial to disperse well the inorganic fillers in the polymer matrix to obtain defect free MM-HFMs with enhanced gas separation performance. The optimization of the hollow fibre fabrication parameters and modification of inorganic fillers to improve the compatibility between inorganic fillers and polymer have been applied to guarantee the uniform dispersion of inorganic fillers and defect free MM-HFMs fabrication. What is more, the PDMS protective layer is commonly coated on the MM-HFMs to further improve the gas separation performance.

### 3.4. Ceramic HFMs

Owing to their high selectivity and high thermal and chemical stability in harsh conditions, ceramic membranes have been studied in many gas separation processes, such as oxygen separation from air (Hashim et al., 2010, 2011; Li et al., 2019), hydrogen recovery (Hashim et al., 2018; Meng et al., 2019; Zhu et al., 2017b), and carbon dioxide separation (Chen et al., 2020; Zhang et al., 2013). What is more, ceramic hollow fibre membrane reactors are used in heterogeneous catalytic phase reactions (García-García et al., 2012; García-García and Li, 2013). Compared to disk membranes, HFMs provide a higher separation area to volume ratio, which makes them attractive for large scale production (Chi et al., 2017). Despite their superior properties and performance at high temperature and pressure, the drawbacks of ceramic membranes are higher costs, a complex preparation process, and low permeation flux for dense inorganic membranes (Zhang et al., 2013; Zhu et al., 2017b). The preparation methods of ceramic HFMs, gas permeation mechanisms in ceramic membranes, and their applications in gas separation processes have been excellently described elsewhere (Athayde et al., 2016; Deibert et al., 2017; Hashim et al., 2010, 2011; Hashim

**Table 6**  
Comparison of gas separation performance of MM-HFMs (SG - single gas, MG - mixed gas).

Membrane materials	Protective layer	Fast gas/slow gas	Permeance of faster gas [GPU]	Selectivity	Testing conditions	Ref.
PSf/0.4 wt.% TNT	PDMS	O <sub>2</sub> /N <sub>2</sub>	269	6.20	25 °C, 3 bar, SG	(Zulhairun et al., 2017)
		H <sub>2</sub> /CH <sub>4</sub>	120	57.86		
		CO <sub>2</sub> /CH <sub>4</sub>	26	25.93		
		CO <sub>2</sub> /N <sub>2</sub>	26	28.76		
PBI/10 wt.% ZIF-8	PDMS	H <sub>2</sub> /CO <sub>2</sub>	107	18.00	150 °C, 7 bar, SG	(Ettxeberria-Benavides et al., 2020a)
PSf/0.1 wt.% fumed silica	-	CO <sub>2</sub> /CH <sub>4</sub>	90.04	32.74	25 °C, 5 bar, SG	(Wahab et al., 2012)
		O <sub>2</sub> /N <sub>2</sub>	15.83	6.35		
PEI/2 wt.% Montmorillonite	PDMS	CO <sub>2</sub> /CH <sub>4</sub>	130	18.35	25 °C, 4 bar, SG	(Jamil et al., 2018)
PSf/5 wt.% Xerogel	PDMS	O <sub>2</sub> /N <sub>2</sub>	17.8	5.95	25 °C, 5 bar, SG	(Magueijo et al., 2013a)
		CO <sub>2</sub> /CH <sub>4</sub>	103.3	32.70		
PSf/0.5 wt.% ZIF-8	PDMS	CO <sub>2</sub> /CH <sub>4</sub>	47.75	25.70	25 °C, 6 bar, SG	(Khan et al., 2020)
PEI/15 wt.% Aminosilane functionalized MIL-53	PDMS	CO <sub>2</sub> /N <sub>2</sub>	30.9	34.7	35 °C, 5 bar, SG	(Zhu et al., 2017a)
PEI/13 wt.% ZIF-8	PDMS	CO <sub>2</sub> /N <sub>2</sub>	26	36	35 °C, 100 psia, SG	(Dai et al., 2012)
PEI/13 wt.% ZIF-8	PDMS	CO <sub>2</sub> /N <sub>2</sub> (20/80 vol%)	26	32	25 °C, 20–50 psia, MG	(Dai et al., 2012)



et al., 2018; Wei et al., 2013; Zhang et al., 2013). This section will briefly introduce the investigation on ceramic HFMs in gas separation processes, since this review mainly focuses on polymeric HFMs.

Dense ceramic oxygen permeation membranes (OPM) are favourable for the oxygen separation from air. The oxygen permeation flux, mechanical and chemical stability, and cost-effectiveness must be considered when developing OPM (Li et al., 2019). Li et al. (Li et al., 2019) introduced an orange-like architecture in the micro-monolithic  $\text{La}_{0.6}\text{Sr}_{0.4}\text{Co}_{0.2}\text{Fe}_{0.8}\text{O}_{3-\delta}$  (LSCF) membranes by changing the geometry of channels in the micro-monolith from a circular shape to a teardrop shape. It was found that such modification in channel geometry not only reduced the effective oxygen diffusive pathway length, but also enhanced the ratio of active circumference, which resulted in high oxygen permeation flux up to  $1.87 \text{ ml min}^{-1} \text{ cm}^{-2}$  at  $950^\circ\text{C}$ . What is more, the prepared membranes possess higher mechanical robustness compared with conventional LSCF hollow fibres (Li et al., 2019). Chi et al. (Chi et al., 2017) prepared mixed ionic electronic conducting 3, 4, 7-bore capillary membranes made of LSCF by the combined phase inversion and sintering technique. It was found that the oxygen permeation flux was similar to that of the single-bore HFMs at a temperature lower than  $900^\circ\text{C}$ . However it was significantly higher than the single-bore HFMs at a higher temperature (Chi et al., 2017). From the aforementioned examples, it can be seen that the trade-off between oxygen permeation and the mechanical properties of ceramic hollow fibres can be tackled by modification of channel geometry in hollow fibres.

Besides the modification of channel geometry, the preparation of an ultrathin selective layer on the porous ceramic hollow fibres is another promising way to increase the gas permeation flux without compromising the mechanical robustness. This is because the porous ceramic hollow fibres not only reduce the thickness of the membrane, but also provide mechanical strength for composite membranes. Graphene based membranes supported on ceramic hollow fibres were prepared for gas separation by Zhu et al. (Zhu et al., 2017b), and Huang et al. (Huang et al., 2017), since graphene and graphene oxide are potential materials for gas separation owing to their special structural and physicochemical properties. Zhu et al. (Zhu et al., 2017b) applied the vacuum-suction impregnation method to assemble the GO flakes on the yttrium-stabilized zirconia (YSZ) hollow fibres to fabricate graphene oxide (GO) membranes supported on porous (YSZ) hollow fibres. It was found that the 2D nano-channels formed by the GO layers provided a molecular sieving function with high gas selectivity. The hydrogen permeance and ideal selectivity of  $\text{H}_2/\text{N}_2$  were 133.4 GPU and 76, respectively (Zhu et al., 2017b). Huang et al. (Huang et al., 2017) prepared a ceramic  $\alpha\text{-Al}_2\text{O}_3$  hollow fibre supported GO membrane by using the vacuum suction method for hydrogen recovery from  $\text{H}_2/\text{CO}_2$  mixture. It was found that the GO membrane fabricated at 30 min showed  $\text{H}_2$  permeance of 300 GPU for both single gas and gas mixture. The ideal selectivity and gas separation factor were 15 and 10, respectively.

MOFs possess large internal surface areas, and uniform and tunable cavities, which make them desirable microporous material for gas adsorption and separation. Silicon nitride hollow fibres are good ceramic supports for membrane preparation because they possess excellent mechanical strength, chemical and thermal stability, and higher surface area (Zhang et al., 2012). Wang et al. (Wang et al., 2016a) fabricated a continuous ZIF-8 membrane on the outer surface of silicon nitride hollow fibres by using a one-step hydrothermal method. The single gas permeation behaviours of  $\text{H}_2$ ,  $\text{N}_2$ , and  $\text{CO}_2$  through ZIF-8 membranes were investigated at  $25^\circ\text{C}$ . It was found that the  $\text{N}_2$  permeance did not change with time, while  $\text{H}_2$  permeance increased firstly and kept steady at 2505 GPU owing to the high storage properties of ZIF-8, and  $\text{CO}_2$  permeance decreased firstly and kept steady at 345 GPU owing to the strong  $\text{CO}_2$  adsorption in ZIF-8. The ideal selectivity of  $\text{H}_2/\text{CO}_2$  and the gas separation factor were 7.26 and 11.67, respectively (Wang et al., 2016a).

The combination of two individual materials to form dual-phase membranes such as ceramic-metallic and ceramic-ceramic membranes is also applied to improve the gas separation performance of ceramic HFMs (Hashim et al., 2018). Chen et al. (Chen et al., 2020) synthesized  $\text{Ce}_{0.8}\text{Sm}_{0.2}\text{O}_{2-\delta}$  (SDC)-carbonate dual-phase HFMs using the phase inversion method for  $\text{CO}_2$  separation at high temperature. It was found that the SDC-carbonate hollow fibre membranes show not only high  $\text{CO}_2$  permeation flux, but also stable permeation behavior. The excellent  $\text{CO}_2$  fluxes can be attributed to a unique and superior structure and a thinner thickness of the hollow fibre membrane (Chen et al., 2020).

#### 4. Final remarks and conclusions

Gas separation is an important technique in many industrial processes from the energy and environment point of view. Membrane technology has been developed and applied in gas separation processes since 1980 owing to its diverse advantages compared with conventional gas separation technologies. Membrane plays a crucial role in gas separation process based on membrane technology. In this text, the fabrication methods and gas separation performances of different kinds of HFMs including asymmetric HFMs, TFC-HFMs, and MM-HFMs have been reviewed. The dope composition possesses a decisive effect on the gas separation performance of fabricated HFMs. Since HFMs are generally fabricated by the dry-jet wet spinning process, the spinning parameters have a significant influence on the morphology and structure of HFMs. Therefore, the optimization of spinning parameters such as bore fluid composition, flow rates of dope and bore fluids, and air gap is an important issue in the fabrication of the defect-free HFMs.

The gas separation of asymmetric HFMs strongly depends on the polymer material and the optimization of spinning parameters. More research should be conducted to develop high performance material for the fabrication of asymmetric HFMs with higher gas separation performance. TFC-HFMs are generally prepared by dip-coating and interfacial polymerization. The gas separation performance is directly influenced by the design of coating solution and coating conditions. To improve further the gas separation performance, the following factors must be considered: (1) material used for coating layer, (2) additives in coating solution and their modification methods, (3) improved interaction between the support hollow fibres and the coating layer, (4) elimination of coating solution intrusion into the substrate. Co-extrusion is a simple method to fabricate dual-layer HFMs in a one-step process. However, the delamination phenomenon must be avoided. To fabricate delamination-free dual-layer HFMs more work is required on the design of the outer dope solution and inner dope solution as well as the optimization of spinning parameters. Ceramic HFMs are able to be used at high temperature and pressure for oxygen separation and hydrogen recovery. Besides the gas separation process, Kang Li's group intensively investigated the performance of ceramic hollow fibre membrane reactors in catalytic gas phase reactions (García-García et al., 2012; García-García and Li, 2013). However, the cost of ceramic membranes is higher and the preparation process is complex. More research should be done to tackle the trade-off relationship between gas permeation flux and mechanical robustness.

As is shown in Table 7, a comprehensive comparison of the gas separation performance of various hollow fibre membranes is presented. MM-HFMs exhibited desirable gas permeance and higher selectivity. The incorporation of nanoparticles into HFMs improves not only the gas separation performance, but also mechanical strength and thermal stability. However, there are still challenges including the agglomeration of nanoparticles, the poor compatibility of polymers and nanoparticles, and the creation of microvoids. Nanoparticles modification has been conducted by different strategies to improve the compatibility with polymers and the uniform dispersion. What is more, the functional groups in modifiers enhance the interaction with gas species. As a result, the gas separation performance is significantly improved. A lot of work has been done on the preparation of flat sheet MMMs for gas separation

Table 7

A comprehensive comparison of gas separation performance of HFMs (SG -Single gas, MG - Mixed gas).

Membrane	Type of HFM	Fast gas/slow gas	Permeance of faster gas [GPU]	Selectivity	Testing conditions	Ref.
PTPESU	Asymmetric	O <sub>2</sub> /N <sub>2</sub>	16	6.5	25 °C, 3.55 bar except CO <sub>2</sub> at 1 bar, SG	(Yong et al., 2018)
		CO <sub>2</sub> /N <sub>2</sub>	85.1	34.0		
		CO <sub>2</sub> /CH <sub>4</sub>	85.1	35.5		
Polyaniline	Asymmetric	O <sub>2</sub> /N <sub>2</sub>	0.49	10.2	25 °C, 1–4 bars, SG	(Hasbullah et al., 2011)
		H <sub>2</sub> /N <sub>2</sub>	5.0	105.6		
		H <sub>2</sub> /CO <sub>2</sub>	5.0	7.9		
Matrimid	Asymmetric	H <sub>2</sub> /N <sub>2</sub>	66.05	74.4	30 °C, 2.3 bar, SG	(David et al., 2012)
		H <sub>2</sub> /CO		42.6		
		H <sub>2</sub> /CO <sub>2</sub>		5		
CTA	Asymmetric	CO <sub>2</sub> /CH <sub>4</sub>	110	22–28	35 °C, 31.3 bar, MG	(Liu et al., 2020)
		H <sub>2</sub> S/CH <sub>4</sub>				
PDMS/PSf	Thin film	O <sub>2</sub> /N <sub>2</sub>	18.31	4.56	28 °C, 5 bar, SG	(Chong et al., 2018)
PEBAX/PSf	composite		12.23	3.94		
PVA/PPO	Thin film	CO <sub>2</sub> /N <sub>2</sub>	791	40	25 °C, 2 bar, MG	(Dai et al., 2019)
	composite					
PDMS/PAN	Thin film	O <sub>2</sub> /N <sub>2</sub>	1000	2	25 °C, 3 bar, SG	(Liang et al., 2017)
	composite	CO <sub>2</sub> /N <sub>2</sub>	5000	11		
sPPSU/PBI	Dual-layer	H <sub>2</sub> /CO <sub>2</sub>	16.7	9.7	90 °C, 14.2 bar, MG	(Naderi et al., 2019)
Matrimid/PES	Dual-layer	O <sub>2</sub> /N <sub>2</sub>	12.57	7.74	25 °C, 5.06 bar, SG	(Ding et al., 2013)
			9.09	6.11		
			5.95	4.61		
TNTs/PSf	Mixed matrix	O <sub>2</sub> /N <sub>2</sub>	269	6.20	25 °C, 3 bar, SG	(Zulhairun et al., 2017)
		H <sub>2</sub> /CH <sub>4</sub>	120	57.86		
		CO <sub>2</sub> /CH <sub>4</sub>	26	25.93		
		CO <sub>2</sub> /N <sub>2</sub>	26	28.76		
ZIF-8/PBI	Mixed matrix	H <sub>2</sub> /CO <sub>2</sub>	107	18	150 °C, 7 bar, SG	(Etxeberria-Benavides et al., 2020a)
fumed silica/PSf	Mixed matrix	CO <sub>2</sub> /CH <sub>4</sub>	90.04	32.74	25 °C, 5 bar, SG	(Wahab et al., 2012)
		O <sub>2</sub> /N <sub>2</sub>	15.83	6.35		
Montmorillonite/PEI	Mixed matrix	CO <sub>2</sub> /CH <sub>4</sub>	130	18.35	25 °C, 4 bar, SG	(Jamil et al., 2017)
GO/YSZ	Ceramic	H <sub>2</sub> /N <sub>2</sub>	133.4	76	20 °C, 1 bar, SG	(Zhu et al., 2017b)
GO/ $\alpha$ -Al <sub>2</sub> O <sub>3</sub>	Ceramic	H <sub>2</sub> /CO <sub>2</sub>	300	15	25 °C, 1 bar, SG	(Huang et al., 2017)
		H <sub>2</sub> /O <sub>2</sub>	300	7.5		
		H <sub>2</sub> /N <sub>2</sub>	300	7.2		
		H <sub>2</sub> /CH <sub>4</sub>	300	6.4		
ZIF-8/Si <sub>3</sub> N <sub>4</sub>	Ceramic	H <sub>2</sub> /CO <sub>2</sub>	2505	7.26	25 °C, 2.5 bar, SG	(Wang et al., 2016a)

in literature. However, the research on MM-HFMs is not sufficient. It is necessary to incorporate nanoparticles into hollow fibre membranes to break the trade-off relationship between gas permeability and selectivity.

### Declaration of Competing Interest

The authors report no declarations of interest.

### Acknowledgements

The Authors would like to acknowledge the support of the National Centre for Research and Development (Poland) [DZP/V4-Korea-1/190/2018].

### References

- Adewole, J., Ahmad, A., Ismail, S., Leo, C., 2013. Current challenges in membrane separation of CO<sub>2</sub> from natural gas: a review. *Int. J. Greenhouse Gas Control* 17, 46–65.
- Askari, M., Yang, T., Chung, T.-S., 2012. Natural gas purification and olefin/paraffin separation using cross-linkable dual-layer hollow fiber membranes comprising  $\beta$ -Cyclodextrin. *J. Membr. Sci.* 423–424, 392–403.
- Athayde, D.D., Souza, D.F., Silva, A.M.A., Vasconcelos, D., Nunes, E.H.M., Diniz da Costa, J.C., Vasconcelos, W.L., 2016. Review of perovskite ceramic synthesis and membrane preparation methods. *Ceram. Int.* 42, 6555–6571.
- Babu, V.P., Kraftschik, B.E., Koros, W.J., 2018. Crosslinkable TEGMC asymmetric hollow fiber membranes for aggressive sour gas separations. *J. Membr. Sci.* 558, 94–105.
- Baig, M.I., Ingole, P.G., Choi, W.K., Park, S.R., Kang, E.C., Lee, H.K., 2016. Development of carboxylated TiO<sub>2</sub> incorporated thin film nanocomposite hollow fiber membranes for flue gas dehydration. *J. Membr. Sci.* 514, 622–635.
- Baker, R.W., 2012. *Membrane Technology and Applications*. John Wiley & Sons.
- Ban, Y., Li, Z., Li, Y., Peng, Y., Jin, H., Jiao, W., Guo, A., Wang, P., Yang, Q., Zhong, C., 2015. Confinement of ionic liquids in nanocages: tailoring the molecular sieving properties of ZIF-8 for membrane-based CO<sub>2</sub> capture. *Angew. Chem., Int. Ed.* 54, 15483–15487.
- Barooh, M., Mandal, B., 2019. Synthesis, characterization and CO<sub>2</sub> separation performance of novel PVA/PG/ZIF-8 mixed matrix membrane. *J. Membr. Sci.* 572, 198–209.
- Biondo, L.D., Duarte, J., Zeni, M., Godinho, M., 2018. A Dual-mode model interpretation of CO<sub>2</sub>/CH<sub>4</sub> permeability in polysulfone membranes at low pressures. *An. Acad. Bras. Cienc.* 90, 1855–1864.
- Cao, C., Wang, R., Chung, T.S., Liu, Y., 2002. Formation of high-performance 6FDA-2, 6-DAT asymmetric composite hollow fiber membranes for CO<sub>2</sub>/CH<sub>4</sub> separation. *J. Membr. Sci.* 209, 309–319.
- Chen, H.Z., Xiao, Y.C., Chung, T.-S., 2011. Multi-layer composite hollow fiber membranes derived from poly(ethylene glycol) (PEG) containing hybrid materials for CO<sub>2</sub>/N<sub>2</sub> separation. *J. Membr. Sci.* 381, 211–220.
- Chen, H.Z., Thong, Z., Li, P., Chung, T.-S., 2014. High performance composite hollow fiber membranes for CO<sub>2</sub>/H<sub>2</sub> and CO<sub>2</sub>/N<sub>2</sub> separation. *Int. J. Hydrogen Energy* 39, 5043–5053.
- Chen, Y., Wang, B., Zhao, L., Dutta, P., Ho, W.W., 2015. New Pebax®/zeolite Y composite membranes for CO<sub>2</sub> capture from flue gas. *J. Membr. Sci.* 495, 415–423.
- Chen, T., Wang, Z., Hu, J., Wai, M.H., Kawi, S., Lin, Y.S., 2020. High CO<sub>2</sub> permeability of ceramic-carbonate dual-phase hollow fiber membrane at medium-high temperature. *J. Membr. Sci.* 597, 117770.
- Cheng, L., Liu, G., Jin, W., 2019. Recent progress in two-dimensional-material membranes for gas separation. *Acta Phys. Chim. Sin.* 35, 1090–1098.
- Chi, Y., Li, T., Wang, B., Wu, Z., Li, K., 2017. Morphology, performance and stability of multi-bore capillary La<sub>0.6</sub>Sr<sub>0.4</sub>Co<sub>0.2</sub>Fe<sub>0.8</sub>O<sub>3.8</sub> oxygen transport membranes. *J. Membr. Sci.* 529, 224–233.
- Choi, S.-H., Sultan, M.M.B., Alsuwailam, A.A., Zuabi, S.M., 2019. Preparation and characterization of multilayer thin-film composite hollow fiber membranes for helium extraction from its mixtures. *Sep. Purif. Technol.* 222, 152–161.
- Chong, K.C., Lai, S.O., Lau, W.J., Thiam, H.S., Ismail, A.F., Roslan, R.A., 2018. Preparation, characterization, and performance evaluation of polysulfone hollow fiber membrane with PEBAX or PDMS coating for oxygen enhancement process. *Polymers* 10, 126.

- Chung, T.-S., Shieh, J.-J., Lau, W.W.Y., Srinivasan, M.P., Paul, D.R., 1999. Fabrication of multi-layer composite hollow fiber membranes for gas separation. *J. Membr. Sci.* 152, 211–225.
- Dai, Y., Johnson, J., Karvan, O., Sholl, D.S., Koros, W., 2012. Ultem®/ZIF-8 mixed matrix hollow fiber membranes for CO<sub>2</sub>/N<sub>2</sub> separations. *J. Membr. Sci.* 401, 76–82.
- Dai, Y., Ruan, X., Bai, F., Yu, M., Li, H., Zhao, Z., He, G., 2016a. High solvent resistance PTFE/PEI hollow fiber composite membrane for gas separation. *Appl. Surf. Sci.* 360, 164–173.
- Dai, Y., Ruan, X., Yan, Z., Yang, K., Yu, M., Li, H., Zhao, W., He, G., 2016b. Imidazole functionalized graphene oxide/PEBA mixed matrix membranes for efficient CO<sub>2</sub> capture. *Sep. Purif. Technol.* 166, 171–180.
- Dai, Z., Ansaloni, L., Deng, L., 2016c. Recent advances in multi-layer composite polymeric membranes for CO<sub>2</sub> separation: a review. *Green Energy Environ.* 1, 102–128.
- Dai, Z., Deng, J., Ansaloni, L., Janakiram, S., Deng, L., 2019. Thin-film-composite hollow fiber membranes containing amino acid salts as mobile carriers for CO<sub>2</sub> separation. *J. Membr. Sci.* 578, 61–68.
- David, O.C., Gorri, D., Nijmeijer, K., Ortiz, I., Urriaga, A., 2012. Hydrogen separation from multicomponent gas mixtures containing CO, N<sub>2</sub> and CO<sub>2</sub> using Matrimid® asymmetric hollow fiber membranes. *J. Membr. Sci.* 419–420, 49–56.
- Deibert, W., Ivanova, M.E., Baumann, S., Guillon, O., Meulenberg, W.A., 2017. Ion-conducting ceramic membrane reactors for high-temperature applications. *J. Membr. Sci.* 543, 79–97.
- Dilshad, M.R., Islam, A., Hamidullah, U., Jamshaid, F., Ahmad, A., Butt, M.T.Z., Ijaz, A., 2019. Effect of alumina on the performance and characterization of cross-linked PVA/PEG 600 blended membranes for CO<sub>2</sub>/N<sub>2</sub> separation. *Sep. Purif. Technol.* 210, 627–635.
- Ding, X., Cao, Y., Zhao, H., Wang, L., Yuan, Q., 2008. Fabrication of high performance Matrimid/polysulfone dual-layer hollow fiber membranes for O<sub>2</sub>/N<sub>2</sub> separation. *J. Membr. Sci.* 323, 352–361.
- Ding, X., Cao, Y., Zhao, H., Wang, L., 2013. Interfacial morphology between the two layers of the dual-layer asymmetric hollow fiber membranes fabricated by co-extrusion and dry-jet wet-spinning phase-inversion techniques. *J. Membr. Sci.* 444, 482–492.
- Ding, L., Wei, Y., Li, L., Zhang, T., Wang, H., Xue, J., Ding, L.-X., Wang, S., Caro, J., Gogotsi, Y., 2018. MXene molecular sieving membranes for highly efficient gas separation. *Nat. Commun.* 9, 1–7.
- Ding, R., Zheng, W., Yang, K., Dai, Y., Ruan, X., Yan, X., He, G., 2020. Amino-functional ZIF-8 nanocrystals by microemulsion based mixed linker strategy and the enhanced CO<sub>2</sub>/N<sub>2</sub> separation. *Sep. Purif. Technol.* 236, 116209.
- Dong, G., Hou, J., Wang, J., Zhang, Y., Chen, V., Liu, J., 2016. Enhanced CO<sub>2</sub>/N<sub>2</sub> separation by porous reduced graphene oxide/Pebax mixed matrix membranes. *J. Membr. Sci.* 520, 860–868.
- Esposito, E., Clarizia, G., Bernardo, P., Jansen, J.C., Sedláková, Z., Izák, P., Curcio, S., Cindio, B., Tasselli, F., 2015. Pebax®/PAN hollow fiber membranes for CO<sub>2</sub>/CH<sub>4</sub> separation. *Chem. Eng. Process.* 94, 53–61.
- Exteberria-Benavides, M., Johnson, T., Cao, S., Zornoza, B., Coronas, J., Sanchez-Lainez, J., Sabetghadam, A., Liu, X., Andres-Garcia, E., Kapteijn, F., 2020a. PBI mixed matrix hollow fiber membrane: Influence of ZIF-8 filler over H<sub>2</sub>/CO<sub>2</sub> separation performance at high temperature and pressure. *Sep. Purif. Technol.* 237, 116347.
- Exteberria-Benavides, M., Johnson, T., Cao, S., Zornoza, B., Coronas, J., Sanchez-Lainez, J., Sabetghadam, A., Liu, X., Andres-Garcia, E., Kapteijn, F., Gascon, J., David, O., 2020b. PBI mixed matrix hollow fiber membrane: influence of ZIF-8 filler over H<sub>2</sub>/CO<sub>2</sub> separation performance at high temperature and pressure. *Sep. Purif. Technol.* 237, 116347.
- Fam, W., Mansouri, J., Li, H., Chen, V., 2017a. Improving CO<sub>2</sub> separation performance of thin film composite hollow fiber with Pebax®1657/ionic liquid gel membranes. *J. Membr. Sci.* 537, 54–68.
- Fam, W., Mansouri, J., Li, H., Chen, V., 2017b. Improving CO<sub>2</sub> separation performance of thin film composite hollow fiber with Pebax® 1657/ionic liquid gel membranes. *J. Membr. Sci.* 537, 54–68.
- Favvas, E.P., Katsaros, F.K., Papageorgiou, S.K., Sapalidis, A.A., Mitropoulos, A.C., 2017. A review of the latest development of polyimide based membranes for CO<sub>2</sub> separations. *React. Funct. Polym.* 120, 104–130.
- Feng, C., Khulbe, K., Matsuura, T., Ismail, A., 2013. Recent progresses in polymeric hollow fiber membrane preparation, characterization and applications. *Sep. Purif. Technol.* 111, 43–71.
- Gao, J., Thong, Z., Wang, K.Y., Chung, T.-S., 2017. Fabrication of loose inner-selective polyethersulfone (PES) hollow fibers by one-step spinning process for nanofiltration (NF) of textile dyes. *J. Membr. Sci.* 541, 413–424.
- Gao, J., Mao, H., Jin, H., Chen, C., Feldhoff, A., Li, Y., 2020. Functionalized ZIF-7/Pebax® 2533 mixed matrix membranes for CO<sub>2</sub>/N<sub>2</sub> separation. *Microporous Mesoporous Mater.*, 110030.
- García-García, F.R., Li, K., 2013. New catalytic reactors prepared from symmetric and asymmetric ceramic hollow fibres. *Appl. Catal.*, A 456, 1–10.
- García-García, F.R., Kingsbury, B.F.K., Rahman, M.A., Li, K., 2012. Asymmetric ceramic hollow fibres applied in heterogeneous catalytic gas phase reactions. *Catal. Today* 193, 20–30.
- George, G., Bhorja, N., AlHallaq, S., Abdala, A., Mittal, V., 2016. Polymer membranes for acid gas removal from natural gas. *Sep. Purif. Technol.* 158, 333–356.
- Gong, X.-Y., Huang, Z.-H., Zhang, H., Liu, W.-L., Ma, X.-H., Xu, Z.-L., Tang, C.Y., 2020. Novel High-Flux Positively Charged Composite Membrane Incorporating Titanium-Based MOFs for Heavy Metal Removal, 398, 125706.
- Guo, A., Ban, Y., Yang, K., Zhou, Y., Cao, N., Zhao, M., Yang, W., 2020. Molecular sieving mixed matrix membranes embodying nano-fillers with extremely narrow pore-openings. *J. Membr. Sci.* 601, 117880.
- Hasbullah, H., Kumbharkar, S., Ismail, A.F., Li, K., 2011. Preparation of polyaniline asymmetric hollow fiber membranes and investigation towards gas separation performance. *J. Membr. Sci.* 366, 116–124.
- Hashim, S.M., Mohamed, A.R., Bhatia, S., 2010. Current status of ceramic-based membranes for oxygen separation from air. *Adv. Colloid Interface Sci.* 160, 88–100.
- Hashim, S.S., Mohamed, A.R., Bhatia, S., 2011. Oxygen separation from air using ceramic-based membrane technology for sustainable fuel production and power generation. *Renewable Sustainable Energy Rev.* 15, 1284–1293.
- Hashim, S.S., Somalu, M.R., Loh, K.S., Liu, S., Zhou, W., Sunarso, J., 2018. Perovskite-based proton conducting membranes for hydrogen separation: a review. *Int. J. Hydrogen Energy* 43, 15281–15305.
- He, H., Li, R., Yang, Z., Chai, L., Jin, L., Alhassan, S.I., Ren, L., Wang, H., Huang, L., 2020. Preparation of MOFs and MOFs derived materials and their catalytic application in air pollution: a review. *Catal. Today*. <https://doi.org/10.1016/j.cattod.2020.1002.1033>.
- Holda, A.K., Vankelecom, I.F., 2015. Understanding and guiding the phase inversion process for synthesis of solvent resistant nanofiltration membranes. *J. Appl. Polym. Sci.* 132, 42130.
- Hu, L., Cheng, J., Li, Y., Liu, J., Zhou, J., Cen, K., 2017. Amino-functionalized surface modification of polyacrylonitrile hollow fiber-supported polydimethylsiloxane membranes. *Appl. Surf. Sci.* 413, 27–34.
- Hu, L., Cheng, J., Li, Y., Liu, J., Zhou, J., Cen, K., 2018. In-situ grafting to improve polarity of polyacrylonitrile hollow fiber-supported polydimethylsiloxane membranes for CO<sub>2</sub> separation. *J. Colloid Interface Sci.* 510, 12–19.
- Hu, C.-C., Cheng, P.-H., Chou, S.-C., Lai, C.-L., Huang, S.-H., Tsai, H.-A., Hung, W.-S., Lee, K.-R., 2020. Separation behavior of amorphous amino-modified silica nanoparticle/polyimide mixed matrix membranes for gas separation. *J. Membr. Sci.* 595, 117542.
- Huang, K., Yuan, J., Shen, G., Liu, G., Jin, W., 2017. Graphene oxide membranes supported on the ceramic hollow fibre for efficient H<sub>2</sub> recovery. *Chin. J. Chem. Eng.* 25, 752–759.
- Huang, G., Isfahani, A.P., Muchtar, A., Sakurai, K., Shrestha, B.B., Qin, D., Yamaguchi, D., Sivaniah, E., Ghalei, B., 2018. Pebax/ionic liquid modified graphene oxide mixed matrix membranes for enhanced CO<sub>2</sub> capture. *J. Membr. Sci.* 565, 370–379.
- Ismail, A., Lorna, W., 2003. Suppression of plasticization in polysulfone membranes for gas separations by heat-treatment technique. *Sep. Purif. Technol.* 30, 37–46.
- Ismail, A., Dunkin, I., Gallivan, S.L., Shilton, S.J., 1999. Production of super selective polysulfone hollow fiber membranes for gas separation. *Polymer* 40, 6499–6506.
- Jamil, A., Ching, O.P., Shariff, A.M., 2017. Mixed matrix hollow fibre membrane comprising polyetherimide and modified montmorillonite with improved filler dispersion and CO<sub>2</sub>/CH<sub>4</sub> separation performance. *Appl. Clay Sci.* 143, 115–124.
- Jamil, A., Oh, P.C., Shariff, A.M., 2018. Polyetherimide-montmorillonite mixed matrix hollow fibre membranes: effect of inorganic/organic montmorillonite on CO<sub>2</sub>/CH<sub>4</sub> separation. *Sep. Purif. Technol.* 206, 256–267.
- Jesswein, I., Hirth, T., Schiestel, T., 2017. Continuous dip coating of PVDF hollow fiber membranes with PVA for humidification. *J. Membr. Sci.* 541, 281–290.
- Jiang, L., Chung, T.-S., Li, D.F., Cao, C., Kulprathipanja, S., 2004. Fabrication of Matrimid/polyethersulfone dual-layer hollow fiber membranes for gas separation. *J. Membr. Sci.* 240, 91–103.
- Jiang, Y., Liu, C., Caro, J., Huang, A., 2019. A new UiO-66-NH<sub>2</sub> based mixed-matrix membranes with high CO<sub>2</sub>/CH<sub>4</sub> separation performance. *Microporous Mesoporous Mater.* 274, 203–211.
- Jo, E.-S., An, X., Ingole, P.G., Choi, W.-K., Park, Y.-S., Lee, H.-K., 2017. CO<sub>2</sub>/CH<sub>4</sub> separation using inside coated thin film composite hollow fiber membranes prepared by interfacial polymerization. *Chin. J. Chem. Eng.* 25, 278–287.
- Jue, M.L., Breedveld, V., Lively, R.P., 2017. Defect-free PIM-1 hollow fiber membranes. *J. Membr. Sci.* 530, 33–41.
- Kardani, R., Asghari, M., Hamedani, N.F., Afsari, M., 2020. Mesoporous copper zinc bimetallic imidazolate MOF as nanofiller to improve gas separation performance of PEBA-based membranes. *J. Ind. Eng. Chem.* 83, 100–110.
- Karimi, S., Firouzfard, E., Khoshchehreh, M.R., 2019. Assessment of gas separation properties and CO<sub>2</sub> plasticization of polysulfone/polyethylene glycol membranes. *J. Pet. Sci. Eng.* 173, 13–19.
- Kentish, S.E., Scholes, C.A., Stevens, G.W., 2008. Carbon Dioxide Separation through Polymeric Membrane Systems for Flue Gas Applications, 1, pp. 52–66.
- Khan, I.U., Othman, M.H.D., Jilani, A., Ismail, A., Hashim, H., Jaafar, J., Zulhairun, A., Rahman, M.A., Rehman, G.U., 2020. ZIF-8 based polysulfone hollow fiber membranes for natural gas purification. *Polym. Test.*, 106415.
- Kumbharkar, S.C., Liu, Y., Li, K., 2011. High performance polybenzimidazole based asymmetric hollow fibre membranes for H<sub>2</sub>/CO<sub>2</sub> separation. *J. Membr. Sci.* 375, 231–240.
- Li, D.F., Chung, T.-S., Wang, R., Liu, Y., 2002. Fabrication of fluoropolyimide/polyethersulfone (PES) dual-layer asymmetric hollow fiber membranes for gas separation. *J. Membr. Sci.* 198, 211–223.
- Li, Y., Cao, C., Chung, T.-S., Pramoda, K.P., 2004. Fabrication of dual-layer polyethersulfone (PES) hollow fiber membranes with an ultrathin dense-selective layer for gas separation. *J. Membr. Sci.* 245, 53–60.
- Li, Y., Chung, T.-S., Huang, Z., Kulprathipanja, S., 2006. Dual-layer polyethersulfone (PES)/BTDA-TDI/MDI co-polyimide (P84) hollow fiber membranes with a submicron PES-zeolite beta mixed matrix dense-selective layer for gas separation. *J. Membr. Sci.* 277, 28–37.



- Li, P., Wang, Z., Qiao, Z., Liu, Y., Cao, X., Li, W., Wang, J., Wang, S., 2015a. Recent developments in membranes for efficient hydrogen purification. *J. Membr. Sci.* 495, 130–168.
- Li, Y., Wang, S., He, G., Wu, H., Pan, F., Jiang, Z., 2015b. Facilitated transport of small molecules and ions for energy-efficient membranes. *Chem. Soc. Rev.* 44, 103–118.
- Li, H., Choi, W., Ingole, P.G., Lee, H.K., Baek, I.H., 2016. Oxygen separation membrane based on facilitated transport using cobalt tetraphenylporphyrin-coated hollow fiber composites. *Fuel* 185, 133–141.
- Li, T., Kamhangdatepon, T., Wang, B., Hartley, U.W., Li, K., 2019. New bio-inspired design for high-performance and highly robust  $\text{La}_{0.6}\text{Sr}_{0.4}\text{Co}_{0.2}\text{Fe}_{0.8}\text{O}_{3-\delta}$  membranes for oxygen permeation. *J. Membr. Sci.* 578, 203–208.
- Liang, C.Z., Yong, W.F., Chung, T.-S., 2017. High-performance composite hollow fiber membrane for flue gas and air separations. *J. Membr. Sci.* 541, 367–377.
- Liang, C.Z., Liu, J.T., Lai, J.-Y., Chung, T.-S., 2018. High-performance multiple-layer PIM composite hollow fiber membranes for gas separation. *J. Membr. Sci.* 563, 93–106.
- Liang, C.Z., Chung, T.-S., Lai, J.-Y., 2019. A review of polymeric composite membranes for gas separation and energy production. *Prog. Polym. Sci.* 97, 101141.
- Liu, L., Chakma, A., Feng, X., 2004a. Preparation of hollow fiber poly(ether block amide)/polysulfone composite membranes for separation of carbon dioxide from nitrogen. *Chem. Eng. J.* 105, 43–51.
- Liu, L., Chakma, A., Feng, X., 2004b. Preparation of hollow fiber poly(ether block amide)/polysulfone composite membranes for separation of carbon dioxide from nitrogen. *Chem. Eng. J.* 105, 43–51.
- Liu, Y., Liu, Z., Morisato, A., Bhuwani, N., Chinn, D., Koros, W.J., 2020. Natural gas sweetening using a cellulose triacetate hollow fiber membrane illustrating controlled plasticization benefits. *J. Membr. Sci.* 601, 117910.
- Ma, C., Koros, W.J., 2018. Physical aging of ester-cross-linked hollow fiber membranes for natural gas separations and mitigation thereof. *J. Membr. Sci.* 551, 214–221.
- Magueijo, V., Anderson, L., Fletcher, A., Shilton, S.J., 2013a. Polysulfone mixed matrix gas separation hollow fibre membranes filled with polymer and carbon xerogels. *Chem. Eng. Sci.* 92, 13–20.
- Magueijo, V.M., Anderson, L.G., Fletcher, A.J., Shilton, S.J., 2013b. Polysulfone mixed matrix gas separation hollow fibre membranes filled with polymer and carbon xerogels. *Chem. Eng. Sci.* 92, 13–20.
- Meng, X., Fan, Y., Zhu, J., Jin, Y., Li, C., Yang, N., Zhao, J., Sunarso, J., Liu, S., 2019. Improving hydrogen permeation and interface property of ceramic-supported graphene oxide membrane via embedding of silicalite-1 zeolite into  $\text{Al}_2\text{O}_3$  hollow fiber. *Sep. Purif. Technol.* 227, 115712.
- Meshkat, S., Kaliaguine, S., Rodrigue, D., 2020. Comparison between ZIF-67 and ZIF-8 in Pebax® MH-1657 mixed matrix membranes for  $\text{CO}_2$  separation. *Sep. Purif. Technol.* 235, 116150.
- Mohammed, S.A., Nasir, A.M., Aziz, F., Kumar, G., Sallehuddin, W., Jaafar, J., Lau, W.J., Yusof, N., Salleh, W.N.W., Ismail, A.F., 2019.  $\text{CO}_2/\text{N}_2$  selectivity enhancement of PEBAX MH 1657/Aminated partially reduced graphene oxide mixed matrix composite membrane. *Sep. Purif. Technol.* 223, 142–153.
- Naderi, A., Chung, T.-S., Weber, M., Maletzko, C., 2019. High performance dual-layer hollow fiber membrane of sulfonated polyphenylsulfone/Polybenzimidazole for hydrogen purification. *J. Membr. Sci.* 591, 117292.
- Nigiz, F.U., Hilmioglu, N.D., 2020. Enhanced hydrogen purification by graphene - Poly(Dimethyl siloxane) membrane. *Int. J. Hydrogen Energy* 45, 3549–3557.
- Ozen, H.A., Ozturk, B., 2019. Gas separation characteristic of mixed matrix membrane prepared by MOF-5 including different metals. *Sep. Purif. Technol.* 211, 514–521.
- Park, H.J., Bhatti, U.H., Nam, S.C., Park, S.Y., Lee, K.B., Baek, I.H., 2019. Nafion/TiO<sub>2</sub> nanoparticle decorated thin film composite hollow fiber membrane for efficient removal of SO<sub>2</sub> gas. *Sep. Purif. Technol.* 211, 377–390.
- Peng, N., Chung, T.-S., Chng, M.L., Aw, W., 2010. Evolution of ultra-thin dense-selective layer from single-layer to dual-layer hollow fibers using novel Extem® polyetherimide for gas separation. *J. Membr. Sci.* 360, 48–57.
- Peng, N., Widjojo, N., Sukitpeneit, P., Teoh, M.M., Lipscomb, G.G., Chung, T.-S., Lai, J.-Y., 2012. Evolution of polymeric hollow fibers as sustainable technologies: past, present, and future. *Prog. Polym. Sci.* 37, 1401–1424.
- Qiao, Z., Wang, Z., Zhao, S., Yuan, S., Wang, J., Wang, S., 2013. High adsorption performance polymers modified by small molecules containing functional groups for  $\text{CO}_2$  separation. *RSC Adv.* 3, 50–54.
- Qin, J.-J., Gu, J., Chung, T.-S., 2001. Effect of wet and dry-jet wet spinning on the shear-induced orientation during the formation of ultrafiltration hollow fiber membranes. *J. Membr. Sci.* 182, 57–75.
- Robeson, L.M., 2008. The Upper Bound Revisited, 320, pp. 390–400.
- Scholes, C.A., Stevens, G.W., Kentish, S.E., 2012. Membrane gas separation applications in natural gas processing. *Fuel* 96, 15–28.
- Seong, M.S., Kong, C.I., Park, B.R., Lee, Y., Na, B.K., Kim, J.H., 2020. Optimization of pilot-scale 3-stage membrane process using asymmetric polysulfone hollow fiber membranes for production of high-purity  $\text{CH}_4$  and  $\text{CO}_2$  from crude biogas. *Chem. Eng. J.* 384, 123342.
- Shamsabadi, A.A., Kargari, A., Bahaheidari, M.B., 2014. Preparation, characterization and gas permeation properties of PDMS/PEI composite asymmetric membrane for effective separation of hydrogen from  $\text{H}_2/\text{CH}_4$  mixed gas. *Int. J. Hydrogen Energy* 39, 1410–1419.
- Shamsabadi, A.A., Seidi, F., Salehi, E., Nozari, M., Rahimpour, A., Soroush, M., 2017. Efficient  $\text{CO}_2$ -removal using novel mixed-matrix membranes with modified TiO<sub>2</sub> nanoparticles. *J. Mater. Chem. A* 5, 4011–4025.
- Sharpe, I.D., Ismail, A.F., Shilton, S.J., 1999. A study of extrusion shear and forced convection residence time in the spinning of polysulfone hollow fiber membranes for gas separation. *Sep. Purif. Technol.* 17, 101–109.
- Shen, J., Liu, G., Huang, K., Li, Q., Guan, K., Li, Y., Jin, W., 2016. UiO-66-polyether block amide mixed matrix membranes for  $\text{CO}_2$  separation. *J. Membr. Sci.* 513, 155–165.
- Siagian, U.W.R., Raksajati, A., Himma, N.F., Khoiruddin, K., Wenten, I.G., 2019. Membrane-based carbon capture technologies: membrane gas separation vs. Membrane contactor. *J. Nat. Gas Sci. Eng.* 67, 172–195.
- Simons, K., Nijmeijer, K., Sala, J.G., van der Werf, H., Benes, N.E., Dingemans, T.J., Wessling, M., 2010.  $\text{CO}_2$  sorption and transport behavior of ODPa-based polyetherimide polymer films. *Polymer* 51, 3907–3917.
- Sukitpeneit, P., Chung, T.-S., 2014. Fabrication and use of hollow fiber thin film composite membranes for ethanol dehydration. *J. Membr. Sci.* 450, 124–137.
- Sun, J., Li, Q., Chen, G., Duan, J., Liu, G., Jin, W., 2019. MOF-801 incorporated PEBA mixed-matrix composite membranes for  $\text{CO}_2$  capture. *Sep. Purif. Technol.* 217, 229–239.
- Tham, H.M., Wang, K.Y., Hua, D., Japip, S., Chung, T.-S., 2017. From ultrafiltration to nanofiltration: hydrazine cross-linked polyacrylonitrile hollow fiber membranes for organic solvent nanofiltration. *J. Membr. Sci.* 542, 289–299.
- Tow, E.W., Warsinger, D.M., Truworthy, A.M., Swaminathan, J., Thiel, G.P., Zubair, S.M., Myerson, A.S., 2018. Comparison of fouling propensity between reverse osmosis, forward osmosis, and membrane distillation. *J. Membr. Sci.* 556, 352–364.
- Tsai, H.-A., Chen, Y.-L., Huang, S.-H., Hu, C.-C., Hung, W.-S., Lee, K.-R., Lai, J.-Y., 2018. Preparation of polyamide/polyacrylonitrile Composite Hollow Fiber Membrane by Synchronous Procedure of Spinning and Interfacial Polymerization, 551, pp. 261–272.
- Ullah Khan, I., Othman, M.H.D., Ismail, A.F., Matsuura, T., Hashim, H., Nordin, N.A.H.M., Rahman, M.A., Jaafar, J., Jilani, A., 2018. Status and improvement of dual-layer hollow fiber membranes via co-extrusion process for gas separation: a review. *J. Nat. Gas Sci. Eng.* 52, 215–234.
- Vinoba, M., Bhagiyalakshmi, M., Alqaheem, Y., Alomair, A.A., Pérez, A., Rana, M.S., 2017. Recent progress of fillers in mixed matrix membranes for  $\text{CO}_2$  separation: a review. *Sep. Purif. Technol.* 188, 431–450.
- Wahab, M.F.A., Ismail, A.F., Shilton, S.J., 2012. Studies on gas permeation performance of asymmetric polysulfone hollow fibre mixed matrix membranes using nanosized fumed silica as fillers. *Sep. Purif. Technol.* 86, 41–48.
- Wang, D., Li, K., Teo, W.K., 2002. Preparation of asymmetric polyetherimide hollow fibre membrane with high gas selectivities. *J. Membr. Sci.* 208, 419–426.
- Wang, M., Wang, Z., Li, S., Zhang, C., Wang, J., Wang, S., 2013. A high performance antioxidant and acid resistant membrane prepared by interfacial polymerization for  $\text{CO}_2$  separation from flue gas. *Energy Environ. Sci.* 6, 539–551.
- Wang, J.-W., Li, N.-X., Li, Z.-R., Wang, J.-R., Xu, X., Chen, C.-S., 2016a. Preparation and gas separation properties of Zeolitic imidazolate frameworks-8 (ZIF-8) membranes supported on silicon nitride ceramic hollow fibers. *Ceram. Int.* 42, 8949–8954.
- Wang, S., Wu, Y., Zhang, N., He, G., Xin, Q., Wu, X., Wu, H., Cao, X., Guiver, M.D., Jiang, Z., 2016b. A highly permeable graphene oxide membrane with fast and selective transport nanochannels for efficient carbon capture. *Energy Environ. Sci.* 9, 3107–3112.
- Wang, M., Wang, Z., Zhao, S., Wang, J., Wang, S., 2017. Recent advances on mixed matrix membranes for  $\text{CO}_2$  separation. *Chin. J. Chem. Eng.* 25, 1581–1597.
- Wang, D., Yao, D., Wang, Y., Wang, F., Xin, Y., Song, S., Zhang, Z., Su, F., Zheng, Y., 2019. Carbon nanotubes and graphene oxide-based solvent-free hybrid nanofluids functionalized mixed-matrix membranes for efficient  $\text{CO}_2/\text{N}_2$  separation. *Sep. Purif. Technol.* 221, 421–432.
- Wei, Y., Yang, W., Caro, J., Wang, H., 2013. Dense ceramic oxygen permeable membranes and catalytic membrane reactors. *Chem. Eng. J.* 220, 185–203.
- Widjojo, N., Chung, T.-S., Kulprathipanja, S., 2008. The fabrication of hollow fiber membranes with double-layer mixed-matrix materials for gas separation. *J. Membr. Sci.* 325, 326–335.
- Wijmans, J.G., Baker, R.W., 1995. The solution-diffusion model: a review. *J. Membr. Sci.* 107, 1–21.
- Woo, K.T., Lee, J., Dong, G., Kim, J.S., Do, Y.S., Hung, W.-S., Lee, K.-R., Barbieri, G., Drioli, E., Lee, Y.M., 2015. Fabrication of thermally rearranged (TR) polybenzoxazole hollow fiber membranes with superior  $\text{CO}_2/\text{N}_2$  separation performance. *J. Membr. Sci.* 490, 129–138.
- Wu, J., Japip, S., Chung, T.-S., 2020. Infiltrating molecular gatekeepers with coexisting molecular solubility and 3D-intrinsic porosity into a microporous polymer scaffold for gas separation. *J. Mater. Chem. A* 8, 6196–6209.
- Xie, K., Fu, Q., Qiao, G.G., Webley, P.A., 2019. Recent progress on fabrication methods of polymeric thin film gas separation membranes for  $\text{CO}_2$  capture. *J. Membr. Sci.* 572, 38–60.
- Xin, Q., Ma, F., Zhang, L., Wang, S., Li, Y., Ye, H., Ding, X., Lin, L., Zhang, Y., Cao, X., 2019. Interface engineering of mixed matrix membrane via  $\text{CO}_2$ -philic polymer brush functionalized graphene oxide nanosheets for efficient gas separation. *J. Membr. Sci.* 586, 23–33.
- Xu, L., Zhang, C., Rungta, M., Qiu, W., Liu, J., Koros, W.J., 2014. Formation of defect-free 6FDA-DAM asymmetric hollow fiber membranes for gas separations. *J. Membr. Sci.* 459, 223–232.
- Xu, J., Wu, H., Wang, Z., Qiao, Z., Zhao, S., Wang, J., 2018. Recent advances on the membrane processes for  $\text{CO}_2$  separation. *Chin. J. Chem. Eng.* 26, 2280–2291.
- Ye, Z., Chen, Y., Li, H., He, G., Deng, M., 2005. Preparation of a novel polysulfone/polyethylene oxide/silicone rubber multilayer composite membrane for hydrogen-nitrogen separation. *Mater. Chem. Phys.* 94, 288–291.
- Yong, W.F., Chung, T.-S., Weber, M., Maletzko, C., 2018. New polyethersulfone (PESU) hollow fiber membranes for  $\text{CO}_2$  capture. *J. Membr. Sci.* 552, 305–314.
- Zhang, J.-W., Fang, H., Hao, L.-Y., Xu, X., Chen, C.-S., 2012. Preparation of silicon nitride hollow fibre membrane for desalination. *Mater. Lett.* 68, 457–459.
- Zhang, Y., Sunarso, J., Liu, S., Wang, R., 2013. Current status and development of membranes for  $\text{CO}_2/\text{CH}_4$  separation: a review. *Int. J. Greenhouse Gas Control* 12, 84–107.

- Zhang, X., Zhang, T., Wang, Y., Li, J., Liu, C., Li, N., Liao, J., 2018. Mixed-matrix membranes based on Zn/Ni-ZIF-8-PEBA for high performance CO<sub>2</sub> separation. *J. Membr. Sci.* 560, 38–46.
- Zhang, J., Xin, Q., Li, X., Yun, M., Xu, R., Wang, S., Li, Y., Lin, L., Ding, X., Ye, H., Zhang, Y., 2019. Mixed matrix membranes comprising aminosilane-functionalized graphene oxide for enhanced CO<sub>2</sub> separation. *J. Membr. Sci.* 570–571, 343–354.
- Zhao, H., Feng, L., Ding, X., Zhao, Y., Tan, X., Zhang, Y., 2018. The nitrogen-doped porous carbons/PIM mixed-matrix membranes for CO<sub>2</sub> separation. *J. Membr. Sci.* 564, 800–805.
- Zhou, H., Su, Y., Chen, X., Luo, J., Tan, S., Wan, Y., 2016. Plasma modification of substrate with poly (methylhydrosiloxane) for enhancing the interfacial stability of PDMS/PAN composite membrane. *J. Membr. Sci.* 520, 779–789.
- Zhu, H., Jie, X., Cao, Y., 2017a. Fabrication of functionalized MOFs incorporated mixed matrix hollow fiber membrane for gas separation. *J. Chem.* 2017, 2548957.
- Zhu, J., Meng, X., Zhao, J., Jin, Y., Yang, N., Zhang, S., Sunarso, J., Liu, S., 2017b. Facile hydrogen/nitrogen separation through graphene oxide membranes supported on YSZ ceramic hollow fibers. *J. Membr. Sci.* 535, 143–150.
- Zhu, H., Jie, X., Wang, L., Kang, G., Liu, D., Cao, Y., 2018. Enhanced gas separation performance of mixed matrix hollow fiber membranes containing post-functionalized S-MIL-53. *J. Energy Chem.* 27, 781–790.
- Zhu, H., Yuan, J., Zhao, J., Liu, G., Jin, W., 2019a. Enhanced CO<sub>2</sub>/N<sub>2</sub> separation performance by using dopamine/polyethyleneimine-grafted TiO<sub>2</sub> nanoparticles filled PEBA mixed-matrix membranes. *Sep. Purif. Technol.* 214, 78–86.
- Zhu, W., Li, X., Sun, Y., Guo, R., Ding, S., 2019b. Introducing hydrophilic ultra-thin ZIF-L into mixed matrix membranes for CO<sub>2</sub>/CH<sub>4</sub> separation. *RSC Adv.* 9, 23390–23399.
- Zulhairun, A.K., Fachrurrazi, Z.G., Nur Izwanne, M., Ismail, A.F., 2015. Asymmetric hollow fiber membrane coated with polydimethylsiloxane–metal organic framework hybrid layer for gas separation. *Sep. Purif. Technol.* 146, 85–93.
- Zulhairun, A., Subramaniam, M., Samavati, A., Ramli, M., Krishparao, M., Goh, P., Ismail, A., 2017. High-flux polysulfone mixed matrix hollow fiber membrane incorporating mesoporous titania nanotubes for gas separation. *Sep. Purif. Technol.* 180, 13–22.

## **Publication II**

**G. Li**, W. Kujawski, K. Knozowska, J. Kujawa, The Effects of PEI Hollow Fiber Substrate Characteristics on PDMS/PEI Hollow Fiber Membranes for CO<sub>2</sub> /N<sub>2</sub> Separation, *Membranes*, 11 (2021) 56.

## Article

# The Effects of PEI Hollow Fiber Substrate Characteristics on PDMS/PEI Hollow Fiber Membranes for CO<sub>2</sub>/N<sub>2</sub> Separation

Guoqiang Li <sup>1</sup>, Wojciech Kujawski <sup>1,2,\*</sup> , Katarzyna Knozowska <sup>1</sup> and Joanna Kujawa <sup>1</sup> <sup>1</sup> Faculty of Chemistry, Nicolaus Copernicus University in Toruń, 7, Gagarina Street, 87-100 Toruń, Poland<sup>2</sup> National Research Nuclear University MEPhI, 31, Kashira Hwy, 115409 Moscow, Russia

\* Correspondence: kujawski@chem.umk.pl; Tel.: +48-566114517

**Abstract:** The CO<sub>2</sub> separation from flue gas based on membrane technology has drawn great attention in the last few decades. In this work, polyetherimide (PEI) hollow fibers were fabricated by using a dry-jet-wet spinning technique. Subsequently, the composite hollow fiber membranes were prepared by dip coating of polydimethylsiloxane (PDMS) selective layer on the outer surface of PEI hollow fibers. The hollow fibers spun from various spinning conditions were fully characterized. The influence of hollow fiber substrates on the CO<sub>2</sub>/N<sub>2</sub> separation performance of PDMS/PEI composite membranes was estimated by gas permeance and ideal selectivity. The prepared composite membrane where the hollow fiber substrate was spun from 20 wt% of dope solution, 12 mL/min of bore fluid (water) flow rate exhibited the highest ideal selectivity equal to 21.3 with CO<sub>2</sub> permeance of 59 GPU. It was found that the dope concentration, bore fluid flow rate and bore fluid composition affect the porous structure, surface morphology and dimension of hollow fibers. The bore fluid composition significantly influenced the gas permeance and ideal selectivity of the PDMS/PEI composite membrane. The prepared PDMS/PEI composite membranes possess comparable CO<sub>2</sub>/N<sub>2</sub> separation performance to literature ones.



**Citation:** Li, G.; Kujawski, W.; Knozowska, K.; Kujawa, J. The Effects of PEI Hollow Fiber Substrate Characteristics on PDMS/PEI Hollow Fiber Membranes for CO<sub>2</sub>/N<sub>2</sub> Separation. *Membranes* **2021**, *11*, 56. <https://doi.org/10.3390/membranes11010056>

Received: 22 December 2020

Accepted: 12 January 2021

Published: 14 January 2021

**Publisher's Note:** MDPI stays neutral with regard to jurisdictional claims in published maps and institutional affiliations.



**Copyright:** © 2021 by the authors. Licensee MDPI, Basel, Switzerland. This article is an open access article distributed under the terms and conditions of the Creative Commons Attribution (CC BY) license (<https://creativecommons.org/licenses/by/4.0/>).

**Keywords:** hollow fiber; PDMS coating; gas separation

## 1. Introduction

With the rapid increase in the global population and the fast development of energy-intensive industries, the consumption of fossil fuels, i.e., coal, petroleum and natural gas, is drastically growing [1]. Consequently, the continuous increase in CO<sub>2</sub> emissions is inevitable. As a result, according to the Intergovernmental Panel on Climate Change (IPCC) reports and the most comprehensive research, the CO<sub>2</sub> concentration in the atmosphere is approaching 400 ppm which is higher than the safe level of CO<sub>2</sub> concentration of 350 ppm [2]. Flue gas containing mainly CO<sub>2</sub> and N<sub>2</sub> from coal-fired power plants occupies 50–60% of the total global CO<sub>2</sub> emission [3]. The excessive CO<sub>2</sub> emission has caused anthropogenic climate change and global warming which has brought about various environmental problems, including rising sea levels, changes in ecosystems, loss of biodiversity and reduction in crop yields [4,5]. Therefore, there is an urgent need to reduce the CO<sub>2</sub> emissions and the CO<sub>2</sub> concentration in the atmosphere. Carbon capture and storage (CCS) is one of the most important technology used to reduce CO<sub>2</sub> emissions [2,6]. In comparison to the traditional CO<sub>2</sub> separation technologies e.g., absorption, adsorption, and cryogenic distillation, membrane technology possesses many advantages such as simple process operation, small footprint, energy efficiency and cost effectiveness [1,5–7].

Hollow fiber membranes have a promising future in various gas separation processes due to their advantages, e.g., high packing density and a self-supporting structure [8–10]. Hollow fibers are generally fabricated by using the dry-jet wet spinning technique. The structure, morphology, outer and inner diameters, wall thickness of hollow fibers were significantly influenced by the fabrication parameters, e.g., air gap length, bore fluid, dope

composition and flow rates of dope and bore fluid [7,11–14]. Hasbullah et al. [12] found that the wall thickness of polyaniline (PAni) hollow fiber decreased while the skin layer thickness increased when the air gap length increased. These findings were attributed to the elongation stress resulting in a more packed structure and longer evaporation time during the dry phase separation in the air gap. Wang et al. [15] found that the addition of methanol, acetone, or a mixture of methanol/acetone into dope solution could tune the morphology of polyetherimide (PEI) hollow fibers resulting in enhanced gas separation performance. Kumbharkar et al. [7] found that increasing the solvent concentration in bore fluid is helpful for the formation of loose skin on the inner surface and the suppression of finger-like macro-voids in the substructure of polybenzimidazole (PBI) hollow fibers. Woo et al. [11] found that the addition of tetrahydrofuran (THF) is beneficial in order to suppress the finger-like macro-voids and to form a dense selective layer. The addition of LiCl salt is good for the suppression of finger-like macro-voids. In terms of the optimization of spinning conditions, the increase in bore flow rate results in an increase in the outer and inner diameter and a decrease in the wall thickness and dense layer thickness of a hollow fiber. The increasing dope flow rate led to larger outer and inner diameters and thicker fiber wall.

The development of membranes with high CO<sub>2</sub> permeance is crucial to industrial applications. Therefore, the preparation of thin-film composite membranes consisting of a thin selective layer on a highly porous substrate, which provides mechanical strength, has attracted more and more attention in recent years [16,17]. To fabricate a defect-free thin film composite membrane, a highly permeable gutter layer can be introduced on the surface of the porous support, and a protective layer is needed to seal the pinholes on the selective layer [3,18,19]. A lot of research has been focused on the preparation of thin film composite hollow fiber membranes for gas separation [20–26].

Polydimethylsiloxane (PDMS) is a rubbery material with high gas permeability due to high flexibility of siloxane linkages and it is the most commonly used coating material for membrane gas separation processes due to its excellent adhesion property to the support. Moreover, PDMS possesses good thermal, chemical and oxidative stability [22,27,28]. Liang et al. [21] fabricated PDMS/PAN (polyacrylonitrile) thin film composite hollow fiber membranes by using the dip coating method. The prepared membranes were used for water vapor removal from humid air and gases. It was found that the composite membrane shows N<sub>2</sub> permeance of about 280 GPU, O<sub>2</sub>/N<sub>2</sub> selectivity of 2.2 and a water vapor permeance ranging from about 800 to 3700 GPU. Liang et al. [29] also prepared crosslinked PDMS/PAN thin film composite hollow fiber membranes for flue gas and air separations. The prepared composite membranes showed excellent O<sub>2</sub> and CO<sub>2</sub> permeances higher than 1000 and 5000 GPU, respectively, while the corresponding selectivities of O<sub>2</sub>/N<sub>2</sub> and CO<sub>2</sub>/N<sub>2</sub> are about 2 and 11, respectively. Roslan et al. [22] fabricated six different types of polysulfone (PSF) hollow fiber membranes from the same dope solution by varying the spinning parameters of air gap length, bore fluid flow rate, and collection speed to investigate the effect of hollow fiber substrate characteristics on the gas separation performance of thin film composite membranes. Subsequently, the prepared hollow fibers were dip coated with PDMS thin layer. It was found that PDMS coating significantly improved the selectivities of PSF hollow fiber membranes for CO<sub>2</sub>/CH<sub>4</sub> and O<sub>2</sub>/N<sub>2</sub> separation. PSF hollow fibers spun at a higher air gap (4 cm) and lower dope extrusion rate (1 mL/min) were found to be the best supports for PDMS coating owing to their good balance between gas permeance and gas selectivity. Chong et al. [30] fabricated PDMS/PSF composite hollow fiber membranes for oxygen enrichment. The prepared PDMS-coated membrane showed oxygen and nitrogen gas permeance of 18.31 and 4.01 GPU, respectively, with oxygen/nitrogen selectivity of 4.56. Li et al. [23] prepared PDMS/PAN hollow fiber composite membranes for the separations of CO<sub>2</sub>/N<sub>2</sub> and O<sub>2</sub>/N<sub>2</sub>. The effects of prewetting agents, morphology and pore size distribution of substrate, and PDMS concentration and viscosity on the gas separation performance of the composite membranes were investigated. It was found that partial PDMS crosslinking and pre-wetting of PAN substrates with

Fluorinert 72 (FC-72) or deionized water before dip coating can mitigate the solution intrusion in the dip coating process.

In this study, PEI hollow fibers were fabricated at various spinning conditions. The flow rate of bore fluid was especially chosen to investigate its effect on hollow fiber structure, since the flow rate of bore fluid was rarely investigated in the literature. PDMS/PEI composite hollow fiber membranes were prepared via the dip coating method. The structure, morphology, outer and inner diameters, wall thickness, and skin layer thickness of hollow fibers were characterized using various techniques to investigate the effect of substrate characteristics on the gas separation performance of the composite membrane.

## 2. Materials and Methods

### 2.1. Materials

Polyetherimide (PEI, Ultem 1000) pellets were kindly provided by Membrain s.r.o. (Stráž pod Ralskem, Czech Republic). N-methyl-2-pyrrolidone (NMP, 99.5%) was purchased from Linegal Chemicals Sp. z o.o. (Warsaw, Poland). Methanol and n-hexane were delivered by Alchem Grupa Sp. z o.o. (Toruń, Poland). Pure CO<sub>2</sub> (99.999%) and N<sub>2</sub> (99.999%) gases were purchased from Air Products Sp. z o.o. (Siewierz, Poland). The fast solidified epoxy resin Araldite 2000 and 3M EPX Quadro Mixing Nozzles were purchased from Farnell (Warsaw, Poland).

Elastosil LR 6240A (containing platinum catalyst) and Elastosil LR 6240B (containing crosslinker) were kindly provided by Wacker Chemie AG Polska Sp. z o.o. (Warsaw, Poland). According to the data provided by the producer, the viscosities of Elastosil LR 6240A and Elastosil LR 6240B are equal to 30–45 and 25–40 Pa s, respectively.

### 2.2. PEI Dope Solution Preparation

Dope solutions possessing various concentrations of PEI (16, 18, 20, 22, and 24 wt%) were prepared by dissolving PEI pellets in NMP solvent in a round bottom flask under refluxing conditions at 60 °C for 24 h. Prior to dissolving PEI pellets into NMP, PEI pellets were dried in the oven at 100 °C to remove residual moisture. The prepared dope solution was transferred into a laboratory screw cap bottle and left for 24 h for degassing.

### 2.3. PEI Hollow Fiber Preparation

The PEI hollow fibers were prepared via the dry-jet wet spinning process by using a home-built spinning system (Figure 1). Polymer concentration, bore fluid composition, and flow rate of bore fluid were chosen as variants and investigated in this study. The names of the fabricated hollow fibers and their corresponding values of variants are gathered in Table 1. The spinning conditions are shown in Table 2. In the spinning process, a gear pump was used to deliver the dope solution at a specific extrusion rate from the stainless steel reservoir to a spinneret. The bore fluid was delivered into the spinneret simultaneously by using a syringe pump. The as-spun hollow fibers went through an air gap and fell free into a coagulation bath containing distilled water at room temperature. The prepared hollow fibers were cut and soaked in another water bath for 2 days to remove the remaining NMP solvent. The solvent exchange was applied as a post-treatment on hollow fibers to avoid the collapse of the hollow fiber structure during the drying process. The hollow fibers were taken out from the water bath and immediately immersed in methanol for 12 h. Then the methanol-wet hollow fibers were immersed in hexane for another 12 h. Finally, hollow fibers were taken from hexane and dried at room temperature before further investigations.



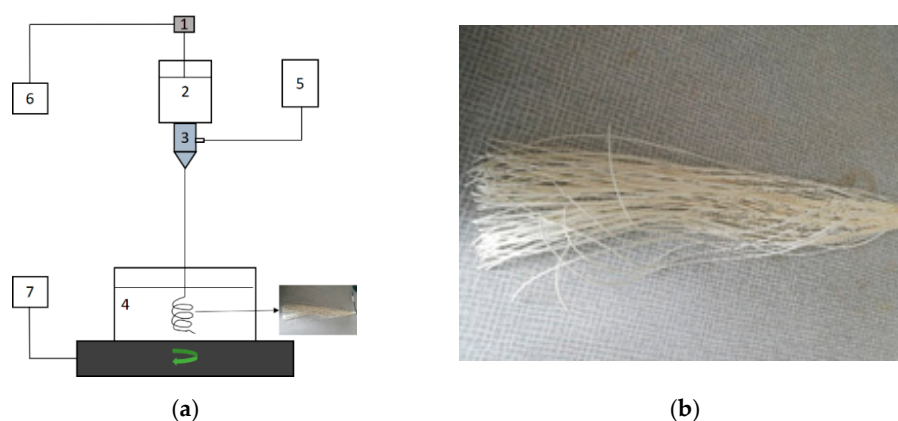


**Figure 1.** (a) Schematic representation of the home-built spinning system: (1) gear pump, (2) tank for spinning solution, (3) spinneret, (4) water coagulation bath, (5) syringe pump and tank for bore fluid, (6) control panel for a gear pump, (7) control panel for rotation of coagulation bath; (b) the prepared hollow fibers.

**Table 1.** The names of prepared hollow fibers and their corresponding fabrication parameters.

Hollow Fibers	PEI (wt%)	Bore Fluid	Flow Rate of Bore Fluid (cm <sup>3</sup> /min)
HF1	16	H <sub>2</sub> O	6
HF2	18	H <sub>2</sub> O	6
HF3-1	20	H <sub>2</sub> O	3
HF3-2	20	H <sub>2</sub> O	6
HF3-3	20	H <sub>2</sub> O	9
HF3-4	20	H <sub>2</sub> O	12
HF3-5	20	H <sub>2</sub> O/NMP * 50/50 (wt%)	9
HF3-6	20	H <sub>2</sub> O/NMP 30/70 (wt%)	9
HF4	22	H <sub>2</sub> O	6
HF5	24	H <sub>2</sub> O	6

\* NMP—N-methyl-2-pyrrolidone.

**Table 2.** Spinning parameters for polyetherimide (PEI) hollow fiber fabrication.

Spinning Parameters	Spinning Conditions
Spinneret dimensions, OD/ID * (mm/mm)	4.8/2.1
Dry air gap length (cm)	25
Dope extrusion rate (mL/min)	7.6
Take up	Free fall
External coagulant	water
Temperature of external coagulant (°C)	25 ± 2
Temperature of spinneret (°C)	25 ± 2

\* OD/ID—outer/inner diameter.

#### 2.4. Fabrication of PDMS/PEI Composite Hollow Fiber Membranes

Elastosil LR 6240 A and Elastosil LR 6240 B in the mass ratio 1:10 were dissolved in hexane to prepare 15 wt% PDMS solution. The solution was prepared by stirring for 2 h at room temperature. The PDMS/PEI composite hollow fiber membranes were fabricated using a dip-coating method. First of all, a 30 cm long PEI hollow fiber was prepared, and one end of the hollow fiber was sealed with epoxy resin. After the solidification of epoxy resin, the other end of the hollow fiber was attached to a metal holder. Then the single PEI hollow fiber was vertically immersed into the PDMS solution for 10 min at room temperature. Finally, the PDMS coated hollow fiber was slowly taken from the coating solution and dried in air for at least 48 h to remove the solvent and fully cure the PDMS.

### 2.5. Characterization of PEI Hollow Fibers and PDMS/PEI Composite Membranes

The morphology of the fabricated PEI hollow fibers and PDMS/PEI composite membranes were analyzed by using Scanning Electron Microscope (SEM)—LEO 1430 VP microscope (Leo Electron Microscopy Ltd., Cambridge, UK). The scanning was performed at an accelerating voltage of 30 keV. To analyze the cross-section of hollow fiber, the sample was prepared by fracturing the hollow fiber in liquid nitrogen. Prior to the analysis, the sample was sputtered with a conductive layer (thickness in the range of 2–6 nm) of Au/Pd (80/20 composition). The inner diameter, outer diameter, wall thickness, outer skin layer thickness, and inner skin layer thickness of hollow fiber were measured from SEM pictures by using ImageJ software. The thicknesses of PDMS layers at the top part and bottom part were also measured by using ImageJ software.

The contact angle (CA) of the inner and outer surfaces of hollow fibers were measured by using a Theta Flex Tensiometer (Biolin Scientific, Gothenburg, Sweden) at room temperature. The sample was prepared by opening the hollow fiber by using a scalpel and mini scissors. Attension Theta (OneAttension Version 4.02, Gothenburg, Sweden) software was used for data acquisition and processing. Water with surface tension equal to 72.5 mN m<sup>-1</sup> was selected as testing liquid.

### 2.6. Module Fabrication and Gas Permeance Measurements

The modules were fabricated according to the following procedure. A total of 2 hollow fibers with a length of 15–20 cm were assembled as a bundle. One hollow fiber bundle was placed in a glass tube. Both ends of the glass tube were sealed with a 5 min fast solidified epoxy resin (Araldite, Winterthur, Switzerland). Then one end of the glass tube was opened by using a scalpel before the complete solidification of epoxy resin. The prepared module was fitted into a home-made apparatus as shown in Figure 2 for gas permeance measurements. Pure N<sub>2</sub> and CO<sub>2</sub> were used for the single gas permeance tests. The trans-membrane pressure was set as 2 bar for all measurements at room temperature 25 °C. To ensure the accuracy of experiments, the gas permeance measurements were conducted 3 times in the stabilized condition. The permeances, P/d, of gases through the hollow fiber module were determined using a bubble flow meter and calculated using Equation (1):

$$\frac{P}{d} = \frac{Q}{\Delta p A} = \frac{Q}{2n\pi r l \Delta p} \quad (1)$$

where P is the permeability (Barrer); d is the thickness of membrane selective layer (cm); Q is the flux of gas permeation rate (cm<sup>3</sup> (STP)/s); Δp is the pressure difference across the membrane (cmHg); A is the effective membrane area (cm<sup>2</sup>); n is the number of hollow fiber; r is the outer radius (cm) of hollow fiber; P/d is the gas permeance expressed in GPU (1 GPU = 10<sup>-6</sup> cm<sup>3</sup> (STP) cm<sup>-2</sup> s<sup>-1</sup> cmHg<sup>-1</sup>).

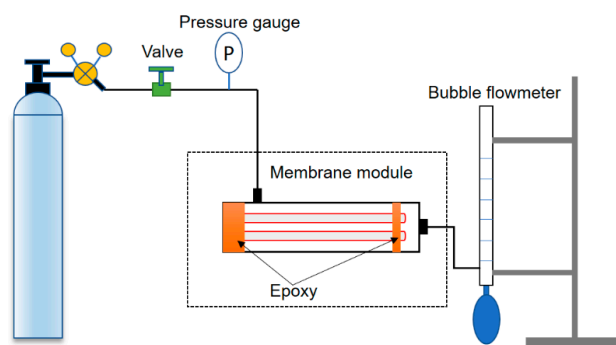


**Figure 2.** The scheme of laboratory set-up for gas permeance measurements of hollow fiber membranes.

The ideal selectivity  $\alpha$  is defined as the permeability coefficient or permeance ratio of two pure gases (Equation (2))

$$\alpha_{12} = \frac{(P/d)_1}{(P/d)_2} = \frac{P_1}{P_2} \quad (2)$$

### 3. Results and Discussion

#### 3.1. PEI Hollow Fiber Substrate

##### 3.1.1. The Effect of Polymer Solution Concentration

The thermodynamic and kinetic principles involved in phase inversion technique such as polymer–solvent interactions, solvent–coagulant interactions, and the concentration and viscosity of dope affect membrane morphology [31,32]. To investigate the influence of concentration of the polymer solution on the hollow fiber formation, hollow fibers were spun from various concentrations of the polymer solution. The rest of the spinning conditions were kept constant (Table 2). Figure 3 shows the cross-section morphology as a function of PEI solution concentration, i.e., 16 wt%, 18 wt%, 20 wt%, 22 wt%, and 24 wt%. The following conclusions can be drawn. Hollow fibers spun from 16 wt%, 18 wt%, and 20 wt% of PEI solution possess similar morphology, i.e., finger-like macrovoids in the bulk of the hollow fibers underneath the inner and outer skin layers, and tear-like macrovoids in the middle part of the hollow fiber wall. However, when the polymer concentration increased from 16 wt% to 20 wt%, the tear-like macrovoids became smaller, and the finger-like macrovoids became shorter (Figure 3A2–C2). This is because the water intrusion is suppressed to some extent, resulting from the greater viscoelasticity of a more concentrated polymer solution [33]. Especially, in the case of hollow fibers spun from 20 wt% of PEI solution, a symmetric structure appeared in the hollow fiber wall (Figure 3C2). The symmetric structure is beneficial to the mechanical stability of hollow fibers which is used as a support layer. Jamil et al. [34] found that NMP has weaker interaction towards PEI, hence, it formed instant demixing and migrated to water coagulant, which created finger-like pores. When the polymer solution concentration increased to 22 wt%, the part with tear-like macrovoids was replaced by a part with sponge-like microporous structure and the finger-like macrovoids near lumen side were longer than the ones near shell sides. The decrease in the length of finger-like macrovoids near the shell side is attributed to the fast formation of relatively dense layer when hollow fibers were passing through the air gap, which impeded the intrusion of nonsolvent (water) into hollow fibers. Hollow fibers spun from 24 wt% PEI solution possess the sponge-like porous structure with a small number of tear-like macrovoids near lumen and shell sides. The sponge-like pores were formed due to the slow exchange of solvent at higher chain orientations [31]. In the hollow fiber fabrication process, the increase in polymer solution can reduce the number and size of macrovoids. Consequently, the macrovoids can be eliminated by increasing the polymer solution concentration. As it is shown in Figure S1, hollow fibers HF1, HF2, HF3-2, HF4, and HF5 possessed a skin layer on the inner and outer surfaces. The formation of skin layers on both the inner and outer side of hollow fibers resulted from the fast precipitation process. Water was used as an inner and outer coagulant in the spinning process. It is a strong nonsolvent that induced the strong kinetics and thermodynamic effects between polymer–solvent and non–solvent (water) during the phase inversion process, which accelerated the precipitation rate the polymer solution [35].

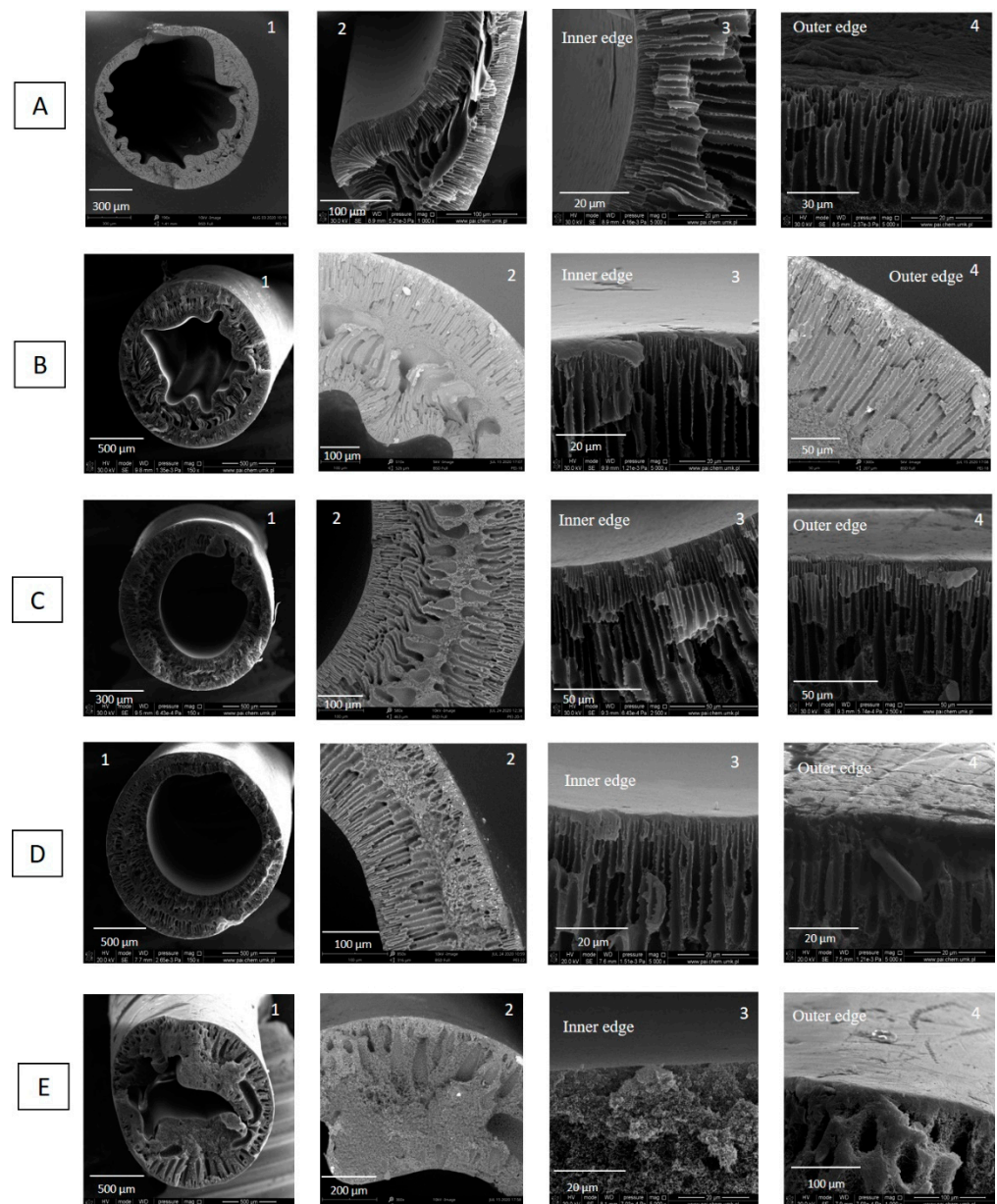


**Figure 3.** SEM micrographs of cross section of PEI hollow fibers spun from various concentrations of polymer solution—(A) HF1—16 wt%, (B) HF2—18 wt%, (C) HF3—20 wt%, (D) HF4—22 wt%, (E) HF5—24 wt% (bore fluid—water and bore fluid flow rate 6 mL/min).

Naim et al. [35] and Bakeri et al. [36] investigated the effect of polymer concentration on the structure and performance of PEI hollow fiber membranes. Bakeri et al. [36] found that the phase separation took place in an earlier stage of solvent–nonsolvent exchange for a higher polymer concentration. However, the higher viscosity of the solution delays the solvent–polymer demixing by slowing down the solvent–nonsolvent exchange process. The thickness and density of the skin layer increased with the increase in polymer concentration. All prepared membranes possessed finger-like macrovoids, which extended from the inner and outer surfaces to the middle of the hollow fiber wall [36]. Naim et al. [35] found that the fine line sponge-like structure was formed in the middle intersection of the finger-like arrangement and varied in terms of the thickness when the polymer concentration increased. Their observation is similar to ours (Figure 3). The finger-like structure of the hollow fibers resulted from the rapid phase inversion process due to the low viscosity of the respective polymer solution. Moreover, water was used as

the internal and external coagulants in the spinning process, the strong non-solvent has accelerated the phase inversion rate. The low viscosity of the polymer solution (13–16 wt%) to some extent contributed to the similarity of the finger-like structure. It is believed that the thermodynamic and kinetics effects played crucial roles in determining the membrane structure which can be manipulated based on the parameters applied in the spinning process, e.g., coagulation medium, air gap, bore fluid composition, spinneret size, and fibers collection methods (spin drum or free falling) [35].

The dimension parameters of hollow fibers i.e., outer diameters, wall thickness, outer skin layer thickness and inner skin layer thickness, were measured by using ImageJ software. As is shown in Figure 4a, the outer diameter increased with the increase in PEI concentration. The outer diameter was in the range of 1400–1600  $\mu\text{m}$  when the PEI concentration was in the range of 18–24 wt%. The influence of dope concentration on the outer diameter of hollow fibers weakened when the dope concentration is higher. The wall thickness of hollow fiber increased from 400  $\mu\text{m}$  to 800  $\mu\text{m}$  when the PEI concentration increased from 16 wt% to 18 wt%. Then it was stabilized at around 800  $\mu\text{m}$  even if the PEI concentration increased from 18 wt% to 22 wt%. HF5 possessed the highest wall thickness equal to 476  $\mu\text{m}$ . The effect of PEI concentration from 16 to 22 wt% on the outer diameter and wall thickness was weakened at higher PEI concentration, which can be explained in terms of viscosity of dope and the phase separation process. The viscosity of the PEI solution increased when the PEI concentration increased [36]. The phase separation took place at an earlier stage of solvent–nonsolvent exchange for a higher polymer concentration [35]. Therefore, the increased viscosity and the faster phase separation restrict the changes of outer diameter and the wall thickness of hollow fibers in the spinning process.

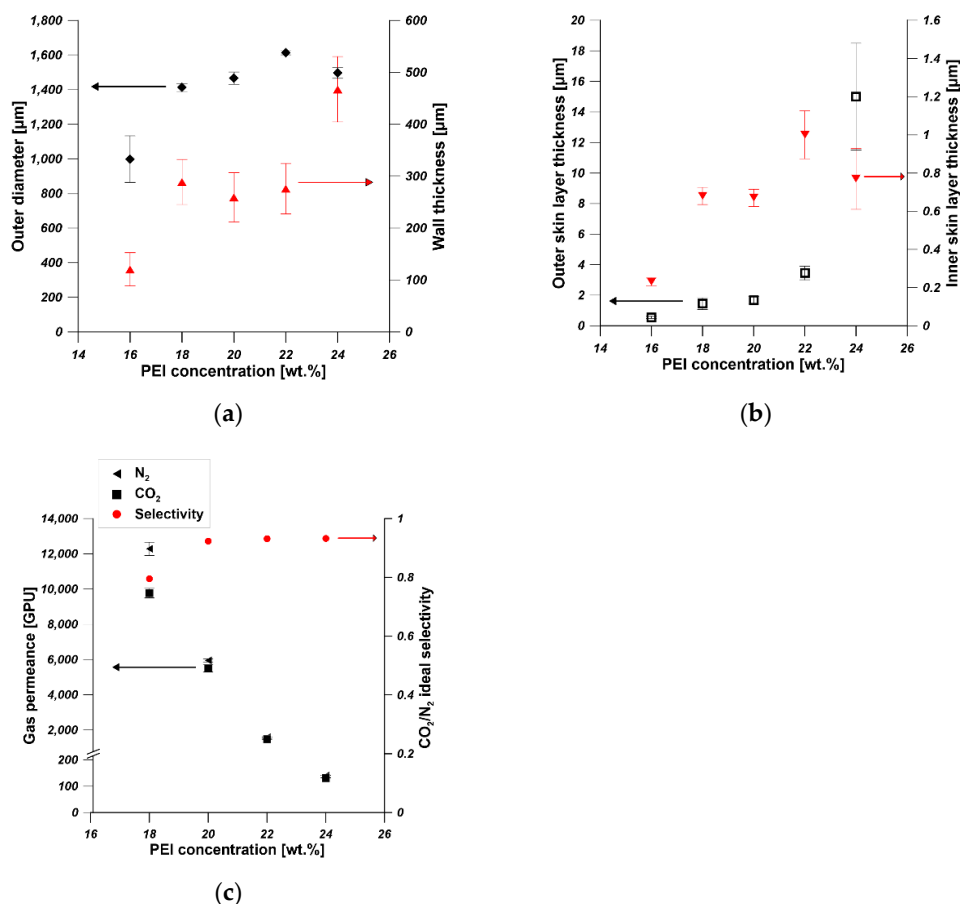


**Figure 4.** The effect of PEI concentration in dope solution on (a) the outer diameter and wall thickness, (b) the skin layer thickness (c) the gas permeance and ideal selectivity of hollow fibers (bore fluid—water and bore fluid flow rate 6 mL/min).



The thicknesses of outer and inner skin layers increased from 0.55  $\mu\text{m}$  to 15  $\mu\text{m}$  and from 0.2  $\mu\text{m}$  to 1  $\mu\text{m}$ , respectively, when the PEI concentration increased from 16 wt% to 24 wt% (Figure 4b). The increase in the skin layers can be attributed to the increased viscosity and slower solvent–nonsolvent exchange rate [36]. The gas permeance test reflecting the skin layer properties showed that the permeances of  $\text{N}_2$  and  $\text{CO}_2$  decreased with the increase in PEI concentration, which is in accordance with the skin layer thickness observed from SEM pictures (Figure 4c). The gas permeance is also influenced by the pore structure of hollow fibers. The finger-like pores promote the gas permeance [31], which is confirmed in Figure 3. The sponge-like hollow fiber showed the lowest  $\text{N}_2$  and  $\text{CO}_2$  permeance between 100 GPU and 200 GPU. The prepared hollow fibers showed  $\text{CO}_2/\text{N}_2$  selectivity lower than one and high  $\text{N}_2$  and  $\text{CO}_2$  permeance except for HF5, which reflected the high porosity of the prepared hollow fibers (Figure 3). During the gas permeance test, the feed gas went from the shell side to the lumen side. The gas permeance of HF1 was too high to be measured, and the HF1 collapsed at 2 bar during the gas permeance test. Therefore, hollow fibers fabricated from 16 wt% of PEI solution are not suitable as mechanical supports of composite membranes.

As was discussed before, hollow fibers fabricated from 20 wt% of PEI solution showed desirable pore structure (Figure 3C) and relatively high gas permeance around 6000 GPU. Therefore, 20 wt% of PEI solution was chosen as the optimal dope for hollow fiber preparation, and further investigation were conducted on hollow fibers fabricated from 20 wt% of PEI solution.

### 3.1.2. The Effect of Bore Fluid Flow Rate

To investigate the influence of bore fluid flow rate on the hollow fiber formation, hollow fibers were spun from 20 wt% PEI solution and at various bore fluid flow rates. The rest of the spinning conditions were kept constant (Table 2). Figure 5 shows the cross-section morphology as a function of bore fluid flow rate, i.e., 3  $\text{cm}^3/\text{min}$ , 6  $\text{cm}^3/\text{min}$ , 9  $\text{cm}^3/\text{min}$ , and 12  $\text{cm}^3/\text{min}$ . It was observed that when the bore fluid flow rate increased, the inner contour of the cross-section became circular in shape (Figure 5C1,D1) from a corrugated one (Figure 5A1,B1) and the wall of hollow fiber became thinner and homogeneous. Bonyadi et al. [37] investigated the corrugation phenomenon in the inner contour of hollow fibers during the non-solvent induced phase separation process. They proposed two possible instability mechanisms to elucidate the deformations of the inner contour of hollow fibers in the spinning process. According to their theory, the instability arose from the elastic, hydrodynamic, mass transfer, and solidification processes. The effects of air-gap distance, bore fluid composition, external coagulant, take-up speed, and dope concentration on the formation of corrugation in the inner contour were explained in detail based on the proposed theory [37]. Their theory could be used to explain the effect of bore fluid flow rate on the corrugation phenomenon in the inner contour in the spinning process. When the bore fluid flow rate was small, the mass transfer between the dope and bore fluid is slow. The bore fluid penetration into the polymer solution was not homogeneous. The polymer solution matrix was divided into regions which have different penetration and contact area with bore fluid. In the region possessing deeper penetration and increased contact area with bore fluid, the solvent–nonsolvent exchange rate between dope and bore fluid is faster and the pressure induced by precipitation in these regions is higher resulting in the deformation of the inner contour [37]. With the increase in bore fluid flow rate, the mass transfer was enhanced, and the solvent–nonsolvent exchange rate between dope and bore fluid became higher and more homogeneous. Therefore, the pressure-induced by precipitation was similar, inhibiting the deformation in the inner contour. On the other hand, the increased solvent–nonsolvent exchange rate resulted in a more rigid elastic cylindrical shell in the inner part of the dope and a more viscous region in the middle part of the dope. Consequently, the initial instabilities were inhibited, and the effect of radial inward shrinkage force generated in the outer coagulant on the deformation of hollow fiber was weakened [37].



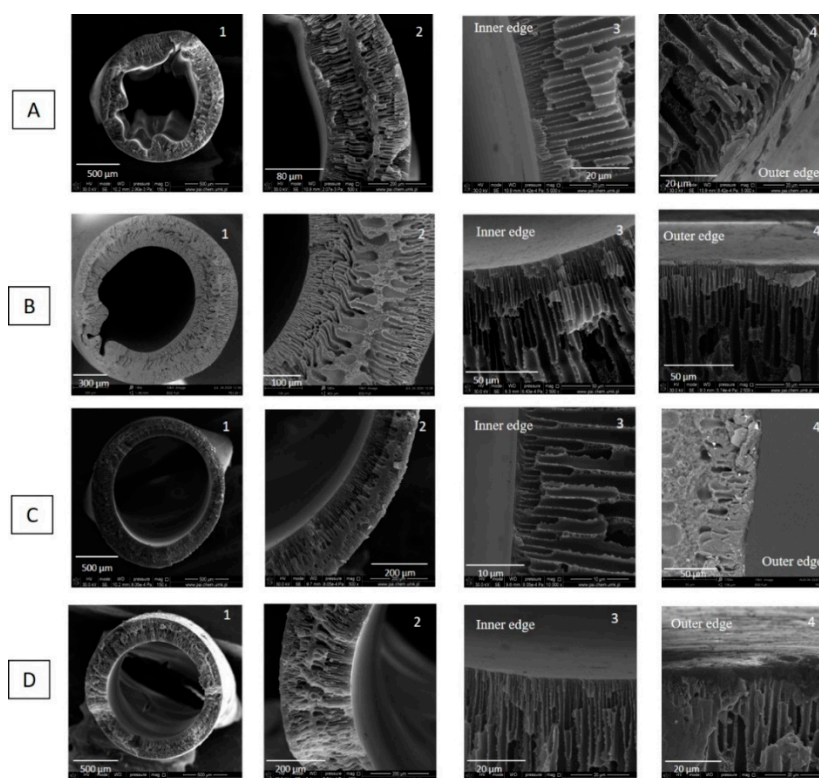


**Figure 5.** SEM micrographs of cross section of PEI hollow fibers spun at various flow rates of bore fluid. (A) HF3-1— $3 \text{ cm}^3/\text{min}$ , (B) HF3-2— $6 \text{ cm}^3/\text{min}$ , (C) HF3-3— $9 \text{ cm}^3/\text{min}$ , (D) HF3-4— $12 \text{ cm}^3/\text{min}$  (PEI concentration—20 wt% and bore fluid—water).

Hollow fibers (HF3-1, HF3-2, HF3-3, and HF3-4) possessed finger-like macrovoids near lumen and shell sides. Wang et al. [38] also observed a typical bulk structure of double rows of finger-like macrovoids with a compact skin at both the outer and inner surface of polyimides hollow fibers spun with water as bore fluid. This is because water is a strong nonsolvent. Both the inner and the external interfaces of the dope undergo instantaneous phase separation, which forms a thin and dense layer on both surfaces of hollow fiber with a finger-like structure of the sublayer. The finger-like macrovoids near the shell side are shorter in comparison with the ones near the lumen side. This is due to the formation of dense outer layer in the air gap impeding the water intrusion and the different contact times between the dope and coagulant (water) since the outer surface of the dope went through an air gap during the spinning process [38]. With an increase in bore fluid flow rate, the finger-like macrovoids near the lumen became longer, which is attributed to the stronger nonsolvent (water) intrusion and the facilitated mass transfer resulting from higher bore fluid flow rate [39]. The hollow fibers spun at a lower bore fluid flow rate ( $3 \text{ cm}^3/\text{min}$ ) possess thicker layers with a microporous structure in the middle part of the hollow fiber wall. The microporous structure in the middle part of hollow fiber wall became thinner with the increase in bore fluid flow rate. The number and size of tear-like macrovoids significantly decreased when the bore fluid flow rate was at 9 and  $12 \text{ cm}^3/\text{min}$ . The increase in flow rate can influence the cross-section profile and the size and shape of macrovoids.

Figure S2 reveals the morphology of inner and outer surfaces of HF3-1, HF3-2, HF3-3, and HF3-4. All hollow fibers possessed outer and inner skin layers since water as a strong nonsolvent was used as the bore fluid. The increase in bore fluid flow rate did not affect the surface morphology of hollow fibers significantly.

Figure 6a shows the effect of bore fluid flow rate on the outer diameter and wall thickness of hollow fibers spun from 20 wt% using water as bore fluid. With the increase in bore fluid flow rate, the outer diameter was slightly influenced, however, the wall thickness

decreased significantly. Consequently, the inner diameter of hollow fibers increased with the increase in bore fluid flow rate. Wang et al. [39] observed the increased inner diameter and the reduced wall thickness of the as-spun polybenzimidazole (PBI) hollow fibers. Bilydukevich et al. [40] also found that the capillary diameter increased and wall thickness decreased with an increase in the rate of bore fluid at a constant polysulfone solution feed rate. This is due to the fact that the solidification rate at the inner surface increases with the increasing bore fluid flow rate since the mass transfer is facilitated. Therefore, an increase in bore fluid flow rate results in the increase in the inner diameter with a reduced wall thickness and slightly stretched outer skin [39]. As Figure 6b shows, the thickness of the outer skin layer was in the range of 1.5–2.5  $\mu\text{m}$ , and the thickness of the inner skin layer decreased from 0.94  $\mu\text{m}$  to 0.28  $\mu\text{m}$ . The slight decrease in inner skin layer is due to the increased solvent–nonsolvent exchange rate resulting from the facilitated mass transfer. Figure 6c shows that hollow fibers spun from 20 wt% using various bore fluid flow rates possessed very high gas ( $\text{N}_2$  and  $\text{CO}_2$ ) permeance in the range of 4500–7000 GPU with no selectivity.

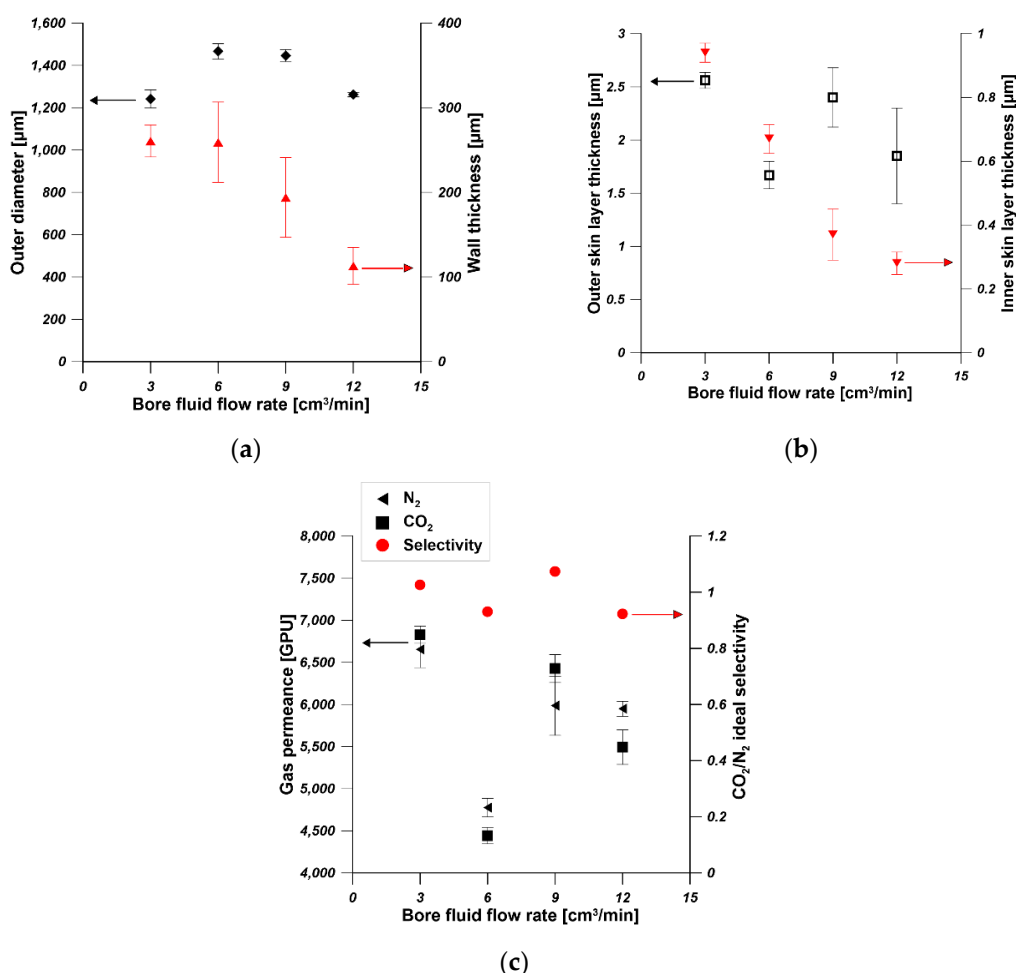


**Figure 6.** The effect of bore fluid flow rate on (a) the outer diameter and wall thickness, (b) the skin layer thickness (c) the gas permeance and ideal selectivity of hollow fibers (PEI concentration—20 wt% and bore fluid—water).

The water contact angle (CA) of the outer surface and inner surface of hollow fibers i.e., HF3-2, HF3-3, and HF3-4, was measured at room temperature. HF3-2, HF3-3, and HF3-4 were spun from 20 wt% PEI solution at a bore fluid flow rate equal to 6 mL/min, 9 mL/min, and 12 mL/min, respectively. As is shown in Figure 7, the CA of the outer surface is between 85° and 89°. Considering the measurement deviation, it can be concluded that the increase in bore fluid flow rate barely affects the outer surface CA since all hollow

fibers went through the same air gap then went into the water coagulant bath. The inner surface CA slightly increased from  $74^\circ$  to  $84^\circ$  when the bore fluid flow rate increased from 6 mL/min to 9 mL/min and 12 mL/min. This is because corrugation exists in the inner surface (seen from cross-section in Figure 5), resulting in slightly different morphology and surface roughness compared to the inner surface of the hollow fiber spun at a higher bore fluid flow rate. It is reported that the surface morphology and roughness affect the contact angle value [41]. The CA of the outer surface and the inner surface is practically the same due to the absence of corrugation on the inner surface (seen from the cross-section in Figure 5) and the use of water as inner and outer coagulant. Similar results were obtained in other research [42–44]. Qtaishat et al. [42] prepared PEI flat sheet membrane from 12 wt% of PEI solution. It was found that the CA for the top layer and the bottom layer was  $80.04^\circ \pm 4.55^\circ$  and  $72.83^\circ \pm 2.62^\circ$ , respectively. Bakeri et al. [43] fabricated PEI hollow fiber membranes from 14.5 wt% PEI solution. They found that the inner surface CA of PEI hollow fiber was  $80.6^\circ \pm 2.5^\circ$ .

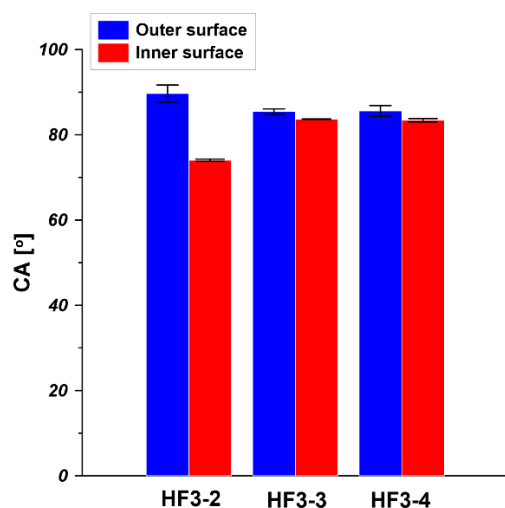


**Figure 7.** Water contact angle (CA) of PEI hollow fibers spun at various bore fluid flow rates (HF3-2—6 mL/min, HF3-3—9 mL/min, HF3-4—12 mL/min, PEI concentration—20 wt% and bore fluid—water).

### 3.1.3. The Effect of Bore Fluid Composition

To investigate the influence of bore fluid composition on the lumen side and the region near the lumen side, hollow fibers were spun from 20 wt% PEI solution using different bore fluids. The rest of the spinning conditions were kept constant (Table 2). Figure 8 shows the cross-section morphology as a function of bore fluid composition, i.e., H<sub>2</sub>O, H<sub>2</sub>O/NMP 50/50 wt%, H<sub>2</sub>O/NMP 30/70 wt%. All hollow fibers possessed finger-like macrovoids near lumen and shell sides, tear-like macrovoids underneath the finger-like macrovoids, and a microporous structure in the middle part of the hollow fiber wall. When the water fraction in bore fluid decreased from 100 wt% to 30 wt%, the finger-like macrovoids near the lumen side became shorter due to the weakened nonsolvent (water) intrusion. The size of tear-like macrovoids increased, and the thickness of the microporous structure in the middle part of hollow fiber walls increased. With the addition of NMP into the bore fluid, the coagulant effect of bore fluid became weaker, resulting in delayed phase separation in the inner region of the dope. What is more, the addition of NMP into the bore fluid inhibited the mass transfer between the inner coagulant and the polymer solutions because the driving force to water inflow and solvent outflow decreased [38,45].

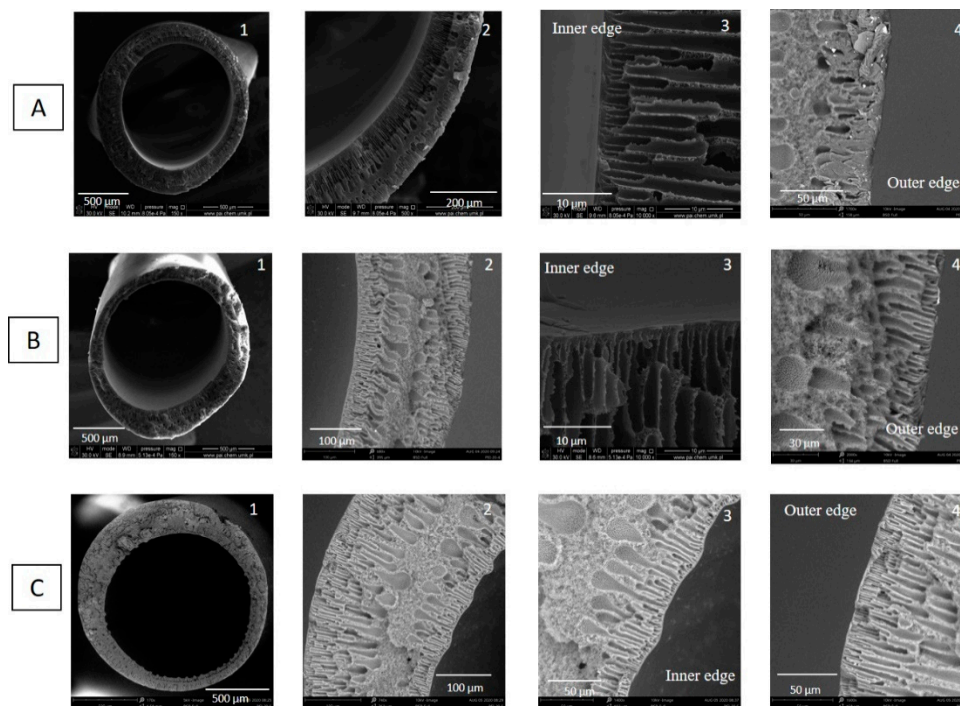


**Figure 8.** SEM micrographs of cross section of PEI hollow fibers spun with various compositions of bore fluid. (A) HF3-3—H<sub>2</sub>O, (B) HF3-5—H<sub>2</sub>O/N-methyl-2-pyrrolidone (NMP) 50/50wt%, (C) HF3-6—H<sub>2</sub>O/NMP 30/70wt% (PEI concentration—20 wt% and bore fluid flow rate—9 mL/min).

Bore fluid directly contacts with the inner region of dope in the spinning process and significantly affects the morphology of the inner surface of hollow fibers. Therefore, the morphology of the inner surface and the inner structure of hollow fibers can be influenced by controlling the composition of bore fluid [38]. Figure S3 reveals the inner and outer surface morphologies of hollow fibers spun with various bore fluids, e.g., H<sub>2</sub>O, H<sub>2</sub>O/NMP 50/50 wt%, H<sub>2</sub>O/NMP 30/70 wt%. The morphologies of outer surfaces of hollow fibers are similar since the as-spun hollow fibers went through the same air gap and into the external coagulant (water) bath. The instantaneous phase separation occurred in this process, and a dense skin layer was formed on the outer surface of hollow fibers. The influence of bore fluid composition on the inner surface morphology can be observed from the SEM pictures. The morphologies of the inner surfaces were slightly different, and pores started appearing with the addition of NMP into bore fluid. Similar results were obtained by Yong et al. [46]. They found that the inner surface porosity increased with the increase in solvent (NMP) concentration in bore fluid. The addition of solvent into bore fluid weakened the coagulant effect and resulted in the delayed phase separation in the inner region of the dope [46].

As Figure 9a shows, the addition of NMP into bore fluid did not affect the outer diameter and wall thickness of hollow fibers. The slight decrease in the inner skin layer thickness resulted from the delayed phase separation process in the inner region of dope. Even the bore fluid did not contact the outer surface of hollow fiber directly, the thickness of the outer skin layer slightly decreased (Figure 9b). It can be seen from Figure 9c that the addition of NMP into bore fluid increased the CO<sub>2</sub> and N<sub>2</sub> permeance from 6500 GPU and 6000 GPU to 9000 GPU and 8000 GPU, respectively. The slight increase in gas permeance might result from the increased porosity on the inner surface of hollow fibers (Figure S3) and the slight decrease in the skin layer on the inner and outer surfaces of hollow fibers (Figure 9b). Similar results were found by Yong et al. [46]. They observed that the fiber spun with a higher solvent (NMP) in the bore fluid possessed a higher O<sub>2</sub> and CO<sub>2</sub> permeance. This phenomenon is directly related to the highly porous inner surface

structure as a consequence of the delay demixing [46]. All hollow fibers possessed very high gas permeance over 6000 GPU, indicating the lower resistance for gas transport.

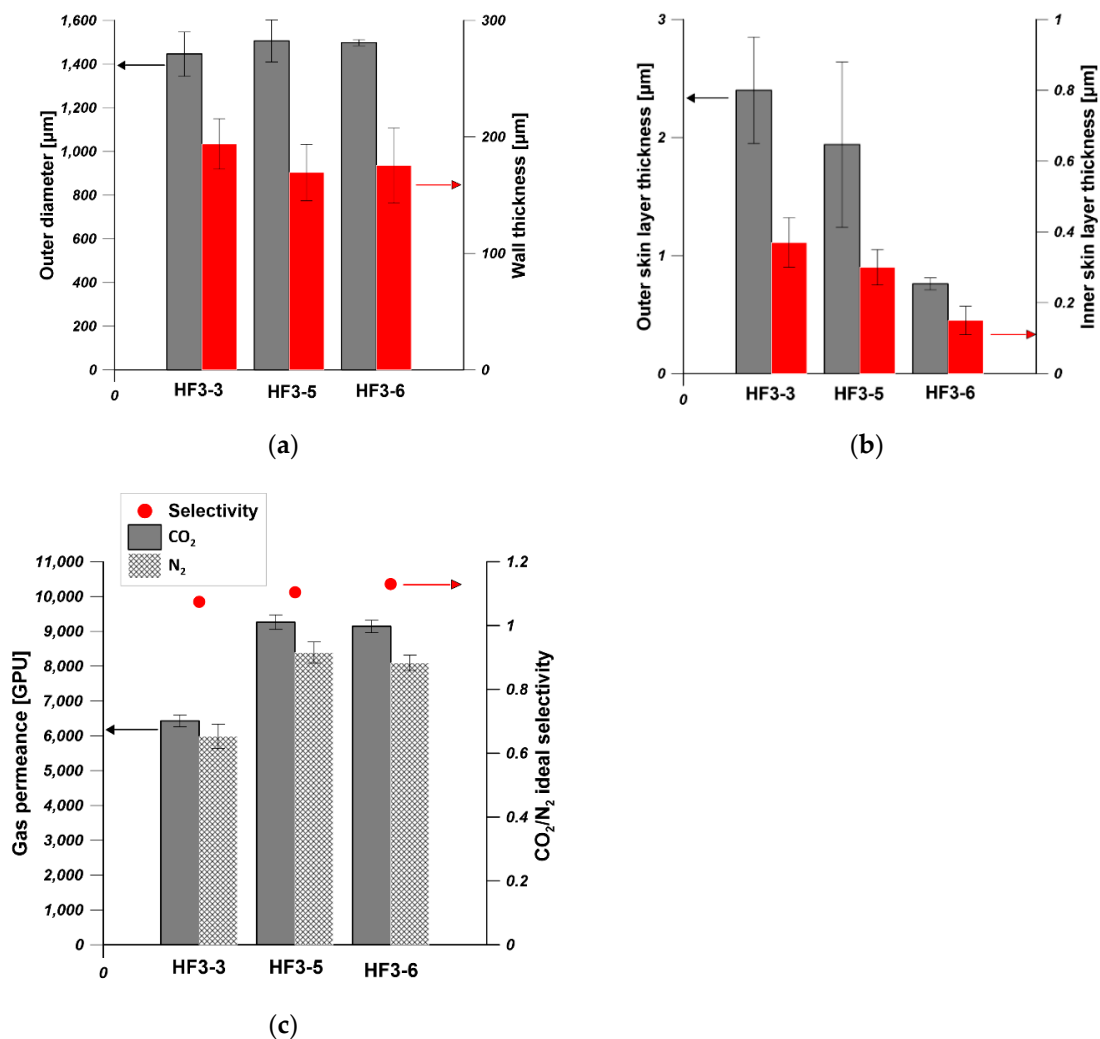


**Figure 9.** The effect of bore fluid composition on (a) the out diameter and wall thickness, (b) the skin layer thickness (c) the gas permeance and ideal selectivity of hollow fibers (HF3-3— $\text{H}_2\text{O}$ , HF3-5— $\text{H}_2\text{O}/\text{NMP}$ —50/50 wt%, and HF3-6— $\text{H}_2\text{O}/\text{NMP}$ —30/70 wt%, PEI concentration—20 wt% and bore fluid flow rate—9 mL/min).

As is shown in Figure 10, the CA of the outer surface is around  $86^\circ$ . The addition of NMP into bore fluid did not influence the CA outer surface since the outer surface was formed at the same spinning condition. However, the addition of NMP into bore fluid should affect the inner surface properties since the inner surface was in direct contact with bore fluid. It was observed that when the NMP content in bore fluid increased from 0 wt% to 50 wt% and 70 wt%, respectively, the CA of the inner surface decreased from  $83^\circ$  to  $78^\circ$  and  $80^\circ$ , respectively. The influence of NMP addition into bore fluid on the CA of the inner surface was due to the change of surface morphology which resulted from the delayed phase separation in the inner region of the dope [46].

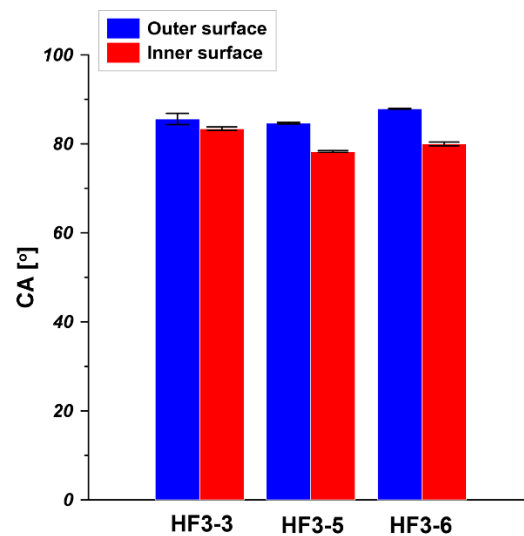


**Figure 10.** Water contact angle (CA) of PEI hollow fibers spun by using H<sub>2</sub>O, H<sub>2</sub>O/NMP—50/50 wt%, and H<sub>2</sub>O/NMP—30/70 wt% as bore fluids for HF3-3, HF3-5, and HF3-6, respectively (PEI concentration—20 wt% and bore fluid flow rate—9 mL/min).

### 3.2. PDMS/PEI Composite Hollow Fiber Membranes

To investigate the effect of hollow fiber substrate characteristics on the gas separation performance of PDMS/PEI composite hollow fiber membranes, a PDMS layer was dip coated on the outer surface of various hollow fibers which were fabricated at different spinning conditions. The designations of PDMS/PEI composite membranes together with the corresponding hollow fiber substrates are gathered in Table 3.

**Table 3.** The designations of polydimethylsiloxane (PDMS)/PEI composite membranes and hollow fiber substrates.

Hollow Fiber Substrate	PDMS/PEI Composite Membrane
HF3-2	M3-2
HF3-3	M3-3
HF3-4	M3-4
HF3-5	M3-5
HF3-6	M3-6

#### 3.2.1. Morphology

The morphology of the PDMS/PEI composite membrane was characterized by using SEM and the Si element identification was performed from the inner surface to the outer surface of the composite membrane by using the line scan mode of EDX (Energy-dispersive X-ray spectroscopy). As it is shown in Figure 11, the PDMS selective layer was successfully coated on the outer surface of hollow fiber support, which is observed from the cross-section and confirmed from the gas separation performance (Figure 14). The element identification confirmed that the PDMS layer was formed on the outer surface of hollow fibers due to the existence of abundant Si elements on the outer surface (Figure 11). Moreover, the Si distribution curve indicates the occurrence of PDMS solution intrusion into hollow fibers in the dip-coating process. The intrusion of PDMS solution into porous support was also studied by Vankelecom et al. [47].



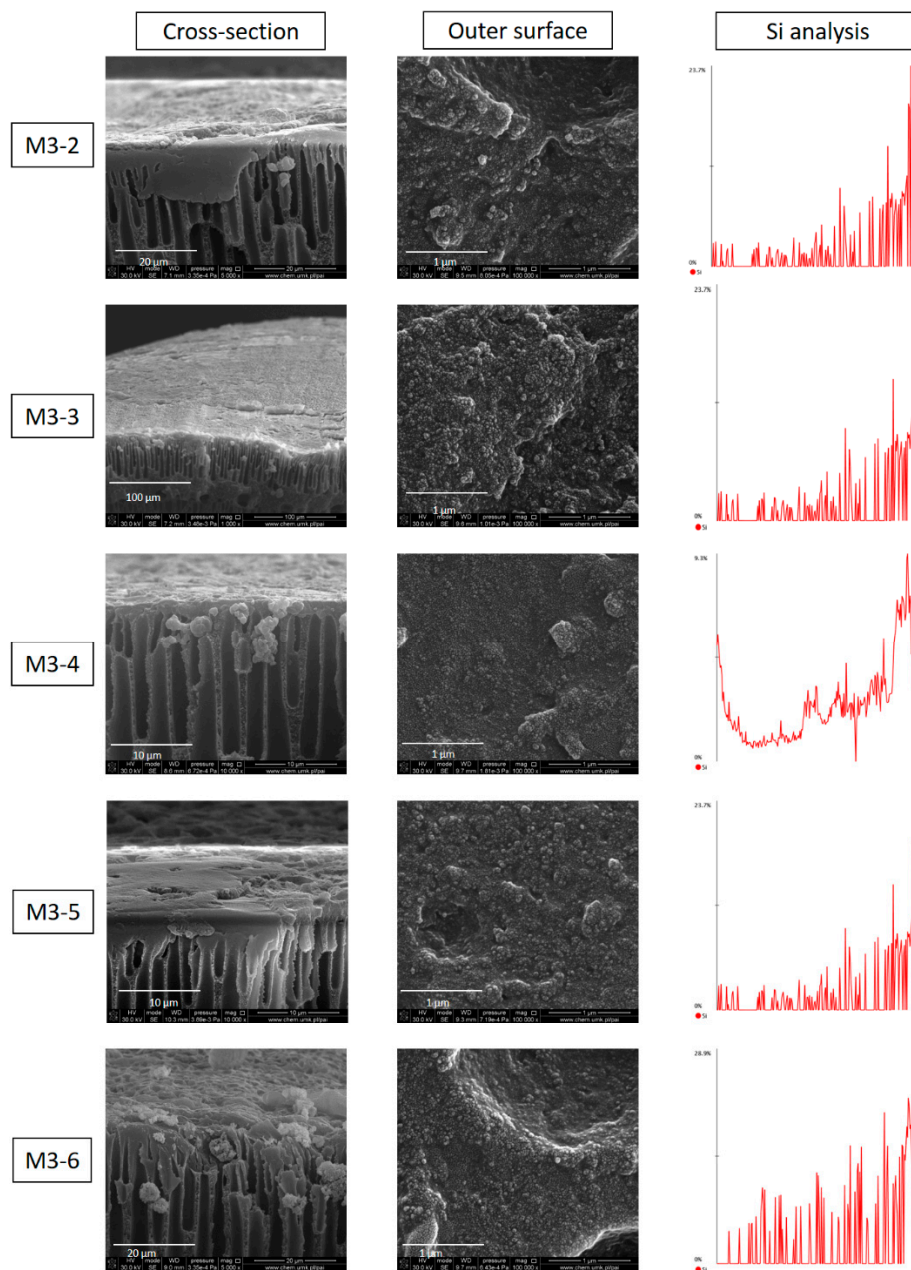


**Figure 11.** The morphology of cross-section and outer surface of a PDMS/PEI composite membrane and the Si distribution made by using a line scan from the inner surface to the outer surface (PDMS concentration—15 wt% and coating time—10 min).

As is shown in Figure 12, the PDMS layer thickness of the top part and bottom part of PDMS/PEI composite hollow fiber membrane is in the range of 1.5–2  $\mu\text{m}$  and 3–4  $\mu\text{m}$ , respectively. The difference in the PDMS layer thickness arose from the dip coating process. In the dip coating process, the bottom part was always close to the solution reservoir while the top part was relatively far from the coating solution. The thickness of the PDMS layer is related to the position of the drying line. The interplay of several parameters e.g., viscous force, solvent evaporation and draining, surface tension, gravity and hydrodynamic factors in the layer deposition region, governs the layer thickness and the position of the drying line [48–50].

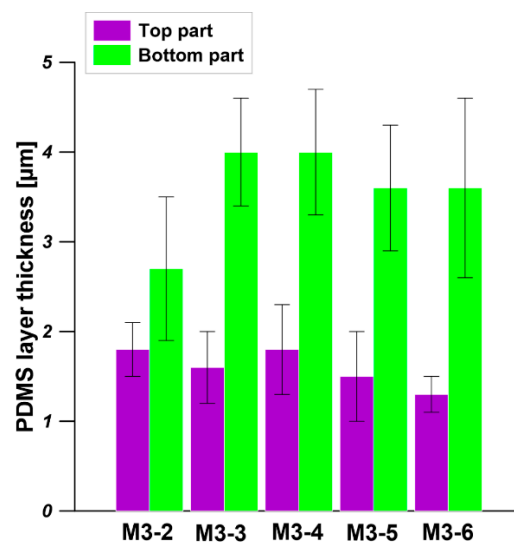


**Figure 12.** The thickness of the PDMS layer measured from the top part and bottom part of the PDMS/PEI composite hollow fiber membrane. The dip coating conditions: PDMS solution concentration—15 wt% and coating time—10 min.

As is shown in Figure 13, the CAs of the outer surfaces of the prepared composite hollow fiber membranes are in the range of  $103^{\circ}$ – $112^{\circ}$  indicating the hydrophobicity of the outer surface. The CAs of the outer surface of hollow fiber substrates are between  $84^{\circ}$  and  $89^{\circ}$  (Figures 7 and 10). The increase in CA is due to the formation of the elective PDMS layer on the outer surface of hollow fiber substrate. Our results are in agreement with the literature values of CA of PDMS membranes [51–54]. Kozowska et al. [51] and Kujawska et al. [52] found that the CA of flat sheet pristine PDMS membrane was  $115^{\circ}$ . While Khorasani et al. [53] and Lin et al. [54] found that the CAs of native PDMS membranes were  $105^{\circ}$  and  $108^{\circ}$ , respectively. It was reported that the wide range of CA values ( $95^{\circ}$ – $120^{\circ}$ ) for PDMS samples results from various experimental conditions, such as surface roughness and type of the substrate surface [52].

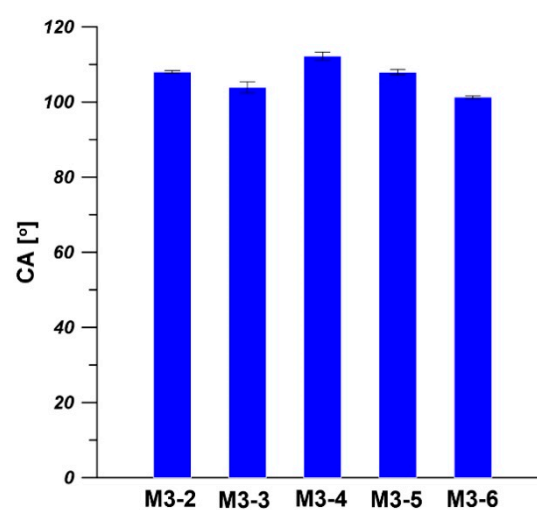


**Figure 13.** Water contact angle (CA) of the outer surface of the PDMS/PEI composite hollow fiber membrane. The dip coating conditions: PDMS solution concentration—15 wt% and coating time—10 min.

### 3.2.2. Gas Separation Performance of the Composite Membranes

Figure 14 shows the CO<sub>2</sub> and N<sub>2</sub> permeances and CO<sub>2</sub>/N<sub>2</sub> ideal selectivity of five types of PEI hollow fibers, spun from 20 wt% of PEI solution at various spinning conditions, coated with PDMS layer. As can be clearly seen, the CO<sub>2</sub>/N<sub>2</sub> ideal selectivity of PEI hollow fibers was significantly enhanced after PDMS coating. The PDMS/PEI composite membranes M3-2, M3-3, M3-4, M3-5, and M3-6 possessed CO<sub>2</sub>/N<sub>2</sub> ideal selectivity of 16, 20, 21, 15, and 10, respectively. The CO<sub>2</sub> permeances of PDMS/PEI composite membranes M3-2, M3-3, M3-4, M3-5, and M3-6 were 41, 45, 59, 161, and 192 GPU, respectively. In comparison to the CO<sub>2</sub> permeance of PEI hollow fibers in the range of 5000–8000 GPU, the CO<sub>2</sub> permeance of PDMS/PEI composite membranes was significantly reduced. These findings indicated that the presence of a PDMS selective layer on the outer surface of PEI hollow fibers plays a crucial role in covering the defects or pores on the surface and forming a gas separation layer successfully. Consequently, the gas transport rate was reduced, and the CO<sub>2</sub>/N<sub>2</sub> ideal selectivity was improved, indicating the trade-off relationship between permeance and selectivity [55]. By comparing the permeances of CO<sub>2</sub> and N<sub>2</sub>, it was found that PDMS coated membranes possessed a higher affinity to CO<sub>2</sub> rather than N<sub>2</sub>. Similar results were found in other research works [22,27]. The gas transport through the PDMS layer can be explained by using the solution–diffusion model. The high permeance of CO<sub>2</sub> in the PDMS layer mainly resulted from the higher solubility coefficient in PDMS [23].

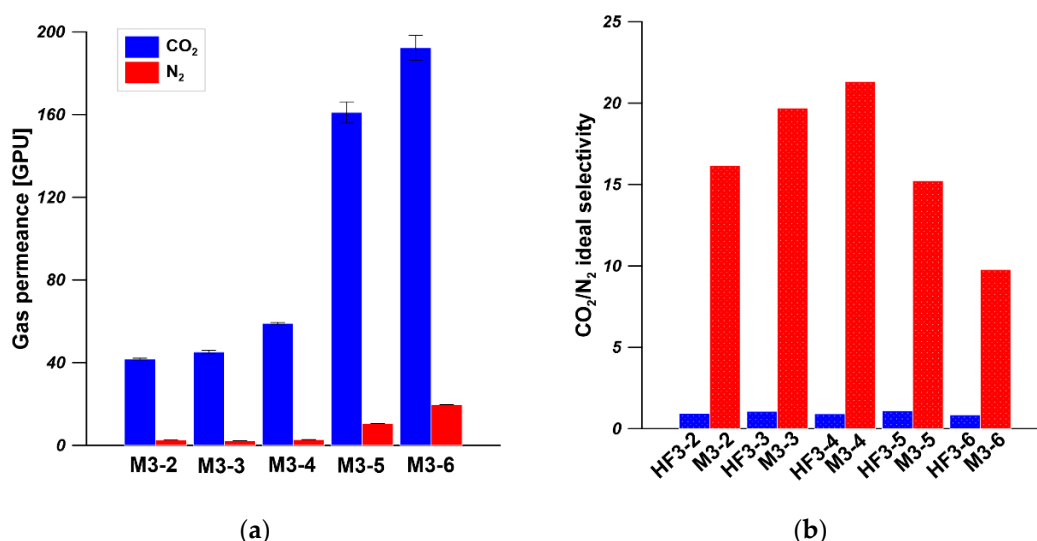


**Figure 14.** (a) The gas permeance of PDMS/PEI composite membranes. (b) The ideal selectivity of PEI hollow fibers and PDMS/PEI composite membranes. The dip coating conditions: PDMS solution concentration—15 wt% and coating time—10 min.

The reported CO<sub>2</sub>/N<sub>2</sub> ideal selectivities of PDMS and PEI membranes are 9.5 and 23–35, respectively [56,57]. M3-4 possessed the CO<sub>2</sub>/N<sub>2</sub> ideal selectivity of 21, which is much higher than the intrinsic selectivity of PDMS. This is because the PDMS coating efficiently sealed the non-selective pinholes (defects) on the skin layer of PEI hollow fibers [22,58]. The obtained CO<sub>2</sub>/N<sub>2</sub> ideal selectivity of 21 is close to the reported CO<sub>2</sub>/N<sub>2</sub> ideal selectivity of PEI membranes. Similar results were obtained in other research works [22,27,58]. Zuhairun et al. [58] dip coated a PDMS layer on the outer surface of polysulfone (PSF) hollow fibers to seal the pinholes and improve the gas separation performance. It was found that the CO<sub>2</sub>/N<sub>2</sub> ideal selectivity was increased from 3.87 for pristine PSF hollow fiber to 31.34 for PDMS coated PSF hollow fiber. Madaeni et al. [27] found that the CO<sub>2</sub>/N<sub>2</sub> ideal selectivity of PDMS coated polyethersulfone (PES) flat sheet membrane increased from 5.9 to 45.5 by increasing the number of coating layers from 2 to 5. This is because the

repetition of coating resulted in good sealing of the defect holes and reduced the unselective gas transport.

PDMS coating is an effective way to prepare composite hollow fiber membranes with high gas separation performance. However, the use of different hollow fiber supports for the coating process might affect the gas separation of the composite hollow fiber membranes. In this study, different types of PEI hollow fiber spun at various spinning conditions were chosen as supports, and the PDMS layer was coated on the outer surface of PEI hollow fibers at the same coating conditions. As is shown in Figure 14, the CO<sub>2</sub> permeances and CO<sub>2</sub>/N<sub>2</sub> ideal selectivities of PDMS/PEI composite membranes M3-2, M3-3, and M3-4 slightly increased when the bore fluid flow rate increased from 6 mL/min to 12 mL/min, indicating that the bore fluid flow rate slightly affects the gas permeance of PDMS/PEI composite membranes, especially at higher bore fluid flow rates i.e., 9 and 12 mL/min. The slight increase in gas permeance with the increase in bore fluid flow rate might result from the weaker PDMS solution intrusion in the dip coating process. This is because the wall thickness of hollow fiber decreased (Figure 6), and the polymer chains became more packed when the bore fluid flow rate was higher. As a result, the PDMS solution intrusion was inhibited to some extent. In the comparison of the CO<sub>2</sub> permeances and CO<sub>2</sub>/N<sub>2</sub> ideal selectivities of PDMS/PEI composite membranes M3-3, M3-5, and M3-6, it was found that the addition of NMP into bore fluid significantly increased the CO<sub>2</sub> permeances from 59 GPU to 192 GPU, while decreasing the CO<sub>2</sub>/N<sub>2</sub> ideal selectivities from 21 to 10. This is attributed to the formation of a more porous inner surface of PEI hollow fiber (S3) and decreased skin layer on the inner and outer surface of PEI hollow fiber (Figure 9). On the other hand, the high PDMS concentration (15 wt%) resulted in less intrusion to the substructure of hollow fibers because of its high bulk viscosity [59]. The effect of the change of substructure and the formation of a more porous inner surface of hollow fiber predominantly resulted in the increase in CO<sub>2</sub> permeances.

As was discussed above, it is concluded that the change of spinning parameters can manipulate the characteristics of structure and morphology of hollow fibers, resulting in significant influence on the CO<sub>2</sub> permeance and selectivity of the prepared composite hollow fiber membranes. In this work, the hollow fibers spun at a higher bore fluid flow rate (12 cm<sup>3</sup>/min) and from bore fluid containing 50 wt% of NMP are desirable hollow fiber substrates for PDMS coating to produce good balance between gas permeance and ideal selectivity. Liang et al. [29] coated PDMS solution (0.3 wt%) on the outer surface of hollow fibers fabricated from various concentrations (17.5, 20.0, 22.5, and 25.0 wt%) of PAN solution and found that the CO<sub>2</sub> permeance decreased from 5000 GPU to 1500 GPU with the increase in PAN concentration, while the CO<sub>2</sub>/N<sub>2</sub> ideal selectivity was maintained around 10 [29]. Li et al. [23] investigated the effects of substrate characteristics on PAN–PDMS composite hollow fiber membranes for CO<sub>2</sub>/N<sub>2</sub> and O<sub>2</sub>/N<sub>2</sub> separation. It was found that when the PAN hollow fiber is made from solvent exchange post treatment, the selectivities of CO<sub>2</sub>/N<sub>2</sub> and O<sub>2</sub>/N<sub>2</sub> of the composite membrane are similar to the PDMS intrinsic selectivities, indicating the formation of a defect-free PDMS layer. When the PAN hollow fiber is made from freeze drying post treatment, the selectivities of CO<sub>2</sub>/N<sub>2</sub> and O<sub>2</sub>/N<sub>2</sub> of the composite membrane are much lower [23].

### 3.2.3. The Comparison of Gas Separation Performance with Literature Data

As is shown in Table 4, the gas separation performances of the prepared PDMS/PEI composite membranes in this work are comparable with the gas separation performances of PDM- coated hollow fiber composite membranes in the literature, indicating the successful formation of a defect-free PDMS selective layer on PEI hollow fibers. The PDMS coated hollow fiber composite membranes either show higher gas permeance with lower selectivity or vice versa. The prepared PDMS/PEI composite membranes in this work followed the same trend since only a PDMS layer was coated on the outer surface of hollow fibers. To break the trade-off relationship between gas permeance and selectivity [55], some other

strategies should be applied, for example, the incorporation of inorganic particles into the polymer matrix [60].

**Table 4.** The comparison of gas separation performance of the prepared composite membranes with the literature.

Membrane Materials	Permeance of CO <sub>2</sub> (GPU)	CO <sub>2</sub> /N <sub>2</sub> Selectivity	Pure Gas Permeance Testing Conditions	Ref.
PDMS/PAN	858	8.4	30 °C, 2 bar	[61]
	1473	8.1		
	1986	6.4		
PDMS/PAN	370	13.0	25 °C, 1 bar	[23]
PDMS/PAN	1926	10.4	25 °C, 2 bar	[62]
PDMS–Cu <sub>3</sub> (BTC) <sub>2</sub> /PSF	109	31.0	25 °C, 5 bar	[58]
PDMS/PSF	64	32	25 °C, 5 bar	[58]
PDMS/PSF	55	35.2	25 °C, 5 bar	[22]
PDMS/PSF	200	33.3	25 °C, 13.6 bar	[63]
PDMS/PES-PI	60	39	25 °C, 4 bar	[64]
PTFPMS/PEI	62	17.2	25 °C, 3 bar	[25]
PDMS/PEI	45	19.7	25 °C, 2 bar	This work
	59	21.3		
	161	16.2		

#### 4. Conclusions

PEI hollow fibers were successfully fabricated by using a dry-jet-wet spinning technique. The polymer concentration significantly influenced the pore structure, skin layer thickness, and outer diameter of hollow fibers, which was confirmed by the significant decrease in gas permeance with the increase in polymer concentration. The bore fluid flow rate imparted predominant effects on the wall thickness and inner skin layer thickness rather than the outer diameter, gas permeance, and the structure of hollow fibers. The addition of NMP into bore fluid resulted in the decrease in the length of finger-like macrovoids near the lumen side due to the weakened nonsolvent intrusion and the decreased driving force of water inflow and solvent outflow. Consequently, the gas permeance of hollow fibers increased due to the formation of more porous inner surface and the decrease in skin layer thickness.

PDMS/PEI composite hollow fiber membranes were successfully prepared by dip-coating PDMS solution on the outer surface of hollow fibers spun from different spinning conditions. The gas separation performance of the composite membranes was affected by the hollow fiber substrates. Composite membranes M3-4 and M3-5 exhibited CO<sub>2</sub> permeance of 59 GPU and 161 GPU, CO<sub>2</sub>/N<sub>2</sub> selectivity of 21.3 and 16.2, respectively. The gas separation performance of M3-4 and M3-5 is comparable to the gas separation performance of PDMS coated hollow fiber membranes in the literature. The PDMS intrusion phenomenon occurred in the dip-coating process and was confirmed by elemental analysis.

**Supplementary Materials:** The following are available online at <https://www.mdpi.com/2077-0375/11/1/56/s1>, Figure S1: SEM micrographs of outer and inner surfaces of PEI hollow fibers spun from different concentrations of polymer solution—(A) HF1—16 wt%, (B) HF2—18 wt%, (C) HF3-2—20 wt%, (D) HF4—22 wt%, (E) HF5—24 wt%. Figure S2: SEM micrographs of outer and inner surface of PEI hollow fibers spun at different flow rates of bore fluid. (A) HF3-1—3 cm<sup>3</sup>/min, (B) HF3-2—6 cm<sup>3</sup>/min, (C) HF3-3—9 cm<sup>3</sup>/min, (D) HF3-4—12 cm<sup>3</sup>/min. Figure S3: SEM micrographs of outer and inner surfaces of PEI hollow fibers spun with different compositions of bore fluid. (A) HF3-3—H<sub>2</sub>O, (B) HF3-5—H<sub>2</sub>O/NMP 50/50 wt%, (C) HF3-6—H<sub>2</sub>O/NMP 30/70 wt%.



**Author Contributions:** Conceptualization, G.L. and W.K.; data curation, K.K. and J.K.; formal analysis, G.L. and K.K.; funding acquisition, W.K.; methodology, G.L., W.K. and J.K.; resources, W.K.; software, K.K. and J.K.; supervision, W.K. and J.K.; validation, W.K.; visualization, G.L. and K.K.; writing—original draft, G.L. and K.K.; writing—review and editing, G.L., W.K. and J.K. All authors have read and agreed to the published version of the manuscript.

**Funding:** This research received no external funding.

**Institutional Review Board Statement:** Not applicable.

**Informed Consent Statement:** Not applicable.

**Data Availability Statement:** Data is contained within the article or supplementary material.

**Conflicts of Interest:** The authors declare no conflict of interest.

## References

1. Wang, Y.; Li, L.; Zhang, X.; Li, J.; Wang, J.; Li, N. Polyvinylamine/amorphous metakaolin mixed-matrix composite membranes with facilitated transport carriers for highly efficient CO<sub>2</sub>/N<sub>2</sub> separation. *J. Membr. Sci.* **2020**, *599*, 117828. [[CrossRef](#)]
2. Rahman, F.A.; Aziz, M.M.A.; Saidur, R.; Bakar, W.A.; Hainin, M.; Putrajaya, R.; Hassan, N.A. Pollution to solution: Capture and sequestration of carbon dioxide (CO<sub>2</sub>) and its utilization as a renewable energy source for a sustainable future. *Renew. Sustain. Energy Rev.* **2017**, *71*, 112–126. [[CrossRef](#)]
3. Ma, C.; Wang, M.; Wang, Z.; Gao, M.; Wang, J. Recent progress on thin film composite membranes for CO<sub>2</sub> separation. *J. CO<sub>2</sub> Util.* **2020**, *42*, 101296. [[CrossRef](#)]
4. Powell, C.E.; Qiao, G.G. Polymeric CO<sub>2</sub>/N<sub>2</sub> gas separation membranes for the capture of carbon dioxide from power plant flue gases. *J. Membr. Sci.* **2006**, *279*, 1–49. [[CrossRef](#)]
5. Kamble, A.R.; Patel, C.M.; Murthy, Z. Polyethersulfone based MMMs with 2D materials and ionic liquid for CO<sub>2</sub>, N<sub>2</sub> and CH<sub>4</sub> separation. *J. Environ. Manag.* **2020**, *262*, 110256. [[CrossRef](#)]
6. Chen, W.; Zhang, Z.; Ho, L.; Yang, C.; Shen, H.; Yang, K.; Wang, Z. Metal-organic framework MOF-801/PIM-1 mixed-matrix membranes for enhanced CO<sub>2</sub>/N<sub>2</sub> separation performance. *Sep. Purif. Technol.* **2020**, *250*, 117198. [[CrossRef](#)]
7. Kumbharkar, S.C.; Liu, Y.; Li, K. High performance polybenzimidazole based asymmetric hollow fibre membranes for H<sub>2</sub>/CO<sub>2</sub> separation. *J. Membr. Sci.* **2011**, *375*, 231–240. [[CrossRef](#)]
8. Tham, H.M.; Wang, K.Y.; Hua, D.; Japip, S.; Chung, T.-S. From ultrafiltration to nanofiltration: Hydrazine cross-linked polyacrylonitrile hollow fiber membranes for organic solvent nanofiltration. *J. Membr. Sci.* **2017**, *542*, 289–299. [[CrossRef](#)]
9. Gao, J.; Thong, Z.; Wang, K.Y.; Chung, T.-S. Fabrication of loose inner-selective polyethersulfone (PES) hollow fibers by one-step spinning process for nanofiltration (NF) of textile dyes. *J. Membr. Sci.* **2017**, *541*, 413–424. [[CrossRef](#)]
10. Li, G.; Kujawski, W.; Válek, R.; Koter, S. A review—The development of hollow fibre membranes for gas separation processes. *Int. J. Greenh. Gas Control.* **2021**, *104*, 103195.
11. Woo, K.T.; Lee, J.; Dong, G.; Kim, J.S.; Do, Y.S.; Hung, W.-S.; Lee, K.-R.; Barbieri, G.; Drioli, E.; Lee, Y.M. Fabrication of thermally rearranged (TR) polybenzoxazole hollow fiber membranes with superior CO<sub>2</sub>/N<sub>2</sub> separation performance. *J. Membr. Sci.* **2015**, *490*, 129–138. [[CrossRef](#)]
12. Hasbullah, H.; Kumbharkar, S.; Ismail, A.F.; Li, K. Preparation of polyaniline asymmetric hollow fiber membranes and investigation towards gas separation performance. *J. Membr. Sci.* **2011**, *366*, 116–124. [[CrossRef](#)]
13. Mubashir, M.; Yeong, Y.F.; Lau, K.K.; Chew, T.L. Effect of spinning conditions on the fabrication of cellulose acetate hollow fiber membrane for CO<sub>2</sub> separation from N<sub>2</sub> and CH<sub>4</sub>. *Polym. Test.* **2019**, *73*, 1–11. [[CrossRef](#)]
14. Bang, Y.; Obaid, M.; Jang, M.; Lee, J.; Lim, J.; Kim, I.S. Influence of bore fluid composition on the physiochemical properties and performance of hollow fiber membranes for ultrafiltration. *Chemosphere* **2020**, *259*, 127467. [[CrossRef](#)]
15. Wang, D.; Li, K.; Teo, W.K. Preparation of asymmetric polyetherimide hollow fibre membrane with high gas selectivities. *J. Membr. Sci.* **2002**, *208*, 419–426. [[CrossRef](#)]
16. Baker, R.W.; Low, B.T. Gas Separation Membrane Materials: A perspective. *Macromolecules* **2014**, *47*, 6999–7013. [[CrossRef](#)]
17. Liang, C.Z.; Chung, T.-S.; Lai, J.-Y. A review of polymeric composite membranes for gas separation and energy production. *Prog. Polym. Sci.* **2019**, *97*, 101141. [[CrossRef](#)]
18. Cabasso, I.; Lundy, K.A. Method of Making Membranes for Gas Separation and the Composite Membranes. U.S. Patent 4,602,922, 29 July 1986.
19. Browall, W.R. Method for Sealing Breaches in Multi-Layer Ultrathin Membrane Composites. U.S. Patent 3,980,456, 14 September 1976.
20. Selyanchyn, R.; Ariyoshi, M.; Fujikawa, S. Thickness effect on CO<sub>2</sub>/N<sub>2</sub> separation in double layer Pebax-1657®/PDMS membranes. *Membranes* **2018**, *8*, 121. [[CrossRef](#)]
21. Liang, C.Z.; Chung, T.-S. Robust thin film composite PDMS/PAN hollow fiber membranes for water vapor removal from humid air and gases. *Sep. Purif. Technol.* **2018**, *202*, 345–356. [[CrossRef](#)]



22. Roslan, R.A.; Lau, W.J.; Sakthivel, D.B.; Khademi, S.; Zulhairun, A.K.; Goh, P.S.; Ismail, A.F.; Chong, K.C.; Lai, S.O. Separation of CO<sub>2</sub>/CH<sub>4</sub> and O<sub>2</sub>/N<sub>2</sub> by polysulfone hollow fiber membranes: Effects of membrane support properties and surface coating materials. *J. Polym. Eng.* **2018**, *38*, 871–880. [[CrossRef](#)]
23. Li, P.; Chen, H.Z.; Chung, T.-S. The effects of substrate characteristics and pre-wetting agents on PAN–PDMS composite hollow fiber membranes for CO<sub>2</sub>/N<sub>2</sub> and O<sub>2</sub>/N<sub>2</sub> separation. *J. Membr. Sci.* **2013**, *434*, 18–25. [[CrossRef](#)]
24. Liu, L.; Chakma, A.; Feng, X. CO<sub>2</sub>/N<sub>2</sub> separation by poly (ether block amide) thin film hollow fiber composite membranes. *Ind. Eng. Chem. Res.* **2005**, *44*, 6874–6882. [[CrossRef](#)]
25. Dai, Y.; Ruan, X.; Bai, F.; Yu, M.; Li, H.; Zhao, Z.; He, G. High solvent resistance PTFPMS/PEI hollow fiber composite membrane for gas separation. *Appl. Surf. Sci.* **2016**, *360*, 164–173. [[CrossRef](#)]
26. Liu, L.; Chakma, A.; Feng, X. Preparation of hollow fiber poly (ether block amide)/polysulfone composite membranes for separation of carbon dioxide from nitrogen. *Chem. Eng. J.* **2004**, *105*, 43–51. [[CrossRef](#)]
27. Madaeni, S.; Badiéh, M.M.S.; Vatanpour, V. Effect of coating method on gas separation by PDMS/PES membrane. *Polym. Eng. Sci.* **2013**, *53*, 1878–1885. [[CrossRef](#)]
28. Kargari, A.; Shamsabadi, A.A.; Bahrami Babaheidari, M. Influence of coating conditions on the H<sub>2</sub> separation performance from H<sub>2</sub>/CH<sub>4</sub> gas mixtures by the PDMS/PEI composite membrane. *Int. J. Hydrogen Energy* **2014**, *39*, 6588–6597. [[CrossRef](#)]
29. Liang, C.Z.; Yong, W.F.; Chung, T.-S. High-performance composite hollow fiber membrane for flue gas and air separations. *J. Membr. Sci.* **2017**, *541*, 367–377. [[CrossRef](#)]
30. Chong, K.C.; Lai, S.O.; Lau, W.J.; Thiam, H.S.; Ismail, A.F.; Roslan, R.A. Preparation, characterization, and performance evaluation of polysulfone hollow fiber membrane with PEBA or PDMS coating for oxygen enhancement process. *Polymers* **2018**, *10*, 126. [[CrossRef](#)]
31. Jamil, A.; Ching, O.P.; Shariff, A.M. Mixed matrix hollow fibre membrane comprising polyetherimide and modified montmorillonite with improved filler dispersion and CO<sub>2</sub>/CH<sub>4</sub> separation performance. *Appl. Clay Sci.* **2017**, *143*, 115–124. [[CrossRef](#)]
32. DashtArzhandi, M.R.; Ismail, A.F.; Matsuura, T.; Ng, B.C.; Abdullah, M.S. Fabrication and characterization of porous polyetherimide/montmorillonite hollow fiber mixed matrix membranes for CO<sub>2</sub> absorption via membrane contactor. *Chem. Eng. J.* **2015**, *269*, 51–59. [[CrossRef](#)]
33. Sukitpaneenit, P.; Chung, T.-S. Molecular elucidation of morphology and mechanical properties of PVDF hollow fiber membranes from aspects of phase inversion, crystallization and rheology. *J. Membr. Sci.* **2009**, *340*, 192–205. [[CrossRef](#)]
34. Jamil, A.; Oh, P.C.; Shariff, A.M. Polyetherimide-montmorillonite mixed matrix hollow fibre membranes: Effect of inorganic/organic montmorillonite on CO<sub>2</sub>/CH<sub>4</sub> separation. *Sep. Purif. Technol.* **2018**, *206*, 256–267. [[CrossRef](#)]
35. Naim, R.; Ismail, A.F. Effect of polymer concentration on the structure and performance of PEI hollow fiber membrane contactor for CO<sub>2</sub> stripping. *J. Hazard. Mater.* **2013**, *250–251*, 354–361. [[CrossRef](#)]
36. Bakeri, G.; Ismail, A.F.; Shariaty-Niassar, M.; Matsuura, T. Effect of polymer concentration on the structure and performance of polyetherimide hollow fiber membranes. *J. Membr. Sci.* **2010**, *363*, 103–111. [[CrossRef](#)]
37. Bonyadi, S.; Chung, T.S.; Krantz, W.B. Investigation of corrugation phenomenon in the inner contour of hollow fibers during the non-solvent induced phase-separation process. *J. Membr. Sci.* **2007**, *299*, 200–210. [[CrossRef](#)]
38. Wang, Z.-Y.; Li, S.; Xu, S.; Tian, L.; Su, B.; Han, L.; Mandal, B. Fundamental understanding on the preparation conditions of high-performance polyimide-based hollow fiber membranes for organic solvent nanofiltration (OSN). *Sep. Purif. Technol.* **2021**, *254*, 117600. [[CrossRef](#)]
39. Wang, Y.; Gruender, M.; Chung, T.S. Pervaporation dehydration of ethylene glycol through polybenzimidazole (PBI)-based membranes. 1. Membrane fabrication. *J. Membr. Sci.* **2010**, *363*, 149–159. [[CrossRef](#)]
40. Bildyukevich, A.; Plisko, T.; Usosky, V. The formation of polysulfone hollow fiber membranes by the free fall spinning method. *Pet. Chem.* **2016**, *56*, 379–400. [[CrossRef](#)]
41. Chau, T.T.; Bruckard, W.J.; Koh, P.T.L.; Nguyen, A.V. A review of factors that affect contact angle and implications for flotation practice. *Adv. Colloid Interface Sci.* **2009**, *150*, 106–115. [[CrossRef](#)]
42. Qtaishat, M.; Rana, D.; Khayet, M.; Matsuura, T. Preparation and characterization of novel hydrophobic/hydrophilic polyetherimide composite membranes for desalination by direct contact membrane distillation. *J. Membr. Sci.* **2009**, *327*, 264–273. [[CrossRef](#)]
43. Bakeri, G.; Matsuura, T.; Ismail, A.F.; Rana, D. A novel surface modified polyetherimide hollow fiber membrane for gas–liquid contacting processes. *Sep. Purif. Technol.* **2012**, *89*, 160–170. [[CrossRef](#)]
44. Naim, R.; Ismail, A.; Matsuura, T.; Rudaini, I.; Abdullah, S. Polyetherimide hollow fiber membranes for CO<sub>2</sub> absorption and stripping in membrane contactor application. *RSC Adv.* **2018**, *8*, 3556–3563. [[CrossRef](#)]
45. Li, Y.; Jin, C.; Peng, Y.; An, Q.; Chen, Z.; Zhang, J.; Ge, L.; Wang, S. Fabrication of PVDF hollow fiber membranes via integrated phase separation for membrane distillation. *J. Taiwan Inst. Chem. Eng.* **2019**, *95*, 487–494. [[CrossRef](#)]
46. Yong, W.F.; Li, F.Y.; Xiao, Y.C.; Chung, T.S.; Tong, Y.W. High performance PIM-1/Matrimid hollow fiber membranes for CO<sub>2</sub>/CH<sub>4</sub>, O<sub>2</sub>/N<sub>2</sub> and CO<sub>2</sub>/N<sub>2</sub> separation. *J. Membr. Sci.* **2013**, *443*, 156–169. [[CrossRef](#)]
47. Vankelecom, I.F.J.; Moermans, B.; Verschueren, G.; Jacobs, P.A. Intrusion of PDMS top layers in porous supports. *J. Membr. Sci.* **1999**, *158*, 289–297. [[CrossRef](#)]
48. Campana, D.M.; Ubal, S.N.; Giavedoni, M.D.; Saita, F.A. Influence of surfactants on dip coating of fibers: Numerical analysis. *Ind. Eng. Chem. Res.* **2016**, *55*, 5770–5779. [[CrossRef](#)]
49. Brinker, C.; Frye, G.; Hurd, A.; Ashley, C. Fundamentals of sol-gel dip coating. *Thin Solid Films* **1991**, *201*, 97–108. [[CrossRef](#)]

50. Dixit, H.N.; Homsy, G. The elastic Landau-Levich problem. *J. Fluid Mech.* **2013**, *732*, 5–28. [[CrossRef](#)]
51. Knozowska, K.; Li, G.; Kujawski, W.; Kujawa, J. Novel heterogeneous membranes for enhanced separation in organic-organic pervaporation. *J. Membr. Sci.* **2020**, *599*, 117814. [[CrossRef](#)]
52. Kujawska, A.; Knozowska, K.; Kujawa, J.; Li, G.; Kujawski, W. Fabrication of PDMS based membranes with improved separation efficiency in hydrophobic pervaporation. *Sep. Purif. Technol.* **2020**, *234*, 116092. [[CrossRef](#)]
53. Khorasani, M.T.; Mirzadeh, H.; Kermani, Z. Wettability of porous polydimethylsiloxane surface: Morphology study. *Appl. Surf. Sci.* **2005**, *242*, 339–345. [[CrossRef](#)]
54. Lin, D.; Zhao, Q.; Yan, M. Surface modification of polydimethylsiloxane microfluidic chips by polyamidoamine dendrimers for amino acid separation. *J. Appl. Polym. Sci.* **2016**, *133*, 43580. [[CrossRef](#)]
55. Robeson, L.M. The upper bound revisited. *J. Membr. Sci.* **2008**, *320*, 390–400. [[CrossRef](#)]
56. Chen, X.Y.; Kaliaguine, S.; Rodrigue, D. Polymer hollow fiber membranes for gas separation: A comparison between three commercial resins. *AIP Conf. Proc.* **2019**, *2139*, 070003.
57. Merkel, T.; Bondar, V.; Nagai, K.; Freeman, B.; Pinnau, I. Gas sorption, diffusion, and permeation in poly (dimethylsiloxane). *J. Polym. Sci. B Polym. Phys.* **2000**, *38*, 415–434. [[CrossRef](#)]
58. Zulfhairun, A.K.; Fachrurrazi, Z.G.; Izwanne, M.N.; Ismail, A.F. Asymmetric hollow fiber membrane coated with polydimethylsiloxane–metal organic framework hybrid layer for gas separation. *Sep. Purif. Technol.* **2015**, *146*, 85–93. [[CrossRef](#)]
59. Liang, C.Z.; Chung, T.S. Ultrahigh flux composite hollow fiber membrane via highly crosslinked PDMS for recovery of hydrocarbons: Propane and propene. *Macromol. Rapid Commun.* **2018**, *39*, 1700535. [[CrossRef](#)]
60. Shi, Y.; Liang, B.; Lin, R.-B.; Zhang, C.; Chen, B. Gas separation via hybrid metal-organic framework/polymer membranes. *Trends Chem.* **2020**, *2*, 254–269. [[CrossRef](#)]
61. Hu, L.; Cheng, J.; Li, Y.; Liu, J.; Zhou, J.; Cen, K. Amino-functionalized surface modification of polyacrylonitrile hollow fiber-supported polydimethylsiloxane membranes. *Appl. Surf. Sci.* **2017**, *413*, 27–34. [[CrossRef](#)]
62. Chen, H.Z.; Thong, Z.; Li, P.; Chung, T.-S. High performance composite hollow fiber membranes for CO<sub>2</sub>/H<sub>2</sub> and CO<sub>2</sub>/N<sub>2</sub> separation. *Int. J. Hydrogen Energy* **2014**, *39*, 5043–5053. [[CrossRef](#)]
63. Wang, D.; Teo, W.K.; Li, K. Preparation and characterization of high-flux polysulfone hollow fibre gas separation membranes. *J. Membr. Sci.* **2002**, *204*, 247–256. [[CrossRef](#)]
64. Kapantaidakis, G.C.; Koops, G.H. High flux polyethersulfone–polyimide blend hollow fiber membranes for gas separation. *J. Membr. Sci.* **2002**, *204*, 153–171. [[CrossRef](#)]

*Supporting Information*

# **The Effects of PEI Hollow Fiber Substrate Characteristics on PDMS/PEI Hollow Fiber Membranes for CO<sub>2</sub>/N<sub>2</sub> Separation**

**Guoqiang Li <sup>1</sup>, Wojciech Kujawski <sup>1,2,\*</sup>, Katarzyna Knozowska <sup>1</sup> and Joanna Kujawa <sup>1</sup>**

<sup>1</sup> Faculty of Chemistry, Nicolaus Copernicus University in Toruń, 7, Gagarina Street, 87-100 Toruń, Poland

<sup>2</sup> National Research Nuclear University MEPhI, 31, Kashira Hwy, 115409 Moscow, Russia

\* Correspondence: kujawski@chem.umk.pl; Tel.: +48-566114517

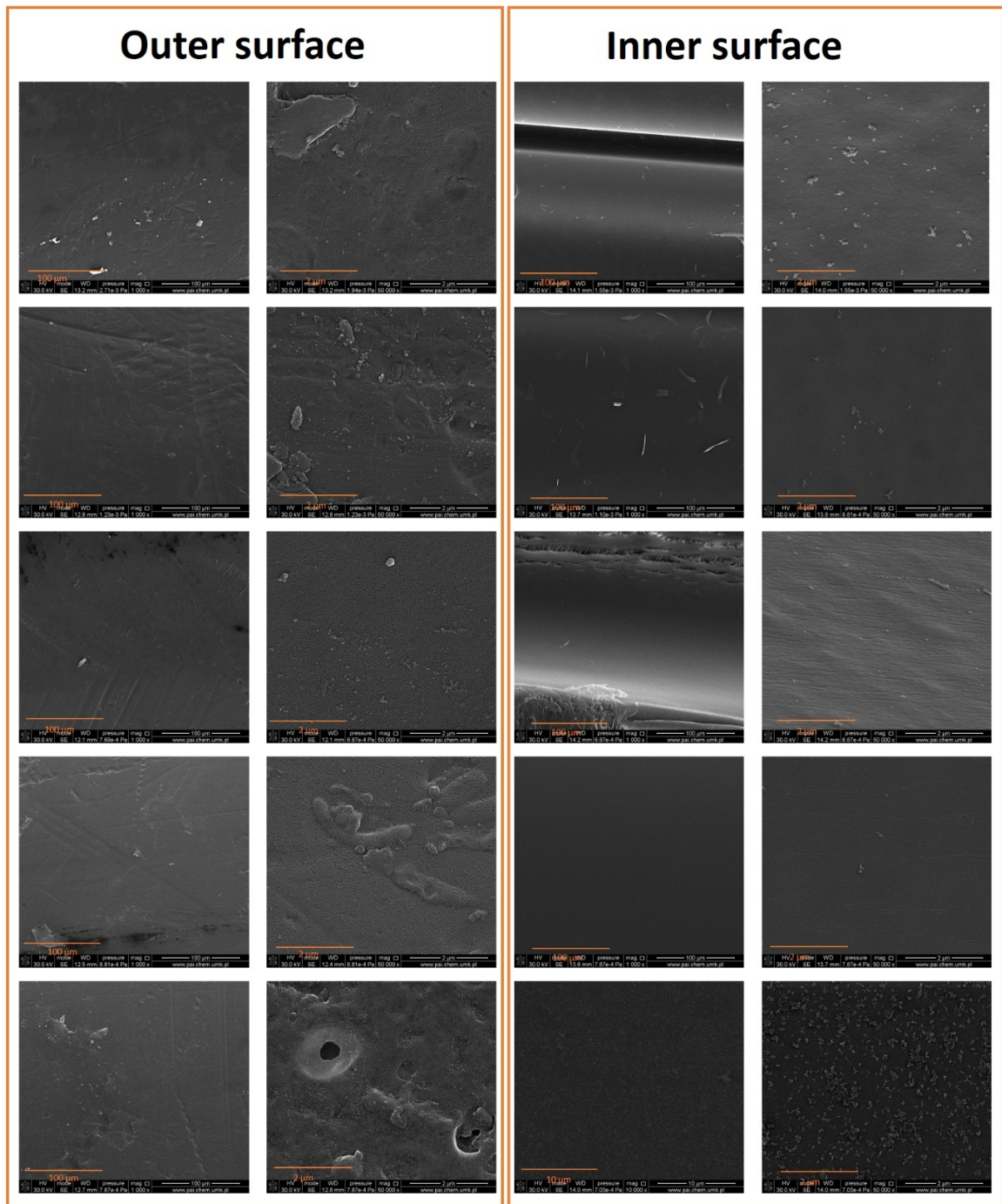


**Figure S1.** SEM micrographs of outer and inner surfaces of PEI hollow fibers spun from different concentrations of polymer solution—(A) HF1—16 wt.%, (B) HF2—18 wt.%, (C) HF3—20 wt.%, (D) HF4—22 wt.%, (E) HF5—24 wt.%.



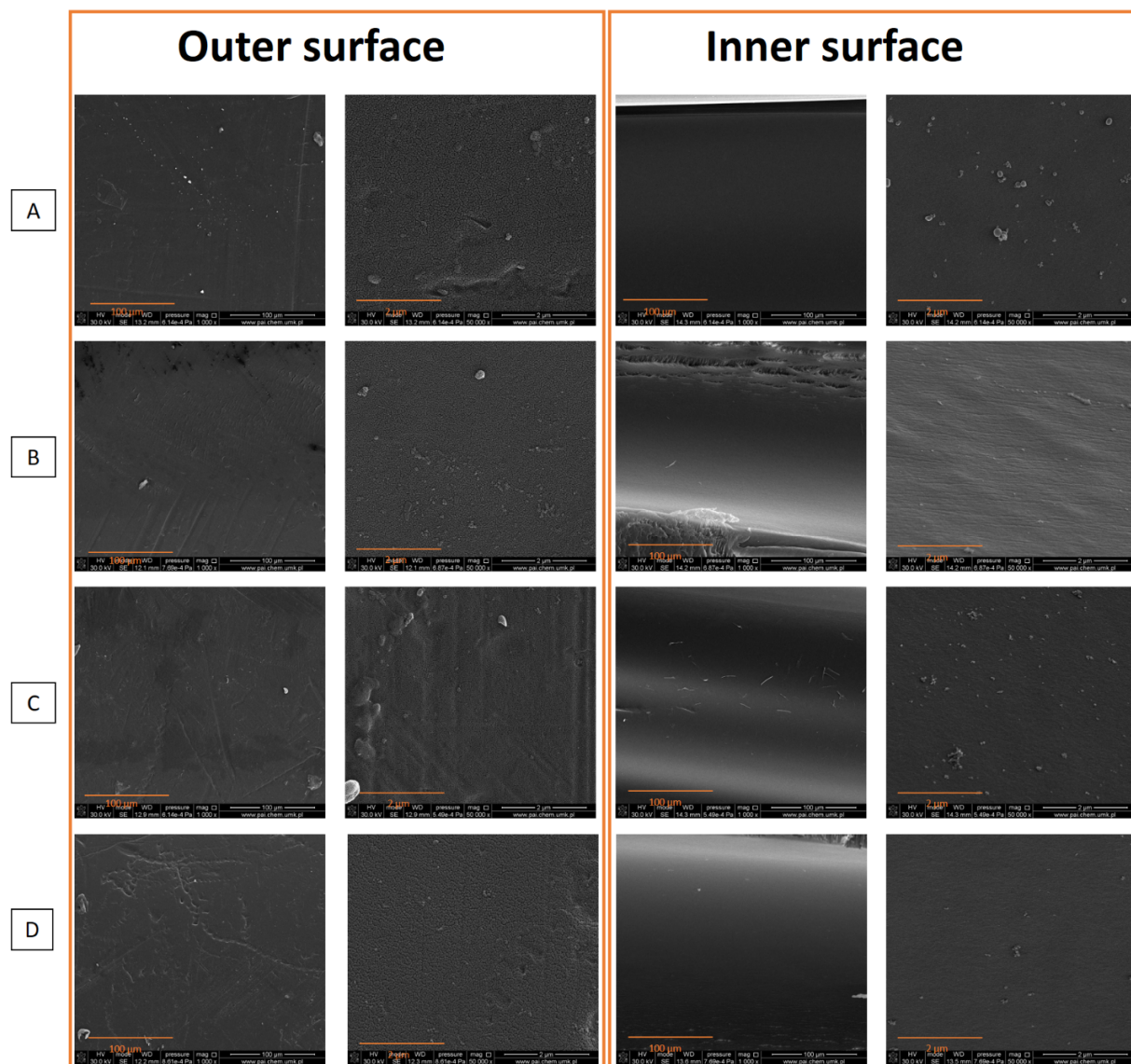


**Figure S2.** SEM micrographs of outer and inner surface of PEI hollow fibers spun at different flow rates of bore fluid. (A) HF3-1—3 cm<sup>3</sup>/min, (B) HF3-2—6 cm<sup>3</sup>/min, (C) HF3-3—9 cm<sup>3</sup>/min, (D) HF3-4—12 cm<sup>3</sup>/min.

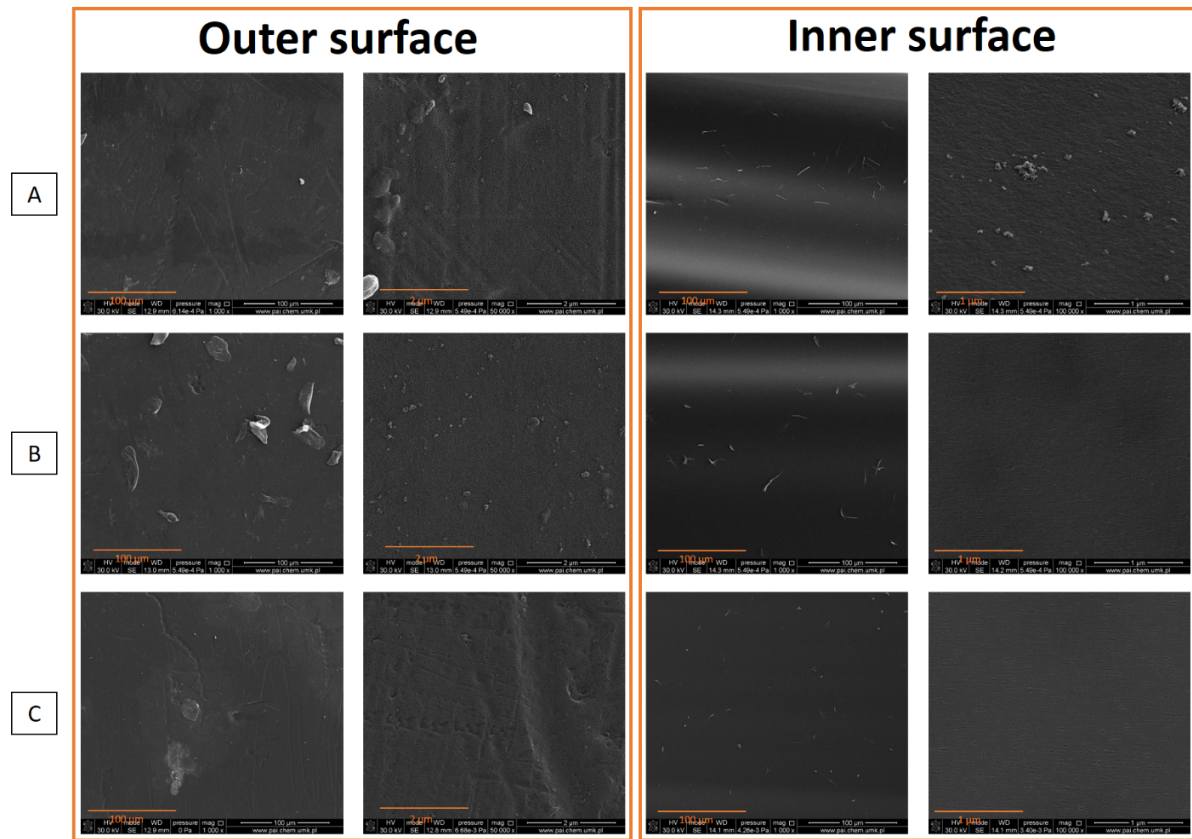


**Figure S3.** SEM micrographs of outer and inner surfaces of PEI hollow fibers spun with different compositions of bore fluid. (A) HF3-3—H<sub>2</sub>O, (B) HF3-5—H<sub>2</sub>O/NMP 50/50 wt.%, (C) HF3-6—H<sub>2</sub>O/NMP 30/70 wt.%.



### **Publication III**

**G. Li**, K. Knozowska 1, J. Kujawa, A. Tonkonogovas, A. Stankevičius, W. Kujawski, Fabrication of Polydimethylsiloxane (PDMS) Dense Layer on Polyetherimide (PEI) Hollow Fiber Support for the efficient CO<sub>2</sub>/N<sub>2</sub> Separation Membranes, *Polymers* 13 (2021) 756.

## Article

# Fabrication of Polydimethylsiloxane (PDMS) Dense Layer on Polyetherimide (PEI) Hollow Fiber Support for the Efficient CO<sub>2</sub>/N<sub>2</sub> Separation Membranes

Guoqiang Li <sup>1</sup>, Katarzyna Knozowska <sup>1</sup>, Joanna Kujawa <sup>1</sup> , Andrius Tonkonogovas <sup>2</sup> , Arūnas Stankevičius <sup>2</sup>  
and Wojciech Kujawski <sup>1,3,\*</sup> 

<sup>1</sup> Faculty of Chemistry, Nicolaus Copernicus University in Toruń, 7, Gagarina Street, 87-100 Toruń, Poland; grantli@doktorant.umk.pl (G.L.); katkno@doktorant.umk.pl (K.K.); joanna.kujawa@umk.pl (J.K.)

<sup>2</sup> Lithuanian Energy Institute, 3, Breslaujos Street, LT-44403 Kaunas, Lithuania; Andrius.Tonkonogovas@lei.lt (A.T.); Arunas.Stankevicius@lei.lt (A.S.)

<sup>3</sup> National Research Nuclear University MEPhI, 31, Kashira Hwy, 115409 Moscow, Russia

\* Correspondence: kujawski@chem.umk.pl; Tel.: +48-566-114-517

**Abstract:** The development of thin layer on hollow-fiber substrate has drawn great attention in the gas-separation process. In this work, polydimethylsiloxane (PDMS)/polyetherimide (PEI) hollow-fiber membranes were prepared by using the dip-coating method. The prepared membranes were characterized by Scanning Electron Microscope (SEM), energy-dispersive X-ray spectroscopy (EDX), and gas permeance measurements. The concentration of PDMS solution and coating time revealed an important influence on the gas permeance and the thickness of the PDMS layer. It was confirmed from the SEM and EDX results that the PDMS layer's thickness and the atomic content of silicon in the selective layer increased with the growth in coating time and the concentration of PDMS solution. The composite hollow-fiber membrane prepared from 15 wt% PDMS solution at 10 min coating time showed the best gas-separation performance with CO<sub>2</sub> permeance of 51 GPU and CO<sub>2</sub>/N<sub>2</sub> ideal selectivity of 21.

**Keywords:** polyetherimide (PEI) hollow-fiber support; thin film composite membranes; dip-coating conditions; polydimethylsiloxane (PDMS) dense layer; gas separation



**Citation:** Li, G.; Knozowska, K.; Kujawa, J.; Tonkonogovas, A.; Stankevičius, A.; Kujawski, W. Fabrication of Polydimethylsiloxane (PDMS) Dense Layer on Polyetherimide (PEI) Hollow Fiber Support for the Efficient CO<sub>2</sub>/N<sub>2</sub> Separation Membranes. *Polymers* **2021**, *13*, 756. <https://doi.org/10.3390/polym13050756>

Academic Editor: Damien Quémener

Received: 13 February 2021

Accepted: 25 February 2021

Published: 28 February 2021

**Publisher's Note:** MDPI stays neutral with regard to jurisdictional claims in published maps and institutional affiliations.



**Copyright:** © 2021 by the authors. Licensee MDPI, Basel, Switzerland. This article is an open access article distributed under the terms and conditions of the Creative Commons Attribution (CC BY) license (<https://creativecommons.org/licenses/by/4.0/>).

## 1. Introduction

CO<sub>2</sub> emission is inevitable owing to the growth of fossil fuel power plants and energy-intensive industries [1]. The excess of CO<sub>2</sub> emission has significantly affected the global warming, sea level rise, and climate changes. Therefore, the conversion, capture, and separation of CO<sub>2</sub> are crucial to tackle the abovementioned environmental problems attracting a plenty of attention in science and engineering in 21st century [2–4]. Several conventional techniques like amine adsorption, Pressure Swing Adsorption (PSA), and cryogenic distillation are used for CO<sub>2</sub> separation [5–7]. However, these processes are energy and cost intensive. Membrane process is an energy efficient technology for CO<sub>2</sub> separation [8]. The characteristics of the membrane process, such as simple operation, small footprint, and low cost, make it more competitive than the conventional gas-separation processes [9].

Both flat sheet and hollow-fiber membranes can be applied for CO<sub>2</sub> separation [8,10,11]. Comparing these two types of membrane configuration, it can be stated, that hollow fibers are easier to be scaled-up, owing to their high packing density and a self-supporting structure [8,12–14]. Polymer materials such as polysulfone (PSf) [15–17], polyetherimide (PEI) [18–21], polyimide (PI) [22,23], polyacrylonitrile (PAN) [24], and polyvinylidene fluoride (PVDF) [25] are commonly applied for the preparation of hollow fibers.

Membranes offering the high gas permeance are crucial to the gas-separation process at industrial scale. To obtain a membrane with high gas permeance and reasonable selectivity,

either the highly permeable materials are used or the thickness of dense selective layer must be reduced. However, highly permeable materials show rather low selectivity, due to the trade-off relationship of polymeric membranes [26]. Therefore, the preparation of asymmetric composite membranes consisting of a thin dense layer and a porous substrate is a desirable method to improve the gas-separation performance of membranes [27].

The dip-coating technique [28–30] and interfacial polymerization (IP) [31–33] are generally applied for the preparation of asymmetric composite membranes. The formation parameters play important roles in the formation of composite membrane with high gas-separation performance. Madaeni et al. [28] prepared polydimethylsiloxane (PDMS) coated polyethersulfone (PES) composite membranes for CO<sub>2</sub> capture. They investigated the coating conditions such as coating temperature, PDMS concentration and the number of sequential coatings. A total of 5 wt% PDMS was reported as an optimal concentration for the dip-coating process. The increase of the coating layer number increased the PDMS layer thickness and selectivity, however, significantly decreased the gas permeance [28]. Li et al. [34] prepared PDMS/polyacrylonitrile (PAN) composite hollow-fiber membranes via the dip-coating method for CO<sub>2</sub>/N<sub>2</sub> separation. It was found that the pre-wetting of PAN substrate could inhibit the intrusion of PDMS enabling the formation of defect-free selective layer [34]. Chen et al. [35] fabricated polyether block amide (Pebax)/PDMS/PAN composite hollow-fiber membranes via the dip-coating method and demonstrated that the prepared membranes could be used for flue gas treatment and hydrogen purification. PDMS was firstly coated on the PAN substrate to act as a gutter layer. The Pebax solution intrusion was minimized due to the PDMS gutter layer. Consequently, high gas permeance was obtained. The coating time and coating solution concentration are very important to the preparation of defect-free multi-layer hollow-fiber membranes [35]. Jo et al. [36] prepared inside coated thin film composite hollow-fiber membranes via interfacial polymerization. It was found that the concentrations of amine solution and acid chloride solution play crucial roles in determining the morphology and gas transport behavior of membranes. The high CO<sub>2</sub>/CH<sub>4</sub> selectivity of the prepared membrane was attributed to the formation of ultrathin film and the properties of binary amino groups [36]. The aforementioned examples demonstrate the need for the creation of thin dense layer on the porous supports for gas separation. The conditions for the preparation of dense thin layer on porous supports are specifically addressed, since the optimization of the fabrication conditions is critically important to the formation of defect-free thin layer. These results from the literature are very close to our research work, since they present the gas-separation performance of PDMS or Pebax layer on various polymer supports.

In addition to the experimental investigation on the gas-separation behavior in the thin-film-composite hollow-fiber membranes, the theoretical and modeling studies are also applied for the study of mass transfer through hollow-fiber membranes in literature. Xiao et al. [37] applied a fractal model for the capillary flow through a single tortuous capillary with rough surfaces in fibrous porous media. Ghobadi et al. [38] conducted a 2D mass-transfer simulation model, using computational fluid dynamics (CFD) for separation of CO<sub>2</sub> from a binary gas mixture of CO<sub>2</sub>/CH<sub>4</sub> by means of polytetrafluoroethylene (PTFE) hollow-fiber membrane contactor.

PDMS and PEI are commercially available polymers. PDMS has been widely used in gas-separation process. The aim of this research was to prepare PDMS/PEI composite hollow fiber membranes via the dip-coating method for CO<sub>2</sub>/N<sub>2</sub> separation. The influences of coating conditions such as the concentration of coating solution, coating time, curing temperature and the number of coating layers on the membrane structure, the gas permeance and ideal selectivity were systematically investigated. The optimization of coating conditions addressed in this study is one of the most outstanding research issues for the fabrication of defect-free thin dense layer on the porous support for gas separation. This experimental work is oriented to the practical application instead of theoretical and modeling studies even though they are also very important to the membrane-based gas-separation processes.

## 2. Experimental

### 2.1. Materials

Polyetherimide (PEI, Ultem 1000) pellets were kindly provided by Membrain (Stráž pod Ralskem, Czech Republic). *N*-methyl-2-pyrrolidone (NMP, 99.5%) was bought from Lineal Chemicals Sp. z o.o. (Warsaw, Poland). Methanol and *n*-hexane were purchased from Alchem Grupa Sp. z o.o. (Toruń, Poland). Pure CO<sub>2</sub> (99.999%) and N<sub>2</sub> (99.999%) gases were purchased from Air Products Sp. z o.o. (Siewierz, Poland). The fast solidified epoxy resin Araldite 2000 and 3M EPX Quadro Mixing Nozzles were delivered by Farnell (Warsaw, Poland). Elastosil LR 6240A (containing platinum catalyst) and Elastosil LR 6240B (containing crosslinker) were provided by Wacker Chemie AG Polska Sp. z o.o. (Warsaw, Poland).

### 2.2. Fabrication of PEI Hollow Fibers

Dope solution with PEI concentration 20 wt% was prepared by dissolving PEI pellets in NMP in a round bottom flask under refluxing condition at 60 °C for 24 h. Prior to dissolving PEI pellets in NMP, they were dried in oven at 100 °C to remove the traces of moisture. The prepared dope solution was transferred into a laboratory screw cap bottle and left for 24 h for degassing. The PEI hollow fibers were prepared via the dry-jet wet spinning process by using a laboratory-built spinning system [8,39]. The spinning conditions are shown in Table 1. In the spinning process, gear pump was used to deliver the dope solution at a specific extrusion rate from the stainless-steel reservoir to a spinneret. The bore fluid was delivered into the spinneret simultaneously by using a syringe pump. The as-spun hollow fibers went through an air gap and free fall into a coagulation bath containing distilled water, at room temperature. The prepared hollow fibers were cut and soaked in another water bath for 2 days, to remove the remaining NMP solvent. The hollow fibers from water bath were immersed into methanol for 12 h. Afterwards, the methanol-wet hollow fibers were immersed into hexane for 12 h. At last, hollow fibers were taken out from hexane and dried at room temperature, before further investigations. The physical properties of PEI hollow fibers have been fully investigated and presented in our previous work [39]; the basic parameters related to the diameters, wall thickness, skin layer thickness, and gas transport properties of hollow fibers are gathered in Table 2.

**Table 1.** Spinning parameters for polyetherimide (PEI) hollow-fiber fabrication.

Spinning Parameters	Spinning Conditions
Spinneret dimensions, outer diameter/inner diameter (mm/mm)	4.8/2.1
Bore fluid	Distilled water
Bore fluid flow rate (mL/min)	9–12
Bore fluid temperature (°C)	25 ± 2
Dry air gap length (cm)	25
Dope extrusion rate (mL/min)	7.6
Take up	Free fall
External coagulant	Water
Temperature of external coagulant (°C)	25 ± 2
Temperature of spinneret (°C)	25 ± 2

**Table 2.** Material and transport characteristics of the prepared hollow-fiber substrate [39].

d <sub>outer</sub> (μm)	d <sub>inner</sub> (μm)	l <sub>wall</sub> (μm)	Outer Skin (μm)	Inner Skin (μm)	CO <sub>2</sub> Permeance (GPU)	CO <sub>2</sub> /N <sub>2</sub> Selectivity
1446 ± 100	1053 ± 81	194 ± 43	2.40 ± 0.90	0.37 ± 0.07	6427	1.07

### 2.3. Dip-Coating Procedure

The coating process was performed on the outer surface of membranes, by applying the following procedure. First of all, PDMS component A and B with mass ratio of 1:10 were dissolved in hexane, to prepare 1.5, 3, 5, 7, 10, 15, and 20 wt% PDMS-coating solution. The solution was prepared by stirring its components for 2 h at room temperature. The PEI hollow fibers were immersed into the PDMS solutions of various concentrations for 10 min at room temperature. To investigate the coating time effect, hollow fibers were immersed into 15 wt% PDMS solution for various coating time of 0.5, 1, 3, 5, 7, 10, and 15 min at room temperature. The PDMS/PEI membranes prepared from 15 wt% PDMS solution and 10 min coating time were cured at various temperatures of 25, 50, 80, and 130 °C for 1 h. Moreover, a sequential coating process was conducted by dip-coating hollow fibers into 15 wt% PDMS solution for 10 min, several times, at room temperature, to investigate the effect of the number of PDMS layers. All the prepared PDMS/PEI composite hollow-fiber membranes were dried in air for at least 48 h, to remove the solvent and to fully cure the PDMS.

### 2.4. Characterization of PDMS/PEI Membranes

The morphology of the fabricated PEI hollow fibers and PDMS/PEI composite membranes were characterized by using Scanning Electron Microscope (SEM)—LEO 1430 VP microscope (Leo Electron Microscopy Ltd., Cambridge, UK). The scanning was performed at an accelerating voltage of 30 keV. To analyze the cross section of hollow fibers, the samples were prepared by fracturing fibers frozen in liquid nitrogen. Prior to the analysis, samples were sputtered with a conductive layer (thickness in the range of 2–6 nm) of Au/Pd (80/20) alloy. The energy-dispersive X-ray spectroscopy (EDX) analysis was conducted by using Phenom Prox/Pro/Pure, Generation 5 (Phenom-Word B. V., Eindhoven, The Netherlands). The PDMS layer thicknesses taken at the top and bottom parts of the prepared composite membranes were measured using SEM photos and ImageJ software (University of Wisconsin, Madison, WI, USA).

### 2.5. Module Preparation and Gas Permeance Measurements

To prepare the module, 2 hollow fibers with a length of 15–20 cm were assembled as a bundle. One hollow-fiber bundle was placed in a glass tube. Briefly, the single hollow-fiber bundle was placed in a glass tube. Both ends of the glass tube were sealed with a 5 min fast solidified epoxy resin (Araldite, Winterthur, Switzerland). Subsequently, one end of the glass tube was opened by using a scalpel before the complete solidification of epoxy resin. The details related to the module preparation are described elsewhere [39]. Pure N<sub>2</sub> and CO<sub>2</sub> were used for the single gas permeance tests. The trans-membrane pressure was set at 2 bar for all measurements, at room temperature, i.e., 25 °C. To ensure the accuracy of experiments, the gas permeance measurements were accomplished 3 times, in the stabilized conditions. A bubble flow meter was used to measure the gas flow rate. The permeances of gases expressed in GPU and the ideal selectivity expressed in the ratio of CO<sub>2</sub> permeance to N<sub>2</sub> permeance were used to estimate the gas-separation performance of PDMS/PEI composite hollow-fiber membranes. The permeances (P/d), of gases through the hollow-fiber module were calculated by using Equation (1):

$$\frac{P}{d} = \frac{Q}{\Delta p A} = \frac{Q}{2n\pi r l \Delta p} \quad (1)$$

where P is the permeability (Barrer), d is the thickness of membrane selective layer (cm), Q is the flux of gas permeation rate (cm<sup>3</sup> (STP)/s), Δp is the pressure difference across the membrane (cmHg), A is the effective membrane area (cm<sup>2</sup>), n is the number of hollow fibers, r is the outer radius (cm) of hollow fiber, and P/d is the gas permeance expressed in GPU (1 GPU = 10<sup>-6</sup> cm<sup>3</sup> (STP) cm<sup>-2</sup> s<sup>-1</sup> cmHg<sup>-1</sup>).

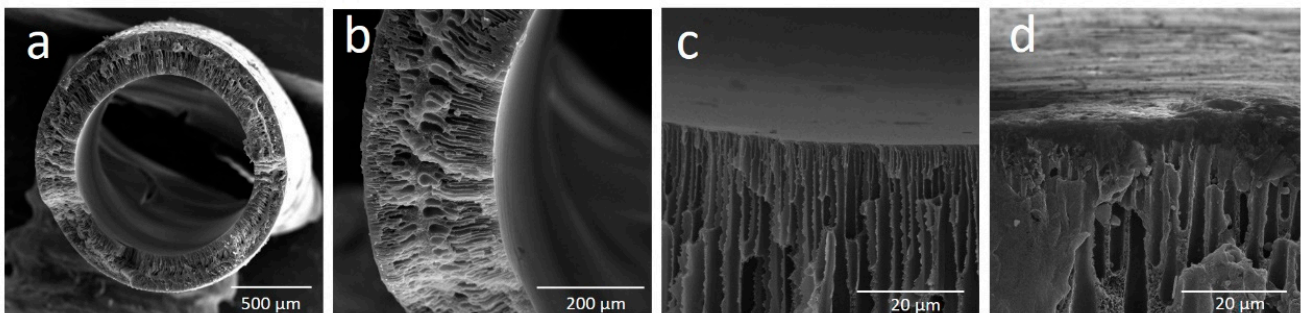
The ideal selectivity,  $\alpha$ , is defined as the permeability coefficients or permeances ratio of two pure gases (Equation (2)):

$$\alpha_{12} = \frac{(P/d)_1}{(P/d)_2} = \frac{P_1}{P_2} \quad (2)$$

### 3. Results and Discussion

#### 3.1. Membrane Morphology

The structure and morphology of the cross-section of the uncoated PEI hollow fibers are shown in Figure 1. Figure 1a presents the overall cross-section of the prepared hollow fiber. The prepared hollow fibers possess finger-like macrovoids near lumen and shell sides, tear-like macrovoids underneath the finger-like macrovoids, microporous structure in the middle of hollow-fiber wall (Figure 1b), and relatively thin dense skin layer on the inner surface (Figure 1c) and outer surface (Figure 1d) of hollow fibers. The resulting membrane morphology is affected by the polymer–solvent interactions, solvent–coagulant interactions and the concentration and viscosity of the dope medium [40,41]. The formation of finger-like and tear-like macrovoids in hollow fibers can be attributed to the water intrusion and the fast mass exchange between the solvent in the polymer solution and water (non-solvent), since distilled water was used as bore fluid and outer coagulant in the spinning process. Water is a strong non-solvent, while NMP has weaker interaction towards PEI; hence, it formed instant phase de-mixing, which created the finger-like and tear-like macrovoids [42]. The finger-like macrovoids near the shell side were shorter than the ones near the lumen side (Figure 1b). This is because of the formation of thin skin dense layer on the outer surface which impeded the water intrusion process. In the spinning process, the as-spun hollow fiber went through an air-gap distance of 25 cm (Table 1), and then to the water coagulant bath; the solvent evaporated during this short time, which increased the viscosity of polymer solution near shell side. As a result, the thin dense skin layer was formed and the solvent/non-solvent exchange process was slowed down.



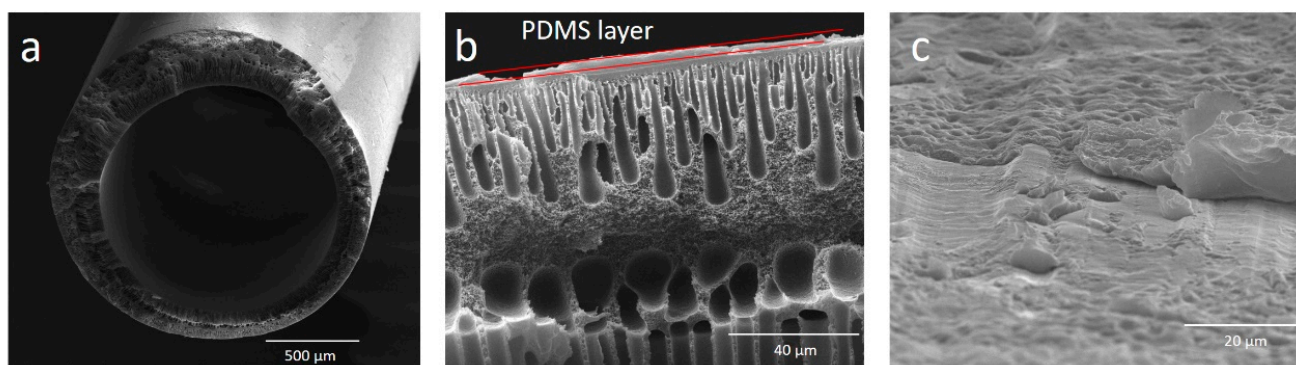
**Figure 1.** SEM pictures of uncoated PEI hollow fibers: (a) overall cross-section, (b) enlarged cross-section, (c) inner side, and (d) outer side.

Figure 2 shows the morphology of PDMS/PEI membranes prepared by using the dip-coating method. The overall cross-section of PDMS/PEI membrane was shown in Figure 2a. It is observed that a thin PDMS selective layer was formed on the outer surface of PEI hollow fibers (Figure 2b,c).

As it is shown in Figure 3, the coating time and the coating solution concentration affect the thickness of PDMS layer. When 15 wt% of PDMS solution was used, the thickness of PDMS layer at the bottom part of PDMS/PEI composite membrane increased from 3 to 4  $\mu\text{m}$ , along with the change of coating time from 1 to 7 min. The further increase in coating time to 15 min did not change the thickness of PDMS layer (Figure 3a). The thickness of PDMS layer at the top part of PDMS/PEI composite membrane slightly increased from 1.9 to 2.5  $\mu\text{m}$ , accompanied by the change of coating time from 1 to 15 min (Figure 3a). With an increase in coating time, more PDMS chains could diffuse and adhere onto the substrate surface and reach a stable state. Therefore, the PDMS layer thickness increased



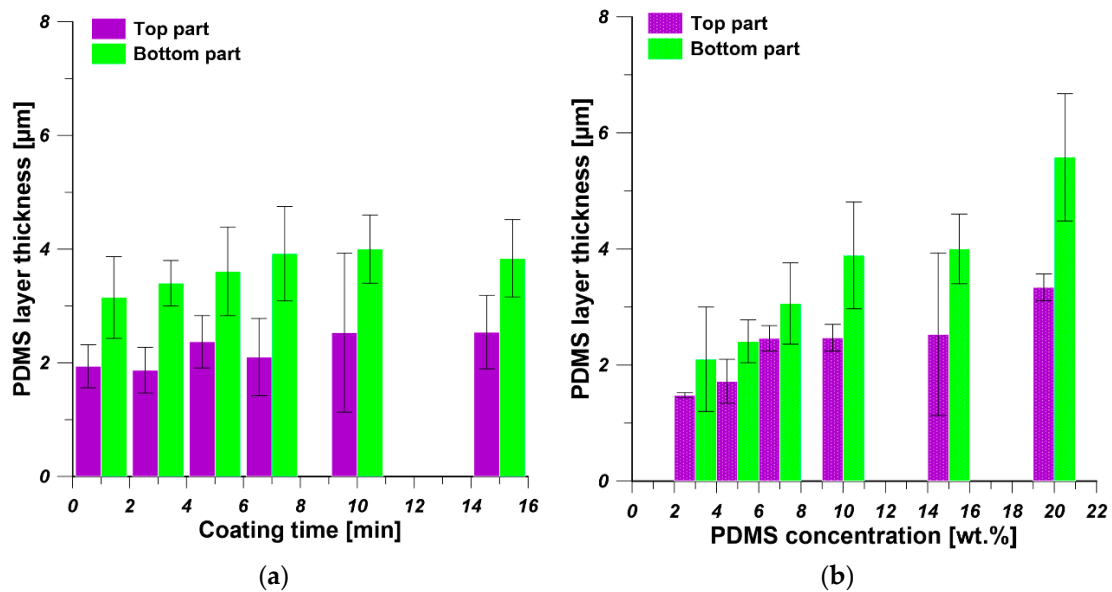
when the coating time increased from 1 to 7 min, while it became constant with the further increase of coating time to 15 min. The coating time has a more significant influence on the PDMS layer thickness at the bottom part than the top part of PDMS/PEI composite membrane. When the coating time is set as 10 min, the thickness of PDMS layer at the top part and the bottom part of PDMS/PEI composite membrane increased from 1.5 and 2  $\mu\text{m}$  to 3.3 and 5.6  $\mu\text{m}$ , along with the growth of PDMS concentration from 3 to 20 wt%, respectively (Figure 3b). According to the Landau–Levich theory, the thickness of coating layer is positively proportional to the viscosity of coating solutions [43]. The viscosity of PDMS solution increased with the concentration increase of PDMS solution. As a result, the thickness of the PDMS layer augmented with an increase in PDMS concentration. It was reported in the literature that the thickness of the coating layer increased with the increase in the concentration of coating solution and coating time [16,28,44,45]. When comparing Figure 3a,b, it is found that the concentration of PDMS solution predominantly affected the thickness of PDMS selective layer. Furthermore, the thickness of PDMS layer at the bottom part is slightly higher than the thickness of PDMS layer at the top part. In the dip-coating process, the interplay of several parameters, e.g., viscous force, solvent evaporation and draining, surface tension, gravity, and hydrodynamic factors in the layer deposition region, governs the layer thickness and the position of the drying front. The bottom part was always close to the solution reservoir, while the top part was relatively far from the coating solution. A wet film with higher concentration was formed at the drying front, due to the higher ratio of surface area to volume, which results in the drawing of solution from surrounding area. When a dry film was formed at the drying front, a capillary force appeared on the solution, resulting in the thickening of the coated film [46–49].



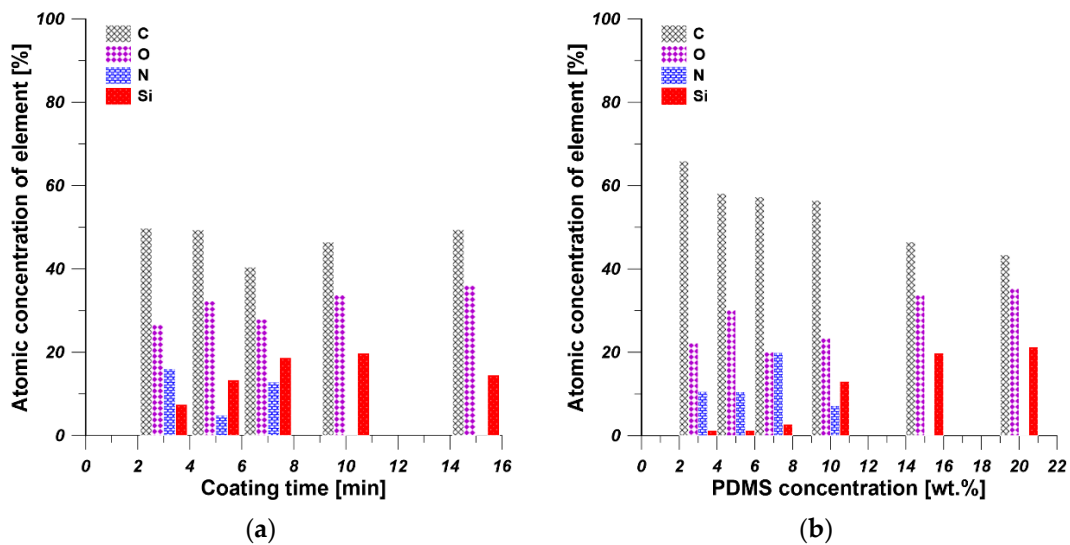
**Figure 2.** SEM pictures of polydimethylsiloxane (PDMS)/PEI membrane prepared from 15 wt% PDMS solution at 10 min coating time: (a) overall cross-section, (b) enlarged cross-section, and (c) outer PDMS coating layer.

Figure 4 shows the EDX results of PDMS/PEI membranes prepared at various coating times and using various concentrations of PDMS solution. The detection of carbon, oxygen, and nitrogen can be attributed to the characteristics of PEI, which contains imide group in its chemical structure. The detection of silicon element indicates the PDMS was successfully coated on the outer surface of substrate. As it is shown in Figure 4a, with an increase in coating time, the atomic concentration of nitrogen and silicon decreased and increased, respectively, which indicates the more desirable formation of PDMS selective layer. When the coating time is over 10 min, a dense PDMS layer completely covered the outer surface of support. These results are consistent with the results of gas permeance of PDMS/PEI membranes prepared at various coating time (Section 3.2.1). As the EDX results in Figure 4b show, the atomic concentration of silicon increased significantly from 1.26% to 21.31%, along with the change of coating solution from 3 to 20 wt%. These results are also consistent with the results of PDMS layer thickness (Figure 3b) and gas permeance of PDMS/PEI membranes prepared from various concentrations of PDMS solution (Section 3.2.2). As discussed above, the silicon concentration increased with the growth of coating time and

PDMS concentration, which is due to the formation of thicker PDMS layer and deposition of more PDMS chains on the support.



**Figure 3.** The thickness of PDMS selective layer: (a) the effect of coating time at constant concentration of PDMS solution equal to 15 wt%; (b) the effect of PDMS concentration at constant coating time equal to 10 min.



**Figure 4.** EDX surface mapping results for PDMS/PEI membranes fabricated (a) by changing the coating time, using PDMS concentration equal to 15 wt%; (b) by using various PDMS concentrations at constant coating time equal to 10 min.

### 3.2. Gas-Separation Performance

The prepared unmodified PEI hollow fibers were highly permeable to  $\text{CO}_2$  and  $\text{N}_2$ , with the ideal selectivity close to 1. To obtain a PDMS/PEI composite hollow-fiber membrane with high selectivity and reasonable gas permeance via the dip-coating method, the optimization of coating conditions plays a crucial role. The influence of the chosen coating conditions on the gas-separation performance of PDMS/PEI composite hollow-fiber membrane is discussed in this section.

### 3.2.1. The Effect of Coating Time

To investigate the influence of coating time on the gas permeance, PDMS/PEI composite membranes were fabricated by immersing PEI supports in 15 wt% of PDMS solution at various time from 0.5 to 15 min and cured at 25 °C. Figure 5a shows the trends of CO<sub>2</sub> and N<sub>2</sub> permeances, and the ideal selectivity of PDMS/PEI membranes prepared at various coating times. It can be realized that the CO<sub>2</sub> and N<sub>2</sub> permeances decreased significantly when the coating time changed from 0.5 to 5 min. Then the CO<sub>2</sub> permeance continued to decrease slightly, while the N<sub>2</sub> permeance leveled off for the coating time in the range of 5 to 15 min. This is because the kinetic diameter of N<sub>2</sub> molecule (0.36 nm) is larger than that of CO<sub>2</sub> molecule (0.33 nm). Moreover, the CO<sub>2</sub> molecules possess higher affinity to PDMS [50]. Hence, CO<sub>2</sub> molecules are transported much faster than N<sub>2</sub> ones, and they are more sensitive to the thickness change of PDMS layer (Figure 3a). On the other hand, the CO<sub>2</sub>/N<sub>2</sub> ideal selectivity increased to the maximal values of 21, when the coating time approached 10 min. Afterwards, the CO<sub>2</sub>/N<sub>2</sub> ideal selectivity decreased only slightly. This is caused by a fact that with an increase of coating time, the defect-free PDMS layer was formed, resulting in the increased value of the ideal selectivity. However, the coated PDMS might be re-dissolved in the solvent when a longer coating time is applied. As a result, defects might be formed and the selectivity was reduced. It is found that 10 min was the optimal coating time for the preparation of PDMS/PEI membranes with a high gas-separation performance. Similar results were also found by Chen et al. [35]. The thickness of PDMS layer of PDMS/PEI composite membrane prepared from 15 wt% of PDMS solution at various coating times was measured. Figure 5b shows the influence of PDMS layer thickness on CO<sub>2</sub> permeance; it can be seen that CO<sub>2</sub> permeance drops with the formation of thicker PDMS layer due to the increased mass transfer resistance [51,52]. According to the solution-diffusion model, the gas permeance is inversely proportional to the thickness of selective layer [53]. It can be seen in Figure 5b that the CO<sub>2</sub> permeance is linearly proportional to the reciprocal of PDMS layer thickness, which revealed the hypothesis that the gas transport through the PDMS layer obeys the solution-diffusion mechanism.

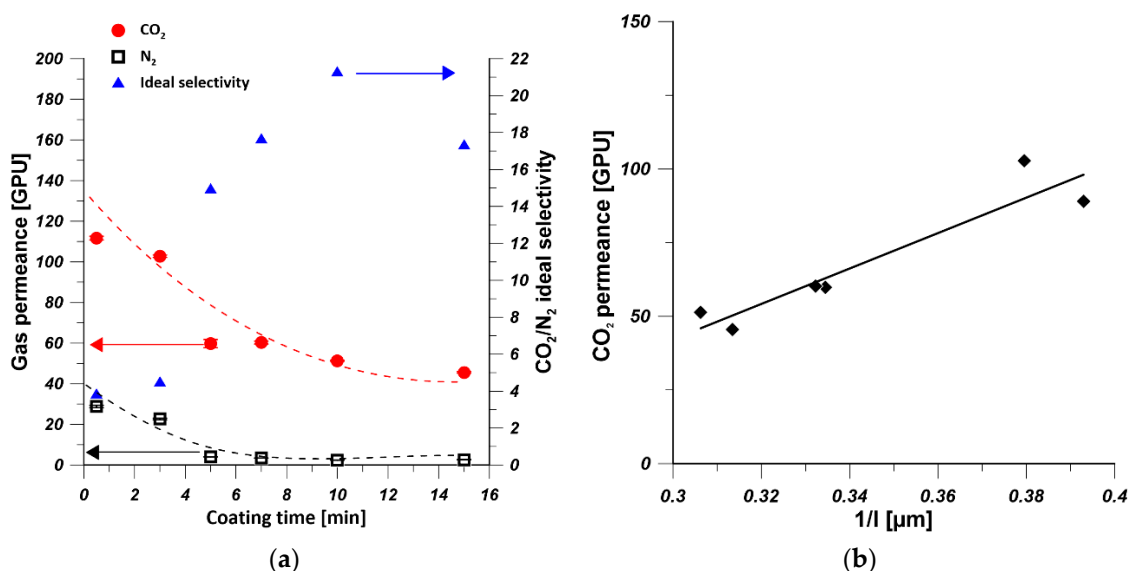


**Figure 5.** (a) The effect of coating time on gas permeance and ideal selectivity of PDMS/PEI membranes prepared from 15 wt% of PDMS solution (the dashed line indicates only the trend of gas permeance change). (b) The influence of PDMS layer thickness ( $l$ ) on CO<sub>2</sub> permeance of PDMS/PEI membranes prepared from various 15 wt% of PDMS solution at various coating time (the average thickness of PDMS layer was calculated based on the thicknesses of PDMS layer at the top and bottom parts).

### 3.2.2. The Effect of PDMS Concentration

As it is shown in Figure 6a, the CO<sub>2</sub> permeance and N<sub>2</sub> permeance dramatically decreased from 1360 GPU to 49 GPU and 2.5 GPU, respectively, when the PDMS concentration changed from 1.5 wt% to 10 wt%. Then the CO<sub>2</sub> permeance was constant at 50 GPU but slightly decreased to 40 GPU with the change of PDMS concentration from 15 wt% to 20 wt%. However, N<sub>2</sub> permeance was leveled off at 2.4 GPU when the PDMS concentration was between 10 and 20 wt%. The decrease in gas permeance was attributed to the increase in PDMS layer thickness (Figure 3b). The CO<sub>2</sub>/N<sub>2</sub> ideal selectivity increased to the maximal values of 21, when the PDMS concentration increased to 15 wt%. However, it decreased when 20 wt% PDMS solution was used for coating. When the PDMS solutions of 1.5, 3, 5, and 7 wt% were used as coating solution, defects might be formed on the PDMS selective layer. These findings are consistent with the EDX mapping results (Figure 4b). When 20 wt% of PDMS solution was used as coating solution, the prepared composite hollow-fiber membrane possessed the lowest CO<sub>2</sub> permeance owing to the formation of a thicker PDMS selective layer (Figure 3b). The decrease of CO<sub>2</sub>/N<sub>2</sub> ideal selectivity can be explained by the relatively larger decrease in CO<sub>2</sub> permeance comparing to the N<sub>2</sub> permeance which resulted from the sensitivity of CO<sub>2</sub> to the change of PDMS layer thickness. Chong et al. [54] found similar results where PDMS/PSf composite hollow-fiber membranes experienced lower O<sub>2</sub> permeance and O<sub>2</sub>/N<sub>2</sub> selectivity due to the formation of thicker PDMS layer which increases the mass transfer resistance. The thickness of PDMS layer of PDMS/PEI composite membrane prepared from various concentrations of PDMS solution at coating time equal to 10 min was measured. As it is shown in Figure 6b, CO<sub>2</sub> permeance is linearly proportional to the reciprocal of PDMS layer thickness which is in good agreement with solution-diffusion model [53]. The decrease in CO<sub>2</sub> permeance was attributed to an increase in the thickness of PDMS selective layer [51,53].

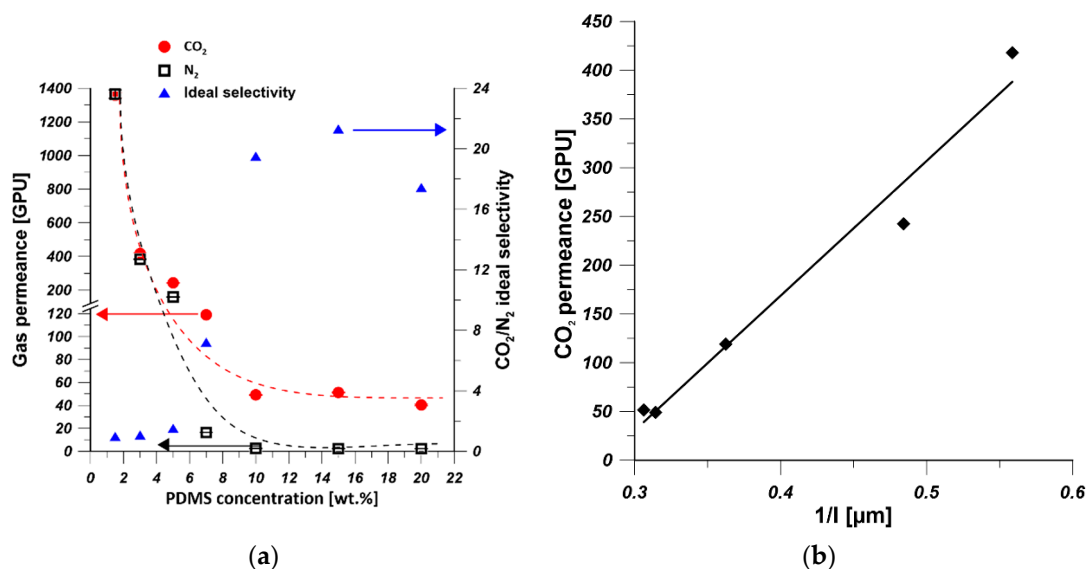


**Figure 6.** (a) The effect of PDMS concentration on gas permeance and ideal selectivity of PDMS/PEI membranes prepared at coating time of 10 min (the dashed line only indicates the trend of gas permeance change). (b) The influence of PDMS layer thickness on CO<sub>2</sub> permeance of PDMS/PEI membranes prepared from various PDMS concentrations, at a coating time of 10 min (the average thickness of PDMS layer was calculated based on the thickness of PDMS layer at the top and bottom parts).

### 3.2.3. The Effect of the Curing Temperature

To investigate the effect of curing temperature on the gas permeance of PDMS/PEI membranes, 15 wt% of PDMS solution was coated on PEI hollow-fiber substrate for 10 min. Subsequently, the coated hollow fibers were transferred to an oven and crosslinked at vari-

ous temperatures, i.e., 25, 50, 80, and 130 °C. As it is shown in Figure 7, the gas permeances of CO<sub>2</sub> and N<sub>2</sub> experienced an increase and decrease trend with the increase in annealing temperature. The PDMS/PEI composite hollow-fiber membranes cured at 25 °C showed the highest CO<sub>2</sub>/N<sub>2</sub> selectivity. Therefore, 25 °C was used as the curing temperature and membranes were annealed in air at 25 °C. Madaeni et al. [28] observed that the CO<sub>2</sub> permeance and CO<sub>2</sub>/N<sub>2</sub> selectivity of PDMS/PES flat sheet membrane decreased slightly with the increase in curing temperature from 25 °C to 200 °C. Kargari et al. [21] found that the curing temperature has little effect on the H<sub>2</sub> and CH<sub>4</sub> permeances and selectivity of PDMS/PEI flat sheet membranes. It can be seen that higher curing temperature could not enhance the gas-separation performance of PDMS coated composite membranes. This is because the viscosity of coating solution decreased with the increase in curing temperature, which resulted in the weakened adhesion between PDMS chain and substrate and the formation of undesirable defects [43].

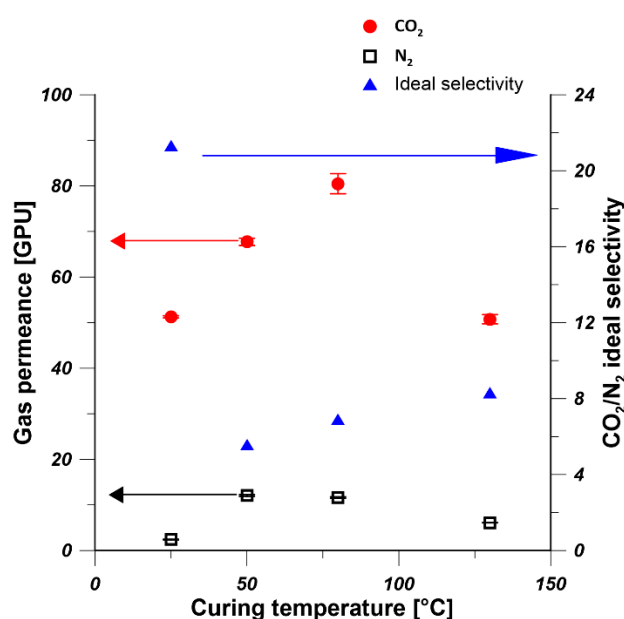


**Figure 7.** Effect of curing temperature on gas permeance and ideal selectivity of PDMS/PEI membranes (PDMS concentration—15 wt% and coating time—10 min).

### 3.2.4. The Effect of the Multiple Coating of PDMS

To investigate the influence of the multiple coating of PDMS layer on the gas permeance of PDMS/PEI membranes, one, two, and three PDMS layers were coated on the hollow-fiber substrate by using 15 wt% PDMS solution for 10 min at 25 °C. As it is shown in Figure 8, when the PDMS coating changed from one time to three times, the N<sub>2</sub> permeance was practically constant, while the CO<sub>2</sub> permeance decreased due to the increase in the thickness of PDMS layer from 3.3 to 5.5 μm. Therefore, CO<sub>2</sub>/N<sub>2</sub> ideal selectivity decreased with the increase in the number of PDMS layers. Similar findings were presented in the work of Selyanchyn et al. [52]. They prepared Pebax/PDMS/porous support thin-film composite flat-sheet membranes, where a PDMS layer was used as a gutter layer and a Pebax layer was used as the selective layer. It was reported that when the thickness of Pebax and PDMS layer increased from 0.29 and 2.3 μm to 0.39 and 10.8 μm, respectively, the CO<sub>2</sub> permeance and CO<sub>2</sub>/N<sub>2</sub> selectivity decreased from 300 GPU and 43 to 180 GPU and 35, respectively. The decrease in gas permeance is owing to the increase of thickness of selective layer. The increased thickness of selective layer imparted more significant influence on CO<sub>2</sub> permeance that it on N<sub>2</sub>, which resulted in the decrease in CO<sub>2</sub>/N<sub>2</sub> selectivity. This is because larger gas molecules are preferentially transported through PDMS selective layer [55]. However, Kargari et al. [21] found that when the number of coating layers increased, the H<sub>2</sub> permeance decreased, while the H<sub>2</sub>/CH<sub>4</sub> selectivity increased.

This is because the defect-free coating layer was developed as the number of coating layer increased, which finally led to a better performance.

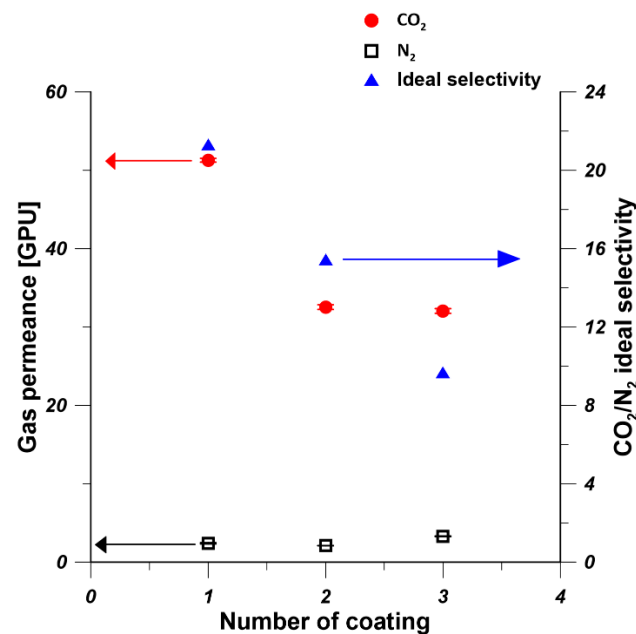


**Figure 8.** Effect of the number of coating layers on gas permeance and ideal selectivity of PDMS/PEI membranes (PDMS concentration—15 wt% and coating time—10 min).

#### 4. Comparison of CO<sub>2</sub> and N<sub>2</sub> Separation with Literature Data

Table 3 summarizes the previously reported works in which thin-film composite membranes have been prepared for CO<sub>2</sub>/N<sub>2</sub> separation. Pebax or PDMS solution with low concentration was generally used as coating solution for the formation of selective layer on porous substrate [34,56]. When the prepared membranes possessed high CO<sub>2</sub> permeance, the CO<sub>2</sub>/N<sub>2</sub> selectivity was low [24,34]. The prepared membranes in this work possess satisfying CO<sub>2</sub>/N<sub>2</sub> separation performance in comparison with the examples from the literature [56], which indicates the PDMS/PEI membranes were successfully fabricated.

**Table 3.** Comparison of the thin film composite hollow-fiber membranes for CO<sub>2</sub>/N<sub>2</sub> separation (HF—hollow fiber and FT—flat sheet).

Membrane	Configuration	Pure Gas Permeance (GPU)		CO <sub>2</sub> /N <sub>2</sub>	Reference
		CO <sub>2</sub>	N <sub>2</sub>		
3 wt% PDMS/PAN	HF	2494	241	10.4	[34]
2 wt% PDMS/PAN	HF	2680	360	9	[34]
3 wt% PDMS/PSf	HF	55	1.56	35	[56]
3 wt% PDMS/PSf	HF	59	1.60	37	[56]
0.3 wt% PDMS/PAN	HF	5138	485	11	[24]
3 wt% PDMS/PSf	HF	200	6	33	[57]
3 wt% PDMS/PES-PI	HF	60	1.54	39	[58]
3 wt% PDMS/PSf	HF	64	2	32	[59]
PEBA/PDMS/PEI	FT	172	3.64	47	[29]
PDMS/PEBA/PDMS/PEI	FT	157	2.46	64	[29]
3 wt% Pebax/PSf	HF	23	0.64	36	[56]
3 wt% Pebax/PSf	HF	30	0.76	39	[56]
5 wt% Pebax/PEI	HF	48	2.00	24	[60]
15 wt% PDMS/PEI	HF	51	2.4	21	This work



## 5. Conclusions

PDMS/PEI composite hollow fiber membranes were successfully fabricated by using the dip-coating method. The thickness of PDMS layer was influenced by the concentration of coating solution and the coating time. The increase in coating time and the concentration of PDMS solution resulted in the decrease in gas permeance, due to the formation of defect-free PDMS layer and the increase in its thickness. The relation between gas permeance and PDMS layer thickness followed the solution-diffusion model. The increase in curing temperature and the number of coating layer imparted adverse effects on the gas-separation performance. The composite hollow fiber membrane prepared from 15 wt.% PDMS solution at 10 min coating time showed the best gas-separation performance with CO<sub>2</sub> permeance of 51 GPU and CO<sub>2</sub>/N<sub>2</sub> selectivity of 21. The gas-separation performance of PDMS/PEI composite hollow fiber membrane is comparable to literature ones.

The prepared PDMS/PEI composite hollow fiber membranes followed the trade-off relationship between permeance and selectivity [26]. To enhance the gas-separation performance by increasing the gas permeance and selectivity simultaneously, 2D nanomaterials, such as surface-modified graphene oxide (GO) containing CO<sub>2</sub>-philic functional groups [61–63] and nitrogen-doped graphene nanosheets [64,65], will be incorporated in the selective coating layer in the further works. Moreover, the conditions for the preparation of mixed matrix hollow fiber membranes [66] will be optimized by using chemometric methods [67].

**Author Contributions:** Conceptualization, G.L. and W.K.; data curation, G.L. and W.K.; formal analysis, G.L., K.K., J.K., A.T., and W.K.; funding acquisition, G.L. and W.K.; investigation, G.L. and K.K.; methodology, G.L., K.K., A.T., and A.S.; supervision, J.K. and W.K.; validation, A.T. and A.S.; visualization, G.L., and K.K.; writing—original draft, G.L.; writing—review and editing, J.K., A.T., A.S., and W.K. All authors have read and agreed to the published version of the manuscript.

**Funding:** This work was supported by the Young Researcher grant for PhD Students of Nicolaus Copernicus University in Toruń, Poland (Faculty of Chemistry, 492/2020).

**Data Availability Statement:** The data presented in this study are available on request from the corresponding author.

**Conflicts of Interest:** The authors declare no conflict of interest.

## References

1. Chen, W.; Zhang, Z.; Hou, L.; Yang, C.; Shen, H.; Yang, K.; Wang, Z. Metal-organic framework MOF-801/PIM-1 mixed-matrix membranes for enhanced CO<sub>2</sub>/N<sub>2</sub> separation performance. *Sep. Purif. Technol.* **2020**, *250*, 117198. [[CrossRef](#)]
2. Ning, H.; Yang, Z.; Wang, D.; Meng, Z.; Li, Y.; Ju, X.; Wang, C. Graphene-based semi-coke porous carbon with N-rich hierarchical sandwich-like structure for efficient separation of CO<sub>2</sub>/N<sub>2</sub>. *Microporous Mesoporous Mater.* **2021**, *311*, 110700. [[CrossRef](#)]
3. Ding, R.; Zheng, W.; Yang, K.; Dai, Y.; Ruan, X.; Yan, X.; He, G. Amino-functional ZIF-8 nanocrystals by microemulsion based mixed linker strategy and the enhanced CO<sub>2</sub>/N<sub>2</sub> separation. *Sep. Purif. Technol.* **2020**, *236*, 116209. [[CrossRef](#)]
4. Aydani, A.; Brunetti, A.; Maghsoudi, H.; Barbieri, G. CO<sub>2</sub> separation from binary mixtures of CH<sub>4</sub>, N<sub>2</sub>, and H<sub>2</sub> by using SSZ-13 zeolite membrane. *Sep. Purif. Technol.* **2021**, *256*, 117796. [[CrossRef](#)]
5. Chang, J.; Hou, C.; Wan, D.; Zhang, X.; Xu, B.; Tian, H.; Wang, X.; Guo, Q. Enhanced CO<sub>2</sub> adsorption capacity of bi-amine co-tethered flue gas desulfurization gypsum with water of hydration. *J. CO<sub>2</sub> Util.* **2020**, *35*, 115–125. [[CrossRef](#)]
6. Riboldi, L.; Bolland, O. Overview on Pressure Swing Adsorption (PSA) as CO<sub>2</sub> Capture Technology: State-of-the-Art, Limits and Potentials. *Energy Procedia* **2017**, *114*, 2390–2400. [[CrossRef](#)]
7. Yousef, A.M.; El-Maghlany, W.M.; Eldrainy, Y.A.; Attia, A. New approach for biogas purification using cryogenic separation and distillation process for CO<sub>2</sub> capture. *Energy* **2018**, *156*, 328–351. [[CrossRef](#)]
8. Li, G.; Kujawski, W.; Válek, R.; Koter, S. A review—The development of hollow fibre membranes for gas separation processes. *Int. J. Greenh. Gas Control.* **2021**, *104*, 103195. [[CrossRef](#)]
9. Xiao, Y.; Chung, T.-S. Grafting thermally labile molecules on cross-linkable polyimide to design membrane materials for natural gas purification and CO<sub>2</sub> capture. *Energy Environ. Sci.* **2011**, *4*, 201–208. [[CrossRef](#)]
10. Xie, K.; Fu, Q.; Qiao, G.G.; Webley, P.A. Recent progress on fabrication methods of polymeric thin film gas separation membranes for CO<sub>2</sub> capture. *J. Membr. Sci.* **2019**, *572*, 38–60. [[CrossRef](#)]
11. Shi, Y.; Liang, B.; Lin, R.-B.; Zhang, C.; Chen, B. Gas Separation via Hybrid Metal–Organic Framework/Polymer Membranes. *Trends Chem.* **2020**, *2*, 254–269. [[CrossRef](#)]

12. Tham, H.M.; Wang, K.Y.; Hua, D.; Japip, S.; Chung, T.-S. From ultrafiltration to nanofiltration: Hydrazine cross-linked polyacrylonitrile hollow fiber membranes for organic solvent nanofiltration. *J. Membr. Sci.* **2017**, *542*, 289–299. [[CrossRef](#)]
13. Gao, J.; Thong, Z.; Wang, K.Y.; Chung, T.-S. Fabrication of loose inner-selective polyethersulfone (PES) hollow fibers by one-step spinning process for nanofiltration (NF) of textile dyes. *J. Membr. Sci.* **2017**, *541*, 413–424. [[CrossRef](#)]
14. Baker, R.W. *Membrane Technology and Applications*; John Wiley & Sons: Hoboken, NJ, USA, 2012.
15. Karimi, S.; Firouzfard, E.; Khoshchehreh, M.R. Assessment of gas separation properties and CO<sub>2</sub> plasticization of polysulfone/polyethylene glycol membranes. *J. Pet. Sci. Eng.* **2019**, *173*, 13–19. [[CrossRef](#)]
16. Chong, K.C.; Lai, S.O.; Lau, W.J.; Thiam, H.S.; Ismail, A.F.; Roslan, R.A. Preparation, characterization, and performance evaluation of polysulfone hollow fiber membrane with PEBA or PDMS coating for oxygen enhancement process. *Polymers* **2018**, *10*, 126. [[CrossRef](#)]
17. Wang, M.; Wang, Z.; Li, S.; Zhang, C.; Wang, J.; Wang, S. A high performance antioxidative and acid resistant membrane prepared by interfacial polymerization for CO<sub>2</sub> separation from flue gas. *Energy Environ. Sci.* **2013**, *6*, 539–551. [[CrossRef](#)]
18. Shamsabadi, A.A.; Kargari, A.; Babaheidari, M.B. Preparation, characterization and gas permeation properties of PDMS/PEI composite asymmetric membrane for effective separation of hydrogen from H<sub>2</sub>/CH<sub>4</sub> mixed gas. *Int. J. Hydrog. Energy* **2014**, *39*, 1410–1419. [[CrossRef](#)]
19. Peng, N.; Chung, T.-S.; Chng, M.L.; Aw, W. Evolution of ultra-thin dense-selective layer from single-layer to dual-layer hollow fibers using novel Extrem<sup>®</sup> polyetherimide for gas separation. *J. Membr. Sci.* **2010**, *360*, 48–57. [[CrossRef](#)]
20. Mousavi, S.A.; Aboosadi, Z.A.; Mansourizadeh, A.; Honarvar, B. Surface modified porous polyetherimide hollow fiber membrane for sweeping gas membrane distillation of dyeing wastewater. *Colloids Surf. A Physicochem. Eng. Asp.* **2020**, 125439. [[CrossRef](#)]
21. Kargari, A.; Shamsabadi, A.A.; Babaheidari, M.B. Influence of coating conditions on the H<sub>2</sub> separation performance from H<sub>2</sub>/CH<sub>4</sub> gas mixtures by the PDMS/PEI composite membrane. *Int. J. Hydrog.* **2014**, *39*, 6588–6597. [[CrossRef](#)]
22. Choi, S.-H.; Jansen, J.C.; Tasselli, F.; Barbieri, G.; Drioli, E. In-line formation of chemically cross-linked P84<sup>®</sup> co-polyimide hollow fibre membranes for H<sub>2</sub>/CO<sub>2</sub> separation. *Sep. Purif. Technol.* **2010**, *76*, 132–139. [[CrossRef](#)]
23. Roy, P.K.; Kumar, K.; Thakkar, F.M.; Pathak, A.D.; Ayappa, K.G.; Maiti, P.K. Investigations on 6FDA/BPDA-DAM polymer melt properties and CO<sub>2</sub> adsorption using molecular dynamics simulations. *J. Membr. Sci.* **2020**, *613*, 118377. [[CrossRef](#)]
24. Liang, C.Z.; Yong, W.F.; Chung, T.-S. High-performance composite hollow fiber membrane for flue gas and air separations. *J. Membr. Sci.* **2017**, *541*, 367–377. [[CrossRef](#)]
25. Fam, W.; Mansouri, J.; Li, H.; Chen, V. Improving CO<sub>2</sub> separation performance of thin film composite hollow fiber with Pebax<sup>®</sup> 1657/ionic liquid gel membranes. *J. Membr. Sci.* **2017**, *537*, 54–68. [[CrossRef](#)]
26. Robeson, L.M. The upper bound revisited. *J. Membr. Sci.* **2008**, *320*, 390–400. [[CrossRef](#)]
27. Liang, C.Z.; Chung, T.-S.; Lai, J.-Y. A review of polymeric composite membranes for gas separation and energy production. *Prog. Polym. Sci.* **2019**, *97*, 101141. [[CrossRef](#)]
28. Madaeni, S.; Badiie, M.M.S.; Vatanpour, V. Effect of coating method on gas separation by PDMS/PES membrane. *Polym. Eng. Sci.* **2013**, *53*, 1878–1885. [[CrossRef](#)]
29. Ren, X.; Ren, J.; Li, H.; Feng, S.; Deng, M. Poly (amide-6-b-ethylene oxide) multilayer composite membrane for carbon dioxide separation. *Int. J. Greenh. Gas Control.* **2012**, *8*, 111–120. [[CrossRef](#)]
30. Liang, C.Z.; Chung, T.-S. Robust thin film composite PDMS/PAN hollow fiber membranes for water vapor removal from humid air and gases. *Sep. Purif. Technol.* **2018**, *202*, 345–356. [[CrossRef](#)]
31. Wong, K.C.; Goh, P.S.; Ismail, A.F. Gas separation performance of thin film nanocomposite membranes incorporated with polymethyl methacrylate grafted multi-walled carbon nanotubes. *Int. Biodeterior. Biodegrad.* **2015**, *102*, 339–345. [[CrossRef](#)]
32. Albo, J.; Wang, J.; Tsuru, T. Gas transport properties of interfacially polymerized polyamide composite membranes under different pre-treatments and temperatures. *J. Membr. Sci.* **2014**, *449*, 109–118. [[CrossRef](#)]
33. Basu, S.; Balakrishnan, M. Polyamide thin film composite membranes containing ZIF-8 for the separation of pharmaceutical compounds from aqueous streams. *Sep. Purif. Technol.* **2017**, *179*, 118–125. [[CrossRef](#)]
34. Li, P.; Chen, H.Z.; Chung, T.-S. The effects of substrate characteristics and pre-wetting agents on PAN–PDMS composite hollow fiber membranes for CO<sub>2</sub>/N<sub>2</sub> and O<sub>2</sub>/N<sub>2</sub> separation. *J. Membr. Sci.* **2013**, *434*, 18–25. [[CrossRef](#)]
35. Chen, H.Z.; Thong, Z.; Li, P.; Chung, T.-S. High performance composite hollow fiber membranes for CO<sub>2</sub>/H<sub>2</sub> and CO<sub>2</sub>/N<sub>2</sub> separation. *Int. J. Hydrog.* **2014**, *39*, 5043–5053. [[CrossRef](#)]
36. Jo, E.-S.; An, X.; Ingole, P.G.; Choi, W.-K.; Park, Y.-S.; Lee, H.-K. CO<sub>2</sub>/CH<sub>4</sub> separation using inside coated thin film composite hollow fiber membranes prepared by interfacial polymerization. *Chin. J. Chem. Eng.* **2017**, *25*, 278–287. [[CrossRef](#)]
37. Xiao, B.; Huang, Q.; Chen, H.; Chen, X.; Long, G. A fractal model for capillary flow through a single tortuous capillary with roughened surfaces in fibrous porous media. *Fractals* **2021**, *29*, 2150017. [[CrossRef](#)]
38. Ghobadi, J.; Ramirez, D.; Khoramfar, S.; Kabir, M.M.; Jerman, R.; Saeed, M. Mathematical modeling of CO<sub>2</sub> separation using different diameter hollow fiber membranes. *Int. J. Greenh. Gas Control.* **2021**, *104*, 103204. [[CrossRef](#)]
39. Li, G.; Kujawski, W.; Knozowska, K.; Kujawa, J. The effects of PEI hollow fiber substrate characteristics on PDMS/PEI hollow fiber membranes for CO<sub>2</sub>/N<sub>2</sub> separation. *Membranes* **2021**, *11*, 56. [[CrossRef](#)] [[PubMed](#)]
40. Jamil, A.; Ching, O.P.; Shariff, A.M. Mixed matrix hollow fibre membrane comprising polyetherimide and modified montmorillonite with improved filler dispersion and CO<sub>2</sub>/CH<sub>4</sub> separation performance. *Appl. Clay Sci.* **2017**, *143*, 115–124. [[CrossRef](#)]

41. DashtArzhandi, M.R.; Ismail, A.F.; Matsuura, T.; Ng, B.C.; Abdullah, M.S. Fabrication and characterization of porous polyetherimide/montmorillonite hollow fiber mixed matrix membranes for CO<sub>2</sub> absorption via membrane contactor. *Chem. Eng. J.* **2015**, *269*, 51–59. [[CrossRef](#)]
42. Jamil, A.; Oh, P.C.; Shariff, A.M. Polyetherimide-montmorillonite mixed matrix hollow fibre membranes: Effect of inorganic/organic montmorillonite on CO<sub>2</sub>/CH<sub>4</sub> separation. *Sep. Purif. Technol.* **2018**, *206*, 256–267. [[CrossRef](#)]
43. Tang, X.; Yan, X. Dip-coating for fibrous materials: Mechanism, methods and applications. *J. Sol Gel Sci. Technol.* **2017**, *81*, 378–404. [[CrossRef](#)]
44. Madaeni, S.S.; Moradi, A.; Kazemi, V. PDMS coated polyethersulphone composite membranes for separation of propylene and nitrogen gas mixtures. *Iran. Polym. J.* **2009**, *18*, 873–879.
45. Wang, L.; Li, Y.; Li, S.; Ji, P.; Jiang, C. Preparation of composite poly(ether block amide) membrane for CO<sub>2</sub> capture. *J. Energy Chem.* **2014**, *23*, 717–725. [[CrossRef](#)]
46. Campana, D.M.; Ubal, S.; Giavedoni, M.D.; Saita, F.A. Influence of Surfactants on Dip Coating of Fibers: Numerical Analysis. *Ind. Eng. Chem. Res.* **2016**, *55*, 5770–5779. [[CrossRef](#)]
47. Brinker, C.J.; Frye, G.C.; Hurd, A.J.; Ashley, C.S. Fundamentals of sol-gel dip coating. *Thin Solid Films* **1991**, *201*, 97–108. [[CrossRef](#)]
48. Kuznetsov, A.V.; Xiong, M. Effect of evaporation on thin film deposition in dip coating process. *Int. Commun. Heat Mass Transf.* **2002**, *29*, 35–44. [[CrossRef](#)]
49. Buapool, S.; Thavarungkul, N.; Srisukhumbowornchai, N.; Termsuksawad, P. Modeling and Analysis of the Effect of Dip-Spin Coating Process Parameters on Coating Thickness Using Factorial Design Method. *Adv. Mater. Sci. Eng.* **2017**, *2017*, 9639306. [[CrossRef](#)]
50. Aguilar-Armenta, G.; Patiño-Iglesias, M.E.; Leyva-Ramos, R. Adsorption kinetic behaviour of pure CO<sub>2</sub>, N<sub>2</sub> and CH<sub>4</sub> in natural clinoptilolite at different temperatures. *Adsorp Sci Technol.* **2003**, *21*, 81–91. [[CrossRef](#)]
51. Firpo, G.; Angeli, E.; Repetto, L.; Valbusa, U. Permeability thickness dependence of polydimethylsiloxane (PDMS) membranes. *J. Membr. Sci.* **2015**, *481*, 1–8. [[CrossRef](#)]
52. Selyanchyn, R.; Ariyoshi, M.; Fujikawa, S. Thickness Effect on CO<sub>2</sub>/N<sub>2</sub> Separation in Double Layer Pebax-1657®/PDMS Membranes. *Membranes* **2018**, *8*, 121. [[CrossRef](#)]
53. Wijmans, J.G.; Baker, R.W. The solution-diffusion model: A review. *J. Membr. Sci.* **1995**, *107*, 1–21. [[CrossRef](#)]
54. Chong, K.C.; Lai, S.O.; Lau, W.J.; Thiam, H.S.; Ismail, A.F.; Zulkhairun, A.K. Fabrication and characterization of polysulfone membranes coated with polydimethylsiloxane for oxygen enrichment. *Aerosol Air Qual Res.* **2017**, *17*, 2735–2742. [[CrossRef](#)]
55. Sadrzadeh, M.; Saljoughi, E.; Shahidi, K.; Mohammadi, T. Preparation and characterization of a composite PDMS membrane on CA support. *Polym. Adv. Technol.* **2010**, *21*, 568–577. [[CrossRef](#)]
56. Roslan, R.A.; Lau, W.J.; Sakthivel, D.B.; Khademi, S.; Zulkhairun, A.K.; Goh, P.S.; Ismail, A.F.; Chong, K.C.; Lai, S.O. Separation of CO<sub>2</sub>/CH<sub>4</sub> and O<sub>2</sub>/N<sub>2</sub> by polysulfone hollow fiber membranes: Effects of membrane support properties and surface coating materials. *J. Polym. Eng.* **2018**, *38*, 871–880. [[CrossRef](#)]
57. Wang, D.; Teo, W.K.; Li, K. Preparation and characterization of high-flux polysulfone hollow fibre gas separation membranes. *J. Membr. Sci.* **2002**, *204*, 247–256. [[CrossRef](#)]
58. Kapantaidakis, G.C.; Koops, G.H. High flux polyethersulfone–polyimide blend hollow fiber membranes for gas separation. *J. Membr. Sci.* **2002**, *204*, 153–171. [[CrossRef](#)]
59. Zulkhairun, A.K.; Fachrurrazi, Z.G.; Izwanne, M.N.; Ismail, A.F. Asymmetric hollow fiber membrane coated with polydimethylsiloxane–metal organic framework hybrid layer for gas separation. *Sep. Purif. Technol.* **2015**, *146*, 85–93. [[CrossRef](#)]
60. Liu, L.; Chakma, A.; Feng, X. CO<sub>2</sub>/N<sub>2</sub> separation by poly (ether block amide) thin film hollow fiber composite membranes. *Ind. Eng. Chem. Res.* **2005**, *44*, 6874–6882. [[CrossRef](#)]
61. Jiang, L.; Meng, Y.; Zhang, W.; Yu, H.; Hou, X. Preparation of NH<sub>2</sub>-SH-GO/SWCNTs based on graphene oxide/single-walled carbon nanotubes for CO<sub>2</sub> and N<sub>2</sub> separation from blast furnace gas. *Microporous Mesoporous Mater.* **2020**, *306*, 110476. [[CrossRef](#)]
62. Ma, S.; Tang, Z.; Fan, Y.; Zhao, J.; Meng, X.; Yang, N.; Zhuo, S.; Liu, S. Surfactant-modified graphene oxide membranes with tunable structure for gas separation. *Carbon* **2019**, *152*, 144–150. [[CrossRef](#)]
63. Xin, Q.; Ma, F.; Zhang, L.; Wang, S.; Li, Y.; Ye, H.; Ding, X.; Lin, L.; Zhang, Y.; Cao, X. Interface engineering of mixed matrix membrane via CO<sub>2</sub>-philic polymer brush functionalized graphene oxide nanosheets for efficient gas separation. *J. Membr. Sci.* **2019**, *586*, 23–33. [[CrossRef](#)]
64. Yang, E.; Goh, K.; Chuah, C.Y.; Wang, R.; Bae, T.-H. Asymmetric mixed-matrix membranes incorporated with nitrogen-doped graphene nanosheets for highly selective gas separation. *J. Membr. Sci.* **2020**, *615*, 118293. [[CrossRef](#)]
65. Shan, M.; Xue, Q.; Jing, N.; Ling, C.; Zhang, T.; Yan, Z.; Zheng, J. Influence of chemical functionalization on the CO<sub>2</sub>/N<sub>2</sub> separation performance of porous graphene membranes. *Nanoscale* **2012**, *4*, 5477–5482. [[CrossRef](#)]
66. Widiastuti, N.; Gunawan, T.; Fansuri, H.; Salleh, W.N.W.; Ismail, A.F.; Szali, N. P84/ZCC Hollow Fiber Mixed Matrix Membrane with PDMS Coating to Enhance Air Separation Performance. *Membranes* **2020**, *10*, 267. [[CrossRef](#)]
67. Bezerra, M.A.; Santos, Q.O.D.; Santos, A.G.; Novaes, C.G.; Ferreira, S.L.C.; de Souza, V.S. Simplex optimization: A tutorial approach and recent applications in analytical chemistry. *Microchem. J.* **2016**, *124*, 45–54. [[CrossRef](#)]

## **Publication IV**

**G. Li**, W. Kujawski, K. Knozowska, J. Kujawa, Thin film mixed matrix hollow fiber membrane fabricated by incorporation of amine functionalized metal-organic framework for CO<sub>2</sub>/N<sub>2</sub> separation, *Materials*, 14 (2021) 3366.

## Article

# Thin Film Mixed Matrix Hollow Fiber Membrane Fabricated by Incorporation of Amine Functionalized Metal-Organic Framework for CO<sub>2</sub>/N<sub>2</sub> Separation

Guoqiang Li <sup>1</sup>, Wojciech Kujawski <sup>1,2,\*</sup> , Katarzyna Knozowska <sup>1</sup> and Joanna Kujawa <sup>1</sup> 

<sup>1</sup> Department of Physical Chemistry and Physical Chemistry of Polymers, Faculty of Chemistry, Nicolaus Copernicus University in Toruń, 7 Gagarina Street, 87-100 Toruń, Poland

<sup>2</sup> Moscow Engineering Physics Institute, National Research Nuclear University MEPhI, 31 Kashira Hwy, 115409 Moscow, Russia

\* Correspondence: kujawski@chem.umk.pl; Tel.: +48-56-6114517

**Abstract:** Membrane separation technology can be used to capture carbon dioxide from flue gas. However, plenty of research has been focused on the flat sheet mixed matrix membrane rather than the mixed matrix thin film hollow fiber membranes. In this work, mixed matrix thin film hollow fiber membranes were fabricated by incorporating amine functionalized UiO-66 nanoparticles into the Pebax<sup>®</sup> 2533 thin selective layer on the polypropylene (PP) hollow fiber supports via dip-coating process. The attenuated total reflection-Fourier transform infrared (ATR-FTIR), scanning electron microscope (SEM), energy-dispersive X-ray spectroscopy (EDX) mapping analysis, and thermal analysis (TGA-DTA) were used to characterize the synthesized UiO-66-NH<sub>2</sub> nanoparticles. The morphology, surface chemistry, and the gas separation performance of the fabricated Pebax<sup>®</sup> 2533-UiO-66-NH<sub>2</sub>/PP mixed matrix thin film hollow fiber membranes were characterized by using SEM, ATR-FTIR, and gas permeance measurements, respectively. It was found that the surface morphology of the prepared membranes was influenced by the incorporation of UiO-66 nanoparticles. The CO<sub>2</sub> permeance increased along with an increase of UiO-66 nanoparticles content in the prepared membranes, while the CO<sub>2</sub>/N<sub>2</sub> ideal gas selectivity firstly increased then decreased due to the aggregation of UiO-66 nanoparticles. The Pebax<sup>®</sup> 2533-UiO-66-NH<sub>2</sub>/PP mixed matrix thin film hollow fiber membranes containing 10 wt% UiO-66 nanoparticles exhibited the CO<sub>2</sub> permeance of 26 GPU and CO<sub>2</sub>/N<sub>2</sub> selectivity of 37.

**Keywords:** thin film hollow fiber membranes; amine functionalized nanoparticles UiO-66-NH<sub>2</sub>; mixed matrix membranes (MMMs); CO<sub>2</sub>/N<sub>2</sub> separation



**Citation:** Li, G.; Kujawski, W.; Knozowska, K.; Kujawa, J. Thin Film Mixed Matrix Hollow Fiber Membrane Fabricated by Incorporation of Amine Functionalized Metal-Organic Framework for CO<sub>2</sub>/N<sub>2</sub> Separation. *Materials* **2021**, *14*, 3366. <https://doi.org/10.3390/ma14123366>

Academic Editor: Anastasios J. Tasiopoulos

Received: 17 May 2021

Accepted: 15 June 2021

Published: 17 June 2021

**Publisher's Note:** MDPI stays neutral with regard to jurisdictional claims in published maps and institutional affiliations.



**Copyright:** © 2021 by the authors. Licensee MDPI, Basel, Switzerland. This article is an open access article distributed under the terms and conditions of the Creative Commons Attribution (CC BY) license (<https://creativecommons.org/licenses/by/4.0/>).

## 1. Introduction

Global warming resulted from greenhouse gas has created serious consequence for the environment, e.g., melting glaciers. In comparison with other greenhouse gases, CO<sub>2</sub> is one of the important contributors to global warming [1]. CO<sub>2</sub> emission increases significantly every year due to the rapid development of industry and the more intensive human activities. The flue gas released by power plant due to the usage of fossil fuels is the main source of CO<sub>2</sub> emission [2]. Therefore, the separation of CO<sub>2</sub> from flue gas mixture to mitigate the CO<sub>2</sub> emission plays an important role in the environment protection and the sustainable development of the industry [3]. Membrane separation technology, physical and chemical adsorption, and cryogenic separation have been used in the CO<sub>2</sub> capture process [1,4,5].

Membrane separation technology is widely considered as an alternative to the traditional intensively energy-consuming technologies for CO<sub>2</sub> separation [6]. Various types of membrane have been used for CO<sub>2</sub> capture from flue gas mixture, such as polymeric membranes [7,8], inorganic membranes [9], and mixed matrix membranes (MMMs) [10–12].



Pebax<sup>®</sup> materials are used for MMMs fabrication because of their advantages, e.g., desirable separation performance and high processability [13]. They are good candidates for polymeric membrane matrix for CO<sub>2</sub>/N<sub>2</sub> separation due to their desirable CO<sub>2</sub> permeance, high ideal selectivity, and tunability of gas separation properties via the incorporation of nanofillers [14]. Pebax<sup>®</sup> 2533 shows higher CO<sub>2</sub> permeability with desirable CO<sub>2</sub>/N<sub>2</sub> selectivity [15]. Therefore, Pebax<sup>®</sup> 2533 was chosen as the polymer matrix for the preparation of thin film mixed matrix hollow fiber membranes in this work. Thin film Pebax<sup>®</sup> 2533/polyetherimide (PEI) composite hollow fiber membranes were fabricated via dip coating method and assembled into a lab-scale hollow fiber module for CO<sub>2</sub>/N<sub>2</sub> separation [13]. In the pure gas permeance test, the prepared membranes exhibited CO<sub>2</sub> and N<sub>2</sub> permeances equal to 48 and 1.6 GPU, respectively, at 23 °C and 790 kPa, while the CO<sub>2</sub> and N<sub>2</sub> permeances are 36 and 1.7 GPU, respectively, in the gas mixture permeance test under the same testing conditions. The CO<sub>2</sub> permeance from gas mixture test was 12 GPU lower than that from pure gas test. However, the N<sub>2</sub> permeance in both cases are practically the same [13].

MMMs containing metal-organic framework (MOF) have been intensively studied to improve the comprehensive gas separation properties of membranes. This is because MOFs possess high surface area, high packing capacity, tunable porosity and pore size, chemical functionality, and enormous varieties, which endows them huge advantages for the incorporation into polymer matrix [16–18]. MOFs are more intensively used in MMMs for various gas separation processes than other porous fillers [5].

MOFs such as the zeolitic imidazolate framework (ZIF) [17–19], Materials Institute Lavoisier (MIL) [20], and University in Oslo (UiO-66) [21,22] are commonly used for the preparation of MMMs for gas separation. Gao et al. [19] incorporated ZIF-7-NH<sub>2</sub>, ZIF-7-OH, and ZIF-7-CH<sub>3</sub>OH into Pebax<sup>®</sup> 2533 matrix to fabricate MMMs. The CO<sub>2</sub> adsorption properties of MMMs was enhanced due to the introduction of functional groups in ZIF-7 framework. All the prepared MMMs showed better CO<sub>2</sub>/N<sub>2</sub> separation performance than the pristine Pebax<sup>®</sup> membranes. The MMM containing 14 wt% ZIF-7-OH particles exhibited high CO<sub>2</sub> permeability equal to 273 Barrer and CO<sub>2</sub>/N<sub>2</sub> selectivity equal to 38, which in comparison to the pristine Pebax<sup>®</sup> membrane increased by 60 and 145%, respectively. Jameh et al. [23] modified ZIF-8 nanoparticles with ethylenediamine (ED) and incorporated them into Pebax<sup>®</sup> 1074 matrix to fabricate MMMs for CO<sub>2</sub> capture. The authors found that the CO<sub>2</sub> adsorption capacity of MMM containing ED modified ZIF-8 was higher than that containing ZIF-8. Consequently, CH<sub>4</sub> and CO<sub>2</sub> permeabilities of the ZIF-8/Pebax<sup>®</sup> MMMs are 9.39 and 134 Barrer, respectively, while for the ED-ZIF-8/Pebax<sup>®</sup> MMMs, the CH<sub>4</sub> and CO<sub>2</sub> permeabilities were 14.2 and 344 Barrer, respectively. Dai et al. [24] incorporated ZIF-8 into polyetherimide (PEI) matrix to prepare dual layer mixed matrix hollow fiber membranes via dry jet-wet spinning technique. It was found that presence of ZIF-8 increased the CO<sub>2</sub> permeance and CO<sub>2</sub>/N<sub>2</sub> ideal selectivity from 13 GPU and 34 to 21 GPU and 39, respectively, in comparison to pure PEI hollow fiber membranes. Etxeberria-Benavides et al. [25] prepared polybenzimidazole (PBI) mixed matrix hollow fiber membranes containing ZIF-8 for H<sub>2</sub>/CO<sub>2</sub> separation. The prepared membranes showed high H<sub>2</sub> permeance of 107 GPU at 7 bar and 70 °C in comparison with 65 GPU of pristine PBI hollow fiber membranes. While the H<sub>2</sub>/CO<sub>2</sub> selectivity was constant. For the mixed gas permeation, the improvement of H<sub>2</sub>/CO<sub>2</sub> separation performance for PBI mixed matrix hollow fibers is hindered at high pressure around 30 bar because of the CO<sub>2</sub> adsorption in ZIF-8, which blocks the H<sub>2</sub> transport [25]. Song et al. [20] prepared Pebax<sup>®</sup> 1657/MIL-101 and Pebax<sup>®</sup> 1657/NH<sub>2</sub>-MIL-101 MMMs for CO<sub>2</sub>/N<sub>2</sub> separation under sub-ambient condition. Authors found that the Pebax<sup>®</sup> 1657/NH<sub>2</sub>-MIL-101 MMM possesses higher CO<sub>2</sub>/N<sub>2</sub> selectivity equal to 95.6 comparing to CO<sub>2</sub>/N<sub>2</sub> selectivity equal to 89.4 for Pebax<sup>®</sup> 1657/MIL-101 MMM. This is because the amino-modified MIL-101 introduced -NH<sub>2</sub> group possessing higher affinity to CO<sub>2</sub>. Therefore, the solubility and adsorption capacity of CO<sub>2</sub> in MMMs were improved [20].



The preparation of flat sheet MMMs containing UiO-66 and UiO-66-NH<sub>2</sub> for gas separation has been also studied [14,21,22]. Shen et al. [14] prepared UiO-66/Pebax<sup>®</sup> 1657 and UiO-66-NH<sub>2</sub>/Pebax<sup>®</sup> 1657 flat sheet MMMs for CO<sub>2</sub>/N<sub>2</sub> separation. It was found that the UiO-66-NH<sub>2</sub> nanoparticles showed higher affinity to carbon dioxide than UiO-66. The dispersibility of nanoparticles in the polymer matrix was improved due to the enhanced hydrogen bonding between fillers and polymer chains. With MOF loading of 10 wt%, UiO-66-NH<sub>2</sub>-Pebax<sup>®</sup> 1657 MMM showed higher CO<sub>2</sub>/N<sub>2</sub> selectivity and slightly lower CO<sub>2</sub> permeability than those of UiO-66-Pebax<sup>®</sup> 1657 membrane [14]. Chuah et al. [21] investigated CO<sub>2</sub>/N<sub>2</sub> separation performance of polyimide-based MMMs containing UiO-66 possessing different functional groups (-HN<sub>2</sub>, -Br, -(OH)<sub>2</sub>). It was found that the functionalized UiO-66 in MMMs can effectively increase the CO<sub>2</sub> diffusivity while suppressing N<sub>2</sub> adsorption [21]. In the above examples, the UiO-66 nanoparticles with various functional groups are synthesized by using pre-synthetic functionalization. It is believed that the further functionalization of UiO-66-NH<sub>2</sub> by using post-synthetic functionalization method can further tune the properties of UiO-66-NH<sub>2</sub>, such as the CO<sub>2</sub> affinity and adsorption capacity, pore size, and surface area. Consequently, the CO<sub>2</sub> capture ability of MMMs is enhanced [22]. Jiang et al. [22] modified UiO-66-NH<sub>2</sub> with imidazole-2-carbaldehyde (ICA) via amine condensation. After modification, the pore volume and BET (Brunauer-Emmett-Teller) area of UiO-66-NH<sub>2</sub> were reduced while the CO<sub>2</sub> affinity and CO<sub>2</sub>/CH<sub>4</sub> adsorption selectivity were increased. It was found that when 10 wt% modified UiO-66-NH<sub>2</sub> was incorporated into Matrimid<sup>®</sup> membranes, the high CO<sub>2</sub>/CH<sub>4</sub> selectivity of 64.7 was obtained, which is 40% higher than the membranes containing UiO-66-NH<sub>2</sub>. As aforementioned, the presence of amine groups improved the CO<sub>2</sub> adsorption capacity for UiO-66-NH<sub>2</sub>, resulting in higher CO<sub>2</sub> solubility of MMMs, consequently, the higher CO<sub>2</sub>/N<sub>2</sub> selectivity. Moreover, UiO-66-NH<sub>2</sub> shows high compatibility with polymer matrix due to the hydrogen bonding between Pebax<sup>®</sup> chains and UiO-66-NH<sub>2</sub>. Hence, UiO-66-NH<sub>2</sub> was incorporated into Pebax<sup>®</sup> 2533 matrix to improve the gas separation properties of thin film mixed matrix hollow fiber membranes in this work.

Microporous polypropylene hollow fiber membranes are suitable to be used as a support for the fabrication of composite hollow fiber membranes due to their desirable properties, e.g., high void volumes, well-controlled porosity, chemical inertness, good mechanical strength, and low cost [26]. Therefore, polypropylene hollow fibers were used as supports for the preparation of thin film mixed matrix hollow fiber membranes in this work.

Hollow fiber membranes have a promising future in various gas separation processes due to their advantages, e.g., high packing density and a self-supporting structure [6,7]. However, the flat sheet MMMs have been intensively studied since the incorporation of fillers, e.g., MOF particles can significantly enhance the gas separation performance of polymeric membranes. Therefore, it is highly necessary to investigate the formation of a selective layer containing filler e.g., MOF particles on the hollow fiber support and their gas separation performance. In this work, the main objective is to develop thin film mixed matrix hollow fiber membranes by incorporating UiO-66-NH<sub>2</sub> filler into the Pebax<sup>®</sup> 2533 selective layer. The effect of UiO-66-NH<sub>2</sub> filler on the morphology, surface chemistry, and CO<sub>2</sub>/N<sub>2</sub> separation performance of the prepared thin film mixed matrix hollow fiber membranes will be investigated.

## 2. Experimental

### 2.1. Materials

Polypropylene (PP) hollow fibers were kindly provided by Faculty of Chemical and Processing Engineering, Warsaw University of Technology (Warsaw, Poland). The PP hollow fibers were prepared via a dry-jet-wet spinning process, using a laboratory made setup. The PP hollow fibers possessed outer diameter of 2.6 mm, internal diameter of 1.8 mm, average pore size of 0.3 μm, and porosity of 50–60% [27]. Pebax<sup>®</sup> 2533 was

provided by Arkema (Colombes, France). Pebax<sup>®</sup> 2533 consists of poly(ethylene oxide)—PEO block (80 wt%) and polyamide—PA-12 block (20 wt%).

Zirconylchloride octahydrate was supplied by Acrb GmbH (Karlsruhe, Germany). 2-aminoterephthalic acid and N,N-dimethylformamide (DMF) were purchased from Sigma Aldrich (Poznań, Poland). Ethanol was purchased from Alchem Grupa Sp. z o.o. (Toruń, Poland). CO<sub>2</sub> (99.999%) and N<sub>2</sub> (99.999%) were purchased from Air Products Sp. z o.o. (Siewierz, Poland). The mixing nozzles and epoxy resin were delivered by Farnell (Warsaw, Poland).

## 2.2. UiO-66-NH<sub>2</sub> Synthesis

To synthesize UiO-66-NH<sub>2</sub>, 4.34 g of 2-aminoterephthalic acid and 7.6 g of zirconylchloride octahydrate were added into 72 mL of DMF. The homogeneous mixture was obtained by stirring (Heating magnetic stirrer, VELP Scientifica, Usmate Velate, Italy) and sonication (BANDELIN SONOREX, BANDELIN electronic GmbH & Co. KG, Berlin, Germany) at room temperature. Then the homogeneous mixture was kept in oven (Memmert GmbH + Co. KG, Schwabach, Germany) at 120 °C for 24 h. Then, the temperature of the mixture decreased to room temperature and centrifuged (High speed centrifuge type 310, Mechanika Precyzyjna, Warsaw, Poland) at 5000 rpm for 15 min. The obtained products were washed three times with DMF and ethanol, respectively. Finally, the obtained products were dried at room temperature and further in the oven at 150 °C for 4 h.

## 2.3. Fabrication of Pristine Pebax/PP and Pebax<sup>®</sup> 2533-UiO-66-NH<sub>2</sub>/PP Thin Film Mixed Matrix Hollow Fiber Membranes

To prepare the pristine Pebax<sup>®</sup> 2533/PP thin film hollow fiber membranes, Pebax<sup>®</sup> 2533 pellets were added into ethanol (90 wt%)/water (10 wt%) solvent. After that, the mixture was stirred at 80 °C for 3 h to obtain 3 and 6 wt% polymer solutions. Then, Pebax<sup>®</sup> 2533 solution was cooled down to 25 °C. The dip-coating technique was used for the preparation of the thin Pebax<sup>®</sup> 2533 layer on the shell side of the PP hollow fiber supports. First of all, a 10 cm long PP hollow fiber was prepared, and one end of the hollow fiber was sealed with epoxy resin. After the solidification of epoxy resin, the other end of the hollow fiber was attached to a metal holder. Then the single PP hollow fiber was vertically immersed into the 3 wt% Pebax<sup>®</sup> 2533 solution for 1 min at room temperature. Finally, the Pebax<sup>®</sup> 2533 coated hollow fiber was slowly taken from the coating solution and dried in air for more than 48 h for solvent evaporation. Afterwards, the second Pebax<sup>®</sup> 2533 thin layer was formed from 6 wt% Pebax<sup>®</sup> 2533 solution by using the same dip coating procedure. The preparation of the pristine Pebax<sup>®</sup> 2533 thin film hollow fiber membrane was schematically illustrated in Figure 1A. The ideal selectivity of Pebax<sup>®</sup> 2533/PP hollow fiber membranes fabricated by a single layer coating of 3 or 6 wt% Pebax<sup>®</sup> 2533 solution was very low (Table S1), indicating the formation of defective Pebax<sup>®</sup> 2533 layer. Therefore, a two-step coating process by using two different concentrations of Pebax<sup>®</sup> 2533 solution was applied in this research.

To prepare the Pebax<sup>®</sup> 2533-UiO-66-NH<sub>2</sub>/PP thin film mixed matrix hollow fiber membranes, a proper amount of UiO-66-NH<sub>2</sub> particles were firstly dispersed into the ethanol/water solution (90:10 wt%/wt%) under continuous stirring for 1 h at 80 °C. Then 30 min sonication process was applied to the UiO-66-NH<sub>2</sub> suspension for better dispersion of UiO-66-NH<sub>2</sub> particles. Afterwards, 10% of the required amount of Pebax<sup>®</sup> 2533 pellets was added to solvent mixture under continuous stirring for 2 h at 80 °C. Finally, the rest of Pebax<sup>®</sup> 2533 pellets was dissolved into the solvent mixture under continuous stirring for 12 h at 80 °C to obtain 6 wt% Pebax<sup>®</sup> 2533 solution containing UiO-66-NH<sub>2</sub>. The dip coating process for the preparation of Pebax<sup>®</sup> 2533-UiO-66-NH<sub>2</sub>/PP thin film mixed matrix hollow fiber membranes is the same as for the preparation of pristine Pebax<sup>®</sup> 2533/PP thin film hollow fiber membranes. The first layer was formed on the PP hollow fiber support from 3 wt% Pebax<sup>®</sup> 2533 solution, and the second layer was formed from the 6 wt% Pebax<sup>®</sup>

2533 solution containing UiO-66-NH<sub>2</sub>. The fabrication of the Pebax<sup>®</sup> 2533-UiO-66-NH<sub>2</sub>/PP mixed matrix thin film hollow fiber membrane was schematically illustrated in Figure 1B.

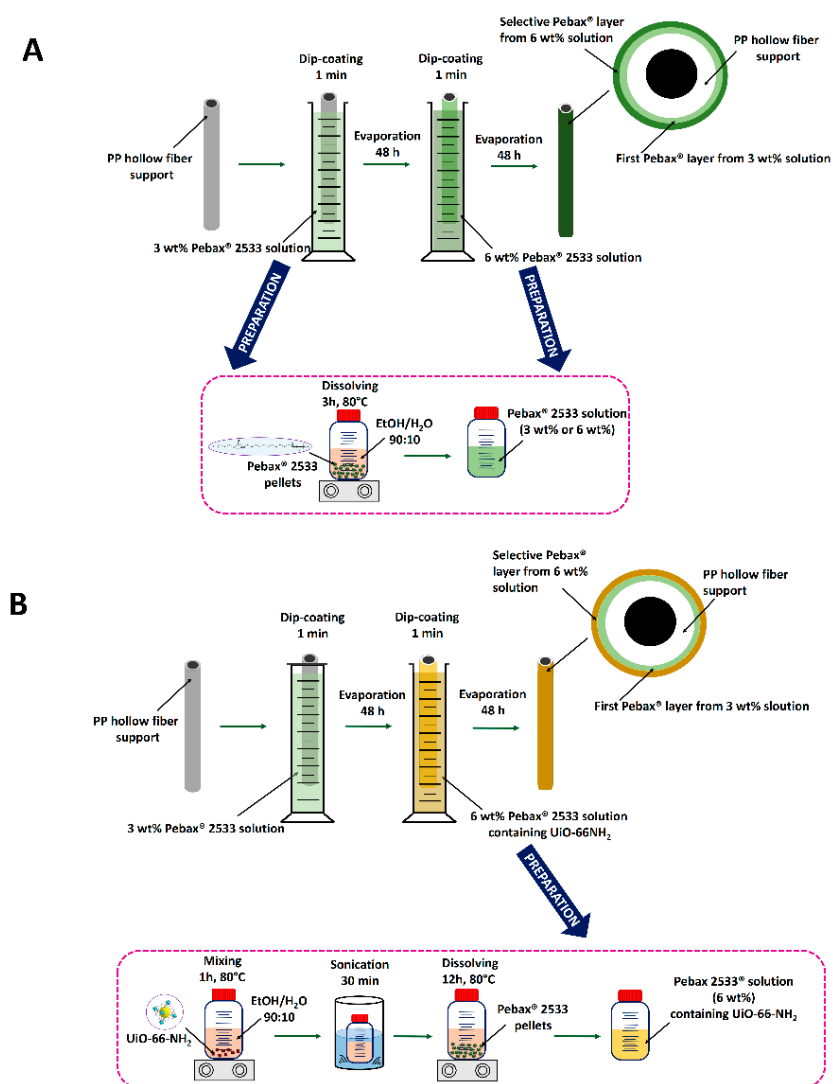


**Figure 1.** Schematic illustration of the preparation of a pristine Pebax<sup>®</sup> 2533 thin film hollow fiber membrane (A) and Pebax<sup>®</sup> 2533-UiO-66-NH<sub>2</sub>/PP mixed matrix thin film hollow fiber membrane (B).

#### 2.4. Characterization

The morphology and element mapping of the UiO-66-NH<sub>2</sub> particles, PP hollow fibers, Pebax<sup>®</sup> 2533/PP and mixed matrix Pebax<sup>®</sup> 2533/PP thin film hollow fiber membranes were analyzed by using scanning electron microscope (SEM) with X-ray spectroscopy (EDX) analysis—Phenom, Generation 5 (Phenom-World B. V., Eindhoven, The Netherlands). The hollow fiber membranes were fractured in liquid nitrogen (Air Products, Siewierz, Poland) to prepare the samples for the cross-section SEM analysis. The Pebax<sup>®</sup> 2533 layer thickness was measured on SEM pictures by using ImageJ software (version 1.8.0\_172, 2020, University of Wisconsin, Madison, WI, USA).

The surface chemistry of UiO-66-NH<sub>2</sub> particles, Pebax<sup>®</sup> 2533/PP and mixed matrix Pebax<sup>®</sup> 2533/PP thin film hollow fiber membranes were analyzed by using FTIR-ATR spectroscopy. The FTIR-ATR spectra were obtained between 500 and 4000 cm<sup>-1</sup> by using spectrometer Nicolet iS10 (Thermo Scientific, Waltham, MA, USA). The transmission mode with resolution of 4 cm<sup>-1</sup> and 256 scans was applied. The obtained data was analyzed by Omnic 9 software (Version 9.2, 2012, Thermo Fisher Scientific, Waltham, MA, USA).

The TGA-DTA analyses for UiO-66-NH<sub>2</sub> particles were conducted by using TA Instrument type SDT 2960 (TA Instrument, Champaign, IL, USA). The measuring temperature was set in the range of 25–950 °C under nitrogen atmosphere. The heating rate was 10 °C/min. The obtained data were analyzed by using TA Universal Analysis software (version: v5.5.24, 2015, TA Instrument, Champaign, IL, USA).

XRD analyses for UiO-66-NH<sub>2</sub> particles were conducted by using Philips X'Pert (Malvern Panalytical, Malvern, UK). The transmission mode was applied. The measured 2θ range was in the range of 5–80°. The X'Celerator Scientific detector (Malvern Panalytical, Malvern, UK) with Cu anode was used.

The nitrogen adsorption/desorption measurements were conducted at −195.7 °C via Gemini VI (Micromeritics Instrument Corp., Norcross, GA, USA). All samples were degassed for 6 h at 110 °C before the measurements. The BET (Brunauer–Emmett–Teller) model was applied for the calculation of surface area.

### 2.5. Gas Permeance Measurements

To measure the gas permeance of hollow fiber membranes, the hollow fiber membranes should be assembled into the module. The module used for the gas permeance measurements of hollow fiber membranes was designed and assembled by the Membranes and Membrane Techniques Research Group in Nicolaus Copernicus University in Toruń, Toruń, Poland. All parts of the module were purchased from Swagelok (Toruń, Poland) (Figure S1). One hollow fiber with a length of 7–10 cm was assembled into the module. A potting process is needed before the assembling of hollow fiber membrane into the module. The details related to the set-up for gas permeance measurements, and the potting process are described elsewhere [7].

The pure gas (N<sub>2</sub> and CO<sub>2</sub>) permeance tests were conducted at 2 bar and 25 °C. Each sample was measured 3 times under stabilized condition for better accuracy. The gas flow rate was measured by using a bubble flow meter (Sigma Aldrich, Poznań, Poland). The permeances (P/d) of gases were calculated by using Equation (1) [7,8]:

$$\frac{P}{d} = \frac{Q}{\Delta p A} = \frac{Q}{2n\pi r l \Delta p} \quad (1)$$

where P is the permeability (Barrer); Q is the flux of gas permeation rate (cm<sup>3</sup> (STP)/s); d is the thickness of membrane selective layer (cm); A is the effective membrane area (cm<sup>2</sup>); Δp is the pressure difference across the membrane (cmHg); r is the outer radius (cm) of hollow fiber; n is the number of hollow fibers; P/d is the gas permeance expressed in GPU (1 GPU = 10<sup>−6</sup> cm<sup>3</sup> (STP) cm<sup>−2</sup> s<sup>−1</sup> cmHg<sup>−1</sup>).

The ideal selectivity α was calculated by using Equation (2) [7,8]:

$$\alpha_{12} = \frac{(P/d)_1}{(P/d)_2} = \frac{P_1}{P_2} \quad (2)$$

## 3. Results and Discussion

### 3.1. Characterization of UiO-66-NH<sub>2</sub>

The SEM and EDX results of the synthesized UiO-66-NH<sub>2</sub> crystals were shown in Figure 2. The UiO-66-NH<sub>2</sub> showed octahedrally rectangular shapes [14]. The particle size of UiO-66-NH<sub>2</sub> is around 50–80 nm (Figure 2b). The elemental composition of synthesized UiO-66-NH<sub>2</sub> was revealed by EDX analysis. UiO-66-NH<sub>2</sub> is composed of Zr, C, O, and N elements (Figure 2c). The EDX results are in good agreement with its crystal structure which consists of Zr<sub>6</sub>-cluster and 2-aminoterephthalic acid linker.

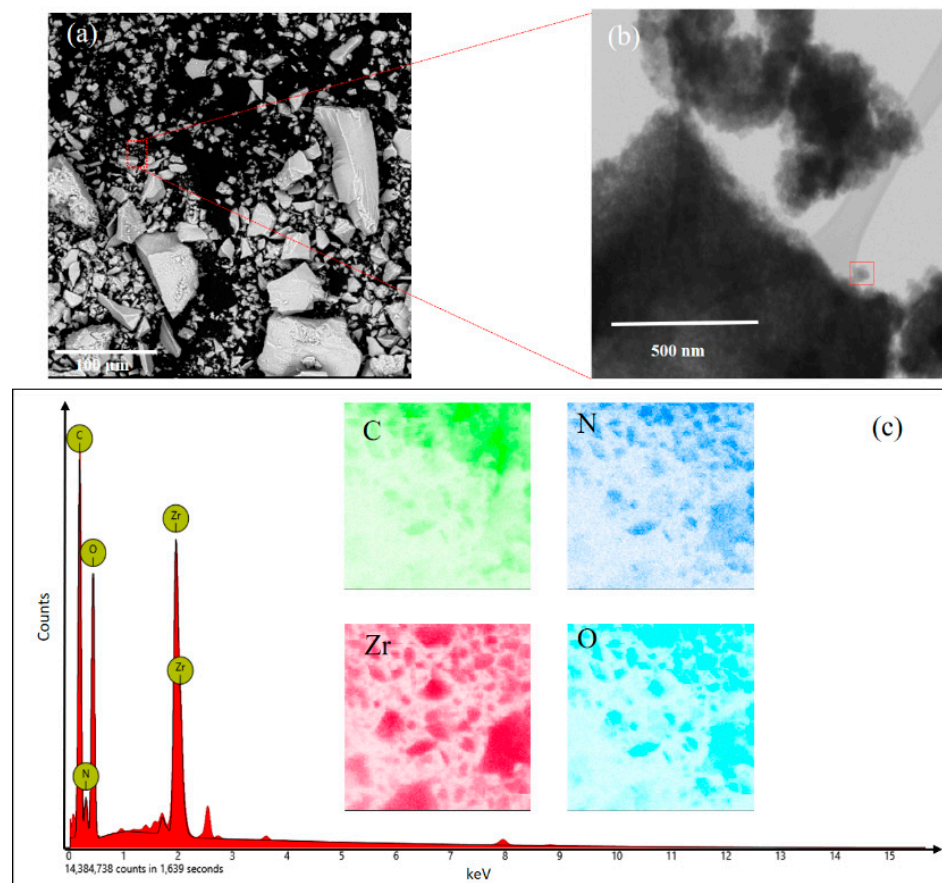


**Figure 2.** SEM (scanning electron microscope) images of synthesized UiO-66-NH<sub>2</sub> particles (a,b). (c) is the corresponding EDX (energy-dispersive X-ray spectroscopy) data and mapping results of the selected area in (a) of UiO-66-NH<sub>2</sub> particles.

As it is shown in Figure 3, the FTIR spectra provided more information about the chemical structure of the prepared UiO-66-NH<sub>2</sub> particles. The intensive peak at 1658 cm<sup>-1</sup> is ascribed to the stretching vibration of C=O group from residual DMF solvent in the MOF structure [28]. Two characteristic peaks at 3454 and 333 cm<sup>-1</sup> can be ascribed to the asymmetric and symmetric stretching vibration of the primary amine group, respectively [29]. Moreover, the peak at 1620 cm<sup>-1</sup> can be ascribed to the N–H bending vibration. What is more, the C–N bonding can be observed at 1257 and 1336 cm<sup>-1</sup> due to the stretching vibration of C–N bond. The peak at 764 cm<sup>-1</sup> can be assigned to the stretching vibration of Zr–O bond. The peak at 1435 cm<sup>-1</sup> can be related to the C–C stretching vibration in the aromatic ring from the 2-aminoterephthalic acid ligand. Moreover, the peaks at 1381 and 1570 cm<sup>-1</sup> can be assigned to the symmetric and asymmetric C–O stretching bonds, respectively, resulting from aromatic and carboxylic groups [30].

The TGA and the DTG curves are presented in Figure 4. The DTG curve was plotted as a function of temperature since it can clearly provide information of the transitions of UiO-66-NH<sub>2</sub>. As it is shown in Figure 4, the TGA and DTG curves of UiO-66-NH<sub>2</sub> show a two-step mass loss. The UiO-66-NH<sub>2</sub> powder underwent first-stage mass loss when the temperature increased to 280 °C. This is because the removal of absorbed moisture, residual solvent and the dehydroxylation of the Zr<sub>6</sub>O<sub>4</sub>(OH)<sub>4</sub> into Zr<sub>6</sub>O<sub>6</sub> [28]. The mass loss at this stage is around 40%. The crystal framework decomposition temperature for UiO-66-NH<sub>2</sub> is around 380 °C indicated by the second-stage mass loss. At the second stage of mass loss, the decomposition of amino terephthalic acid ligand occurred and ZrO<sub>2</sub> was formed [14]. Finally, when the temperature arrived at 650 °C, UiO-66-NH<sub>2</sub> nanoparticles showed the largest mass loss around 68%. Cao et al. [31] also found that the decomposition of amino terephthalic acid ligand in UiO-66-NH<sub>2</sub> nanoparticles occurred



from 380 °C. When the temperature reaches 650 °C, the UiO-66-NH<sub>2</sub> has the largest mass loss of approximately 65% [31]. The N<sub>2</sub> adsorption-desorption isotherm measured at 77 K was used to determine the specific area and pore structure of UiO-66-NH<sub>2</sub> (Figure 5). The adsorption hysteresis was observed due to the network effects and various forms of pore blocking [32], which could have resulted from the high increasing rate of temperature during the synthesis process. The BET (Brunauer-Emmett-Teller) surface area, adsorption average pore diameter, and BJH (Barrett-Joyner-Halenda) pore volume of the synthesized UiO-66-NH<sub>2</sub> were 349.35 m<sup>2</sup>/g, 2.35 nm, and 0.49 cm<sup>3</sup>/g, respectively. Our results are in good agreement with the earlier reports [33,34].

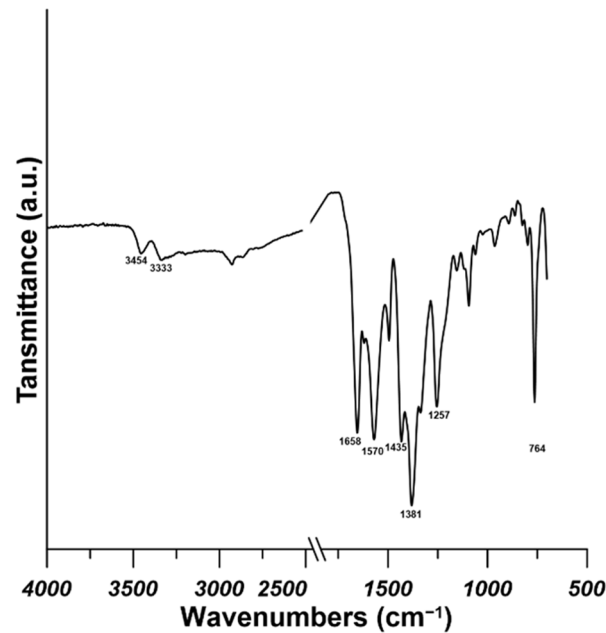


Figure 3. FTIR (fourier transform infrared) spectra of UiO-66-NH<sub>2</sub>.

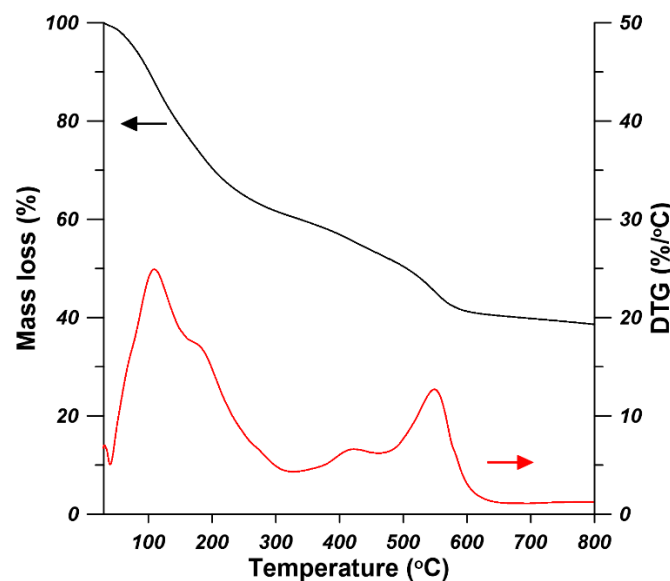


Figure 4. TGA (thermal gravimetric analysis) curves of UiO-66-NH<sub>2</sub>.

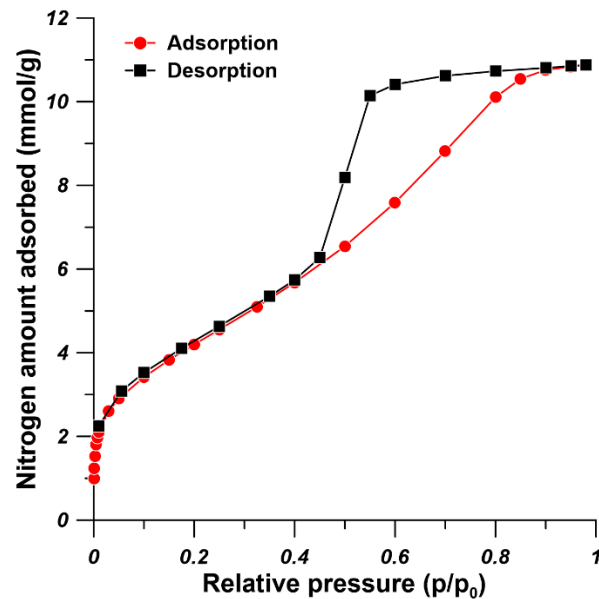


Figure 5.  $N_2$  adsorption and desorption curves of UiO-66-NH<sub>2</sub>.

The XRD analysis has been performed to prove that UiO-66-NH<sub>2</sub> has been successfully synthesized. The formation of MOF was evidenced by the observation of characteristic intensive peaks at  $2\theta$  equal to  $7.5^\circ$  (111) and  $8.8^\circ$  (002) (Figure 6). The experimental results are in a good accordance to the theoretical diffractogram, calculated based on the single crystal data (Figure 6) (ref code: SURKAT, deposit nr: 1405751) [35] with the implementation of Mercury software (Mercury 4. 2. 0., 2019, Cambridge Crystallographic Data Centre, Cambridge, UK).

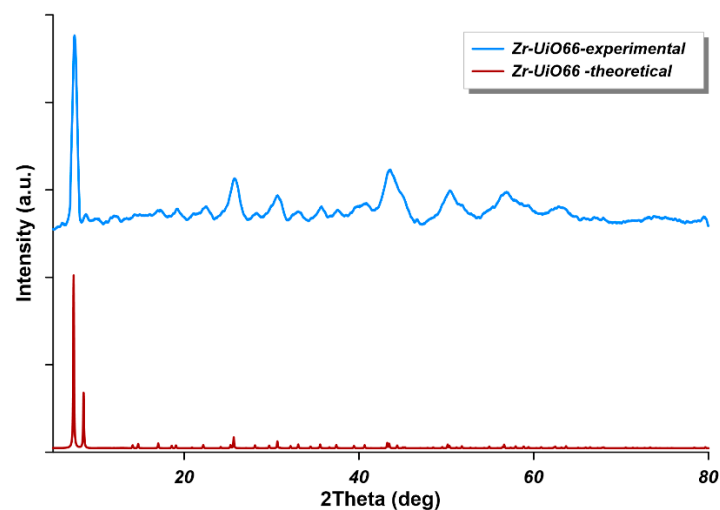


Figure 6. XRD (X-Ray diffraction) pattern of UiO-66-NH<sub>2</sub> (the blue curve) and the theoretical XRD pattern of UiO-66 MOF (metal-organic frameworks) (the red curve).

### 3.2. Membrane Characterization

The cross-section SEM and surface images of the polypropylene (PP) hollow fiber support, pristine Pebax<sup>®</sup> 2533 membrane, and thin film mixed matrix hollow fiber membranes were shown in Figure 7. The Pebax<sup>®</sup> 2533 thin layer was successfully coated on the shell side of PP hollow fibers by using a dip-coating method. As it is shown in Figure 7A, the PP hollow fiber supports possess porous structure (A1 and A2) and porous outer surface (A3 and A4). The porosity of PP hollow fiber is 50–60% and the average pore size is  $0.3 \mu\text{m}$  [27]. After dip-coating with 3 and 6 wt% Pebax<sup>®</sup> 2533 solutions, a defect-free Pebax<sup>®</sup> 2533

selective layer was fabricated on the shell side of PP hollow fiber support (Figure 7B). When UiO-66-NH<sub>2</sub> was incorporated into the Pebax<sup>®</sup> 2533 matrix, the thin film mixed matrix membrane was successfully formed on the outer surface of PP hollow fiber support (Figure 7C–G). The loading amount of UiO-66-NH<sub>2</sub> nanoparticles did not influence the thickness of Pebax<sup>®</sup> 2533-UiO-66-NH<sub>2</sub> hybrid selective layer since the coating Pebax<sup>®</sup> 2533 solution was kept constant at 6 wt%. The thickness of the Pebax<sup>®</sup> 2533-UiO-66-NH<sub>2</sub> hybrid selective layer was in the range of 5.40–6.97 μm (Table S2). When comparing the morphology of the prepared hollow fiber membranes, the roughness of the shell side increased with the increase of the UiO-66-NH<sub>2</sub> content from 0 to 50 wt% (Figure 7B4–G4). When the content of UiO-66-NH<sub>2</sub> was low (5 and 10 wt%), the homogeneous dispersion of UiO-66-NH<sub>2</sub> particles into Pebax<sup>®</sup> 2533 matrix was observed (Figure 7B,C). At the high content of MOF particles (15, 20, and 50 wt%), the aggregation of UiO-66-NH<sub>2</sub> in the polymeric matrix was observed (Figure 7E–G and Figure S2). It is reported that the MOF aggregation in polymeric matrix could lead to the formation of non-selective defects during the fabrication process [36]. Similar phenomenon was observed by Sutrisna et al. [33]. In their work, Pebax<sup>®</sup> 1657-UiO-66/PVDF thin film mixed matrix hollow fiber membranes were prepared for CO<sub>2</sub> separation. When the filler content was in the range of 10–50 wt%, no significantly aggregation was observed. However, the significant UiO-66 particle aggregation was observed when 80 wt% of UiO-66 was incorporated into the Pebax<sup>®</sup> 1657 matrix [33].

To investigate the chemical structure of pure PP hollow fiber support and the prepared thin film mixed matrix hollow fiber membranes, FTIR analysis was conducted. The FTIR spectra of PP hollow fiber support and the prepared Pebax<sup>®</sup> 2533-UiO-66-NH<sub>2</sub>/PP thin film mixed matrix hollow fiber membranes in the range of 650–4000 cm<sup>-1</sup> were shown in Figure 8. As the FTIR spectra of PP shows, the peak at 841 cm<sup>-1</sup> was attributed to C–CH<sub>3</sub> stretching vibration. The peaks at 973, 998, and 1168 cm<sup>-1</sup> were attributed to –CH<sub>3</sub> rocking vibration. The symmetric bending vibration of –CH<sub>3</sub> group was observed at 1376 cm<sup>-1</sup>. The –CH<sub>3</sub> asymmetric stretching vibration was observed at 2951 cm<sup>-1</sup>. Besides the peaks related to methyl group in PP, the peaks at 1456, 2839, and 2919 cm<sup>-1</sup> are designated to –CH<sub>2</sub>– symmetric bending, –CH<sub>2</sub>– symmetric stretching and –CH<sub>2</sub>– asymmetric stretching, respectively. Our FTIR results are in good agreement with the literature values [37,38]. After the formation of Pebax<sup>®</sup> 2533 layer on the shell side of PP hollow fiber support, the characteristic peaks of the –CH<sub>3</sub> group from PP disappeared. The characteristic peaks at 1109, 1640, 1734, and 3308 cm<sup>-1</sup>, are assigned to the stretching vibration of the C–O–C group of the PEO segment part, the N–H–C=O stretching vibration, the –O–C=O group, and the –N–H– stretching vibration of the polyamide block in Pebax<sup>®</sup> 2533, respectively [33,39]. The FTIR spectra of the prepared Pebax<sup>®</sup> 2533-UiO-66-NH<sub>2</sub>/PP thin film mixed matrix hollow fiber membranes are similar to the FTIR spectra of pristine Pebax<sup>®</sup> 2533/PP hollow fiber membranes, which demonstrates that there were no strong chemical interaction between UiO-66-NH<sub>2</sub> fillers and Pebax<sup>®</sup> 2533 matrix. It was found that the red shift of FTIR characteristic peak related to the –N–H– stretching vibration occurred when the UiO-66-NH<sub>2</sub> particles were incorporated into Pebax<sup>®</sup> 2533 due to the formation of hydrogen bonding [14,40]. However, the peaks related to the –N–H– stretching vibration for the mixed matrix membrane containing 0, 5, 10, 15, 20, and 50 wt% of UiO-66-NH<sub>2</sub> are 3308, 3297, 3297, 3296, 3307, and 3307 cm<sup>-1</sup>, respectively (Figure 8A). The –N–H– peak shift for PA (polyamide) segment is negligible due to the difficulty in the thin composite layer characterization [33]. As it is shown in the FTIR spectra in the range of 700–800 cm<sup>-1</sup> (Figure 8C), a peak related to the stretching vibration of Zr–O bond around 764 cm<sup>-1</sup> was observed, which indicates the serious aggregation of UiO-66-NH<sub>2</sub> particles in the mixed matrix hollow fiber membranes. This finding is in good agreement with the SEM results (Figure 7G).

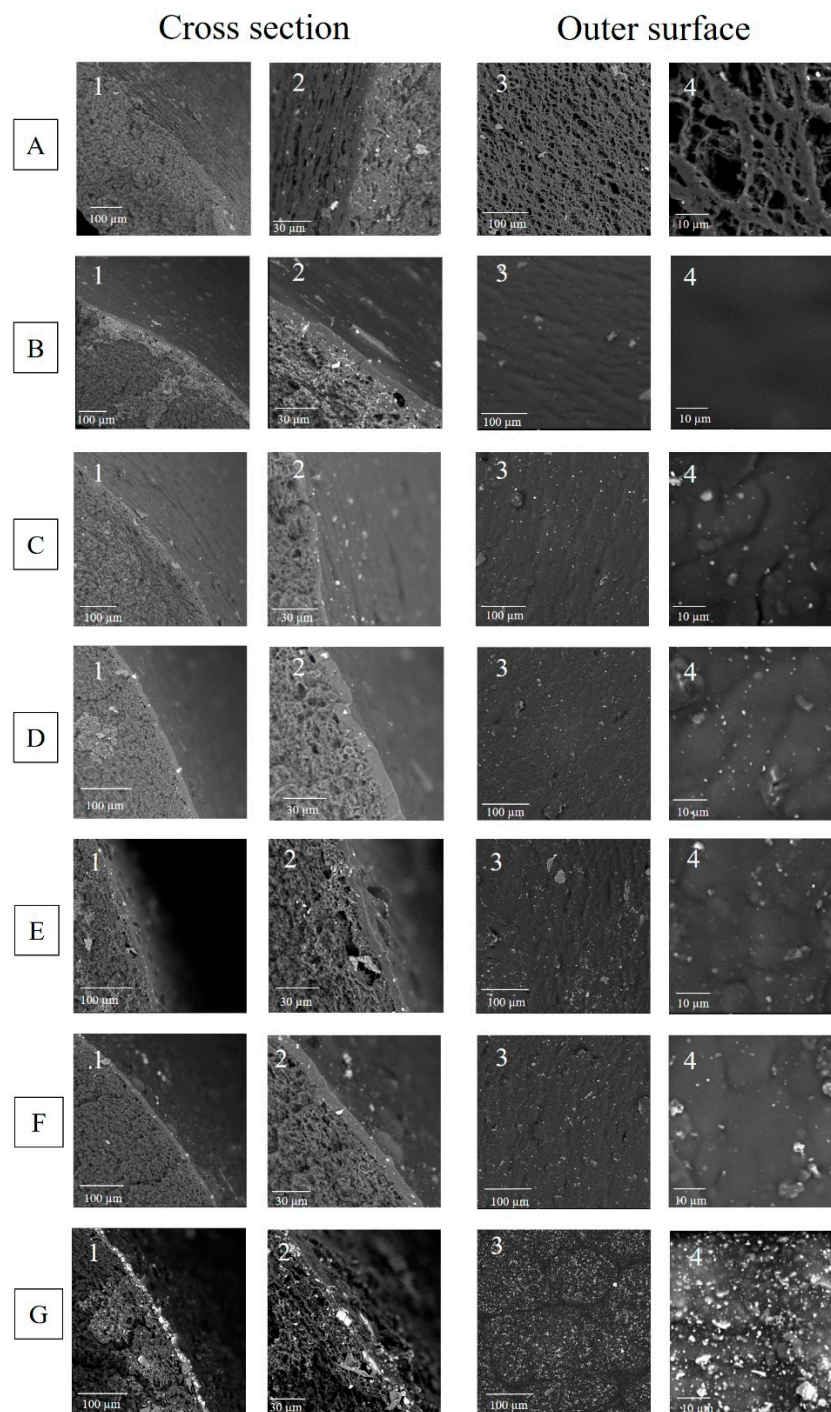


**Figure 7.** SEM pictures of cross-section (1 and 2) and outer surface (3 and 4) of Pebax<sup>®</sup> 2533-UiO-66-NH<sub>2</sub>/PP thin film mixed matrix hollow fiber membranes—(A) PP hollow fiber support, (B) 0 wt% UiO-66-NH<sub>2</sub>, (C) 5 wt% UiO-66-NH<sub>2</sub>, (D) 10 wt% UiO-66-NH<sub>2</sub>, (E) 15 wt% UiO-66-NH<sub>2</sub>, (F) 20 wt% UiO-66-NH<sub>2</sub>, and (G) 50 wt% UiO-66-NH<sub>2</sub>.

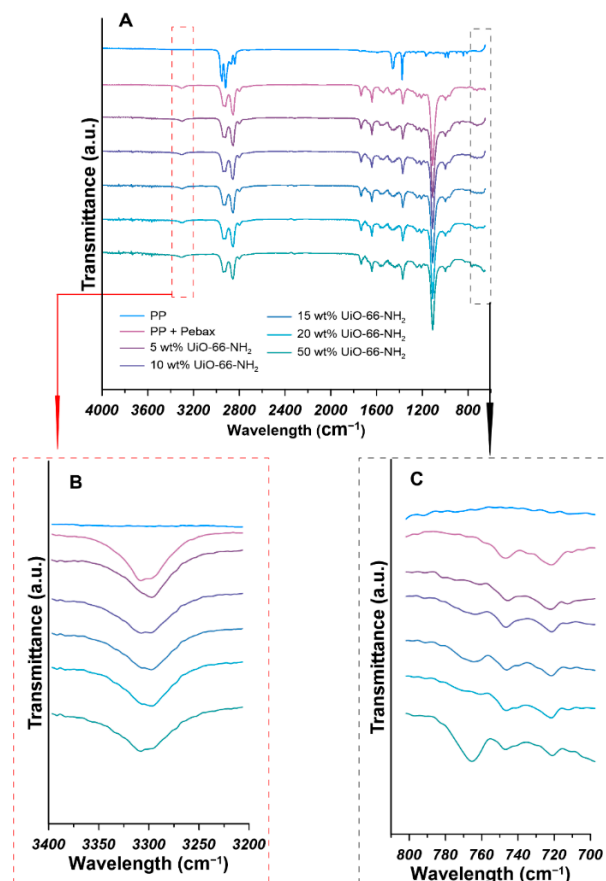


**Figure 8.** FTIR (Fourier transform infrared) spectra of Pebax<sup>®</sup> 2533-UiO-66-NH<sub>2</sub>/PP thin film mixed matrix hollow fiber membranes (A) (the enlarged FTIR spectra in the wavelength range 3400–3200 cm<sup>-1</sup> and 800–700 cm<sup>-1</sup> are shown in (B) and (C), respectively).

### 3.3. The Effect of UiO-66-NH<sub>2</sub> Loading on Gas Separation Performance

The gas separation behaviors of the prepared thin film mixed matrix hollow fiber membranes were studied by the gas permeation measurements. The CO<sub>2</sub> and N<sub>2</sub> permeance through the prepared membranes were measured at 2 bar and 25 °C. As it is shown in Figure 9, the UiO-66-NH<sub>2</sub> content in the Pebax<sup>®</sup> 2533 matrix influenced the gas permeance and the ideal selectivity of Pebax<sup>®</sup> 2533-UiO-66-NH<sub>2</sub>/PP thin film mixed matrix hollow fiber membranes. As can be seen from Figure 9A, when the UiO-66-NH<sub>2</sub> content increased from 0 to 50 wt%, the CO<sub>2</sub> permeance increased significantly from 19 to 30 GPU. The N<sub>2</sub> permeance barely increased when the UiO-66-NH<sub>2</sub> content increased from 0 to 10 wt%. However, the N<sub>2</sub> permeance increased to 0.91, 1.14, and 1.42 GPU when the UiO-66-NH<sub>2</sub> content increased to 15, 20, and 50 wt%, respectively. As it is shown in Figure 9B, the CO<sub>2</sub>/N<sub>2</sub> ideal selectivity firstly increased from 30 to 37 when the UiO-66-NH<sub>2</sub> content increased from 0 to 10 wt%. Then the CO<sub>2</sub>/N<sub>2</sub> ideal selectivity decreased to 21 when the UiO-66-NH<sub>2</sub> content increased to 50 wt%.



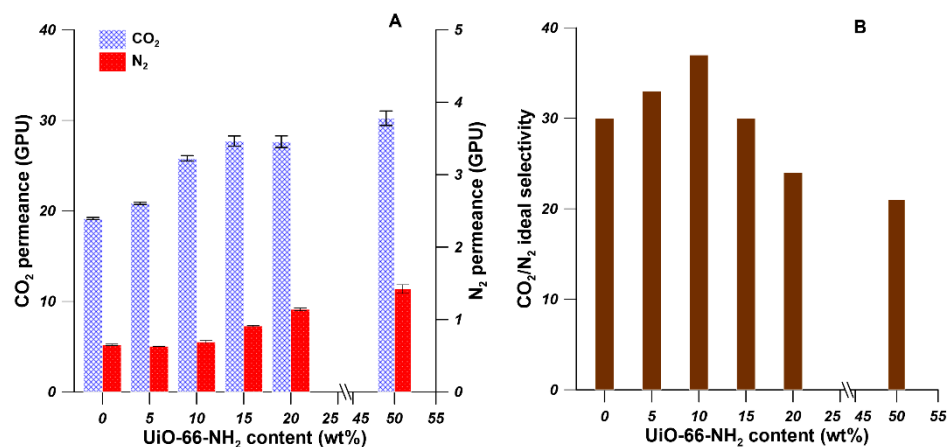


**Figure 9.** The effect of UiO-66-NH<sub>2</sub> content on the CO<sub>2</sub> and N<sub>2</sub> permeances (A) and CO<sub>2</sub>/N<sub>2</sub> ideal selectivity (B) of Pebax<sup>®</sup> 2533-UiO-66-NH<sub>2</sub>/PP thin film mixed matrix hollow fiber membranes.

As discussed above, when the UiO-66-NH<sub>2</sub> content increased to 10 wt%, both the CO<sub>2</sub> permeance and CO<sub>2</sub>/N<sub>2</sub> ideal selectivity increased while the N<sub>2</sub> permeance was practically unchanged, which indicates the formation of defect-free thin mixed matrix membrane on the PP hollow fiber support. The enhanced CO<sub>2</sub> permeance and CO<sub>2</sub>/N<sub>2</sub> ideal selectivity were ascribed to the interrupted chain packing in the polymer matrix [41] and the CO<sub>2</sub>-philic nature of UiO-66-NH<sub>2</sub> [42]. In comparison to the pure Pebax<sup>®</sup> 2533 thin film hollow fiber membrane, the CO<sub>2</sub> permeance and CO<sub>2</sub>/N<sub>2</sub> ideal selectivity of Pebax<sup>®</sup> 2533-UiO-66-NH<sub>2</sub>/PP thin film mixed matrix hollow fiber membrane containing 10 wt% UiO-66-NH<sub>2</sub> increased by 35 and 23%, respectively. The kinetic diameters for CO<sub>2</sub> and N<sub>2</sub> molecules are 0.33 and 0.36 nm, respectively. The CO<sub>2</sub> mobility is higher than the N<sub>2</sub> mobility in Pebax<sup>®</sup> membranes due to smaller size and higher condensability of CO<sub>2</sub> molecules, and the CO<sub>2</sub>-philic ether group in Pebax<sup>®</sup> polymer chains [14]. The CO<sub>2</sub> permeance increased with the addition of UiO-66-NH<sub>2</sub> nanoparticles. The N<sub>2</sub> permeance increased slightly when the UiO-66-NH<sub>2</sub> content increased from 0 to 10 wt%. However, when the UiO-66-NH<sub>2</sub> content was higher than 10 wt%, the N<sub>2</sub> permeance started to increase significantly, resulting in the decrease in CO<sub>2</sub>/N<sub>2</sub> ideal selectivity. For instance, when 20 and 50 wt% of UiO-66-NH<sub>2</sub> was incorporated into the Pebax<sup>®</sup> 2533 matrix, the CO<sub>2</sub> permeance increased 9% while the N<sub>2</sub> permeance increased 25%. Consequently, the CO<sub>2</sub>/N<sub>2</sub> ideal selectivity was less than that of pure Pebax<sup>®</sup> 2533 membranes. This can be explained by the severe agglomeration of UiO-66-NH<sub>2</sub> when large amounts of UiO-66-NH<sub>2</sub> particles were incorporated into polymeric matrix. Consequently, the non-selective interface defects were formed, resulting in the deterioration of gas separation of Pebax<sup>®</sup> 2533-UiO-66-NH<sub>2</sub>/PP thin film mixed matrix hollow fiber membranes. The agglomeration of nanoparticles in the mixed matrix membranes have been documented in the literature [14,41,43]. Shen et al. [14] prepared Pebax<sup>®</sup> 1657 based mixed matrix membranes containing UiO-66 and UiO-66-NH<sub>2</sub> nanoparticles for CO<sub>2</sub> separation. It was found that CO<sub>2</sub>/N<sub>2</sub> selectivity started to decrease due to the filler agglomeration when the UiO-66 and UiO-66-NH<sub>2</sub> loading is higher than 7.5 and 10 wt%, respectively. Jiao et al. [43] synthesized polyethyleneimine (PEI) modified ZIF-8 and incorporated the PEI-ZIF-8 particle into Pebax<sup>®</sup> 1657 matrix to prepare mixed matrix membranes for CO<sub>2</sub>/N<sub>2</sub> separation. It was found that the composite membrane with 5 wt% PEI-ZIF-8 shows the best gas separation performance with CO<sub>2</sub> permeance equal to 13 GPU and CO<sub>2</sub>/N<sub>2</sub> selectivity equal to 49. The filler agglomeration occurred resulting in rigidified interface.

#### 3.4. Comparison of the Pebax<sup>®</sup>-Based Mixed Matrix Membranes Incorporating Various Nanoparticles in CO<sub>2</sub>/N<sub>2</sub> Gas Separation

The performance of the prepared Pebax<sup>®</sup> 2533-UiO-66-NH<sub>2</sub>/PP thin film mixed matrix hollow fiber membranes were compared with Pebax<sup>®</sup>-based mixed matrix membranes

containing various types of fillers (Table 1). The gas separation performance of Pebax<sup>®</sup> 2533-UiO-66-NH<sub>2</sub>/PP thin film mixed matrix hollow fiber membrane containing 10 wt% UiO-66-NH<sub>2</sub> is comparable with previous reported Pebax<sup>®</sup>-based mixed matrix membranes containing various types of fillers in literature [14,33,40,44–52]. The prepared membrane shows a high CO<sub>2</sub>/N<sub>2</sub> ideal selectivity equal to 37 with a CO<sub>2</sub> permeance 25.81 GPU at feed pressure 2 bar. The addition of UiO-66-NH<sub>2</sub> enhances the CO<sub>2</sub>/N<sub>2</sub> separation performance mainly due to the good interfacial compatibility and the CO<sub>2</sub>-philic nature of UiO-66-NH<sub>2</sub>. Sutrisna et al. [33] fabricated UiO-66-NH<sub>2</sub>/Pebax<sup>®</sup> 1657 based hollow fiber composite membranes with high CO<sub>2</sub> permeance equal to 338 GPU and high CO<sub>2</sub>/N<sub>2</sub> selectivity equal to 57. Their work showed better CO<sub>2</sub>/N<sub>2</sub> separation performance, which can be attributed to the lower Pebax<sup>®</sup> 1657 coating solution, and the application of poly [1-(trimethylsilyl) prop-1-yne] (PTMSP) as a gutter layer. The lower coating solution concentration could result in smaller selective layer thickness. The smooth PTMSP gutter layer can prevent the intrusion of Pebax<sup>®</sup> into pores of support layer, resulting in a thin selective layer. As a result, the prepared UiO-66-NH<sub>2</sub>/Pebax<sup>®</sup> 1657 based hollow fiber composite membranes showed very high gas separation performance. As it is shown in Table 1, the thin film mixed matrix membranes possess comparable CO<sub>2</sub>/N<sub>2</sub> selectivity but much higher CO<sub>2</sub> permeance than that of dense flat sheet mixed matrix membranes. Therefore, the gas separation performances of thin film mixed matrix membranes are better than the dense flat sheet membranes.

**Table 1.** The comparison of gas separation performances of Pebax<sup>®</sup>-based mixed matrix membranes with different fillers.

Support Polymer	Hybrid Coating Material	Filler Content (wt%)	Configuration	Feed Gas	CO <sub>2</sub> (GPU)	N <sub>2</sub> (GPU)	CO <sub>2</sub> /N <sub>2</sub> Selectivity	Ref.
PVDF/PTMSP	UiO-66-NH <sub>2</sub> /Pebax <sup>®</sup> 1657	50	Hollow fiber	Pure gas	338	5.93	57	[33]
PSF	Fe(DA)/Pebax <sup>®</sup> 1657	3	Hollow fiber	Pure gas	90.00	1.61	56	[44]
PVDF	ZIF-8/Pebax <sup>®</sup> 1657	30	Hollow fiber	Pure gas	350.00	10.94	32	[40]
PVDF	GO/Pebax <sup>®</sup> 1657	0.1	Hollow fiber	Pure gas	415.00	9.65	43	[46]
PSF	GO/Pebax <sup>®</sup> 1657	0.4	Hollow fiber	Pure gas	28.08	0.66	43	[47]
PAN	ZIF-7/Pebax <sup>®</sup> 1657	34	Flat sheet	Pure gas	39.00	0.37	105	[45]
PVDF	UiO-66-NH <sub>2</sub> /Pebax <sup>®</sup> 1657	20	Flat sheet	Pure gas	125 Barrer	-	25	[14]
-	ZIF-8/Pebax <sup>®</sup> 1657	20	Dense flat sheet	Pure gas	2.80	0.07	41	[48]
-	NH <sub>2</sub> -MIL-53/Pebax <sup>®</sup> 1657	10	Dense flat sheet	Pure gas	1.60	0.03	55	[49]
-	NaY/Pebax <sup>®</sup> 1657	10	Dense flat sheet	Pure gas	3.60	0.10	35	[50]
-	ZIF-7/Pebax <sup>®</sup> 2533	14	Dense flat sheet	Pure gas	198 Barrer	8.74 Barrer	22.6	[19]
-	ZIF-7-NH <sub>2</sub> /Pebax <sup>®</sup> 2533	14	Dense flat sheet	Pure gas	206 Barrer	7.53 Barrer	27.3	[19]
-	ZIF-8@GO/Pebax <sup>®</sup> 2533	6	Dense flat sheet	Pure gas	249 Barrer	5.23 Barrer	47.6	[51]
-	Zn/Ni-ZIF-8/Pebax <sup>®</sup> 2533	10	Dense flat sheet	Pure gas	321 Barrer	7.5 Barrer	42.8	[52]
PP	UiO-66-NH <sub>2</sub> /Pebax <sup>®</sup> 2533	10	Hollow fiber	Pure gas	25.81	0.69	37	This work

PVDF—polyvinylidene difluoride, PTMSP—poly [1-(trimethylsilyl) prop-1-yne], PSF—polysulfone, PAN—polyacrylonitrile, PP—polypropylene.

#### 4. Conclusions

Pebax<sup>®</sup> 2533-UiO-66-NH<sub>2</sub>/PP mixed matrix thin film hollow fiber membranes were successfully fabricated by using dip coating method. The pre-treatment of PP hollow fibers by dip-coating with 3 wt% Pebax<sup>®</sup> 2533 solution could smoothen the outer surface of hollow fiber supports, which facilitated the formation of defect-free selective layer. The incorporation of UiO-66-NH<sub>2</sub> nanoparticles into the Pebax<sup>®</sup> 2533 coating solution affected the morphology, surface chemistry, and gas separation performance of Pebax<sup>®</sup> 2533-UiO-66-NH<sub>2</sub>/PP mixed matrix thin film hollow fiber membranes confirmed by SEM analysis, FTIR analysis, and gas permeance measurements, respectively. The aggregation of UiO-66-NH<sub>2</sub>

nanoparticles was observed at higher amounts of UiO-66-NH<sub>2</sub> nanoparticles in the Pebax<sup>®</sup> 2533 matrix. The filler aggregation should be tackled by post-synthetic modification of UiO-66-NH<sub>2</sub> nanoparticles. The CO<sub>2</sub> permeance increased with the increase of the loading amount of UiO-66 nanoparticles, while the CO<sub>2</sub>/N<sub>2</sub> ideal gas selectivity firstly increased then decreased due to the aggregation of UiO-66 nanoparticles. The Pebax<sup>®</sup> 2533-UiO-66-NH<sub>2</sub>/PP mixed matrix thin film hollow fiber membranes containing 10 wt% UiO-66 nanoparticles exhibited the best gas separation performance with CO<sub>2</sub> permeance of 26 GPU and CO<sub>2</sub>/N<sub>2</sub> selectivity of 37.

**Supplementary Materials:** The following are available online at <https://www.mdpi.com/article/10.3390/ma14123366/s1>, Figure S1: Hollow fiber module for testing gas permeance of hollow fiber membranes (This module is designed by the Membranes and Membrane Techniques Research Group in Nicolaus Copernicus University in Toruń. All the components of this module including housing part, end caps, and ports are purchased from Swagelok), Figure S2: The Zr element mapping and element analysis of Pebax<sup>®</sup>2533-UiO-66-NH<sub>2</sub>/PP thin film mixed matrix hollow fiber membranes by EDX. (a) 15 wt% UiO-66-NH<sub>2</sub>, (b) 20 wt% UiO-66-NH<sub>2</sub>, (c) 50 wt% UiO-66-NH<sub>2</sub>, Table S1: The gas permeance and ideal selectivity of thin film hollow fiber membranes fabricated from single concentration of coating solution, Table S2: The thickness of the Pebax/UiO-66-NH<sub>2</sub> hybrid layer measured from the top part and bottom part of the prepared mixed matrix thin film hollow fiber membrane. The bottom part is close to the coating solution while the top part is close to the metal holder during the dip-coating process.

**Author Contributions:** Conceptualization, G.L. and W.K.; Data curation, G.L. and K.K.; Formal analysis, G.L., W.K., K.K. and J.K.; Funding acquisition, G.L. and W.K.; Investigation, G.L.; Methodology, G.L., W.K. and J.K.; Resources, W.K.; Software, K.K. and J.K.; Supervision, W.K. and J.K.; Validation, G.L.; Visualization, G.L. and K.K.; Writing—original draft, G.L.; Writing—review & editing, G.L., W.K. and K.K. All authors have read and agreed to the published version of the manuscript.

**Funding:** This work was supported by the Young Researcher grant for PhD Students of Nicolaus Copernicus University in Toruń, Poland (Faculty of Chemistry, 492/2020).

**Institutional Review Board Statement:** Not applicable.

**Informed Consent Statement:** Not applicable.

**Data Availability Statement:** The data presented in this study are available on request from the corresponding author.

**Conflicts of Interest:** The authors declare no conflict of interest.

## References

1. Al Mesfer, M.K.; Danish, M. Breakthrough adsorption study of activated carbons for CO<sub>2</sub> separation from flue gas. *J. Environ. Chem. Eng.* **2018**, *6*, 4514–4524. [[CrossRef](#)]
2. Wang, K.; Xu, H.; Yang, C.; Qiu, T. Machine learning-based ionic liquids design and process simulation for CO<sub>2</sub> separation from flue gas. *Green Energy Environ.* **2020**. [[CrossRef](#)]
3. Polat, H.M.; Kavak, S.; Kulak, H.; Uzun, A.; Keskin, S. CO<sub>2</sub> separation from flue gas mixture using [BMIM][BF<sub>4</sub>]/MOF composites: Linking high-throughput computational screening with experiments. *Chem. Eng. J.* **2020**, *394*, 124916. [[CrossRef](#)]
4. Gilassi, S.; Taghavi, S.M.; Rodrigue, D.; Kaliaguine, S. Techno-Economic Analysis of a Hybrid System for Flue-Gas Separation: Combining Membrane and Enzymatic-Absorption Processes. *Chem. Eng. Process. Process. Intensif.* **2021**, *159*, 108222. [[CrossRef](#)]
5. Kamble, A.R.; Patel, C.M.; Murthy, Z. A review on the recent advances in mixed matrix membranes for gas separation processes. *Renew. Sustain. Energy Rev.* **2021**, *145*, 111062. [[CrossRef](#)]
6. Li, G.; Kujawski, W.; Válek, R.; Koter, S. A review—The development of hollow fibre membranes for gas separation processes. *Int. J. Greenh. Gas. Control.* **2021**, *104*, 103195. [[CrossRef](#)]
7. Li, G.; Kujawski, W.; Knozowska, K.; Kujawa, J. The Effects of PEI Hollow Fiber Substrate Characteristics on PDMS/PEI Hollow Fiber Membranes for CO<sub>2</sub>/N<sub>2</sub> Separation. *Membranes* **2021**, *11*, 56. [[CrossRef](#)]
8. Li, G.; Knozowska, K.; Kujawa, J.; Tonkonogovas, A.; Stankevičius, A.; Kujawski, W. Fabrication of Polydimethylsiloxane (PDMS) Dense Layer on Polyetherimide (PEI) Hollow Fiber Support for the Efficient CO<sub>2</sub>/N<sub>2</sub> Separation Membranes. *Polymers* **2021**, *13*, 756. [[CrossRef](#)] [[PubMed](#)]
9. Liu, B.; Tang, C.; Li, X.; Wang, B.; Zhou, R. High-performance SAPO-34 membranes for CO<sub>2</sub> separations from simulated flue gas. *Microporous Mesoporous Mater.* **2020**, *292*, 109712. [[CrossRef](#)]

10. Ilicak, I.; Boroglu, M.S.; Durmus, A.; Boz, I. Influence of ZIF-95 on structure and gas separation properties of polyimide-based mixed matrix membranes. *J. Nat. Gas. Sci. Eng.* **2021**, *91*, 103941. [[CrossRef](#)]
11. Wang, Q.; Dai, Y.; Ruan, X.; Zheng, W.; Yan, X.; Li, X.; He, G. ZIF-8 hollow nanotubes based mixed matrix membranes with high-speed gas transmission channel to promote CO<sub>2</sub>/N<sub>2</sub> separation. *J. Membr. Sci.* **2021**, *630*, 119323. [[CrossRef](#)]
12. Saqib, S.; Rafiq, S.; Muhammad, N.; Khan, A.L.; Mukhtar, A.; Ullah, S.; Nawaz, M.H.; Jamil, F.; Zhang, C.; Ashokkumar, V. Sustainable mixed matrix membranes containing porphyrin and polysulfone polymer for acid gas separations. *J. Hazard. Mater.* **2021**, *411*, 125155. [[CrossRef](#)]
13. Liu, L.; Chakma, A.; Feng, X. CO<sub>2</sub>/N<sub>2</sub> Separation by Poly(Ether Block Amide) Thin Film Hollow Fiber Composite Membranes. *Ind. Eng. Chem. Res.* **2005**, *44*, 6874–6882. [[CrossRef](#)]
14. Shen, J.; Liu, G.; Huang, K.; Li, Q.; Guan, K.; Li, Y.; Jin, W. UiO-66-polyether block amide mixed matrix membranes for CO<sub>2</sub> separation. *J. Membr. Sci.* **2016**, *513*, 155–165. [[CrossRef](#)]
15. Casadei, R.; Baschetti, M.G.; Yoo, M.J.; Park, H.B.; Giorgini, L. Pebax<sup>®</sup> 2533/Graphene Oxide Nanocomposite Membranes for Carbon Capture. *Membranes* **2020**, *10*, 188. [[CrossRef](#)] [[PubMed](#)]
16. Liu, C.; Wang, J.; Wan, J.; Yu, C. MOF-on-MOF hybrids: Synthesis and applications. *Co-Ord. Chem. Rev.* **2021**, *432*, 213743. [[CrossRef](#)]
17. Chen, S.; Li, X.; Duan, J.; Fu, Y.; Wang, Z.; Zhu, M.; Li, N. Investigation of highly efficient adsorbent based on Ni-MOF-74 in the separation of CO<sub>2</sub> from natural gas. *Chem. Eng. J.* **2021**, *419*, 129653. [[CrossRef](#)]
18. Kujawa, J.; Al-Gharabli, S.; Muzioł, T.M.; Knozowska, K.; Li, G.; Dumée, L.F.; Kujawski, W. Crystalline porous frameworks as nano-enhancers for membrane liquid separation—Recent developments. *Co-Ord. Chem. Rev.* **2021**, *440*, 213969. [[CrossRef](#)]
19. Gao, J.; Mao, H.; Jin, H.; Chen, C.; Feldhoff, A.; Li, Y. Functionalized ZIF-7/Pebax<sup>®</sup> 2533 mixed matrix membranes for CO<sub>2</sub>/N<sub>2</sub> separation. *Microporous Mesoporous Mater.* **2020**, *297*, 110030. [[CrossRef](#)]
20. Song, C.; Li, R.; Fan, Z.; Liu, Q.; Zhang, B.; Kitamura, Y. CO<sub>2</sub>/N<sub>2</sub> separation performance of Pebax/MIL-101 and Pebax/NH<sub>2</sub>-MIL-101 mixed matrix membranes and intensification via sub-ambient operation. *Sep. Purif. Technol.* **2020**, *238*, 116500. [[CrossRef](#)]
21. Chuah, C.Y.; Lee, J.; Song, J.; Bae, T.-H. CO<sub>2</sub>/N<sub>2</sub> Separation Properties of Polyimide-Based Mixed-Matrix Membranes Comprising UiO-66 with Various Functionalities. *Membranes* **2020**, *10*, 154. [[CrossRef](#)] [[PubMed](#)]
22. Jiang, Y.; Liu, C.; Caro, J.; Huang, A. A new UiO-66-NH<sub>2</sub> based mixed-matrix membranes with high CO<sub>2</sub>/CH<sub>4</sub> separation performance. *Microporous Mesoporous Mater.* **2019**, *274*, 203–211. [[CrossRef](#)]
23. Jameh, A.A.; Mohammadi, T.; Bakhtiari, O. Preparation of PEBAX-1074/modified ZIF-8 nanoparticles mixed matrix membranes for CO<sub>2</sub> removal from natural gas. *Sep. Purif. Technol.* **2020**, *231*, 115900. [[CrossRef](#)]
24. Dai, Y.; Johnson, J.; Karvan, O.; Sholl, D.S.; Koros, W. Ultem<sup>®</sup>/ZIF-8 mixed matrix hollow fiber membranes for CO<sub>2</sub>/N<sub>2</sub> separations. *J. Membr. Sci.* **2012**, *401–402*, 76–82. [[CrossRef](#)]
25. Etxeberria-Benavides, M.; Johnson, T.; Cao, S.; Zornoza, B.; Coronas, J.; Sanchez-Lainez, J.; Sabetghadam, A.; Liu, X.; Andres-Garcia, E.; Kapteijn, F.; et al. PBI mixed matrix hollow fiber membrane: Influence of ZIF-8 filler over H<sub>2</sub>/CO<sub>2</sub> separation performance at high temperature and pressure. *Sep. Purif. Technol.* **2020**, *237*, 116347. [[CrossRef](#)]
26. Xu, Z.-K.; Dai, Q.-W.; Liu, Z.-M.; Kou, R.-Q.; Xu, Y.-Y. Microporous polypropylene hollow fiber membranes: Part II. Per-vaporation separation of water/ethanol mixtures by the poly (acrylic acid) grafted membranes. *J. Membr. Sci.* **2003**, *214*, 71–81. [[CrossRef](#)]
27. Szwaszt, M.; Zalewski, M.; Prokopowicz, L.; Khoshgrudi, R.N. Novel Mixed Matrix Membrane for gas mixture separation. In *Monographs of the Environmental Engineering Committee Polish Academy of Sciences: Membranes and Membrane Processes in Environmental Protection*; Konieczny, K., Korus, I., Eds.; Polska Akademia Nauk, Komitet Inżynierii Środowiska: Warsaw, Poland, 2014; pp. 89–99.
28. Zhu, J.; Wu, L.; Bu, Z.; Jie, S.; Li, B.-G. Polyethyleneimine-Modified UiO-66-NH<sub>2</sub>(Zr) Metal–Organic Frameworks: Preparation and Enhanced CO<sub>2</sub> Selective Adsorption. *ACS Omega* **2009**, *4*, 3188–3197. [[CrossRef](#)]
29. Hou, J.; Luan, Y.; Tang, J.; Wensley, A.M.; Yang, M.; Lu, Y. Synthesis of UiO-66-NH<sub>2</sub> derived heterogeneous copper (II) catalyst and study of its application in the selective aerobic oxidation of alcohols. *J. Mol. Catal. A Chem.* **2015**, *407*, 53–59. [[CrossRef](#)]
30. Zhang, X.; Zhang, Y.; Wang, T.; Fan, Z.; Zhang, G. A thin film nanocomposite membrane with pre-immobilized UiO-66-NH<sub>2</sub> toward enhanced nanofiltration performance. *RSC Adv.* **2019**, *9*, 24802–24810. [[CrossRef](#)]
31. Cao, Y.; Zhang, H.; Song, F.; Huang, T.; Ji, J.; Zhong, Q.; Chu, W.; Xu, Q. UiO-66-NH<sub>2</sub>/GO Composite: Synthesis, Characterization and CO<sub>2</sub> Adsorption Performance. *Materials* **2018**, *11*, 589. [[CrossRef](#)]
32. Thommes, M.; Kaneko, K.; Neimark, A.V.; Olivier, J.P.; Rodriguez-Reinoso, F.; Rouquerol, J.; Sing, K.S.W. Physisorption of gases, with special reference to the evaluation of surface area and pore size distribution (IUPAC Technical Report). *Pure Appl. Chem.* **2015**, *87*, 1051–1069. [[CrossRef](#)]
33. Sutrisna, P.D.; Hou, J.; Zulkifli, M.Y.; Li, H.; Zhang, Y.; Liang, W.; D’Alessandro, D.M.; Chen, V. Surface functionalized UiO-66/Pebax-based ultrathin composite hollow fiber gas separation membranes. *J. Mater. Chem. A* **2017**, *6*, 918–931. [[CrossRef](#)]
34. Tambat, S.N.; Sane, P.K.; Suresh, S.; Varadan, N.; Pandit, A.B.; Sontakke, S.M. Hydrothermal synthesis of NH<sub>2</sub>-UiO-66 and its application for adsorptive removal of dye. *Adv. Powder Technol.* **2018**, *29*, 2626–2632. [[CrossRef](#)]
35. Trickett, C.A.; Gagnon, K.J.; Lee, S.; Gándara, F.; Bürgi, H.-B.; Yaghi, O.M. Definitive Molecular Level Characterization of Defects in UiO-66 Crystals. *Angew. Chem. Int. Ed.* **2015**, *54*, 11162–11167. [[CrossRef](#)] [[PubMed](#)]



36. Bi, X.; Zhang, Y.; Zhang, F.; Zhang, S.; Wang, Z.; Jin, J. MOF Nanosheet-Based Mixed Matrix Membranes with Metal–Organic Coordination Interfacial Interaction for Gas Separation. *ACS Appl. Mater. Interfaces* **2020**, *12*, 49101–49110. [[CrossRef](#)]
37. Gopanna, A.; Mandapati, R.N.; Thomas, S.P.; Rajan, K.; Chavali, M. Fourier transform infrared spectroscopy (FTIR), Raman spectroscopy and wide-angle X-ray scattering (WAXS) of polypropylene (PP)/cyclic olefin copolymer (COC) blends for qualitative and quantitative analysis. *Polym. Bull.* **2019**, *76*, 4259–4274. [[CrossRef](#)]
38. Gonzalez-Canche, N.G.; Flores-Johnson, E.A.; Cortes, P.; Carrillo, J.G. Evaluation of surface treatments on 5052-H32 aluminum alloy for enhancing the interfacial adhesion of thermoplastic-based fiber metal laminates. *Int. J. Adhes. Adhes.* **2018**, *82*, 90–99. [[CrossRef](#)]
39. Bernardo, P.; Clarizia, G. Enhancing Gas Permeation Properties of Pebax<sup>®</sup> 1657 Membranes via Polysorbate Nonionic Surfactants Doping. *Polymers* **2020**, *12*, 253. [[CrossRef](#)] [[PubMed](#)]
40. Sutrisna, P.D.; Hou, J.; Li, H.; Zhang, Y.; Chen, V. Improved operational stability of Pebax-based gas separation membranes with ZIF-8: A comparative study of flat sheet and composite hollow fibre membranes. *J. Membr. Sci.* **2017**, *524*, 266–279. [[CrossRef](#)]
41. Nafisi, V.; Hägg, M.-B. Development of dual layer of ZIF-8/PEBAX-2533 mixed matrix membrane for CO<sub>2</sub> capture. *J. Membr. Sci.* **2014**, *459*, 244–255. [[CrossRef](#)]
42. Biswas, S.P.; Van Der Voort, P. A General Strategy for the Synthesis of Functionalised UiO-66 Frameworks: Characterisation, Stability and CO<sub>2</sub> Adsorption Properties. *Eur. J. Inorg. Chem.* **2013**, *2013*, 2154–2160. [[CrossRef](#)]
43. Jiao, C.; Li, Z.; Li, X.; Wu, M.; Jiang, H. Improved CO<sub>2</sub>/N<sub>2</sub> separation performance of Pebax composite membrane containing polyethyleneimine functionalized ZIF-8. *Sep. Purif. Technol.* **2021**, *259*, 118190. [[CrossRef](#)]
44. Li, Y.; Wang, S.; Wu, H.; Wang, J.; Jiang, Z. Bioadhesion-inspired polymer–inorganic nanohybrid membranes with enhanced CO<sub>2</sub> capture properties. *J. Mater. Chem.* **2012**, *22*, 19617–19620. [[CrossRef](#)]
45. Li, T.; Pan, Y.; Peinemann, K.-V.; Lai, Z. Carbon dioxide selective mixed matrix composite membrane containing ZIF-7 nano-fillers. *J. Membr. Sci.* **2013**, *425–426*, 235–242. [[CrossRef](#)]
46. Zhang, Y.; Shen, Q.; Hou, J.; Sutrisna, P.D.; Chen, V. Shear-aligned graphene oxide laminate/Pebax ultrathin composite hollow fiber membranes using a facile dip-coating approach. *J. Mater. Chem. A* **2017**, *5*, 7732–7737. [[CrossRef](#)]
47. Roslan, R.A.; Lau, W.J.; Lai, G.S.; Zulkhairun, A.K.; Yeong, Y.F.; Ismail, A.F.; Matsuura, T. Impacts of Multilayer Hybrid Coating on PSF Hollow Fiber Membrane for Enhanced Gas Separation. *Membranes* **2020**, *10*, 335. [[CrossRef](#)] [[PubMed](#)]
48. Zheng, W.; Ding, R.; Yang, K.; Dai, Y.; Yan, X.; He, G. ZIF-8 nanoparticles with tunable size for enhanced CO<sub>2</sub> capture of Pebax based MMMs. *Sep. Purif. Technol.* **2019**, *214*, 111–119. [[CrossRef](#)]
49. Meshkat, S.; Kaliaguine, S.; Rodrigue, D. Mixed matrix membranes based on amine and non-amine MIL-53(Al) in Pebax<sup>®</sup>MH-1657 for CO<sub>2</sub> separation. *Sep. Purif. Technol.* **2018**, *200*, 177–190. [[CrossRef](#)]
50. Zheng, Y.; Wu, Y.; Zhang, B.; Wang, Z. Preparation and characterization of CO<sub>2</sub>-selective Pebax/NaY mixed matrix membranes. *J. Appl. Polym. Sci.* **2020**, *137*, 48398. [[CrossRef](#)]
51. Dong, L.; Chen, M.; Li, J.; Shi, D.; Dong, W.; Li, X.; Bai, Y. Metal-organic framework-graphene oxide composites: A facile method to highly improve the CO<sub>2</sub> separation performance of mixed matrix membranes. *J. Membr. Sci.* **2016**, *520*, 801–811. [[CrossRef](#)]
52. Zhang, X.; Zhang, T.; Wang, Y.; Li, J.; Liu, C.; Li, N.; Liao, J. Mixed-matrix membranes based on Zn/Ni-ZIF-8-PEBA for high performance CO<sub>2</sub> separation. *J. Membr. Sci.* **2018**, *560*, 38–46. [[CrossRef](#)]



Supplementary Material

# Thin Film Mixed Matrix Hollow Fiber Membrane Fabricated by Incorporation of Amine Functionalized Metal-Organic Framework for CO<sub>2</sub>/N<sub>2</sub> Separation

Guoqiang Li <sup>1</sup>, Wojciech Kujawski <sup>1,2,\*</sup>, Katarzyna Knozowska <sup>1</sup> and Joanna Kujawa <sup>1</sup>

<sup>1</sup> Department of Physical Chemistry and Physical Chemistry of Polymers, Faculty of Chemistry, Nicolaus Copernicus University in Toruń, 7 Gagarina Street, 87-100 Toruń, Poland

<sup>2</sup> Moscow Engineering Physics Institute, National Research Nuclear University MEPhI, 31 Kashira Hwy, 115409 Moscow, Russia

\* Correspondence: kujawski@chem.umk.pl; Tel.: +48-56-6114517

**Table S1.** The gas permeance and ideal selectivity of thin film hollow fiber membranes fabricated from single concentration of coating solution.

Sample	CO <sub>2</sub> Permeance (GPU)	N <sub>2</sub> Permeance (GPU)	CO <sub>2</sub> /N <sub>2</sub> Selectivity
Pebax <sup>®</sup> -6-1-PP*	62.80 ± 0.59	25.92 ± 0.40	2.4
Pebax <sup>®</sup> -3-1-PP*	376.46 ± 14.02	234.82 ± 9.23	1.6
Pebax <sup>®</sup> -3-4-PP*	51.85 ± 1.68	28.16 ± 0.55	1.84

\* Pebax<sup>®</sup>-x-y-PP indicates the selective thin layer was formed from x wt% Pebax<sup>®</sup> 2533 solution with y layers.

**Table S2.** The thickness of the Pebax/UiO-66-NH<sub>2</sub> hybrid layer measured from the top part and bottom part of the prepared mixed matrix thin film hollow fiber membrane. The bottom part is close to the coating solution while the top part is close to the metal holder during the dip-coating process.

Membrane	Thickness of Selective Layer (µm)		
	Upper Part	Bottom Part	Average
Pristine Pebax	6.06 ± 0.49	7.61 ± 1.17	6.97 ± 1.19
5 wt% UiO-66-NH <sub>2</sub>	3.58 ± 0.66	7.49 ± 1.01	5.36 ± 0.97
10 wt% UiO-66-NH <sub>2</sub>	5.58 ± 0.83	8.15 ± 0.86	7.36 ± 1.46
15 wt% UiO-66-NH <sub>2</sub>	5.06 ± 0.68	6.35 ± 0.70	5.40 ± 0.88
20 wt% UiO-66-NH <sub>2</sub>	6.70 ± 0.33	8.26 ± 1.07	6.82 ± 1.16
50 wt% UiO-66-NH <sub>2</sub>	4.76 ± 0.76	8.89 ± 1.83	6.83 ± 2.51

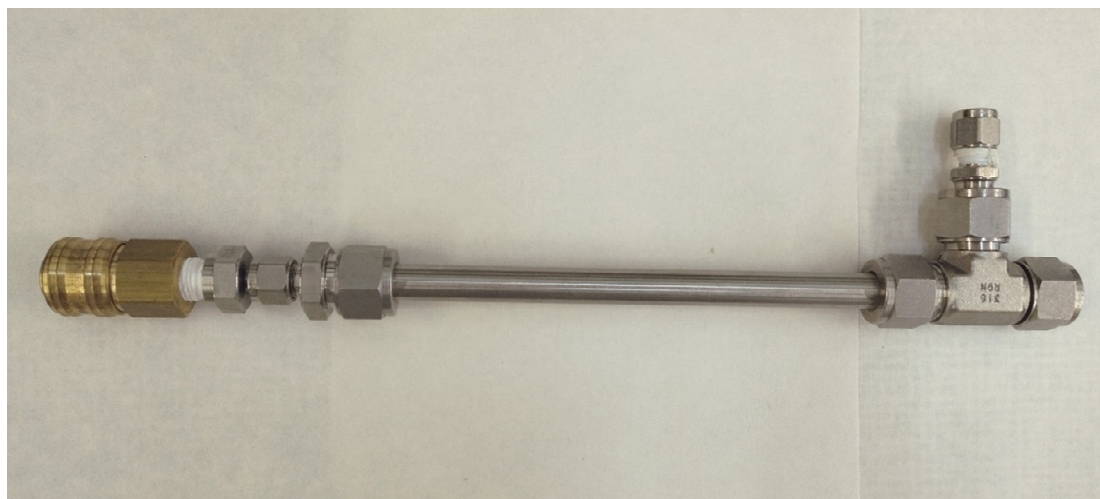
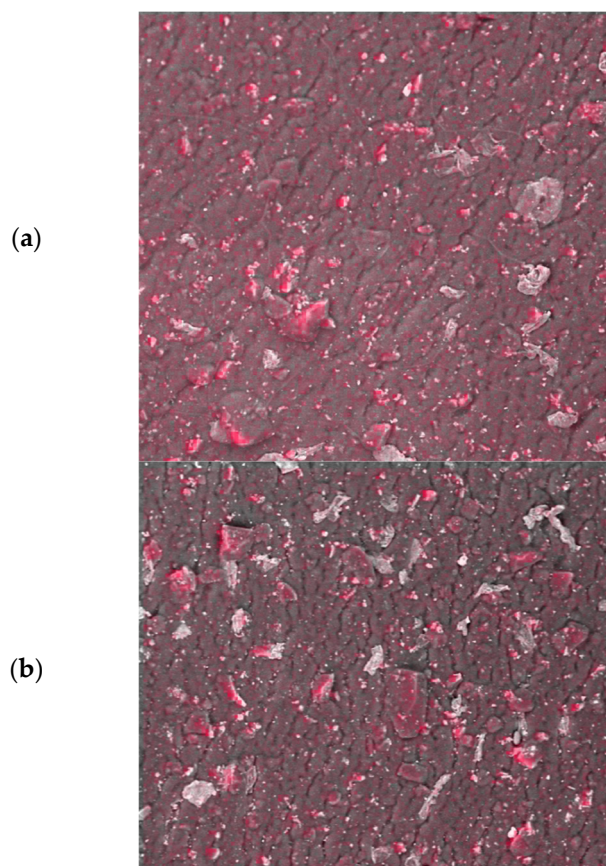
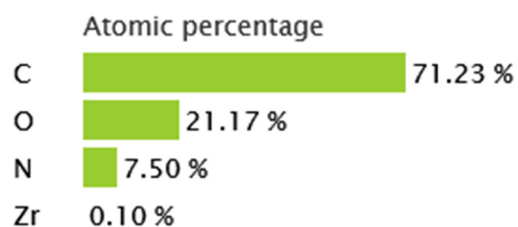
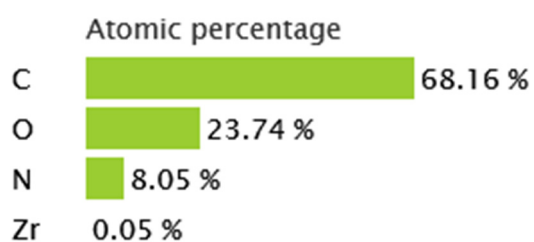


**Figure S1.** Hollow fiber module for testing gas permeance of hollow fiber membranes (This module is designed by the Membranes and Membrane Techniques Research Group in Nicolaus Copernicus University in Toruń. All the components of this module including housing part, end caps, and ports were purchased from Swagelok, Solon, OH, SUA).

#### Zr element mapping



#### Element analysis of UiO-66-NH<sub>2</sub> Pebax® 2533-UiO-66-NH<sub>2</sub>/PP membranes



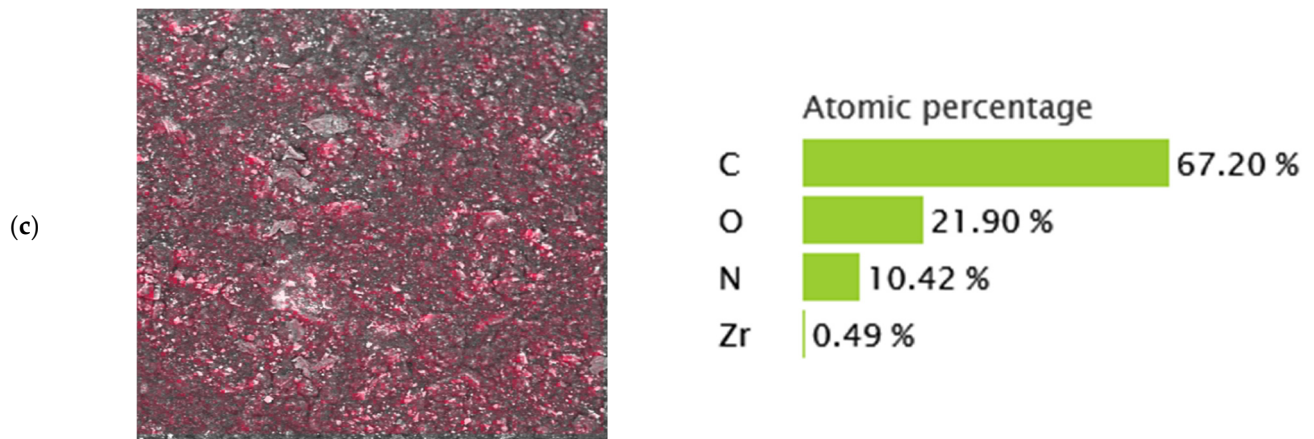


**Figure S2.** The Zr element mapping and element analysis of Pebax® 2533-UiO-66-NH<sub>2</sub>/PP thin film mixed matrix hollow fiber membranes by EDX. (a) 15 wt% UiO-66-NH<sub>2</sub>, (b) 20 wt% UiO-66-NH<sub>2</sub>, (c) 50 wt% UiO-66-NH<sub>2</sub>.

## **Publication V**

**G. Li**, W. Kujawski, A. Tonkonogovas, K. Knozowska, J. Kujawa, E. Olewnik-Kruszkowska, N. Pedišius, A. Stankevičius, Evaluation of CO<sub>2</sub> separation performance with enhanced features of materials - Pebax® 2533 mixed matrix membranes containing ZIF-8-PEI@[P(3)HIm][Tf<sub>2</sub>N], Chemical Engineering Research and Design, 181 (2022) 195-208.

Available online at [www.sciencedirect.com](http://www.sciencedirect.com)

Chemical Engineering Research and Design

journal homepage: [www.elsevier.com/locate/cherd](http://www.elsevier.com/locate/cherd)


# Evaluation of CO<sub>2</sub> separation performance with enhanced features of materials – Pebax® 2533 mixed matrix membranes containing ZIF-8-PEI@[P(3)HIm][Tf<sub>2</sub>N]

Guoqiang Li<sup>a</sup>, Wojciech Kujawski<sup>a,\*</sup>, Andrius Tonkonogovas<sup>b</sup>, Katarzyna Knozowska<sup>a</sup>, Joanna Kujawa<sup>a</sup>, Ewa Olewnik-Kruszkowska<sup>a</sup>, Nerijus Pedišius<sup>b</sup>, Arūnas Stankevičius<sup>b</sup>

<sup>a</sup> Nicolaus Copernicus University in Toruń, Faculty of Chemistry, 7 Gagarina Street, 87-100 Toruń, Poland

<sup>b</sup> Lithuanian Energy Institute, 3 Breslaujos Street, Kaunas 44403, Lithuania

## ARTICLE INFO

### Article history:

Received 17 February 2022

Received in revised form 7 March 2022

Accepted 14 March 2022

Available online 17 March 2022

### Keywords:

MMMs

ZIF-8

Ionic liquids

Post-synthetic modification

CO<sub>2</sub> capture

## ABSTRACT

Zeolitic imidazolate framework (ZIF-8) was functionalized by polyethyleneimine (PEI) and subsequently decorated with ionic liquid (IL) – [P(3)HIm][Tf<sub>2</sub>N]. ZIF-8-PEI@IL/Pebax® 2533 mixed matrix membranes (MMMs) were fabricated to enhance the CO<sub>2</sub> capture performance of Pebax membranes. The amino groups and IL in ZIF-8-PEI improved the gas separation performance of the MMMs due to the additional CO<sub>2</sub> transporting pathways by using the reversible reaction with amino groups and the high affinity between IL and CO<sub>2</sub>. The modified ZIF-8 particles demonstrated enhanced interfacial interactions and compatibility between fillers and polymer matrix due to the presence of amino groups and IL, confirmed by the enhanced gas separation performance, improved elongation at break, and tensile strength of MMMs. Comparing with the pristine membranes, CO<sub>2</sub> permeability of MMMs containing 15 wt% ZIF-8-PEI@IL increased by 123% to 285 Barrer, and the CO<sub>2</sub>/N<sub>2</sub> and CO<sub>2</sub>/CH<sub>4</sub> ideal selectivity increased from 17 and 12 to 76 and 25, respectively.

© 2022 Institution of Chemical Engineers. Published by Elsevier Ltd. All rights reserved.

## 1. Introduction

CO<sub>2</sub> separation plays a critical role in environment protection, the development of green energy and energy security (Cui et al., 2021; Kujawski et al., 2020; Gouveia et al., 2021). In comparison to the traditional CO<sub>2</sub> capture technologies, e.g. pressure-swing adsorption (Abd et al., 2021), amine absorption (Ji et al., 2021) and cryogenic distillation (Yousef et al., 2018), membrane technology is gaining more and more attention owing to its lower energy consumption, higher flexibility, smaller footprint, and higher efficiency (Liu et al., 2021; Li et al., 2021a).

Pebax® 2533 is a thermoplastic elastomer containing 20 wt % of polyamide (PA) aliphatic hard block providing mechanical strength and 80 wt% of amorphous polyether (PE) soft block facilitating the transport of CO<sub>2</sub> molecules. Pebax® 2533 is regarded as a promising material for the fabrication of membranes for CO<sub>2</sub> separation processes, showing acceptable CO<sub>2</sub> permeability with desirable CO<sub>2</sub>/N<sub>2</sub> selectivity (Li et al., 2021a; Kim et al., 2020). However, the properties of polymeric membranes are restricted by the typical trade-off relation between gas permeability and selectivity, expressed by the Robeson upper bound (Dal-Cin et al., 2008). The fabrication of mixed matrix membranes (MMMs) is an efficient way to overcome the trade-off relation in polymeric membranes applied in gas separation processes (Kamble et al., 2021; Singh et al., 2021; Shah Buddin and Ahmad, 2021). MMMs could integrate the processability of polymer matrix and the

\* Corresponding author.

E-mail address: [kujawski@chem.umk.pl](mailto:kujawski@chem.umk.pl) (W. Kujawski).

<https://doi.org/10.1016/j.cherd.2022.03.023>

0263-8762/© 2022 Institution of Chemical Engineers. Published by Elsevier Ltd. All rights reserved.



excellent gas transport and selective properties of fillers, resulting in both higher gas permeability and better selectivity (Shah Buddin and Ahmad, 2021; He et al., 2022).

Metal organic frameworks (MOFs) have been intensively utilized as fillers in MMMs for enhancing gas separation performance owing to their large surface area, inorganic-organic structural properties and the possible tuning functionality (Wu et al., 2021). Among various types of MOFs, zeolitic imidazolate framework (ZIF-8) consisting of zinc ion centers coordinated with 2-methyl imidazolate has drawn attention in CO<sub>2</sub> separation due to its intrinsic properties and the small aperture equal to 3.4 Å which is bigger than the kinetic diameter of CO<sub>2</sub> (3.3 Å) but smaller than the kinetic diameter of N<sub>2</sub> (3.6 Å) and CH<sub>4</sub> (3.8 Å) (Chi et al., 2015; Nafisi and Hägg, 2014a). Nafisi and Hägg (Nafisi and Hägg, 2014b) prepared ZIF-8 Pebax® 2533 MMMs for CO<sub>2</sub> separation. It was found that with the increase of ZIF-8 content, the CO<sub>2</sub> permeability increased while the CO<sub>2</sub>/N<sub>2</sub> selectivity decreased. The decreasing selectivity in MMMs containing ZIF-8 is related to the poor compatibility between ZIF-8 and polymer matrix, resulting in the formation of interfacial voids and defects (Zheng et al., 2019).

To fabricate ZIF-8 incorporated MMMs with higher CO<sub>2</sub> permeability and selectivity, it is crucial to modify ZIF-8 with CO<sub>2</sub>-philic groups (Song et al., 2021). Moreover, the modified ZIF-8 can improve the compatibility between filler and polymer matrix due to the enhanced intermolecular interaction, e.g., hydrogen bond (Nordin et al., 2015; Ding et al., 2020; Zhu et al., 2021). Atash Jameh et al. (2020) modified ZIF-8 with ethylenediamine (ED) and prepared Pebax® 1074/ED-ZIF-8 MMMs. It was found that there was not any agglomeration observed when 30 wt% of ED-ZIF-8 was incorporated into MMMs in comparison to 20 wt% for ZIF-8. At the filler content of 30 wt%, Pebax® 1074/ED-ZIF-8 MMMs showed CO<sub>2</sub> permeability equal to 344 Barrer and ideal CO<sub>2</sub>/CH<sub>4</sub> selectivity equal to 24.2 which were 157% and 69%, respectively, higher than those for Pebax® 1074/ZIF-8 MMMs. The enhanced gas separation performance for MMMs containing modified ZIF-8 was related to the high affinity of ED for CO<sub>2</sub>, resulting in the increased CO<sub>2</sub>/CH<sub>4</sub> selectivity. Lv et al. (2021) synthesized bio-inspired ZIF (Bio-ZIF) by introducing amino groups into ZIF-8 via the ligand exchange reaction between 3-amino-1,2,4-triazole (Atz) and Hmin of ZIF-8 via post-synthetic modification method. The synthesized Bio-ZIF was incorporated into Pebax® 1657 to prepare MMMs for CO<sub>2</sub> separation. When 12 wt% Bio-ZIF was incorporated, the prepared MMMs exhibited high CO<sub>2</sub> permeability equal to 542 Barrer and high CO<sub>2</sub>/CH<sub>4</sub> selectivity equal to 40, which surpassed the 2008 Robert upper bound (Lv et al., 2021). This is because the amino groups in Bio-ZIF can react with CO<sub>2</sub> to form zwitterion as an intermediate during the reversible reaction, resulting in the increase of CO<sub>2</sub> permeability.

As discussed above, the CO<sub>2</sub> affinity of ZIF-8 and the compatibility between ZIF-8 and polymer matrix could be enhanced by introducing amino groups into ZIF-8. It is hypothesized that the increase of the number of amino groups in the modifier might further enhance these properties for ZIF-8. Therefore, Jiao et al. (2021) synthesized polyethyleneimine (PEI) functionalized ZIF-8 (PEI-ZIF-8) via in-situ method by using Hmin and PEI mixed linker. The prepared PEI-ZIF-8 was incorporated into Pebax® 1657 matrix for MMMs preparation. It was found that the MMMs with 5 wt% PEI-ZIF-8 exhibited CO<sub>2</sub> permeance of 13 GPU (Gas Permeation Unit, 1 GPU = 10<sup>-6</sup> cm<sup>3</sup>(STP)/(cm<sup>2</sup> s cmHg)) and CO<sub>2</sub>/N<sub>2</sub>

selectivity of 49 which were much higher than the pristine membranes. The improved gas separation performance for MMMs was ascribed to the porous structure and higher affinity with CO<sub>2</sub> of PEI-ZIF-8, the large density of amine groups from PEI providing facilitated CO<sub>2</sub> transport path and enhancing interfacial compatibility.

Ionic liquids (ILs) have been used as additives and gas carriers for the improvement of gas separation performance of membranes due to their preferential solubility of CO<sub>2</sub> over N<sub>2</sub> and CH<sub>4</sub> and low volatility (Rynkowska et al., 2018; Hao et al., 2013). To enhance the interfacial adhesion between fillers and polymer matrix and avoid the formation of non-selective interfacial voids, Li et al. (2016) synthesized ZIF-8 and confined ionic liquid (IL) 1-butyl-3-methylimidazolium bis(trifluoromethylsulfonyl)imide ([bmim][Tf<sub>2</sub>N]) into ZIF-8 cages. It was found that the gas separation performance and the mechanical properties of IL@ZIF-8/Pebax® 1657 MMMs were simultaneously improved.

Both the PEI modification and the ionic liquid decoration can improve the gas separation performance and enhance the compatibility between fillers and polymer matrix. Therefore, in this work, the PEI modification and the ionic liquid decoration are combined to modify ZIF-8. The PEI modified ZIF-8 will be decorated with ionic liquid 1-allyl-3H-imidazolium bis(trifluoromethanesulfonyl)imide ([P(3)HIm][Tf<sub>2</sub>N]) owing to its high CO<sub>2</sub> solubility and its role as a sealant to optimize the interfacial morphology between polymer matrix and nanofillers (Nath and Henni, 2020). The prepared ZIF-8-PEI@IL particles will be incorporated into Pebax® 2533 matrix for MMMs preparation to improve the gas separation performance. The amino groups from PEI will provide facilitated CO<sub>2</sub> transport path and enhance the compatibility between filler and polymer matrix via hydrogen bond with Pebax® 2533. Moreover, PEI polymer chains located on ZIF-8 could prevent the excessive occupation of IL in ZIF-8. The reduced pore volume and aperture size of the modified ZIF-8 should modulate the gas transporting pathways of the prepared MMMs.

## 2. Experimental

### 2.1. Materials

Zinc nitrate hexahydrate (Zn(NO<sub>3</sub>)<sub>2</sub>·6H<sub>2</sub>O, 98%), 2-methylimidazole (Hmin, 99%), N,N-dimethylformamide (DMF), and branched polyethyleneimine (PEI, 25000 Mw) (Fig. S1a) were purchased from Sigma Aldrich (Poznań, Poland). Methanol (99.8%) and ethanol (99.8%) were purchased from Alchem Grupa Sp. z o.o. (Toruń, Poland).

Ionic liquid of 1-allyl-3H-imidazolium bis(trifluoromethanesulfonyl)imide ([P(3)HIm][Tf<sub>2</sub>N], 99%) (Fig. S1b) was purchased from SOLVIONIC (Toulouse, France).

Pebax® 2533 (80 wt% of poly(ethylene oxide) – PEO block and 20 wt% of polyamide – PA-12 block) was kindly provided by Arkema (Colombes, France).

### 2.2. Synthesis of ZIF-8, ZIF-8-PEI, and ZIF-8-PEI@IL

ZIF-8 was synthesized according to the modified method reported by Wee et al. (2013). 11.75 g of Zn(NO<sub>3</sub>)<sub>2</sub>·6 H<sub>2</sub>O and 25.92 g of 2-methylimidazole were dissolved in 200 mL of DMF. The 2-methylimidazole solution was added into zinc nitrate solution under strong stirring for 10 min. After mixing, the spontaneous precipitation was observed. The

mixture solution was transferred into a 1 L Schott bottle and placed in oven for 4 h at 140 °C (Fig. S2). Subsequently, the temperature of the mixture decreased to room temperature. The as-synthesized product was collected by centrifugation. The obtained products were repeatedly washed three times by dispersing in DMF and ethanol in an ultrasonic bath and recovered by centrifugation. Finally, the obtained products were dried at 100 °C.

ZIF-8 was modified with PEI via wet impregnation strategy (Xian et al., 2015). ZIF-8 was heated at 150 °C for 12 h to remove adsorbed and coordinated water. 0.25 g PEI was dissolved in anhydrous 10 mL methanol by stirring and sonication. Then, 1 g ZIF-8 was slowly added into PEI solution under stirring for 30 min. After that, the obtained gel was allowed to stand overnight at room temperature. The final product ZIF-8-PEI was dried in an oven for 12 h at 100 °C (Fig. S2).

To synthesize ZIF-8-PEI@IL, 0.5 g [P(3)HIm][Tf<sub>2</sub>N] was dissolved in 15 g anhydrous ethanol to obtain IL solution. Then, 0.5 g ZIF-8-PEI was added to the IL solution to react with IL under stirring at 80 °C for 12 h (Fig. S2). The obtained ZIF-8-PEI@IL was collected via centrifugation and washed three times with ethanol and dried in an oven at 100 °C for 12 h.

### 2.3. Membrane fabrication

ZIF-8-PEI@IL/Pebax® 2533 MMMs were prepared by using the solution casting and solvent evaporation method. First of all, ZIF-8-PEI@IL (0.15 g, 0.3 g, 0.45 g, or 0.6 g) was dispersed in ethanol (90 wt%)/water (10 wt%) solvent homogeneously under strong stirring at 80 °C for 1 h followed by a sonication for 30 min. Pebax® 2533 (3 g) pellets were dissolved in the ZIF-8-PEI@IL suspension in two steps. In the first step, a small amount of Pebax® 2533 pellets were dissolved under strong stirring at 80 °C for 3 h. In the second step, the rest of Pebax® 2533 pellets were added into the above solution under stirring at 80 °C for 12 h to obtain the final 6 wt% Pebax® 2533 solution containing filler. The determined amount of obtained solution was poured into a clean Teflon dish with a glass cover to allow the slow solvent evaporation. The cast membrane was left at room temperature for 3 days, dried at 60 °C following overnight, and then peeled off from Teflon dish (Fig. S3). For the comparison, ZIF-8/Pebax® 2533 and ZIF-8-PEI/Pebax® 2533 MMMs and pristine Pebax® 2533 membranes were prepared following the same procedure.

### 2.4. Characterization of fillers and membranes

The morphologies of prepared nanoparticles and membranes were characterized by using Scanning Electron Microscope (SEM), applying LEO 1430 VP microscope (Leo Electron Microscopy Ltd., Cambridge, UK) at 30 keV. ImageJ software was used to evaluate the particle size and membrane thickness from SEM pictures.

The pristine and modified ZIF-8 were characterized by using scanning transmission electron microscopy (STEM) with HAADF detector (FEI Europe B.V, Eindhoven, the Netherlands).

Fourier Transform Infrared-Attenuated Total Reflectance (FTIR-ATR) spectra of prepared nanoparticles and membranes were obtained by using Nicolet iS10 (Thermal Scientific, Waltham, USA) spectrometer in the range of 400–4000 cm<sup>-1</sup>. All obtained spectra were analyzed using Omnic 9 software (Thermo Fisher Scientific, Waltham, USA).

X-Ray Diffraction (XRD) analyses for the pristine and modified ZIF-8 were conducted by utilizing Philips X'Pert (Malvern Panalytical, Malvern, UK). The transmission mode and 2θ range of 5–80° were applied. The X'Celerator Scientific detector (Malvern Panalytical, Malvern, UK) with Cu anode was used.

The nitrogen adsorption/desorption measurements for the pristine and modified ZIF-8 were conducted at –195.7 °C via Gemini VI (Micromeritics Instrument Corp., Norcross, GA, USA). All samples were degassed for 6 h at 110 °C before the measurements.

Thermal properties of the prepared nanoparticles and membranes were characterized by using a Jupiter STA 449 F5 (Netzsch, Germany) thermogravimetric analyzer. Thermogravimetric analysis (TGA) measurements were performed in the temperature range of 25–950 °C with heating rate of 10 °C/min under the nitrogen atmosphere. Moreover, the FTIR Vertex 70 V spectrometer (Bruker Optik, Germany) was combined with TGA analysis for nanoparticles to analyze gas products online.

Mechanical properties of the prepared membranes were measured by using the mechanical testing equipment (Shimadzu EZ-Test ZE-SX, Shimadzu, Kyoto, Japan). The prepared samples were placed between two clips. The initial force and the testing speed are 0.1 N and 1 cm/min, respectively. The obtained results were used to determine the tensile strength (MPa) and elongation at break (%) by using the Trapezium X Texture software.

### 2.5. Gas permeation measurements

The gas permeation tests for pure gas of CO<sub>2</sub>, N<sub>2</sub>, CH<sub>4</sub>, and H<sub>2</sub> were conducted at 2 bar and temperature of 24, 35, 40 and 45 °C by using a home-made equipment which has been described in detail elsewhere (Yousef et al., 2021). The effective membrane area in the module is 12.56 cm<sup>2</sup>. Each membrane sample was measured 3 times under stabilized condition for better accuracy. The gas flow rate was recorded by using a bubble flow meter. The gas permeability P (1 Barrer = 10<sup>-10</sup> cm<sup>3</sup> (STP) cm cm<sup>-2</sup> s<sup>-1</sup> cmHg<sup>-1</sup>) was calculated by using Eq. (1) (Jiao et al., 2021):

$$P = \frac{Ql}{\Delta pA} \quad (1)$$

where Q is the gas flow rate (cm<sup>3</sup>(STP)/s); l is the membrane thickness (cm); Δp is the pressure difference across the membrane (cmHg); A is the active membrane area (cm<sup>2</sup>) (Jiao et al., 2021; Gao et al., 2020).

The ideal selectivity α<sub>12</sub> was calculated by using Eq. (2) (Li et al., 2021a):

$$\alpha_{12} = \frac{P_1}{P_2} \quad (2)$$

## 3. Results and discussion

### 3.1. Characterization of modified ZIF-8

The morphology of ZIF-8, ZIF-8-PEI, and ZIF-8-PEI@IL was investigated by SEM, STEM and TEM techniques and results are shown in Figs. 1 and S4. The synthesized ZIF-8 particles possessed rhombic dodecahedron morphology (Fig. 1). After PEI modification and IL decoration, the edges between particles have been weakened, indicating the successful

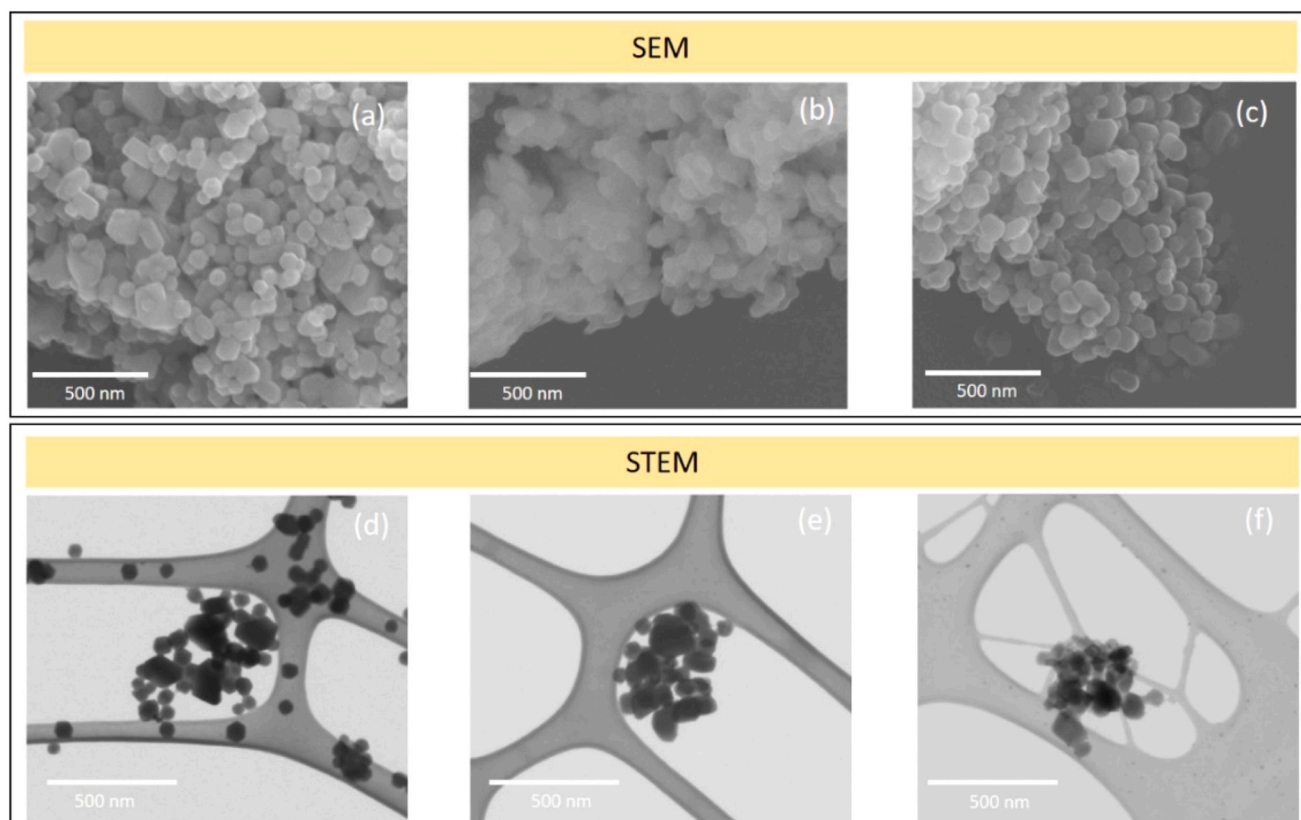


Fig. 1 – SEM and STEM images of ZIF-8 (a, d), ZIF-8-PEI (b, e), and ZIF-8-PEI@IL (c, f).

attachment of PEI polymer chains and decoration of IL as lubricant between ZIF-8 particles (Fig. S4). The morphology of ZIF-8 particles was barely changed after PEI modification and IL decoration. The pristine and modified ZIF-8 particles possess a particle size of 80 – 190 nm evaluated from SEM images by using ImageJ software. The PEI modification and IL decoration barely changed the particle size of ZIF-8. The particle size was also measured by using dynamic light scattering (DLS) technique. As shown in Fig. S5, the average particle size of ZIF-8, ZIF-8-PEI, and ZIF-8-PEI@IL are 115 nm, 424 nm, and 499 nm, respectively, along with the range of particle size distribution of 80–160 nm, 360–750 nm, and 424–750 nm, respectively. For ZIF-8-PEI, and ZIF-8-PEI@IL, the particle size measured by using DLS is larger than that measured from SEM image. This is because DLS measures the hydrodynamic size which is the size of the nanoparticle together with the solvation layer around the particle (Anderson et al., 2013). According to the element analysis by using Energy Dispersive X-Ray Analysis (EDX) mapping (Fig. S6), the F and S elements from [P(3)HIm][Tf<sub>2</sub>N] were found in ZIF-8-PEI@IL particles, indicating the successful decoration of IL on ZIF-8.

XRD measurements were conducted to investigate the crystal structure of the pristine and modified ZIF-8. As shown in Fig. 2, the characteristic peaks of ZIF-8 were also found in ZIF-8-PEI and ZIF-8-PEI@IL, indicating that the crystal structure of ZIF-8 was preserved after the PEI modification and IL decoration. However, the intensity of the characteristic peaks of ZIF-8 gradually decreased after the PEI modification and IL decoration owing to the decrease of electron density resulting from the presence of PEI polymer chains and IL in the cage and on the surface of ZIF-8 (Liu et al., 2020). On the other hand, the decrease of surface area (Table S1) and the slight change of the morphology of ZIF-8-PEI and ZIF-8-PEI@

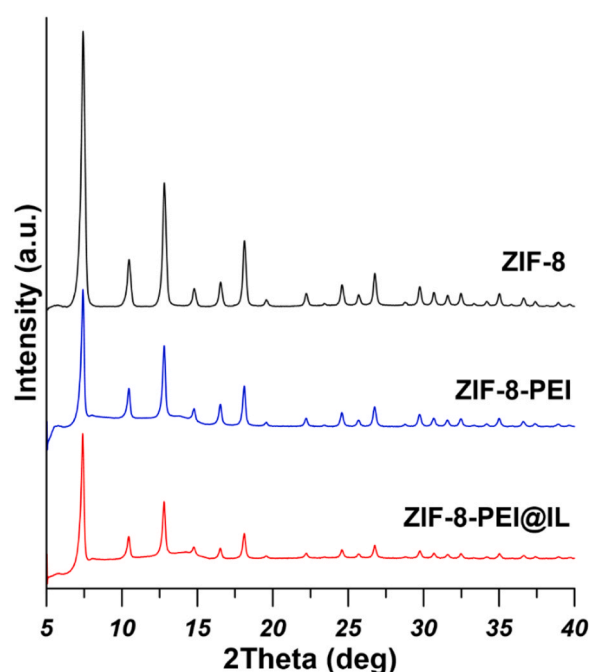


Fig. 2 – XRD patterns of ZIF-8, ZIF-8-PEI, and ZIF-8-PEI@IL.

IL (Figs. 1b, c and S4e, f) could also result in the decrease of peak intensity (Inoue and Hirasawa, 2013).

The N<sub>2</sub> adsorption and desorption isotherms and the particle size distribution of ZIF-8, ZIF-8-PEI, and ZIF-8-PEI@IL were presented in Figs. 3 and S7. The pristine and modified ZIF-8 exhibited the type-I adsorption behavior, indicating the microporous structure of the prepared fillers (ALothman, 2012; Leofanti et al., 1998). The microporous structure of ZIF-8 was preserved after the PEI surface modification and ILs



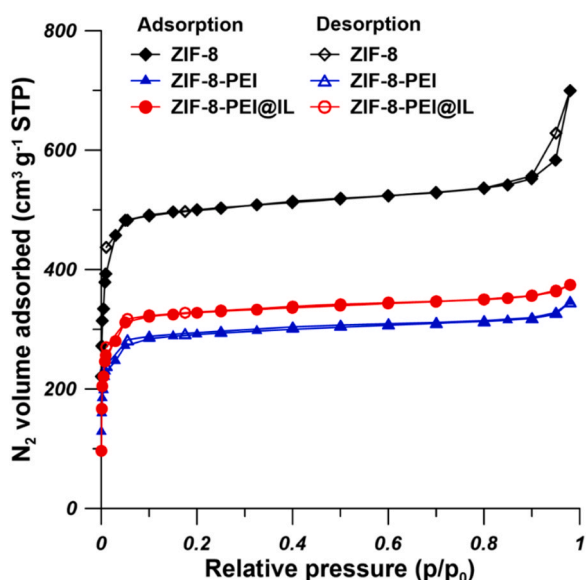


Fig. 3 –  $N_2$  adsorption and desorption isotherms of ZIF-8, ZIF-8-PEI, and ZIF-8-PEI@IL at 77 K.

decoration, which is consistent with the previous reported studies (Li et al., 2016; Menezes et al., 2020). As it is shown in Table S1, the Brunauer, Emmett and Teller (BET) surface area, total pore volume, micropore volume and average pore size of synthesized ZIF-8 are comparable with the previous literatures (Zheng et al., 2019; Jiao et al., 2021; Menezes et al., 2020). For ZIF-8-PEI, the BET surface area, total pore volume and average pore size decreased due to the impregnation of PEI in ZIF-8. Jiao et al. (2021) also found the decrease of BET surface area from  $1628.8 \text{ m}^2/\text{g}$  to  $998.0 \text{ m}^2/\text{g}$  after the PEI modification for ZIF-8. For ZIF-8-PEI@IL, the BET surface area, total pore volume and average pore size are comparable to ZIF-8-PEI. Further investigation on the micropore volume and mesopore volume (Table S1) showed that the increase of total volume was mainly determined by the increase of mesopore volume, since the micropore volume barely changed. The PEI chains in the mesopore was replaced by ILs resulting in the increase of mesopore volume since the size of ILs is smaller than PEI.

The FTIR spectra were used to characterize the chemical structure of ZIF-8, ZIF-8-PEI, and ZIF-8-PEI@IL (Fig. 4). For pristine ZIF-8, the peaks at  $3135 \text{ cm}^{-1}$  and in the range of  $3000\text{--}2800 \text{ cm}^{-1}$  can be ascribed to C-H stretching vibration from the imidazole ring and the methyl group in the linker, respectively (Nafisi and Hägg, 2014b). The peak at  $1585 \text{ cm}^{-1}$  can be attributed to the C=N stretching vibration. The peaks at  $1456 \text{ cm}^{-1}$  and  $1382 \text{ cm}^{-1}$  are related to the stretching vibration of the entire imidazole ring. The peaks in the range of  $1310\text{--}900 \text{ cm}^{-1}$  can be assigned to the in-plane bending of the imidazole ring. The peaks at  $759 \text{ cm}^{-1}$  and  $693 \text{ cm}^{-1}$  are related to the aromatic C-H bending. The most importantly, the presence of a strong peak at  $420 \text{ cm}^{-1}$  indicated the Zn-N stretching in ZIF-8 (Nordin et al., 2015). For ZIF-8-PEI, in addition to the characteristic peaks of ZIF-8, the increase of the intensity of peaks at  $2827 \text{ cm}^{-1}$  and  $2935 \text{ cm}^{-1}$  corresponding to aliphatic C-H stretching vibration indicates the successful attachment of PEI polymer chains. The peak representing the hydrogen bond and the amino stretching vibration from PEI was found at  $3300 \text{ cm}^{-1}$ . Moreover, the peaks at  $1458 \text{ cm}^{-1}$  and  $1585 \text{ cm}^{-1}$  are also associated with N-H vibration of primary and secondary amino groups, respectively (Kasprzak et

al., 2015). For  $[\text{P}(3)\text{HIm}][\text{Tf}_2\text{N}]$ , peaks at  $3158 \text{ cm}^{-1}$ ,  $1579 \text{ cm}^{-1}$ ,  $1452 \text{ cm}^{-1}$ ,  $1347 \text{ cm}^{-1}$  are attributed to the aromatic C-H stretching, C=N stretching, C=C stretching, and C-N stretching from  $[\text{P}(3)\text{HIm}]$  cation, respectively. Peaks at  $1186 \text{ cm}^{-1}$ ,  $1134 \text{ cm}^{-1}$ , and  $1055 \text{ cm}^{-1}$  were related to the C-F stretching, S=O stretching, and S-N-S stretching from  $[\text{Tf}_2\text{N}]$  anion (Abdollahi et al., 2018). It was found that the characteristic peaks of  $514 \text{ cm}^{-1}$ ,  $572 \text{ cm}^{-1}$ ,  $615 \text{ cm}^{-1}$ ,  $654 \text{ cm}^{-1}$ ,  $1055 \text{ cm}^{-1}$ ,  $1186 \text{ cm}^{-1}$ ,  $1452 \text{ cm}^{-1}$ , and  $1579 \text{ cm}^{-1}$  from  $[\text{P}(3)\text{HIm}][\text{Tf}_2\text{N}]$  were present in ZIF-8-PEI@IL, indicating the successful decoration of ILs on ZIF-8. Moreover, peaks at  $1452 \text{ cm}^{-1}$  and  $1579 \text{ cm}^{-1}$  showed a blue shift in ZIF-8-PEI@IL, which indicates the strong interaction between ZIF-8 and ILs (Liu et al., 2020).

TGA measurements for the ZIF-8, ZIF-8-PEI, and ZIF-8-PEI@IL were performed in the temperature range from  $25 \text{ }^\circ\text{C}$  to  $950 \text{ }^\circ\text{C}$  under the nitrogen atmosphere. FTIR spectrometer was combined with TGA to analyze gas products. As it is shown in Fig. 5, there was a slight mass loss in at  $100\text{--}200 \text{ }^\circ\text{C}$ , indicating the removal of residual molecules of  $\text{H}_2\text{O}$ , DMF, ethanol, and methanol. For ZIF-8, the main mass loss occurred at  $550\text{--}900 \text{ }^\circ\text{C}$  due to the thermal decomposition of ZIF-8, which confirmed the high thermal stability of synthesized ZIF-8 (Zheng et al., 2019). For ZIF-8-PEI, the first main mass loss started at around  $200 \text{ }^\circ\text{C}$  and ended at around  $500 \text{ }^\circ\text{C}$ , which is attributed to the thermal decomposition of PEI polymer chains (K. Li et al., 2015). The second main mass loss is seen in the temperature range of  $550\text{--}900 \text{ }^\circ\text{C}$ , which is attributed to the thermal decomposition of ZIF-8. Similar to ZIF-8-PEI, the first main mass loss ( $200\text{--}500 \text{ }^\circ\text{C}$ ) of ZIF-8-PEI@IL was related to the decomposition of PEI polymer chains and ILs (Xu and Cheng, 2021), while the second mass loss ( $500\text{--}900 \text{ }^\circ\text{C}$ ) indicates the decomposition of ZIF-8. As it is shown in Figs. S8 and S9, the characteristic peaks at  $3000\text{--}3400 \text{ cm}^{-1}$  could be assigned to the produced gases of  $\text{NH}_3$ ,  $\text{CH}_4$ ,  $\text{C}_2\text{H}_4$ ,  $\text{C}_2\text{H}_6$  and  $\text{H}_2\text{O}$  vapor. The characteristic peaks at  $731\text{--}741 \text{ cm}^{-1}$  and  $2200\text{--}2400 \text{ cm}^{-1}$  could be attributed to  $\text{CO}_2$ . The characteristic peaks at  $1078 \text{ cm}^{-1}$  and  $1151\text{--}1160 \text{ cm}^{-1}$  could be related to  $\text{SO}_2$  and  $\text{H}_2\text{S}$ . The weak peak at  $4068 \text{ cm}^{-1}$  is related to HF. The increase of the intensity of peaks at  $3000\text{--}3400 \text{ cm}^{-1}$ ,  $731\text{--}741 \text{ cm}^{-1}$ , and  $2200\text{--}2400 \text{ cm}^{-1}$  indicates the successful attachment of PEI chains on ZIF-8 since PEI mainly contains C and N (Fig. S8b). The presence of peaks at  $1078 \text{ cm}^{-1}$ ,  $1151\text{--}1160 \text{ cm}^{-1}$ , and  $4068 \text{ cm}^{-1}$  indicates the successful decoration of ILs on ZIF-8 owing to the presence of F, O, and S in ILs.

### 3.2. Characterization of MMMs

FTIR spectra of pristine Pebax® 2533 membrane and MMMs containing 10 wt% of ZIF-8, ZIF-8-PEI or ZIF-8-PEI@IL were presented in Fig. S10. The pristine Pebax® 2533 membranes exhibited the characteristic peak at  $1109 \text{ cm}^{-1}$  which is ascribed to the C–O–C bond from the PEO segment of Pebax® 2533. Peaks at  $3298$ ,  $1734$ , and  $1640 \text{ cm}^{-1}$  are assigned to the -N-H- stretching vibration, out-of-plane H-N-C=O vibration of amide, and O-C=O stretching vibration of carboxylic acid, respectively (Nafisi and Hägg, 2014b). After the addition of ZIF-8, ZIF-8-PEI or ZIF-8-PEI@IL into the Pebax® 2533 matrix, new peaks at  $693$ ,  $759$ ,  $1150$ ,  $1312$ ,  $1340$ , and  $1456 \text{ cm}^{-1}$  which are related to the aromatic C-H bending, the in-plane bending of imidazole ring, and the stretching vibration of the entire imidazole ring of ZIF-8 were found in the FTIR spectra. Moreover, the FTIR spectra of MMMs exhibited a shift of the

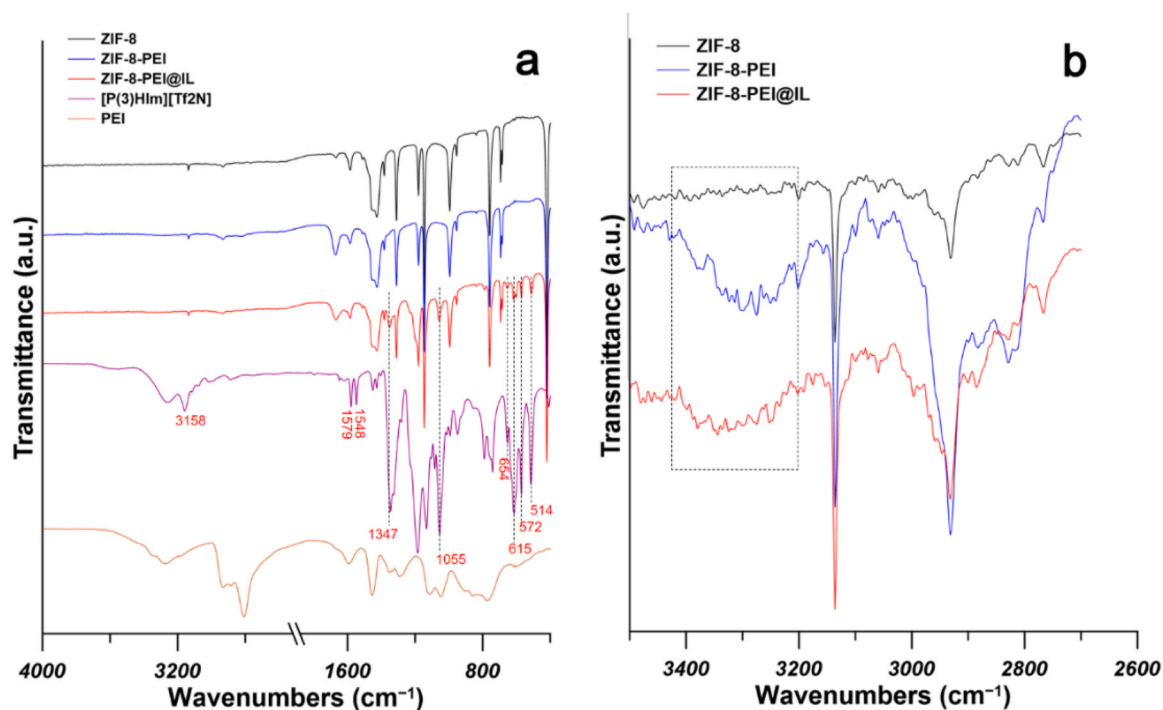


Fig. 4 – FTIR spectra of ZIF-8, ZIF-8-PEI, and ZIF-8-PEI@IL. (a) Full wavenumber range of 400–4000  $\text{cm}^{-1}$  and (b) high wavenumber range of 2700–3600  $\text{cm}^{-1}$ .

characteristic peaks at 3298, 1734, and 1640  $\text{cm}^{-1}$  corresponding to the bonds of  $-\text{N}-\text{H}-$ ,  $\text{H}-\text{N}-\text{C}=\text{O}$ , and  $\text{O}-\text{C}=\text{O}$ , respectively, to 3307, 1732, and 1639  $\text{cm}^{-1}$ , respectively (Fig. S10). The shift of the characteristic peaks for Pebax® 2533 indicates the stronger molecular interactions between fillers e.g., the methyl groups, amine groups, N atoms on imidazole rings from ZIF-8-PEI@IL and the polymer chains in Pebax® 2533 (Liu et al., 2021; Jiao et al., 2021). FTIR spectra of MMMs containing various amount of ZIF-8-PEI@IL were shown in Fig. S11. It was found that the intensity of characteristic peaks of ZIF-8 at 693 and 759  $\text{cm}^{-1}$  increased with the increase of ZIF-8-PEI@IL content in MMMs.

The morphology of surface and cross-section of pristine Pebax® 2533 membrane and the prepared MMMs were investigated by SEM (Figs. 6 and 7). All the prepared membranes possess the thickness in the range of 60 – 100  $\mu\text{m}$ . As

it is shown in Fig. 6(a–d), the surface of pristine Pebax® 2533 membrane is smooth while the surfaces of MMMs are rough. This is because the crystallinity of the polyether and polyamide blocks decreased after the addition of fillers (Zhang et al., 2018). No defects were observed on the membrane surface. As it is shown in Fig. 6(f and j), the slight agglomeration was observed when 10 wt% ZIF-8 was incorporated into Pebax® 2533 matrix. However, there were no visible voids at the interface between ZIF-8 agglomerates and polymer, indicating the good compatibility between ZIF-8 and polymer. As it is shown in Fig. 6(g, h, k, and l), no agglomeration was observed when 10 wt% of ZIF-8-PEI or ZIF-8-PEI@IL was incorporated into Pebax® 2533 matrix, indicating the homogeneous distribution of modified ZIF-8 in polymer matrix. It was concluded that the surface modification could further improve the compatibility between ZIF-8 and polymer by

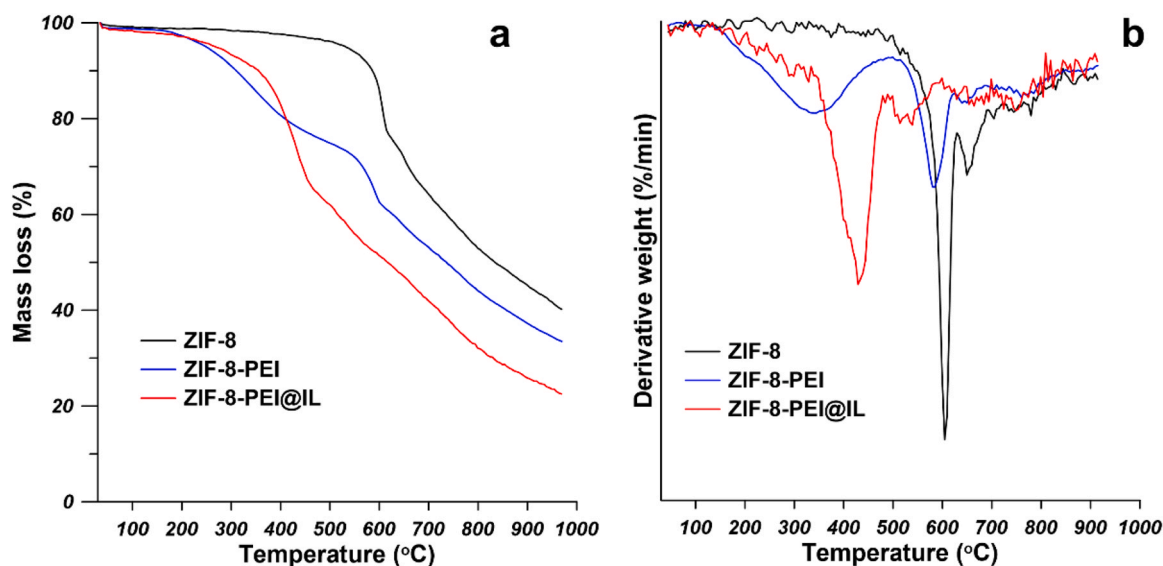
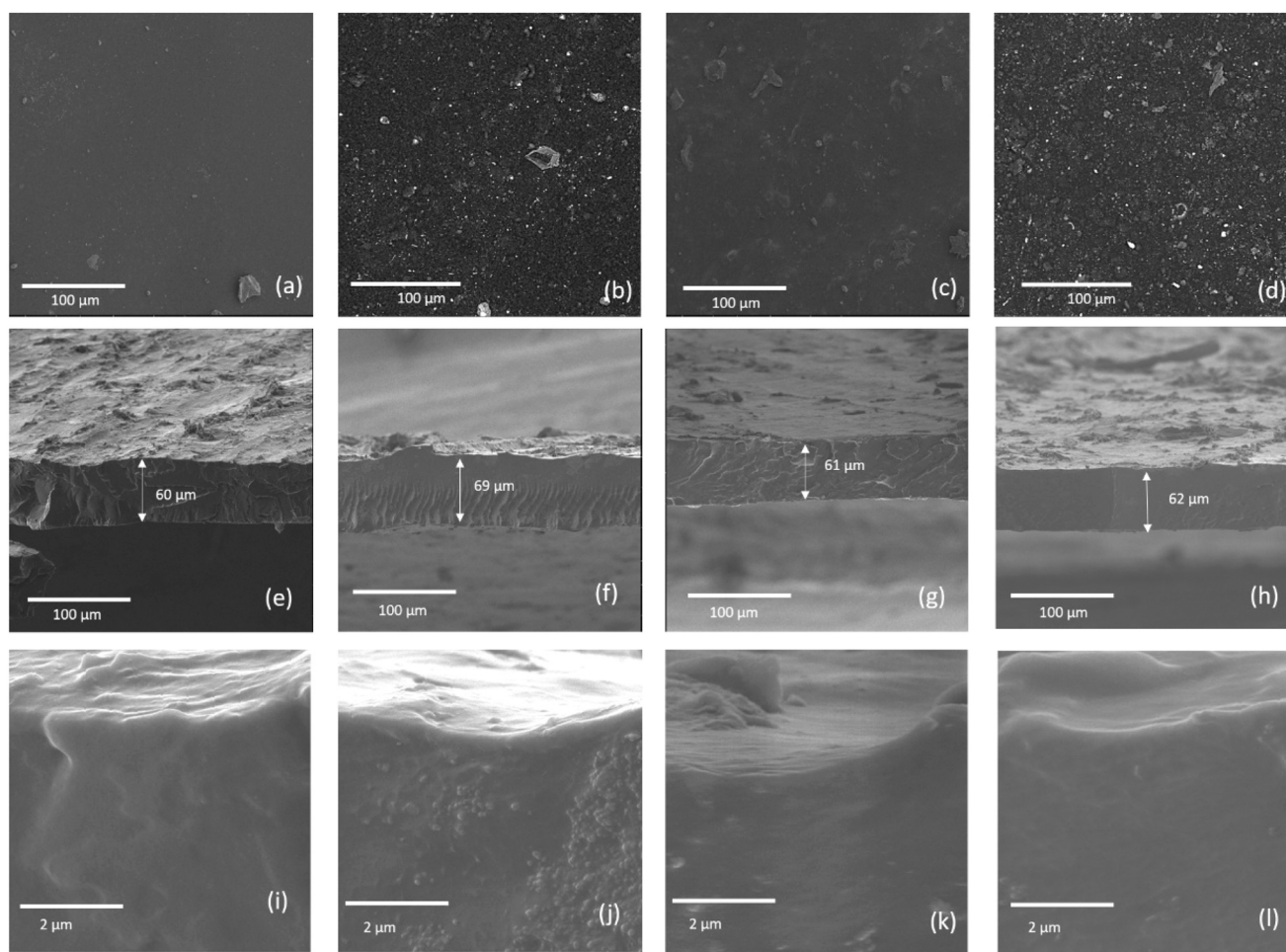


Fig. 5 – (a) TGA and (b) DTG curves of ZIF-8, ZIF-8-PEI, and ZIF-8-PEI@IL.





**Fig. 6** – SEM images of surface (top row) and cross-section (middle and bottom rows) of the pristine Pebax® 2533 membrane (a, e, and i); MMMs with 10 wt% ZIF-8 (b, f, and j); MMMs with 10 wt% ZIF-8-PEI (c, g, and k); and MMMs with 10 wt% ZIF-8-PEI@IL (d, h, and l).

enhancing the molecular interaction, *e.g.* hydrogen bond between modified filler and polymer chains and applying ILs as sealant to inhibit the formation of interfacial voids (Li et al., 2016). Consequently, the prepared MMMs are dense and defect-free, which results in a high gas separation performance.

As shown in Fig. 7(a-e), the surfaces of MMMs became rougher with the increase of ZIF-8-PEI@IL content, which was also confirmed by AFM images (Fig. S12). As shown in Fig. 7(l-n), the ZIF-8-PEI@IL particles were dispersed homogeneously in polymer matrix at low filler content. No large agglomerates and interfacial voids were observed. However, the mild agglomeration of ZIF-8-PEI@IL particles was found in MMMs with 20 wt% loading. Nevertheless, no interfacial voids were observed in the prepared MMMs.

The thermal stability of pristine Pebax® 2533 membrane, MMMs containing different types of fillers and MMMs containing different amount of ZIF-8-PEI@IL was evaluated (Fig. S13). It was found that the thermal stability of Pebax® 2533 membrane was barely influenced after the incorporation of nanofillers. All the prepared membranes were thermally stable up to 300 °C which is far higher than the experimental temperatures (24, 35, 40, and 45 °C). The thermal decomposition of the polymer chains occurred at 420 °C. The decomposition of PEI chains and ILs occurred at 340 °C (Fig. S13).

The elongation at break and tensile strength were determined to investigate the effect of the prepared nanofillers on the mechanical properties of MMMs. As it is shown in Fig. 8, all the prepared membranes are flexible due to their high elongation at break with sufficient mechanical resistance for gas permeance tests. The pristine Pebax® 2533 membranes showed the tensile strength equal to 9.6 MPa and the elongation at break equal to 840%. The mechanical strength of the Pebax membranes was mainly determined by the rigid hydrophobic PA parts, while the elongation at break was mainly determined by the soft PE parts (Li et al., 2016). The MMMs containing 10 wt% of ZIF-8, ZIF-8-PEI, and ZIF-8-PEI@IL showed the tensile strength equal to 10.1 MPa, 10.6 MPa, and 10.2 MPa, respectively, whereas the elongation at break was equal to 780%, 996%, and 960%, respectively (Fig. 8a). In comparison to the pristine Pebax® 2533 membranes and MMMs containing ZIF-8, MMMs containing ZIF-8-PEI, and ZIF-8-PEI@IL exhibited higher tensile strength and elongation at break, which indicates the good dispersion and improved compatibility of modified ZIF-8 owing to the formation of hydrogen bonds between the modified ZIF-8 and the polymer matrix. Therefore, the interaction force between the modified ZIF-8 and polymer chains increased resulting in the improved mechanical properties of MMMs (Liu et al., 2021). As it is shown in Fig. 8b, both the elongation at break and the tensile strength increased with the increase of ZIF-8-PEI@IL

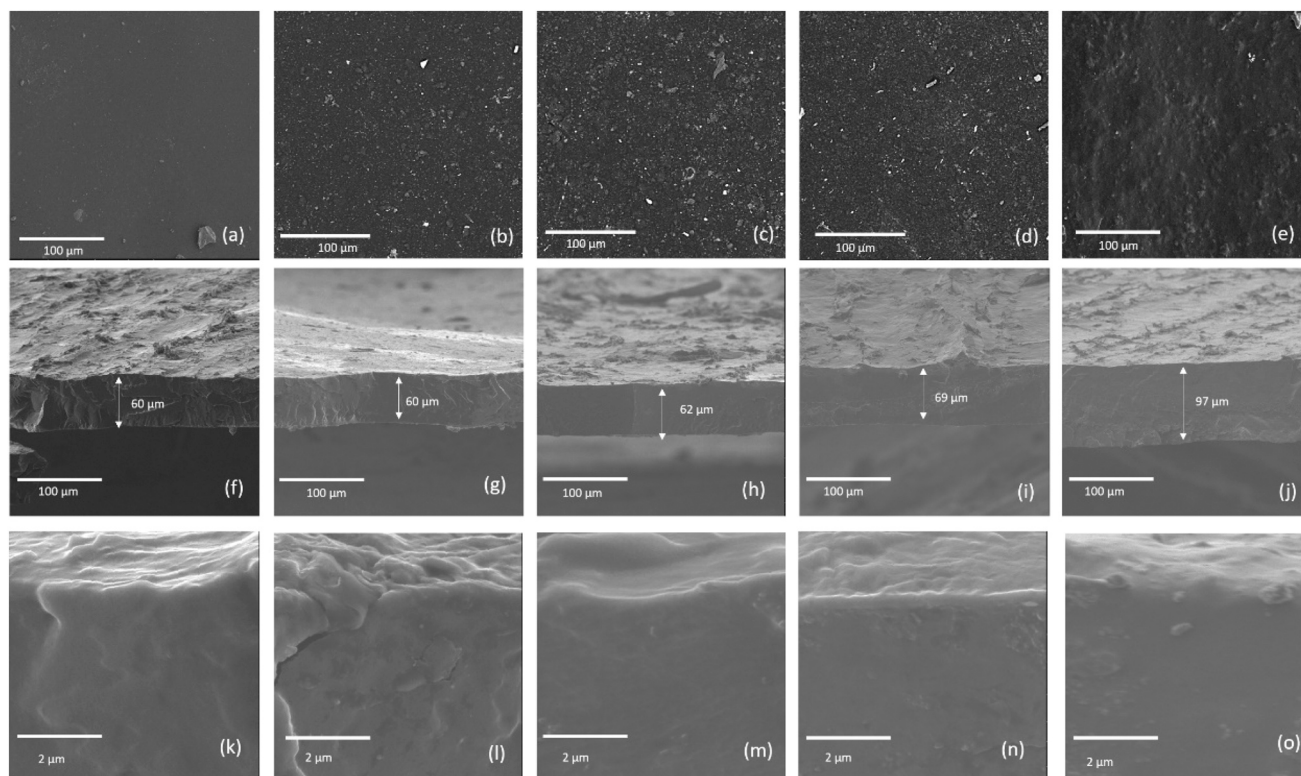


Fig. 7 – SEM images of surface (top row) and cross-section (middle and bottom rows) of the pristine Pebax® 2533 membrane (a, f, and k); MMMs with 5 wt% (b, g, and l), 10 wt% (c, h, and m), 15 wt% (d, i, and n), and 20 wt% (e, j, and o) of ZIF-8-PEI@IL.

up to 15 wt%. The further increase of filler content to 20 wt% resulted in the significant decrease of the elongation at break (45%) and the tensile strength (24%), in comparison to pristine Pebax® 2533 membranes. This is because the nanofiller agglomeration occurred at higher nanofiller content as it is shown in the SEM images (Fig. 7). The interface between nanofillers and polymer matrix became rigidified due to the agglomeration of nanofillers, resulting in the decrease of crystallinity of MMMs (Liu et al., 2021; Behroozi and Pakizeh, 2017).

### 3.3. Gas permeation measurements of MMMs

#### 3.3.1. The effect of filler type on gas permeability and ideal selectivity

The pure gas permeability and the ideal selectivity of CO<sub>2</sub>/N<sub>2</sub>, CO<sub>2</sub>/CH<sub>4</sub>, and CO<sub>2</sub>/H<sub>2</sub> of pristine Pebax® 2533 membranes and MMMs containing 10 wt% of ZIF-8, ZIF-8-PEI, or ZIF-8-PEI@IL were presented in Fig. 9. All the prepared MMMs showed higher CO<sub>2</sub> permeability and ideal selectivity than the pristine Pebax® 2533 membrane. Therefore, the incorporation of

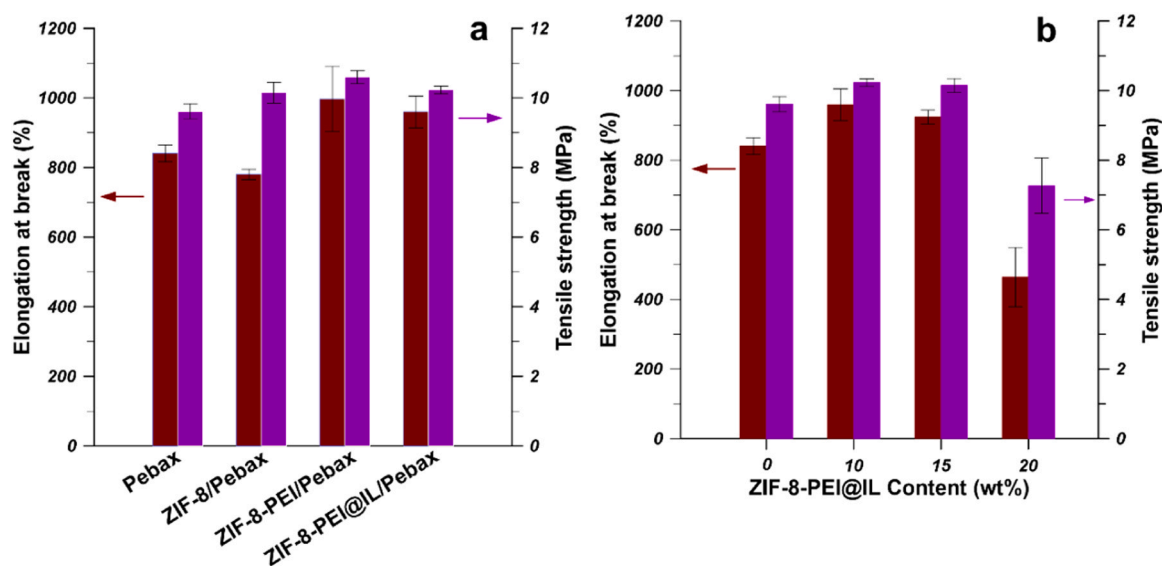
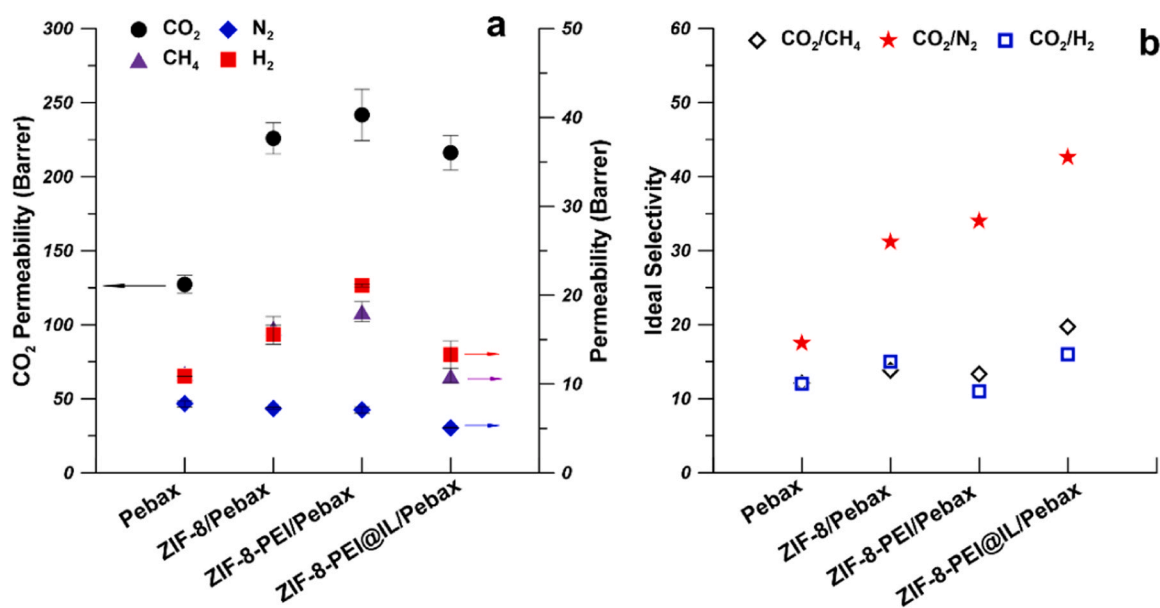


Fig. 8 – Mechanical properties of (a) pristine Pebax® 2533 membranes and MMMs containing 10 wt% of ZIF-8, ZIF-8-PEI, and ZIF-8-PEI@IL, and (b) MMMs containing different amount of ZIF-8-PEI@IL.



**Fig. 9 – (a) Gas permeability and (b) ideal selectivity of MMMs containing various types of fillers (filler content 10 wt%, experimental condition: 24 °C and 2 bar).**

pristine and modified ZIF-8 could improve the gas separation performance of membranes. In the pristine Pebax® 2533 membrane, it was found that the H<sub>2</sub> permeability is lower than the CO<sub>2</sub> permeability even though the kinetic diameter of H<sub>2</sub> (0.29 nm) is smaller than CO<sub>2</sub> (0.33 nm). This is because PEO chains show strong dipole-quadrupole interactions with polar gases such as CO<sub>2</sub>. Moreover, CO<sub>2</sub> possesses high condensability. Therefore, the gas permeability is mainly determined by gas solubility in Pebax® 2533 (Bernardo and Clarizia, 2020). After the incorporation of porous pristine and modified ZIF-8, CO<sub>2</sub> permeability was significantly enhanced due to the smaller kinetic diameter than the ZIF-8 aperture (0.34 nm) and the strong interaction between filler and CO<sub>2</sub> molecules (Liu et al., 2021). H<sub>2</sub> permeability was higher than that of pristine Pebax® 2533 membrane owing to the smaller kinetic diameter and transporting path provided by ZIF-8. Even though the kinetic diameter of CH<sub>4</sub> (0.38 nm) is higher than that of N<sub>2</sub> (0.36 nm), CH<sub>4</sub> permeability is higher than N<sub>2</sub> permeability. This is because the solubility coefficient of CH<sub>4</sub> is higher than that of N<sub>2</sub> when the ZIF-8 was incorporated into Pebax® 2533 (Li et al., 2017). N<sub>2</sub> permeability is the lowest because N<sub>2</sub> possesses lowest solubility coefficient and bigger kinetic diameter than the ZIF-8 aperture (Li et al., 2017). As a result, the CO<sub>2</sub>/N<sub>2</sub> selectivity increased much more significantly than CO<sub>2</sub>/CH<sub>4</sub> and CO<sub>2</sub>/H<sub>2</sub> selectivity.

Among these three types of porous fillers, ZIF-8-PEI@IL showed the most desirable effect on the CO<sub>2</sub> separation performance of MMMs. MMMs containing ZIF-8-PEI@IL exhibited the highest selectivity of CO<sub>2</sub>/N<sub>2</sub>, CO<sub>2</sub>/CH<sub>4</sub> and CO<sub>2</sub>/H<sub>2</sub> which are equal to 43, 20 and 16, respectively and high CO<sub>2</sub> permeability equal to 216 Barrer (Fig. 9). The high CO<sub>2</sub> permeability of MMMs containing ZIF-8-PEI@IL was resulted from the presence of ZIF-8-PEI@IL pores, the additional facilitated transport path for CO<sub>2</sub> molecules, the enhanced interfacial compatibility between fillers and Pebax® 2533 polymer chains, and the enhanced CO<sub>2</sub> affinity to fillers by ILs (Jiao et al., 2021). Specifically, the pores from fillers provide additional paths for such gas molecules as CO<sub>2</sub>. The presence of PEI containing plenty of primary and secondary

amino groups as CO<sub>2</sub> carriers endows the MMMs with facilitated transport mechanism for CO<sub>2</sub> molecules (Y. Li et al., 2015). The reversible reactions between primary and secondary amino groups and CO<sub>2</sub> molecules are shown by Eqs. (3) and (4) (Li et al., 2015):



where R' is hydrogen atom or other organic groups. Moreover, the amino groups improved the interfacial compatibility via the interaction with Pebax® 2533 chains, such as the interaction between -NH<sub>2</sub> and C=O in the PA segment and the interaction between N-H and C-O in the PEO segment of Pebax® 2533 (Jiao et al., 2021). CO<sub>2</sub> exhibited high solubility in ILs ([P(3)HIm][Tf<sub>2</sub>N]) (Zoubeik et al., 2016). Therefore, the ILs decoration improved the CO<sub>2</sub> affinity of ZIF-8, which is beneficial to the increase of CO<sub>2</sub> permeability of MMMs. What is also important, ILs could be used as sealants between fillers and polymer chains to enhance their compatibility (Li et al., 2016).

MMM containing ZIF-8-PEI@IL exhibited the highest ideal selectivity owing to the high CO<sub>2</sub> permeability and lower permeability of N<sub>2</sub>, CH<sub>4</sub>, and H<sub>2</sub>, comparing with MMMs containing ZIF-8 or ZIF-8-PEI. On one hand, the low permeability of big gas molecular (N<sub>2</sub>, and CH<sub>4</sub>) was related to the reduced pore volume and aperture size of modified ZIF-8, which decreased the gas adsorption capacity of fillers. Consequently, the molecular sieving properties of MMMs were enhanced (Li et al., 2016). The permeability of hydrogen is low because hydrogen is non-polar gas which shows low solubility coefficient in the Pebax® 2533 based MMMs (Jansen et al., 2013). On the other hand, the incorporation of ZIF-8-PEI@IL into Pebax® 2533 matrix significantly increased the CO<sub>2</sub> permeability. Therefore, MMMs containing ZIF-8-PEI@IL exhibited the highest ideal selectivity. According to the above discussion, the probable pathways of gas molecules (CO<sub>2</sub>, N<sub>2</sub>, and CH<sub>4</sub>) are visualized in Fig. S14.



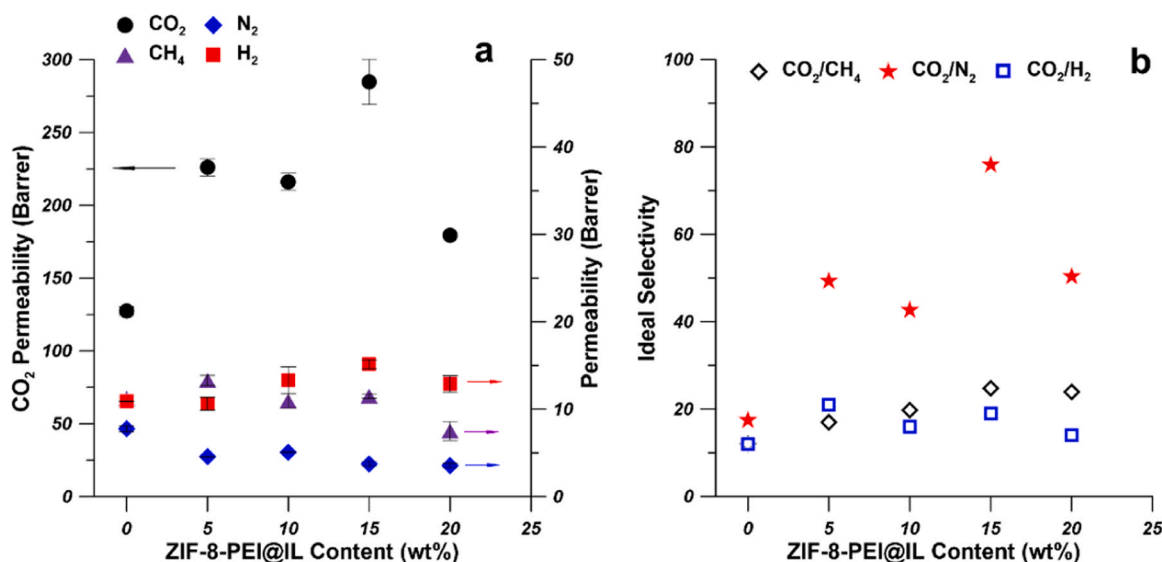


Fig. 10 – (a) Gas permeability and (b) ideal selectivity of MMMs containing various amount of ZIF-8-PEI@IL (experimental condition: 24 °C and 2 bar).

### 3.3.2. The effect of filler content on gas permeability and ideal selectivity

MMMs containing ZIF-8-PEI@IL showed the best gas separation performance considering the permeability and selectivity. Therefore, the effects of amount of ZIF-8-PEI@IL on the gas permeability and selectivity of MMMs have been investigated. As it is shown in Fig. 10a, in comparison to pristine Pebax® 2533 membrane, CO<sub>2</sub> permeability significantly increased when ZIF-8-PEI@IL was incorporated. Moreover, CO<sub>2</sub> permeability increased to a peak value of 285 Barrer with the increase of filler content to 15 wt% owing to the gas molecule transport path provided by porous ZIF-8-PEI@IL, the additional facilitated transport path for CO<sub>2</sub> molecules, and the enhanced CO<sub>2</sub> affinity to fillers by ILs (Jiao et al., 2021). The further increase of ZIF-8-PEI@IL resulted in the decrease of CO<sub>2</sub> permeability which can be related to the agglomeration of fillers which might hinder at the center of polymer chains and block the passage of the gas molecules (Liu et al., 2021). Similar relationship between CO<sub>2</sub> permeability and filler content in MMMs was reported by Jiao et al. (2021). In their research, as PEI-ZIF-8 content increased in Pebax® 2533 matrix, CO<sub>2</sub> permeance and selectivity firstly increased and subsequently decreased. It was suggested that the decline in CO<sub>2</sub> permeance resulted from the over-loading of PEI-ZIF-8 fillers which produced rigidified interface (Jiao et al., 2021).

The gas permeability of CH<sub>4</sub> and N<sub>2</sub> decreased slightly while the H<sub>2</sub> permeability increased slightly with the increase of filler content in MMMs due to the size sieving effect (Li et al., 2016). The permeabilities of CH<sub>4</sub>, N<sub>2</sub>, and H<sub>2</sub> were changed slightly because they are non-polar gas molecules possessing low solubility coefficient in Pebax® 2533-based MMMs (He et al., 2021; Zhao et al., 2014). According to the solution diffusion mechanism, the gas permeability through Pebax® 2533-based MMMs is mainly determined by solubility coefficient rather than the diffusion coefficient (Li et al., 2021b). Consequently, the selectivity of CO<sub>2</sub>/N<sub>2</sub> and CO<sub>2</sub>/CH<sub>4</sub> increased with the increase of filler content in MMMs (Fig. 10b). At 15 wt% of ZIF-8-PEI@IL, MMMs exhibited the highest gas selectivity equal to 76 and 25 for CO<sub>2</sub>/N<sub>2</sub> and CO<sub>2</sub>/CH<sub>4</sub>, respectively. It was found that the incorporation of ZIF-8-PEI@IL did not increase the CO<sub>2</sub>/H<sub>2</sub> selectivity significantly, indicating the effect of ZIF-8 fillers on CO<sub>2</sub>/H<sub>2</sub> separation

performance of Pebax® 2533 based MMMs is limited owing to the nature of Pebax® 2533 polymer matrix.

### 3.3.3. The effect of temperature on gas permeability and ideal selectivity

The gas permeability and selectivity at various temperatures (24, 35, 40, and 45 °C) were tested to investigate the effect of temperature on the gas separation performance of pristine Pebax® 2533 membranes and the prepared MMMs containing ZIF-8-PEI@IL. As it is shown in Fig. 11, with an increase of temperature, gas (CO<sub>2</sub>, N<sub>2</sub>, CH<sub>4</sub> and H<sub>2</sub>) permeability of pristine Pebax® 2533 membranes and prepared MMMs increased, while the selectivity of all membranes exhibited a decreasing trend. The decline of gas selectivity of membranes with increasing temperature can be explained in the following way. On one hand, the movement of polymer chains was enhanced at higher temperature, leading to the increase of the free volume and the formation of less selective membranes allowing bigger molecules to permeate through membranes (Gou et al., 2021). On the other hand, the increment of diffusion rate of molecules with smaller molecular weight was more significant than for molecules with bigger molecular weight, while the solubility coefficient of gas molecules in membrane decreased at higher temperature (Gülmüş and Yilmaz, 2007). Therefore, the gas selectivity decreased with the increase of temperature.

Additionally, the effect of temperature on gas permeability can be estimated by using the Arrhenius Eq. (5) (Bernardo and Clarizia, 2020):

$$P_i = P_{i,0} \exp\left(\frac{-E_p}{RT}\right) \quad (5)$$

where  $P_i$  is the permeability of component  $i$ ,  $P_{i,0}$  is pre-exponential factor,  $E_p$  is the activation energy,  $R$  is the gas constant, and  $T$  is the operation temperature in Kelvin. It was found that the  $E_p$  values of all tested gases in the prepared MMMs were higher than the those in pristine Pebax® 2533 membranes (Table S2), indicating the change of the energy barrier of gas permeation through membranes resulted from the incorporation of ZIF-8-PEI@IL (Sun et al., 2019). The  $E_p$  value of CO<sub>2</sub> in both the pristine Pebax® 2533 membrane and MMMs is the lowest, which suggests the lower activation

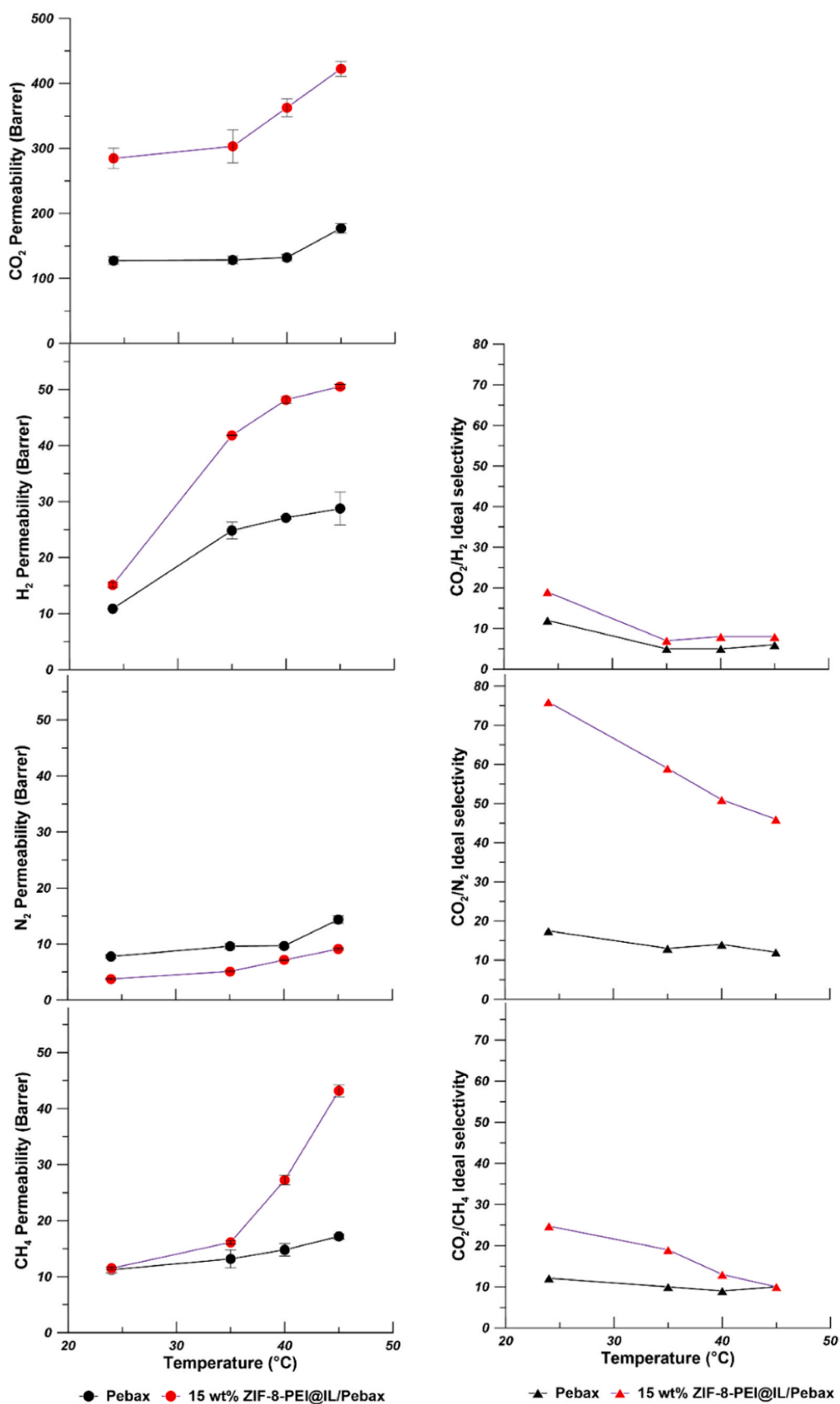
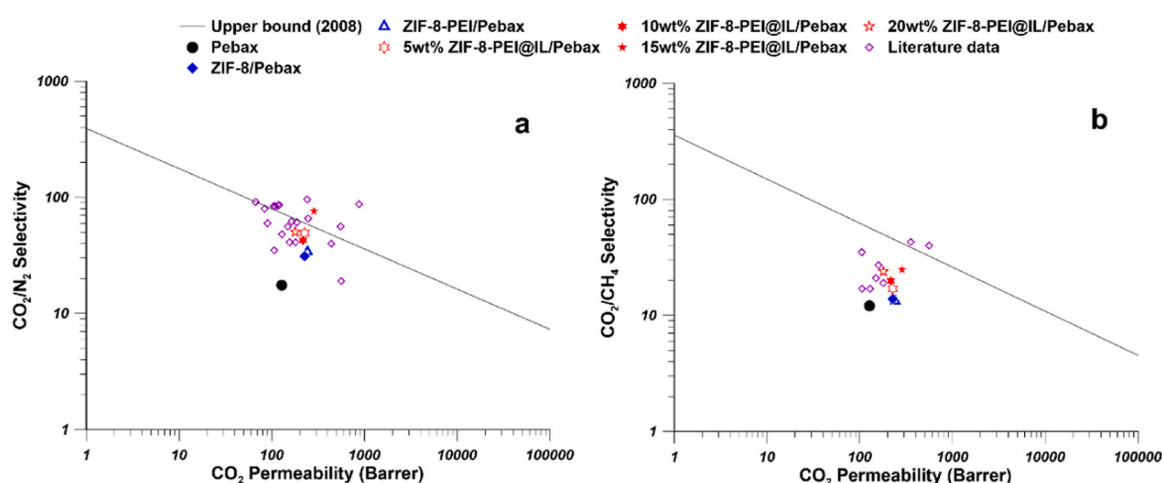


Fig. 11 – Gas permeability and selectivity of pristine Pebax® 2533 membrane and MMMs containing 15 wt% of ZIF-8-PEI@IL at various temperatures.





**Fig. 12** – The comparison of the performance of MMMs with Robeson upper bound (2008) for (a)  $\text{CO}_2/\text{N}_2$  and (b)  $\text{CO}_2/\text{CH}_4$  (the gas permeability and selectivity in this work were obtained by using pure gas testing; the literature data were taken from Table S3).

energy of  $\text{CO}_2$  permeating through the membranes. The obtained results are consistent with the previous reports which revealed that larger gas molecules exhibited higher activation energy of permeation through membranes (Stevens et al., 2020). The orders of  $E_p$  were  $\text{N}_2 > \text{CH}_4 > \text{H}_2 > \text{CO}_2$  and  $\text{CH}_4 > \text{N}_2 > \text{H}_2 > \text{CO}_2$  for pristine Pebax® 2533 membrane and prepared MMMs, respectively (Table S2). The high values of activation energy of permeation for  $\text{N}_2$  and  $\text{CH}_4$  indicate that the permeability of these bigger and less permeable gases were strongly affected by temperature change (Lasseguette et al., 2018).  $\text{CO}_2$  possessed the lowest  $E_p$  and superior solubility in Pebax® 2533 membrane and prepared MMMs. With the increase of temperature, gas solubility decreased, while  $\text{CO}_2$  permeability is mainly dominated by solubility in Pebax® 2533 based membranes (Lasseguette et al., 2018). Therefore, the  $\text{CO}_2$  permeability was less influenced by the increase of temperature than  $\text{N}_2$  and  $\text{CH}_4$ , resulting in the decline of  $\text{CO}_2/\text{N}_2$  and  $\text{CO}_2/\text{CH}_4$  selectivity.

### 3.3.4. The comparison with literature data of MMMs

The gas permeability and selectivity of prepared MMMs were compared with the Robeson's upper bound (Robeson, 2008). As it is shown in Fig. 12, ZIF-8-PEI@IL/Pebax® 2533 MMMs exhibited much higher permselectivity than pristine Pebax® 2533 membranes for  $\text{CO}_2/\text{N}_2$  and  $\text{CO}_2/\text{CH}_4$  separations. The  $\text{CO}_2/\text{N}_2$  separation performance of prepared ZIF-8-PEI@IL/Pebax® 2533 MMMs surpassed the Robeson's upper bound (2008). While the  $\text{CO}_2/\text{CH}_4$  separation performance of prepared ZIF-8-PEI@IL/Pebax® 2533 MMMs is approaching the Robeson's upper bound (2008). MMMs containing 15 wt% ZIF-8-PEI@IL showed the best gas separation performance for  $\text{CO}_2/\text{N}_2$  and  $\text{CO}_2/\text{CH}_4$  separations. The prepared MMMs containing 15 wt% ZIF-8-PEI@IL showed high  $\text{CO}_2$  permeability equal to 285 Barrer along with  $\text{CO}_2/\text{N}_2$  selectivity of 76 and  $\text{CO}_2/\text{CH}_4$  selectivity of 25. As it is shown in Table S3 and Fig. 12, the performance of MMMs containing 15 wt% ZIF-8-PEI@IL is comparable with reported performances of Pebax based MMMs. Consequently, the modification of ZIF-8 with PEI along with the decoration of ILs is an encouraging way to improve the gas separation performance of MMMs via the additional gas molecules transport pathways, improved filler affinity to  $\text{CO}_2$  and enhancement of compatibility between filler and polymer matrix.

## 4. Conclusions

ZIF-8-PEI@P(3)HIm][Tf<sub>2</sub>N] composite fillers were designed and prepared for the successful fabrication of Pebax® 2533-based MMMs for  $\text{CO}_2$  separation. The crystal structure of ZIF-8 was preserved, while the BET surface area, total pore volume, and average pore diameter decreased after modification due to the presence of PEI and ILs in ZIF-8. It was found that the compatibility between filler and polymer matrix was significantly enhanced owing to the enhanced molecular interactions between amino groups in PEI and Pebax polymer chains. Moreover, the decoration of ILs on ZIF-8-PEI further optimized the interfacial morphology of MMMs by inhibiting the formation of interfacial voids. As a result, the mechanical properties of MMMs were enhanced, confirmed by the increased elongation at break and tensile strength. In comparison to the pristine Pebax® 2533 membranes, the ZIF-8-PEI@IL/Pebax® 2533 MMMs exhibited significant improvement of gas separation performance due to the size sieving effect of ZIF-8-PEI@IL, the additional facilitated  $\text{CO}_2$  molecules transport path from amino groups on PEI, and the enhanced  $\text{CO}_2$  affinity to fillers by ILs.  $\text{CO}_2$  permeability of MMMs containing 15 wt% ZIF-8-PEI@IL increased 123% to 285 Barrer, and the  $\text{CO}_2/\text{N}_2$  and  $\text{CO}_2/\text{CH}_4$  ideal selectivity increased from 17 and 12 to 76 and 25, respectively.

## Declaration of Competing Interest

The authors declare that they have no known competing financial interests or personal relationships that could have appeared to influence the work reported in this paper.

## Acknowledgements

This work was supported by the PROM project, funded by Polish National Agency for Academic Exchange NAWA (agreement no.: PPI/PRO/2019/1/00015/U/00001)

## Appendix A. Supplementary material

Supplementary data associated with this article can be found in the online version at [doi:10.1016/j.cherd.2022.03.023](https://doi.org/10.1016/j.cherd.2022.03.023).

## References

- Abdollahi, S., Mortaheb, H.R., Ghadimi, A., Esmaeili, M., 2018. Improvement in separation performance of Matrimid®5218 with encapsulated [Emim][Tf2N] in a heterogeneous structure: CO<sub>2</sub>/CH<sub>4</sub> separation. *J. Membr. Sci.* 557, 38–48.
- Abd, A.A., Othman, M.R., Naji, S.Z., Hashim, A.S., 2021. Methane enrichment in biogas mixture using pressure swing adsorption: process fundamental and design parameters. *Mater. Today Sustain.* 11–12, 100063.
- ALothman, Z.A., 2012. A review: fundamental aspects of silicate mesoporous materials. *Materials* 5, 2874–2902.
- Anderson, W., Kozak, D., Coleman, V.A., Jämting, Å.K., Trau, M., 2013. A comparative study of submicron particle sizing platforms: accuracy, precision and resolution analysis of poly-disperse particle size distributions. *J. Colloid Interface Sci.* 405, 322–330.
- Atash Jameh, A., Mohammadi, T., Bakhtiari, O., 2020. Preparation of PEBAX-1074/modified ZIF-8 nanoparticles mixed matrix membranes for CO<sub>2</sub> removal from natural gas. *Sep. Purif. Technol.* 231, 115900.
- Behroozi, M., Pakizeh, M., 2017. Study the effects of Cloisite15A nanoclay incorporation on the morphology and gas permeation properties of Pebax2533 polymer. *J. Appl. Polym. Sci.* 134, 45302.
- Bernardo, P., Clarizia, G., 2020. Enhancing gas permeation properties of Pebax® 1657 membranes via polysorbate nonionic surfactants doping. *Polymers* 12, 253.
- Chi, W.S., Hwang, S., Lee, S.-J., Park, S., Bae, Y.-S., Ryu, D.Y., Kim, J.H., Kim, J., 2015. Mixed matrix membranes consisting of SEBS block copolymers and size-controlled ZIF-8 nanoparticles for CO<sub>2</sub> capture. *J. Membr. Sci.* 495, 479–488.
- Cui, L., Liu, M., Yuan, X., Wang, Q., Ma, Q., Wang, P., Hong, J., Liu, H., 2021. Environmental and economic impact assessment of three sintering flue gas treatment technologies in the iron and steel industry. *J. Clean. Prod.* 311, 127703.
- Dal-Cin, M.M., Kumar, A., Layton, L., 2008. Revisiting the experimental and theoretical upper bounds of light pure gas selectivity–permeability for polymeric membranes. *J. Membr. Sci.* 323, 299–308.
- Ding, R., Zheng, W., Yang, K., Dai, Y., Ruan, X., Yan, X., He, G., 2020. Amino-functional ZIF-8 nanocrystals by microemulsion based mixed linker strategy and the enhanced CO<sub>2</sub>/N<sub>2</sub> separation. *Sep. Purif. Technol.* 236, 116209.
- Gao, J., Mao, H., Jin, H., Chen, C., Feldhoff, A., Li, Y., 2020. Functionalized ZIF-7/Pebax® 2533 mixed matrix membranes for CO<sub>2</sub>/N<sub>2</sub> separation. *Microporous Mesoporous Mater.* 297, 110030.
- Gouveia, A.S.L., Yáñez, M., Alves, V.D., Palomar, J., Moya, C., Gorri, D., Tomé, L.C., Marrucho, I.M., 2021. CO<sub>2</sub>/H<sub>2</sub> separation through poly(ionic liquid)–ionic liquid membranes: the effect of multicomponent gas mixtures, temperature and gas feed pressure. *Sep. Purif. Technol.* 259, 118113.
- Gou, M., Zhu, W., Sun, Y., Guo, R., 2021. Introducing two-dimensional metal-organic frameworks with axial coordination anion into Pebax for CO<sub>2</sub>/CH<sub>4</sub> separation. *Sep. Purif. Technol.* 259, 118107.
- Gülmüs, S.A., Yilmaz, L., 2007. Effect of temperature and membrane preparation parameters on gas permeation properties of polymethacrylates. *J. Polym. Sci. Part B Polym. Phys.* 45, 3025–3033.
- Hao, L., Li, P., Yang, T., Chung, T.-S., 2013. Room temperature ionic liquid/ZIF-8 mixed-matrix membranes for natural gas sweetening and post-combustion CO<sub>2</sub> capture. *J. Membr. Sci.* 436, 221–231.
- He, R., Cong, S., Xu, S., Han, S., Guo, H., Liang, Z., Wang, J., Zhang, Y., 2021. CO<sub>2</sub>-philic mixed matrix membranes based on low-molecular-weight polyethylene glycol and porous organic polymers. *J. Membr. Sci.* 624, 119081.
- He, S., Zhu, B., Li, S., Zhang, Y., Jiang, X., Hon Lau, C., Shao, L., 2022. Recent progress in PIM-1 based membranes for sustainable CO<sub>2</sub> separations: polymer structure manipulation and mixed matrix membrane design. *Sep. Purif. Technol.* 284, 120277.
- Inoue, M., Hirasawa, I., 2013. The relationship between crystal morphology and XRD peak intensity on CaSO<sub>4</sub>·2H<sub>2</sub>O. *J. Cryst. Growth* 380, 169–175.
- Jansen, J.C., Clarizia, G., Bernardo, P., Bazzarelli, F., Friess, K., Randová, A., Schauer, J., Kubicka, D., Kacirková, M., Izak, P., 2013. Gas transport properties and pervaporation performance of fluoropolymer gel membranes based on pure and mixed ionic liquids. *Sep. Purif. Technol.* 109, 87–97.
- Jiao, C., Li, Z., Li, X., Wu, M., Jiang, H., 2021. Improved CO<sub>2</sub>/N<sub>2</sub> separation performance of Pebax composite membrane containing polyethyleneimine functionalized ZIF-8. *Sep. Purif. Technol.* 259, 118190.
- Ji, L., Zhang, L., Zheng, X., Feng, L., He, Q., Wei, Y., Yan, S., 2021. Simultaneous CO<sub>2</sub> absorption, mineralisation and carbonate crystallisation promoted by amines in a single process. *J. CO<sub>2</sub> Util.* 51, 101653.
- Kamble, A.R., Patel, C.M., Murthy, Z.V.P., 2021. A review on the recent advances in mixed matrix membranes for gas separation processes. *Renew. Sustain. Energy Rev.* 145, 111062.
- Kasprzak, A., Popławska, M., Bystrzejewski, M., Łabędź, O., Grudziński, I.P., 2015. Conjugation of polyethylenimine and its derivatives to carbon-encapsulated iron nanoparticles. *RSC Adv.* 5, 85556–85567.
- Kim, S.Y., Cho, Y., Kang, S.W., 2020. Correlation between functional group and formation of nanoparticles in PEBAX/Ag salt/al salt complexes for olefin separation. *Polymers* 12, 667.
- Kujawski, W., Li, G., Van der Bruggen, B., Pedišius, N., Tonkonogij, J., Tonkonogovas, A., Stankevičius, A., Šereika, J., Jullok, N., Kujawa, J., 2020. Preparation and characterization of polyphenylsulfone (PPSU) membranes for biogas upgrading. *Materials* 13, 2847.
- Lasseguette, E., Malpass-Evans, R., Carta, M., McKeown, N.B., Ferrari, M.-C., 2018. Temperature and pressure dependence of gas permeation in a microporous Tröger's base polymer. *Membranes* 8, 132.
- Leofanti, G., Padovan, M., Tozzola, G., Venturelli, B., 1998. Surface area and pore texture of catalysts. *Catal. Today* 41, 207–219.
- Liu, N., Cheng, J., Hou, W., Yang, X., Zhou, J., 2021. Pebax-based mixed matrix membranes loaded with graphene oxide/core shell ZIF-8@ZIF-67 nanocomposites improved CO<sub>2</sub> permeability and selectivity. *J. Appl. Polym. Sci.* 138, 50553.
- Liu, B., Li, D., Yao, J., Sun, H., 2020. Improved CO<sub>2</sub> separation performance and interfacial affinity of mixed matrix membrane by incorporating UiO-66-PEI@[bmim][Tf2N] particles. *Sep. Purif. Technol.* 239, 116519.
- Li, K., Jiang, J., Tian, S., Yan, F., Chen, X., 2015. Polyethyleneimine–nano silica composites: a low-cost and promising adsorbent for CO<sub>2</sub> capture. *J. Mater. Chem. A* 3, 2166–2175.
- Li, Y., Wang, S., He, G., Wu, H., Pan, F., Jiang, Z., 2015. Facilitated transport of small molecules and ions for energy-efficient membranes. *Chem. Soc. Rev.* 44, 103–118.
- Li, G., Kujawski, W., Knozowska, K., Kujawa, J., 2021a. Thin film mixed matrix hollow fiber membrane fabricated by incorporation of amine functionalized metal-organic framework for CO<sub>2</sub>/N<sub>2</sub> separation. *Materials* 14, 3366.
- Li, G., Kujawski, W., Válek, R., Koter, S., 2021b. A review - the development of hollow fibre membranes for gas separation processes. *Int. J. Greenh. Gas Control* 104, 103195.
- Li, H., Tuo, L., Yang, K., Jeong, H.-K., Dai, Y., He, G., Zhao, W., 2016. Simultaneous enhancement of mechanical properties and CO<sub>2</sub> selectivity of ZIF-8 mixed matrix membranes: interfacial toughening effect of ionic liquid. *J. Membr. Sci.* 511, 130–142.
- Li, M., Zhang, X., Zeng, S., Bai, L., Gao, H., Deng, J., Yang, Q., Zhang, S., 2017. Pebax-based composite membranes with high gas transport properties enhanced by ionic liquids for CO<sub>2</sub> separation. *RSC Adv.* 7, 6422–6431.
- Lv, X., Huang, L., Ding, S., Wang, J., Li, L., Liang, C., Li, X., 2021. Mixed matrix membranes comprising dual-facilitated bio-inspired filler for enhancing CO<sub>2</sub> separation. *Sep. Purif. Technol.* 276, 119347.

- Menezes, T., Santos, K., Franceschi, E., Borges, G., Dariva, C., Egues, S., De Conto, J., Santana, C., 2020. Synthesis of the chiral stationary phase based on functionalized ZIF-8 with amylose carbamate. *J. Mater. Res.* 35, 2936–2949.
- Nafisi, V., Hägg, M.-B., 2014a. Gas separation properties of ZIF-8/6FDA-durene diamine mixed matrix membrane. *Sep. Purif. Technol.* 128, 31–38.
- Nafisi, V., Hägg, M.-B., 2014b. Development of dual layer of ZIF-8/PEBAX-2533 mixed matrix membrane for CO<sub>2</sub> capture. *J. Membr. Sci.* 459, 244–255.
- Nath, D., Henni, A., 2020. Solubility of carbon dioxide (CO<sub>2</sub>) in four bis (trifluoromethyl-sulfonyl)imide (Tf<sub>2</sub>N) based ionic liquids. *Fluid Phase Equilibria* 524, 112757.
- Nordin, N.A.H.M., Racha, S.M., Matsuura, T., Misdan, N., Abdullah Sani, N.A., Ismail, A.F., Mustafa, A., 2015. Facile modification of ZIF-8 mixed matrix membrane for CO<sub>2</sub>/CH<sub>4</sub> separation: synthesis and preparation. *RSC Adv.* 5, 43110–43120.
- Robeson, L.M., 2008. The upper bound revisited. *J. Membr. Sci.* 320, 390–400.
- Rynkowska, E., Fatyeyeva, K., Kujawski, W., 2018. Application of polymer-based membranes containing ionic liquids in membrane separation processes: a critical review. *Rev. Chem. Eng.* 34, 341–363.
- Shah Buddin, M.M.H., Ahmad, A.L., 2021. A review on metal-organic frameworks as filler in mixed matrix membrane: Recent strategies to surpass upper bound for CO<sub>2</sub> separation. *J. CO<sub>2</sub> Util.* 51, 101616.
- Singh, S., Varghese, A.M., Reinalda, D., Karanikolos, G.N., 2021. Graphene-based membranes for carbon dioxide separation. *J. CO<sub>2</sub> Util.* 49, 101544.
- Song, Y., He, M., Zhao, J., Jin, W., 2021. Structural manipulation of ZIF-8-based membranes for high-efficiency molecular separation. *Sep. Purif. Technol.* 270, 118722.
- Stevens, K.A., Moon, J.D., Borjigin, H., Liu, R., Joseph, R.M., Riffle, J.S., Freeman, B.D., 2020. Influence of temperature on gas transport properties of tetraaminodiphenylsulfone (TADPS) based polybenzimidazoles. *J. Membr. Sci.* 593, 117427.
- Sun, J., Li, Q., Chen, G., Duan, J., Liu, G., Jin, W., 2019. MOF-801 incorporated PEBA mixed-matrix composite membranes for CO<sub>2</sub> capture. *Sep. Purif. Technol.* 217, 229–239.
- Wee, L.H., Lescouet, T., Ethiraj, J., Bonino, F., Vidruk, R., Garrier, E., Packet, D., Bordiga, S., Farrusseng, D., Herskowitz, M., 2013. Hierarchical zeolitic imidazolate framework-8 catalyst for monoglyceride synthesis. *ChemCatChem* 5, 3562–3566.
- Wu, D., Zhang, P.-F., Yang, G.-P., Hou, L., Zhang, W.-Y., Han, Y.-F., Liu, P., Wang, Y.-Y., 2021. Supramolecular control of MOF pore properties for the tailored guest adsorption/separation applications. *Coord. Chem. Rev.* 434, 213709.
- Xian, S., Xu, F., Ma, C., Wu, Y., Xia, Q., Wang, H., Li, Z., 2015. Vapor-enhanced CO<sub>2</sub> adsorption mechanism of composite PEI@ZIF-8 modified by polyethyleneimine for CO<sub>2</sub>/N<sub>2</sub> separation. *Chem. Eng. J.* 280, 363–369.
- Xu, C., Cheng, Z., 2021. Thermal stability of ionic liquids: current status and prospects for future development. *Processes* 9, 337.
- Yousef, A.M., El-Maghlany, W.M., Eldrainy, Y.A., Attia, A., 2018. New approach for biogas purification using cryogenic separation and distillation process for CO<sub>2</sub> capture. *Energy* 156, 328–351.
- Yousef, S., Šereika, J., Tonkonogovas, A., Hashem, T., Mohamed, A., 2021. CO<sub>2</sub>/CH<sub>4</sub>, CO<sub>2</sub>/N<sub>2</sub> and CO<sub>2</sub>/H<sub>2</sub> selectivity performance of PES membranes under high pressure and temperature for biogas upgrading systems. *Environ. Technol. Innov.* 21, 101339.
- Zhang, X., Zhang, T., Wang, Y., Li, J., Liu, C., Li, N., Liao, J., 2018. Mixed-matrix membranes based on Zn/Ni-ZIF-8-PEBA for high performance CO<sub>2</sub> separation. *J. Membr. Sci.* 560, 38–46.
- Zhao, D., Ren, J., Li, H., Hua, K., Deng, M., 2014. Poly(amide-6-b-ethylene oxide)/SAPO-34 mixed matrix membrane for CO<sub>2</sub> separation. *J. Energy Chem.* 23, 227–234.
- Zheng, W., Ding, R., Yang, K., Dai, Y., Yan, X., He, G., 2019. ZIF-8 nanoparticles with tunable size for enhanced CO<sub>2</sub> capture of Pebax based MMMs. *Sep. Purif. Technol.* 214, 111–119.
- Zhu, C., Peng, Y., Yang, W., 2021. Modification strategies for metal-organic frameworks targeting at membrane-based gas separations. *Green Chem. Eng.* 2, 17–26.
- Zoubeik, M., Mohamedali, M., Henni, A., 2016. Experimental solubility and thermodynamic modeling of CO<sub>2</sub> in four new imidazolium and pyridinium-based ionic liquids. *Fluid Phase Equilibria* 419, 67–74.

## Supplementary material

Evaluation of CO<sub>2</sub> separation performance with enhanced features of materials - Pebax<sup>®</sup> 2533 mixed matrix membranes containing ZIF-8-PEI@[P(3)HIm][Tf<sub>2</sub>N]

Guoqiang Li<sup>1</sup>, Wojciech Kujawski<sup>1,\*</sup>, Andrius Tonkonogovas<sup>2</sup>, Katarzyna Knozowska<sup>1</sup>, Joanna Kujawa<sup>1</sup>, Ewa Olewnik-Kruszkowska<sup>1</sup>, Nerijus Pedišius<sup>2</sup>, Arūnas Stankevičius<sup>2</sup>

<sup>1</sup> Nicolaus Copernicus University in Toruń, Faculty of Chemistry, 7 Gagarina Street, 87-100 Toruń, Poland

<sup>2</sup> Lithuanian Energy Institute, 3 Breslaujos Street, Kaunas 44403, Lithuania

\* Corresponding author: Wojciech Kujawski, kujawski@chem.umk.pl

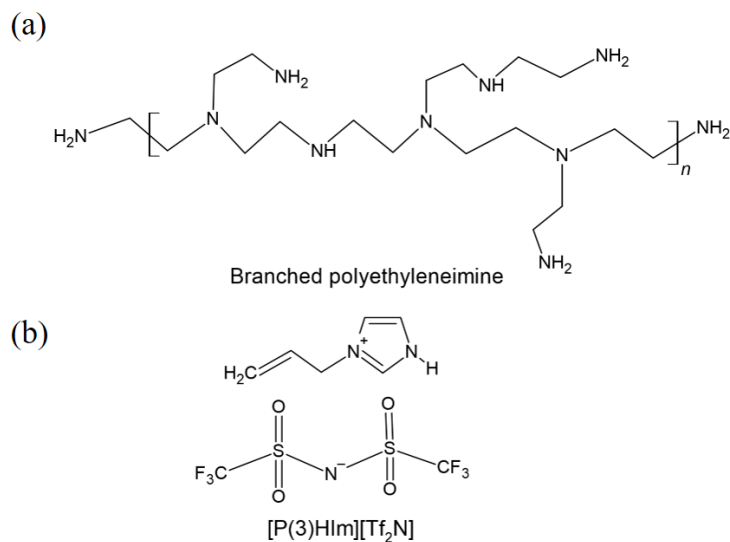


Figure S1. Chemical structures of (a) branched PEI and (b) [P(3)HIm][Tf<sub>2</sub>N] ionic liquid.

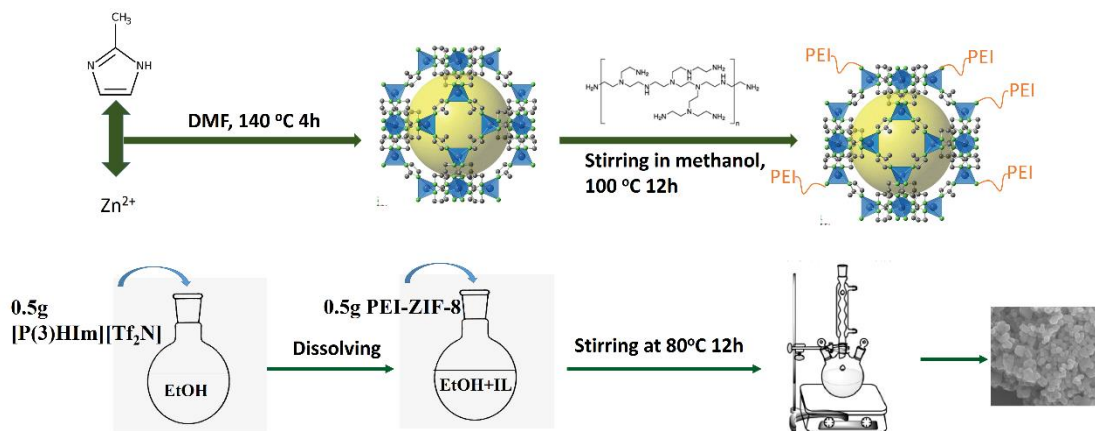


Figure S2. Schematic illustration of the preparation of ZIF-8, ZIF-8-PEI, and ZIF-8-PEI@IL.

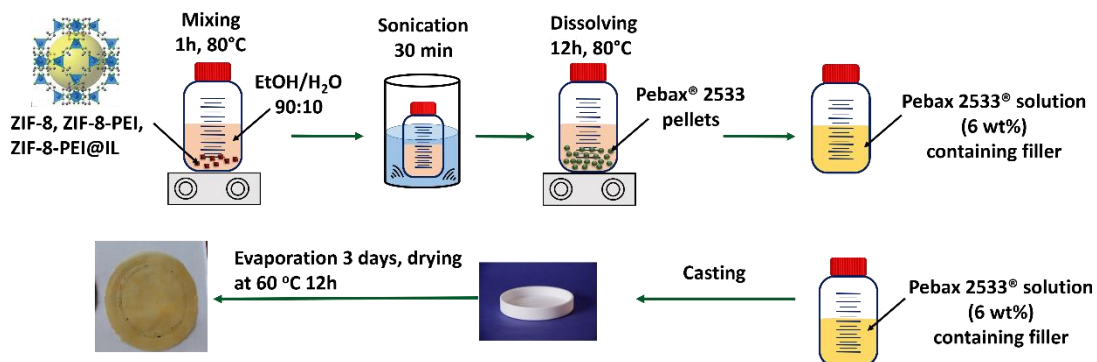


Figure S3. Schematic illustration of the preparation of MMMs.



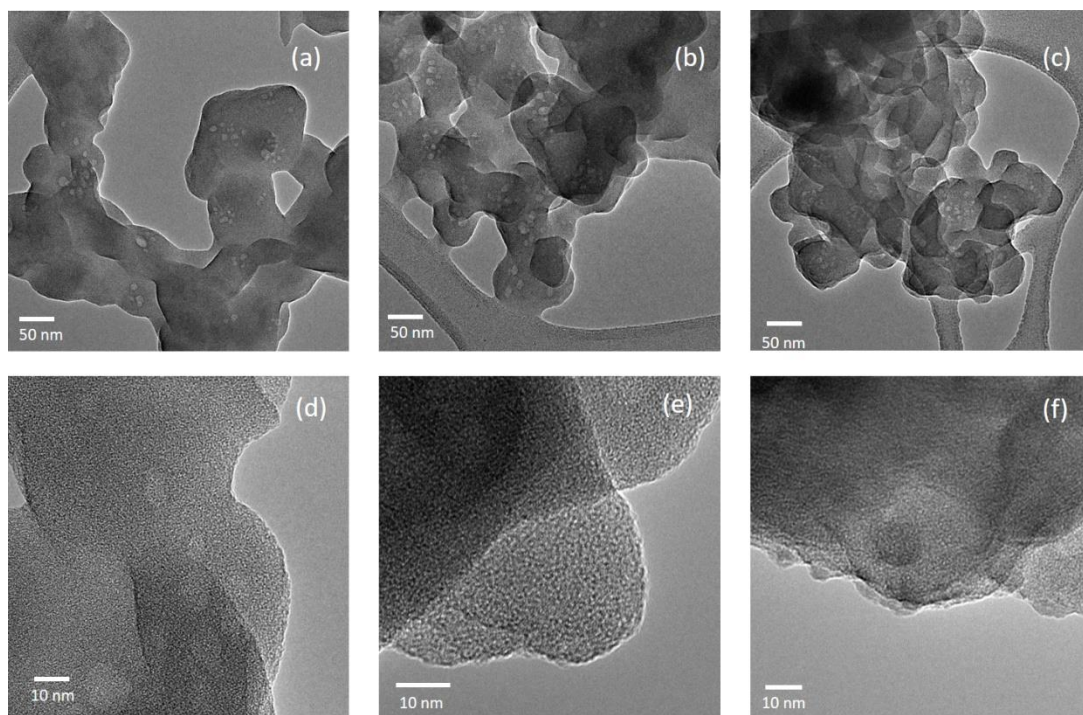


Figure S4. TEM images of ZIF-8 (a, d), ZIF-8-PEI (b, e), and ZIF-8-PEI@IL (c, f).

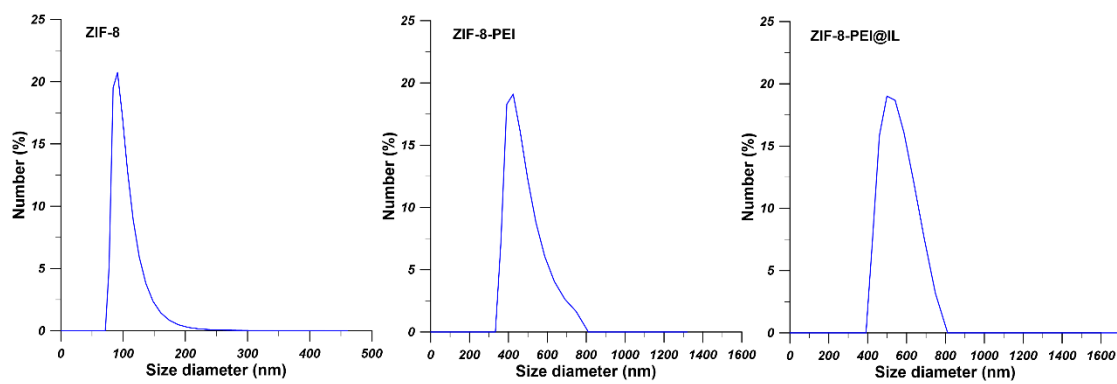


Figure S5. DLS results for ZIF-8, ZIF-8-PEI, and ZIF-8-PEI@IL.

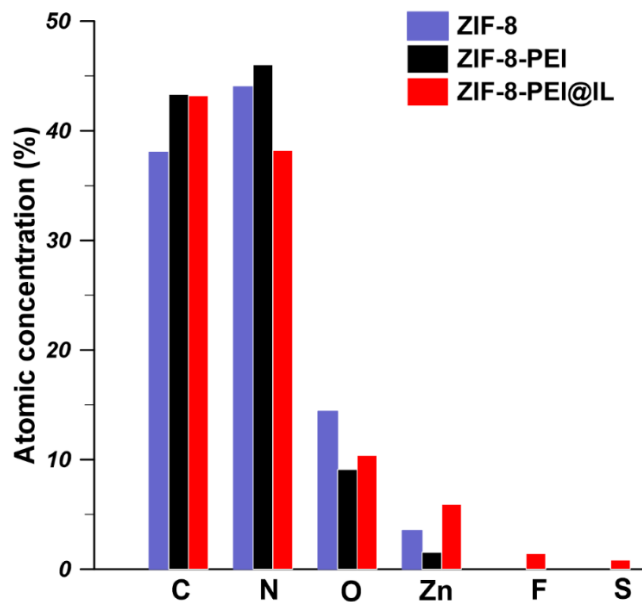


Figure S6. The results of element analysis for ZIF-8, ZIF-8-PEI, and ZIF-8-PEI@IL by using EDX

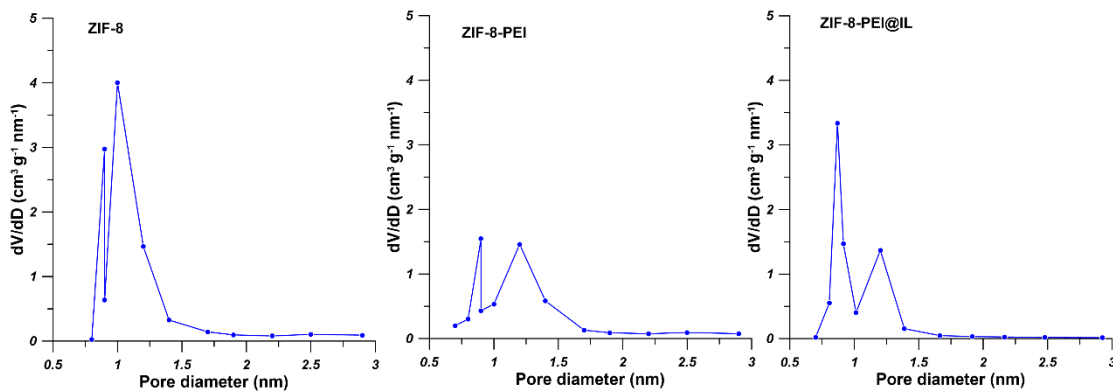


Figure S7. The pore size distribution of ZIF-8, ZIF-9-PEI, and ZIF-8-PEI@IL

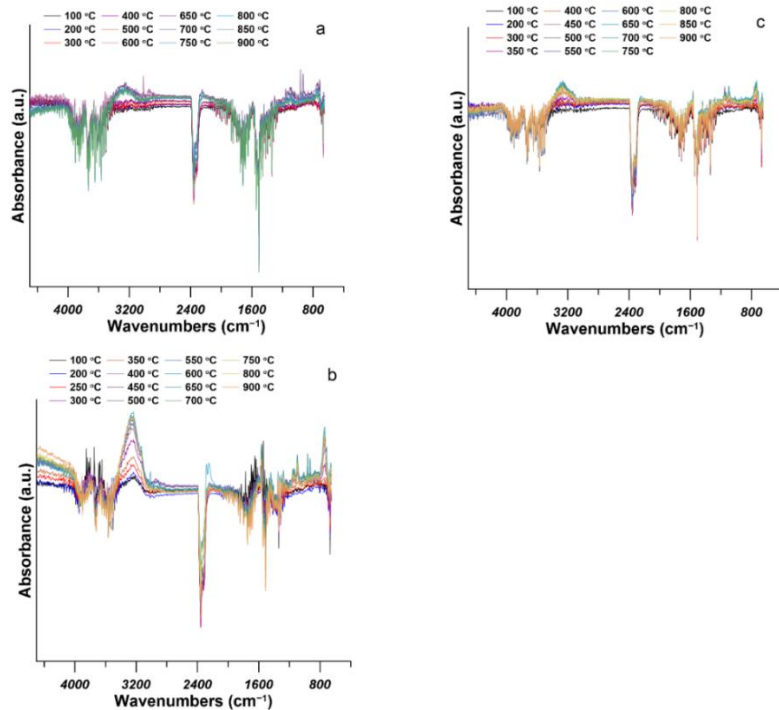


Figure S8. FTIR spectra at various temperatures of gas products generated in TGA processes for (a) ZIF-8, (B) ZIF-8-PEI, and (c) ZIF-8-PEI@IL.

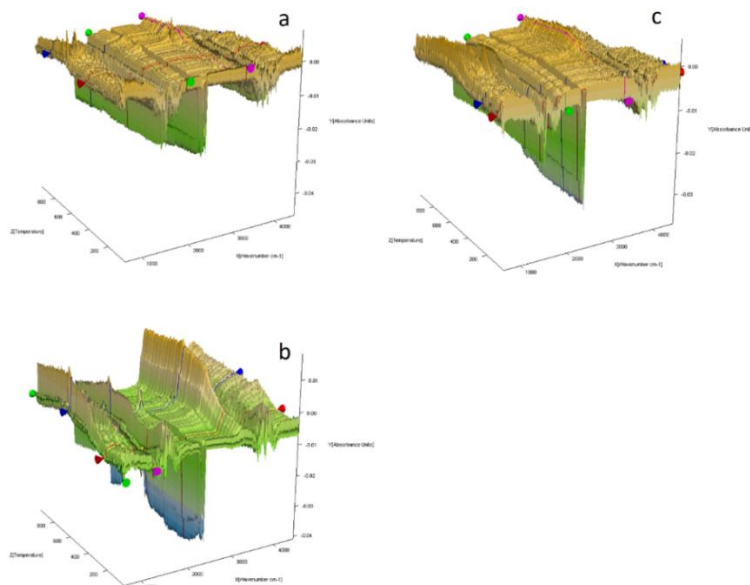


Figure S9. 3D FTIR spectra of gas products generated in TGA processes for (a) ZIF-8, (b) ZIF-8-PEI, and (c) ZIF-8-PEI@IL.

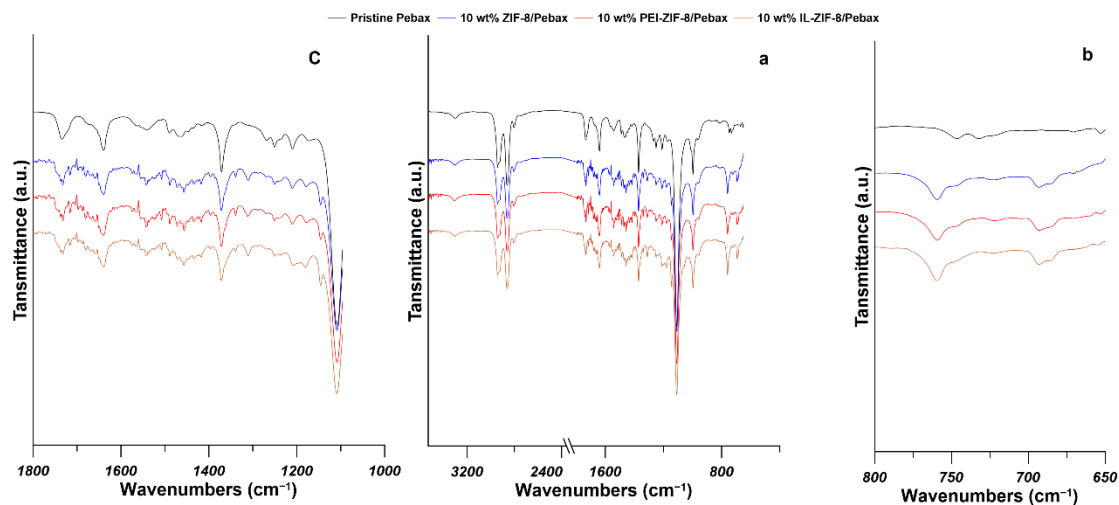


Figure S10. FTIR spectra of pristine Pebax and the prepared MMMs containing 10 wt% of ZIF-8, ZIF-8-PEI, and ZIF-8-PEI@IL.

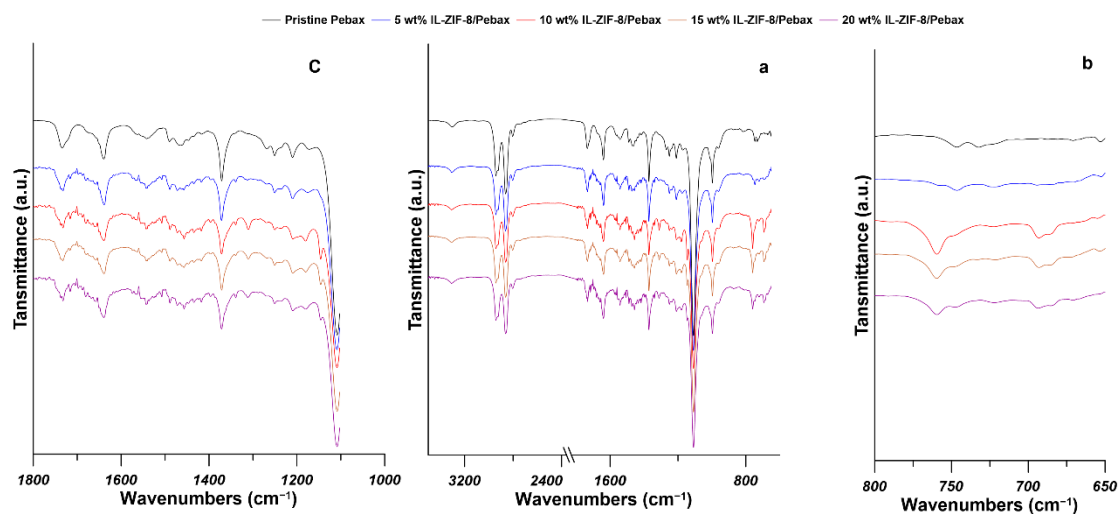


Figure S11. FTIR spectra of pristine Pebax and the prepared MMMs containing different amount of ZIF-8-PEI@IL.

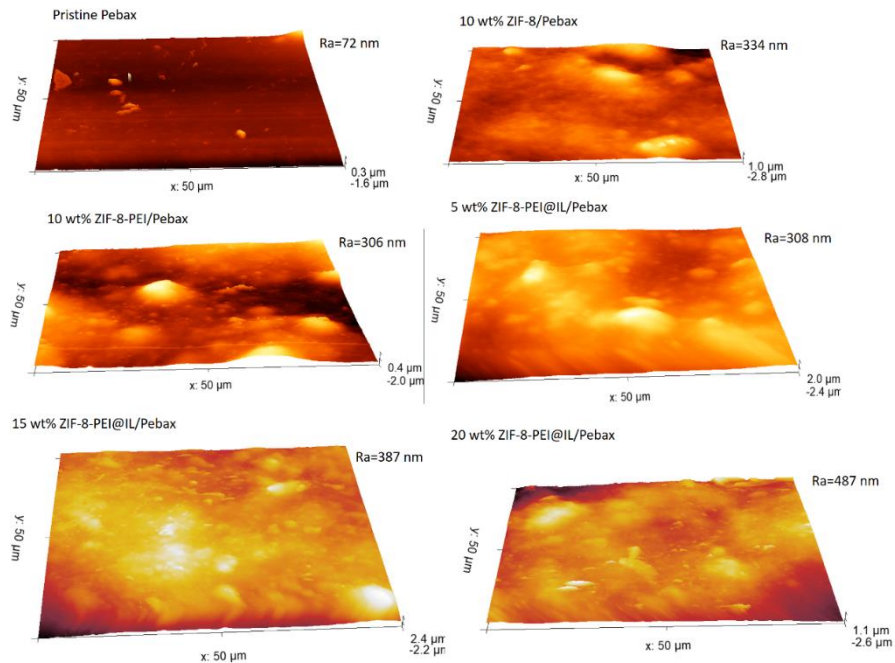


Figure S12. AFM images of pristine Pebax and the prepared MMMs.

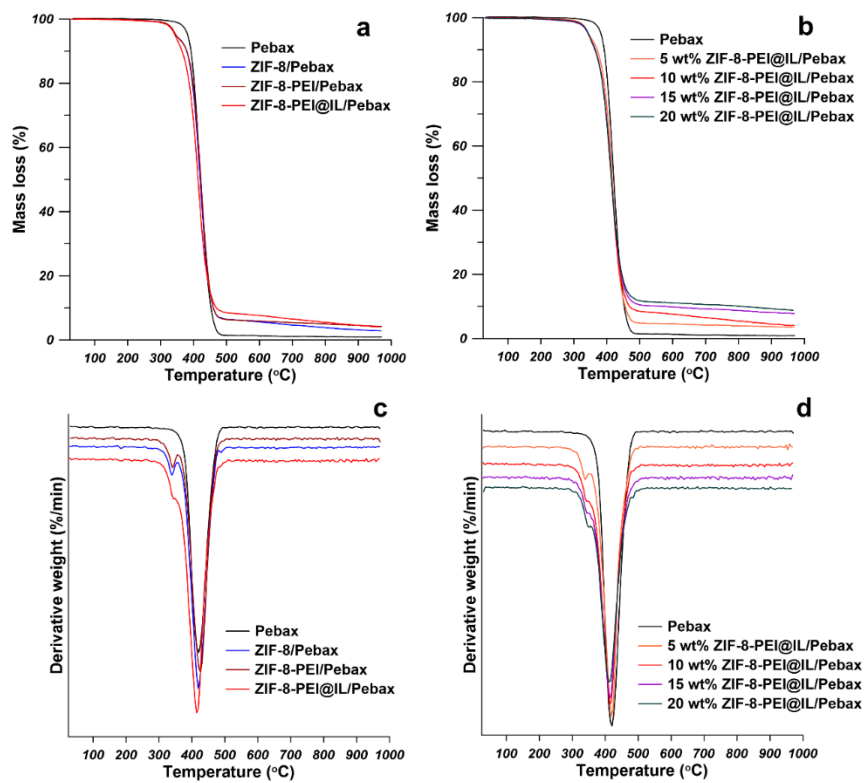


Figure S13. TGA and DTG curves of pristine Pebax<sup>®</sup> 2533 membrane, MMMs containing different



types of fillers (a, c) and MMMs containing different amount of ZIF-8-PEI@IL (b, d).

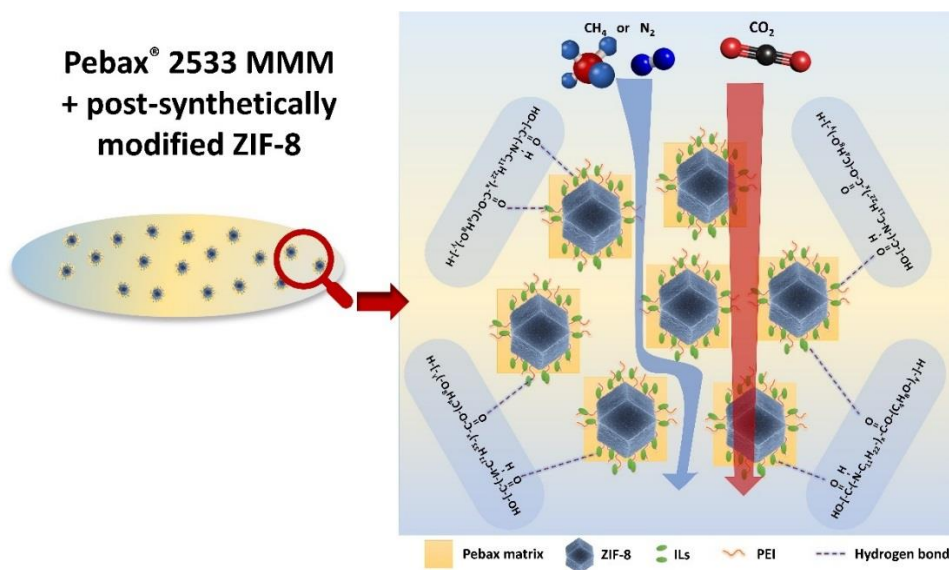


Figure S14. Pathways for CO<sub>2</sub> N<sub>2</sub> and CH<sub>4</sub> transport through the ZIF-8-PEI@IL/ Pebax<sup>®</sup> 2533 MMMs.

Table S1. Textural properties of ZIF-8, ZIF-8-PEI, and ZIF-8-PEI@IL

Samples	BET (m <sup>2</sup> /g)	V <sub>Total</sub> (cm <sup>3</sup> /g)	V <sub>Micro</sub> (cm <sup>3</sup> /g)	V <sub>Meso</sub> (cm <sup>3</sup> /g)	F <sub>Micro</sub> (%)	Average pore diameter (nm)
ZIF-8	1604	1.83	0.75	1.08	40.98	1.05
ZIF-8-PEI	940	0.96	0.41	0.55	42.71	0.96
ZIF-8-PEI@IL	1053	1.53	0.48	1.05	31.37	0.84

V<sub>Micro</sub>: Micropore volume calculated by using the t-plot method.

V<sub>Meso</sub>: Mesopore volume calculated from the subtraction of micropore volume from total pore volume.

F<sub>Micro</sub>: The fraction of micropore volume = (micropore volume/total pore volume)\*100%.

Table S2. Activation energy  $E_p$  of the pristine Pebax<sup>®</sup> 2533 membrane and MMM containing 15 wt% ZIF-8-PEI@IL.

	Activation energy $E_p$ (kJ/mol)			
	CO <sub>2</sub>	CH <sub>4</sub>	N <sub>2</sub>	H <sub>2</sub>
Pebax <sup>®</sup> 2533	9.84	15.40	19.88	11.90
15 wt% ZIF-8-PEI@IL/ Pebax <sup>®</sup> 2533	14.32	47.54	33.06	15.46

Table S3. Summary of gas separation performances of Pebax-based MMMs.

Fillers	Filler content (wt%)	$P_{CO_2}$ (Barrer)	$\alpha_{CO_2/N_2}$	$\alpha_{CO_2/CH_4}$	Experimental	Ref.
					condition: P (bar)/T (°C)	
MIL-53	10	129	48	17	10/35	[1]
NH <sub>2</sub> -MIL-53	10	149	56	21	10/35	[1]
UiO-66	7.5	90	60	-	3/20	[2]
UiO-66-NH <sub>2</sub>	10	84	80	-	3/20	[2]
ZIF-8	20	156	41	-	1/20	[3]
ZIF-8	15	106	35	17	1/23	[4]
ZIF-8	10	180	41	19	3/25	[5]
ZIF-7-CH <sub>3</sub> OH	10	562	19	-	4.5/25	[6]
2D MOF	4	355	-	43	1/25	[7]
CFA-1	3	869	87		1/30	[8]
Zn/Ni-ZIF-8	15	440	40	-	2/25	[9]
NH <sub>2</sub> -ZIF-8	6	164	62	-	1/25	[10]

Bio-ZIF	12	560	-	40	2/25	[11]
IL@ZIF-8	15	105	84	35	1/25	[12]
[Bmim][PF6]@ZIF-8	25	117	85	-	2/25	[13]
MWCNTs@ZIF-8	8	186	61	-	5/35	[14]
NPC	5	553	56	-	2/25	[15]
N-FLG	4	240	96	-	2/25	[16]
CNs	0.5	120	86	-	10/25	[17]
NOHMs	15	247	66	-	2/25	[18]
2D MFI zeolite	5	159	-	27	2/25	[19]
MoS <sub>2</sub>	5	67	91	-	2/30	[20]
ZIF-90@C <sub>3</sub> N <sub>4</sub>	8	110	84	-	2/25	[21]
PEI-ZIF-8	5	13 GPU	49	-	1/25	[22]
ZIF-8-PEI@IL	15	285	76	25	2/24	This wor k

MIL – Materials of Institut Lavoisier, UiO – University of Oslo, ZIF – Zeolitic imidazolate framework, CFA – Coordination Framework Augsburg, MWCNTs – Multi-wall carbon nanotubes, NPC – nitrogen-doped porous carbons, CNs – microporous carbon nanospheres, NOHMs – nanoparticle organic hybrid materials, N-FLG – N-doped few-layer graphene.

## References

- [1] S. Meshkat, S. Kaliaguine, D. Rodrigue, Mixed matrix membranes based on amine and non-amine MIL-53(Al) in Pebax® MH-1657 for CO<sub>2</sub> separation, *Separation and Purification Technology*, 200 (2018) 177-190.
- [2] J. Shen, G. Liu, K. Huang, Q. Li, K. Guan, Y. Li, W. Jin, UiO-66-polyether block amide mixed matrix membranes for CO<sub>2</sub> separation, *Journal of Membrane Science*, 513 (2016) 155-165.
- [3] W. Zheng, R. Ding, K. Yang, Y. Dai, X. Yan, G. He, ZIF-8 nanoparticles with tunable size for enhanced CO<sub>2</sub> capture of Pebax based MMMs, *Separation and Purification Technology*, 214 (2019) 111-119.
- [4] M. Li, X. Zhang, S. Zeng, L. bai, H. Gao, J. Deng, Q. Yang, S. Zhang, Pebax-based composite membranes with high gas transport properties enhanced by ionic liquids for CO<sub>2</sub> separation, *RSC Advances*, 7 (2017) 6422-6431.
- [5] P.D. Sutrisna, J. Hou, H. Li, Y. Zhang, V. Chen, Improved operational stability of Pebax-based gas separation membranes with ZIF-8: A comparative study of flat sheet and composite hollow fibre membranes, *Journal of Membrane Science*, 524 (2017) 266-279.
- [6] J. Gao, H. Mao, H. Jin, C. Chen, A. Feldhoff, Y. Li, Functionalized ZIF-7/Pebax® 2533 mixed matrix membranes for CO<sub>2</sub>/N<sub>2</sub> separation, *Microporous and Mesoporous Materials*, 297 (2020) 110030.
- [7] M. Gou, W. Zhu, Y. Sun, R. Guo, Introducing two-dimensional metal-organic frameworks with axial coordination anion into Pebax for CO<sub>2</sub>/CH<sub>4</sub> separation, *Separation and Purification Technology*, 259 (2021) 118107.
- [8] W. Zheng, Z. Tian, Z. Wang, D. Peng, Y. Zhang, J. Wang, Y. Zhang, Dual-function biomimetic carrier based facilitated transport mixed matrix membranes with high stability for efficient CO<sub>2</sub>/N<sub>2</sub>

separation, *Separation and Purification Technology*, 285 (2022) 120371.

[9] X. Zhang, T. Zhang, Y. Wang, J. Li, C. Liu, N. Li, J. Liao, Mixed-matrix membranes based on Zn/Ni-ZIF-8-PEBA for high performance CO<sub>2</sub> separation, *Journal of Membrane Science*, 560 (2018) 38-46.

[10] R. Ding, W. Zheng, K. Yang, Y. Dai, X. Ruan, X. Yan, G. He, Amino-functional ZIF-8 nanocrystals by microemulsion based mixed linker strategy and the enhanced CO<sub>2</sub>/N<sub>2</sub> separation, *Separation and Purification Technology*, 236 (2020) 116209.

[11] X. Lv, L. Huang, S. Ding, J. Wang, L. Li, C. Liang, X. Li, Mixed matrix membranes comprising dual-facilitated bio-inspired filler for enhancing CO<sub>2</sub> separation, *Separation and Purification Technology*, 276 (2021) 119347.

[12] H. Li, L. Tuo, K. Yang, H.-K. Jeong, Y. Dai, G. He, W. Zhao, Simultaneous enhancement of mechanical properties and CO<sub>2</sub> selectivity of ZIF-8 mixed matrix membranes: Interfacial toughening effect of ionic liquid, *Journal of Membrane Science*, 511 (2016) 130-142.

[13] Z. Guo, W. Zheng, X. Yan, Y. Dai, X. Ruan, X. Yang, X. Li, N. Zhang, G. He, Ionic liquid tuning nanocage size of MOFs through a two-step adsorption/infiltration strategy for enhanced gas screening of mixed-matrix membranes, *Journal of Membrane Science*, 605 (2020) 118101.

[14] X. Li, S. Yu, K. Li, C. Ma, J. Zhang, H. Li, X. Chang, L. Zhu, Q. Xue, Enhanced gas separation performance of Pebax mixed matrix membranes by incorporating ZIF-8 in situ inserted by multiwalled carbon nanotubes, *Separation and Purification Technology*, 248 (2020) 117080.

[15] Y. Wang, Z. Ma, X. Zhang, J. Li, Y. Zhou, Z. Jin, N. Li, Mixed-matrix membranes consisting of Pebax and novel nitrogen-doped porous carbons for CO<sub>2</sub> separation, *Journal of Membrane Science*, 644 (2022) 120182.

[16] T.-C. Huang, Y.-C. Liu, G.-S. Lin, C.-H. Lin, W.-R. Liu, K.-L. Tung, Fabrication of pebax-



1657-based mixed-matrix membranes incorporating N-doped few-layer graphene for carbon dioxide capture enhancement, *Journal of Membrane Science*, 602 (2020) 117946.

[17] H. Wang, W. Zheng, X. Yang, M. Ning, X. Li, Y. Xi, X. Yan, X. Zhang, Y. Dai, H. Liu, G. He, Pebax-based mixed matrix membranes derived from microporous carbon nanospheres for permeable and selective CO<sub>2</sub> separation, *Separation and Purification Technology*, 274 (2021) 119015.

[18] D. Wang, S. Song, W. Zhang, Z. He, Y. Wang, Y. Zheng, D. Yao, Y. Pan, Z. Yang, Z. Meng, Y. Li, CO<sub>2</sub> selective separation of Pebax-based mixed matrix membranes (MMMs) accelerated by silica nanoparticle organic hybrid materials (NOHMs), *Separation and Purification Technology*, 241 (2020) 116708.

[19] Q. Zhang, M. Zhou, X. Liu, B. Zhang, Pebax/two-dimensional MFI nanosheets mixed-matrix membranes for enhanced CO<sub>2</sub> separation, *Journal of Membrane Science*, 636 (2021) 119612.

[20] Y.-C. Liu, C.-Y. Chen, G.-S. Lin, C.-H. Chen, K.C.W. Wu, C.-H. Lin, K.-L. Tung, Characterization and molecular simulation of Pebax-1657-based mixed matrix membranes incorporating MoS<sub>2</sub> nanosheets for carbon dioxide capture enhancement, *Journal of Membrane Science*, 582 (2019) 358-366.

[21] F. Guo, D. Li, R. Ding, J. Gao, X. Ruan, X. Jiang, G. He, W. Xiao, Constructing MOF-doped two-dimensional composite material ZIF-90@C<sub>3</sub>N<sub>4</sub> mixed matrix membranes for CO<sub>2</sub>/N<sub>2</sub> separation, *Separation and Purification Technology*, 280 (2022) 119803.

[22] C. Jiao, Z. Li, X. Li, M. Wu, H. Jiang, Improved CO<sub>2</sub>/N<sub>2</sub> separation performance of Pebax composite membrane containing polyethyleneimine functionalized ZIF-8, *Separation and Purification Technology*, 259 (2021) 118190.

## **Publication VI**

**G. Li**, W. Kujawski, K. Knozowska, J. Kujawa, Pebax® 2533/PVDF thin film mixed matrix membranes containing MIL-101 (Fe)/GO composite for CO<sub>2</sub> capture, RSC Advances, 12 (2022) 29124-29136.


 Cite this: *RSC Adv.*, 2022, 12, 29124

# Pebax® 2533/PVDF thin film mixed matrix membranes containing MIL-101 (Fe)/GO composite for CO<sub>2</sub> capture

Guoqiang Li, Wojciech Kujawski, \* Katarzyna Knozowska and Joanna Kujawa

MIL-101 (Fe) and MIL-GO composites were successfully synthesized and used as fillers for the preparation of Pebax® 2533/PVDF thin film MMMs for CO<sub>2</sub>/N<sub>2</sub> separation. The defect-free Pebax® 2533/PVDF thin film MMMs were fabricated by casting the Pebax solution containing fillers on the PVDF support. The presence of GO nanosheets in the reaction solution did not destroy the crystal structure of MIL-101 (Fe). However, the BET surface area and total pore volume of MIL-GO decreased dramatically, comparing with MIL-101 (Fe). The incorporation of MIL-GO-2 into Pebax matrix simultaneously increased the CO<sub>2</sub> permeability and the CO<sub>2</sub>/N<sub>2</sub> ideal selectivity of Pebax® 2533/PVDF thin film MMMs mainly owing to the porous structure of MIL-GO-2, and the tortuous diffusion pathways created by GO nanosheets. MMMs containing 9.1 wt% MIL-GO-2 exhibited the highest CO<sub>2</sub> permeability equal to 303 barrer (1 barrer = 10<sup>-10</sup> cm<sup>3</sup> (STP) cm cm<sup>-2</sup> s<sup>-1</sup> cmHg<sup>-1</sup>) and the highest CO<sub>2</sub>/N<sub>2</sub> ideal selectivity equal to 24. Pebax-based MMMs containing composite fillers showed higher gas separation performance than the Pebax-based MMMs containing single filler (GO or MOFs). Therefore, the synthesis and utilization of 3D@2D composite filler demonstrated great potential in the preparation of high-performance MMMs for gas separation processes.

 Received 14th August 2022  
 Accepted 4th October 2022

 DOI: 10.1039/d2ra05095a  
[rsc.li/rsc-advances](http://rsc.li/rsc-advances)

## 1. Introduction

CO<sub>2</sub> emission has been increasing dramatically owing to the rapid industrialization and the fast development of economy in the world, which has resulted in the extreme climate and global warming.<sup>1,2</sup> Therefore, it is of global concern to decrease the CO<sub>2</sub> emission by separating CO<sub>2</sub> from N<sub>2</sub> and other gases owing to the environmental and economic incentives for the utilization of the separated CO<sub>2</sub>.<sup>3</sup> Membrane technology has shown great potential in gas separation processes due to its high modularity and compactness, low energy consumption, and low operating costs.<sup>3-5</sup> Moreover, it is tolerable for the feed composition to change since there is no phase change or solvent regeneration process.<sup>3</sup>

Polymeric membranes have been widely used in gas separation processes owing to their high processability and reasonable cost of polymer materials. However, it is challenging to prepare polymeric membranes possessing the high gas separation performance owing to the trade-off relationship between the permeability and the selectivity which is represented by the Robeson upper bound.<sup>6,7</sup> The preparation of mixed matrix membranes (MMM) is an effective solution to surpass the Robeson upper bound.<sup>7</sup> The incorporation of nanomaterials into polymeric matrix can create the additional continuous gas transport channels, resulting in the

enhancement of gas separation performance of MMMs.<sup>8</sup> Various inorganic nanomaterials have been used as fillers in MMMs preparation, such as zeolites,<sup>9</sup> metal-organic frameworks (MOFs),<sup>10</sup> graphene oxide (GO),<sup>11</sup> and carbon nanotubes (CNTs).<sup>12</sup> Fillers refer to the inorganic materials like nanoparticles that are incorporated into MMMs in order to enhance the membrane performance.

Among various fillers used in MMMs preparation, MOFs have been intensively investigated since MOFs possess high surface area, tunable porosity and pore size, and chemical functionality.<sup>13</sup> MOFs can be modified with CO<sub>2</sub>-philic chemicals, such as ionic liquids (ILs),<sup>14</sup> isophthalic dihydrazide (IPD),<sup>15</sup> and polyethyleneimine (PEI),<sup>16</sup> to enhance their affinity to CO<sub>2</sub> molecules in order to improve the CO<sub>2</sub> permeability and selectivity of MMMs. Chen *et al.*<sup>14</sup> synthesized [Bmim][NTf<sub>2</sub>] modified MOF-801 *via* wet impregnation and prepared MMMs by incorporating the synthesized filler into polymers of intrinsic microporosity PIM-1 matrix. It was found that the CO<sub>2</sub> permeability of IL@MOF/PIM-5% MMMs increased by 130% and the CO<sub>2</sub>/N<sub>2</sub> selectivity increased by 45%, comparing with the pristine PIM-1 membranes. The enhancement of the gas separation performance was owing to the high porosity and good CO<sub>2</sub> affinity of IL@MOF-801 fillers, which significantly increased the diffusion rate of CO<sub>2</sub>. Moreover, the selectivity of MMMs increased owing to the reduction of pore volume of IL@MOF-801 composites. Shi *et al.*<sup>15</sup> modified zeolitic imidazolate framework (ZIF-8) nanoparticles by coating isophthalic dihydrazide (IPD) molecular layer onto their surfaces by using

Nicolaus Copernicus University in Toruń, Faculty of Chemistry, 7 Gagarina Street, Toruń 87-100, Poland. E-mail: [wkujawski@umk.pl](mailto:wkujawski@umk.pl)



coordination interaction. Subsequently, the modified IPD@ZIF-8 nanoparticles were incorporated into 6FDA-Durene polyimide (PI) matrix for the MMMs preparation. It was found that the modified IPD@ZIF-8 nanoparticles showed enhanced interfacial compatibility between fillers and PI matrix owing to the formed hydrogen bond. As a result, the prepared MMMs containing high loading content (45 wt%) showed high CO<sub>2</sub> permeability equal to 4133 barrer which increased by 154%, comparing with the pristine PI membranes. Jiao *et al.*<sup>16</sup> synthesized PEI modified ZIF-8 (PEI-ZIF-8) by using Hmin and PEI mixed linker. The prepared PEI-ZIF-8 was incorporated into Pebax® 1657 matrix to fabricate MMMs. It was found that the MMMs with 5 wt% PEI-ZIF-8 exhibited increased CO<sub>2</sub> permeance equal to 13 GPU and increased CO<sub>2</sub>/N<sub>2</sub> selectivity equal to 49. The improved gas separation performance for MMMs was ascribed to the porous structure and higher affinity with CO<sub>2</sub> of PEI-ZIF-8, the large density of amine groups from PEI providing facilitated CO<sub>2</sub> transport path and the enhanced interfacial compatibility.

GO as a two-dimensional (2D) material has been used in the preparation of MMMs owing to its high aspect ratio, high mechanical and thermal properties, facile preparation, and tunable surface modification.<sup>17</sup> In MMMs, GO nanosheets improve the gas diffusivity selectivity by creating tortuous pathways which allow small gas molecules to transport through membranes more easily than big gas molecules.<sup>17</sup> Therefore, the incorporation of MOF/GO composite filler into MMMs is an effective way to enhance their gas separation performance due to the synergistic effects of MOF and GO.<sup>17,18</sup>

Dong *et al.*<sup>17</sup> synthesized ZIF-8@GO composite filler and incorporate it into Pebax matrix to prepare MMMs for gas separation. It was found that MMMs containing 6 wt% of ZIF-8@GO demonstrated the CO<sub>2</sub> permeability of 249 barrer and CO<sub>2</sub>/N<sub>2</sub> ideal selectivity of 47.6 which are 191% and 174% higher than those of pristine Pebax membranes, respectively. Moreover, the gas separation performance of MMMs containing ZIF-8@GO is higher than that of MMMs containing ZIF-8 or GO. The enhancement of gas separation of MMMs containing ZIF-8@GO was mainly due to the synergistic effects of ZIF-8 and GO. The higher free volume, higher CO<sub>2</sub> adsorption, and lower crystallinity of MMMs enhanced the CO<sub>2</sub> permeability. The high porosity of ZIF-8 could increase the solubility selectivity, while the tortuous diffusion pathways created by GO nanosheets could increase the diffusivity selectivity. Chen *et al.*<sup>19</sup> synthesized ZIF-8@GO composite fillers with different reaction time by using the *in situ* growth method and incorporated it into a CO<sub>2</sub>-philic, comb copolymer for the MMMs preparation. It was found that the reaction time of ZIF-8@GO plays a crucial role in improving the gas separation performance of MMMs. MMMs containing ZIF-8@GO synthesized from 6 h reaction time showed the highest CO<sub>2</sub> permeability of 475 barrer and CO<sub>2</sub>/N<sub>2</sub> ideal selectivity of 58.2. Yang *et al.*<sup>18</sup> synthesized ZIF-8@GO composite fillers by continuously forming a ZIF-8 layer on the GO surface to overcome the stacking and folding issues of GO in MMMs. The prepared ZIF-8@GO composite fillers were incorporated into Pebax matrix to fabricate MMMs. The MMMs containing 20 wt% of ZIF-8@GO exhibited the best gas

separation performance evidence by CO<sub>2</sub> permeability of 136.2 barrer and CO<sub>2</sub>/N<sub>2</sub> ideal selectivity of 77.9. In comparison to the pristine Pebax membranes, the CO<sub>2</sub> permeability and CO<sub>2</sub>/N<sub>2</sub> ideal selectivity increased by 66% and 60%, respectively. In comparison to the MMMs containing GO nanosheets, the CO<sub>2</sub> permeability increased by 75%, while the selectivity was not changed. It was found that the high porosity of ZIF-8 decreased the mass transfer resistance of GO by providing the transporting pathways around GO nanosheets for gas molecules, resulting in the increase of CO<sub>2</sub> permeability. The CO<sub>2</sub>/N<sub>2</sub> selectivity was enhanced by abundant oxy-groups on GO surface.

According to the aforementioned literature survey, ZIF-8/GO composites have been intensively studied in the preparation of MMMs for gas separation.<sup>17–19</sup> The study of other MOF/GO composites is highly needed to explore the effects of MOF/GO composites on the gas separation performance of MMMs. MOFs consisting of the high-valence metal sites (Fe<sup>3+</sup>) and the strong polarizing terephthalic acid can improve their molecular interaction with CO<sub>2</sub> molecules possessing quadrupole moment due to the electrical difference.<sup>20</sup> Moreover, the utilization of high-valence metal cation endows MOFs with high water-resistance. The nontoxic MIL-101 (Fe) showed higher adsorption capacity for CO<sub>2</sub> than N<sub>2</sub>.<sup>20</sup> It was more often reported that the phase transition exists in the synthesis of the amino-functionalized NH<sub>2</sub>-MIL-101 (Fe), comparing with the synthesis of MIL-101 (Fe).<sup>21</sup> However, this work intends to utilize the porous structure of MIL-101 (Fe) to provide additional pathways for gas molecules. The investigation of the crystal phase transition is not the focus of this work. MIL-101 (Fe)/GO has been used as catalyst and adsorbent for the water treatment processes.<sup>22,23</sup> To our best knowledge, it is the first time to synthesize MIL-101 (Fe)/GO composite fillers and investigate their effects on the membrane-based gas separation process. Therefore, MIL-101 (Fe)/GO composite fillers will be synthesized and incorporated into Pebax® 2533 matrix to prepare MMMs for CO<sub>2</sub>/N<sub>2</sub> separation in this work.

## 2. Experimental

### 2.1. Materials

Ferric chloride hexahydrate (FeCl<sub>3</sub>·6H<sub>2</sub>O), terephthalic acid (H<sub>2</sub>BDC), *N,N*-dimethylformamide (DMF), and Graphene oxide powder (GO), 15–20 sheets, 4–10% edge-oxidized were purchased from Sigma Aldrich (Poznań, Poland). Methanol (99.8%) and ethanol (99.8%) were purchased from Alchem Grupa Sp. z o.o. (Toruń, Poland). Pebax® 2533 was kindly provided by Arkema (Colombes, France). Hydrophobic PVDF (polyvinylidene difluoride) membrane (Durapore Membrane Filter, 0.22 μm) were purchased from Merck (Darmstadt, Germany). CO<sub>2</sub> (99.999%) and N<sub>2</sub> (99.999%) were purchased from Air Products Sp. z o.o. (Siewierz, Poland).

### 2.2. Synthesis of MIL-101 (Fe) and MIL-GO fillers

MIL-101 (Fe) fillers were synthesized by using a solvothermal method.<sup>22</sup> 2.922 g ferric chloride hexahydrate and 0.854 g



terephthalic acid were dissolved in 60 mL DMF by stirring at room temperature for 1 h. Subsequently, the mixture solution was transferred into a Schott bottle and placed in oven at 120 °C for 24 hours. After cooling down to room temperature, the obtained composite fillers were collected by centrifugation and washed repeatedly with DMF and ethanol. Finally, the obtained composite fillers were dried in oven at 70 °C overnight and activated at 150 °C for 10 h.

To synthesize MIL-GO composite fillers, 1.461 g ferric chloride hexahydrate and 0.427 g terephthalic acid were dissolved in 30 mL DMF by stirring at room temperature for 1 h. Subsequently, a specific amount of GO was dispersed into 6 mL ethanol by using ultrasonic bath for half an hour. Then, the prepared GO dispersion was added into the above solution. After the complete mixing in the ultrasonic bath for half an hour, the mixture solution was transferred into Schott bottle and placed in oven at 120 °C for 24 hours. When the reaction is completed, the Schott bottle was cooled down to room temperature. The obtained composite fillers were collected by centrifugation and washed repeatedly with DMF and ethanol. Finally, the obtained composite fillers were dried in oven at 70 °C overnight and activated at 150 °C for 10 h. The content of GO in the composite filler was calculated by using the mass ratio of GO to GO, ferric chloride hexahydrate, and terephthalic acid. In this work, MIL-GO composite fillers containing 2 wt%, 5 wt%, and 10 wt% of GO were prepared and designated as MIL-GO-2, MIL-GO-5, and MIL-GO-10, respectively.

### 2.3. Membrane preparation

To prepare pristine Pebax® 2533/PVDF thin film membranes and MMMs, the casting solution of Pebax® 2533 solution (6 wt%) containing a specific amount of fillers were prepared firstly. The detailed procedure of the Pebax® 2533 solution preparation can be found elsewhere.<sup>13</sup> Pristine Pebax® 2533/PVDF membrane and MMMs were fabricated by casting a certain amount of the prepared solutions on the PVDF support by using the automatic film applicator. The casting knife with a 0.4 mm slit was used in this work. The casting speed is maintained at 10 mm s<sup>-1</sup> for the preparation of all membranes. The freshly cast membranes were firstly dried at 25 °C for 24 h then further dried in an oven at 60 °C for 8 h to completely evaporate solvent. The composition of the selective layer, and

the codes of the prepared membranes were listed in Table 1. In the nomenclature of the prepared membranes, P represents Pebax® 2533, M represents MIL-101 (Fe), G represents GO. For instance, 9-PMG2 presents Pebax-based MMMs containing 9.1 wt% MIL-GO-2 composite filler.

### 2.4. Material characterization

The morphologies of the synthesized MIL-101 (Fe), MIL-GO composite fillers and membranes were characterized by using Scanning Electron Microscope (SEM), LEO 1430 VP microscope (Leo Electron Microscopy Ltd, Cambridge, UK).

FTIR-ATR spectra of the synthesized MIL-101 (Fe), MIL-GO composite fillers and membranes were obtained by using Nicolet iS10 (Thermal Scientific, Waltham, USA) spectrometer in the range of 400–4000 cm<sup>-1</sup>.

XRD analyses for the synthesized MIL-101 (Fe), and MIL-GO composite fillers were conducted by utilizing Philips X'Pert (Malvern Panalytical, Malvern, UK). The transmission mode and 2θ range of 5–80° were applied.

The nitrogen adsorption/desorption measurements for the synthesized MIL-101 (Fe), and MIL-GO composite fillers were conducted at –195.7 °C via Gemini VI (Micromeritics Instrument Corp., Norcross, GA, USA). All samples were degassed for 6 h at 110 °C before the measurements.

Thermal properties of the synthesized MIL-101 (Fe), MIL-GO composite fillers and membranes were analyzed by using a Jupiter STA 449 F5 (Netzsch, Germany) thermogravimetric analyzer. TGA measurements were conducted from 25 °C to 950 °C under the nitrogen atmosphere.

### 2.5. Gas permeation measurements

The gas permeation tests for pure gas of CO<sub>2</sub>, and N<sub>2</sub>, were conducted at 2–4 bar and 20 °C by using a home-made equipment (Fig. 1).<sup>24</sup> The effective membrane area in the module is 2.11 cm<sup>2</sup>. Each membrane was measured 3 times for a better accuracy. The gas flow rate was recorded by using a bubble flow meter. The gas permeability *P* (1 barrer = 10<sup>-10</sup> cm<sup>3</sup> (STP) cm cm<sup>-2</sup> s<sup>-1</sup> cmHg<sup>-1</sup>) was calculated by using eqn (1):<sup>16</sup>

$$P = Ql/\Delta pA \quad (1)$$

**Table 1** Compositions and fabrication conditions of the prepared Pebax-based MMMs

Membrane	Composition of selective layer (wt%)		
	Pebax® 2533	Filler type	Filler content
Pebax® 2533/PVDF	100	—	0
9-PM/PVDF	90.9	MIL-101 (Fe)	9.1
9-PMG2/PVDF	90.9	MIL-GO-2	9.1
9-PMG5/PVDF	90.9	MIL-GO-5	9.1
9-PMG10/PVDF	90.9	MIL-GO-10	9.1
5-PMG2/PVDF	95.2	MIL-GO-2	4.8
13-PMG2/PVDF	87.0	MIL-GO-2	13.0

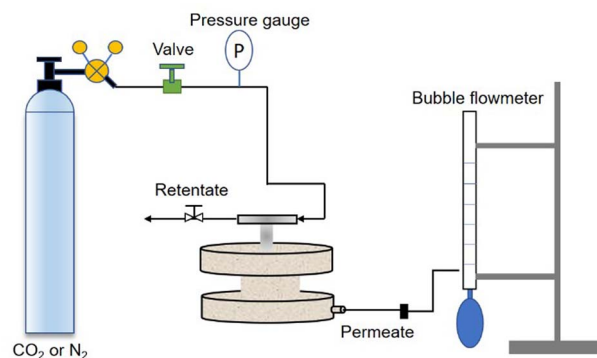


**Fig. 1** The illustration of the laboratory permeation system for gas permeance measurements of flat sheet membranes.





where  $Q$  is the gas flow rate ( $\text{cm}^3(\text{STP}) \text{s}^{-1}$ );  $l$  is the membrane thickness (cm);  $\Delta p$  is the pressure difference across the membrane (cmHg);  $A$  is the active membrane area ( $\text{cm}^2$ ).<sup>4,16</sup>

The ideal selectivity  $\alpha_{12}$  was calculated by using eqn (2):<sup>13</sup>

$$\alpha_{12} = P1/P2 \quad (2)$$

### 3. Results and discussion

#### 3.1. Characterization of MIL-101 (Fe) and MIL-GO fillers

SEM images of GO, MIL-101 (Fe), MIL-GO-2, MIL-GO-5, and MIL-GO-10 are shown in Fig. 2. The flakes of graphene sheets were observed for GO (Fig. 2(a and f)). MIL-101 (Fe) and MIL-GO-2 showed a regular octahedral structure (Fig. 2(b, c, g and h)). The crystal structure of MIL-101 (Fe) was perfectly preserved with addition of a small amount (2 wt%) of GO. However, with the increase of GO amount (5 and 10 wt%) in the MIL-GO composites, it can be clearly seen that the MIL-101 (Fe) particles possessing a spherical shape instead of the octahedral structure were formed on the GO sheets, which indicates the distortion of MIL-101 (Fe) crystals. The MIL-101 (Fe) crystal size in MIL-GO-5, and MIL-GO-10 composites is much smaller than that in pristine MIL-101 (Fe), and MIL-GO-2 composite (Fig. 2(d, e, i and j)). According to the estimation from SEM images, the MIL-101 (Fe) crystal size in pristine MIL-101 (Fe), and MIL-GO-2 composite is 0.6–1.0  $\mu\text{m}$ , and 0.9–2.0  $\mu\text{m}$ , respectively. While the MIL-101 (Fe) crystal size in MIL-GO-5, and MIL-GO-10 composites is 0.15–0.30  $\mu\text{m}$ . This is because the GO sheets restrained the possible growth orientation of MIL-101 (Fe) crystal, which results in the formation of smaller and irregular MIL-101 (Fe) crystals on the surface of GO sheets.<sup>22</sup>

The XRD patterns of GO, MIL-101 (Fe), MIL-GO-2, MIL-GO-5, and MIL-GO-10 are presented in Fig. 3. The characteristic peaks of the synthesized MIL-101 (Fe) in the range of 5–25° were in good agreement with these of the previously reported MIL-101 (Fe),<sup>22,25</sup> indicating the good crystallinity of the prepared MIL-101 (Fe). Specifically, the observed peaks at 2 theta values of 5.81, 9.11, 9.50, 18.94, and 22.15° correspond to the (111), (220),

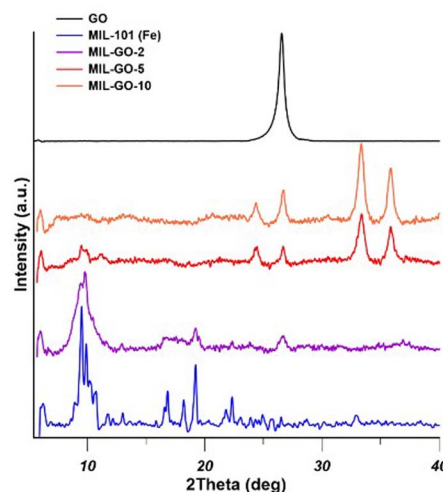


Fig. 3 XRD patterns of GO, MIL-101 (Fe), and MIL-GO fillers.

(311), (511), and (825) crystal planes.<sup>22</sup> From the XRD patterns of MIL-GO-2, and MIL-GO-5, it can be seen the characteristic peaks of MIL-101 (Fe) were observed, while the intensity of the characteristic peaks of MIL-101 (Fe) decreased, indicating the crystal structure of MIL-101 (Fe) was preserved in at low content of GO. However, the characteristic peaks of MIL-101 (Fe) disappeared from the XRD pattern of MIL-GO-10. This is because the high GO content might limit the crystallization of MIL-101 (Fe) crystal and result in the distortion of MIL-101 (Fe) induced by the dispersed GO,<sup>26,27</sup> since most peaks from MIL-101 (Fe) disappeared except some new peaks produced in the composite filler and the peaks from GO (Fig. 3). Similar changes of XRD patterns were observed in MIL-88A(Fe)/GO,<sup>27</sup> and MOF-5/GO.<sup>28</sup> In this work, the characteristic peak for GO is at 2 theta value of 26° which represents (002) of the applied multi-layer GO with interlayer spacing of 0.336 nm according to the Bragg's law.<sup>29</sup> The typical characteristic peak of GO at 2 theta value of 10–12° was not observed since the amount of oxygen groups mainly located at the edges in the purchased GO sample is low.<sup>30</sup>

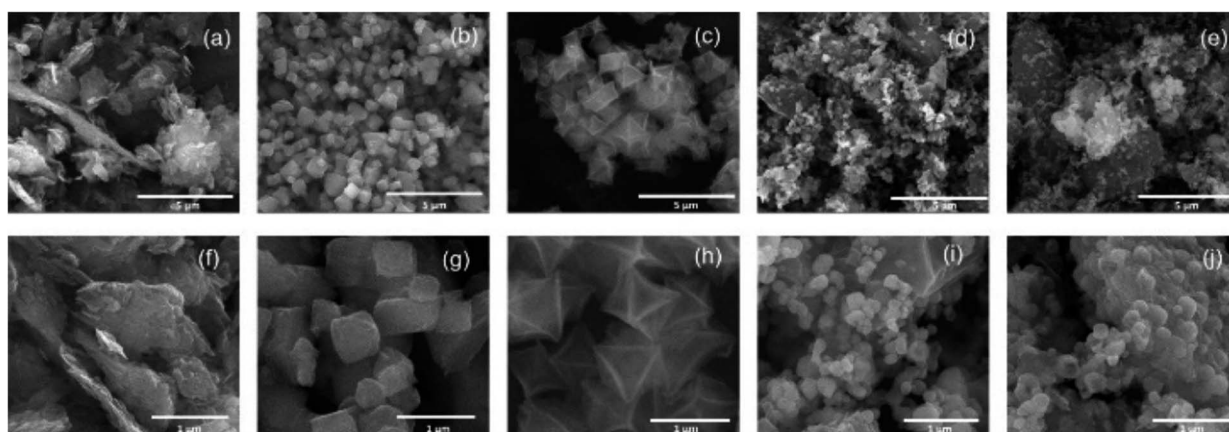


Fig. 2 SEM images of GO (a and f), MIL-101 (Fe) (b and g), MIL-GO-2 (c and h), MIL-GO-5 (d and i), and MIL-GO-10 (e and j).



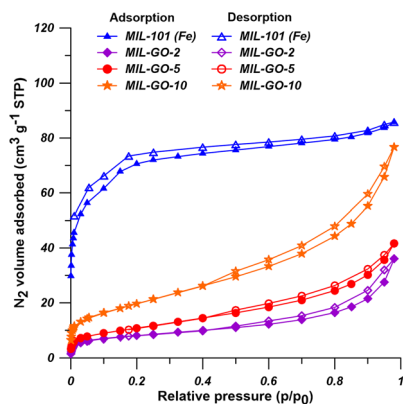


Fig. 4  $N_2$  adsorption/desorption isotherms of MIL-101 (Fe), MIL-GO-2, MIL-GO-5, and MIL-GO-10.

Fig. 4 and Table 2 show the  $N_2$  adsorption/desorption isotherms and the textural properties of MIL-101 (Fe), MIL-GO-2, MIL-GO-5, and MIL-GO-10. According to IUPAC classification, the  $N_2$  adsorption/desorption isotherms of the prepared MIL-101 (Fe) are ascribed to I-type adsorption isotherms indicating the presence of microporous structure in MIL-101 (Fe). While the  $N_2$  adsorption/desorption isotherms of MIL-GO are assigned as II-type adsorption isotherms, implying the microporous and mesoporous structure in MIL-GO fillers.<sup>31</sup> The BET surface area of MIL-101 (Fe) is  $239 \text{ m}^2 \text{ g}^{-1}$  which is comparable to the reported ones.<sup>22,25</sup> Liu *et al.*<sup>22</sup> and Zhao *et al.*<sup>25</sup> found that the BET surface area of MIL-101 (Fe) is  $608 \text{ m}^2 \text{ g}^{-1}$  and  $199 \text{ m}^2 \text{ g}^{-1}$ , respectively. Zorainy *et al.*<sup>32</sup> found the BET surface area of MIL-101 (Cr) and mixed-metal MIL-101(Cr/Fe) is over  $2000 \text{ m}^2 \text{ g}^{-1}$ . Comparing with MIL-101 (Cr), the low BET surface area of the synthesized MIL-101 (Fe) could be attributed to the smaller crystal size of MIL-101 (Cr) than the synthesized MIL-101 (Fe). The texture properties and the crystal size of MIL-101 (Fe) are significantly influenced by the synthesis conditions.<sup>21</sup> In comparison to MIL-101 (Fe), the BET surface area, the total pore volume and the micropore volume decreased dramatically (Table 2), which can be ascribed to the coverage of MIL-101 (Fe) by nonporous GO sheets with low surface area.<sup>33</sup> Moreover, the mesopores were formed due to the addition of GO sheets in MIL-101 (Fe) synthesis process indicated by the presence of type H3 hysteresis loop in the  $N_2$  adsorption/desorption isotherms of MIL-GO fillers.<sup>34,35</sup> It was noticed that the BET surface area and total pore volume of MIL-GO composite filler increased slightly

when the GO content increased from 2 wt% to 10 wt%. Similar trend was observed by Liu *et al.*<sup>27</sup> In their work, the specific surface area of MIL-88A (Fe)/GO composite material increased with the increase of GO content since the addition of GO affects the crystallization process of MOF.<sup>27</sup>

Fig. 5 shows the TGA and DTG curves of GO, MIL-101 (Fe), and MIL-GO composites fillers. The total weight loss for GO is 8.6%, resulting from the decomposition of the epoxy groups and carboxylic groups, which indicated the high thermal stability of GO. For MIL-101 (Fe), the weight loss at 30–100 °C could be attributed to the evaporation of the adsorbed water and ethanol. The weight loss occurred at 100–350 °C due to the removal of DMF molecules and the free terephthalates in the pores of MIL-101 (Fe). Finally, the significant weight loss occurred from 350 °C to 760 °C, which could be resulted from the decomposition of the organic ligands, resulting in the collapse of the frameworks.<sup>22,36</sup> The MIL-GO composites fillers shared the similar thermal behavior with MIL-101 (Fe). Comparing to the total weight loss of 66% and the temperature of complete decomposition at 760 °C for MIL-101 (Fe), MIL-GO-2 exhibited the total weight loss of 67% and the temperature of complete decomposition at 720 °C. However, with the increase of the GO content in the MIL-GO composite fillers, the total weight loss decreased while the temperature of complete decomposition increased. MIL-GO-10 showed the highest temperature of complete decomposition of 975 °C, but the lowest total weight loss of 45%. It is found that the synthesized MIL-101 (Fe), and MIL-GO composites fillers showed high thermal stability. Moreover, the addition of GO can further increase their thermal stability.

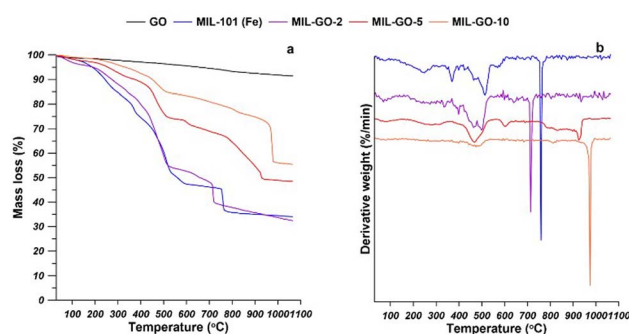


Fig. 5 TGA-DTG curves of GO, MIL-101 (Fe), and MIL-GO fillers.

Table 2 Textural properties of MIL-101 (Fe), MIL-GO-2, MIL-GO-5, and MIL-GO-10<sup>a</sup>

Samples	BET ( $\text{m}^2 \text{ g}^{-1}$ )	$V_{\text{Total}}$ ( $\text{cm}^3 \text{ g}^{-1}$ )	$V_{\text{Micro}}$ ( $\text{cm}^3 \text{ g}^{-1}$ )	$V_{\text{Meso}}$ ( $\text{cm}^3 \text{ g}^{-1}$ )	Average pore diameter (nm)
MIL-101 (Fe)	239	0.186	0.109	0.077	1.24
MIL-GO-2	29	0.070	0.002	0.068	2.95
MIL-GO-5	40	0.076	0.004	0.072	3.31
MIL-GO-10	72	0.139	0.007	0.132	3.27

<sup>a</sup>  $V_{\text{Micro}}$ : micropore volume calculated by using the *t*-plot method.  $V_{\text{Meso}}$ : mesopore volume calculated from the subtraction of micropore volume from total pore volume.



The FTIR of GO, MIL-101 (Fe), and MIL-GO composites fillers are presented in Fig. 6. For GO, the peaks at  $3400\text{ cm}^{-1}$ ,  $2120\text{ cm}^{-1}$ , and  $1720\text{ cm}^{-1}$  could be related to the bands of  $-\text{OH}$  and  $\text{C}=\text{O}$  in carboxyl groups. The peak at  $1618\text{ cm}^{-1}$  could be related to  $-\text{OH}$  in the absorbed water.<sup>22</sup> For MIL-101 (Fe) and MIL-GO composites fillers, the peak at  $542\text{ cm}^{-1}$  was related to the Fe-O bond, and the peaks at  $746\text{ cm}^{-1}$  and  $1018\text{ cm}^{-1}$  were assigned to C-H bending in benzene and C-O-C vibration, respectively. Peaks at  $1387\text{ cm}^{-1}$  and  $1599\text{ cm}^{-1}$  could be originated from the symmetric and asymmetric vibrations of carboxyl bond ( $-\text{COO}-$ ). The peak at  $1653\text{ cm}^{-1}$  might be originated from the  $\text{C}=\text{O}$  bond in carboxyl group. The observed characteristic peaks for the synthesized MIL-101 (Fe) are in agreement with other reported literature.<sup>22,23</sup> The characteristic peaks of MIL-101 (Fe) were mostly found in the MIL-GO composite fillers, which indicates the successful formation of MIL-101 (Fe) with the presence of GO. However, the difference of IR spectra between MIL-101 (Fe) and MIL-GO composite can be observed. For example, the intensity of peak at  $1653\text{ cm}^{-1}$  decreased as the GO content in MIL-GO composite increased. This is because the oxygen functional groups on GO surface can react with the carboxyl groups on MIL-101 (Fe), resulting in the reduction of  $\text{C}=\text{O}$  bonds of free carboxyl groups. The red shift of peaks  $1599\text{ cm}^{-1}$  and  $542\text{ cm}^{-1}$  was observed due to the interference of the GO characteristic peaks and the stronger interaction between MIL-101 (Fe) and GO.<sup>23</sup>

### 3.2. Characterization of MMMs

The morphology of cross-section and top surface of pristine Pebax® 2533 membrane and MMMs containing different types of fillers was shown by SEM images presented in Fig. 7. The surface of pristine Pebax® 2533 membrane is smooth while the surface became rough after the incorporation of MIL-101 (Fe) and MIL-GO composite fillers into the polymer matrix. However, the MMMs containing 9.1 wt% MIL-GO-2 and MIL-GO-5 possessed less rough surface than the MMMs containing 9.1 wt% MIL-101 (Fe) and MIL-GO-10, indicating the more

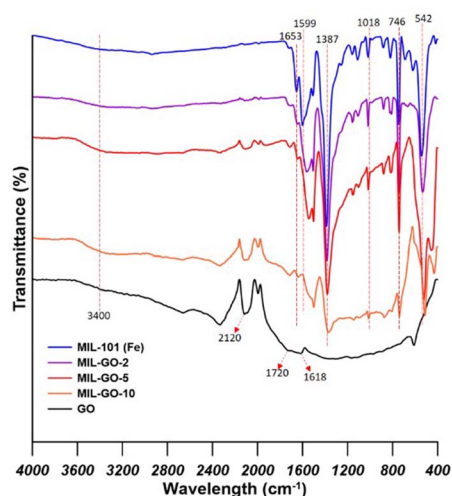


Fig. 6 FTIR spectra of GO, MIL-101 (Fe), and MIL-GO fillers.

desirable dispersion of MIL-GO-2 and MIL-GO-5 in polymer matrix. Most importantly, no defects were observed on the surfaces of all the prepared membrane. As shown in the cross-section of the prepared MMMs, there were no visible filler agglomeration nor voids at the interface between fillers and polymer matrix, which indicates the homogenous distribution of MIL-101 (Fe) and MIL-GO composite fillers in polymer matrix.

The morphology of cross-section and top surface of pristine Pebax® 2533 membrane and MMMs containing different content of MIL-GO-2 composite filler was shown by SEM images presented in Fig. 8. The surfaces of MMMs became rougher with the increasing content of MIL-GO-2 composite filler. As shown in the cross-section of the prepared MMMs, the MIL-GO-2 composite fillers were dispersed homogeneously in polymer matrix at low filler content. No interfacial voids and visible agglomerates were observed. However, the filler agglomeration was observed when the filler content reached 13.0 wt%. Nevertheless, no interfacial voids were observed in the prepared MMMs.

The thermal properties of the prepared Pebax® 2533/PVDF MMMs were investigated by using TGA and DTG analysis. As it is shown in Fig. 9, the prepared MMMs exhibited similar TGA curves and the thermal weight loss rate curves, comparing to the pristine Pebax® 2533/PVDF membranes. Two main steps of weight loss were observed for the pristine Pebax® 2533/PVDF membranes and the prepared MMMs. The first step of weight loss occurred between  $350\text{ }^{\circ}\text{C}$  to  $450\text{ }^{\circ}\text{C}$ , which is resulted from the decomposition of polymer chains from Pebax® 2533.<sup>24</sup> The second step of weight loss occurred in the temperature range of  $438\text{ }^{\circ}\text{C}$ – $500\text{ }^{\circ}\text{C}$ , mainly due to the degradation of PVDF polymer chains.<sup>37</sup> It can be found that the incorporation of the prepared fillers into Pebax® 2533/PVDF composite MMMs did not change their thermal properties significantly. However, taking into consideration of the first DTG peak temperature which indicates the maximum rate of the weight loss in Pebax, it was found that the first DTG peak temperature increased from  $415\text{ }^{\circ}\text{C}$  for pristine Pebax® 2533/PVDF membranes to  $425\text{ }^{\circ}\text{C}$ – $430\text{ }^{\circ}\text{C}$  for the prepared MMMs containing 9 wt% of different types of fillers. MMMs containing 9 wt% of MIL-GO-2 composite filler showed the highest DTG peak temperature of  $430\text{ }^{\circ}\text{C}$ . It was also found the with the increase of MIL-GO-2 composite filler, the first DTG peak temperature increased. However, the second DTG peak temperature of MMMs remained the same as the pristine Pebax® 2533/PVDF membranes, since the prepared fillers were incorporated into the Pebax selective layer. The higher DTG peak temperature in the prepared MMMs indicated the slight enhancement of thermal stability of MMMs due to the limited thermal motion of polymer chains induced by the incorporated fillers.<sup>17</sup>

The FT-IR spectra of PVDF support, the pristine Pebax® 2533/PVDF thin film membranes and the prepared MMMs containing 9.1 wt% of MIL-101 (Fe), MIL-GO-2, MIL-GO-5, or MIL-GO-10 were shown in Fig. 10a. As can be seen, after the formation of Pebax selective layer on PVDF support, the characteristic peaks for PVDF disappeared, e.g., the peaks at  $1403\text{ cm}^{-1}$  corresponding to the C-H stretching vibration,  $1181\text{ cm}^{-1}$



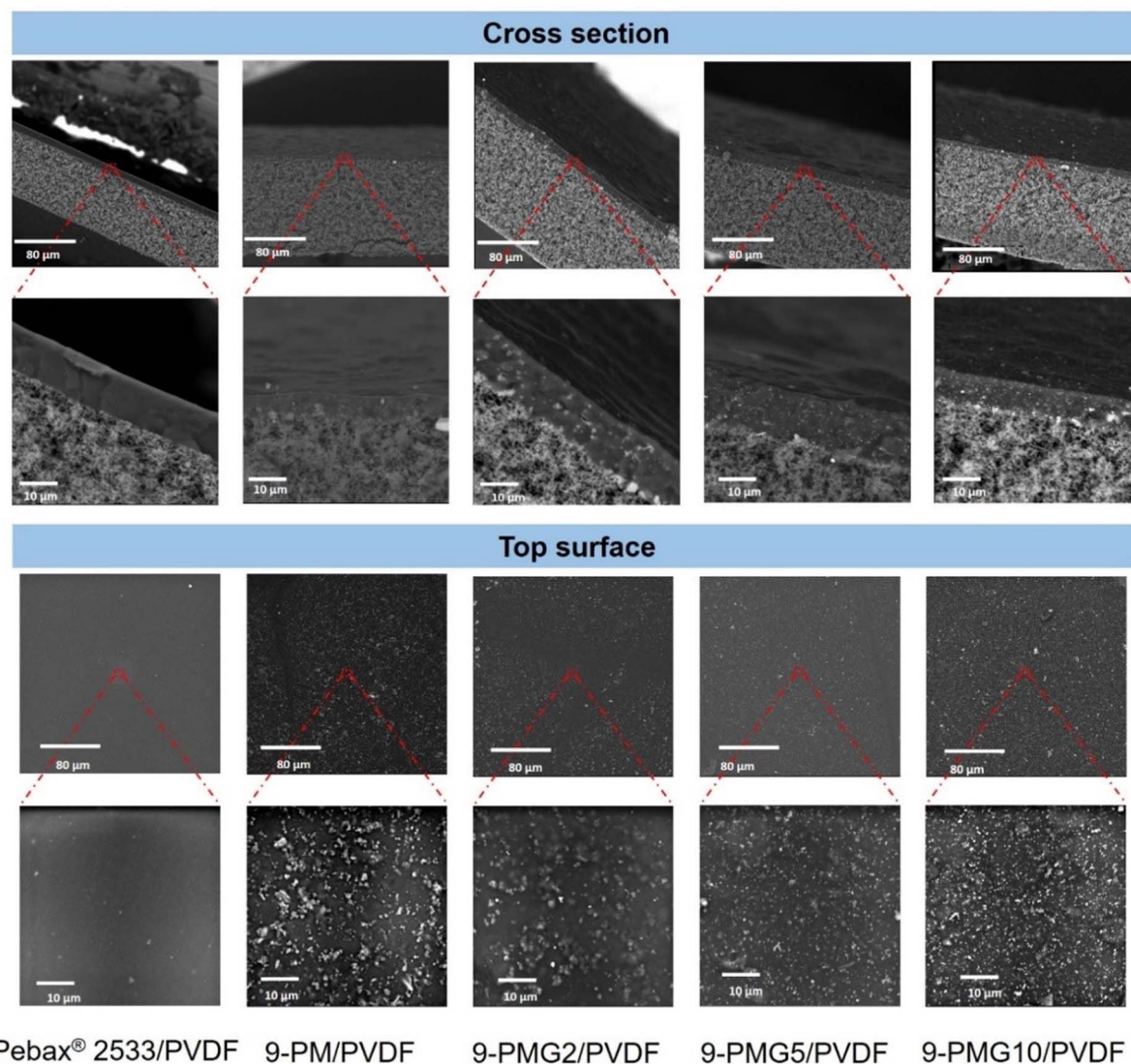


Fig. 7 SEM images of cross-section and surface of the pristine Pebax® 2533 membrane; MMMs with 9.1 wt% of MIL-101 (Fe); MIL-GO-2; MIL-GO-5; and MIL-GO-10, respectively.

and  $1275\text{ cm}^{-1}$  corresponding to the stretching of C–F bonds,<sup>38</sup> and  $764\text{ cm}^{-1}$  attributed to the bending of C–F bonds.<sup>39</sup> On the contrary, the characteristic peaks for Pebax were generated, *e.g.*, the peaks at  $1109\text{ cm}^{-1}$ ,  $3298\text{ cm}^{-1}$ ,  $1734\text{ cm}^{-1}$ , and  $1640\text{ cm}^{-1}$  which were ascribed to the C–O–C bond from the PEO segment, the –N–H– stretching vibration, out-of-plane H–N–C=O vibration of amide, and O–C=O stretching vibration of carboxylic acid, respectively.<sup>24</sup> The peaks at  $746\text{ cm}^{-1}$  and  $1018\text{ cm}^{-1}$  which were related to the C–H bending in benzene and C–O–C vibration from MIL-101 (Fe) were generated in FT-IR spectra of the prepared MMMs. Moreover, with the increase of GO content in MIL-GO composite fillers, the intensity of the peak at  $747\text{ cm}^{-1}$  corresponding to the C–H bending in benzene decreased, while the intensity of the peak at  $1019\text{ cm}^{-1}$  corresponding to C–O–C vibration was the highest in MMMs containing MIL-GO-2 composite filler, which indicates the interaction between MIL-101 (Fe) and GO. These changes in intensity of peaks at  $746$

$\text{cm}^{-1}$  and  $1018\text{ cm}^{-1}$  observed from the FT-IR spectra for MMMs are consistent with that in the FT-IR spectra for the prepared fillers. The FT-IR spectra of the prepared MMMs containing various amount of MIL-GO-2 were presented in Fig. 10b. It was found that the intensity of characteristic peaks of MIL-GO-2 at  $746\text{ cm}^{-1}$  and  $1018\text{ cm}^{-1}$  increased with the increase of MIL-GO-2 composite filler content in MMMs.

### 3.3. Evaluation of gas separation performance of MMMs

**3.3.1. The effect of filler types.** Single gas permeation measurements were conducted to estimate the gas permeation performance of the prepared MMMs. In this study, permeability of pure gas ( $\text{CO}_2$  and  $\text{N}_2$ ) was determined at 2 bar and  $20\text{ }^\circ\text{C}$ . The effect of different fillers, *e.g.* MIL-101 (Fe), MIL-GO-2, MIL-GO-5, and MIL-GO-10 on the permeability of  $\text{CO}_2$  and  $\text{N}_2$ , and the ideal selectivity of MMMs was shown in Fig. 11. It can be seen that the incorporation of fillers into Pebax® 2533 significantly



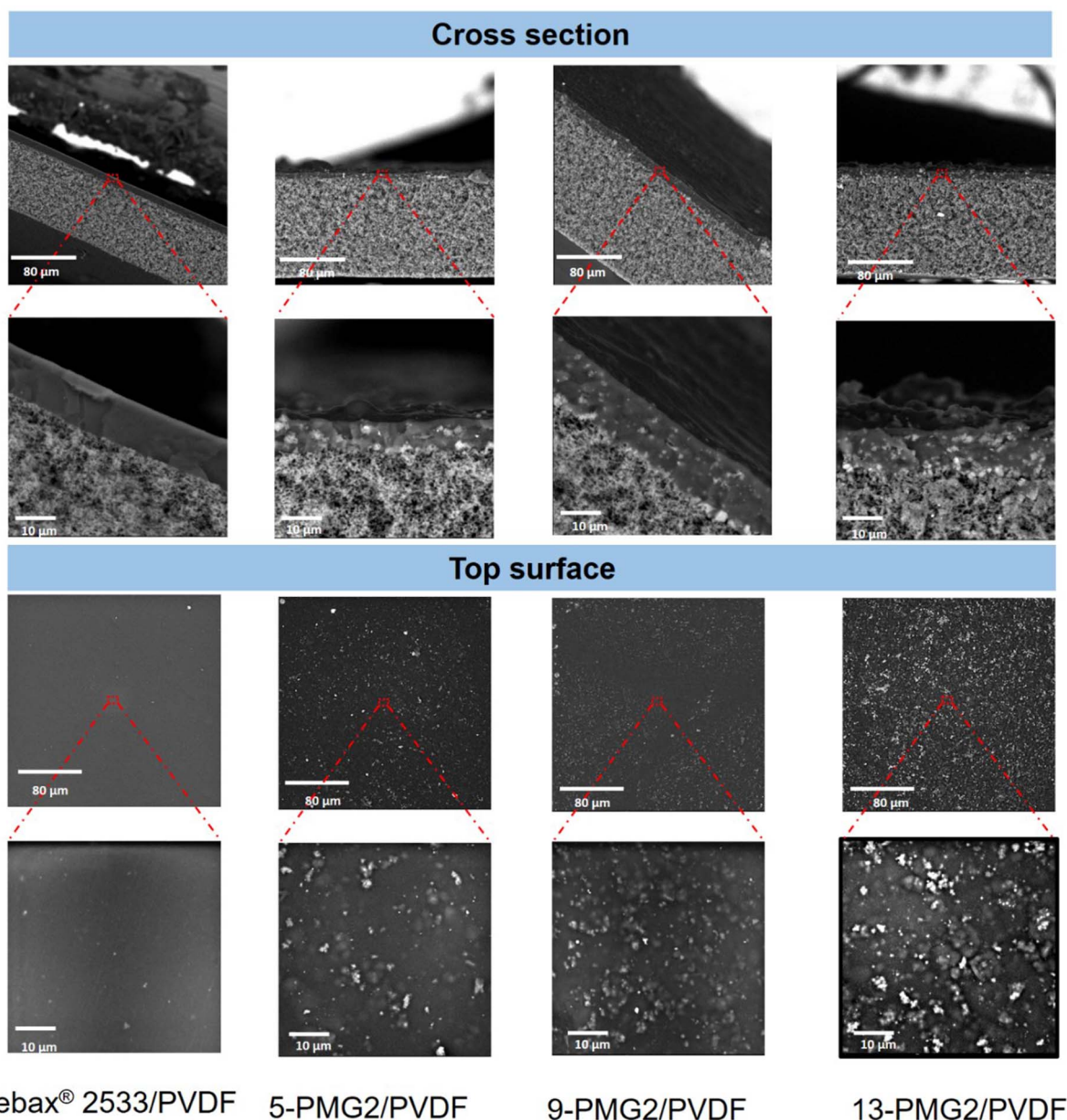


Fig. 8 SEM images of cross-section and surface of the pristine Pebax® 2533 membrane; MMMs with 4.8 wt%, 9.1 wt%, and 13.0 wt% of MIL-GO-2 composite filler.

influenced the gas transport properties of the prepared membranes. MMMs containing 9.1 wt% MIL-101 (Fe) exhibited  $\text{CO}_2$  permeability equal to 323 barrer ( $1 \text{ barrer} = 10^{-10} \text{ cm}^3 \text{ (STP) cm cm}^{-2} \text{ s}^{-1} \text{ cmHg}^{-1}$ ) which is 59% higher than that of pristine Pebax membranes. While the  $\text{CO}_2/\text{N}_2$  ideal selectivity equal to 17 was barely changed. The increase of  $\text{CO}_2$  permeability can be explained by the following reasons. The incorporation of MIL-101 (Fe) disrupted the arrangement of polymer chains, resulting in the easier transport of gas molecules through membranes. Moreover, MIL-101 (Fe) provided additional free volume for gas molecules transport due to the high porosity and flexible framework of MIL-101 (Fe), which facilitated the transport of  $\text{CO}_2$  through MMMs.<sup>17,40</sup> The ideal

selectivity was slightly influenced after the incorporation of MIL-101 (Fe) due to the simultaneous enhancement of gas permeability of  $\text{CO}_2$  and  $\text{N}_2$ , resulting from the porous structure and larger pore diameter (Table 2) than the diameter of  $\text{CO}_2$  (0.33 nm) and  $\text{N}_2$  (0.36 nm).

The incorporation of MIL-101 (Fe) into the Pebax® 2533 membranes has demonstrated the positive effect on the  $\text{CO}_2$  permeability without the sacrifice of  $\text{CO}_2/\text{N}_2$  ideal selectivity. To obtain the simultaneous enhancement of  $\text{CO}_2$  permeability and  $\text{CO}_2/\text{N}_2$  ideal selectivity, the MIL-GO composite fillers were synthesized and incorporated into Pebax® 2533 membranes due to the porous structure of MIL-101 (Fe) and high respect ratio of GO nanosheets. The effect of the mass ratio of GO to





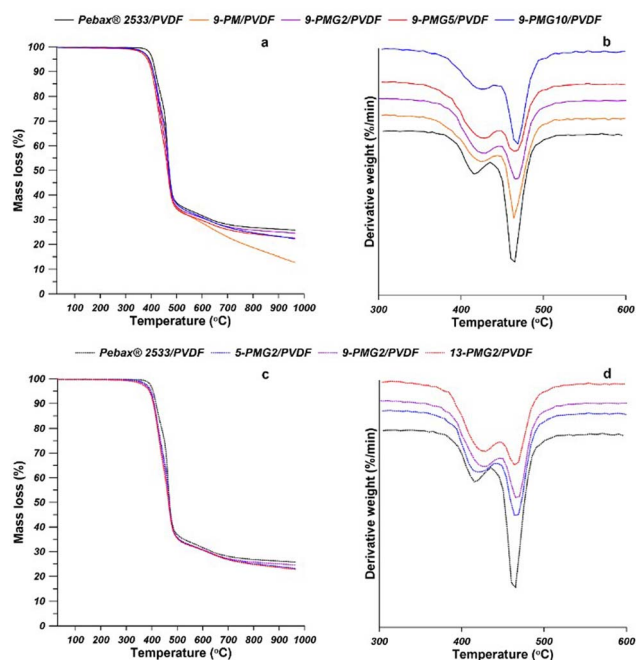


Fig. 9 TGA and DTG curves of MMMs containing 9 wt% of different types of fillers (a and b) and MMMs containing different content of MIL-GO-2 filler (c and d).

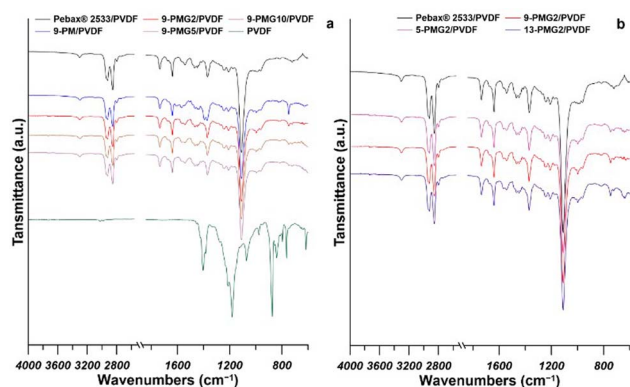


Fig. 10 FT-IR spectra of MMMs containing 9 wt% of different types of fillers (a) and MMMs containing different content of MIL-GO-2 filler (b).

MIL-GO composite filler on the gas permeation properties of MMMs was investigated by using the  $\text{CO}_2$  permeability and  $\text{CO}_2/\text{N}_2$  ideal selectivity of MMMs containing 9.1 wt% of MIL-GO-2, MIL-GO-5, or MIL-GO-10. It can be seen that the presence of MIL-GO-2 and MIL-GO-5 in MMMs showed enhancing effects on the  $\text{CO}_2$  permeability and  $\text{CO}_2/\text{N}_2$  ideal selectivity. On the contrary, the incorporation of MIL-GO-10 showed adverse effects on the gas separation properties of MMMs. In comparison to the pristine Pebax® 2533 membranes, the  $\text{CO}_2$  permeability (equal to 303 barrer) of MMMs containing 9.1 wt% MIL-GO-2 was 50% higher. Moreover, the  $\text{CO}_2/\text{N}_2$  ideal selectivity (equal to 24) of MMMs containing 9.1 wt% MIL-GO-2 was 41% higher than that of pristine Pebax® 2533 membranes and the highest among the prepared MMMs. However, the MMMs

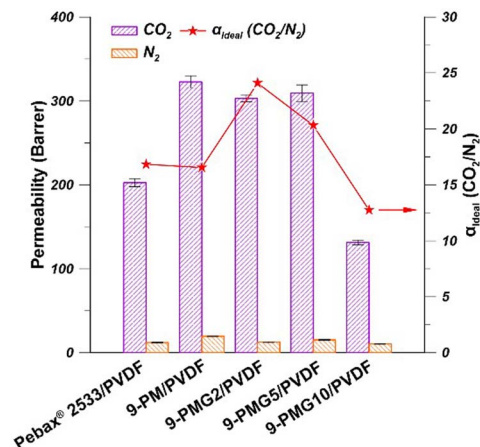


Fig. 11 Gas permeability and ideal selectivity of MMMs containing various types of fillers (filler content 9.1 wt%, experimental condition: 20 °C and 2 bar, the red line indicates only the trend of the ideal selectivity change).

containing 9.1 wt% MIL-GO-10 showed worse gas separation performance than that of pristine Pebax® 2533 membranes, evidenced by the lower  $\text{CO}_2$  permeability (equal to 131 barrer) and the lower  $\text{CO}_2/\text{N}_2$  ideal selectivity (equal to 13).

In order to account for the high  $\text{CO}_2$  permeability and  $\text{CO}_2/\text{N}_2$  ideal selectivity, it is crucial to elucidate the gas molecules transporting mechanism in MMMs containing MIL-GO-2 composite fillers. Solution diffusion model is mainly used as the transport mechanism for gas molecules in the prepared Pebax-based MMMs.<sup>19,41</sup> The incorporation of MIL-GO-2 composite filler into Pebax® 2533 membranes could affect the solubility and diffusivity of gas molecules in the prepared MMMs, resulting in the high  $\text{CO}_2$  permeability and  $\text{CO}_2/\text{N}_2$  ideal selectivity. First of all, the porous structure of MIL-101 (Fe) could increase the diffusion of gas molecules ( $\text{CO}_2$  and  $\text{N}_2$ ). Second, the incorporation of MIL-GO-2 could induce the additional free volume and the rearrangement of polymer chain packing in the MMMs, which facilitates the transport of gas molecules ( $\text{CO}_2$  and  $\text{N}_2$ ).<sup>40</sup> These two factors result in the enhancement of permeability of  $\text{CO}_2$  and  $\text{N}_2$  after the incorporation of MIL-GO-2 into Pebax® 2533 membranes (Fig. 11). However, the enhancement of  $\text{CO}_2$  permeability was more significant than the enhancement of the  $\text{N}_2$  permeability due to the smaller kinetic diameter of  $\text{CO}_2$  (0.33 nm) than that of  $\text{N}_2$  (0.36 nm). Third, the polar functional groups present in GO improved the affinity of  $\text{CO}_2$  to MIL-GO-2 composite filler, which increased the solubility of  $\text{CO}_2$  in MMMs due to the higher condensability of  $\text{CO}_2$ . The critical temperature of  $\text{CO}_2$  (304.2 K) is higher than that of  $\text{N}_2$  (126.1 K), resulting in higher condensability and solubility of  $\text{CO}_2$  in MMMs.<sup>19,42</sup> Last but not least, the tortuous diffusion pathways were formed by GO nanosheets due to their high aspect ratio, which significantly increased the diffusional resistance for larger  $\text{N}_2$  molecules rather than smaller  $\text{CO}_2$  molecules.<sup>17,43</sup> Moreover, the inter-distance between GO nanosheets is 0.34 nm, which allowed the easier transport of smaller  $\text{CO}_2$  molecules.<sup>43</sup> Based on the



above discussion on the effects of MIL-GO-2 on the gas molecules transporting mechanism in MMMs, the increased CO<sub>2</sub>/N<sub>2</sub> ideal selectivity was mainly resulted from the synergistic effect of MIL-101 (Fe) and GO. The porous structure of MIL-GO-2, the additional free volume in MMMs and the higher affinity to CO<sub>2</sub> of MIL-GO-2 strongly enhanced the CO<sub>2</sub> permeability rather than N<sub>2</sub> permeability. The highly tortuous diffusion paths and the inter-distance between GO nanosheets inhibited the N<sub>2</sub> transport through MMMs. These factors collectively result in the increased CO<sub>2</sub>/N<sub>2</sub> ideal selectivity.

When MIL-GO-10 containing higher GO ratio was incorporated into Pebax® 2533 membranes, the CO<sub>2</sub> permeability decreased dramatically and the N<sub>2</sub> permeability decreased slightly (Fig. 11). The reduction of gas permeability in MMMs containing MIL-GO-10 could be related to the decreased porosity and GO behavior of MIL-GO-10 composite filler. Casadei *et al.*<sup>44</sup> reported that the incorporation of GO into Pebax® 2533 membranes substantially decreased the permeability of CO<sub>2</sub> and N<sub>2</sub> since GO nanosheets created high tortuosity of diffusion path due to their high aspect ratio and low intrinsic permeability.<sup>44</sup> Moreover, it is reported that the stacked and folded morphology of GO sheets in MMMs could create the dead end zone and barrier structures, impairing the gas permeability.<sup>18</sup> According to the above discussion, the probable pathways of gas molecules in MMMs containing GO, MIL-101 (Fe) or MIL-GO composite fillers are visualized in Fig. 12.

**3.3.2. The effect of MIL-GO-2 content.** MMMs containing MIL-GO-2 demonstrated the best gas separation performance among the prepared MMMs. Therefore, the effect of MIL-GO-2 content on the gas permeability and ideal selectivity was investigated. As it is shown in Fig. 13, both the CO<sub>2</sub> permeability and CO<sub>2</sub>/N<sub>2</sub> ideal selectivity have been significantly increased, while the N<sub>2</sub> permeability was not influenced when the MIL-GO-2 content increased to 9.1 wt%. MMMs containing 9.1 wt% MIL-GO-2 composite filler exhibited the highest CO<sub>2</sub> permeability equal to 303 barrer and CO<sub>2</sub>/N<sub>2</sub> ideal selectivity equal to 24, which were 50% and 41% higher than those of pristine Pebax® 2533 membranes, respectively. The high gas separation performance of MMMs containing 9.1 wt% MIL-GO-2 composite filler was attributed to the multiple effects of the porous structure of MIL-GO-2, the additional free volume in MMMs, the higher affinity to CO<sub>2</sub> of MIL-GO-2, the highly tortuous diffusion paths and the inter-distance between GO nanosheets. More details about the analysis of gas transport

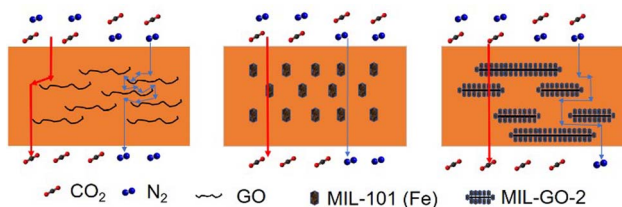


Fig. 12 Schematic diagram of the possible gas transport path in MMMs containing GO, MIL-101(Fe), or MIL-GO-2 composite fillers.

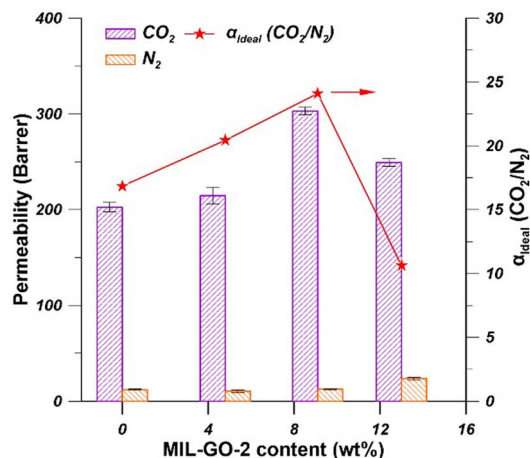


Fig. 13 Gas permeability and ideal selectivity of MMMs containing various amount of MIL-GO-2 (experimental condition: 20 °C and 2 bar).

mechanism in MMMs containing MIL-GO-2 composite filler can be found in Section 3.3.1. The further increase of MIL-GO-2 content in MMMs to 13.0 wt% resulted in the decrease of CO<sub>2</sub> permeability and CO<sub>2</sub>/N<sub>2</sub> ideal selectivity. This could be related to the over-loading of MIL-GO-2, resulting in filler agglomeration and rigidified interface between filler and polymer chains.<sup>43,45</sup>

**3.3.3. The effect of feed pressure.** The effect of feed pressure on gas permeability and CO<sub>2</sub>/N<sub>2</sub> ideal selectivity of pristine Pebax® 2533 membranes, MMMs containing 9.1 wt% MIL-101 (Fe), and MMMs containing 9.1 wt% MIL-GO-2 composite filler was also estimated. As shown in Fig. 14, the gas

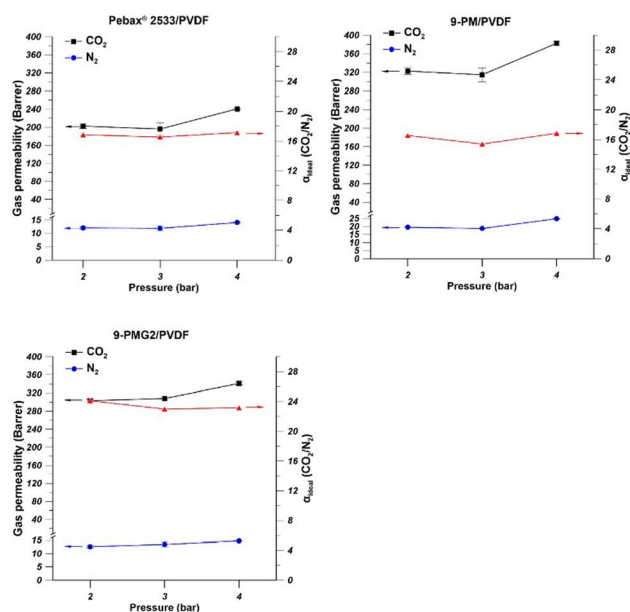


Fig. 14 Gas permeability and selectivity of pristine Pebax® 2533/PVDF membrane, MMMs containing 9.1 wt% of MIL-101 (Fe), and MMMs containing 9.1 wt% of MIL-GO-2 composite filler at various feed pressures.



permeability and CO<sub>2</sub>/N<sub>2</sub> ideal selectivity of these three types of membranes exhibited the same behavior. When the feed pressure increased from 2 bar to 4 bar, the gas permeability of CO<sub>2</sub> and N<sub>2</sub> increased, while the CO<sub>2</sub>/N<sub>2</sub> ideal selectivity was almost unchanged or slightly decreased. Similar results were reported by Guo *et al.*<sup>46</sup> In their research, ZIF-90@C<sub>3</sub>N<sub>4</sub> composite filler was synthesized and incorporated into Pebax® 1657 membranes for CO<sub>2</sub>/N<sub>2</sub> separation. It was found that both CO<sub>2</sub> permeability and N<sub>2</sub> permeability of MMMs containing 8 wt% ZIF-90@C<sub>3</sub>N<sub>4</sub> increased to a certain extent when the feed pressure increased from 2 bar to 6 bar. The ideal selectivity was almost unchanged due to the high-efficiency screening capabilities of composite fillers.<sup>46</sup> In comparison to the N<sub>2</sub> permeability, CO<sub>2</sub> permeability was enhanced more significantly with the increase of feed pressure. This is because CO<sub>2</sub> possesses a smaller kinetic diameter (0.33 nm) and higher condensability.<sup>19,42</sup> In Pebax® 2533-based membranes, the solution-diffusion mechanism is the main separation principle. When the feed pressure increased, the solubility and diffusion rate of the gas molecules in membranes will increase, resulting in the increase of gas permeability.<sup>46</sup> Comparing the CO<sub>2</sub> permeability of these three types of membranes, it can be found that the increment of CO<sub>2</sub> permeability for MMMs containing 9.1 wt% MIL-GO-2 composite filler was less than that for the other two types of membranes. These results indicated that the performance of MMMs containing 9.1 wt% MIL-GO-2 composite filler was less sensitive to the feed pressure change.

**3.3.4. Comparison with other Pebax-based MMMs reported in literature.** The gas separation performance of the prepared MMMs in this work was comparable with other reported Pebax-based MMMs for CO<sub>2</sub>/N<sub>2</sub> separation presented in Table 3. The prepared MIL-GO-2-Pebax® 2533/PVDF MMMs showed higher CO<sub>2</sub> permeability (303 barrer) than that of the reported Pebax-based MMMs containing singer filler (GO or MOFs),<sup>40,43,47–51</sup> along with the moderate CO<sub>2</sub>/N<sub>2</sub> ideal selectivity (24). The

moderate CO<sub>2</sub>/N<sub>2</sub> ideal selectivity obtained in this work can be explained by the type of Pebax matrix. Pebax® 2533 consists of poly(ethylene oxide)-PEO block (80 wt%) and polyamide-PA block (20 wt%), while the Pebax® 1657 consists of poly(ethylene oxide)-PEO block (60 wt%) and polyamide-PA block (40 wt%).<sup>48,52</sup> In comparison to the Pebax® 1657 membranes, the Pebax® 2533 membranes showed higher CO<sub>2</sub> permeability but lower CO<sub>2</sub>/N<sub>2</sub> ideal selectivity due to the higher content of PEO block which possesses high mobility of polyether chains and strong affinity to CO<sub>2</sub> molecules.<sup>52</sup> Therefore, the reported Pebax® 1657-based MMMs showed relatively higher CO<sub>2</sub>/N<sub>2</sub> ideal selectivity but relatively lower CO<sub>2</sub> permeability.<sup>40,43,47–51</sup> Taking into consideration the gas permeability and ideal selectivity, Pebax-based MMMs containing composite fillers<sup>17,18,46,53</sup> showed higher gas separation performance than those of the Pebax-based MMMs containing singer filler (GO or MOFs).<sup>40,43,47–51</sup> Therefore, the synthesis and utilization of 3D@2D composite filler demonstrated great potential in the preparation of high-performance MMMs for gas separation processes.

## 4. Conclusions

MIL-101 (Fe) and MIL-GO composites were successfully synthesized and used as fillers for the preparation of Pebax® 2533/PVDF thin film MMMs for CO<sub>2</sub>/N<sub>2</sub> separation. The crystal structure of MIL-101 (Fe) and MIL-GO composites was confirmed by XRD pattern. Comparing with MIL-101 (Fe), the BET surface area and total pore volume of MIL-GO composites significantly decreased owing to the coverage of MIL-101 (Fe) by nonporous GO sheets with low surface area. The defect-free Pebax® 2533/PVDF thin film MMMs were successfully fabricated, indicating the homogeneous dispersion of the synthesized fillers in Pebax matrix. It was found that the incorporation of MIL-GO (Fe) into Pebax matrix significantly increased the

Table 3 Summary of gas separation performances of Pebax-based MMMs

Fillers	Filler content (wt%)	$P_{\text{CO}_2}$ (barrer)	$\alpha_{\text{CO}_2/\text{N}_2}$	Experimental condition: $P$ (bar)/ $T$ (°C)	Ref.
MIL-53	10	129	48	10/35	47
NH <sub>2</sub> -MIL-53	10	149	56	10/35	47
MIL-101	15	71	47	1.5/20	40
NH <sub>2</sub> -MIL-101	5	74	43	1.5/20	40
UiO-66	7.5	90	60	3/20	48
ZIF-8	15	106	35	1/23	49
ZIF-7-CH <sub>3</sub> OH	10	562	19	4.5/25	54
Zn/Ni-ZIF-8	15	440	40	2/25	55
ZIF-90@C <sub>3</sub> N <sub>4</sub>	8	110	84	2/25	46
GO	2	108	48	7/35	50
GO	2	100	68	2/30	51
GO	0.02	371	24	1/35	44
Reduced GO	5	119	104	2/30	43
MXene	1	148	63	2/30	51
ZIF-8@GO	6	249	47	1/25	17
ZIF-8@GO	20	136	78	3/25	18
CuBDC-ns@MoS <sub>2</sub>	2.5	123	69	4/35	53
MIL-GO-2	9.1	303	24	2/20	This work





CO<sub>2</sub> permeability without changing the CO<sub>2</sub>/N<sub>2</sub> ideal selectivity of Pebax selective layer. While the incorporation of MIL-GO-2 into Pebax matrix simultaneously increased the CO<sub>2</sub> permeability and the CO<sub>2</sub>/N<sub>2</sub> ideal selectivity of Pebax selective layer. The improvement of the gas separation performance of MMMs resulted from the additional gas molecules pathway provided by MIL-GO-2, the additional free volume and the rearrangement of polymer chains in Pebax matrix, the high affinity of MIL-GO-2 to CO<sub>2</sub>, and the tortuous diffusion pathways created by GO nanosheets. The prepared Pebax® 2533/PVDF thin film MMMs containing 9.1 wt% MIL-GO-2 demonstrated the highest CO<sub>2</sub> permeability equal to 303 barrer (1 barrer = 10<sup>-10</sup> cm<sup>3</sup> (STP) cm cm<sup>-2</sup> s<sup>-1</sup> cmHg<sup>-1</sup>) and the highest CO<sub>2</sub>/N<sub>2</sub> ideal selectivity equal to 24.

## Author contributions

Conceptualization, G. L. and W. K.; data curation, G. L. and K. K.; formal analysis, G. L., W. K., K. K. and J. K.; funding acquisition, G. L. and W. K.; investigation, G. L.; methodology, G. L., W. K. and J. K.; resources, W. K.; software, K. K. and J. K.; supervision, W. K. and J. K.; validation, G. L.; visualization, G. L. and K. K.; writing—original draft, G. L.; writing—review & editing, G. L., W. K. and K. K. All authors have read and agreed to the published version of the manuscript.

## Conflicts of interest

There are no conflicts to declare.

## Acknowledgements

This work was supported by the fund from Excellence Initiative – Research University – Nicolaus Copernicus University in Torun (Emerging Field and Grants4NCUStudents).

## Notes and references

- Q. Sohaib, A. Muhammad, M. Younas and M. Rezakazemi, *Sep. Purif. Technol.*, 2020, **241**, 116677.
- N. Hajilary, M. Rezakazemi and A. Shahi, *Mater. Sci. Energy Technol.*, 2020, **3**, 218–224.
- A. Arabi Shamsabadi, M. Rezakazemi, F. Seidi, H. Riazi, T. Aminabhavi and M. Soroush, *Prog. Energy Combust. Sci.*, 2021, **84**, 100903.
- C. Ma, M. Wang, Z. Wang, M. Gao and J. Wang, *J. CO<sub>2</sub> Util.*, 2020, **42**, 101296.
- S. Bandehali, A. Moghadassi, F. Parvizian, S. M. Hosseini, T. Matsuura and E. Joudaki, *J. Energy Chem.*, 2020, **46**, 30–52.
- H. Rajati, A. H. Navarchian, D. Rodrigue and S. Tangestaninejad, *Chem. Eng. Process.*, 2021, **168**, 108590.
- L. M. Robeson, *J. Membr. Sci.*, 2008, **320**, 390–400.
- A. R. Kamble, C. M. Patel and Z. V. P. Murthy, *Renewable Sustainable Energy Rev.*, 2021, **145**, 111062.
- M. M. Zagho, M. K. Hassan, M. Khraisheh, M. A. A. Al-Maadeed and S. Nazarenko, *Chem. Eng. J. Adv.*, 2021, **6**, 100091.
- M. M. H. Shah Buddin and A. L. Ahmad, *J. CO<sub>2</sub> Util.*, 2021, **51**, 101616.
- M. Vinoba, M. Bhagiyalakshmi, Y. Alqaheem, A. A. Alomair, A. Pérez and M. S. Rana, *Sep. Purif. Technol.*, 2017, **188**, 431–450.
- S. S. Swain, L. Unnikrishnan, S. Mohanty and S. K. Nayak, *Int. J. Hydrogen Energy*, 2017, **42**, 29283–29299.
- G. Li, W. Kujawski, K. Knozowska and J. Kujawa, *Materials*, 2021, **14**, 3366.
- W. Chen, Z. Zhang, C. Yang, J. Liu, H. Shen, K. Yang and Z. Wang, *J. Membr. Sci.*, 2021, **636**, 119581.
- Y. Shi, S. Wu, Z. Wang, X. Bi, M. Huang, Y. Zhang and J. Jin, *Sep. Purif. Technol.*, 2021, **277**, 119449.
- C. Jiao, Z. Li, X. Li, M. Wu and H. Jiang, *Sep. Purif. Technol.*, 2021, **259**, 118190.
- L. Dong, M. Chen, J. Li, D. Shi, W. Dong, X. Li and Y. Bai, *J. Membr. Sci.*, 2016, **520**, 801–811.
- K. Yang, Y. Dai, X. Ruan, W. Zheng, X. Yang, R. Ding and G. He, *J. Membr. Sci.*, 2020, **601**, 117934.
- B. Chen, C. Wan, X. Kang, M. Chen, C. Zhang, Y. Bai and L. Dong, *Sep. Purif. Technol.*, 2019, **223**, 113–122.
- H. R. Mahdipoor, R. Halladj, E. Ganji Babakhani, S. Amjad-Iranagh and J. Sadeghzadeh Ahari, *Colloids Surf., A*, 2021, **619**, 126554.
- M. Y. Zorainy, M. Gar Alalm, S. Kaliaguine and D. C. Boffito, *J. Mater. Chem. A*, 2021, **9**, 22159–22217.
- Z. Liu, W. He, Q. Zhang, H. Shapour and M. F. Bakhtari, *ACS Omega*, 2021, **6**, 4597–4608.
- J. Lin, H. Hu, N. Gao, J. Ye, Y. Chen and H. Ou, *J. Water Process. Eng.*, 2020, **33**, 101010.
- G. Li, W. Kujawski, A. Tonkonogovas, K. Knozowska, J. Kujawa, E. Olewnik-Kruszkowska, N. Pedišius and A. Stankevičius, *Chem. Eng. Res. Des.*, 2022, **181**, 195–208.
- F. Zhao, Y. Liu, S. B. Hammouda, B. Doshi, N. Guijarro, X. Min, C.-J. Tang, M. Sillanpää, K. Sivula and S. Wang, *Appl. Catal., B*, 2020, **272**, 119033.
- C. Petit and T. J. Bandoz, *Adv. Funct. Mater.*, 2011, **21**, 2108–2117.
- N. Liu, W. Huang, X. Zhang, L. Tang, L. Wang, Y. Wang and M. Wu, *Appl. Catal., B*, 2018, **221**, 119–128.
- C. Petit and T. J. Bandoz, *Adv. Mater.*, 2009, **21**, 4753–4757.
- M. Seredych, C. Petit, A. V. Tamashausky and T. J. Bandoz, *Carbon*, 2009, **47**, 445–456.
- F. Besharat, M. Manteghian, G. Gallone and A. Lazzeri, *Nanotechnology*, 2020, **31**, 155701.
- M. D. Donohue and G. L. Aranovich, *Adv. Colloid Interface Sci.*, 1998, **76–77**, 137–152.
- M. Y. Zorainy, H. M. Titi, S. Kaliaguine and D. C. Boffito, *Dalton Trans.*, 2022, **51**, 3280–3294.
- C. Yang, X. You, J. Cheng, H. Zheng and Y. Chen, *Appl. Catal., B*, 2017, **200**, 673–680.
- J. Zhu, H. Zhang, Q. Liu, C. Wang, Z. Sun, R. Li, P. Liu, M. Zhang and J. Wang, *J. Taiwan Inst. Chem. Eng.*, 2019, **99**, 45–52.
- K. S. W. Sing and R. T. Williams, *Adsorpt. Sci. Technol.*, 2004, **22**, 773–782.



- 36 M.-L. Chen, S.-Y. Zhou, Z. Xu, L. Ding and Y.-H. Cheng, *Molecules*, 2019, **24**, 3718.
- 37 W. Li, H. Li and Y.-M. Zhang, *J. Mater. Sci.*, 2009, **44**, 2977–2984.
- 38 Z. Zeng, D. Yu, Z. He, J. Liu, F.-X. Xiao, Y. Zhang, R. Wang, D. Bhattacharyya and T. T. Y. Tan, *Sci. Rep.*, 2016, **6**, 20142.
- 39 S. Govender, W. Przybylowicz and P. Swart, *Desalin. Water Treat.*, 2009, **9**, 272–278.
- 40 C. Song, R. Li, Z. Fan, Q. Liu, B. Zhang and Y. Kitamura, *Sep. Purif. Technol.*, 2020, **238**, 116500.
- 41 J. G. Wijmans and R. W. Baker, *J. Membr. Sci.*, 1995, **107**, 1–21.
- 42 Q. Xin, Z. Li, C. Li, S. Wang, Z. Jiang, H. Wu, Y. Zhang, J. Yang and X. Cao, *J. Mater. Chem. A*, 2015, **3**, 6629–6641.
- 43 G. Dong, J. Hou, J. Wang, Y. Zhang, V. Chen and J. Liu, *J. Membr. Sci.*, 2016, **520**, 860–868.
- 44 R. Casadei, M. Giacinti Baschetti, M. J. Yoo, H. B. Park and L. Giorgini, *Membranes*, 2020, **10**, 188.
- 45 S. Khoshhal Salestan, K. Pirzadeh, A. Rahimpour and R. Abedini, *J. Environ. Chem. Eng.*, 2021, **9**, 105820.
- 46 F. Guo, D. Li, R. Ding, J. Gao, X. Ruan, X. Jiang, G. He and W. Xiao, *Sep. Purif. Technol.*, 2022, **280**, 119803.
- 47 S. Meshkat, S. Kaliaguine and D. Rodrigue, *Sep. Purif. Technol.*, 2018, **200**, 177–190.
- 48 J. Shen, G. Liu, K. Huang, Q. Li, K. Guan, Y. Li and W. Jin, *J. Membr. Sci.*, 2016, **513**, 155–165.
- 49 M. Li, X. Zhang, S. Zeng, L. bai, H. Gao, J. Deng, Q. Yang and S. Zhang, *RSC Adv.*, 2017, **7**, 6422–6431.
- 50 D. Zhao, J. Ren, Y. Qiu, H. Li, K. Hua, X. Li and M. Deng, *J. Appl. Polym. Sci.*, 2015, **132**, 42624.
- 51 F. Shi, J. Sun, J. Wang, M. Liu, Z. Yan, B. Zhu, Y. Li and X. Cao, *J. Membr. Sci.*, 2021, **620**, 118850.
- 52 L. Liu, A. Chakma and X. Feng, *Ind. Eng. Chem. Res.*, 2005, **44**, 6874–6882.
- 53 N. Liu, J. Cheng, W. Hou, C. Yang, X. Yang and J. Zhou, *Sep. Purif. Technol.*, 2022, **282**, 120007.
- 54 J. Gao, H. Mao, H. Jin, C. Chen, A. Feldhoff and Y. Li, *Microporous Mesoporous Mater.*, 2020, **297**, 110030.
- 55 X. Zhang, T. Zhang, Y. Wang, J. Li, C. Liu, N. Li and J. Liao, *J. Membr. Sci.*, 2018, **560**, 38–46.

